Exploiting DNA repair defects in high-grade serous ovarian carcinoma

Ksenija Nesic

OCRID iD: https://orcid.org/0000-0001-9972-9819

Submitted in total fulfilment of the requirements

for the degree of Doctor of Philosophy

February 2020

Walter and Eliza Hall Institute of Medical Research

Department of Medical Biology

The University of Melbourne

Abstract

High-Grade Serous Ovarian Carcinoma (HGSOC) is the most common subtype of ovarian cancer, and is the leading cause of ovarian cancer death. This subtype is molecularly characterised by frequent loss of Homologous Recombination (HR) DNA repair, making it susceptible to Poly-ADP ribose polymerase (PARP) inhibitor treatment. Despite the efficacy of PARP inhibitors (PARPi) in treating HGSOC, disease recurrence is common. A poor understanding of PARPi toxicity and resistance mechanisms has limited improvements in overall survival of patients. This project utilised HGSOC Patient-Derived Xenograft (PDX) and *in vitro* models to determine underlying mechanisms of PARPi sensitivity and resistance.

Characterisation of the HGSOC PDX cohort led to the discovery of 2 models with HR gene secondary mutations, thereby explaining the poor PARPi responses of these tumours. Loss of the Classical Non-Homologous End-Joining (C-NHEJ) DNA repair pathway was also investigated but was not supported as a mechanism of resistance in PDX, or in a genome-wide PARPi-resistance CRISPR screen using a *BRCA2*-mutant cell line. The CRISPR screen revealed *PARP1* mutations as the top hit, but no C-NHEJ mutation hits. CRISPR screens have also been optimised for a *BRCA1*-mutant cell line and a unique *BRCA1* methylated cell line, to enable future validation in different HRD contexts. HR gene methylation analysis in the HGSOC PDX models revealed distinct *BRCA1* promoter methylation profiles, subsequently found to represent “homozygous” and “heterozygous” methylation states. Our group demonstrated that all copies of *BRCA1* must be methylated for gene silencing and PARPi response, and that methylation can be lost under treatment pressure in patients. I then investigated this mechanism in two HGSOC PDX models with *RAD51C* promoter methylation. *RAD51C* promoter methylation was found to have homogeneous or heterogeneous patterns, and both caused gene silencing and PARPi response in the PDX, that could be lost under treatment pressure. One third of patient samples tested appear to have a heterogeneous *RAD51C* methylation profile and, like the PDX, some responded to chemotherapy. To assess whether global methylation profiles influenced HR gene methylation stability, I carried out genome-wide methylation array analysis of PDX models and clinical samples. Analysis of cyclically PARPi re-treated *RAD51C* methylated tumours from one PDX model demonstrated increasing global losses in methylation with each treatment cycle.

Through characterisation of the HGSOC PDX cohort and *in vitro* CRISPR screens, I have uncovered both well-established mechanisms of resistance (e.g. secondary mutations), and less studied mechanisms of sensitivity and resistance, such as loss of *RAD51C* methylation and *PARP1* loss. These models provide a platform for further study of these PARPi resistance mechanisms, including potential therapeutics to prevent or overcome their development in the clinic.

Declaration

This is to certify that:

(i) This thesis comprises only my original work towards the PhD except where indicated in the Preface,

(ii) Due acknowledgement has been made in the text to all other material used,

(iii) This thesis is less than 100,000 words in length, exclusive of tables, maps, bibliographies and appendices



Signature: ……

Ksenija Nesic

The Walter and Eliza Hall Institute of Medical Research

Department of Medical Biology

The University of Melbourne

Parkville, Victoria 3052

Australia

14 February 2020

Preface

Chapter 1. 100% author contribution

Chapter 2. 100% author contribution

Chapter 3. 90% author contribution

Drug responses for PDX models (excluding 134183, WEHI-PH039, 34931, 34939, 34939B, 134206 and 23133) were characterised before the start of my PhD project by Dr Monique Topp, Dr Valerie Heong, Dr Gwo Yaw-Ho, Elizabeth Lieschke, Dr Alison Hardley and Dr Robert Holian (Kondrashova et al., 2018; Topp et al., 2014). Animal experiments were managed and performed by Dr Olga Kondrashova, Dr Cassandra Vandenberg, Silvia Stoev and Kathy Barber with support from bioservices staff.

Chapter 4. 90% author contribution

Western blots and IHC were run by the Kaufmann group (Mayo Clinic, MN, USA). PEO1 A2 cell line was sourced from the Kaufmann group (AlHilli et al., 2016).

Chapter 5. 95% author contribution

MAYO-PH039 PDX was characterised by the Kaufmann group (Mayo Clinic, MN, USA). DNA bisulfite conversions and MS-HRM assays were performed by the Dobrovic group (Oliva Newton John Cancer Research Institute). RNAseq data was analysed by Matthew Wakefield. Initial analysis of targeted RAD51C sequencing and SNP array data was done by Olga Kondrashova.

Chapter 6. 95% author contribution

EPIC methylation arrays were performed by the Southey group (Monash University/ University of Melbourne).

Thus, the author's overall contribution to work in this thesis was > 90%.

The following publications fully or partially arising from the work in this thesis have been prepared during this study:

- Kondrashova O, Topp M, **Nesic K**, Lieschke E, Ho G, Harrell M, Zapparoli G, Hadley A, Holian R, Boehm E, Heong V, Sanij E, Pearson R, Krai J, Johnson N, McNally O, Ananda S, Alsop K, Hutt K, Kaufmann S, Lin K, Harding T, Traficante N, Australian Ovarian Cancer Study, DeFazio A, McNeish I, Bowtell D, Swisher E, Dobrovic A, Wakefield M, Scott C. Methylation of all BRCA1 copies predicts response to the PARP inhibitor rucaparib in ovarian carcinoma. Nature Communications. 2018 Sep 28;9(1):3970. doi: 10.1038/s41467-018-05564-z.

- **Nesic K**, Wakefield M, Kondrashova O, Scott CL, McNeish IA. Targeting DNA repair: the genome as a potential biomarker. The Journal of pathology. 2018 Apr;244(5):586-97. doi: 10.1002/path.5025.

- Wakefield MJ, **Nesic K**, Kondrashova O, Scott CL. Diverse mechanisms of PARP inhibitor resistance in ovarian cancer. Biochimica et biophysica acta. Reviews on cancer. 2019 Dec;1872(2):188307. doi: 10.1016/j.bbcan.2019.08.002.

Funding for this work was provided by the Australian Government Research Training Program Stipend Scholarship (formerly Australian Postgraduate Award), The Stafford Fox Medical Research Foundation and the Bev Gray Ovarian Cancer Scholarship.

Acknowledgements

I would like to express my deep appreciation and gratitude to my PhD supervisors Professor Clare Scott, Dr Matthew Wakefield and Dr Olga Kondrashova who made this work possible. Thank you for providing me with the opportunity to take on and complete this research project, and for the endless support, patience and guidance you have offered throughout this process. I have grown so much, both personally and professionally, since starting this project. Thanks to your wonderful supervision and the positive work environment you have cultivated within our group.

I would like to thank all members of the Scott Laboratory, both past and present. I could not have asked for a more positive and supportive group of people to work with for the last 4 years. I would like to thank Olga Kondrashova, Elizabeth Kyran, Elizabeth Lieshcke and Ellen Mathieson in particular for being great friends and colleagues during the difficult periods. I cherish the time we spent working together, and I hope we remain good friends long into the future. I would also like to thank the staff in WEHI bioservices, the genomics group and flow cytometry core for their support during my project, and our brilliant collaborators in the laboratories of Professor Scott Kaufmann, Professor Elizabeth Swisher and Professor Alexander Dobrovic. I wish to thank members of the 2017 and 2018 WESA student committees for their friendship and encouragement. I also wish to acknowledge the Stem Cells and Cancer Division for their kindness, helpfulness and valuable insights over the years.

I would like to thank all the women with ovarian cancer who participated in this study, making this work possible, and the Australian Ovarian Cancer Study (AOCS) for providing access to precious human ovarian cancer samples. I am also extremely grateful for the financial support I received through the Australian Postgraduate Award and the Bev Gray scholarship, which provided my PhD stipend.

In closing, I would like to thank my parents, Nina and Dragan, for supporting me during the PhD and for everything leading up to that point. Your love and support created the foundation for all of my growth and achievement, and I would not be here without you. Thank you to my beautiful sister Caterina, and my wonderful partner Alex for brightening my life and always being there for me when I really needed it.

Abbreviations

AOCS	Australian Ovarian Cancer Study
alt-EJ	Alternative end-joining
BER	Base excision repair
BET	Bromodomain and Extra-Terminal motif
Bp	Basepairs
BPM	Prophylactic bilateral mastectomy
BRCA	Breast cancer susceptibility genes
C-NHEJ	Classical non-homologous end joining
CA125	Cancer-antigen 125
CASCADE	**CA**ncer Ti**S**sue **C**ollection **A**fter **DE**ath
CDK	Cyclin-dependent kinase
Chr	Chromosome
CI	Confidence interval
CN	Copy number
cnLOH	Copy number-neutral loss of heterozygosity
CoQ	Co-enzyme Q
CR	Complete response
CRISPR	Clustered regularly interspaced short palindromic repeats
D11q	BRCA1 delta-11q isoform
ddPCR	droplet digital Polymerase Chain Reaction
DPBS	Dulbecco's phosphate buffered saline
DSB	Double-strand breaks
EGF	Epidermal growth factor
EMA	European Medicines Agency
EOC	Epithelial ovarian cancer
EpCAM	Epithelial cell adhesion molecule
FACS	Fluorescence activated cell sorting
FCS	Foetal calf serum
FDA	Food and Drug Administration
FIGO	International Federation of Gynaecology and Obstetrics
GO	Gene ontology
H&E	Hematoxylin and eosin
H3K27me3	Histone 3 Lysine 27 tri-methylation
H3K4me1	Histone 3 Lysine 4 mono-methylation
H3K9me3	Histone 3 Lysine 9 tri-methylation
HGSOC	High Grade Serous Ovarian Carcinoma
HPF1	Histone PARylation factor 1
HR	Homologous recombination
HRa	Hazard ratio for progression or death
HRC	Homologous recombination competent

HRD	Homologous recombination deficient
ICGC	International Cancer Genome Consortium
ICLs	Interstrand crosslinks
IHC	Immunohistochemistry
Kb	Kilobases
KO	Knock out
LFC	Log fold change
LLS	"Left left shift" curve
LOH	Loss of heterozygosity
LR-PCR	Long-range polymerase chain reaction
LS	"Left shift" curve
LTH	Long Term Harvest
MAPK	Mitogen-activated protein kinase
me*BRCA1*	methylated *BRCA1* promoter
MECOM	MDS1 and EVI1 Complex Locus
meCpG	Methylated CpG site
me*RAD51C*	methylated *RAD51C* promoter
MLPA	Multiplex ligation-dependent probe amplification
MS-HRM	Methylation specific high resolution melt
MS-PCR	Methylation specific polymerase chain reaction
NF1	Neurofibromin 1
NGS	Next generation sequencing
NHEJ	Non-homologous end-joining repair
NPC	Nuclear pore complex
NSG	Non-obese diabetic severe combined immunodeficient (NOD-SCID) interleukin-2 receptor (IL-2r)-null recipient
Nt	nucleotides
OC	Ovarian cancer
OS	Overall survival
PARG	Poly(ADP-ribose) glycohydrolase
PARP	Poly(ADP)-ribose polymerase
PARPi	PARP inhibitors
PCR	Polymerase Chain Reaction
PD	Progressive disease
PD-1	Programmed cell death protein 1
PD-L1	Programmed death-ligand 1
PDX	Patient derived xenograft
PFA	Paraformaldehyde
PFI	Platinum free interval
PFS	Progression Free Survival
PI	Propidium iodide
PI3Ks	phosphoinositide 3-kinases

PR	Partial Response
qPCR	Quantitative polymerase chain reaction
qRT-PCR	Quantitative real-time polymerase chain reaction
RB1	Retinoblastoma 1
RFU	Relative fluorescence units
RNA	Ribonucleic acid
RNAseq	RNA sequencing
rRNA	Ribosomal RNA
RRSO	Bilateral risk reducing salphingo-oophorectomy
SD	Stable Disease
SEER	The Surveillance, Epidemiology, and End Results program of the National Cancer Institute
siRNA	Small interfering RNA
snoRNA	Small nucleolar RNA
SNV	Single nucleotide variant
SSA	Single-strand annealing
SSU	Small Subunit Processome
STH	Short-term harvest
SV	Structural variants
TCGA	The Cancer Genome Atlas
TFI	Treatment free interval
TFST	Time to first subsequent therapy
TIC	Tubal intraepithelial carcinoma
TIL	Tumour-infiltrating lymphocytes
TNBC	Triple-negative breast cancer
TP53	Tumour Protein 53
TTH	Time To Harvest
TTP	Time To Progression
VEGF	Vascular endothelial growth factor
VEGFR	VEGF receptor
WB	Western blot
WEHI	Walter and Eliza Hall Institute
WGS	Whole genome sequencing
WT	Wild-type

Table of contents

1 Introduction 21

1.1 High-grade serous ovarian carcinoma 22
1.1.1 High-grade serous ovarian carcinoma pathology 22
1.1.2 Early diagnosis and screening of high-grade serous ovarian carcinoma 23
1.1.3 Standard treatment of high-grade serous ovarian carcinoma 24
1.1.4 Targeted treatment of high-grade serous ovarian carcinoma with VEGF inhibitors 25
1.1.5 Targeted treatment of high-grade serous ovarian carcinoma with PARP inhibitors 26

1.2 Molecular features of high grade serous ovarian carcinoma 34
1.2.1 Loss of p53 function 34
1.2.2 Homologous recombination DNA repair deficiency 35
1.2.3 Loss of tumour suppressors RB1 and NF1 38
1.2.4 Oncogene amplifications 39

1.3 Predicting response to PARP inhibitors 40
1.3.1 Importance of BRCA1 and BRCA2 genes in HGSOC therapy 40
1.3.2 Impacts of non-BRCA HR defects on HGSOC therapy 41
1.3.3 Impact of BRCA1 or RAD51C promoter methylation on HGSOC therapy 43
1.3.4 Limitations of HR gene testing in the clinic 43
1.3.5 Genomic scarring as a marker of HR deficiency in HGSOC 45

1.4 Proposed mechanisms of PARP inhibitor sensitivity 46
1.4.1 PARP inhibitors and base excision repair 47
1.4.2 PARP1 trapping and replication fork collapse 47
1.4.3 Competing DNA repair pathways/ de-regulated non-homologous end joining 49
1.4.4 Combining different models of PARPi action 51

1.5 Mechanisms of PARP inhibitor resistance 52
1.5.1 Homologous recombination pathway reversion 52
1.5.2 C-NHEJ pathway loss 54
1.5.3 Replication fork protection 54
1.5.4 Contribution of other signalling pathways 56
1.5.5 Drug efflux 57

1.6 Evolution of PARP inhibitor resistance 58

1.7 Project Rationale and Aims 59

2 Materials and Methods 61

2.1 Molecular methods 61
2.1.1 DNA purification from tissues and cell pellets 61
2.1.2 Ethanol precipitation of DNA 61
2.1.3 Quantification of double-stranded DNA 61
2.1.4 Murine vs Human PCR 62
2.1.5 TP53 molecular identification check next generation sequencing libraries 62
2.1.6 Mutation reversion analysis using amplicon sequencing 63
2.1.7 Mutation reversion analysis using amplicon Long Range PCR-based sequencing 64
2.1.8 Targeted sequencing of DCLRE1C CRISPR mutation 65
2.1.9 Methylation-specific High Resolution Melt 66
2.1.10 RAD51C bisulfite amplicon sequencing 66
2.1.11 Agarose gel electrophoresis 67
2.1.12 AmpureXP library clean-up 67
2.1.13 NexteraXT and amplicon library pooling and sequencing 68
2.1.14 Brunello CRISPR library pooling and sequencing 68
2.1.15 Zymo RNA extraction 71
2.1.16 BRCA1 exon skipping quantitative PCR protocol 71
2.1.17 RAD51C quantitative real-time PCR 72
2.1.18 RAD51C immunoblotting 73

2.1.19 RNA sequencing of PDX 73
2.1.20 RAD51C copy number assessment by MLPA-seq 74

2.2 *In vitro* and cell culture protocols 76
2.2.1 Cell line culture 76
2.2.2 Cell viability assays 77
2.2.3 Cell counting 77
2.2.4 Genome-wide PARPi-resistance CRISPR screens 78
2.2.5 DNA repair foci in PDX tumours 82
2.2.6 PDX DNA repair foci imaging 84
2.2.7 DNA repair foci in cell lines 85

2.3 *In vivo* Patient Derived Xenograft protocols 86
2.3.1 Generation of PDX models 86
2.3.2 Establishment of WEHI-PH039 PDX lineages A and B 87
2.3.3 Immunohistochemistry 87
2.3.4 PDX in vivo single-agent treatments 87
2.3.5 PDX 134183 and WEHI-PH039 in vivo rucaparib re-treatments 88
2.3.6 In vivo data analysis 89

2.4 *In silico* protocols 89
2.4.1 Molecular landscape summary of HGSOC PDX cohort 89
2.4.2 Illumina Infinium EPIC and 450K array analysis 90
2.4.3 Analysis of CRISPR screen data using CRISPRAnalyzeR software 90
2.4.4 TP53 and reversion mutation analysis 91
2.4.5 Targeted RAD51C bisulfite sequencing analysis 91
2.4.6 MLPA-seq analysis 91

3 Characterisation of HGSOC PDX cohort 92

3.1 Introduction 92

3.2 Chapter 3 hypotheses 95

3.3 Chapter 3 aims 95

3.4 Results 96
3.4.1 Summary of HGSOC PDX cohort 96
3.4.2 Secondary and reversion mutation screening 104
3.4.3 BRCA1 methylation zygosity 113
3.4.4 Constitutional BRCA1 methylation and BRCA1 methylation stability 114
3.4.5 RAD51C methylation in PDX models 118
3.4.6 BRCA1 D11q isoform testing 118
3.4.7 Screening for C-NHEJ gene mutations 138
3.4.8 CHD4 mutation in PDX #134019 139

3.5 Discussion 142
3.5.1 Reversion mutation screening is crucial for understanding platinum and PARPi responses in PDX 142
3.5.2 Tumour heterogeneity influences PARPi responses 143
3.5.3 The power of PDX models for the study of HR gene methylation 144
3.5.4 No PARP1 or C-NHEJ pathway mutations detected in PDX 144
3.5.5 Re-treatment studies to drive resistance 145
3.5.6 Measuring HR competence in PDX 146
3.5.7 Future studies of immune interactions in HGSOC PDX 146
3.5.8 Further characterisation of PDX models 147

4 DNA repair pathways and PARPi sensitivity and resistance 148

4.1 Introduction 148
4.1.1 Role of C-NHEJ 148
4.1.2 Pre-clinical HGSOC models with C-NHEJ loss 149

4.2 Chapter 4 hypotheses 152

4.3 Chapter 4 aims 152

4.4 Results 153
4.4.1 C-NHEJ loss and PARPi resistance 153
4.4.2 Characterisation of Artemis-deficient cell line 153
4.4.3 Identification of PARPi resistance through pooled CRISPR screen 176

4.5 Discussion 195
4.5.1 PEO1A2 cell line characterisation raises questions 195
4.5.2 Inconsistent C-NHEJ profiles of PDX 134013 tumours 195
4.5.3 Rationale for genome-wide PARPi resistance CRISPR screens 196
4.5.4 C-NHEJ pathway hits absent in CRISPR screen 196
4.5.5 Other hits absent in CRISPR screen 197
4.5.6 Interpretation of enriched gene hits 197
4.5.7 Interpretation of depleted gene hits 202
4.5.8 In silico validation of hits 204
4.5.9 Future CRISPR screens 205

5 *RAD51C* promoter methylation and PARPi response 207

5.1 Introduction 207

5.2 Chapter 5 hypotheses 211

5.3 Chapter 5 aims 211

5.4 Results 212
5.4.1 PDX 134183 characterisation 212
5.4.2 MAYO-PH039 characterisation 218
5.4.3 WEHI-PH039 characterisation 219
5.4.4 DNA repair capacity of RAD51C methylated PDX models 225
5.4.5 Bisulfite capture sequencing using methyl-BROCA 231
5.4.6 Driving RAD51C methylation loss in PDX 134183 239
5.4.7 Driving RAD51C methylation loss in PDX WEHI-PH039 241
5.4.8 RAD51C promoter methylation and gene expression in PDX 245
5.4.9 RAD51C copy-number analysis in PDX 134183 and WEHI-PH039 251
5.4.10 Targeted bisulfite meRAD51C sequencing 252
5.4.11 Patterns of RAD51C methylation in clinical samples 258

5.5 Discussion 264
5.5.1 Analysis of new PDX lineages 265
5.5.2 Further optimization of the DNA repair foci assay 265
5.5.3 Interpretation of DNA repair foci results 266
5.5.4 Potential of targeted meRAD51C sequencing assay 267
5.5.5 Patterns of meRAD51C in clinical samples 268
5.5.6 Mechanisms influencing DNA methylation states at RAD51C promoter 269

6 Genome-wide DNA methylation profiling of HGSOC PDX models 270

6.1 Introduction 270
6.1.1 PDX samples selected for EPIC array 273

6.2 Chapter 6 hypotheses: 275

6.3 Chapter 6 aims: 275

6.4 Results 276
6.4.1 Validation of EPIC array for PDX samples 276
6.4.2 Clustering of PDX samples run on EPIC array 277
6.4.3 RAD51C and BRCA1 gene promoter methylation patterns 279
6.4.4 Methylation patterns of other genes 282
6.4.5 Global methylation profiles of PDX 287
6.4.6 Differential methylation analysis in RAD51C-methylated PDX models 288
6.4.7 Gene ontology terms for MAYO-PH039 differential methylation analysis 298
6.4.8 Differential methylation analysis in BRCA1-methylated PDX models 300

6.4.9 Searching for signatures: ICGC differential methylation analysis 304
6.4.10 Searching for signatures: ICGC manual methylation analysis 312

6.5 Discussion 319
6.5.1 RAD51C and BRCA1 methylation profiles of PDX 319
6.5.2 Methylation profiles of other genes 319
6.5.3 Characterisation of PDX by global methylation profiles 320
6.5.4 Global methylation losses in MAYO-PH039 with niraparib re-treatment 320
6.5.5 Gene ontology analysis of MAYO-PH039 treated samples 321
6.5.6 Differential methylation analysis of homozygous vs heterozygous BRCA1 methylated PDX 322
6.5.7 ICGC sample methylation analysis 323

7 Discussion and Conclusions 325

7.1 Introduction 325

7.2 Outcomes of PhD project 326
7.2.1 PDX are a valuable resource for the study of PARPi sensitivity and resistance HGSOC 327
7.2.2 Types of PARPi resistance mechanisms observed in PDX models 330
7.2.3 Genome-wide PARPi resistance CRISPR screens may uncover novel biological aspects of PARPi action 332
7.2.4 RAD51C promoter methylation influences PARPi responses 333
7.2.5 Relationship between DNA methylation stability and underlying histone marks 334

7.3 Closing remarks 335

8 References 337

9 Appendices 368

List of Figures

Figure 1.1. Homologous recombination DNA repair pathway. 37
Figure 1.2. The classical NHEJ pathway. 51
Figure 1.3. Competing DNA DSB repair pathways. 52
Figure 1.4. Evolution of PARPi and platinum resistance. 58
Figure 3.1. Summary of genomic profiles for all HGSOC PDX models. 101
Figure 3.2. Two in-house sequencing approaches designed for secondary mutation screening. 107
Figure 3.3. Takara polymerase outperforms Phusion polymerase in LR-PCR optimization. 108
Figure 3.4. BRCA1 revertant PDX 34931 is cisplatin and PARPi resistant. 111
Figure 3.5. Correcting BRCA2 secondary mutation in PDX 34931 112
Figure 3.6. Relative BRCA1 expression in meBRCA1 homozygous and heterozygous models. 114
Figure 3.7. BRCA1 methylation can be lost following chemotherapy in patients. 115
Figure 3.8. Hypothesis for constitutional methylation and stability of tumour methylation under treatment pressure. 116
Figure 3.9. BRCA1 isoform qPCR primer design. 120
Figure 3.10. Two lineages with different PARPi sensitivity derived from PDX 134056. 122
Figure 3.11. Direct comparison of PDX 134056 lineage #56S and #56R rucaparib 300mg/kg responses. 123
Figure 3.12. No elevated BRCA1 D11q expression in PDX 134056 LTH tumours. 124
Figure 3.13. BRCA1 exon 11-containing transcript expression in LTH PDX 134056 lineage #56S and #56R tumours. 125
Figure 3.14. "BRCA1 All" expression in LTH PDX 134056 lineage #56S and #56R tumours. 126
Figure 3.15. Slightly elevated BRCA1 D11q expression in PDX 134056 STH tumours. 128
Figure 3.16. BRCA1 exon 11-containing transcript expression in STH PDX 134056 lineage #56S and #56R tumours. 129
Figure 3.17. "BRCA1 All" expression in STH PDX 134056 lineage #56S and #56R tumours. 130
Figure 3.18. Western blot for BRCA1 isoforms in PDX 134056 lineage #56S and #56R tumours. 131
Figure 3.19. BRCA1 D11q expression in PDX 56 associated with higher passage number in the 56R. 132
Figure 3.20. PDX 134056 rescue lineage #56cis is refractory to PARPi. 133
Figure 3.21. BRCA1 D11q isoform expression in LTH PDX 134056 lineage #56cis tumours. 134
Figure 3.22. PDX 134206 is sensitive to cisplatin and rucaparib. 135
Figure 3.23. BRCA1 D11q isoform expression in LTH PDX 134206 tumours. 136
Figure 3.24. BRCA1 exon 11-containing transcript expression in LTH PDX 134206 tumours. 137
Figure 3.25. "BRCA1 All" expression in LTH PDX 134056 lineage #56cis tumours. 138
Figure 3.26. Consequences of CHD4 mutation c.4226_4236del (p.Asn1410Thrfs*4). 139
Figure 3.27. In vivo cisplatin and rucaparib responses of PDX 134019. 140
Figure 4.1. PEO1A2 is relatively rucaparib resistant. 155
Figure 4.2. PEO1A2 is relatively cisplatin resistant. 155
Figure 4.3. PEO1A2, like PEO1, has impaired RAD51 foci formation following DNA damage. 157
Figure 4.4. IGV visualisation of PEO1A2 CRISPR mutations in Artemis gene (DCLRE1C). 158
Figure 4.5. PDX 134013 C-NHEJ lineage 1 rucaparib and cisplatin responses. 160
Figure 4.6. PDX 134013 C-NHEJ lineage 2 rucaparib and cisplatin responses. 161
Figure 4.7. PDX 134013 C-NHEJ lineage 3 rucaparib and cisplatin responses. 162
Figure 4.8. PDX 134013 C-NHEJ lineage 4 rucaparib and cisplatin responses. 163
Figure 4.9. Comparison of PDX 134013 C-NHEJ lineage rucaparib 450mg/kg responses. 165
Figure 4.10. Comparison of PDX 134013 C-NHEJ lineage rucaparib 300mg/kg responses. 166
Figure 4.11. Comparison of PDX 134013 C-NHEJ lineage tumour growth rates. 167
Figure 4.12. Key of XRCC4 staining intensity used to score PDX samples. 169
Figure 4.13. Key of Ku70 staining intensity used to score PDX samples. 170
Figure 4.14. Key of Ku80 staining intensity used to score PDX samples. 171
Figure 4.15. Key of DNA-PKcs staining intensity used to score PDX samples. 172

Figure 4.16. Outline of in vitro PARPi resistance CRISPR screen design. 177
Figure 4.17. In vitro rucaparib responses in cell lines screened for CRISPR screen experiment..... 179
Figure 4.18. In vitro cisplatin responses in cell lines screened for CRISPR screen experiment. 179
Figure 4.19. BRCA1 splice site mutation c.4096+1C>A detected at 100% frequency in COV362 cell line. 180
Figure 4.20. WEHI-CS62 rucaparib and cisplatin responses. 181
Figure 4.21. Example FACS plots of second mCherry sort for WEHI-CS62Cas9 cell line. 182
Figure 4.22. Cisplatin and rucaparib responses of PEO1 Cas9 unchanged compared to PEO1 cell line. 184
Figure 4.23. Cisplatin and rucaparib responses of UWB1.289 Cas9 unchanged compared to UWB1.289 cell line. 184
Figure 4.24. Cisplatin and rucaparib responses of WEHI-CS62 Cas9 unchanged compared to WEHI-CS62 cell line. 185
Figure 4.25. Growth and doubling rate curves of cell lines used for CRISPR screen. 186
Figure 4.26. WEHI-CS62 Cas9 cells appear more dispersed in culture than the PEO1 Cas9 and UWB1.289 Cas9 cells 187
Figure 4.27. Gene count summary for PEO1 (BRCA2-mutant) CRISPR screen samples. 191
Figure 4.28. Example CRISPRAnalyzeR output for significantly enriched guides in PEO1 post-PARPi (DESeq2). 192
Figure 4.29. MAGeCK enriched guide results for BRCA1 and BRCA2 genes reveal one enriched single guide-RNA (sgRNA) detected in BRCA2. 193
Figure 5.1. PDX MAYO-PH039 niraparib re-treatment experiments. 210
Figure 5.2. PDX 134183 is sensitive to cisplatin at a 4mg/kg dose. 213
Figure 5.3. PDX 134183 shows some response to the PARPi rucaparib. 214
Figure 5.4. PDX 134183 shows some response to the PARPi niraparib. 215
Figure 5.5. MS-PCR and MS-HRM show that PDX 134183 harbours RAD51C promoter methylation. 216
Figure 5.6. No RAD51C message or protein expression found in RNAseq and immunoblotting analysis of PDX 134183 treated and untreated samples. 217
Figure 5.7. MS-HRM reveals heterogeneous meRAD51C of PDX MAYO-PH039. 218
Figure 5.8. WEHI-PH039 Lineage A vs B in vivo cisplatin responses. 220
Figure 5.9. WEHI-PH039 Lineage A vs B in vivo rucaparib 300mg/kg responses. 221
Figure 5.10. WEHI-PH039 Lineage A vs B in vivo rucaparib 450mg/kg responses. 222
Figure 5.11. WEHI-PH039 Lineage A vs B in vivo niraparib responses. 223
Figure 5.12. PH039 lineage A vs B RAD51C methylation patterns by MS-HRM. 224
Figure 5.13. PDX tumour digested and FACS-sorted cells can be stained for DNA repair foci on cytospin slides and imaged on confocal microscope. 226
Figure 5.14. Improved separation of live and dead fixed cell populations using fixable stain. 227
Figure 5.15. PDX tumour digested and FACS-sorted cells can be attached to 96-well plates for foci staining and imaging on OPERA platform. 228
Figure 5.16. PDX 134183 does not form RAD51 DNA repair foci following DNA damage. 229
Figure 5.17. PH039 Lineage A and B have impaired RAD51 DNA repair foci forming capacity following DNA damage. 230
Figure 5.18. Example PDX 134183 meRAD51C profiles by methyl-BROCA. 233
Figure 5.19. Tumour heterogeneity influences meRAD51C measurements. 234
Figure 5.20. Tumour with 50% meRAD51C loss is 100% PDX 134183 based on TP53 mutation. 235
Figure 5.21. Methyl-BROCA profile reveals some RAD51C CpG sites less methylated than others in untreated MAYO-PH039. 236
Figure 5.22. Vehicle-treated PDX 134183 sample #8269 has heterogeneous meRAD51C profile. 237
Figure 5.23. PDX 134183 sample meRAD51C profile that matches that of MAYO-PH039. 238
Figure 5.24. Rucaparib and cisplatin retreatments of PDX 134183. 239
Figure 5.25. Example MS-HRM curve of rucaparib-treated 134183 sample with ~50% meRAD51C loss. 241
Figure 5.26. Rucaparib and cisplatin retreatments of PDX WEHI-PH039. 243

Figure 5.27. Example MS-HRM curve of rucaparib-treated WEHI-PH039 Lineage A sample with >50% meRAD51C loss. 244
Figure 5.28. Example MS-HRM curve of rucaparib-treated WEHI-PH039 Lineage A sample with 100% meRAD51C loss. 244
Figure 5.29. Example MS-HRM curve of rucaparib-treated WEHI-PH039 Lineage B sample with 100% meRAD51C loss. 245
Figure 5.30. Untreated PDX 134183 samples lack detectable RAD51C gene expression while some post-treatment samples demonstrate elevated RAD51C gene expression. 246
Figure 5.31. PDX 134183 tumours with meRAD51C loss have increased RAD51C expression compared to tumours without meRAD51C loss. 247
Figure 5.32. PARPi-treated PH039 Lineage A tumours regain RAD51C gene expression. 248
Figure 5.33. WEHI-PH039 Lineage A tumours with meRAD51C loss have increased RAD51C expression compared to tumours without meRAD51C loss. 249
Figure 5.34. No RAD51C gene expression detected in highly methylated PH039 Lineage B samples. 250
Figure 5.35. No apparent bias in targeted meRAD51C sequencing 253
Figure 5.36. Long-term storage of bisulfite-converted DNA samples does not affect results of meRAD51C sequencing. 255
Figure 5.37. WEHI-PH039 Lineage A and B have slightly different methylation profiles due to differential methylation of single CpG site. 256
Figure 5.38. High degree of RAD51C epiallele heterogeneity in source PDX MAYO-PH039. 257
Figure 5.39. Unmethylated RAD51C promoter epialleles first detected after cycle 1 of niraparib in MAYO-PH039. 258
Figure 5.40. Example MS-HRM curves and corresponding meRAD51C amplicon plots of clinical samples. 262
Figure 5.41. Not all patient samples with heterogeneous meRAD51C have the same unmethylated CpG sites as PDX PH039. 263
Figure 5.42. Majority of meRAD51C epialleles detected in clinical samples are highly methylated, containing ≥40% methylated CpG sites. 263
Figure 6.1. Contaminating murine DNA in PDX DNA samples does not significantly affect methylation measurements. 276
Figure 6.2. Global methylation value distributions of control samples. 277
Figure 6.3. PDX samples cluster together on MDS plot of dimensions 1 vs 2. 278
Figure 6.4. MDS clustering reveals WEHI-CS62 cell line has different methylation profile to PDX #134062. 278
Figure 6.5. WEHICS62 cell line has substantially different methylome to PDX #134062 tumours. 279
Figure 6.6. Methylation heatmap of all RAD51C CpG probes in EPIC array. 280
Figure 6.7. Methylation heatmap of all BRCA1 CpG probes in EPIC array. 281
Figure 6.8. EPIC array RAD51C CpG probes associated with gene silencing. 283
Figure 6.9. EPIC array BRCA1 CpG probes associated with gene silencing. 284
Figure 6.10. Methylation heatmap of all MLH1 CpG probes in EPIC array. 285
Figure 6.11. Methylation heatmap of all CDH13 CpG probes in EPIC array. 286
Figure 6.12. Methylome profiling of HGSOC PDX models by all CpG regions. 287
Figure 6.13. Methylome profiling of HGSOC PDX models by CpG islands. 288
Figure 6.14. Treated PDX MAYO-PH039 samples appear to lose methylation at differentially methylated CpG probes globally. 290
Figure 6.15. Treated PDX MAYO-PH039 samples appear to lose methylation at differentially methylated CpG probes, including chromosome 17. 291
Figure 6.16. Increasing global methylation loss with each subsequent round of niraparib treatment in PDX MAYO-PH039. 292
Figure 6.17. Increasing global methylation losses associated with increasing rounds of niraparib treatment in PDX MAYO-PH039 are not specific to a single epigenomic region. 293
Figure 6.18. Some differentially methylated CpG probes in MAYO-PH039 gain methylation. 294
Figure 6.19. Global distribution of differentially methylated CpG probes for PDX 134183 treated vs untreated samples. 295

Figure 6.20. Trend towards gain of methylation in differentially methylated CpG probes for PDX 134183 treated samples compared to untreated samples. 296
Figure 6.21. Subtle gains of methylation in differentially methylated CpG probes in PDX 134183 treated samples. 297
Figure 6.22. No global trends observed comparing differentially methylated CpG probes in homozygous and heterozygous PDX. 301
Figure 6.23. No trends observed comparing differentially methylated CpG probes in homozygous and heterozygous PDX across chromosome 17. 302
Figure 6.24. PDX 134062 has reduced methylation of CpG probes from BRCA1 homozygous vs heterozygous differentially methylation analysis 303
Figure 6.25. No batch effects produced by array for ICGC samples. 305
Figure 6.26. No batch effects produced by slide for ICGC samples. 306
Figure 6.27. BRCA1 methylation heatmap of ICGC samples indicates 16 samples with possible homozygous or heterozygous BRCA1 promoter methylation. 308
Figure 6.28. RAD51C methylation heatmap of ICGC samples indicates four samples with RAD51C promoter methylation. 309
Figure 6.29. CpG probes associated with RAD51C promoter methylation in 450K differential methylation analysis are not methylated in EPIC array PDX samples. 311
Figure 6.30. Four sample clusters identified in manual BRCA1 clustering analysis of ICGC samples. 313
Figure 6.31. Apparent association between identified clusters and broad BRCA1 methylation patterns. 314
Figure 6.32. Apparent association between identified clusters and methylation of BRCA1 CpG probes relevant to gene silencing. 315

List of Tables

Table 1.1. Genes alterations reported to cause PARPi sensitivity in vitro or in vivo. 42
Table 2.1. Human vs murine PCR primer mix details. 62
Table 2.2. TP53 sample identity check primers. 63
Table 2.3. Primers for amplicon-based NGS reversion mutation screening. 64
Table 2.4. Region-specific primers for LR-PCR-based NGS reversion mutation screening. 65
Table 2.5. Primers for amplicon-based DCLRE1C mutation screening. 66
Table 2.6. Primers for targeted bisulfite sequencing of the RAD51C promoter. 66
Table 2.7. Brunello NGS library preparation primers. 70
Table 2.8. Control and BRCA1 region qPCR primers. 71
Table 2.9. MLPA-seq RAD51C gene probes 74
Table 2.10. MLPA-seq control gene probes 75
Table 2.11. MR media composition. 76
Table 2.12. FV media composition. 77
Table 2.13. Reagents used for lentiviral packaging of FUCas9Cherry plasmid DNA. 79
Table 2.14. Reagents used for lentiviral packaging of Brunello plasmid DNA. 79
Table 2.15. PDX tumour digestion media composition. 82
Table 2.16. Summary of the single agent compound dosing regimens used for in vivo drug studies. . 88
Table 3.1. Cisplatin and PARPi (rucaparib) responses of chemonaïve HGSOC PDX models. 97
Table 3.2. Cisplatin and PARPi (rucaparib) responses of pre-treated HGSOC PDX models. 99
Table 3.3. Mutational features of chemonaïve HGSOC PDX models. 102
Table 3.4. Mutational features of pre-treated HGSOC PDX models. 103
Table 3.5. Summary of all mutation reversion screening results. 110
Table 3.6. Patient 34931 completed treatments. 111
Table 3.7. P-values of BRCA1 revertant PDX 34931 in vivo responses. 112
Table 3.8. Reversion mutation screening results for patient and PDX 134206 tumours. 113
Table 3.9. Results of constitutional methylation analysis in patients with meBRCA1 HGSOC. 117
Table 3.10. PDX 134056 lineage #56S and #56R rucaparib response p-values. 123
Table 3.11. P-values of PDX 134056 rescue lineage #56cis in vivo responses. 133
Table 3.12. P-values of PDX 134206 in vivo responses. 135
Table 3.13. PDX 134019 and 134019B samples screened for CHD4 deletion. 141
Table 4.1. Summary of C-NHEJ western blot results for HRD PDX models. 150
Table 4.2. Established PDX 134013 C-NHEJ loss lineages 151
Table 4.3. Summary of all cell lines discussed in this chapter. 154
Table 4.4. PDX 134013 C-NHEJ lineage treatment response summary. 164
Table 4.5. P-values of PDX 134013 C-NHEJ lineage rucaparib 450mg/kg response comparisons. . 165
Table 4.6. P-values of PDX 134013 C-NHEJ lineage growth rate comparison. 167
Table 4.7. IHC results of PDX 134027 and 134056 test samples. 173
Table 4.8. WB and IHC data discordant for PDX 134013 C-NHEJ lineage source tumours. 175
Table 4.9. Minimum lethal dose of puromycin for each Cas9 cell line. 182
Table 4.10. Infection efficiency calculations reveal 1:40 dilution of virus is optimal for all Cas9 cell lines. 183
Table 4.11. Summary of doubling rates of cell lines used for CRISPR screen. 186
Table 4.12. All CRISPR Brunello infections demonstrate a high library diversity following puromycin selection. 189
Table 4.13. Number of missing genes or sgRNAs for each PEO1 CRISPR screen sample. 191
Table 4.14. Significantly enriched gene hits and corresponding p-values across all analyses. 193
Table 4.15. Significantly depleted gene hits and corresponding p-values across all analyses. 194
Table 5.1. Summary of PDX 134183 in vivo treatment responses compared to control. 213
Table 5.2. P-values of WEHI-PH039 Lineage A vs B in vivo cisplatin response differences. 220
Table 5.3. P-values of WEHI-PH039 Lineage A vs B in vivo rucaparib 300mg/kg response differences. 221

Table 5.4. P-values of WEHI-PH039 Lineage A vs B in vivo rucaparib 450mg/kg response differences. 222
Table 5.5. P-values of WEHI-PH039 Lineage A vs B in vivo niraparib 100mg/kg response differences. 223
Table 5.6. Vehicle-treated WEHI-PH039 Lineage B samples slightly more methylated at RAD51C promoter than Lineage A samples. 224
Table 5.7. Mean RAD51 foci value comparison between irradiated PDX groups. 230
Table 5.8. Samples selected for methyl-BROCA analysis. 232
Table 5.9. Results of meRAD51C loss MS-HRM screening in PDX 134183 tumours by treatment. 240
Table 5.10. WEHI-PH039 samples grow too fast for standard treatments. 242
Table 5.11. WEHI-PH039 Lineage A loses meRAD51C more readily than Linage B. 243
Table 5.12. RAD51C gene expression observed in PH039 Lineage A tumours with meRAD51C loss. 248
Table 5.13. WEHI-PH039 Lineage B meRAD51C LS and LLS profiles result in RAD51C gene silencing. 250
Table 5.14. MLPA-seq results for RAD51C copy number are inconclusive. 251
Table 5.15. Both PDX models have one copy of RAD51C per cell in WGS analysis. 252
Table 5.16. Both PDX models have one copy of RAD51C per cell in SNP array analysis. 252
Table 5.17. Summary of clinical information and meRAD51C profiles of PDX and patient samples. 261
Table 6.1. Samples analysed using EPIC array. 273
Table 6.2. Enrichment of cell-cell interaction GO terms in CpG probes that gain methylation under niraparib pressure in MAYO-PH039. 298
Table 6.3. Enrichment of neuronal pathway GO terms in CpG probes that lose methylation under niraparib pressure in MAYO-PH039. 299
Table 6.4. CpG probes outside RAD51C promoter that are possibly associated with RAD51C methylation. 310
Table 6.5. BRCA1 clusters are associated with sample tumour purity rather than unique BRCA1-associated methylation signatures. 316
Table 6.6. Potential BRCA1 methylation zygosity of AOCS patient samples based on 450K array results and tumour purity estimates. 317

1 Introduction

Of all gynaecological malignancies, ovarian cancer (OC) is the leading cause of death worldwide (Banerjee et al., 2011). Despite being relatively rare, OC is highly lethal, with most women diagnosed succumbing to the disease (Hunn et al., 2012; Topp et al., 2014). This is in large due to the late presentation of disease, often only after the cancer has metastasized (Hunn et al., 2012; Lengyel, 2010). The 5-year relative survival for OC is currently below 50% for all stages, having improved modestly over the last few decades (Torre et al., 2018).

Contrary to its name, OC is not a single disease, but rather a heterogeneous collection of distinct diseases that happen to share an anatomical location. These diseases have distinct patterns of spread, risk factors, molecular profiles, prognosis and responses to chemotherapy (Gilks, 2010; Prat, 2012a, 2012b). Aggressive de-bulking surgery combined with platinum-based chemotherapy has long been the primary treatment approach for all subtypes, but a growing understanding of OC subtypes is allowing the development of more targeted and effective therapies (Vaughan et al., 2011).

The best example of this is the use of Poly-ADP ribose polymerase (PARP) inhibitors in the treatment of cancers deficient in Homologous Recombination (HR) DNA repair, such as those with *BRCA1* and *BRCA2* mutations. High-Grade Serous Ovarian Carcinoma (HGSOC) is the most common OC subtype, and is frequently HR deficient (HRD). The PARPi Olaparib was the first to be approved as maintenance therapy by the Food and Drug Administration (FDA) in the United States in 2014 following a number of successful clinical trials (Gelmon et al., 2010; Gelmon et al., 2011; Kim et al., 2015; Ledermann et al., 2012). Many of these trials demonstrated marked improvements in Progression Free Survival (PFS) for the majority of *BRCA1/2*-mutation carrying patients treated with PARPi, but have also extended overall survival in some patients, with rare cases where complete remission is achieved (Coleman et al., 2017; Ledermann et al., 2014; Pilié et al., 2019; Swisher et al., 2017). However, despite the demonstrated efficacy of PARPi in treating HRD HGSOC, many responses are not durable and disease recurrence is common. Predicting which patients will derive benefit has been a challenge, with *BRCA1/2* mutations not being necessary for response in some instances, or in other cases not being sufficient. Overcoming this has been challenging, as the underlying mechanism of PARPi cytotoxicity remains elusive, with different roles of the PARP1 enzyme having been implicated. Many different mechanisms of PARPi resistance have also been

reported, with reversion or secondary mutations that correct the primary HR defect being the best studied in patients. The majority of other resistance mechanisms have been described pre-clinically, and have been more challenging to validate in patient cohorts. Whether some of these mechanisms exist in the clinic, or only experimentally, requires clarification. Furthermore, the evolution of PARPi resistance within a tumour is not fully understood. Two models have been proposed; one of spontaneous evolution of resistant clones, and one of acquired resistance forming under platinum or PARPi treatment pressure. Knowing whether both models are relevant, or whether one prevails in the clinic, would have significant implications for how and which treatments are delivered.

Thus, understanding what makes a tumour sensitive or resistant to PARPi would enable development of more effective therapeutic strategies in the clinic, and allow for better stratification and selection of cancer patients in PARPi clinical trials.

1.1 High-grade serous ovarian carcinoma

Ovarian cancer is not a single disease, but is instead comprised of multiple cancer subtypes, all with their own unique pathological features and molecular drivers. My PhD project has focussed on the epithelial histotype, high-grade serous ovarian carcinoma.

1.1.1 High-grade serous ovarian carcinoma pathology

Epithelial ovarian carcinomas (EOCs) are the most common ovarian cancer histotype (Prat, 2012b). Five main types of EOC have been described thus far based on the histopathology, immunohistochemistry, and molecular features of the tumour: High-grade serous ovarian carcinomas (HGSOC), endometrioid carcinomas, clear cell carcinomas, mucinous carcinomas, and low-grade serous ovarian carcinomas (LGSOC) (Gilks, 2010; McCluggage, 2011; Prat, 2012a, 2012b; Vaughan et al., 2011). The most common EOC histology is serous, representing approximately 80% of all EOCs (Pilié et al., 2019). These tumours are more aggressive, and often present at an advanced stage. High-grade and low-grade serous carcinomas are biologically distinct (Singer et al., 2002). The grade describes the observed pathological abnormality of the cells, which is reflective of the underlying molecular progression of the ovarian carcinoma. This can be either through great genomic instability leading to metastasis with unclear precursor lesions (high-grade), or via a step-wise mutation pathway, like the

adenoma-carcinoma sequence described for colorectal cancer, resulting in less invasive tumours (low-grade) (Landen et al., 2008; Leslie et al., 2002).

HGSOCs are the most common EOC and are highly aggressive, with the majority of EOC deaths associated with this subtype (Verhaak et al., 2013). HGSOC and other EOC subtypes were long believed to all originate from the ovarian surface epithelium (OSE), despite the OSE not resembling a true, differentiated epithelium on a molecular level (Erickson, Conner & Landen, 2013). However, mounting evidence suggests that secretory epithelial cells of the distal fallopian tube are frequently progenitors of HGSOC (Falconer et al., 2015; Kindelberger et al., 2007; Kuhn et al., 2012; Perets et al., 2013; Piek et al., 2001a). In studies of HGSOC prevention, removal of the ovaries and fallopian tubes (bilateral salpingo-oophorectomy) has been shown to reduce disease risk by 80% in *BRCA1/2* mutation carriers (Domchek et al., 2010; Rebbeck et al., 2009).

1.1.2 Early diagnosis and screening of high-grade serous ovarian carcinoma

Early cancer diagnosis is a key determinant of clinical outcomes, with earlier detection leading to better prognosis for patients across most cancer types (Rubin et al., 2011). Indeed, this is the case for OC, where the approximately 15% of women presenting with International Federation of Gynaecological Oncology (FIGO) stage I disease (cancer is localized within the ovaries or fallopian tubes) have a 5-year survival of >90%. Most of these women can be cured by surgery without the need for neo-adjuvant chemotherapy. Unfortunately, due to a lack of reliable early screening or diagnostic methods, the majority of women (~59%) are diagnosed at FIGO stages III-IV, after cancer has metastasized, where the 5-year survival drops to less than 30% (Radziszewska et al., 2018; Raja et al., 2012). At this stage, surgery must be combined with neo-adjuvant chemotherapy to combat the metastasized disease.

OC is usually asymptomatic until later stages of disease (Ledermann et al., 2013), making early diagnosis extremely difficult. This is in part due to its anatomical location, but also the non-specific symptoms associated with the disease, such as abdominal bloating, frequent need to urinate and reduced appetite (Goff et al., 2007). Thus, approximately 60% of women are diagnosed with stage III, metastatic disease, while only 15% are diagnosed at stage I, and 21% at stage II (Howlader et al., 2019).

There are currently few useful diagnostic tools available for early OC. Existing tests for detecting and monitoring OC include pelvic examinations, ultrasound and molecular biomarkers such as CA125, but these are not considered specific or sensitive enough to be implemented as reliable screening/diagnostic tools. In fact, current evidence indicates that screening for OC's using these methods does not decrease mortality, but does increase rates of unnecessary surgery (Mathieu et al., 2018).

In the context of early stage EOC, implementation of sensitive and specific liquid biopsy tests would be transformative, as too many women are either being exposed to unnecessary invasive procedures or only receiving a diagnosis once it is too late (Mari et al., 2019). Thus, there is currently a significant body of work being done to uncover novel reliable biomarkers of disease that can be detected in a non-invasive way, for example in liquid biopsies (Cohen et al., 2018; Elias et al., 2017; Shewell et al., 2018). Unfortunately, many of these tests are still in the early stages of development and it is unclear when and if such tests will become widely available (Mari et al., 2019). For now, there is much focus on improving treatment options for women who are diagnosed at late stages of disease and understanding the biology of the disease to inform test development.

1.1.3 Standard treatment of high-grade serous ovarian carcinoma

De-bulking surgery combined with platinum-based chemotherapy has long been the standard treatment approach for all ovarian cancers, despite fundamental differences between disease subtypes (Bowtell et al., 2015). Optimal de-bulking surgery is considered one of the most important positive prognostic factors in the outcome of women with OC (Polterauer et al., 2012). However, chemotherapy continues to play a crucial role in HGSOC management given that most patients experience cancer recurrence even following complete surgical resection (Marth et al., 2017; Scarabelli et al., 2000).

Platinum-based chemotherapy has been used since the late 1970s to treat OC, with trials of various compound combinations over the years, leading to a carboplatin and paclitaxel combination (administered every 3 weeks) becoming the 'backbone' of advanced OC treatment, due to its lower toxicity profile compared to previous platinum-based approaches (Raja et al., 2012; Vaughan et al., 2011). Paclitaxel (taxol) was formally described as an anti-neoplastic agent in the early 1990s. This compound is a "taxane", and thus promotes the

assembly and stabilization of microtubules in cancer cells, leading to mitotic arrest (Long, 1994). It was two significant clinical trials around this time that demonstrated a regimen of paclitaxel and cisplatin outperformed the formerly used combination of cisplatin and cyclophosphamide in OC (McGuire et al., 1996; Piccart et al., 2000). Subsequent clinical trials showed that replacing cisplatin with carboplatin in combination with paclitaxel had the same efficacy but better safety profiles and ease of administration (du Bois et al., 2003; Ozols et al., 2003).

Since these trials, multiple chemotherapy-based strategies have been tested to further improve outcomes for women with advance OC. These have included the substitution of paclitaxel with other drugs (e.g. docetaxel or pegylated liposomal doxorubicin) (Vasey et al., 2004), or addition of other drugs to the paclitaxel and carboplatin combination (i.e. triple-combinations) (Bookman, 2010). Despite these efforts, carboplatin-paclitaxel remains the mainstay of chemotherapeutic treatment in advanced EOC (Vaughan et al., 2011).

Unfortunately, HGSOCs tend to have a favourable response to platinum-based therapy initially, but cycles of relapse and acquired resistance tend to follow (Bowtell et al., 2015; Erickson et al., 2013). The median time to progression still sits within a range of 12–18 months (contingent on residual disease post-surgery), with a 5-year overall survival (OS) of <35% for all stages of EOC (Marth et al., 2017). Fortunately, following decades of limited advances in OC chemotherapy, 2014 saw the FDA approval of the first targeted therapies for OC – the vascular endothelial growth factor (VEGF) inhibitor Avastin (bevacizumab; Roche) and the PARPi Lynparza (olaparib; AstraZeneca).

1.1.4 Targeted treatment of high-grade serous ovarian carcinoma with VEGF inhibitors

Angiogenesis has a known pathogenic role in solid tumour growth and metastasis, and this led to the development of anti-angiogenic drugs as a targeted therapy. Of these therapies, the most promising has been a humanized monoclonal IgG antibody that targets vascular endothelial growth factor receptor (VGEF), bevacizumab (Avastin) (Marchetti et al., 2019).

Bevacizumab was approved as first-line therapy in advanced (stage III-IV) epithelial ovarian, fallopian tube, or primary peritoneal cancers in combination with carboplatin and paclitaxel by

the European Medicines Agency (EMA) in late 2011, by Australia's Therapeutic Goods Administration (TGA) in 2014 and mid 2018 by the US FDA (Marchetti et al., 2019).

This was following the success of two randomized and controlled phase III clinical trials (GOG-0213 and OCEANS) where improvements in PFS of up to 3.4 months were reported (Aghajanian et al., 2015; Coleman et al., 2017). Although OS benefits were observed in these studies, they were not statistically significant (Aghajanian et al., 2015; Coleman et al., 2017). However, it was later found in the ICON7 trial (phase III randomised trial of bevacizumab combined with carboplatin-paclitaxel in the first line setting) that a subset of patients can derive some OS benefit from bevacizumab – those with high-risk disease, such as bulky or sub-optimally debulked disease, or with presence of ascites. (Oza et al., 2015b; Perren et al., 2011).

1.1.5 Targeted treatment of high-grade serous ovarian carcinoma with PARP inhibitors

PARPi have transformed the clinical management of *BRCA*-mutant EOC, having demonstrated outstanding efficacy in this cancer subtype. Although PARPi were originally developed as chemo-/radio- sensitizing drugs, the exciting finding that inhibition of PARP1 is particularly cytotoxic to *BRCA1/2*-null cells *in vitro* (Bryant et al., 2005; Farmer et al., 2005) resulted in subsequent clinical approvals of PARPi as a new class of targeted drugs for *BRCA*-mutant cancers. This highly specific sensitivity of *BRCA*-mutated cancer cells to PARPi is an excellent example of 'synthetic lethality' as a mechanism. This term was first coined in the 1940s through experimentation in Drosophila (Dobzhansky, 1946), and it describes a phenomenon where loss of two genes/pathways together is lethal, while loss of either one on its own is viable. Other examples of synthetic lethality in the context of DNA repair are reviewed by (Nickoloff et al., 2017). In the last decade, multiple clinical studies have demonstrated that tumours carrying *BRCA*-mutations are more sensitive to both PARPi and platinum-based chemotherapy, and that such mutations are associated with improved overall survival in the short-term (5 years), particularly in *BRCA2* mutant cases (Candido-dos-Reis et al., 2015; Lheureux et al., 2017b). Germline *BRCA1/2* mutation testing has thus become a key stratification factor in the clinical management of OC patients, including in PARPi clinical trials. (Audeh et al., 2010; Coleman et al., 2017; Ledermann et al., 2012; Mirza et al., 2016; Swisher et al., 2017).

As with platinum-chemotherapy, HGSOC is well-matched to PARPi therapy, because around 50% are thought to be HRD, although responses are neither guaranteed, nor durable. As both therapies exploit deficiencies in DNA repair, platinum responses are often found to predict responses to PARPi in the clinic (Audeh et al., 2010). Unfortunately, there are few therapeutic options available to HGSOC patients once they stop responding to platinum-based agents and PARPi. Thus, there is an urgent need to develop approaches to either evade or overcome platinum and PARPi resistance. This requires a better understanding of the molecular drivers of sensitivity and resistance to these therapies.

1.1.5.1 Current clinical indications for PARP inhibitors

PARPi have the features of an ideal maintenance therapy due to their low toxicity profiles and high efficacy in platinum-sensitive/HRD patients. Maintenance therapy is designed to be administered over an extended period of time in order to prevent cancer recurrence for advanced cancer patients whilst they remain in remission, or to prolong the time taken to first progression for patients in their first remission.

Maintenance therapy was first proven effective in the platinum-sensitive relapsed setting. In the olaparib clinical trial, Study 19, which included both patients with *BRCA*-mutated and *BRCA*-wildtype (WT) HGSOC, a prolongation of PFS of 8.4 months compared with 4.8 months in the placebo group was observed (hazard ratio for progression or death [HRa] of 0.35; 95% confidence interval [CI] of 0.25-0.49; $p<0.001$) (Ledermann et al., 2012). The benefit for *BRCA1/2* mutation carriers was subsequently shown to be 11.2 months (95% CI of 8.3–not calculable) vs 4.3 months in the *BRCA*-WT group (95% CI of 3.0–5.4; HRa 0.18 [0.10–0.31]; $p<0.0001$) (Ledermann et al., 2014). Subsequent studies of niraparib in NOVA (Mirza et al., 2016) and of rucaparib in ARIEL3 (Coleman et al., 2017) also showed positive PFS for both the *BRCA*-mutant cohorts and HRD cohorts in the platinum sensitive relapsed setting for high-grade EOC.

Thus, as a result of these and additional data, olaparib, rucaparib and niraparib were approved in the US and Europe for maintenance monotherapy therapy in platinum-sensitive HGSOC, with monotherapy only available for patients following multiple lines of chemotherapy. The EMA (Europe) has only approved these PARPi as maintenance treatment for patients with

platinum-sensitive, relapsed HGSOC. Of these, only rucaparib is indicated as the third-line treatment in *BRCA*-mutant ovarian cancer.

Olaparib is FDA-approved as a fourth-line treatment for *BRCA*-mutated advanced OC, as well as maintenance therapy for recurrent OC and as first-line maintenance therapy for newly-diagnosed *BRCA*-mutant advanced OC. The FDA has indicated rucaparib as both third-line treatment for *BRCA*-mutant OC and as maintenance treatment for recurrent ovarian cancer, while niraparib is only indicated as maintenance treatment in recurrent ovarian cancer (Jiang et al., 2019).

In Australia, olaparib is indicated for maintenance in patients with platinum-sensitive relapsed *BRCA*-mutant (germline or somatic) OC who are currently responding (completely or partially) to platinum chemotherapy, with at least two prior lines of platinum therapy completed.

These initial maintenance trials in relapsed disease demonstrated impressive efficacy of this new class of drug, and led to subsequent first-line trials of PARP inhibitors. These exciting results also have prompted suggestions that maintenance therapies, such as PARPi, may eventually lead to EOC being treated more like a chronic disease, rather than a terminal one, in the future.

1.1.5.2 PARP inhibitors in the first-line treatment setting

How PARPi would perform as an alternative neoadjuvant/adjuvant treatment to platinum-based chemotherapy, allowing some patients to avoid the need for chemotherapy, remains to be established. It is possible that PARPi may provide patients with *BRCA*-mutant EOC similar therapeutic benefits, or better, as platinum chemotherapy, but without the associated toxicities/side-effects. However, we would need to be able to predict which ovarian cancers are going to be super-responsive to PARPi alone, not requiring the addition of chemotherapy, thus ensuring such a randomised trial of PARPi compared to chemotherapy followed by PARPi maintenance remains ethically appropriate. As yet, we do not have the capacity to accurately predict which cases these would be prospectively, although we are beginning to investigate appropriately (Lheureux et al., 2017a; Saner et al., 2019). Trials designed to test this theory are unlikely to be pursued in the near future because it would place women at risk of not receiving life-prolonging platinum-based chemotherapy. Instead, the focus of upcoming trials is more

likely to be in refining the role of PARPi maintenance therapy in the first-line combination setting, ensuring we make it available to more patients who may derive potentially life-prolonging benefit.

Indeed, results from the SOLO-1 trial, a phase III study of olaparib maintenance monotherapy in *BRCA*-mutated FIGO Stage III-IV ovarian cancer post-first line platinum-chemotherapy, showed that the PFS benefit in the olaparib maintenance group substantially exceeded that of the same treatment group in the SOLO-2 trial (following platinum-sensitive relapse) (Moore et al., 2018). The median Progression Free Survival (PFS) was 36 months longer in the olaparib arm than in the placebo arm, and the median Time to First Subsequent Therapy (TFST) or death was 51.8 months for the olaparib-treated group and only 15.1 months in the placebo control group (Moore et al., 2018). These differences are unprecedented – simply unlike anything ever seen before in ovarian cancer for any other class of therapeutic.

The SOLO1 first-line maintenance trial, reported in September 2018, was confirmed and supported by three other first-line maintenance studies, which reported *BRCA*-mutant sub-groups in September 2019 (the PRIMA, VELIA and PAOLA trials) (Coleman et al., 2019; González-Martín et al., 2019; Ray-Coquard et al., 2019). In addition, the PRIMA trial also reported an HRD-subgroup (including, but not limited to, *BRCA*-mutant patients) in which the niraparib-treated group had a median PFS of 21.9 months compared with 10.4 months in the placebo group (HRa of 0.43; 95% CI of 0.31-0.59; P<0.001) (González-Martín et al., 2019). In the VELIA trial, in which patients were treated with veliparib throughout their first-line chemotherapy and during the maintenance period, the HRD positive group had a median PFS of 31.9 months when treated with veliparib compared with 20.5 months when treated with placebo (starting from the beginning of chemotherapy treatment; HRa of 0.57; 95% CI of 0.43-0.76; p<0.001) (Coleman et al., 2019). For the PAOLA trial, in which patients received either bevacizumab with olaparib or bevacizumab alone, patients with HRD had a median PFS of 37.2 months for olaparib/bevacizumab versus 17.1 months for bevacizumab alone (HRa 0.33 with 95% CI, 0.25 to 0.45) (Ray-Coquard et al., 2019). These trials all suggested that perhaps there was PARPi efficacy beyond HRD, and that platinum sensitivity was the best selection criterion for PARPi, as did the three PARPi trials in the platinum sensitive relapsed setting; Study 19 (Ledermann et al., 2012) (Friedlander et al., 2018), NOVA (Mirza et al., 2016) and ARIEL3 (Coleman et al., 2017). As discussed elsewhere in this thesis, this may relate more to the inadequacy of current HRD biomarker tests, than to the possibility that a truly HR

competent ovarian cancer could respond to a single agent PARPi. However, for now, the jury is out. Platinum sensitivity is still considered a hallmark of PARPi response; although more and more, HRD testing is starting to be used and PARPi treatment accessed, both in the relapsed and first-line maintenance setting if a woman can access PARPi or afford to pay for it herself.

The unprecedented magnitude of the first-line PARPi maintenance data certainly suggest that olaparib has greater benefit in *BRCA*-mutation carriers as a first-line maintenance treatment than it does as a third-line relapsed treatment and, therefore, should be given to patients in an earlier treatment setting (Friedlander et al., 2018; Moore et al., 2018; Pujade-Lauraine et al., 2017). Furthermore, the PARPi talazoparib has shown great promise in the neoadjuvant setting in *BRCA*-mutant triple-negative breast cancer as a single agent, significantly reducing disease with manageable toxicity (Litton et al., 2019). However, this study was in a small cohort of patients and remains to be confirmed in a larger trial (Litton et al., 2019). Thus, the future of PARPi maintenance therapy should be in earlier treatment settings.

1.1.5.3 Long-term responders to PARP inhibitors

Some patients have been known to respond for up to 7 years on PARPi maintenance therapy, with no significant side-effects reported (Lheureux et al., 2017b). These patients are often termed “long-term responders” or “super-responders”, and although most have *BRCA*-mutant cancer, there are some lacking *BRCA*-mutations that still show exceptional PARPi responses (Ledermann et al., 2014; Lheureux et al., 2017b). *BRCA*-mutation status and platinum chemotherapy response are currently still the best predictors of an initial PARPi response, though there is still no precise means of predicting the durability of response for patients.

The complexity of cancer as a disease results in complexity when trying to explain exceptional responses of patients, with unique combinations of multiple factors influencing outcomes for each individual case. These factors include the genetic background of the tumour, whether there are druggable targets within the tumour, the patient’s immune response, their lifestyle and access to quality care (Saner et al., 2019). Even when considering responses to PARPi in HGSOC, patients with *BRCA2*-mutant tumours, for example, can have extremely different clinical progression and outcomes. It is not enough to only consider one facet of the tumour. The Exceptional Responders Initiative (ERI), launched by the National Cancer Institute (NCI)

in 2014, aims to address this by characterizing the molecular underpinnings of exceptional responders, including HGSOC patients (Printz, 2015). Thus, identification of biomarkers for PARPi response durability remains an active area of research (Saner et al., 2019).

1.1.5.4 Combining PARPi with other therapies

The complexity and heterogeneity of HGSOC supports a rationale for combination therapies to urgently target different aspects of the biology of the disease, which would be expected to prove more successful than single agent approaches. There are currently multiple therapies that are being studied in combination with PARPi for treatment of HGSOC, with some examples described in this section.

Anti-angiogenic agents initially offered some PFS benefits as a monotherapy in EOC and have since been investigated in combination with PARPi. PARPi have been shown to have anti-angiogenic effects as single agents in pre-clinical models (Tentori et al., 2007). Other pre-clinical studies have shown that hypoxia can reduce the HR capacity of cancer cells (Bindra et al., 2005; Bindra et al., 2004; Chan et al., 2010; Hegan et al., 2010). It was, therefore, hypothesized that anti-angiogenic agents may synergize with PARPi. So far, combination of anti-angiogenic cediranib (a VEGFR inhibitor) combined with olaparib has been assessed in a cohort of recurrent ovarian cancer/triple-negative breast cancer patients. Manageable dose-limiting toxicities were detected in phase I (Liu et al., 2013), and the phase II trial revealed significant clinical benefits in the combination arm compared to olaparib monotherapy arm (Liu et al., 2014). Interestingly, *BRCA*-WT patients appeared to also derive benefit from this combination therapy, with extended PFS and OS observed (Liu et al., 2014). Initially it was thought that this was due to the hypoxia induced by cediranib causing reduced HR DNA repair. However, a recent study has demonstrated that cediranib directly supresses the HR pathway by downregulating gene expression core HR factors *BRCA1/2* and *RAD51*, thereby inducing HRD in tumour cells (Kaplan et al., 2019).

Similar findings have been observed for the combination of VEGFR inhibitor Bevacizumab with niraparib in a phase II trial of patients with platinum-sensitive recurrent ovarian cancer, where the combination therapy demonstrated improved PFS in patients regardless of HRD status and PFI (Mirza et al., 2019). The addition of olaparib to bevacizumab maintenance following first-line platinum chemotherapy with bevacizumab was also found to increase PFS

significantly compared to single agent bevacizumab maintenance, as described above in the phase III trial PAOLA-1 in advanced ovarian cancer. However, it is unclear whether this benefit was due to PARPi and VEGFR inhibitor synergy or PARPi alone, given lack of an olaparib single-agent maintenance arm in this trial (Ray-Coquard et al., 2019).

Cancer immunotherapy using immune checkpoint inhibitors (e.g. anti-PD-1 and anti-PD-L1 antibodies) has shown to be extremely effective in treatment of multiple cancer type known to generally exhibit high mutational burden (e.g. melanoma) (Samstein et al., 2019). This high mutational load has been shown to correlate with tumour antigenicity, which in turn leads to recruitment of more tumour-infiltrating lymphocytes (TILs). High immune checkpoint PD-1 or PD-L1 expression allows tumour cells to evade death by TILs, but means that these cells can be sensitive to immune checkpoint blockade (Riley et al., 2019).

HRD tumours have been shown to have a higher neo-antigen capacity compared to HR competent cancers and have increased expression of PD-1 and PD-L1 in tumour-associated immune cells compared to HR-proficient tumours (Strickland et al., 2016). HR proficient tumours with low TIL counts have also been found to have very poor prognosis, while *BRCA*-mutant tumours with high TIL counts were found to have a very good prognosis (Strickland et al., 2016). Furthermore, PARPi have been found to be immunosuppressive by increasing PD-L1 expression in breast cancer models, with combination therapy of PARPi and anti-PD-L1 therapy found to effectively overcome this attenuated anticancer immunity (Jiao et al., 2017). However, PARPi have also been found to be immune-stimulating by causing accumulation of cytosolic DNA fragments, which in turn activate the DNA-sensing cyclic GMP-AMP synthase and stimulator of interferon genes (cGAS-STING) pathway (Ding et al., 2018; Shen et al., 2019). This pathway stimulates production of type I interferons which induces anti-tumour immunity independent of *BRCA*-mutation status. These effects of PARPi were found to be further enhanced by immune checkpoint blockade using anti-PD-L1 antibody (Shen et al., 2019). These pre-clinical findings all strongly supported a rationale for combining PARPi with PD-1/PDL-1 inhibitors to treat HRD cancers. A phase I/II trial (TOPACIO) of PARPi niraparib in combination with pembrolizumab (anti-PD-1 antibody) in platinum resistant ovarian cancer has demonstrated some benefit of the combination therapy and warrants further investigation (Konstantinopoulos et al., 2018)

Other combination therapy approaches being explored include targeting cell cycle checkpoints, for example using CHK1, ATR, ATM or WEE1 inhibitors, which have been shown to synergize with PARPi by increasing DNA replication stress (Kim et al., 2017; Parmar et al., 2019).

Targeting the same vulnerability in HGSOC cells has also been explored as a potential approach for combination therapies. For example, HGSOC are particularly sensitive to both platinum agents and PARPi due to their frequent HR DNA repair defects, meaning that the same vulnerability is being exploited by both therapies. Although targeting HRD tumours with both platinum-based chemotherapies and PARPi simultaneously results in greater toxicity to the tumour, this combination has not become common practice because it was not shown to be efficacious in Study 41, at least partly due to overlapping hematologic toxicities (Balmana et al., 2014; Dent et al., 2013; Oza et al., 2015a). Changes in dosing are overcoming this limitation and showing promise for the combination of platinum compounds and PARPi in future (Lampert et al., 2019).

1.1.5.5 PARP inhibitors for cancer prevention

Due to their relatively high tolerability and manageable side-effects, PARPi have also been suggested for use in a preventative setting for women with germline *BRCA*-defects. Women carrying germline *BRCA*-mutations are at a much higher risk of developing breast and ovarian cancer. Currently, the most effective preventative strategies available to these women are prophylactic surgery to remove both fallopian tubes and ovaries (bilateral risk reducing salphingo-oophorectomy (RRSO)), their breasts (prophylactic bilateral mastectomy (BPM)) or both. However, these procedures are physically and psychologically taxing for women, affecting the onset of menopause, their fertility, and body image (Salhab et al., 2010; van de Ven et al., 2017a).

The prophylactic potential of PARPi has been explored pre-clinically in genetically engineered mouse models with stochastic loss of *TP53* and *BRCA1* (To et al., 2014; van de Ven et al., 2017b). In these studies it was found that both chronic and intermittent olaparib treatment significantly delayed the formation of mammary tumours. Intermittent dosing of PARPi in the clinic would have several advantages as a preventative strategy, such as reducing the side-

effects, the cost and possibly the development of chemo-resistant clones (To et al., 2014; van de Ven et al., 2017b).

Although there is extensive clinical data demonstrating the long-term safety of olaparib as a maintenance therapy, there have been no long-term clinical trials confirming the efficacy and safety of PARPi as a preventative measure. Myelodysplastic syndrome and acute myeloid leukaemia are the most serious adverse events that are reported in patients treated with PARPi, however these are rare (incidence of 0·5%–1·4%) and usually only occur after long-term treatment. Furthermore, all patients who developed these secondary malignancies had received platinum-based chemotherapy or other DNA-damaging therapies previously, meaning that it is currently unclear whether PARP inhibitors were solely responsible for these potentially devastating carcinogenic effects (LaFargue et al., 2019). Thus, although PARPi as a prevention is an attractive option, more work must be done before PARPi can be considered a viable option for ovarian and breast cancer prevention in high risk populations.

1.2 Molecular features of high grade serous ovarian carcinoma

Compared to other subtypes of OC, HGSOC's are molecularly characterized by a high degree of genomic instability, and loss of tumour suppressor p53 function is nearly ubiquitous (Ahmed et al., 2010; TCGA, 2011).

1.2.1 Loss of p53 function

The human *TP53* gene encodes p53, a highly conserved tumour suppressor protein that is involved in cellular responses to stress, and is the most frequently mutated gene in human cancer (Ahmed et al., 2010; Brosh et al., 2009; Kondrashova et al., 2018). This has made p53 an attractive target for cancer therapy. Many compounds targeting mutant p53 have been developed, though they are still in early phase clinical trials (Lieschke et al., 2019; Parrales et al., 2015). The p53 signalling network is generally inactive in cells, but becomes active upon sensing cellular stress or damage. Stressed cells are more likely to experience genomic instability and transform into cancer. The p53 pathway prevents the transformation of these stressed cells by either suppressing cell cycle progression or inducing apoptosis (Vogelstein et al., 2000).

Loss of normal p53 function by missense or inactivating mutations within the *TP53* gene is one of the earliest known events in the evolution of HGSOCs, and is reported in close to 100% of HGSOC cases (Ahmed et al., 2010; TCGA, 2011).

Both intense p53 protein staining and *TP53* mutations have been observed in Tubal Intraepithelial Carcinoma (TIC) and dysplastic fallopian tubes, suggesting that the distal fallopian tube is the likely precursor lesions for HGSOC. However, though such "p53 signature" lesions are much more numerous in patients with Li-Fraumeni syndrome, they are not associated with increased ovarian cancer risk (Xian et al., 2010). Thus, although these lesions appear to be necessary for HGSOC formation, they do not appear to be sufficient, or even rate-limiting (like *BRCA*-mutations) (Bowtell, 2010).

Most *TP53* mutations are missense and affect the DNA-binding domain of the protein. These can be recessive, requiring loss of both wild-type alleles, though dominant negative/gain-of-function mutations are common (de Vries et al., 2002; Petitjean et al., 2007). Missense mutations in p53 have been shown to provide a selective growth advantage compared to p53 null tumours (Dittmer et al., 1993), though approximately 50% of human cancers with such mutations also experience loss of the remaining wild-type allele, suggesting that lack of any wild-type p53 further promotes tumorigenesis (de Vries et al., 2002).

1.2.2 Homologous recombination DNA repair deficiency

Loss of high fidelity HR DNA repair is common in many cancers, and frequently observed in HGSOC. Loss of this pathway causes genomic instability that drives carcinogenesis (Moynahan et al., 2010).

The HR pathway has several critical roles within the cell; it repairs DNA double-strand breaks (DSBs), which are one of the most dangerous types of lesion DNA can encounter, as a single DSB can cause cell death if left unrepaired (van Gent et al., 2001). HR also repairs inter-strand crosslinks (ICLs), which obstruct DNA replication and transcription if unrepaired, making them extremely toxic to cells. In addition, HR is critical in supporting the recovery of stalled or collapsed replication forks, which in turn contributes to DNA damage tolerance of cells (Li et al., 2008).

There are multiple competing repair pathways that can take over repair of DSBs when they form, with the two primary pathways in mammalian cells being HR and Classical non-homologous end joining (C-NHEJ). The repair pathway that takes over depends largely on the availability of each pathway, which normally comes down to stage of cell cycle, but in the context of cancer also depends on which pathways remain intact. HR DNA repair is considered high fidelity, given it depends on the sister chromatid which acts as a sequence template (**Figure 1.1**). This means that, in mammalian cells, HR can only occur during S/G2 phases of the cell cycle when both sister chromatids are present. Furthermore, crucial HR proteins BRCA2 and RAD51 are only expressed during the S and G2 phases of the cell cycle, so HR cannot occur in G0/G1 (Chen et al., 2008).

It is estimated that up to half of all HGSOCs can have defects in the HR pathway (i.e. HR-deficiency- HRD), as a result of either germline *BRCA1/2* mutation (15%), somatic *BRCA1/2* mutation (6%) or mutation or epigenetic silencing of HR genes *BRCA1/RAD51C* (20%) (Alsop et al., 2012; Pennington et al., 2014; Roy et al., 2012; TCGA, 2011).

Although *BRCA1* and *BRCA2* are the best known breast and ovarian cancer risk genes, many other genes involved in the HR pathway (**Figure 1.1**) have also been found to contribute to hereditary breast and ovarian cancer risk when inactivated. These include core HR pathway genes *MRE11*, *BARD1*, *BRIP1*, *RAD50*, *RAD51C*, *RAD51D*, *NBS1* and *PALB2*, as well as the DNA damage checkpoint genes *ATM* and *CHEK2* (Loveday et al., 2011; Meindl et al., 2010; Rafnar et al., 2011; Walsh et al., 2011).

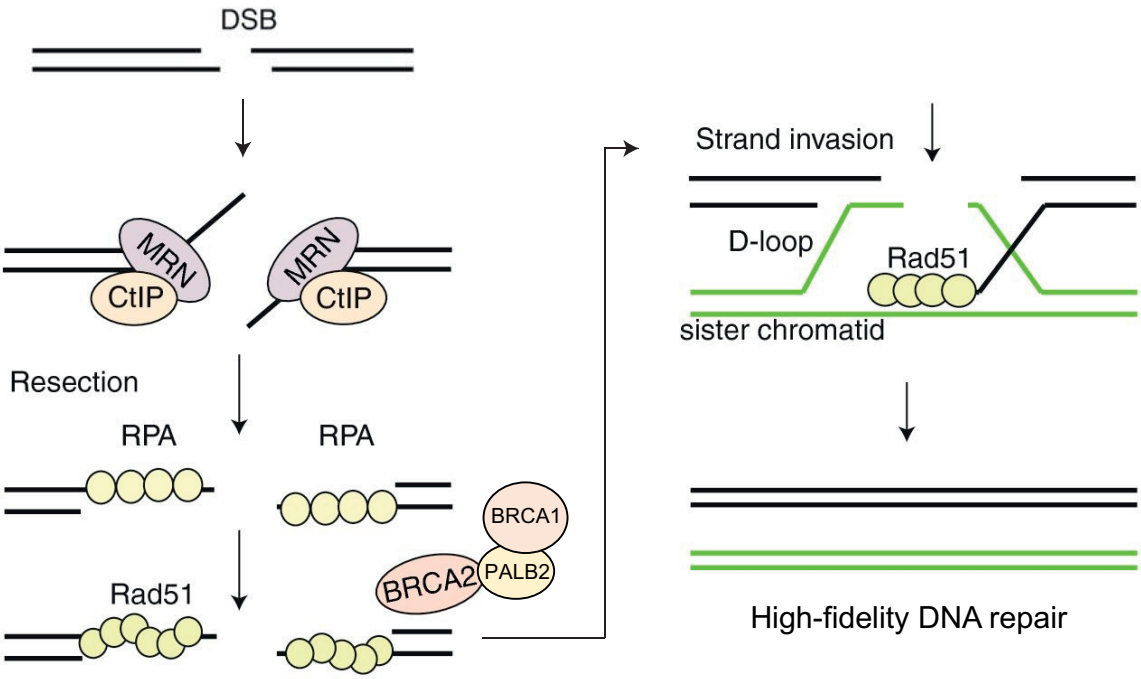


Figure 1.1. Homologous recombination DNA repair pathway.
Figure adapted from (Brandsma et al., 2012). HR repair is activated upon DSB detection by the MRE11-Rad50-Nbs1 (MRN) complex. Briefly, Nbs1 recruits its binding partners MRE11 and Rad50 to the nucleus where they are able to bind to the DNA DSB (Stracker et al., 2011). MRN then activates the serine/threonine kinase ataxia telangiectasia mutated (ATM), which plays a critical role in DNA damage checkpoint activation via Chk2 and p53 and in HR DNA repair (Lavin, 2008). Once activated, ATM undergoes auto-phosphorylation, and initiates sequential phosphorylation and recruitment of several HR proteins, including BRCA1, to sites of DNA damage (Polo et al., 2011; Roy et al., 2012). Phosphorylated CtIP is also recruited to the MRN complex where it can activate the exonuclease function MRE11 (Brosh, 2013; Chen et al., 2008; Paull, 2010; Sartori et al., 2007). MRE11 resects each DNA strand to generate short, 3' single-strand DNA overhangs. These are then resected further (up to several thousand nucleotides) by exonucleases ExoI, DNA2 and the BLM helicase (Huertas, 2010; Mimitou et al., 2011). These long single stranded DNA regions are rapidly coated with replication protein A (RPA) to prevent secondary structures from forming, and protect them from exonucleases (Zou et al., 2006). Partner and localizer of BRCA2 (PALB2) then forms a bridge between BRCA1 and BRCA2, and this complex facilitates loading of RAD51 onto the single-stranded DNA by displacing RPA. The complex of RAD51 family proteins (including RAD51C and RAD51D) and single-stranded DNA form nucleofilaments that enable homology searching and invasion of homologous sister chromatid DNA sequences. Resected DNA ends are thus annealed to complementary DNA sequences (forming Holliday junctions), and missing DNA sequence is copied and ligated using the intact homologous strand as a template (Holloman, 2011; Wyman et al., 2004). HR efficiency is reduced or altered when any of these proteins are mutated at critical residues or epigenetically silenced, thus the repair process can be disrupted at any stage.

1.2.3 Loss of tumour suppressors RB1 and NF1

Other less frequent, but recurrent, events in HGSOC include loss of the tumour suppressor genes *RB1* and *NF1* (Patch et al., 2015; TCGA, 2011). The retinoblastoma 1 (*RB1)* gene was first identified as a tumour suppressor in childhood malignancies of osteosarcoma and retinoblastoma (Friend et al., 1986). The *RB1* gene product, RB, was later found to be the target of various viral onco-proteins, including human papillomavirus E7 proteins. The fact that *RB* overexpression was found to cause G1 phase arrest in cells, and *RB* loss caused accelerated G1 transition provided further evidence that RB is involved in control of cell proliferation (Goodrich et al., 1991; Herrera et al., 1996; Huang et al., 1988). The *RB1* and *TP53* tumour suppressor pathways are the most commonly inactivated in human cancers, and their combined loss is sufficient to induce transformation of somatic cells from various tissue types (Sage, 2012). The mechanism by which RB exerts its tumour suppressor function is believed to be largely connected to its inhibition of E2F family transcription factors, in turn preventing G1/S phase transition.

Another critical role of RB1 in cell cycle control is not related to its transcriptional repression activity. Instead it involves the stabilization of the cell-cycle inhibitor $p27^{Kip1}$ via inhibition of SKP2, a component of the SCF ubiquitin E3-ligase (Carrano et al., 1999; Wang et al., 2010). High levels of p27 enable direct inhibition of Cdk2 activity and slow cell cycle progression (Sage, 2012). The *RB1* pathway appears to be deregulated in over 60% of HGSOC cases (TCGA, 2011), with 15-17% of HGSOC having somatic mutations or gene-breakage in the *RB1* gene (Bowtell et al., 2015; Patch et al., 2015; TCGA, 2011). Recent work has shown that HGSOC with concurrent *BRCA*-mutation and *RB1* loss appear to be enriched in exceptional chemotherapy responders and long-term survivors, though the precise mechanisms underpinning this have not yet been established (Garsed et al., 2018). Another recent study reports $p16^{Ink4a}$ staining combined with RB1 status is useful in predicting clinical outcome for patients treated with first-line platinum-based chemotherapy (Milea et al., 2014). Patients with homogeneous $p16^{Ink4a}$ staining and RB1 loss were found to have a significant increase in overall survival, suggesting an increase in sensitivity to cytotoxic therapy (Milea et al., 2014).

The NF1 (neurofibromin) protein is a key regulator of Ras family proteins, small monomeric GTPase proteins with central roles in cell proliferation and differentiation (Bollag et al., 1992; Kano et al., 2016). Activating mutations in Ras genes, such as *KRAS* and *NRAS*, contribute to

the development of many different cancers. Ras proteins exist in inactive (GDP-bound) and active (GTP-bound) states. NF1 regulates the activity of Ras proteins by accelerating conversion of GTP-bound Ras to the inactive GDP-bound form (Bollag et al., 1992). Active Ras proteins have a high affinity for Raf family effector proteins that activate the mitogen-activated protein kinase (MAPK) pathway or phosphoinositide 3-kinases (PI3Ks), promoting cell survival and proliferation (Kano et al., 2016). Inactivating mutations of the *NF1* gene have been observed in 20% of HGSOC (Patch et al., 2015), and the pathway is altered in 45% of HGSOC cases (TCGA, 2011). Targeting of Ras oncoproteins to treat cancers has proven difficult, with no effective inhibitors of Ras having yet reached the clinic (Baker et al., 2013; Berndt et al., 2011; O'Bryan, 2019).

1.2.4 Oncogene amplifications

Large amplifications in the *MYC, MECOM* and *CCNE1* oncogenes each occur in more than 20% of HGSOC tumours (TCGA, 2011).

MYC (also known as c-Myc) is a proto-oncogene encoding a transcription factor that regulates a broad range of pathways such as cell proliferation and cellular metabolism. MYC overexpression (including via gene amplification) has been reported in up to 70% of human malignancies, and is a frequent occurrence in ovarian cancer (Li et al., 2012; TCGA, 2011). Fortunately, ovarian cancer patients with high tumour MYC expression have improved platinum chemotherapy responses (Iba et al., 2004). This may be due to increased genomic instability observed in high-MYC tumours (Li et al., 2012).

MECOM (MDS1 and EVI1 Complex Locus) amplifications are associated with expression of both EVI1 and MDS1/EVI1 mRNA/proteins, though EVI1 is better characterized. Interestingly, MDS1/EVI1 transcript levels have been shown to be associate with a favourable prognosis in patients, while EVI1 transcript levels are associated with a poor patient survival (Nanjundan et al., 2007). Potential targeted therapies for MECOM amplifications (aurintricarboxylic acid and arsenic trioxide) have been described, but not validated (TCGA, 2011).

CCNE1 amplifications and HRD (e.g. *BRCA1* and *BRCA2* mutations) appear to be mutually exclusive (Etemadmoghadam et al., 2013b; Patch et al., 2015; TCGA, 2011). HGSOC with

CCNE1 amplifications are, therefore, not susceptible to PARPi and platinum-based chemotherapy, and tend to have a poor prognosis (Etemadmoghadam et al., 2009; Nakayama et al., 2010). CDK2 inhibitors (such as dinaciclib) are currently being investigated for the treatment of *CCNE1* amplified HGSOC (Au-Yeung et al., 2017; Etemadmoghadam et al., 2013a).

BRD4 amplifications are another frequent event in HGSOC and, like *CCNE1* amplifications, are mutually exclusive with *BRCA1/2* mutations. Thus, patients with *BRD4*-amplified tumours are currently left with limited therapeutic options, beyond platinum-based chemotherapy. *BRD4* amplifications have recently been found to facilitate oncogenic gene expression programs in HGSOC, including enhanced *E2F1* and *MYC* gene expression signatures (Rhyasen et al., 2018). Fortunately, their reliance on excess BRD4 can make these cells sensitive to BET (Bromodomain and Extra-Terminal motif) inhibitors, which target the bromodomains of BET family proteins such as BRD4 (Rhyasen et al., 2018), presenting a therapeutic opportunity for patients with such tumours in future.

1.3 Predicting response to PARP inhibitors

1.3.1 Importance of BRCA1 and BRCA2 genes in HGSOC therapy

BRCA1 and *BRCA2* were first described as breast cancer susceptibility genes in the mid 1990s (Miki et al., 1994; Wooster et al., 1995; Wooster et al., 1994), and they each play fundamental, but differing, roles in HR (Moynahan et al., 1999; Orelli et al., 2001). The clinical significance of *BRCA*-mutations has been most obvious in the management of OC. It is estimated that up to half of all HGSOCs contain functional HRD at diagnosis (Mukhopadhyay et al., 2010; TCGA, 2011), most commonly caused by either germline *BRCA*-mutations (~8–12% in *BRCA1* and ~5–7% in *BRCA2*) or somatic *BRCA*-mutations (~3% in either *BRCA1* or *BRCA2*) (Alsop et al., 2012; TCGA, 2011; Walsh et al., 2011). An additional 5–20% of HGSOCs are considered HRD, due to other factors such as silencing of *BRCA1* or *RAD51C* via promoter hypermethylation (generally considered mutually exclusive of HR gene mutations, other than large scale structural variants and copy number changes) (Catteau et al., 1999; TCGA, 2011). *BRCA2* promoter methylation in HGSOC is rare, and, unlike in *BRCA1*, does not result in reduced gene expression (Collins et al., 1997). The importance of *BRCA1* methylation zygosity for PARPi response was recently demonstrated in a study of *BRCA1* homozygously and

heterozygously methylated HGSOC tumours, including clinical cases from the ARIEL2 part 1 trial of the PARPi rucaparib (Kondrashova et al., 2018). This study determined that all copies of the *BRCA1* promoter must be methylated, and therefore silenced, for HR to be inactive and for PARPi to be effective.

As women with *BRCA1/2* mutant cancers have demonstrated improved survival and response to cytotoxic chemotherapy (Alsop et al., 2012; TCGA, 2011), *BRCA*-mutation testing has become a key stratification factor in many OC clinical trials, and a routine clinical practice for management of OC patients (Audeh et al., 2010; Ledermann et al., 2014; Tutt et al., 2010).

1.3.2 Impacts of non-BRCA HR defects on HGSOC therapy

Although loss of *BRCA1/2* function through mutation or epigenetic silencing is the most common cause of HRD, PARPi therapy has also demonstrated efficacy in tumours with loss of HR by other means, a trait also known as 'BRCAness' (Lord et al., 2017; Turner et al., 2004). It is estimated that approximately half of HGSOCs are functionally HRD at time of diagnosis (Mukhopadhyay et al., 2010; TCGA, 2011), but germline/somatic *BRCA*-mutations only account for 20% of this. The Cancer Genome Atlas (TCGA) Network study has attributed the remaining 30% to defects in Fanconi anaemia genes, DNA damage repair/checkpoint genes, *EMSY* amplification, or loss of *PTEN* (TCGA, 2011). Loss of multiple other DNA repair genes has indeed been associated with PARPi lethality *in vitro* or *in vivo* (**Table 1.1**). Nevertheless, more reliable evidence of HRD and PARPi sensitivity is available for *RAD51C* (Kondrashova et al., 2017; McCabe et al., 2006; Swisher et al., 2017), *RAD51D* (Kondrashova et al., 2017), *ATM* (McCabe et al., 2006; Menisser-de Murcia et al., 2001), *NBN* (Swisher et al., 2017), and *PALB2* (Villarroel et al., 2011). In contrast, there is currently conflicting evidence for PARPi sensitivity cause by *PTEN* loss (Fraser et al., 2012; Mendes-Pereira et al., 2009) and *EMSY* amplification (Kondrashova et al., 2019; Wilkerson et al., 2011).

Table 1.1. Genes alterations reported to cause PARPi sensitivity in vitro or in vivo.
*Table adapted from (Nesic et al., 2018). *reported in clinical trials.*

Gene altered	Evidence from models	Publications
ATM	*in vitro* and *in vivo**	(Aguilar-Quesada et al., 2007; Mateo et al., 2015; McCabe et al., 2006)
ATR	*in vitro* only	(Lord et al., 2008; McCabe et al., 2006)
BRCA1	*in vitro* and *in vivo**	(Alsop et al., 2012; Farmer et al., 2005; Swisher et al., 2017; Walsh et al., 2011)
BRCA2	*in vitro* and *in vivo**	(Alsop et al., 2012; Bryant et al., 2005; Swisher et al., 2017; Walsh et al., 2011)
CCDC6	*in vitro* only	(Turner et al., 2008)
CDK12	*in vitro*	(Bajrami et al., 2014; Joshi et al., 2014)
CDK5	*in vitro* and *in vivo**	(Lord et al., 2008; Mateo et al., 2015)
CHK1	*in vitro* only	(McCabe et al., 2006)
CHK2	*in vitro* only	(McCabe et al., 2006)
CTIP	*in vitro* only	(Gaymes et al., 2013)
DDB1	*in vitro* only	(Lord et al., 2008)
DSS1	*in vitro* only	(McCabe et al., 2006)
FANCA	*in vitro* and *in vivo**	(Mateo et al., 2015; McCabe et al., 2006)
FANCC	*in vitro* only	(McCabe et al., 2006)
FANCD2	*in vitro* only	(McCabe et al., 2006)
FANCF	*in vitro* and *in vivo**	(Mateo et al., 2015; McCabe et al., 2006)
HPF1	*in vitro* only	(Gibbs-Seymour et al., 2016).
LIG1	*in vitro* only	(Lord et al., 2008)
MRE11	*in vitro* only	(Gaymes et al., 2013)
NBN	*in vivo**	(Swisher et al., 2017)
NBS1	*in vitro* only	(McCabe et al., 2006)
PALB2	*in vitro* and *in vivo**	(Buisson et al., 2010; Gaymes et al., 2013; Smith et al., 2015; Villarroel et al., 2011)
PCNA	*in vitro* only	(Lord et al., 2008)
PLK3	*in vitro* only	(Turner et al., 2008)
PNKP	*in vitro* only	(Turner et al., 2008)
PTEN	*in vitro* and *in vivo**	(Mateo et al., 2015; Mendes-Pereira et al., 2009)
RAD51B	*in vitro* only	(McCabe et al., 2006)
RAD51C	*in vitro* and *in vivo**	(Kondrashova et al., 2017; McCabe et al., 2006; Swisher et al., 2017)
RAD51D	*in vitro and in vivo**	(Kondrashova et al., 2017; Loveday et al., 2011; McCabe et al., 2006; Swisher et al., 2017)
RAD54	*in vitro* only	(McCabe et al., 2006)
RPA1	*in vitro* only	(McCabe et al., 2006)
STK22C	*in vitro* only	(Turner et al., 2008)
STK36	*in vitro* only	(Turner et al., 2008)
USP1	*in vitro* only	(Turner et al., 2008)
USP11	*in vitro* only	(Turner et al., 2008)
XAB2	*in vitro* only	(Lord et al., 2008)
XPF	*in vitro* only	(Ali et al., 2020; Mesquita et al., 2019)
XRCC1	*in vitro* only	(Lord et al., 2008)

1.3.3 Impact of BRCA1 or RAD51C promoter methylation on HGSOC therapy

BRCA1 and *RAD51C* are, so far, the only HR genes where promoter methylation has been shown to correlate with reduced gene expression (Esteller et al., 2000; George et al., 2013; Patch et al., 2015; TCGA, 2011). Promoter methylation in these genes tends to be mutually exclusive of HR gene mutations, (Bernards et al., 2018; Esteller et al., 2000; George et al., 2013; Patch et al., 2015; TCGA, 2011), and has been associated with genomic signatures related to *BRCA*-defects (George et al., 2013; Polak et al., 2017). However, the impacts of *BRCA1* and *RAD51C* promoter methylation on platinum or PARP inhibitor responses in HGSOC have long been debated, with mixed reports on its effects on overall survival in clinical studies (Bernards et al., 2018; Cancer Genome Atlas Research et al., 2013; Lheureux et al., 2017b; Ruscito et al., 2014; Swisher et al., 2009; Swisher et al., 2017).

There is now evidence to suggest that previous studies may have been limited by several technical factors related to measuring and estimating methylation in tumours. In cases of *BRCA1* methylation, it has been shown that *BRCA1* methylation zygosity is critical for predicting HR capacity and PARPi/platinum response. Methylation of all *BRCA1* copies is required for PARPi response, where loss of methylation in a single *BRCA1* copy is sufficient to restore HR capacity and lead to platinum and PARPi resistance (Kondrashova et al., 2018). Measuring zygosity accurately, however, relies on quantitative methylation assays and careful assessment of tumour purity and gene copy number (Kondrashova et al., 2018). Previous studies lacked either one, or both of these factors making it impossible to accurately quantify the proportion of methylated *BRCA1*epialleles in tumours (Cunningham et al., 2014). The same principles may apply to *RAD51C* promoter methylation, but this is yet to be established.

1.3.4 Limitations of HR gene testing in the clinic

A key finding of some early phase PARPi clinical trials was that some patients without *BRCA*-mutations still derived clinical benefit, and this was supported by some pre-clinical data (Gelmon et al., 2011). This suggested that mutation testing beyond the BRCA genes may be useful in identifying other patients that may derive benefit from PARPi therapy (Coleman et al., 2017; Kondrashova et al.; Kondrashova et al.; Konstantinopoulos et al., 2010; Lord et al., 2017; Swisher et al., 2017; Turner et al., 2004). However, less than 10% of other core HR genes are found to have mutations following relapse in HGSOC, and current gene sequencing

panels cannot detect HR gene promoter methylation, as this require additional tests such as methylation-specific polymerase chain reaction (MS-PCR) (Laird et al., 2004) or pyrosequencing (Ronaghi et al., 1998). Thus, even expanded HR gene panel sequencing can still miss patients that may respond to PARPi therapy (Konstantinopoulos et al., 2010; Marquard et al., 2015; Swisher et al., 2017).

Moreover, despite extensive testing and characterisation of the *BRCA1/2* genes for pathogenic (class 4–5) mutations, variants of uncertain significance (VUSs; class 2–3) are still detected in these genes (Richards et al., 2015). VUS pose a significant clinical problem. Given their effects on disease risk, prognosis and treatment response are unclear, resolving them requires functional experimental work, followed by difficult discussions with patients and families (Millot et al., 2012).

As the cost of next-generation sequencing (NGS) continues to fall, and somatic/germline gene testing becomes more common, more VUSs are being reported in commonly assessed genes, and other less-characterized genes that are now also being interrogated (Cheon et al., 2014). Unfortunately, traditional experimental approaches have not been able to keep up with the vast number of VUS being reported for these genes in the clinic (Findlay et al., 2018; Landrum et al., 2015). However, a novel approach for resolving VUS in *BRCA1* using CRISPR genome editing technology has recently been described (Findlay et al., 2018). This assay exploited the dependence of human haploid HAP1 cells on the *BRCA1* gene, by performing saturation CRISPR genome editing to target 96.5% of all single-nucleotide variants across 13 exons in cells from this cell line. Functionally critical sites were uncovered by measuring cell viability in exposed cells. Using this approach, authors were able to functionally characterize nearly 4000 *BRCA1* variants, uncover over 400 non-functional missense *BRCA1* mutations, and approximately 300 variants that disrupted gene expression (Findlay et al., 2018). This is a powerful approach, and may also prove useful for the characterisation of VUS in other genes, such as *BRCA2.*

Another approach for addressing uncertainty around VUS in *BRCA1/2* relies on looking at the functional consequences of HRD on the genome, rather than just the mutation itself. Such methods are discussed in more detail in the following section.

1.3.5 Genomic scarring as a marker of HR deficiency in HGSOC

Many HGSOCs will present with *BRCA* mutant-like genomic scarring, despite no detection of known HR gene mutations (Konstantinopoulos et al., 2010; Marquard et al., 2015). Recently, the international phase 2 trial of PARPi rucaparib (ARIEL2 part 1) has demonstrated the utility of these genomic signatures as surrogate markers of HRD that can identify *BRCA* wild-type patients that may benefit from PARPi therapy. The next generation sequencing (NGS)-based Foundation One (Foundation Medicine) test was used to measure the percentage of genome-wide loss of heterozygosity (LOH) in each patient tumour, and it was found that a cut-off of ≥16% LOH could be used to identify patients who may have a durable response to rucaparib (Coleman et al., 2017; Swisher et al., 2017). This approach may aid in identification of patients that would benefit from PARPi therapy despite not having detectable HR gene mutations. However, this does not change the problem of non-durable responses and drug resistance. Addressing these limitations requires a deeper understanding of how PARPi actually work.

In addition to LOH-based assays, tests based on Single Nucleotide Variant (SNV) signatures may also be used for HRD detection. Alexandrov et al. (2013) studied the six classes of SNV (T > A, T > G, T > C, C > A, C > G, and C > T,), plus the nucleotides to either side (5′ and 3′) of the mutated base. This resulted in 96 possible classes of nucleotide changes that were assessed. This SNV analysis uncovered 21 distinct signatures across 30 cancer types (Alexandrov et al., 2013). It was found that all signatures contained various classes of SNV changes, and that multiple signatures could be identified in a single tumour type. Signature 3, characterized by a high number of indels (up to 50 bp), was found to be strongly associated with the presence of *BRCA1/2* mutations. Interestingly, some cancers containing high representation of SNV signature 3 in their genomes were lacking *BRCA* mutations (Alexandrov et al., 2013).

Complex copy-number (CN) and structural variants (SV) have also been used to define genomic HRD signatures in breast cancer (Nik-Zainal et al., 2016). From this work, three rearrangement signatures associated with HRD repair were identified. These were characterized by tandem duplications or deletions, and included one associated with *BRCA1* defects, another with *BRCA1* or *BRCA2* defects and a third signature where the cause is

unknown. Following up on this work, the Nik-Zainal group developed the HRDetect test, which relies on the weighted quantification of six genomic features; SNV signature 3, SNV signature 8, deletions with microhomology, rearrangement signatures 3 and 5 and degree of LOH. This test was found to detect *BRCA*-deficient tumours with 98.7% sensitivity, and outperformed LOH-based assays (Davies et al., 2017). Unfortunately, HRDetect relies on deep-coverage WGS, making it unsuitable for use outside of a research setting for the time being.

As genomic scarring is a reflection of historical rather than present DNA repair capacity, the role of genomic signatures should predominantly be applied to the analysis of cancers at diagnosis, to aid in choice of subsequent treatment approaches. However, using rapid and low-cost methods, in future it may be possible to detect changes in HR state (e.g. reversion mutations) by monitoring changes in genomic scarring. Other challenges in the application of these HRD signatures in the clinic remain, with further prospective studies required to determine optimal thresholds for each test, which would ultimately reveal their clinical utility.

1.4 Proposed mechanisms of PARP inhibitor sensitivity

Poly(ADP-ribosyl)ation (PARylation) is one of the earliest covalent post-translational modifications affecting proteins responding to DNA strand breaks, and is also a key mechanism in regulation of a range of other cellular processes including telomere homeostasis, chromatin remodeling, transcription, differentiation and cell death (De Vos et al., 2012). PARylation is catalyzed by certain members of the PARP superfamily, of which PARP1 is the best studied. PARP1 is capable of transferring successive ADP-ribose units to itself and to acceptor proteins, including histones, using NAD^+ as a substrate. This is a rapid reaction, but the results are transient, due to the catabolic activity of poly(ADP-ribose) glycohydrolase (PARG) (Gagne et al., 2006; Min et al., 2009).

PARP1 has a critical role in maintaining genomic integrity by coordinating the processing and resolution of various types of DNA lesions, including damaged DNA bases, single strand breaks (SSBs), DSBs, DNA cross-links and stalled replication forks (Krishnakumar et al., 2010; Trucco et al., 1998). PARP1 promotes DNA repair and cell survival when DNA damage levels are low. Extensive DNA damage, on the other hand, can trigger PARP1-mediated cell death via two mechanisms: depletion of cellular energy (ATP) pools by NAD^+ consumption

causing necrosis, and apoptosis-inducing factor (AIF)-dependent apoptosis (Bouchard et al., 2003; Kim et al., 2005). Inhibition of PARP1 using PARPi has been shown to specifically kill HRD cancer cells via synthetic lethality, where loss of HR or inhibition of PARP1 alone are tolerated, but together cause catastrophic genomic instability and cell death.

Despite years of clinical use for the treatment of HRD HGSOC, we are still refining our understanding of the mechanisms by which PARPi trigger synthetic lethality in these tumours. Over the years, various theories have been put forward by different groups, with some gaining traction as others fade.

1.4.1 PARP inhibitors and base excision repair

Initially, it was believed that it was PARP1's essential role in base excision DNA repair (BER) that causes PARPi-induced cellular toxicity in the absence of HR DNA repair (Dantzer et al., 1999; De Vos et al., 2012). In fact this was the rationale for testing PARPi in *BRCA2*-deficient cell lines in the first place (Bryant et al., 2005). In this model, PARP1 inhibition leads to loss of BER, resulting in an accumulation of unrepaired single-strand breaks (SSBs) that are converted to DSBs. HRD cells are unable to cope with the increased DSBs, and undergo apoptosis (Iglehart et al., 2009; Yap et al., 2011).

However, accumulation of SSBs was not observed in PARPi-treated HRD cells (Fraser et al., 2012; Gottipati et al., 2010), though perhaps the transition from SSB to DSB was too rapid to detect with technology available at the time. Furthermore, knockdown of the crucial BER protein XRCC1, which is directly downstream of PARP1 in this pathway, does not kill HRD cells in the same way (Patel et al., 2011). These observations casted doubt over this model as the true mechanism of PARPi-HRD synthetic lethality.

1.4.2 PARP1 trapping and replication fork collapse

There is now growing evidence that PARPi action occurs via 'trapping' of the PARP1 protein at sites of DNA damage during DNA replication, leading to stalled and collapsed DNA replication forks (Ding et al., 2016; Gogola et al., 2018; Neelsen et al., 2015; Ray Chaudhuri et al., 2016; Saleh-Gohari et al., 2005). Normally, upon binding to damaged DNA, PARP1 generates negatively charged PAR chains on target proteins, including itself. As these chains

grow in length on PARP1, affinity of PARP1 for DNA is lowered, eventually allowing the protein to be released. PARylation is then removed by the glycohydrolase PARG, which allows PARP1 reactivation. Under cell-free conditions, PARP1 protein that is unable to catalyze PARylation remains bound to damaged DNA and prevents repair (Satoh et al., 1992).

PARPi have been shown to trap PARP1 and PARP2 on DNA, and this is more cytotoxic than PARP loss and the consequent accumulation of unrepaired single strand breaks (Murai et al., 2012; Murai et al., 2014; Strom et al., 2011). Furthermore, genetic loss of PARP1 has also been shown to eliminate the cytotoxicity of PARPi, supporting the notion that PARP trapping is the crucial to the mechanism of synthetic lethality in HR deficient cancers (Murai et al., 2014). Various PARPi have been shown to have different "trapping" potencies, and this is unrelated to their relative catalytic inhibition potency (Murai et al., 2012). Talazoparib is the most potent PARP-trapper, followed by olaparib and rucaparib, and least potent being veliparib and niraparib (Hopkins et al., 2019; Murai et al., 2012). However, although trapping may be important mechanistically, PARP trapping potency does not appear to correlate with mono-therapeutic activity both clinically and pre-clinically (Hopkins et al., 2019). However, in the clinic this may be because of lower PARPi dosing of stronger PARP-trappers due to reduced maximum tolerated doses (Pommier et al., 2016). Furthermore, a recent study of these PARPi has revealed that they have different specificities for killing HRD cells *in vitro*, with olaparib being the most specific HRD toxicity, while talazoparib cytotoxicity was less restricted to HRD cells (Leo et al., 2018).

It has been proposed that PARP trapping exerts its toxic effects predominantly via collapse of stalled DNA replication forks, which prevent cells from replicating their DNA and entering mitosis (Ding et al., 2016; Gogola et al., 2018; Neelsen et al., 2015; Ray Chaudhuri et al., 2016; Saleh-Gohari et al., 2005). Faithful reproduction of the genome relies on the completion of DNA replication, and one obstacle that must be dealt with during this process is replication fork stalling. Cells have evolved a network of protein interactions that serve to stabilize, repair and restart these stalled replication forks. Under normal conditions, PARP1 regulates DNA replication fork progression rates, and also prevents the premature restart of reversed replication forks (Berti et al., 2013; Ray Chaudhuri et al., 2012; Sugimura et al., 2008; Zellweger et al., 2015). When PARP inhibition occurs in the absence of functional HR, replication forks are degraded and a larger proportion of single strand breaks are processed into DSBs, leading to unrepaired DNA damage that can carry over into cell division (Ding et al.,

2016; Gogola et al., 2018; Neelsen et al., 2015; Ray Chaudhuri et al., 2016; Saleh-Gohari et al., 2005).

This model is supported by observations that *PARP1* silencing in HRD cells does not cause the same degree of toxicity (Bryant et al., 2005), as well as the localization of PARP1 to stalled replication forks (Gogola et al., 2018). PARylation of PARP1, which modulates its binding to DNA and its release, has also been shown to be necessary for synthetic lethality (Gogola et al., 2018). Furthermore, PARPi-treated HRD cells have been shown to have an increased dependence on the ATR/CHK1 pathway for survival, as CHK1 and ATR inhibitors targeting cell cycle checkpoint and inducing replication stress have been shown to synergize with PARPi (Kim et al., 2017).

1.4.3 Competing DNA repair pathways/ de-regulated non-homologous end joining

There is now an abundance of evidence in the literature that suggests DNA repair pathway balance is the key mechanism of PARPi-HRD synthetic lethality, namely de-regulation of the C-NHEJ DNA DSB repair pathway.

Unlike HR, C-NHEJ is considered an error-prone DNA repair pathway as it is not homology-directed, causing chromosomal rearrangements and mutations when unregulated (Ceccaldi et al., 2015; Ceccaldi et al., 2016; Patel et al., 2011). Regulated C-NHEJ, however, has a critical, evolutionarily conserved role in diversity generating V(D)J recombination in developing lymphocytes (Malu et al., 2012). It can occur at any stage of the cell cycle, but is especially active during the G1 phase (Burma et al., 2006). During C-NHEJ, DNA DSB ends are simply joined together, sometimes following limited processing, resulting in fast but inaccurate DNA repair (Lieber, 2010; Lieber et al., 2004). Based on multiple studies, C-NHEJ appears to be necessary for PARPi cytotoxicity in HRD cells, and loss of C-NHEJ causes PARPi resistance *in vitro* (AlHilli et al., 2016; McCormick et al., 2017; Patel et al., 2011; Williamson et al., 2012) and in Patient Derived Xenografts (PDX) (AlHilli et al., 2016). In the absence of HR, loss of PARP1 may de-represses C-NHEJ and cause catastrophic genomic instability (Patel et al., 2011).

Though multiple associations of PARP1 with various proteins involved in the HR and C-NHEJ have been observed, additional data suggests these are probably not indicative of PARP1's

direct involvement in these pathways, but rather a regulatory role that limits these pathways and promotes alternative end joining (alt-EJ)(Magnusson et al., 1990; Schreiber et al., 1995; Schultz et al., 2003; Semionov et al., 1999; Sousa et al., 2012; Waldman et al., 1991). Alt-EJ is slower than C-NHEJ, and considered more error-prone (Ceccaldi et al., 2016 2015; Wang et al.; Wang et al., 2006). It is a poorly understood DNA DSB mechanism that often relies on micro-homologies at the break sites, which is why it is sometimes referred to as microhomology-mediated end joining. Interestingly, these types of microhomologies are enriched in HRD cancers, and are therefore a defining characteristic of HRD-associated mutational signatures (Alexandrov et al., 2018; Nesic et al., 2018). Polymerase theta (Polθ, encoded by *POLQ* gene), another alt-EJ protein, is upregulated in many HGSOCs (Ceccaldi et al., 2015; Tothill et al., 2008), and its loss has recently been demonstrated to be cytotoxic in the absence of HR DNA repair (Ceccaldi et al., 2015; Dai et al., 2016; Mateos-Gomez et al., 2015; Shima et al., 2004).

As both POLQ and PARP1 are involved in alt-NHEJ DSB repair and their loss is synthetic lethal in a HRD setting suggests that alt-EJ serves as a critical back-up repair mechanism when HR is lost. Indeed, HRD cells have been found to have hyperactive PARP1 activity, and upregulated PolQ (Ceccaldi et al., 2015; Ceccaldi et al., 2016; Gottipati et al., 2010).

HRD cancers may rely more heavily on this pathway, thus its loss renders cancer cells non-viable, sparing healthy HR competent (HRC) cells. To confirm that it is alt-EJ loss that is responsible for PARP1 and PolQ loss synthetic lethality in HRD cells, the same results should be seen when other critical alt-EJ proteins are lost or inhibited. The limited reports in the literature have, thus far, only attempted this in alt-EJ proteins that are not considered crucial, or are functionally redundant (e.g. XRCC1 and ligase I and III) (Boboila et al., 2012; Mateos-Gomez et al., 2015; Patel et al., 2011; Simsek et al., 2011).

Synthetic lethality with HRD has also been reported for the RAD52 protein, which participates in the single-strand annealing (SSA) DNA repair pathway and, like PolQ, is upregulated in HRD cells (Feng et al., 2011; Lok et al., 2013; Sullivan-Reed et al., 2018). This further supports the model of competing DNA repair pathway loss leading to de-regulated C-NHEJ and synthetic lethality.

1.4.4 Combining different models of PARPi action

Whether these models of PARPi-HRD synthetic lethality are all at play, or whether some are more relevant than others remains to be determined. Given the diverse roles of HR DNA repair in maintaining genomic stability, it is possible that multiple models are valid, and that it is the cumulative effect of all parts that leads to the potency and selectivity of PARPi in HRD ovarian cancer cells.

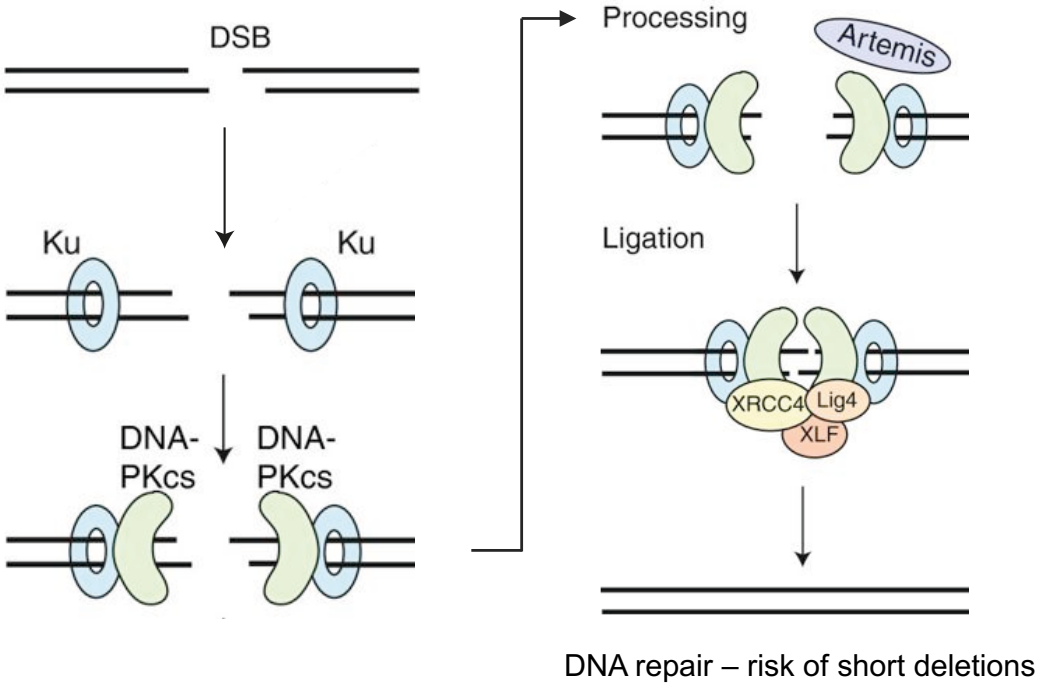


Figure 1.2. The classical NHEJ pathway.

Figure adapted from (Brandsma et al., 2012). Upon DNA DSB detection, the C-NHEJ proteins Ku70 and Ku80 heterodimerise and bind to the ends of each DNA strand. They then recruit DNA-PKs, a serine/threonine kinase which can then phosphorylate itself and other repair proteins. This signals the presences of the DSB to other C-NHEJ proteins, including the 5′–3′ exonuclease Artemis. Artemis then executes nucleolytic processing to resolve complex, incompatible DNA DSB ends. This process can, however, result in gaps that either lead to loss of genetic information (deletions) or are filled by DNA polymerases μ and λ (Davis et al., 2013). Final ligation is performed by a complex of XRCC4 and DNA ligase 4, and XLF. All of these

proteins, excluding the DNA polymerases, are critical for C-NHEJ (Betermier et al., 2014 2014; Burma et al., 2006; Lieber et al., 2004).

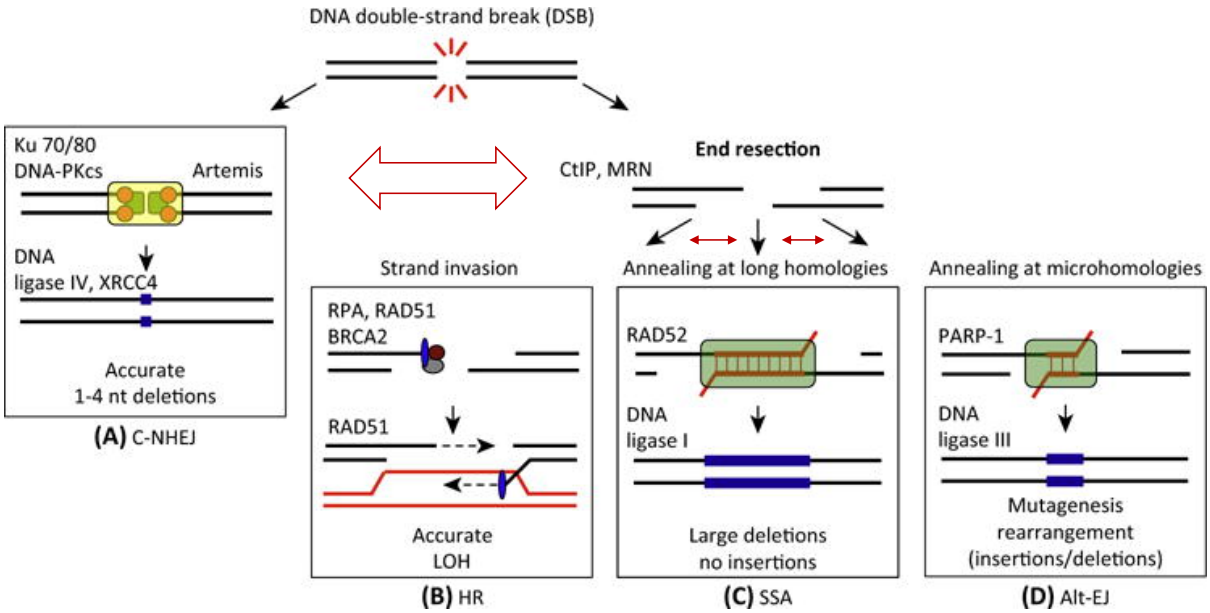


Figure 1.3. Competing DNA DSB repair pathways.
Figure adapted from (Ceccaldi et al., 2016). (A–D) Following a DSB, DNA end resection is the initial factor determining which DNA DSB pathway is subsequently activated. Defects or blocks in end-resection mechanisms lead to C-NHEJ repair being favoured. DSB end-resection results in one of three pathways taking over: HR, SSA and alt-EJ. These pathways compete with one another, and result in different genetic outcomes or signatures; HR is high fidelity but can result in LOH, while SSA can lead to large deletions, and alt-EJ is considered mutagenic, leading to insertions and deletion. Nt, - nucleotides.

1.5 Mechanisms of PARP inhibitor resistance

Our understanding of the true mechanism of PARPi action in HRD cells may not be complete, but certain mechanisms of resistance are well defined. PARPi resistance is a major problem, limiting response time and the benefit patients gain from this targeted therapy.

1.5.1 Homologous recombination pathway reversion

HRD cells that become HR competent become resistant to PARPi. Secondary (reversion) mutations that correct primary defects in *BRCA1* and *BRCA2* and restore HR protein function are a well described mechanism of PARPi and platinum resistance. These have been reported

to occur *in vitro*, and in patients post-chemotherapy (Barber et al., 2013; Edwards et al., 2008; Norquist et al., 2011; Patch et al., 2015; Sakai et al., 2009; Sakai et al., 2008) and PARPi (Kondrashova et al., 2017). Recently, a patient with acquired platinum resistance and no response to the PARPi olaparib was found to have 11 independent secondary *BRCA1* mutations at various metastatic sites following warm autopsy, highlighting the high degree of heterogeneity within this tumour type (Patch et al., 2015).

Secondary mutations can either be single nucleotide changes that correct a primary missense mutation, or insertion/deletion mutations (indels) that restore the open reading frame of a gene following a primary indel. Knowing whether a patient carries secondary HR gene mutations is useful for prognosis and has important implications for treatment, as patients with reversions would not be expected to respond to PARPi. Using genomic scarring as a surrogate marker of HRD in patients is now possible, and has the advantage of identifying patients that do not have *BRCA1/2* mutations but may still benefit from PARPi therapy. However, genomic scarring does not disappear once a HR defect is corrected. Thus, such assays may need to be supplemented with tests for reversion mutations.

RAD51 foci formation (which is a marker of functional and active HR DNA repair) has been previously reported in *BRCA*-mutant PDX models of breast and ovarian cancer, despite no secondary mutations being detected (Cruz et al., 2016). Indeed, other mechanisms of HR defect reversion have been reported, though their contribution in the clinic is yet to be determined (Cruz et al., 2016). For example, mutations in the BRCT domain of *BRCA1* cause misfolding of the BRCA1 protein, and its subsequent degradation by proteases. Stabilization of misfolded BRCA1 proteins via HSP90 has been shown to restore partial BRCA1 function in HR, and confer resistance to PARPi (Johnson et al., 2013). HSP90 inhibitors may be useful in reversing PARPi resistance in tumours with such *BRCA1* BRCT domain mutations.

Another mechanism of HR defect reversion is the expression of alternative HR protein isoforms that may partially compensate for loss of the canonical HR protein. This mechanism has been shown to contribute to PARPi resistance in cells with deleterious mutations in the 11q region of *BRCA1,* which is spliced out in the D11q (also known as Δ11q) *BRCA1* isoform (Wang et al., 2016). However, despite having a poorer prognosis relative to HGSOC patients with *BRCA1* mutations outside of 11q, no correlation between D11q *BRCA1* expression and

PARPi resistance was seen in patients with *BRCA1* 11q mutations (Wang et al., 2016). This example further highlights the complex biology of these tumours, and the challenges in tailoring treatments for HGSOC patients.

1.5.2 C-NHEJ pathway loss

As discussed in section 1.4.3 of this chapter, C-NHEJ may have a key role in PARPi sensitivity, and loss of the pathway has been described as a resistance mechanism in some contexts. Loss of early C-NHEJ pathway proteins 53BP1, RIF1 and members of the shieldin complex (REV7, RINN1 and RINN2) has been shown to cause PARPi resistance in BRCA1-deficient cells, but not BRCA2-deficient cells (Boersma et al., 2015, Bunting et al., 2010, Lord and Ashworth, 2017, Xu et al., 2015; Gupta et al., 2018). In these cases, HR DNA repair has been shown to be restored following loss of early C-NHEJ proteins, suggesting that BRCA1 competes with these proteins to promote DSB end-resection and HR. Upon their loss, HR DNA repair can occur, even in the absence of BRCA1. Interestingly, 53BP1 has been shown to not be essential for C-NHEJ.

It remains to be seen whether loss of other downstream C-NHEJ proteins can have the same effect, perhaps even in other HRD contexts, such as BRCA2 or RAD51C loss. It is possible that cells completely lacking the two major DNA DSB repair pathways, HR and C-NHEJ, are not viable.

1.5.3 Replication fork protection

Given that one of the models of PARPi sensitivity is PARP trapping, which causes an increase in DSBs due to collapsed replication forks, stabilization of stalled replication forks has thus been proposed as a mechanism of PARPi resistance. According to the fork-protection theory of PARPi resistance, stalled replication forks are especially unstable in HRD cells treated with PARPi, collapsing into DNA DSBs, which then cannot be repaired by high fidelity HR DNA repair, leading to genomic instability and toxicity. Mechanisms that prevent fork collapse in this context would, therefore, lead to resistance. Some such mechanism has recently been described (Ding et al., 2016; Ray Chaudhuri et al., 2016; Rondinelli et al., 2017; Schlacher et al., 2012).

Apart from their role in HR DNA repair, BRCA1 and BRCA2 play another critical role in protecting cells from genomic instability via their involvement in replication fork stabilization. This pathway is initiated by upregulation of the checkpoint kinase pathway proteins ATR and CHK1, which in turn leads to loading of BRCA1 and BRCA2 at the stalled replication fork. These proteins protect the exposed DNA ends of stalled replication forks from degradation by various nucleases, including DNA2, MRE11, EXO1, and MUS81 (Ding et al., 2016; Ray Chaudhuri et al., 2016; Rondinelli et al., 2017; Schlacher et al., 2012). Stabilization of replication forks can, however, be achieved in the absence of BRCA1 and BRCA2 by other mechanisms. Loss of either CHD genes (e.g. CHD4), SNF2-family fork re-modelers (e.g. SMARCAL1), RADX, PTIP and PARP1 is believed to limit MRE11 access to single-stranded DNA ends at stalled replication forks and prevent fork collapse when PARP1 is inhibited, leading to fork stability and PARPi resistance. Loss of the break-induced replication (BIR) pathway, triggered by MUS81-dependant fork degradation, has also been shown to cause PARPi resistance in some *BRCA2*-mutant contexts, as does loss of the RAD51 antagonist, RADX. This type of PARPi resistance does not rely on restored HR repair.

Cells with replication fork-protected PARPi resistance mechanisms have also been shown to better tolerate cisplatin and topotecan, suggesting that fork stabilization provides a general resistance to chemotherapies that induce replication stress. In the clinic, low expression of MUS81, PTIP, RADX and SMARCAL1 have been shown to correlate with poor survival outcomes in patients with *BRCA1/2* cancers (Dungrawala et al., 2017; Ray Chaudhuri et al., 2016; Rondinelli et al., 2017; Taglialatela et al., 2017).

Mutations or single-nucleotide polymorphisms in PARP1 found in human cancers have also been suggested as a potential mechanism of PARPi resistance due to their effects on PARP trapping (Montoni et al., 2013) and this was recently confirmed using genome-wide and targeted PARPi resistance CRISPR screens (Pettitt et al., 2018). Pettitt et al., found that mutations lying both within and outside the PARP1 DNA-binding domain can alter PARP1 trapping and lead to PARPi resistance. Authors reported on one clinical case of PARPi resistance with a *PARP1* mutation (c.1771C>T, p.R591C), where the mutation was shown *in vitro* to prevent PARP trapping. Interestingly, PARP1 loss was only found to be tolerated in cancer cell lines with mutations in the exon 11q region of *BRCA1* (Δ11q *BRCA1* mutants), where some residual BRCA1 function was present. *BRCA1* or *BRCA2* knockdown in these Δ11q cell lines with added PARP1 mutations (introduced by CRISPR) negatively impacted on

cell survival, suggesting that some HR activity is required for cell survival in the presence of *PARP1* mutations.

Other groups have suggested that it is instead PARP1's role in recruiting MRE11 nuclease to stalled replication forks that leads to fork protection and PARPi resistance following loss of PARP1, rather than loss of PARP trapping (Ding et al., 2016; Ray Chaudhuri et al., 2016). It is quite possible that both of these play a role in PARPi resistance caused by loss of PARP1.

1.5.4 Contribution of other signalling pathways

Elevated oncoprotein activity has been associated with platinum resistance in various cell lines (Youn et al., 2004) and in patients (Kolasa et al., 2009; Mignogna et al., 2016). As *RB1* and *NF1* are frequently lost in HGSOC, it is possible that deregulation of oncogenes downstream of these tumour suppressors may contribute to PARPi resistance.

Interestingly, RB1 loss has been shown to correlate with exceptional chemotherapy responses and extended survival in HGSOC with *BRCA*-mutations (Garsed et al., 2018). The co-occurrence of these two independent molecular defects appears to sensitize cancers to chemotherapy, though the mechanism by which this occurs is not yet established. It is possible that perhaps disinhibited cell cycle progression following RB1 loss is causing elevated DNA replication stress that is, in turn, sensitizing these cells to DNA-damaging chemotherapy (Mateo et al., 2019).

The effects of RB1 and HR loss on PARPi therapy has not yet been established. However, phosphorylated RB1 is known to repress the activity E2F transcription factors, and loss of E2F7 has recently been shown to cause PARPi resistance in BRCA2-deficient cells via increased expression of RAD51 (a target for E2F7-mediated transcriptional repression). Increased RAD51 levels were shown to enhance both HR DNA repair and replication fork stability in these BRCA2-deficient cells (Clements et al., 2018). In this model, hyperphosphorylation of RB1 may lead to PARPi resistance via E2F7 loss, though this has not yet been reported.

The Ras-Raf-MEK-ERK and PI3K-AKT-mTOR signalling pathways are the most frequently altered in solid tumours. These pathways can become hyperactive via activating mutations in Ras, Raf or PIK3CA oncogenes, or by loss of tumour suppressors such as NF1 and PTEN

(Jokinen et al., 2015). In contrast to RB1 loss, reduced NF1 expression is a poor prognostic indicator in ovarian carcinoma, and is associated with reduced 5-year patient survival (Qiao et al., 2019).

MEK inhibitors have recently been shown to synergize with PARPi in cell lines via downregulation of HR and checkpoint reduction independent of *BRCA*-status (Sun et al., 2017), and this is now being investigated in early phase clinical trials (e.g. NCT03162627). The direct effects of NF1 loss on PARPi responses, however, are not established.

Given frequent aberration of Ras-Raf-MEK-ERK and PI3K-AKT-mTOR signalling pathways in multiple cancer types, much focus has been placed in therapeutically targeting these pathways directly. Targeting of the Ras GTPases directly modulated by NF1 has proved a difficult task, though new Raf kinase inhibitors currently in clinical trials (such as Rigosertib and BGB283) show great promise (Athuluri-Divakar et al., 2016; Tang et al., 2015). Another approach developed to combat oncogenic PI3K-AKT-mTOR and Ras-Raf-MEK-ERK signalling has been the dual targeting of each pathway using downstream PI3K and MEK inhibitors (Jokinen et al., 2015).

1.5.5 Drug efflux

Various copper influx and efflux transporters are known to contribute to platinum resistance in ovarian and cervical cancer cells (Nakayama et al., 2004; Samimi et al., 2004; Zisowsky et al., 2007). Similar findings have been reported for ATP-binding cassette (ABC) drug efflux transporters in platinum and PARPi resistance. For example, *ABCG2* (ABC transporter breast cancer resistance protein) and *ABCB1* (P-glycoprotein/ multidrug-resistant protein 1; MDR1), affect the uptake of the oral rucaparib (Durmus et al., 2015). *ABCB1* translocations causing significantly increased gene expression have been reported in approximately 8% of platinum-treated HGSOC recurrent samples compared to pre-treatment (Patch et al., 2015). Increased *ABCB1* expression in mouse mammary tumours has also been shown to cause resistance to PARPi (Henneman et al., 2015).

Unfortunately, existing MDR1 inhibitors have not been clinically successful thus far due to considerably increased toxicity when combined with paclitaxel (Binkhathlan et al., 2013; Lhomme et al., 2008). In future, for patients with evidence of *ABCB1* overexpression, it may

be possible to prioritize treatments with chemotherapies or novel PARP inhibitors that are not substrates of MDR1.

1.6 Evolution of PARP inhibitor resistance

What triggers the formation of the PARPi and platinum resistant lesions in the clinic is not established. Two models of how resistance develops have been proposed: 1) the pre-existing resistant clone/tumour heterogeneity model, and 2) the acquired resistant clone model (**Figure 1.4**) (Barber et al., 2013; Norquist et al., 2011).

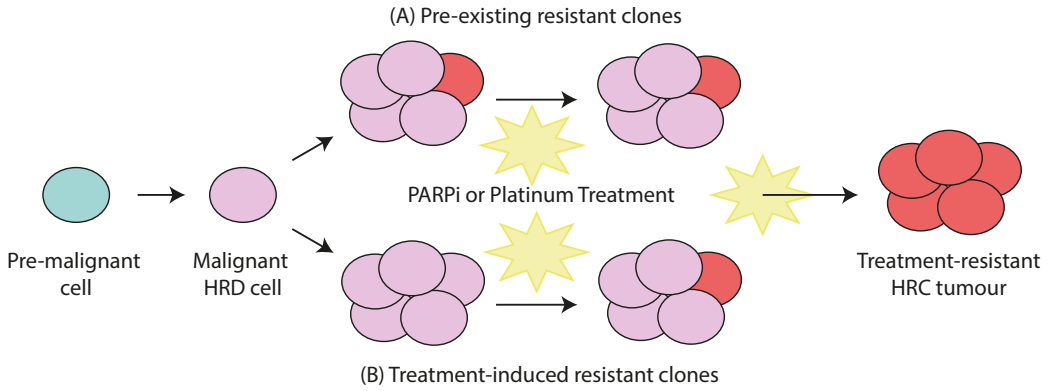


Figure 1.4. Evolution of PARPi and platinum resistance.
*When PARPi or platinum resistant clones develop in a primarily HRD tumour, for example via restored HR DNA repair, they are further selected for under treatment pressure. The result of selection is a PARPi- and platinum-resistant, recurrent tumour, at which point there are few therapeutic options left for a patient. It is unclear whether these lesions exist **(A)** prior to chemotherapy in patients, or whether **(B)** they require treatment pressure to form.*

The high degree of clonal diversity, as measured by genomic methods, in chemonaïve HGSOC supports a model of pre-existing resistance (Bowtell et al., 2015). Indeed, loss of BRCA2 leads to error-prone DNA DSB repair, and it has been proposed that this error prone repair leads to tumour heterogeneity and may generate secondary mutations in clones that are then simply selected for under platinum or PARPi pressure (Ashworth, 2008; Tutt et al., 2001). Then again, platinum chemotherapy is a DNA damaging agent, and may also increase the chances of such events. *In vitro*, patient-derived HRD cancer cell lines can be driven to resistance under platinum or PARPi pressure (Johnson et al., 2013; Sakai et al., 2008), and secondary HR gene mutations have only been described in patients treated with platinum chemotherapy (with or

without PARPi) previously (Barber et al., 2013; Norquist et al., 2011; Patch et al., 2015; Sakai et al., 2009; Sakai et al., 2008). Even in patients where chemonaïve and post-platinum/PARPi samples are available, it has not been possible to tell whether resistance in these patients was present at undetectable levels prior to chemotherapy, or whether chemotherapy triggered the formation of resistant lesions that were then selected for. Knowing which model prevails in the clinic may have a significant impact on how patients are treated. For example, if DNA-damaging platinum chemotherapy is found to increase the frequency of stabilized replication forks or restored HR, patients may be given PARPi, or an alternative drug, combination therapy in the first line setting.

1.7 Project Rationale and Aims

Given frequent late stage diagnosis and limited treatment options for women with HGSOC, precision therapy using PARPi offers hope to many patients. However, although some women demonstrate highly durable and impressive PARPi responses, there are still many who either never respond or eventually develop drug resistance (Audeh et al., 2010; Gelmon et al., 2011; Kaufman et al., 2015; Ledermann et al., 2014; Swisher et al., 2017).

This is most likely because we do not fully understand the underlying mechanisms of PARPi synthetic lethality and resistance, which in turn limits the development of novel treatment strategies to exploit the cancer's DNA repair defects.

Broadly, this project will involve the characterisation of pre-clinical models, including a cohort of HGSOC Patient-Derived Xenografts (PDX) and panel of HGSOC cell lines with various HR pathway defects. These will then be screened for underlying mechanisms of PARPi sensitivity and resistance, followed by more comprehensive validation of some of these mechanisms. As follows are the specific aims related to each chapter:

Chapter 3 aims:

- To investigate the contribution of HR gene secondary and reversion mutations to PARPi resistance within the HGSOC PDX cohort
- To investigate the contribution of alternative *BRCA1* isoforms to PARPi resistance within the HGSOC PDX cohort
- To screen for other DNA repair mutations that may be influencing PARPi responses within the HGSOC PDX models

Chapter 4 aims:

- Explore the role of C-NHEJ loss in PARP inhibitor resistance in *in vitro* and *in vivo* setting.
- Uncover novel PARPi-resistance genes/pathways using *in vitro* genome-wide CRISPR screens across multiple HRD contexts (*BRCA1/2*-mutation and *BRCA1* methylation)
- Find which PARPi-resistance hits are specific to certain HRD contexts, and which are common across all contexts

Chapter 5 aims:

- Characterisation of novel HGSOC PDX models with *RAD51C* promoter methylation
- Drive *RAD51C* promoter methylation loss in these models using PARPi or cisplatin and screen for heterozygous methylation patterns
- Search for heterozygous *RAD51C* promoter methylation patterns in patient samples, to see if this state is associated with platinum/PARPi resistance

Chapter 6 aims:

- Characterize global methylation profiles of HGSOC PDX models with *RAD51C* or *BRCA1* promoter methylation
- Search for changes in global methylation profiles of PDX tumours following PARPi-treatment
- Search for global methylation signatures that may be associated with *RAD51C* or *BRCA1* promoter methylation profiles

2 Materials and Methods

2.1 Molecular methods

2.1.1 DNA purification from tissues and cell pellets

For PDX tumours, less than 25mg of snap frozen tissue was homogenized in 80µl of GIBCO Dulbecco's Phosphate-Buffered Saline (DPBS; Thermo Fisher Scientific, Cat# 14190250) using a stainless-steel grinding ball and the TissueLyser II (Qiagen, Cat# 85300) set at 20ghrz for 4 minutes. The QIAamp DNA Mini Kit (Qiagen, Cat# 51306) was used to extract high quality DNA from the homogenized tissue samples according to the manufacturer's protocol. Cell pellets were re-suspended in DPBS to a final volume of 200µl, and high quality DNA was extracted according to the QIAamp DNA Mini Kit (Qiagen, Cat# 51306) manufacturer's protocol.

2.1.2 Ethanol precipitation of DNA

Ethanol precipitation was used to purify and/or concentrate low concentration genomic DNA samples. Briefly, 1/10 volume of 3M sodium acetate was added to the DNA sample, followed by addition of 2.5x of the total volume of pre-chilled 100% ethanol. Samples were left in -30 to -80°C for 1 hour, and were then centrifuged for at least 30 minutes at 20,000g at 4°C. Supernatant was removed without disturbing the pellet, and 1ml of pre-chilled 70% ethanol added. Samples centrifuged for at least 5 minutes at 20,000g at 4°C. Supernatant was removed without disturbing the pellet, and pellets allowed to air-dry (time varied between pellets). Pellets then re-suspended in 50µL of 1xTE buffer/water and incubated for 5-10 minutes at room temperature.

2.1.3 Quantification of double-stranded DNA

Qubit dsDNA high sensitivity (HS) assay (Invitrogen, Cat#Q32854) was used to quantitate the double-stranded DNA in genomic DNA samples and in each NGS libraries prior to equimolar normalization. The assay was performed according to manufacturer's protocol.

2.1.4 Murine vs Human PCR

This PCR uses primers specific to human and murine *TP53* gene to estimate the amount of contaminating murine tissue in DNA samples to be sequenced by NGS (**Table 2.1**). Briefly, 2µl of 10ng/µl DNA was added to 8µl HotStarTaq Master mix (Qiagen, Cat#203443), 8µl of primer mix, and 2µl of molecular grade H_2O. Reactions were incubated at 95°C for 15 minutes, followed by 30 cycles of 95°C for 30 seconds, 62°C for 40 seconds, 72°C for 40 seconds. Reactions then incubated at 72°C for 10 minutes, and stored at 4°C until prepared for agarose gel electrophoresis.

Table 2.1. Human vs murine PCR primer mix details.

Primer pair (and product size)	Forward and reverse primer sequences (5' to 3')	Concentration (µM)	Volume for Primer Mix (µl)
TP53 human 1 (100bp)	tcacatgagtgagagggtctg ggtgtggccaccatcttg	5	100
TP53 human 2 (230bp)	caggtcctacctgtcccatt gcccacctcttaccgatttc	2	100
TP53 mouse 1 (158bp)	ctctaggctggaggctgaaa taatggcagtggtggtgatg	1	100
TP53 mouse 2 (295bp)	gagaaccactgtcggaggag ttcaccccaaagtcacctct	1	100

2.1.5 TP53 molecular identification check next generation sequencing libraries

To ensure the identity of HGSOC PDX DNA samples is correct, an in-house Next Generation Sequencing (NGS)-based test that exploits the unique TP53 mutations of each of our PDX is used to confirm PDX identity of each sample when required (**Table 2.2**). Libraries are prepared using a nested PCR, that creates region-specific, ready-to-sequence amplicons for the Illumina platform.

Briefly, for the inner PCR reaction, 4µl of 10ng/µl DNA was added to 8µl HotStarTaq Master mix (Qiagen, Cat#203443), 2µl of 2µM primer mix, and 6µl of molecular grade H_2O. Reactions were incubated at 95°C for 15 minutes, followed by 15 cycles of 95°C for 30 seconds, 62°C for 40 seconds, 72°C for 40 seconds. Reactions were then incubated at 72°C for 10 minutes, and stored at 4°C.

Table 2.2. TP53 sample identity check primers.
Primer sequences obtained from the TP53 IARC website (Bouaoun et al., 2016).

Primers from IARC Website	Primer Sequences (lower case) with Nextera Adapters	Inner Product Size (bp)
TP53 Exon 2-3 Forward	TCGTCGGCAGCGTCAGATGTGTATAAGAGACAGtctcatgctggatccccact	362
TP53 Exon 2-3 Reverse	GTCTCGTGGGCTCGGAGATGTGTATAAGAGACAGagtcagaggaccaggtcctc	
TP53 Exon 4 Forward	TCGTCGGCAGCGTCAGATGTGTATAAGAGACAGtgaggacctggtcctctgac	413
TP53 Exon 4 Reverse	GTCTCGTGGGCTCGGAGATGTGTATAAGAGACAGagaggaatcccaaagttcca	
TP53 Exon 5-6 Forward	TCGTCGGCAGCGTCAGATGTGTATAAGAGACAGtgttcacttgtgccctgact	467
TP53 Exon 5-6 Reverse	GTCTCGTGGGCTCGGAGATGTGTATAAGAGACAGttaacccctcctcccagaga	
TP53 Exon7 Forward	TCGTCGGCAGCGTCAGATGTGTATAAGAGACAGcttgccacaggtctccccaa	237
TP53 Exon 7 Reverse	GTCTCGTGGGCTCGGAGATGTGTATAAGAGACAGaggggtcagaggcaagcaga	
TP53 Exon 8-9 Forward	TCGTCGGCAGCGTCAGATGTGTATAAGAGACAGttgggagtagatggagcct	445
TP53 Exon 8-9 Reverse	GTCTCGTGGGCTCGGAGATGTGTATAAGAGACAGagtgttagactggaaacttt	
TP53 Exon 10 Forward	TCGTCGGCAGCGTCAGATGTGTATAAGAGACAGcaattgtaacttgaaccatc	260
TP53 Exon 10 Reverse	GTCTCGTGGGCTCGGAGATGTGTATAAGAGACAGggatgagaatggaatcctat	
TP53 Exon 11 Forward	TCGTCGGCAGCGTCAGATGTGTATAAGAGACAGagaccctctcactcatgtga	245
TP53 Exon 11 Reverse	GTCTCGTGGGCTCGGAGATGTGTATAAGAGACAGtgacgcacacctattgcaag	

In the outer PCR, unique combinations of Nextera XT Index Kit v2 set B or set C (Illumina, Cat# FC-131-2002 or FC-131-2003) primers were added to enable Illumina NGS and sample multiplexing. Briefly, 2µl of inner PCR product was added to 8µl HotStarTaq Master mix, 1µl of each Nextera XT Index Kit v2 set B primers (2 per sample; Illumina), and 8µl of molecular grade H_2O. These reactions were then incubated at 98°C for 30 seconds, followed by 20 cycles of 98°C for 10 seconds, 63°C for 15 seconds, 72°C for 30 seconds. Reactions were then incubated at 72°C for 10 minutes, and stored at 4°C.

2.1.6 Mutation reversion analysis using amplicon sequencing

A nested PCR was used to generate amplicon NGS libraries for mutations reversion screening. Briefly, 2µl of 5ng/µl DNA was added to 4µl of Phusion 5x HF buffer (Thermo Fisher Scientific), 4µl of 2.5mM deoxynucleotide (dNTP) mix (Genesearch), 2µl of 2µM primer pool (table), and 0.2µl Phusion Hot Start Flex DNA Polymerase (Thermo Fisher Scientific). This inner PCR was incubated at 98°C for 30 seconds, followed by 15 cycles of 98°C for 10 seconds, primer-specific Ta°C (see **Table 2.3**) for 15 seconds, 72°C for 30 seconds. Reactions were then incubated at 72°C for 10 minutes, and stored at 4°C. Then 2µl of inner PCR product was added to 8µl HotStarTaq Master mix (Qiagen), 1µl of each Nextera XT Index Kit v2 set B or set C barcoding primer (Illumina, Cat# FC-131-2002 or FC-131-2003), and 8µl of molecular grade H_2O. These reactions were then incubated at 98°C for 30 seconds, followed by 20 cycles of

98°C for 10 seconds, 63°C for 15 seconds, 72°C for 30 seconds. Reactions were then incubated at 72°C for 10 minutes, and stored at 4°C.

Table 2.3. Primers for amplicon-based NGS reversion mutation screening.
**All PDX models screened, except for one cell line – COV362. Product size excludes Illumina adaptors and barcodes, but includes targeted primers.*

PDX	Primary Mutation	Primers	Primer sequence	Product size (bp)	Annealing Temperature (Ta) C°
23133	*BRCA1*: c.181T>G	*BRCA1* forward primer **(illumina adaptors bold)**	**TCGTCGGCAGCGTCAGATGTGTATAAGAG ACAG**TGATGAATGGTTTTATAGGAACG	286	58.5
		BRCA1 reverse primer **(illumina adaptors bold)**	**GTCTCGTGGGCTCGGAGATGTGTATAAGA GACAG**GGCTCTTAAGGGCAGTTGTG		
134206	*BRCA1*:c.3817C>T	*BRCA1* forward primer **(illumina adaptors bold)**	**TCGTCGGCAGCGTCAGATGTGTATAAGAG ACAG**TGCACTGTGAAGAAAACAAGC	233	58
		BRCA1 reverse primer **(illumina adaptors bold)**	**GTCTCGTGGGCTCGGAGATGTGTATAAGA GACAG**ACCGTTGCTACCGAGTGTCT		
134141B	*BRCA1*:c.5346G>A	*BRCA1* forward primer **(illumina adaptors bold)**	**TCGTCGGCAGCGTCAGATGTGTATAAGAG ACAG**CTGACAGGGCACCCAATACT	229	58
		BRCA1 reverse primer **(illumina adaptors bold)**	**GTCTCGTGGGCTCGGAGATGTGTATAAGA GACAG**GGTAGAGGGCCTGGGTTAAG		
34931	*BRCA2*:c.1313dupA	*BRCA2* forward primer **(illumina adaptors bold)**	**TCGTCGGCAGCGTCAGATGTGTATAAGAG ACAG**GTCTTTGGCCTGTGAATGGT	255	58
		BRCA2 reverse primer **(illumina adaptors bold)**	**GTCTCGTGGGCTCGGAGATGTGTATAAGA GACAG**GGCTAGAAATACGTGGCAAA		
COV362*	*BRCA1*:c.4095+1G>T	*BRCA1* forward primer **(illumina adaptors bold)**	**TCGTCGGCAGCGTCAGATGTGTATAAGAG ACAG**GTGCTCCCCAAAAGCATAAA	193	58
		BRCA1 reverse primer **(illumina adaptors bold)**	**GTCTCGTGGGCTCGGAGATGTGTATAAGA GACAG**GTCTGAAAGCCAGGGAGTTG		

2.1.7 Mutation reversion analysis using amplicon Long Range PCR-based sequencing

Long-Range PCR (LR-PCR) was used to cover target regions in PDX 134019, 134019B and 134148. Briefly, 2µl of 50ng/µl DNA was added to 11.25µl of molecular-grade H_2O, 2.5µl of 25mM $Mg2^+$, 2.5µl of 2.5µM Primer mix (**Table 2.4**), 2.5µl 10x LA buffer, and 0.25µl TaKaRa LA Taq polymerase (Takara Bio Inc). Reactions were incubated at 94°C for 1 minute, followed by 30 cycles of 94°C for 15 seconds, primer-specific Ta°C (**Table 2.4**) for 30 seconds, 68°C for 15 seconds. Reactions were then incubated at 72°C for 10 minutes, and stored at 4°C. LR-PCR products were then processed using the Nextera XT DNA Library Preparation Kit (Illumina, cat # FC-131-1002) according to according to the manufacturer's protocol.

Table 2.4. Region-specific primers for LR-PCR-based NGS reversion mutation screening.
Product size excludes Illumina adaptors and barcodes, but includes targeted primers.

PDX	Primary Mutation	Primers	Primer sequence	Product size (bp)	Annealing Temperature (Ta) C°
134019/ 134019B	*BRCA2*: c.2323delT (p.775fs*8)	*BRCA2* forward primer	CCAATATCCCCCAGTGAATG	13,737	62.8
		BRCA2 reverse primer	ACTTAGGGGCAAAAGGCACT		
134148	*BLM*: c.2206_2212TATCTGA>TTAGATTC (p.Y736fs*5)	*BLM* forward primer	TGCCCTAATTCTTGCCTTTG	4979	63.6
		BLM reverse primer	CTGCCATCGGGTTACAACTT		

2.1.8 Targeted sequencing of DCLRE1C CRISPR mutation

To confirm the presence of the *DCLRE1C* (Artemis) mutation introduced using targeted CRISPR in (AlHilli et al., 2016) to create the PEO1A2 cell line, targeted amplicon NGS was performed.

For the inner PCR reaction, 5µl of 4ng/µl DNA was added to 2µl 10x PCR buffer (Qiagen, Cat# 203203), 8µl of 2µM primer mix (**Table 2.5**), 0.4µl of 10µM dNTP mix, 4.5µl of molecular grade H_2O and 0.1µl HotStarTaq DNA Polymerase (Qiagen, Cat# 203203). Reactions were incubated at 95°C for 15 minutes, followed by 17 cycles of 95°C for 30 seconds, 57.5°C for 40 seconds, 72°C for 40 seconds. Reactions then incubated at 72°C for 10 minutes, and stored at 4°C.

In the outer PCR, unique combinations of Nextera XT Index Kit v2 set B or set C primers (Illumina, Cat# FC-131-2002 or FC-131-2003) were added to enable Illumina NGS and sample multiplexing. Briefly, 2µl of inner PCR product was added to 2µl 10x PCR buffer (Qiagen, Cat# 203203), 1.4µl of 10µM dNTP mix, 12.5µl of molecular grade H_2O and 0.1µl HotStarTaq DNA Polymerase (Qiagen, Cat# 203203) and 1µl of each Nextera XT barcoding primer (Illumina, Cat# FC-131-2002 or FC-131-2003). These reactions were then incubated at 95°C for 15 minutes, followed by 20 cycles of 95°C for 30 seconds, 63°C for 40 seconds, 72°C for 40 seconds. Reactions then incubated at 72°C for 10 minutes, and stored at 4°C.

Table 2.5. Primers for amplicon-based DCLRE1C mutation screening.

Product size excludes Illumina adaptors and barcodes, includes targeted primers.

Cell line	Primers	Primer sequence	Product size (bp)	Annealing Temperature (Ta) C°
PEO1 A2	*DCLRE1C* forward primer **(illumina adaptors bold)**	**TCGTCGGCAGCGTCAGATGTGTATAAGAG ACAG**CCTTTGAGAGGCTGAAGAGC	267	57.5
	DCLRE1C reverse primer **(illumina adaptors bold)**	**GTCTCGTGGGCTCGGAGATGTGTATAAGA GACAG**AGTTCTTTCGAGGGGCAGAT		

2.1.9 Methylation-specific High Resolution Melt

Methylation-specific High Resolution Melt (MS-HRM) was performed by collaborators at the Olivia Newton John Cancer Centre (ONJCC, Melbourne). Up to 1µg of PDX or cell line DNA was sent to the A. Dobrovic group at the ONJCC, where MS-HRM was carried out as previously described (Snell et al., 2008) using primers targeting genomic region hg38 chr17:58,692,488-58,692,629 (the *RAD51C* promoter).

2.1.10 RAD51C bisulfite amplicon sequencing

The primers used in *RAD51C*-targeted MS-HRM (described in section 2.1.9) were modified (**Table 2.6**) in order to create an Illumina NGS-based test that would allow interrogation of individual CpG sites and amplicons (alleles) within *RAD51C*-methylated PDX samples. Bisulfite-converted DNA (bisDNA) samples were the left-over material from the MS-HRM experiments conducted by the A. Dobrovic group at the ONJCC. The bisDNA was not quantitated prior to PCR, but was instead quantitated and normalized prior to NGS.

Table 2.6. Primers for targeted bisulfite sequencing of the RAD51C promoter.

Product size excludes Illumina adaptors and barcodes, includes targeted primers.

Primers	Primer sequence	Product size (bp)	Annealing Temperature (Ta) C°
bisRAD51C forward primer **(illumina adaptors bold)**	**TCGTCGGCAGCGTCAGATGTGTATAAGAGACA G**GAAAATTTAtAAGAtTGCGtAAAGtTGtAAGG	142	60
bisRAD51C reverse primer **(illumina adaptors bold)**	**GTCTCGTGGGCTCGGAGATGTGTATAAGAGAC AG**CTAACCCCGaAaCAaCCAAACTCC		

For the inner PCR reaction, 4µl of bisDNA was added to 2µl 10x PCR buffer (Qiagen, Cat# 203203), 2µl of 10µM primer mix (**Table 2.6**), 0.4µl of 10µM dNTP mix, 11.5µl of molecular grade H_2O and 0.1µl HotStarTaq DNA Polymerase (Qiagen, Cat# 203203). Reactions were incubated at 95°C for 15 minutes, followed by 15 cycles of 95°C for 30 seconds, 60°C for 40 seconds, 72°C for 40 seconds. Reactions then incubated at 72°C for 10 minutes, and stored at 4°C.

In the outer PCR, unique combinations of Nextera XT Index Kit v2 set B or set C primers (Illumina, Cat# FC-131-2002 or FC-131-2003) were added to enable Illumina NGS and sample multiplexing. Briefly, 2µl of inner PCR product was added to 2µl 10x PCR buffer (Qiagen, Cat# 203203), 0.4µl of 10µM dNTP mix, 13.5µl of molecular grade H_2O, 0.1µl HotStarTaq DNA Polymerase (Qiagen, Cat# 203203) and 1µl of each Nextera XT Index Kit v2 set B or set C barcoding primer (Illumina, Cat# FC-131-2002 or FC-131-2003). These reactions were then incubated at 95°C for 15 minutes, followed by 20 cycles of 94°C for 30 seconds, 60°C for 40 seconds, 72°C for 40 seconds. Reactions were then incubated at 72°C for 10 minutes, and stored at 4°C.

2.1.11 Agarose gel electrophoresis

Amplicon PCR products were visualized on a 2% agarose gel using SYBR safe DNA gel stain (Thermo Fisher Scientific, Cat# S33102). Electrophoresis is run at 100V for 30-40 minutes and gels are imaged (1.5 second exposure) using the ChemiDoc XRS system (BioRad). LR-PCR products were visualized on a 0.5% agarose gel using SYBR safe DNA gel stain (Thermo Fisher Scientific, Cat# S33102). Electrophoresis is run at 100V for 70 minutes and gels are imaged (1.5 second exposure) using the ChemiDoc XRS system (BioRad).

2.1.12 AmpureXP library clean-up

Agencourt AMPure XP (Beckman Coulter, Cat#10136224) beads were used to remove PCR contaminants and size-select for target amplicons (based on AMPure XP: PCR product ratio) according to manufacturer's protocol. A ratio of 0.9:1 was used for amplicon libraries (18µl AmpureXP beads added to 20µl PCR product), and a 0.4:1 ampureXP ratio was used for LR-PCR libs (10µl AmpureXP beads added to 25µl LR-PCR product). Libraries were eluted in 20µl of 1x TE buffer (Sigma-Aldrich, Cat#93283).

2.1.13 NexteraXT and amplicon library pooling and sequencing

The D1000 ScreenTape System (Agilent, Cat#5067- 5582 and 5067- 5583) was used to assess the size profile of NexteraXT libraries according to manufacturer's protocol. NGS libraries were quantitated using the Qubit dsDNA high sensitivity (HS) assay, normalized to 2nM and pooled. These pools were then sequenced in the WEHI genomics core laboratory on the Illumina MiSeq using a MiSeq Nano Reagent Kit v2 (300 cycle; Illumina; Cat# MS-102-2002) according to manufacturer's protocol.

2.1.14 Brunello CRISPR library pooling and sequencing

DNA extractions of cells collected during CRISPR screens were performed using the Quick-DNA Midiprep plus kit (Zymo Research Cat# D4075) according to manufacturer's instructions. Briefly, frozen pellets of ~20 million cells each were resuspended in 3ml of DPBS in 50ml falcon tube. Then 3ml BioFluid & Cell Buffer (Red) and 100µl of Protinase K were added to the solution. Samples were then pulse vortexed for 15 seconds to mix solution, and then incubated at 55°C in a water bath overnight.

The following day, 6ml of Genomic Lysis Buffer was added to each sample, and they were pulse vortexed for 15 seconds to mix solution. Resulting lysates were then transferred to a Zymo-Spin V-E Column placed within a 50ml tube (ensuring the column was screwed in securely so it does not detach during spins). Tubes were capped and then centrifuged for 5 minutes at 1000g (or 2000g if lysates not passing through column), and flow-through discarded. 9ml of DNA Pre-Wash Buffer was then added to each column, samples were centrifuged for 5 minutes at 1000-2000g, and resulting flow-through discarded. 7ml gDNA Wash Buffer was then added to each column, samples were centrifuged for 5 minutes at 1000-2000g, and resulting flow-through discarded. Reservoirs were the removed and discarded, and columns placed onto a collection tube. Tubes were then centrifuged for 1 minute at 12,000g in micro-centrifuge to remove any residual buffer.

Columns were then transferred to new collection tubes and 200µl gDNA Wash Buffer added to them. Tubes were then centrifuged at 12000g for 1 minute in a micro-centrifuge, and flow-through discarded. Columns were then transferred to clean 1.5ml tubes for DNA elution. 150µl

of DNA elution buffer was added to each column and incubates 5 minutes at room temperature. Samples were then centrifuged at 12000g for 1 minute to elute DNA. These two steps were repeated to produce 300µl of eluted DNA. Resulting DNA was quantitated using the Qubit dsDNA high sensitivity (HS) assay (Invitrogen, Cat#Q32854).

A single-step PCR was used to create Brunello NGS libraries using primers outlined in ***Table 2.7***. DNA was diluted to 100ng/µl and 15µl was added to 50µl of Taq 2X Master Mix (NEB; cat# M0270L), 5µl of each 10µM primer dilution (**Table 2.7**) and 25µl of molecular grade H_2O. Reactions were incubated at 95°C for 1 minute, followed by 25 cycles of 95°C for 30 seconds, 53°C for 30 seconds, 72°C for 30 seconds. Reactions then incubated at 72°C for 10 minutes, and stored at 4°C.

Resulting libraries were cleaned up using a 0.9:1 Ampure XP beads to PCR product ratio (45µl beads into 50µl PCR product). Libraries were then quantitated using the Qubit dsDNA HS assay (Invitrogen, Cat#Q32854), and the size of each library was assessed using the Agilent D1000 ScreenTape System according to manufacturer's instructions (ScreenTape: Cat# 5067-5582, D1000 Reagents: Cat# 5067- 5583). Libraries were pooled equally based on molarity (calculated using DNA concentrations and average library size). Pooled libraries were sequenced on the Illumina Nextseq500 platform by the WEHI genomics hub using a TG NextSeq® 500/550 v2 High Output Kit (75 cycles; Cat# TG-160-2005).

Resulting FASTQ files were run through a custom in-house pipeline to report all detected unique Brunello guide sequences, their corresponding genes and read counts. This resulted in a single Excel (Microsoft) file per sample.

Table 2.7. Brunello NGS library preparation primers.

Unique forward and reverse primer combinations were used create uniquely barcoded Illumina NGS libraries for multiplexed sequencing in a single step. Bp= base-pairs.

Forward primers	5' to 3' sequence	length (bp)
AR069-Fwd_37_Brie-P5	AATGATACGGCGACCACCGAGATCTACACTCTTTCCCTACACGACGCTCTTCCGATCTaAACTCACCTTGTGGAAAGGACGAAACACCG	89
AR070-Fwd_38_Brie-P5	AATGATACGGCGACCACCGAGATCTACACTCTTTCCCTACACGACGCTCTTCCGATCTcgtAAGAGATCTTGTGGAAAGGACGAAACACCG	91
AR071-Fwd_39_Brie-P5	AATGATACGGCGACCACCGAGATCTACACTCTTTCCCTACACGACGCTCTTCCGATCTtcAAGGACACTTGTGGAAAGGACGAAACACCG	90
AR072-Fwd_40_Brie-P5	AATGATACGGCGACCACCGAGATCTACACTCTTTCCCTACACGACGCTCTTCCGATCTcAATCCGTCTTGTGGAAAGGACGAAACACCG	89
AR073-Fwd_41_Brie-P5	AATGATACGGCGACCACCGAGATCTACACTCTTTCCCTACACGACGCTCTTCCGATCTacgAATGTTGCTTGTGGAAAGGACGAAACACCG	91
AR074-Fwd_42_Brie-P5	AATGATACGGCGACCACCGAGATCTACACTCTTTCCCTACACGACGCTCTTCCGATCTgaACACGACCTTGTGGAAAGGACGAAACACCG	90
AR075-Fwd_43_Brie-P5	AATGATACGGCGACCACCGAGATCTACACTCTTTCCCTACACGACGCTCTTCCGATCTtACAGATTCTTGTGGAAAGGACGAAACACCG	89
AR076-Fwd_44_Brie-P5	AATGATACGGCGACCACCGAGATCTACACTCTTTCCCTACACGACGCTCTTCCGATCTgtaAGATGTACTTGTGGAAAGGACGAAACACCG	91
AR078-Fwd_45_Brie-P5	AATGATACGGCGACCACCGAGATCTACACTCTTTCCCTACACGACGCTCTTCCGATCTtcAGCCATGCTTGTGGAAAGGACGAAACACCG	90
AR079-Fwd_46_Brie-P5	AATGATACGGCGACCACCGAGATCTACACTCTTTCCCTACACGACGCTCTTCCGATCTgAGGCTAACTTGTGGAAAGGACGAAACACCG	89
AR080-Fwd_47_Brie-P5	AATGATACGGCGACCACCGAGATCTACACTCTTTCCCTACACGACGCTCTTCCGATCTtacATAGCGACTTGTGGAAAGGACGAAACACCG	91
AR081-Fwd_48_Brie-P5	AATGATACGGCGACCACCGAGATCTACACTCTTTCCCTACACGACGCTCTTCCGATCTagATCATTCCTTGTGGAAAGGACGAAACACCG	90
Reverse primers	**5' to 3' sequence**	**length (bp)**
AR029-Rev_65_Brie-P7	CAAGCAGAAGACGGCATACGAGATCGGTCTCGGCATTCCTGCTGAACCGCTCTTCCGATCTaATTGAGGATCTACTATTCTTTCCCCTGCACTGT	95
AR030-Rev_66_Brie-P7	CAAGCAGAAGACGGCATACGAGATCGGTCTCGGCATTCCTGCTGAACCGCTCTTCCGATCTcgtCAACCACATCTACTATTCTTTCCCCTGCACTGT	97
AR031-Rev_67_Brie-P7	CAAGCAGAAGACGGCATACGAGATCGGTCTCGGCATTCCTGCTGAACCGCTCTTCCGATCTtcCAAGACTATCTACTATTCTTTCCCCTGCACTGT	96
AR032-Rev_68_Brie-P7	CAAGCAGAAGACGGCATACGAGATCGGTCTCGGCATTCCTGCTGAACCGCTCTTCCGATCTcCAATGGAATCTACTATTCTTTCCCCTGCACTGT	95
AR033-Rev_69_Brie-P7	CAAGCAGAAGACGGCATACGAGATCGGTCTCGGCATTCCTGCTGAACCGCTCTTCCGATCTacgCACTTCGATCTACTATTCTTTCCCCTGCACTGT	97
AR034-Rev_70_Brie-P7	CAAGCAGAAGACGGCATACGAGATCGGTCTCGGCATTCCTGCTGAACCGCTCTTCCGATCTgaCAGCGTTATCTACTATTCTTTCCCCTGCACTGT	96
AR035-Rev_71_Brie-P7	CAAGCAGAAGACGGCATACGAGATCGGTCTCGGCATTCCTGCTGAACCGCTCTTCCGATCTtCATACCAATCTACTATTCTTTCCCCTGCACTGT	95
AR036-Rev_72_Brie-P7	CAAGCAGAAGACGGCATACGAGATCGGTCTCGGCATTCCTGCTGAACCGCTCTTCCGATCTgtaCCAGTTCATCTACTATTCTTTCCCCTGCACTGT	97

2.1.15 Zymo RNA extraction

Less than 25mg of snap frozen tissue was homogenized in 600µl TRI reagent (Zymo Research, Cat# R2050-1-50) using a stainless steel grinding ball and the TissueLyser II (QIAGEN, Cat# 85300) set at 20ghrz for 4 minutes. High quality RNA was then extracted from tissue lysates using the Direct-zol RNA MiniPrep (Zymo Research, Cat# R2050) according to the manufacturer's protocol. Resulting RNA was quantitated using the NanoDrop 2000 UV-Vis Spectrophotometer (Thermo Fisher Scientific, Cat# ND-2000), and quality checked using the RNA ScreenTape System (Agilent, Cat# 5067-5576, 5067-5577 and 5067-5578) according to manufacturer's protocol.

2.1.16 BRCA1 exon skipping quantitative PCR protocol

SuperScript III Reverse Transcriptase (Invitrogen, Cat# 18080085) was used to convert RNA to cDNA according to the manufacturer's protocol. A volume of 2µl cDNA diluted to 5ng/µl was added to 5µl SYBR Green PCR Master Mix (Thermo Fisher Scientific), 2.5ul molecular-grade H_2O and 0.5µl of the relevant 2µM primer mix (**Table 2.8**).

Table 2.8. Control and BRCA1 region qPCR primers.

HPRT, B-ACTIN, SDHA and GAPDH were used as housekeeper control primers. BRCA1 All primer set amplifies most common isoforms of BRCA1 (including those with and without exon 11). BRCA1 +exon 11 primer set specifically amplify BRCA1 transcripts containing all of exon 11. The BRCA1 Δ11θ primer set specifically amplifies BRCA1 transcripts without the 11q region.

Target transcript	Forward primer 5' to 3'	Reverse primer 5' to 3'	Product size (bp)
HPRT1	GTTATGGCGACCCGCAG	ACCCTTTCCAAATCCTCAGC	107
ACTB	GCACAGAGCCTCGCCTT	GTTGTCGACGACGAGCG	93
SDHA	GGACCTGGTTGTCTTTGGTC	CCAGCGTTTGGTTTAATTGG	93
GAPDH	GGTGTGAACCATGAGAAG	CCACAGTTTCCCGGAG	189
BRCA1 All	GCAGAGGTTGAAGATGGTATGTT	CCAAGGCAAGATCTAGAGGGA	137
BRCA1 +exon 11	TAAGCCAGGCTGTTTGCTTT	GAAATCAGTTTGGATTCTGCAA	297
BRCA1 D11q	TGCTGCTTCACCCTGATACT	TGCAGTGTGGGAGATCAAGA	210

Plates were incubated on the ABI 7900 (Applied Biosystems) or the ViiA 7 Real-Time PCR System (Thermo Fisher Scientific) at 95°C for 10 minutes, 40 cycles of 95°C for 15 seconds and 60°C for 1 minute, followed by 95°C for 15 seconds, 60°C for 15 seconds and 95°C for 15

seconds. Resulting Ct values were normalized to the averaged value housekeeper control primers in Excel (Microsoft). Fold change values were calculated for each sample. These values were then graphed in PRISM7 (GraphPad), and the standard deviation calculated. P-values were generated using an unpaired t test with Welch's correction in the PRISM7 (GraphPad) software.

2.1.17 RAD51C quantitative real-time PCR

The TaqMan™ RNA-to-CT™ 1-Step Kit (Cat# 4392653) was used to quantify *RAD51C* and *GAPDH* RNA levels in samples. Briefly, RNA samples were diluted to 10ng/µl in molecular-grade H_2O, and 5µl of this dilution was added per well of a MicroAmp™ Optical 384-Well Reaction Plate with Barcode (Thermo Fisher Scientific, Cat# 4343814). Three wells were prepared per sample per probe (6 in total per sample). Then 5µl of the following master-mix was prepare for each probe/sample, and was added to the corresponding sample wells: 5µl of TaqMan kit master mix, 1µl of molecular-grade H_2O, 0.5µl of *RAD51C* probe Hs00427442_m1 (Life Technologies, Cat# 4331182) or *GAPDH* (Life Technologies, Cat# 4333764F) probe and 0.25µl of TaqMan kit enzyme.

Plates were centrifuged for 1 minute at 300g, and were then incubated on the ABI 7900 (Applied Biosystems) or the ViiA 7 Real-Time PCR System (Thermo Fisher Scientific) and run on a standard TaqMan RNA protocol:

Stage 1:
    48°C for 15 minutes
    95°C for 10 minutes
Stage 2 (repeated 40x):
    95°C for 15 seconds
    60°C for 1 minute *hold
Stage 3:
    95°C for 15 seconds
    60°C for 15 seconds
    95°C for 20 seconds *ramp *hold
*data collection points

Ct values were then exported for analysis in an Excel file (Microsoft). Here, the ΔCt values were calculated: Ct(*RAD51C*) - Ct(*GAPDH*); and fold change: $2^{-\Delta Ct}$. Graphs were then plotted in PRISM 8 (GraphPad).

2.1.18 RAD51C immunoblotting

PDX #183 tumours protein lysates were prepared using 2D lysis buffer containing protease inhibitor PMSF (7M urea, 2M Thiourea, 4% CHAPS in 0.1M Tris buffer with 4.6% 100mM PMSF). Tumour tissue samples were either homogenized manually using a mortar and pestle and then resuspended in 300µl of 2D lysis buffer, or were homogenized in 300µl of 2D lysis buffer using the TissueLyser II (Qiagen, Cat# 85300) set at 20ghrz for 4 minutes. Samples were then sonicated in buffer at a 15% amplitude for 10 seconds. Samples were then centrifuged at ≥8000g at 4°C for 20 minutes. Supernatant containing protein was then transferred to two fresh 1.5ml Eppendorf tubes (~150µl each). Samples were then stored in the -80°C freezer until ready to quantitate.

Protein in each sample was quantified using the Pierce™ BCA Protein Assay Kit according to manufacturer's instructions (Thermo Fisher Scientific, #23225). Equal protein loads of 8µg were resolved on 8–16% Criterion™ TGX Stain-Free™ Protein Gel (Bio-rad) under reducing conditions. Protein was transferred to PVDF membranes using Bio-rad criterion wet transfer method (Bio-rad), then probed with primary antibody anti-RAD51C (Santa Cruz, sc-56214; 1/200 in 5% BSA), followed by peroxidase-labelled secondary antibody (SouthernBiotech, 1010-05; 1/5000 in 5% BSA). Membranes were then stripped and probed with anti-beta actin (Abcam, ab8229; 1/2000 in 5% BSA), followed by peroxidase-labelled secondary antibody (Santa Cruz, sc-2020; 1/5000 anti- goat in 5% BSA) for loading control. Blots were visualized on the ChemiDoc Imaging System (biorad) using enhanced chemi-luminescence (Amersham ECL Prime, GE Healthcare Life Sciences) according to manufacturer's instructions.

2.1.19 RNA sequencing of PDX

RNA sequencing library preparation and data analysis were performed as previously described (Kondrashova et al., 2018).

2.1.20 RAD51C copy number assessment by MLPA-seq

MLPA-seq was performed as previously described (Kondrashova et al., 2015b), using *RAD51C* probes outlined in **Table 2.9** (MRC Holland, Cat# P260-025R) and control probes outlined in **Table 2.10** (Kondrashova et al., 2015b).

Table 2.9. MLPA-seq RAD51C gene probes

Probe name	Probe & Adapter Anchor		Chromosomal position
RAD51C_ex2_Nilmn	Left	TCGTCGGCAGCGTCAGATGTGTATAAGAGACAGTCTGGAACTTCTTGAGCAGGAGCATACCCAGGGCTTCA	chr17:54127407-54127484
	Right	/5Phos/TAATCACCTTCTGTTCAGCACTAGATGATATTCTTGGGGGTCTGTCTCTTATACACATCTCCGAGCCCACGAGAC	
RAD51C_ex6_Nilmn	Left	TCGTCGGCAGCGTCAGATGTGTATAAGAGACAGCTGACTGTATTTGTCTTGTTCACTGGTTAATCTTAGCACTA	chr17:54153266-54153352
	Right	/5Phos/AGCACAGTACCGTTAGATACTGATTGTTCCTTTTAGTTATTTAACACTGTCTCTTATACACATCTCCGAGCCCACGAGAC	
RAD51C_ex9_Nilmn	Left	TCGTCGGCAGCGTCAGATGTGTATAAGAGACAGCGTTGTTACTTCTGCATGTTCATTGCAAACAGAA	chr17:54166499-54166566
	Right	/5Phos/GGTTCCTTGAGCACCCGGAAACGGTCACGAGACCCCTGTCTCTTATACACATCTCCGAGCCCACGAGAC	

Table 2.10. MLPA-seq control gene probes

Control probe name	Probe & Adapter Anchor		Chromosomal position
CFTR_a_Nilmn	Left	TCGTCGGCAGCGTCAGATGTGTATAAGAGACAGCTCTTGCACCTCTTCTTCTGTCTCCTCTT	chr7:117307078-117307150
	Right	/5Phos/TCAGAGCAGCAATCTGGGGCTTAGACTTGCACTTGCTTGAGTTCCTGTCTCTTATACACATCTCCGAGCCCACGAGAC	
GCH1_a_Nilmn	Left	TCGTCGGCAGCGTCAGATGTGTATAAGAGACAGGATGAGATGGTGATTGTGAAGGACATAGAC	chr14:55332047-55332119
	Right	/5Phos/ATGTTTTCCATGTGTGAGCATCACTTGGTTCCATTTGTTGGAACTGTCTCTTATACACATCTCCGAGCCCACGAGAC	
JAG1_a_Nilmn	Left	TCGTCGGCAGCGTCAGATGTGTATAAGAGACAGGGATCGCCTGCTCAAAGGTAGGACAT	chr20:10622384-10622447
	Right	/5Phos/GATGGCTGCCGCAGTTCACCTGTGTTCTGGAATCAGGGCTGTCTCTTATACACATCTCCGAGCCCACGAGAC	
OPTN_a_Nilmn	Left	TCGTCGGCAGCGTCAGATGTGTATAAGAGACAGGTTCCTCGCCATAAGGAGGTGGT	chr10:13142648-13142708
	Right	/5Phos/TACAGACACGCCTGTGGGAGACATGGGACCACTACCCGCTGTCTCTTATACACATCTCCGAGCCCACGAGAC	
GPC3_1_Nilmn	Left	TCGTCGGCAGCGTCAGATGTGTATAAGAGACAGGACAGAACTGGCCTATGATCTGGATGT	chrX:132670260-132670326
	Right	/5Phos/GGATGATGCGCCTGGAAACAGTCAGCAGGCAACTCCGAAGCTGTCTCTTATACACATCTCCGAGCCCACGAGAC	
IL1B_1_Nilmn	Left	TCGTCGGCAGCGTCAGATGTGTATAAGAGACAGGCTGGTTCCCTGCCCACAGACCT	chr2:113590971-113591021
	Right	/5Phos/TCCAGGAGAATGACCTGAGCACCTTCTTCCTGTCTCTTATACACATCTCCGAGCCCACGAGAC	
PANK2_1_Nilmn	Left	TCGTCGGCAGCGTCAGATGTGTATAAGAGACAGTATGGAGGGGACTATGAGAGGTTTGGA	chr20:3893229-3893286
	Right	/5Phos/CTGCCAGGCTGGGCTGTGGCTTCAAGGTAAGCTGTCTCTTATACACATCTCCGAGCCCACGAGAC	
FLCN_1_Nilmn	Left	TCGTCGGCAGCGTCAGATGTGTATAAGAGACAGGCGGAAGAAGAGGAAGGTGGCATTCAGAT	chr17:17131259-17131319
	Right	/5Phos/GAACAGTCGGATGCGTGCGCACAGCCCCGCAGCTGTCTCTTATACACATCTCCGAGCCCACGAGAC	

2.2 *In vitro* and cell culture protocols

2.2.1 Cell line culture

All cell lines were routinely tested and shown to be negative for *Mycoplasma*. Cell lines were authenticated by STR profiling in April 2017 and November 2019.

Cell lines PEO1 and PEO4 were obtained from F. Couch (Mayo Clinic) in 2013, and the PEO1A2 cell line published in (AlHilli et al., 2016) was obtained from S. Kaufmann (Mayo Clinic) in 2017. Cell lines UWB1.289 and UWB1.289+BRCA1 were obtained from the D. Bowtell group (Peter MacCallum Cancer Centre) in 2018. The OVCAR8 cell line was obtained from the NCI, while the COV362 cell line was ordered from Cell Bank Australia in 2017 (cat# 07071910). The UWB1.289 and UWB1.289+BRCA1 cell lines were cultured in "MR" media: 50% RPMI-1640 (Corning) and 50% Complete Mammary Epithelial Growth Medium (Clonetics/ Lonza, CC-3150) supplemented with 3% Fetal Calf Serum (FCS; **Table 2.11**), though the UWB1.289+BRCA1 cells had 200µg/ml Geneticin/G418 (Thermo Fisher Scientific, Cat# 11811031) added to media to maintain selection of the *BRCA1*-transfected cells. Cells were grown in 5% CO_2 atmosphere at 37 °C.

Table 2.11. MR media composition.

Component	Stock Concentration	Catalog number	Supplier	Storage	Volumes combined
RPMI 1640 Medium, GlutaMAX™ supplement	1x	61870127	Gibco	4ºC	500ml
Complete Mammary Epithelial Growth Medium	1x	CC-3150	Clonetics/ Lonza	4ºC / -30ºC	500ml
Fetal Bovine Serum	100x	F9423	Sigma-Aldrich	-30ºC	30.9ml

All other cell lines were cultured in "FV" media: DMEM/F12, GlutaMAX (Gibco) with 5µg/ml insulin, 50ng/ml EGF, and 1µg/ml hydrocortisone, 1% penicillin and streptomycin and 5% FCS (**Table 2.12**) in a 5% CO_2 atmosphere at 37 °C.

Adherent cells were detached from culture flasks using Trypsin-EDTA Solution 1X (Sigma-Aldrich, Cat# 59430C-100ML).

Table 2.12. FV media composition.

Component	Stock Concentration	Catalog number	Supplier	Storage	Volumes combined
DMEM/F-12, GlutaMAX™ supplement	1x	10565018	Gibco	4ºC	500ml
Fetal Bovine Serum	100x	F9423	Sigma-Aldrich	-30ºC	50ml
Insulin	1g/ml	11 376 497 001	Sigma-Aldrich	-30ºC	2.5ml
EGF	0.5mg/ml	E9644	Sigma-Aldrich	-30ºC	50µl
Hydrocortisone	0.5mg/ml	H0396	Sigma-Aldrich	-30ºC	1ml
Penicillin and streptomycin	100x	15140-122	Gibco	-30ºC	5ml

2.2.2 Cell viability assays

Cells were plated in CELLSTAR® 96 well plates (Greiner, Cat# M1062), at densities related to their growth rates:

- 500 cells per well for PEO1, PEO1A2 and UWB1.289 +BRCA1
- 1000 cells for COV362 and UWB1.289
- 1500 cells per well for PEO4 and PEO4 RAD51C KO

Drugs were added the following day at the given concentrations (for a total volume of 150µl per well), and cells were incubated at 37°C in 5% CO_2 for 7 days. CellTiter-Glo® Luminescent (CTG) Cell Viability Assay (Promega, Cat# G7572) was then used to measure viability of cells. Cells were removed from the incubator and left to cool to room temperature for approximately 30 minutes. Then 50µl of CTG reagent (1 in 4 dilution) was added to each well, and plates were placed on an orbital shaker for 2 minutes to mix reagents. Plates were then incubated for 10 minutes at room temperature, before measuring luminescence on the Chameleon Microplate Reader (LabLogic systems).

2.2.3 Cell counting

Cells were counted using either a hemocytometer, or on the on the Moxi Z miniature automated cell counter (Dittami et al., 2012) using Moxi Z Cell Count Type M Cassettes (ORFLO, Cat# MXC001).

2.2.4 Genome-wide PARPi-resistance CRISPR screens

2.2.4.1 Preparing the Cas9/Brunello-packaged virus

HEK 293T cells were cultured in FV media (without penicillin streptomycin), before being trypsinized and plated 6 x 10^6 cells in 12ml per 10cm plate, making 2 plates. These cells were then incubated at 37°C in 5% CO2 overnight, allow cells to settle. The following day, 41µl of Lipofectamine 3000 Transfection Reagent (Thermo Fisher Scientific, Cat# L3000008) was added to 1.5ml of OptiMEM media (Gibco, Cat# 31985070) to create reaction "mix A". Then a separate reaction "mix B" was made by adding 35µl of p3000 (Thermo Fisher Scientific, Cat# L3000008) to 1.5ml of OptiMEM media (Gibco, Cat# 31985070) and reagents in **Table 2.13** for packaging FUCas9Cherry (Cas9 and mCherry) plasmid DNA and **Table 2.14** for packaging Brunello plasmid DNA.

FUCas9Cherry plasmid DNA (Addgene #70182), viral component plasmids pMDL (Addgene #12251), VSVg (Addgene #12259) and RSV-REV (Addgene #12253) were provided by the Herold Lab (WEHI). Human CRISPR Knockout Pooled Library Brunello plasmid DNA (Addgene Cat# 73178) was provided by E. Surgenor of the Huntington group (WEHI).

To create the plasmid DNA: lipid complex, 1.5ml of mix A was mixed with 1.5ml of mix B to create "mix C". This mixture was then incubated for 10-20 minutes at room temperature. HEK 293T cells were then transfected with the packaged lentivirus. After incubation, 6ml of FV media from each HEK 293T cell dish was removed and 3ml of mix C was added to each dish. Cells were then incubated for 6 hours at 37°C in 5% CO_2. The media-virus mixture was then removed and replaced with 12ml of regular FV media and cells incubated at 37°C in 5% CO_2 for 24 hours. Packaged lentivirus was harvested at 24 hours post-transfection. All viral supernatant (12ml) was removed and replaced with fresh FV media (12ml). The viral supernatant was centrifuged at 800g for 10 minutes at room temperature to remove cellular debris. The resulting clarified supernatant was then filtered through a 45µm pore to remove any remaining cellular debris. This material was stored at 4°C. At 52 hours post-transfection, this process was repeated, for a total of 24ml of packaged virus produced per dish of infected cells. The virus was dispensed as 5ml aliquots in 10ml tubes and stored in the -80 freezer until required for infections.

Table 2.13. Reagents used for lentiviral packaging of FUCas9Cherry plasmid DNA.

Reagent	Concentration (µg/µl)	µg required per mix B reaction	µl added per mix B reaction
pMDL	1.4	5	3.6
RSV-REV	0.85	2.5	2.9
VSVg	2.3	3	1.3
Plasmid DNA (Cas9)	1.7	5	2.9

Table 2.14. Reagents used for lentiviral packaging of Brunello plasmid DNA.

Reagent	Concentration (µg/µl)	µg required per mix B reaction	µl added per mix B reaction
pMDL	1.4	5	3.6
RSV-REV	0.85	2.5	2.9
VSVg	2.3	3	1.3
Plasmid DNA (Brunello)	2	5	2.5

2.2.4.2 Generation of Cas9 cell lines

Previously prepared Cas9-packaged virus was thawed. Then 200,000 cells were plated in each well of 24-well plate in 500µl (4 replicate wells). Then 8µg/mL polybrene was added to neat viral solution, and 1ml of this solution was added to each well with cells. An uninfected control plate was also prepared, where MR/FV media was added instead of virus. All plates were then centrifuged at 800g for 1 hour at 32°C to spin infect cells. Plates were then incubated overnight at 37°C in 5% CO_2. The following day, virus/media was removed and cells were washed twice in DPBS. Fresh MR/FV media was then added to each well and plates were incubated overnight at 37°C in 5% CO_2. Cells were then washed again in DPBS, detached using trypsin, washed again using DPBS, and sorted for mCherry fluorescence on the BD FACSAria™ III sorter at the WEHI Cytometry facility; uninfected/negative control cells (with and without DAPI stain), and infected mCherry positive cells collected in 1ml FCS. Resulting mCherry/Cas9 positive cells were then cultured for 6-7 days before repeating the Fluorescence Activated Cell Sorting (FACS) protocol (second sort to enrich further for Cas9-positive cells).

2.2.4.3 Puromycin selection toxicity assessment

In order to find the optimal concentration of puromycin to use in selection of PEO1 cas9 cells with guides in the Brunello CRISPR screen (i.e. a concentration that is not overly toxic and just enough to kill all uninfected cells to avoid creating bias in the screen), toxicity curves were generated for each cell line. Uninfected cas9 cell lines were plated onto two (duplicate) 12-well cell culture plates using their standard split-rate (adjusted for change in surface area) for a total volume of 2ml. Cells were then incubated at 37°C in 5% CO_2 overnight, allow cells to settle. The following day, puromycin (Invivogen, Cat# ant-pr-1), diluted to 100µg/ml in DPBS, was added to the 2ml of FV/MR media (depending on cell line used) per well to create final puromycin concentrations of 1, 0.9, 0.8, 0.7, 0.6, 0.5, 0.4, 0.3, 0.2, 0.1 and 0µg/ml. Note - the initial puromycin concentration range tested on the PEO1 cell line (0-5µg/ml) was too high, with the lowest concentration (0.5µg/ml) killing all cells. Wells were checked under 4x and 10x magnification after 3 days to assess cell death in each well. The lowest puromycin concentration causing complete cell death in the well was assess visually, and used as the selecting concentration in the Brunello CRISPR screen for each cell line.

2.2.4.4 Infection efficiency calculations

Infection efficiency represents the percentage of infected cells per reaction. To uncover the dilution of Brunello virus required for a 30-50% infection efficiency for the CRISPR PARPi resistance screen, 200,000 cells were plated in each well of a 24-well plate in a volume of <100µl. A lentiviral dilution series containing 8µg/mL polybrene was created: neat, 1:1, 1:2, 1:3, 1:4, 1:5, 1:10, 1:15, 1:20, 1:30, 1:40, no virus. 1.5 mL of each lentiviral dilution was added per well with cells. Cells were spin infected by centrifugation at 800g for 1 hour at 32°C. Plates were then incubated overnight at 37°C in 5% CO_2. The following day, the virus was removed and cells were washed twice with DPBS. Fresh FV media was added to the cells and plates were incubated overnight at 37°C in 5% CO_2. The following day, cells were washed with DPBS again, the trypsinized and counted. 2000 cells were seeded in 75µl per well on a CELLSTAR® 96 well plate (Greiner, Cat# M1062), with 4 wells seeded per lentiviral dilution/condition. Cells were left to settle at 37°C in 5% CO_2 for 1 hour before adding 75µl of puromycin in FV media (0.8µg/ml for PEO1 and UWB1.289 and 1.4µg/ml for WEHI-CS62) to 2 wells, and add 75µl of regular FV media to the other 2 wells (control). Plates were incubated at 37°C in 5% CO_2 for 3 days. CTG assay was then used to measure the viability of the cells, and MOI calculated

by dividing the infected cell viability by the control cell viability for each lentiviral dilution in Excel (Microsoft).

2.2.4.5 Brunello library CRISPR infections

Cas9-expressing versions of each cell line were expanded in Millicell HY 5-layer cell culture T-1000 flasks (MERCK, Cat# PFHYS1008) to produce enough cells for Brunello CRISPR guide library infections. Once expanded, 70-100 million cells (70 million WEHI-CS62 Cas9 cells, 100 million PEO1/UWB1.289 Cas9 cells) were dissociated using trypsin and resuspended in 96mL of FV media with 1:40 diluted Brunello virus containing 8µg/mL polybrene (2.4ml thawed virus, 76.8µl of 10mg/ml polybrene). These cells were plated across 16 x 6-well plates (2ml per well) per infection replicate/experiment. Also, 4.3 million infected/uninfected cells were plated in a T75 flask each as puromycin selection controls. All infection plates were then centrifuged at 800g for 1 hour at 32°C to spin infect cells (8 plates per spin, two spins required). Plates were then incubated overnight at 37°C in 5% CO_2.

The following day, virus/media was removed and cells were washed twice in DPBS before being dissociated and total cells transferred into multilayer flasks for cell culture. Puromycin selection was then performed (24 hours post infection) using 0.8µg/mL for PEO1 Cas9 and 1.4µg/mL for WEHI-CS62/UWB1.289 Cas9 cells. At least 30 million cells were maintained per passage for 7 days of puromycin selection/culture.

Total cells were then harvested and 2 cell pellets of 20 million cells each were snap frozen for DNA extraction and library diversity assessment. Remaining cells were used to make viable DMSO (10%) freezings of 25 million cells per vial, and these would be thawed for downstream CRISPR screen rucaparib treatment experiments.

2.2.4.6 Brunello library CRISPR drug treatments

25 million PEO1 Cas9 Brunello cells were thawed and 12.5 million cells were plated per treatment/control flask. Rucaparib/DMSO control were first added to flasks 2 days after cell plating, marking the beginning of treatment. PEO1 Cas9 Brunello cells were then treated for 1 month with escalating doses of rucaparib (EC50 for 2 weeks and then EC75 for 2 weeks). Escalating doses were used to prevent excessive cell death, given that these assays were run

longer than the CTG experiments used to calculated the used EC50 and EC75 values. DMSO control flasks (equivalent volume to DMSO added in rucaparib-treated flasks) were run in parallel, to be used in the final analysis.

A minimum of 12.5 million cells were maintained per passage for 3 weeks (week 4 had a minimum of 3 million cells passaged due to limited availability of 5-layer flasks). Thus 20 million cells from each treatment were harvested and snap frozen on weeks 1, 2 and 3, while 3 million cells were harvested at week 4. Cells were stored at -80°C until DNA extractions. The 3 week timepoint was chosen for initial analysis.

2.2.5 DNA repair foci in PDX tumours

PDX tumours, harvested either untreated or 4 hours post-5Gy irradiation *in vivo*, were dissociated by mincing followed by a 45 minute incubation at 37°C in 3ml/tumour of the digestion media outlined in **Table 2.15**.

Table 2.15. PDX tumour digestion media composition.

Component	Stock Concentration	Catalog number	Supplier	Storage	Volume per x1 tumour (µl)
DMEM/F-12, GlutaMAX™ supplement	**1x**	10565018	Gibco	4ºC	2658
Pronase	**10mg/ml**	10165921001	Sigma-Aldrich	-30ºC	420
DNAse	**1mg/ml**	10104159001	Sigma-Aldrich	-30ºC	300

After digestion, cells were pipetted through 100µm cell strainer into a 50ml falcon tube. 10ml DPBS was used to wash the empty digest tube and then this wash solution was pipetted through strainer (to wash through any left-over single cells). The single cell suspension was centrifuged (5 minutes, 1200rpm), and supernatant poured off. Cells were washed in 20ml DPBS to remove any FCS that may interfere with the fixable live-dead stain in subsequent steps. The cell suspension was centrifuged (5 minutes, 300g) and supernatant poured off again. Cells were then resuspended in 200µl DPBS with 2µl of LIVE/DEAD Fixable Aqua Dead Cell Stain Kit, for 405 nm excitation (Invitrogen, Cat# L34957). Cells were incubated for 10 minutes on ice in the dark, and then centrifuged (5 minutes, 300g). Supernatant was carefully removed, and

cells were resuspended in 400µl blocking solution (2.4G2 supernatant diluted 1:2 in 3% FCS in DPBS, or 7% FCS in DPBS) for a 15 minute incubation on ice. To create an unstained (LIVE/DEAD-only) control, 100µl of this mix was put aside. The remaining 300µl of cells were stained with 3-6µl of human-specific EpCam-647 antibody (clone VU1D9; Cell Signalling Technologies, Cat#5447) or 15µl of EpCam-APC (clone EBA-1, BD, Cat#347200) for a minimum dilution of 1:100 or 1:20 antibody respectively. Stained cells were incubated for 25 minutes on ice, then centrifuged (5 minutes, 300g). Stained and unstained cells were washed with 200-600µl of FACS buffer (3% FCS in DPBS) and centrifuged (5 minutes, 300g). Cells were then fixed with 200-1000µl of 4% Paraformaldehyde for 5 minutes, and centrifuged (5 minutes, 300g). Fixed cells were then washed with 200-600µl of FACS buffer (3% FCS in DPBS) and centrifuged (5 minutes, 300g) to remove the fixative, then stored in ~200µl FACS buffer in cold room until the FACS sort (either the following day, or two days later).

Cells were sorted at the WEHI Flow Cytometry core, and collected in FACS tubes with 1ml of FBS (whole inside of the tube was coated the with FBS to prevent cells sticking to the plastic). The selected population was the EpCam-647/APC positive (epithelial cells) and LIVE/DEAD-aqua negative (alive following digestion). Example of gating shown in **Figure 5.14**.

The resulting fixed epithelial (HGSOC tumour) cells were centrifuged (5 minutes, 300g) and washed with 1ml of DPBS. These cells were then centrifuged (5 minutes, 300g) and ultra-concentrated in 10µl of DPBS. The resulting 10µl of high concentration cell mix for each tumour was then used to coat 4 separate wells of a CellCarrier-96 Ultra Microplates (PerkinElmer, Cat# 6055302), ensuring the entire surface of each well was covered before transferring the mix to coat the next well. Left-over cells were stored in immunofluorescent foci (IFF) buffer (2% FBS and 1% BSA in DPBS) at 4°C as a back-up, and were usable for immunofluorescent staining for up to a week. Despite fixation, the quality of immunofluorescent staining was found to decline over storage time. It is possible that there are more suitable storage solutions that could be tested in future.

Cells were then spun at 1800g for 10 minutes to help the cells dry/stick to the surface of the wells. Other methods of sticking the cells to wells that were tested, such as leaving the cells in plate to settle in DPBS over 2-7 days at 4°C or centrifuging cells/wells in >50µl DPBS, were not as successful. Cells needed to be dried and spun onto the well surface to ensure they did not detach in subsequent steps of the experiment.

Once cells were centrifuged and dried to the well surface, they were immediately permeabilized using 100µl per well of 0.2% Triton-X, incubated for 10 minutes at room temperature (some cells often lost at this stage). Cells were then washed 3 times with 150µl DPBS per well, and blocked in IFF buffer for 1 hour (room temperature). Cells were then washed 3 times with 150µl DPBS per well. Cells were then incubated with mouse anti-human Geminin (ab104306 Abcam) diluted 1:100 in IFF buffer for 1 hour (room temperature). Cells were washed again 3 times with 150µl DPBS per well, and the incubated overnight at 4°C with either rabbit anti-human RAD51 (Abcam, Cat# ab133534) or rabbit anti-human γH2AX (Phospho-Histone H2A.X (Ser139), clone 20E3; Cell Signalling Technology, cat# #9718), diluted 1:250 and 1:200 in IFF buffer respectively. The following day, cells were washed 3 times with 150µl DPBS per well and then incubated for 30 minutes at room temperature with a mix of Goat anti-Rabbit IgG (H+L) Cross-Adsorbed Secondary Antibody, Alexa Fluor 488 (Invitrogen, Cat# A-11008) and Goat anti-Mouse IgG (H+L) Highly Cross-Adsorbed Secondary Antibody, Alexa Fluor 546 (Invitrogen, Cat# A-11030) – both diluted 1:800 in IFF buffer, combined with 1 drop of Hoechst 33342 Ready Flow™ Reagent (Invitrogen, Cat# R37165) per ml of solution. Cells were then washed once in 150µl of DPBS and left in 150µl of DPBS until imaging.

2.2.6 PDX DNA repair foci imaging

Cells stained for DNA repair foci on CellCarrier-96 Ultra Microplates (PerkinElmer, Cat# 6055302) were imaged on the Opera Phenix™ High Content Screening System (PerkinElmer, Cat# HH14000000). The imaging settings were as follows: Optical mode was set to confocal with an imaging plane of 1.5µm using a 40x water immersion. There were 197 fields of view captured per well. The channels Alexa 488, Alexa 568 and HOECHST 33342 were used to measure RAD51/γH2AX, geminin and nuclear stains respectively. Files were then exported automatically to the WEHI Columbus server (PerkinElmer), a data storage and analysis system.

A custom foci analysis pipeline was then set up on Columbus using the following settings: Find nuclei was set to method C with a >30µm^2 area threshold and standard morphology properties. Nuclei were then filtered based on an area of 50-150µm^2 and a roundness of >0.9 to make the "assay nuclei" group. This group was then further filtered based on a geminin staining intensity mean (Alexa 568) of >800. The "find spots" protocol was then applied, using method C to filter

for spots with a mean intensity of >2500 within the geminin positive group. The defined outputs for the Microsoft Excel export file were total cell nuclei, geminin positive nuclei and geminin positive nuclei with >5 foci. The analysis of % foci-positive cells was then performed in Microsoft Excel using the proportion of nuclei with >5 foci divided by the total number of geminin positive nuclei per sample. These results were then plotted using the PRISM7 (GraphPad) software.

2.2.7 DNA repair foci in cell lines

Cells were plated (10,000 cells for PEO1, PEO1A2 or 20,000 cells for PEO4) per well in 500µl FV media cells in Nunc Lab-Tek Chamber Slide™ system chamber slides (MERCK, Cat# C7182-1CS). Cells were left to settle and adhere to wells for 3 days. Two replicate wells were prepared per slide/condition (1, 3 and 6 hours post-irradiation).

After 3 days, cells were irradiated at the same time using 5Gy and fixed at either at 1, 3 or 6 hour post-irradiation using 4% PFA, wells incubated for 10 minutes at room temperature. Wells were then washed twice with DPBS (500µl per well for all washes) and stored in DPBS with 0.05% azide at 4°C for up to 7 days until ready for immunofluorescent staining.

Fixed cells were permeabilized using cells were permeabilized using 500µl per well of 0.2% Triton-X, incubated for 20 minutes at room temperature. Cells were then washed three times in DPBS to remove detergent, with each wash incubated for 5 minutes at room temperature. Cells were then blocked using IFF buffer for 1 hour (room temperature). Cells were then washed three times in DPBS before staining.

Cells were then incubated with mouse anti-human Geminin (ab104306 Abcam) diluted 1:100 in IFF buffer for 1 hour (room temperature). Cells were washed again three times with DPBS and the incubated for 1 hour at room temperature with Goat anti-Mouse IgG (H+L) Highly Cross-Adsorbed Secondary Antibody, Alexa Fluor 546 (Invitrogen, Cat# A-11030) diluted 1:800 in IFF buffer. Cells were washed again three times with DPBS and the incubated for 1 hour at room temperature with rabbit anti-human RAD51 (Abcam, Cat# ab133534) diluted 1:250 in IFF buffer. Cells were washed again three times with DPBS and the incubated for 1 hour at room temperature with Goat anti-Rabbit IgG (H+L) Cross-Adsorbed Secondary Antibody, Alexa Fluor 488 (Invitrogen, Cat# A-11008) diluted 1:800 in IFF buffer. Cells were washed again three times with DPBS and the incubated for 1 hour at room temperature anti-

γH2AX-rabbit antibody conjugated to Alexa Fluor 647 (cell signalling #9720) diluted 1:200 in IFF buffer. Cells were washed again two times with DPBS and then incubated in Hoechst 33342 Ready Flow™ Reagent (Invitrogen, Cat# R37165) diluted as 2 drops/mL in DPBS for 5 minutes at room temperature. Cells were finally washed once in DPBS, and then mounted using Fluoromount-G mounting solution (Southern Biotech, Cat# 0100-01). Slides were imaged using the Zeiss LSM780 confocal microscope system.

Images were exported as .czi files that were analysed manually for cells with >5 foci per geminin positive cell using Fiji (ImageJ) imaging software. A minimum of 100 cells were analysed per well. Cell counts were imported into the PRISM7 (GraphPad) software to create figures.

2.3 *In vivo* Patient Derived Xenograft protocols

2.3.1 Generation of PDX models

The use of animals in PDX experiments had approval from the Melbourne Health Animal Ethics Committee and the WEHI Animal Ethics Committee. Immuno-compromised non-obese diabetic–severe combined immunodeficient, interleukin -2 receptor-γ-null (NOD-SCID-IL-2rγ; NSG) mice aged between 6 to 8 weeks were sourced from the WEHI KEW animal breeding facility. Under general anaesthesia, 1-3 mm^3 fresh tumour tissue fragments were transplanted subcutaneously into the flank of each NSG mouse.

Tumour growth was assessed using digital callipers (measuring 2 perpendicular axes) once weekly prior to reaching tumour treatment size (between 180mm^3 and 300mm^3) and twice weekly once the mouse had commenced treatment (except for PDX model PH039 which was so fast growing it commenced treatments between 180mm^3 to 250mm^3, and required measurement three times weekly during treatments). The tumour measurements were digitally recorded directly into the StudyLog system, and tumour volume was automatically calculated using the following equation;
Tumour volume (mm^3) = 0.5236 x [larger diameter (mm) x smaller diameter ($(mm)^2$)].

Mice were sacrificed once the tumour volume reached 700mm^3, or ethical endpoint, and details of the experiment harvest were recorded. Standard harvested tumours were divided into several

pieces for further transplantation into new recipient mice (enabling serial propagation), snap frozen for molecular analyses (such as DNA, RNA or protein extractions), minced and cryopreserved in 10% DMSO, and fixed in neutral-buffered formalin for histology assessment. Tumours harvested for PDX foci experiments had several pieces snap frozen and fixed in neutral-buffered formalin, but remaining tumour material was digested for specific FACS staining protocols (see section 2.2.5).

2.3.2 Establishment of WEHI-PH039 PDX lineages A and B

The HGSOC PDX model WEHI-PH039 was originally derived from cryopreserved PDX MAYO-PH039 material obtained from collaborator, Dr Haluska (Mayo Clinic, USA) (Weroha et al. 2014). The sample was thawed and subcutaneously transplanted into 6 NSG mice (T2 generation), 3 which were used to establish serial propagation at the time (2015). Cryopreserved material from two of the original T2 tumours were thawed and subcutaneously transplanted to create lineages A (mouse 1467) and B (mouse 1471) of WEHI-PH039 in 2018.

2.3.3 Immunohistochemistry

Formalin fixed tumour samples were sent for in-house automatic immunostaining using the Ventana BenchMark Ultra (Roche Diagnostics, USA) at the WEHI histology laboratory. Clones used for immunostaining are as previously published (Topp et al., 2014).

C-NHEJ protein immunohistochemistry (IHC) was performed by the Kaufmann group (Mayo Clinic, MN USA) using internally optimized protocols. Digitized whole slide IHC images (in .svs file format) were provided to our group via secure file transfer. Images were analysed using the Aperio ImageScope software (v12.3.3; Leica Biosystems).

2.3.4 PDX in vivo single-agent treatments

Recipient mice bearing T2–T9 (passage 2 to passage 9) tumours were randomly assigned to treatment when tumour volume reached 180–300mm^3 (or 180–250mm^3 for fast-growing model PH039). Cisplatin treatment was administered via intra-peritoneal (IP) injection at a dose of 4mg/kg on day 1, day 4 and day 8, and this dosing was based on the previously established maximum tolerated dose (MTD) for the tumour-bearing NSG mice in our cohort. The regimen

for rucaparib treatment was oral gavage once daily, 5 days a week (Monday–Friday) for 3 weeks at 150mg/kg, 300mg/kg, or 450mg/kg doses. Niraparib was also administered by oral gavage once daily, 5 days a week (Monday–Friday) for 3 weeks at a dose of 100mg/kg. The Olaparib treatment regimen was IP injection of drug, 5 days a week (Monday–Friday) for 3 weeks at doses of 1mg/mouse, 2mg/mouse or 3mg/mouse. Vehicle for these studies was DPBS, given by IP and (intravenous) IV injection on day 1, day 8 and day 18 (**Table 2.16**).

Tumours were measured twice per week (or three times per week for PH039) and measurements were automatically recorded in the StudyLog software (StudyLog Systems).

Table 2.16. Summary of the single agent compound dosing regimens used for in vivo drug studies.

Compounds and doses	Dosing regimen	Route	Vehicle	Supplier
Cisplatin 4mg/kg	4mg/kg on days 1, 8 and 18	Intra-peritoneal injection	DPBS	Clifford Hallam Healthcare Pty Ltd (Hospital grade)
Rucaparib 150mg/kg	150mg/kg five times a week for 21 days	Oral gavage	0.5% Methylcellulose	Collaboration with Clovis Oncology
Rucaparib 300mg/kg	300mg/kg five times a week for 21 days	Oral gavage	0.5% Methylcellulose	Collaboration with Clovis Oncology
Rucaparib 450mg/kg	450mg/kg five times a week for 21 days	Oral gavage	0.5% Methylcellulose	Collaboration with Clovis Oncology
Niraparib 100mg/kg	100mg/kg five times a week for 21 days	Oral gavage	0.5% Methylcellulose	MedChemExpress
Olaparib 1mg/dose	1mg five times a week for 21 days	Intra-peritoneal injection	10% β-hydroxy-cyclodextrin	MedChemExpress
Olaparib 2mg/dose	2mg five times a week for 21 days	Intra-peritoneal injection	10% β-hydroxy-cyclodextrin	MedChemExpress
Olaparib 3mg/dose	3mg five times a week for 21 days	Intra-peritoneal injection	10% β-hydroxy-cyclodextrin	MedChemExpress

2.3.5 PDX 134183 and WEHI-PH039 in vivo rucaparib re-treatments

The rucaparib re-treatment strategy for PDX 134183 (#183); tumours were treated with two cycles of rucaparib (300mg/kg) in the first mouse/passage, with the first cycle being three weeks of once-daily oral gavage 5 days a week (Monday–Friday) for three weeks, and the second cycle being the same for two weeks starting when tumours reached a 500mm^3 volume. Tumours were then transplanted into new mice, and the protocol repeated in these mice for cycles three and four. The cisplatin re-treatment strategy for PDX 134183 (#183); tumours were re-treated with a lower dose of cisplatin (1mg/kg) each time tumour volume reached 300mm^3 for up to 6 doses per mouse, and this was repeated across two passages. A summary

can be found in **Figure 5.24**. The rucaparib re-treatment strategy for PDX WEHI-PH039 lineages: tumours were treated with two cycles of rucaparib (450mg/kg) in the first mouse/passage, with the first cycle being three weeks of once-daily oral gavage 5 days a week (Monday–Friday) for three weeks, and the second cycle being the same for two weeks starting when tumours reached a 300mm^3 volume. Tumours were then transplanted into new mice, and the protocol repeated in these mice for cycles three and four. The cisplatin re-treatment strategy for PDX WEHI-PH039 lineages; tumours were re-treated with a lower dose of cisplatin (1mg/kg) each time tumour volume reached 300mm^3 for up to 6 doses per mouse, and this was repeated across two passages. A summary can be found in **Figure 5.26**.

2.3.6 In vivo data analysis

Raw *in vivo* data for each PDX was extracted from the StudyLog database in an Excel spreadsheet format containing individual tumour volume measurements. The SurvivalVolume v1.2 (Wakefield, 2016) software package was then used generate the mean tumour volume vs time graphs (with 95% CI error bars), which includes individual tumour measurements. A Kaplan Meier (KM) graph was also generated for each model using 600mm^3 as the volume threshold for end of experiment harvest. Median TTH was also automatically generated from the KM analysis in the software. SurvivalVolume also created Pair wise Log Rank statistical tests to compare the outcome of each treatment arm. Time to progression (TTP) was defined as the time (in days) from beginning of treatment to an increase in average tumour volume of >20% from the nadir and was used to categorise PDX as sensitive (TTP ≥100 days), resistant (TTP <100 days) or refractory (TTP <8 days for cisplatin or <21 for rucaparib). TTP was calculated based on measurements of at least 3 tumours, and excluded any PDX that stopped measurements before treatment completion. Complete response (CR), Partial Response (PR), Stable Disease (SD) and Progressive disease (PD) are defined as previously described (Kondrashova et al., 2018).

2.4 *In silico* protocols

2.4.1 Molecular landscape summary of HGSOC PDX cohort

PDX molecular landscape summary was generated using the OncoPrint function (ComplexHeatmap package) in R based on BROCA and Foundation medicine sequencing

results generated prior to and during my PhD project. Input file was in Excel (Microsoft) file format.

2.4.2 Illumina Infinium EPIC and 450K array analysis

Infinium MethylationEPIC and HumanMethylation450K beadchip data was analysed using the missMethyl package in R (Phipson et al., 2016). Raw data files (IDAT format) were imported into R using the minfi package (Aryee et al., 2014). M-values and β values were extracted from objects created by minfi. SWAN (subset-quantile within array normalization) was performed on M-values, and poor quality probes were filtered out using the detection *p-value* (p <0.01). Normalized M-values were then extracted and used to create MDS plots using the plotMDS function (limma package) and Q-Q plots using the qqplot function (EnvStats package).

Comparisons between groups were performed by creating a contrast matrix of selected samples in R, and testing for differential methylation using the lmFit and eBayes functions (limma) using normalized M-values as input data. Differentially methylated probes were ranked using the decideTests function (limma), and the top 50,000 (adjustable value) differentially methylated probes for the comparison could be extracted using the topTable function (limma). A log fold change (LFC) threshold was also applied (specified for each analysis in results).

Annotation of differentially methylated probes, associated gene names and epigenomic regions was performed using the "IlluminaHumanMethylation" -EPICanno.ilm10b2.hg19 (EPIC array) or -450kanno.ilmn12.hg19 (450K array) annotation files. The ggPlot package was used to visualize the resulting data (using geom_point, geom_boxplot or geom_line functions).

2.4.3 Analysis of CRISPR screen data using CRISPRAnalyzeR software

CRISPRAnalyzeR was used to analyse the Brunello CRISPR screen data using 6 different analysis pipelines simultaneously (Winter et al., 2017). To import CRISPR sequencing data into the online CRISPRAnalyzeR software (http://crispr-analyzer.dkfz.de/), Excel (Microsoft) files (from custom in-house pipeline) containing all detected unique Brunello guide sequences were manipulated in R to produce read count file (.txt) files in the required CRISPR Analyzer format. "Brunello" was selected as the screening library, and the read count files were imported

into CRISPRAnalyzeR. Replicate samples were placed in treated (rucaparib) or untreated (DMSO control) groups, and HGNC gene identifier was chosen as the output format.

Default settings were used for individual analysis pipelines; Wilcox analysis = *p*-value threshold of 0.05 and 300 randomly picked sgRNAs; DESeq2 analysis = *p*-value threshold of 0.001; MAGeCK analysis = *p*-value threshold of 0.05; sgRSEA analysis = *p*-value threshold of 0.05; EdgeR analysis = *p*-value threshold of 0.05; BAGEL essential genes analysis = lowest cut-off of -50 and highest cut-off of 100 (Winter et al., 2017).

2.4.4 TP53 and reversion mutation analysis

FASTQ files were aligned to human genome build 38 (GRCh38, hg38) using BWA-MEM. The resulting bam files were then uploaded to Integrative Genomics Viewer (IGV, Broad Institute), where target regions could be assessed for the presence/absence and proportion of the PDX-specific TP53 mutation, or for the presence/absence and proportion of secondary mutations in PDX or cell lines.

2.4.5 Targeted RAD51C bisulfite sequencing analysis

Analysis of targeted *RAD51C* bisulfite sequencing data was performed by a bioinformatician using AmpliVar Genotyping workflow (Hsu et al., 2015). Briefly, unique amplicon reads spanning targeted RAD51C region were grouped and counted. A custom Python script was used for follow-up analysis and visualisation of the AmpliVar grouped amplicon data.

2.4.6 MLPA-seq analysis

Analysis of MLPA-seq data was performed as previously described (Kondrashova et al., 2015b). Target and control probes are described in section 2.1.20.

3 Characterisation of HGSOC PDX cohort

3.1 Introduction

OC is a highly heterogeneous disease, made up of various clinical and molecular subtypes, all with different pathologies, tumour progression, cell of origin, drug response and risk factors. EOC is the most common histotype of OC, accounting for over 85% of all cases (Sankaranarayanan et al., 2006). EOC can be further divided into 5 main histological sub-types: HGSOC, LGSOC, Endometrioid, Clear Cell Carcinoma and Mucinous, though the mutational landscape can vary greatly even within these subtypes.

This heterogeneity has long hampered progress in the detection and treatment of disease, given it was not fully appreciated until the advent of the -omics era, which allowed comprehensive molecular characterisation of the various OC subtypes. For example, we now not only know that HGSOC is the most chromosomally unstable subtype of EOC with universal *TP53* mutations and frequent loss of the HR DNA repair pathway, but it can also be stratified further based on its global transcriptional profiles into 4 molecular subtypes – C1 (a high stromal response), C2 (a high immune signature), C4 (a low stromal response), and C5 (mesenchymal, with a low immune signature) (Beaufort et al., 2014; Tan et al., 2013; TCGA, 2011; Tothill et al., 2008).

Another shift that occurred with the ability to better define HGSOC at a molecular level, was that pre-clinical models could now be screened and compared, in order to find those that best match the cancer subtype of interest. Many cell lines that were heavily used as models of HGSOC in the past have, in recent years, been found to not represent HGSOC at a molecular level, and are instead likely to be other subtypes of ovarian cancer (Domcke et al., 2013). For example, the two most commonly used cell line models for HGSOC, SK-OV-3 and A2780, were found to more closely resemble other histological subtypes. Furthermore, many immortalized (non-cancer) cells lines derived from normal OSE may not be the best models for HGSOC given mounting evidence that the cell of origin is in fact from the fallopian tube (Lee et al., 2007; Li et al., 2007; Piek et al., 2001b).

Although comprehensive molecular characterisation of cell lines is now possible, even properly characterized cell lines have their limitations. Cancer cell lines are invaluable for the

study of cancer biology and discovery of new therapies, but they lack the high level of heterogeneity found in patient tumours, with some degree of selection being necessary for the cells to grow on a 2D surface in culture. They also do not represent the complex 3D structure of the original tumour, and interactions that may occur with the tumour microenvironment.

PDX can be derived directly from patient tumours following surgery and transplanted into immune-compromised mice, without the need for *in vitro* expansion or manipulation. Though they can be derived from patient tumours that have been digested prior to xeno-transplantation, extensive digestion may affect surface tumour cell markers or alter the landscape of tumours initiating factors (Scott et al., 2013). Xenografts from fragments provide a more realistic disease model for researchers, given their complexity and heterogeneity, and have been shown to accurately recapitulate disease progression, histopathology, gene expression, genetic defects and drug responses in corresponding patients (Bankert et al., 2011; Elkas et al., 2002; Kolfschoten et al., 2000; Tentler et al., 2012; Topp et al., 2014). PDX are also a renewable resource, allowing multiple studies to be undertaken on the same tumour, often in parallel.

PDX from fragments are generated by engrafting fresh tumour tissue (1–2 × 1–3 mm^3) pieces either subcutaneously or orthotopically into immuno-deficient mice. Engraftment rates for the initial transplant (T1) range between 25 to 80% depending on the tumours type (Elkas et al., 2002), and growth to ethical harvest size (~700–1500 mm^3) usually takes 2–6 months (Morton et al., 2007). Once harvested, tumours are directly re-transplanted and expanded as later serial generations (T2, T3) which can then be used for a range of pre-clinical studies. Fresh patient or PDX tumours can also be minced and cryo-preserved in DMSO for thawing and transplantation at a later date, offering renewability of the resource. HGSOC PDX tumours can also be derived from ascites and have proven useful in multiple studies, though it is not yet established whether these PDX truly represent the heterogeneity or full disease spectrum of those derived from solid tumours (Indraccolo et al., 2006; Stewart et al., 2011).

In the past, a major concern regarding PDX in the literature was the lack of detail provided for methods and lack of important molecular characterisation provided in some papers (Scott et al., 2013). Understanding the full spectrum of PDX features and how they compare to the patient cancer is critical in generating meaningful and translatable pre-clinical research.

Since 2011, our group has generated and carefully curated a large cohort of HGSOC PDX. Multiple PDX models derived from chemonaïve patients (134011, 134013, 134019, 134027, 134054, 134056 and 134062) have been previously characterized by their molecular features and *in vivo* responses to cisplatin (Topp et al., 2014). This PDX cohort has since been expanded and characterized for responses to other treatments, and now consists of tumours derived from patients before and after chemotherapy and/or PARPi therapy treatment. These have been characterized by both their mutational landscape, treatment responses and immunohistochemistry. In my PhD, this cohort has been primarily used for the study of PARPi sensitivity and resistance mechanisms, with a heavy focus on defining *bone fide* HR defects and the various DNA repair modifications cells develop to escape PARPi synthetic lethality. The purity of these PDX tumour samples makes it much easier to screen for and study certain drug resistance mechanisms that may be harder to detect and resolve in patient samples where contaminating normal human stroma is often present.

This chapter describes the detailed molecular characterisation of the HGSOC PDX cohort in an attempt to uncover molecular features influencing PARPi responses in each model. This careful characterisation is especially important given the complexity of the HR pathway, with multiple relevant core factors, and the complex interactions that occur between HR and other DNA repair pathways that may impact PARPi responses. Furthermore, this chapter also attempts to use the HGSOC PDX to validate certain mechanisms of PARPi resistance reported in other pre-clinical models.

3.2 Chapter 3 hypotheses

1. Mechanisms that impair HR DNA repair will cause PARPi sensitivity in HGSOC PDX models

2. Mechanisms that restore the HR pathway will cause PARPi resistance in HGSOC PDX models

3. Mechanisms that do not restore the HR pathway, such as C-NHEJ pathway mutations or mutations that stabilize replication forks will cause PARPi resistance in HGSOC PDX models

3.3 Chapter 3 aims

1. To investigate the contribution of HR gene secondary and reversion mutations to PARPi resistance within the HGSOC PDX cohort

2. To investigate the contribution of alternative *BRCA1* isoforms to PARPi resistance within the HGSOC PDX cohort

3. To screen for other DNA repair pathway mutations that may be influencing PARPi responses within the HGSOC PDX models

3.4 Results

3.4.1 Summary of HGSOC PDX cohort

3.4.1.1 PDX HR status and treatment responses

Large gene panel sequencing tests (BROCA or Foundation One) were used to screen for HR gene mutations in PDX models. *BRCA1* and *RAD51C* methylation were screened for using methylation specific PCR (MS-PCR) or methylation specific high resolution melt (MS-HRM).

Treatment data was available for nine HRD models derived from chemonaïve patients, and four models from chemonaïve patients without any detectable defects in the HR pathway (**Table 3.1**). Of the chemonaïve HRD models with treatment data, two models had *BRCA1* mutations, two had *BRCA1* promoter methylation (me*BRCA1*), two had *BRCA2* mutations, two had *RAD51C* promoter methylation (me*RAD51C*) and one had a *BLM* mutation (**Table 3.1**).

The two *BRCA1*-mutant PDX models 134054 and 134056 were found to have different responses to cisplatin and PARPi, with 134056 being more sensitive to both treatments compared to 134054 (**Table 3.1**). PDX 134011 and 134062 were both homozygous for me*BRCA1*, but 134011 was sensitive to cisplatin while 134062 was refractory. PDX 134062 was, however, responsive to rucaparib, and while PDX 134011 rucaparib response could not be assessed *in vivo*, clinical data showed that the patient did respond to rucaparib (Kondrashova et al., 2018). The *BRCA2*-mutant PDX 134019 was supremely sensitive to both cisplatin and rucaparib, with complete responses achieved for both drugs (**Table 3.1**). *BRCA2*-mutant PDX 134013, on the other hand, was less sensitive to both cisplatin and rucaparib, with a partial response and stable disease achieved for each treatment respectively (**Table 3.1**). The two PDX with me*RAD51C*, 134183 and PH039, were both sensitive to cisplatin, and were responsive to rucaparib. However, two lineages of PH039 with different rucaparib responses were uncovered – Lineage A (PH039-A) being less responsive than Lineage B (PH039-B) (**Table 3.1**). These me*RAD51C* models are described in more detail in chapter 5.

Table 3.1. Cisplatin and PARPi (rucaparib) responses of chemonaïve HGSOC PDX models.

*P-values are based on log-rank test. TTH – time to harvest; TTP – time to progression (based on n=3 or more mice); CR – complete response; PR – partial response; SD – stable disease; PD – progressive disease; NA – not applicable, indicates PDX models that were lost before sufficient treatment data could be generated. ^ rucaparib 450mg/kg used; *No tumour regressions or stabilization of disease was achieved despite significant p-value.*

PDX #	HR gene defect	Median TTH vehicle	PDX cisplatin response				PDX rucapraib 300mg/kg response			
			Response	Median TTH (days)	Average TTP (days)	*p* -value	Response	Median TTH (days)	Average TTP (days)	*p* -value
Chemo-naïve patient - HR defective HGSOC										
134011	*BRCA1* methylation	46	Sensitive, CR	>120	>120	<0.001	NA			
134013	*BRCA2:* c.5517delA	43	Resistant, PR	>120	99	<0.001	Response, SD	81	32	0.01
134019	*BRCA2:* c.2323delT	22	Sensitive, CR	>120	>120	<0.001	Response, CR	>120	>120	<0.001
134054	*BRCA1:* c.5095C>T	32	Resistant, SD	78	50	0.010	Refractory, PD	36	8	0.900
134056	*BRCA1:* c.894_895delTG	15	Sensitive, CR	>120	113	<0.001	Response, SD	95	53	<0.001
134062	*BRCA1* methylation	18	Resistant/Refractory, SD	60	46	<0.001	Response, SD	71	50	<0.001
134148	*BLM:* c.2207_2212delinsTAGATTC	50	Resistant, SD	116	72	<0.001	Refractory, PD	60	15	0.443
134183	*RAD51C* methylation	50	Sensitive, CR	183	145	<0.001	Response, SD	74	43	0.015
PH039-A	*RAD51C* methylation	8	Sensitive, CR	137	>120	<0.001	Response, SD	57	43	<0.001
PH039-B	*RAD51C* methylation	15	Sensitive, CR	109	85	0.001	Response, PR	67	60	0.067
Chemo-naïve patient - HR competent (BROCA WT and no *BRCA1* methylation)										
134027	BROCA WT	22	Resistant, PR	109	57	0.001	Refractory, PD	36	8	0.887
134029	BROCA WT	25	Refractory, PD	32	8	0.128	Refractory, PD	32	8	0.306
134080	BROCA WT	53	Sensitive, CR	>120	>120	0.021	Refractory, PD	64	15	0.021*
134201	BROCA WT	25	Resistant, PR	99	57	<0.001	Refractory, PD	46	8	<0.001*

The one PDX with a *BLM* mutation was found to be resistant to cisplatin and refractory to rucaparib. *BLM* c.2207_2212delinsTAGATTC is the most common mutation causing Bloom syndrome in the Ashkenazi Jewish population. BLM is known to be involved in the HR pathway, but appears to be a negative regulator of this pathway, with loss of BLM causing increased sister chromatid exchanges (Patel et al., 2017). Thus, PDX 134148 may have de-regulated HR, rather than HRD. Indeed, the lack of PARPi response in this model supports this (**Table 3.1**).

All chemonaïve PDX models where no HR defects have been detected are refractory to rucaparib treatment, as expected. However, 134080 is sensitive to cisplatin, while 134027 and 134201 have a partial response (**Table 3.1**).

Treatment data was also available for seven PDX derived from pre-treated patients with HR defects, and two without HR defects (**Table 3.2**). These included models with *BRCA2* mutations (134019B and 34931), *BRCA1* mutations (23133, 134206 and 134153C) and two models with heterozygous me*BRCA1* (134048 and 134169; **Table 3.2**).

PDX 134019B was derived from the same patient as PDX 134019, but following 1st – line platinum chemotherapy. This PDX was, however, still very sensitive to both cisplatin and rucaparib (**Table 3.2**). The other *BRCA2*-mutant PDX derived from a pre-treated CASCADE warm autopsy patient (post 7-lines of platinum), in contrast, was refractory to both cisplatin and rucaparib (**Table 3.2**). This PDX was found to have two mutations in *BRCA2* (c.1313dupA and c.1299_1331del33), with one predicted to be a reversion mutation which is described in more detail in subsequent sections. The *BRCA1*-mutant models were all responsive to rucaparib, with 134206 showing a complete response, while 23133 and 134153C both achieved stable disease (**Table 3.2**). 134206 was also the most sensitive to cisplatin (complete response) while 23133 and 134153C were resistant with stable disease. PDX models 134048 and 134169 were found to have heterozygous me*BRCA1*, and were both refractory to rucaparib treatment. PDX 134048 was resistant to cisplatin, with stabilization of disease, while 134169 was refractory (**Table 3.2**). The two PDX without detected HR mutations, 134111 and 34939, were refractory to cisplatin treatment, and 134111 was also refractory to rucaparib (rucaparib data for 34939 was not available).

Table 3.2. Cisplatin and PARPi (rucaparib) responses of pre-treated HGSOC PDX models.

*P-values are based on log-rank test. TTH – time to harvest; TTP – time to progression (based on n=3 or more mice); CR – complete response; PR – partial response; SD – stable disease; PD – progressive disease; NA – not applicable, indicates PDX models that were lost before sufficient treatment data could be generated. **estimates given most mice were censored before harvest tumour volume. ^ rucaparib 450mg/kg used; *No tumours regressions or stabilization of disease was achieved despite significant p-value; **All treated mice censored early due to weight-loss or sickness, TTH measurements may not be reliable.*

PDX #	HR gene defect	Median TTH vehicle	PDX cisplatin response				PDX rucapraib 300mg/kg response			
			Response	Median TTH (days)	Average TTP (days)	*p* -value	Response	Median TTH (days)	Average TTP (days)	*p* -value
Pre-treated patient - HR defective HGSOC										
134019B	*BRCA2:* c.2323delT	22	Sensitive, CR	116	106	<0.001	Response, CR	102	85	<0.001
134048	*BRCA1* methylation (heterozygous)	36	Resistant, SD	>120	43	<0.001	Refractory, PD	67	8	0.095
134169	*BRCA1* methylation (heterozygous)	29	Refractory, PD	67	8	0.077	Refractory^, PD	36	8	0.924
23133	*BRCA1:* c.181T>G	81	Resistant, SD	200	92	0.033	Response^, SD	148	26	0.391
134206	*BRCA1:* c.3817C>T	39	Sensitive, CR	60**	>103**	0.010	Response, CR	76**	>120	<0.001
134153C	*BRCA1:* c.5503C>T	32	Resistant, SD	57	40	0.019	Response, SD	50	19	0.254
34931	BRCA2:c.1313dupA / c.1299_1331del33 (reversion)	36	Refractory, PD	81	5	0.065	Refractory, PD	53	8	0.196
Pre-treated patient - (BROCA WT and no BRCA1 methylation)										
134111	BROCA WT	46	Refractory, PD	74	5	0.004	Refractory, PD	46	12	0.229
34939	BROCA WT	36	Refractory, PD	116	4	0.003	NA			

3.4.1.2 Other genomic features of PDX models

Sequencing data from the BROCA and Foundation One tests uncovered a great degree of heterogeneity between the genomic profiles of these HGSOC PDX models. Some models, such as PDX 134029, 134201 and 34931, appear to have less stable genomes enriched with oncogenic amplifications and translocations (**Figure 3.1**; **Table 3.3**; **Table 3.4**). PDX 134029 and 134201 are both HR competent models that are refractory to PARPi, while PDX 34931 was derived from an initially HR deficient cancer (*BRCA2* mutation detected during 4th line of chemotherapy) that developed a *BRCA2* reversion mutation (PDX derived post 7th line of chemotherapy). Thus all three models with this profile are HR competent.

In contrast, models, such as 134011 and 134019, appear to lack genome rearrangements (based on the given gene panel tests) but have multiple gene mutations, while models 134183 and PH039 harbour relatively few deleterious genomic events (**Figure 3.1**; **Table 3.3**; **Table 3.4**). Whole genome sequencing of these models may, however, reveal more genome rearrangements that were not detected by BROCA or foundation medicine.

Approximately 30% (7/23) of all PDX models screened had *RB1* defects. PDX 134011, 134019 and 134056 all had HR defects combined with *RB1* loss, and were all found to be sensitive to cisplatin and responsive to rucaparib. This aligns with recent reports that concurrent *BRCA*-mutation and *RB1* loss causes exceptional chemotherapy responses in the clinic (Garsed et al., 2018).

Interestingly, PDX 134019 and 134019B derived from the same patient pre- and post-chemotherapy respectively, have the same *TP53* and *BRCA2* mutations but different additional oncogenic events (**Table 3.3**; **Table 3.4**). 134019 has an *RB1* deletion and a *NOTCH1* mutation while 134019B has an *NF1* splice site mutation and a *BRD4_NOTCH3* fusion detected by the Foundation One test. It is possible that these additional oncogenic hits were not early events in the tumour, and were therefore only within some sub-populations of cells. Perhaps this tumour heterogeneity led to different population being selected for under platinum pressure in the clinic, leading to PDX with slightly different genomic profiles.

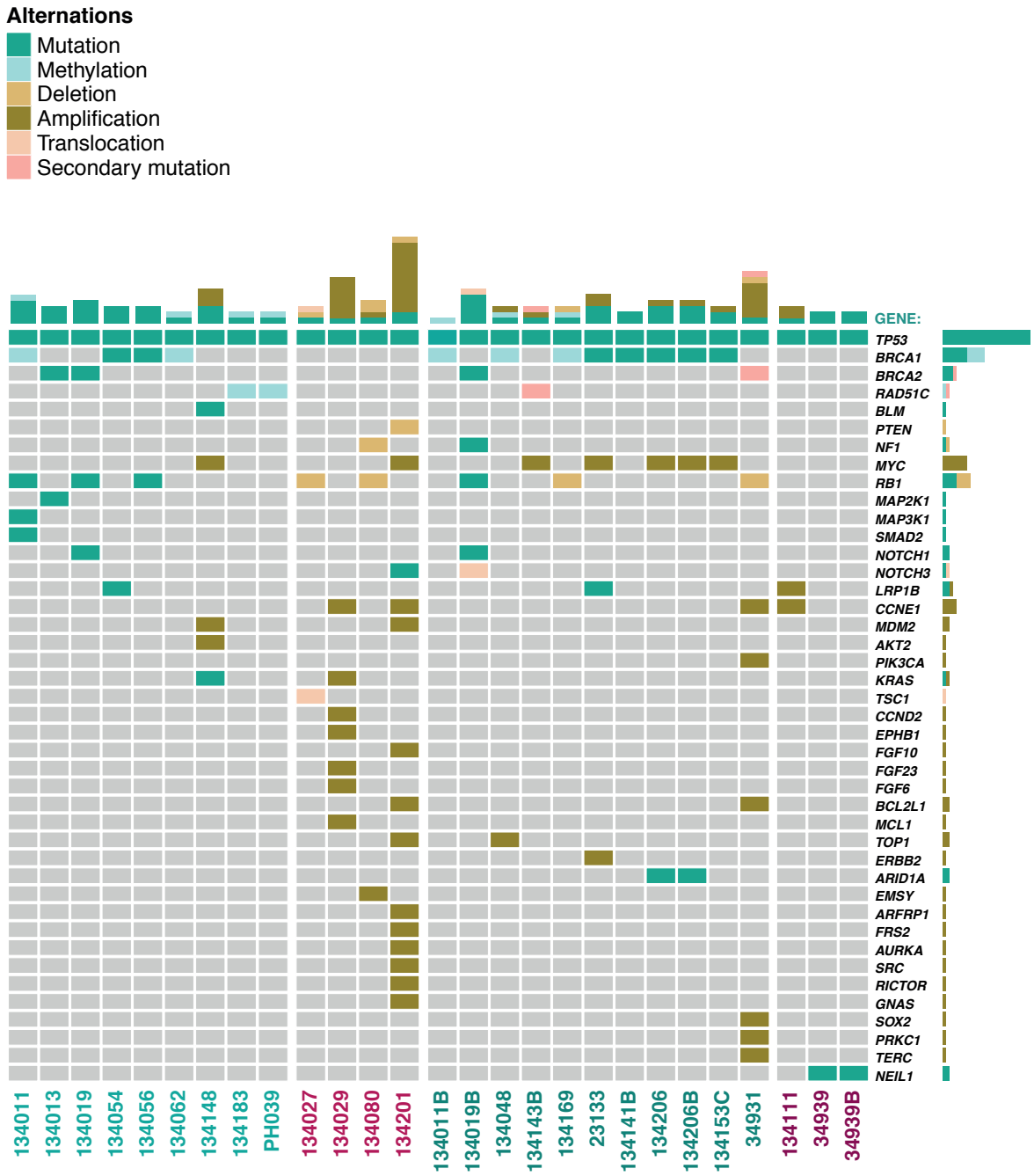


Figure 3.1. Summary of genomic profiles for all HGSOC PDX models.

Genomic alterations for PDX models where genomic data was available (based on data from the BROCA or Foundation One gene panel tests). PDX models listed along x-axis: Models 134011 to 134201 are derived from chemonaive patients, and models 134011B to 34939B are from pre-treated patients. Models highlighted in green indicate HRD models and those in red indicate HR Competent (HRC) models. Short deletions/insertions are classified as "mutations" in this summary, while "deletions" are defined as larger-scale events that remove 1 or more exons of a gene.

Table 3.3. Mutational features of chemonaïve HGSOC PDX models.

Genomic alterations for PDX models where genomic data was available. Based on data from the BROCA or Foundation One gene panel tests and BRCA1/RAD51C promoter MS-HRM. Mutation nomenclature based on human genome assembly 38 (hg38).

PDX #	*TP53* mutation	HR gene defect	Other oncogenic events
Chemo-naïve patient - HR defective HGSOC			
134011	c.592G>T	*BRCA1* methylation (homozyogous)	*RB1* deletion, *MAP3K1* deletion, SMAD2 splice-site mutation
134013	c.654_662del	*BRCA2:* c.5517delA	*MAP2K1* mutation
134019	c.463A>C	*BRCA2:* c.2323delT	*RB1* deletion, *NOTCH1* mutation
134054	c.596_600del	*BRCA1:* c.5095C>T	*LRP1B* mutation
134056	c.963del	*BRCA1:* c.894_895delTG	*RB1* truncation
134062	c.581T>G	*BRCA1* methylation (homozyogous)	*CCNE1* overexpression; *FGF12, NFKBIA, NKX2-1* and *ZNF217* amplifications, *CTNNA1* loss, *EZH2* translocation
134148	c.273G>A	*BLM:* c.2207_2212delinsTAGATTC	*MDM2, AKT2, MYC* amplification; *KRAS* mutation
134183	c.661G>T	*RAD51C* methylation	None detected
Chemo-naïve patient - HR competent (BROCA WT and no BRCA1 methylation)			
134027	c.470_471insCGT	BROCA WT	*RB1* loss, Hh over-expression, *TSC1* deletion
134029	c.840A>C	BROCA WT	*CCND2, CCNE1, EPHB1, FGF23, FGF6, KRAS, MCL1* amplifications
134080	c.672G>T	BROCA WT	*RB1* loss, *NF1* loss
134201	c.422G>A	BROCA WT	*MDM2, ARFRP1, CCNE1, FRS2, TOP1, AURKA, SRC, MYC, ZNF217, BCL2L1, FGF10, RICTOR* and *GNAS* amplificaations, *NOTCH3* mutation, *PTEN* deletion

Table 3.4. Mutational features of pre-treated HGSOC PDX models.

Genomic alterations for PDX models where genomic data was available. Based on data from the BROCA or Foundation One gene panel tests and BRCA1/RAD51C promoter MS-HRM. Mutation nomenclature based on human genome assembly 38 (hg38).

PDX #	*TP53* mutation	PDX derived post patient treatements:	HR gene defect	Other oncogenic events
HR defective HGSOC				
134019B	c.463A>C	Post 1st-line platinum	*BRCA2:* c.2323delT	*NF1* splice site mutation, *BRD4_NOTCH3* fusion
134048	c.814G>A	Post 3rd-line platinum	*BRCA1* methylation (heteryzyogous)	*TOP1* amplification
134143B	c.151_154delinsAA	Post 1st-line platinum and rucaparib (ARIEL2)	*RAD51C:* c.577C>T	*MYC* amplification, *ARID2* truncation, *LRP1B* deletion, *STK11* mutation
134169	c.380C>T	Ascitic tap post 2nd-line platinum	*BRCA1* methylation (heteryzyogous)	*RB1* region loss
23133	c.716A>G	Post 6th-line chemotherapy and olaparib	*BRCA1:* c.181T>G	*ERBB2, MYC* amplifications
134141B	c.818G>A	Post 1st-line platinum and rucaparib (ARIEL2)	*BRCA1:* c.5346G>A	None detected
134206	c.451C>T	Post 1st-line platinum	*BRCA1:* c.3817C>T	*MYC* amplification, *ARID1A* mutation
134206B	c.451C>T	Post 2nd-line platinum and olaparib (SOLACE)	*BRCA1:* c.3817C>T	*MYC* amplification, *ARID1A* mutation
134153C	c.314_315delinsTT	Post 2nd-line platinum and olaparib (SOLACE)	*BRCA1:* c.5503C>T	*MYC* amplification
34931	c.743G>A	Cascade post 9th-line chemotherapy	*BRCA2:* c.1313dupA and c.1299_1331del33 (reversion 50%)	*SOX2, CCNE1, BCL2L1, PIK3CA, PRKCI* and *TERC* amplifications, *RB1* deletion
HR competent (BROCA WT and no *BRCA1* methylation)				
134111	c.700T>A	Post 4th-line platinum	BROCA WT	*CCNE1* amplification, *LRP1B* deletion

Only 2/23 (~ 9%) of all PDX models screened had *NF1* defects, the BROCA WT PDX 134080 and *BRCA2*-mutant 134019B (**Table 3.3**; **Table 3.4**). This does not reflect published data where *NF1* gene mutations have been observed in 20% of HGSOC (Patch et al., 2015).

There were 6/23 (~26%) PDX models in the sequenced HGSOC cohort with *MYC* oncogene amplifications, and these appeared to be enriched in the pre-treated patient group (4 PDX models - 134143B, 23133, 134206/134206B, 134153C; **Table 3.3**; **Table 3.4**). Of these models, treatment data was only available for 23133, 134206 and 134153C, all of which have *BRCA1* mutations and were shown to be responsive to rucaparib (**Table 3.1**; **Table 3.2**). A full list of samples sent for BROCA sequencing during my PhD, and the genes covered by the panel versions, is provided in appendix A-D.

Given that some less durable PARPi responses could not be explained simply by HR status, for example why PDX 134056 or 134013 being less sensitive to rucaparib compared to PDX 134019, I started exploring other mechanisms of PARPi resistance in these models.

3.4.2 Secondary and reversion mutation screening

As reversion and secondary mutations in HR genes are one of the most commonly reported mechanisms of resistance in the clinic, screening for these mutations using targeted next generation sequencing (NGS) was integrated as part our PDX cohort characterisation process. PDX with primary mutations in HR genes were screened using Sanger sequencing, the NGS BROCA gene panel, targeted NGS approaches in-house (developed as part of my PhD project), or by the Foundation Medicine T5 NGS assay. A total of 11 PDX models from the HGSOC cohort were screened for reversion mutations in total, and 7 of these were screened by me using targeted sequencing approaches.

3.4.2.1 PDX models chosen for screening

Of the seven models that I screened during my PhD, there were two models derived from chemonaïve patients (134019 and 134148) and five PDX from post-chemotherapy patients (134019B, 134206, 23133, 34931 and 134141B). Some of these PDX had been tested previously using other sequencing methods, but none of these methods could provide the

sensitivity and depth of sequencing coverage afforded by targeted NGS. Thus some models were screened again, in case secondary mutations were missed by other approaches.

BRCA2-mutant PDX 134019 (**Table 3.3**) was very rucaparib sensitive, as was 134019B (derived from the same patient post 1st line platinum chemotherapy), though PDX 134019B did have a shorter time to progression than 134019 (TTP; 85 days vs >120 respectively; **Table 3.1**; **Table 3.2**). Thus, there was a possibility that some 134019B tumours had developed some PARPi resistant cells that may be detected following *in vivo* rucaparib treatment pressure. Three rucaparib-treated and 3 vehicle-treated PDX 134019 samples were chosen for screening, while 4 cisplatin-treated, 3 rucaparib-treated and 4 vehicle-treated PDX 134019B samples were also chosen.

BLM-mutant PDX 134148 (**Table 3.3**) was grouped as HRD, given that the BLM helicase participates in HR DNA repair (though *BLM* deficiency has not been established as a cause of HRD). This model was resistant to cisplatin and refractory to rucaparib (**Table 3.1**), thus, there was a chance that this model's poor response to rucaparib was due to correcting secondary mutations in *BLM*. Three rucaparib-treated and 2 vehicle-treated tumours from this model were chosen for screening.

PDX 23133 was derived from a pre-treated patient (**Table 3.4**), and was found to be resistant to cisplatin and had a modest responses to rucaparib treatment *in vivo*, with stabilization of disease observed for both treatments (**Table 3.2**). This PDX harbours a pathogenic point mutation in *BRCA1*, and was thus screened for reversion mutations at this locus.

BRCA1-mutant PDX 134206 (**Table 3.4**) was found to be very cisplatin and rucaparib sensitive, with complete responses achieved for both drugs (**Table 3.2**). However, at time of screening this treatment data was not yet available, thus several untreated samples from this model were tested. This PDX was also from a patient who had completed one line of chemotherapy, and was thus included for reversion mutations screening.

PDX 34931 was derived from a patient who had undergone 7 lines of platinum therapy. A *BRCA2*-mutation was detected at the 4th line of chemotherapy, so there was a chance a secondary mutation had developed in subsequent lines of therapy (**Table 3.4**). This PDX was later found to be refractory to both cisplatin and rucaparib treatments *in vivo* (**Table 3.2**),

suggesting that there may be some underlying platinum/PARPi resistance mechanism in this model.

PDX 134141B was derived from a patient who had been treated with 1st-line platinum chemotherapy and rucaparib (in the ARIEL2 clinical trial). This model was found to have a *BRCA1* mutation (c.5346G>A) and no secondary mutations in the post-progression biopsy (**Table 3.4**). To confirm this finding, 3 early passage untreated 134141B tumours were included in screening.

3.4.2.2 Sequencing approaches

Two targeted in-house sequencing approaches were required for reversion mutation screening, depending on the type of primary mutation. Primary frameshift mutations shift the reading frame of a gene, often causing premature protein termination by the creation of novel stop codons. Correcting secondary frameshift mutations (including large deletions) can, therefore, be some distance upstream or downstream of the primary mutation, as long as the reading frame is corrected and the resulting protein function is not significantly affected by these mutations. Therefore, a broader genomic region should be interrogated when screening for these secondary mutations, to ensure that they are not missed. To address this, I designed long-range PCR-based (LR-PCR) library preparations for several PDX with primary frameshift mutations – PDX 134019, 134019B and 134148 (**Table 3.3**; **Table 3.4**; **Figure 3.2**). In contrast, missense mutations do not affect the reading frame of the gene, but only the codon within which they are found. Thus, only that codon and the local region around it (in case of a small in-frame deletion removing the pathogenic primary mutation) need to be considered. For such primary mutations, a targeted amplicon sequencing approach was used (**Figure 3.2**).

LR-PCRs generate larger products, and therefore require different enzymes and cycling conditions compared to smaller amplicon-based PCRs. My initial optimization experiments were done using the high fidelity Phusion flex polymerase, successfully used in the amplicon-based assays. However, this polymerase was found to be unsuitable for LR-PCRs I was running (**Figure 3.3A**). I went on to test the Takara LA Taq kit, and found it worked well with both LR-PCR primer sets (**Figure 3.3B**). Compared to the amplicon assays, the LR-PCRs also required more input DNA and primers and longer PCR extension times (see methods section for details).

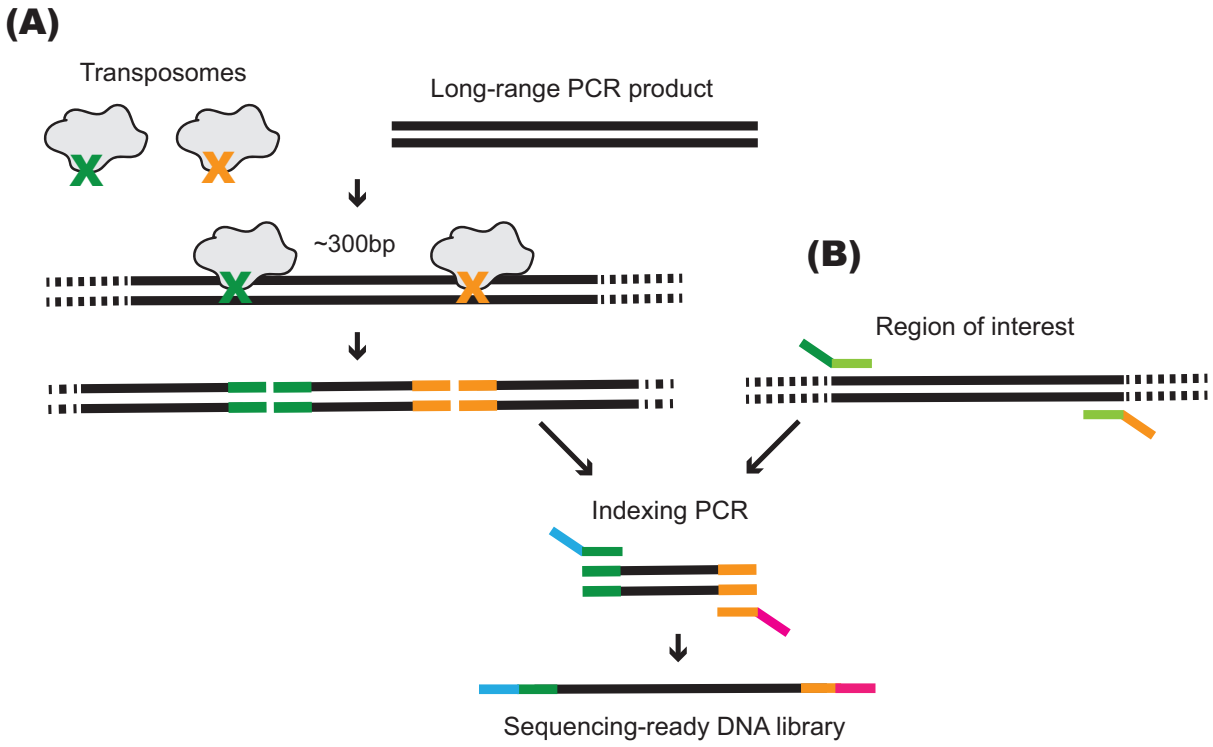


Figure 3.2. Two in-house sequencing approaches designed for secondary mutation screening.

(A) *Long-range PCR products, required for interrogation of primary frame-shift mutations, were processed using the Illumina NexteraXT library preparation kit, which uses transposomes to cut DNA and insert Illumina adaptor primers. Resulting DNA fragments are ~300 basepairs (bp) in size, and are then barcoded with Illumina index primers to produce sequencing-ready libraries.* ***(B)*** *The amplicon approach is a relatively simple two-step PCR, where the primary region of interest is first amplified using targeted primers containing Illumina-adaptors at either the 5' or 3' end. Resulting PCR products are then barcoded in a second PCR reaction with Illumina index primers to produce sequencing-ready libraries.*

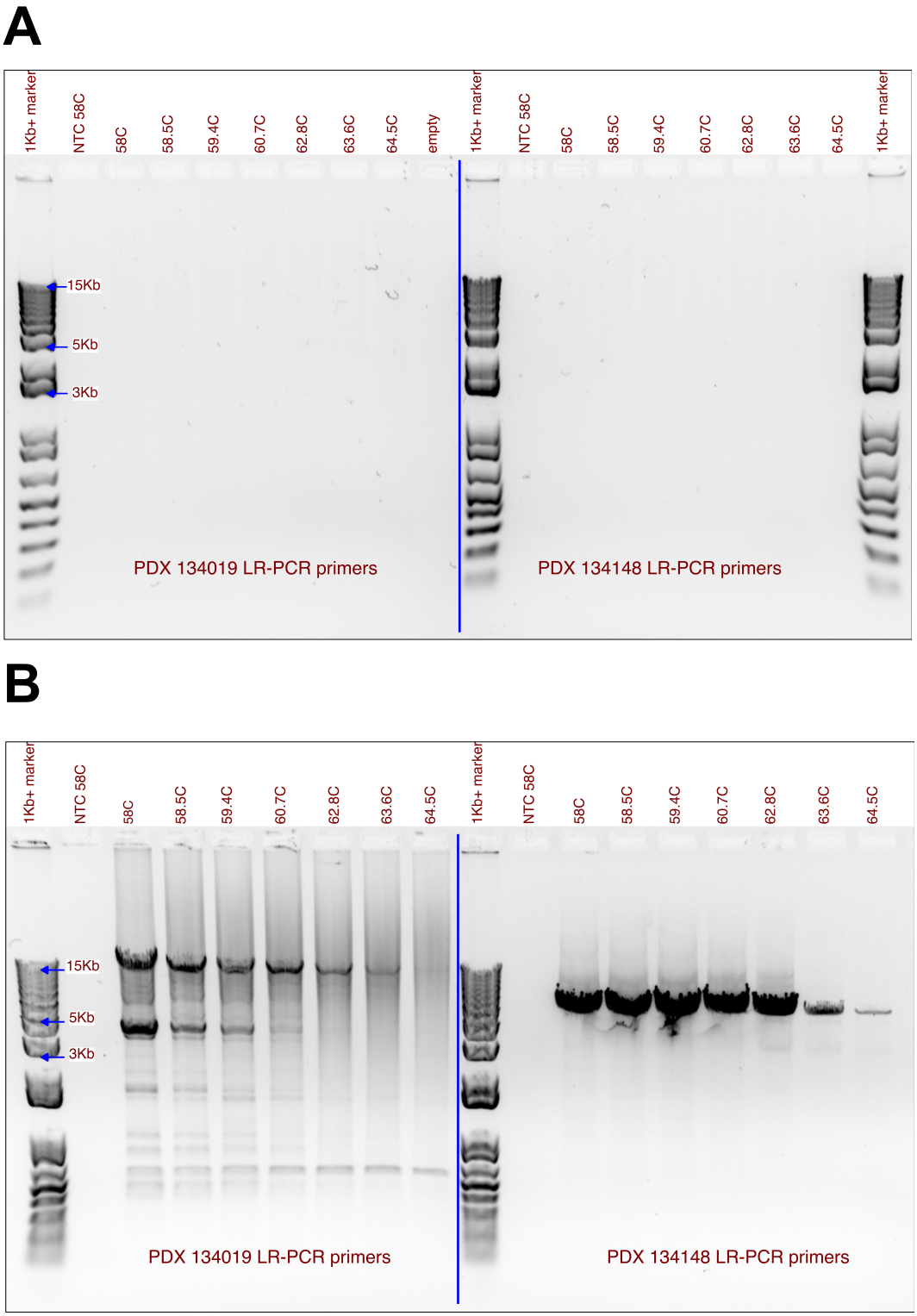


Figure 3.3. Takara polymerase outperforms Phusion polymerase in LR-PCR optimization.
LR-PCR optimization results of ***(A)*** *Phusion polymerase and* ***(B)*** *Takara polymerase using the same DNA and primer inputs and thermocycling protocols. PDX 134147 sample #6093 used as a control for all PCRs; Annealing temperatures 58°C -64.5°C presented; Kb= kilobases.*

3.4.2.3 Reversion mutations detected

There were no reversion mutation detected in PDX models 134019, 134148,134019B, 134206, 23133 or 134141B screened using targeted sequencing (**Table 3.5**). Of the seven models I screened, only one was found to harbour a HR gene secondary mutation – PDX 34931. This PDX was derived from a CASCADE warm autopsy patient who had received 9 lines of chemotherapy, 6 of which were platinum-based, but no PARPi (**Table 3.6**). The PDX was found to be refractory to both cisplatin and PARPi (**Table 3.2**).

A *BRCA2*:c.1313dupA (primary mutation, 50%) and c.1299_1331del33 (secondary mutation, 50%) were found by me initially in BROCA data sent to us from collaborators (**Table 3.4**). I then confirmed this result using the targeted amplicon sequencing assay (**Table 3.5**). Given that the location of secondary mutation was detected in BROCA sequencing, a targeted amplicon sequencing assay could thus be used, instead of a LR-PCR-based approach I would have normally used to screen for secondary frameshift mutations, like this one. All samples tested contained the secondary mutation (**Table 3.5**).

The primary mutation *BRCA2*:c.1313dupA causes a frameshift of 13 codons, with a premature termination codon at the 14th position (p.Asp348Glufs*14), thereby significantly truncating the protein, removing critical protein domains with nonsense-mediated decay predicted (Schwarz et al., 2014). The secondary mutation creates an in-frame deletion of 33 base-pairs, removing 11 amino acids (KRKKDFLTSEN) but still producing a protein, albeit truncated (NM_000059.3:p.Lys434_Asn444del; **Figure 3.5**). This mutation occurs in exon 10 of *BRCA2*, which does not code for any known functional protein domains (**Figure 3.5**) (Roy et al., 2012).

Though no reversion mutations were found in PDX 134206 (established post-1st line chemotherapy in patient) using my in-house targeted amplicon sequencing method, it is possible that patient samples 134206B (biopsy post-second-line platinum and olaparib) and 134206C (surgery post-third-line platinum and olaparib) in patient 134206 may contain a reversion mutation to wild-type. Unfortunately, no PDX were successfully generated from 134206B and 134206C, thus only the patient samples were available for testing.

Table 3.5. Summary of all mutation reversion screening results.

*Summarized findings of the reversion mutation screening experiments. PDX 34931 was the only PDX model found to have a reversion mutation in this project, initially by BROCA and validated by in-house amplicon sequencing. This table only shows PDX samples and those that were successfully sequenced. * marks the assays designed and run by me during my PhD. A full list of all samples, including baseline human tumour samples and samples that failed sequencing, can be found in appendix E.*

PDX model	Primary mutation	Tumours with reversion mutation/ total tested	Treatments tested	Sequencing Method Used
134013	*BRCA2* :c.5517delA	0/7	Cisplatin, Rucaparib 300mg/kg, Vehicle	Sanger Sequencing
134019	*BRCA2* :c.2323delT	0/13	Cisplatin, Rucaparib 150/ 300mg/kg, Vehicle	Sanger sequencing, LR-PCR-based NGS*
134019B	*BRCA2* :c.2323delT	0/10	Cisplatin, Rucaparib 300mg/kg, Vehicle	LR-PCR-based NGS*
134054	*BRCA1* :c.5095C>T	0/5	Rucaparib 300mg/kg, Vehicle	Sanger Sequencing
134056	*BRCA1* :c.894_895delTG	0/40	Cisplatin, Rucaparib 150/ 300/ 450mg/kg, Vehicle	Sanger sequencing, amplicon-based NGS
134148	*BLM* :c.2207_2212delinsTAGATTC	0/9	LDCy, LDCy+Rucaparib 300mg/kg, Rucaparib 300/ 450mg/kg, Vehicle	LR-PCR-based NGS*
23133	*BRCA1* :c.181T>G	0/9	Cisplatin, Rucaparib 450mg/kg, Vehicle	Amplicon-based NGS*
134141B	*BRCA1* :c.5346G>A	0/1	Untreated	Amplicon-based NGS*
34931	*BRCA2* :c.1313dupA	4/4	Untreated	Amplicon-based NGS*
134206	*BRCA1* :c.3817C>T	0/3	Untreated	Amplicon-based NGS*

Table 3.6. Patient 34931 completed treatments.

Nine lines of chemotherapy completed in total, with 6 of these being platinum-based.

Patient 34931 treatments	Treatment line	Status
Carboplatin + Paclitaxel	1	Completed
Gemcitabine + Carboplatin	2	Completed
Carboplatin + Cediranib/placebo (ICON6)	3	Completed
Caelyx	4	Completed
Paclitaxel	5	Completed
Carboplatin	6	Completed
Docetaxel	7	Completed
Carboplatin	8	Completed
Cisplatin	9	Completed

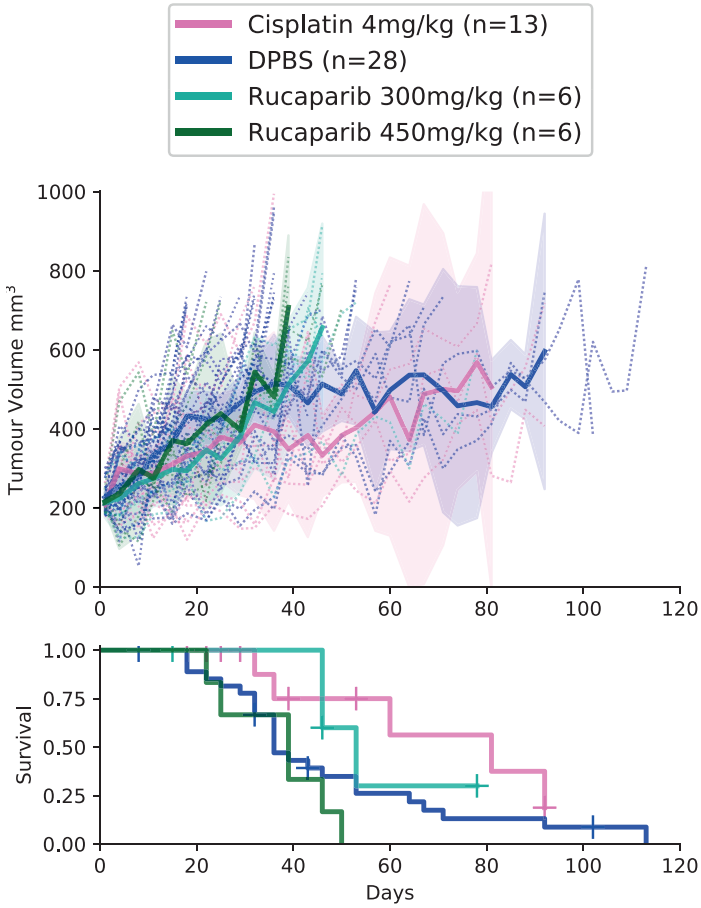


Figure 3.4. BRCA1 revertant PDX 34931 is cisplatin and PARPi resistant.

PDX 34931 is refractory to cisplatin and rucaparib (300mg/kg and 450mg/kg doses). Tumour volume data presented is individual tumour measurements (dashed lines), with mean (bold line) +/- 95% CI (shaded area).

Table 3.7. P-values of BRCA1 revertant PDX 34931 in vivo responses.

Referencing data presented in Figure 3.4. P-values calculated using Pairwise Log Rank Tests. Median TTH= median time (days) to harvest.

Treatment	*p* -value	Median TTH
DPBS	NA	36
Cisplatin 4mg/kg	0.07	81
Rucaparib 300mg/kg	0.20	53
Rucaparib 450mg/kg	0.33	39

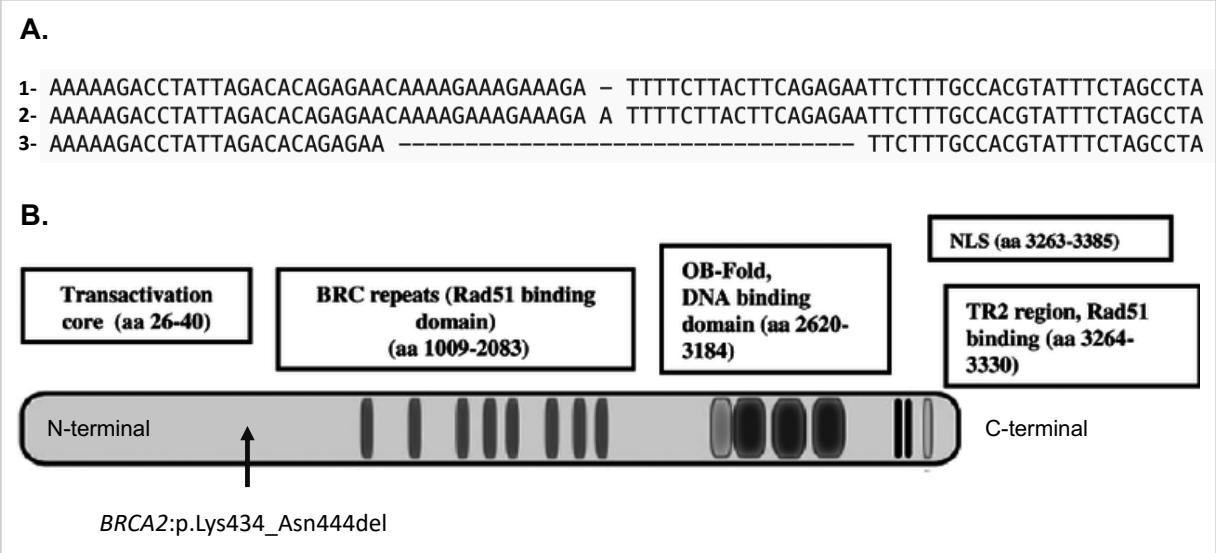


Figure 3.5. Correcting BRCA2 secondary mutation in PDX 34931

(A) *Line 1 shows the WT sequence (82 nucleotide) of BRCA2 surrounding the primary mutation (BRCA2:c.1313dupA) shown in line 2. Line 3 shows the in-frame secondary mutation BRCA2:c.1299_1331del33.* ***(B)*** *Figure adapted from (Roy et al., 2012). The PDX 34931 primary (p.Asp348Glufs*14) and correcting secondary (p.Lys434_Asn444del) BRCA2 mutations sit within a region where there are no known functional protein domains, between the transactivation core and RAD51 binding domains.*

Given the primary mutation is a missense mutation in *BRCA1,* reversion to wild-type sequence is possible. The primary mutation was only detected in 134206B and 134206C at 88% and 57% respectively, with remaining sequence being wild-type (**Table 3.8**). This is possibly a reversion mutation, but may also be due to reduced tumour purity in these patient samples. Unfortunately, there were no SNPs within the sequenced region that would allow phasing of potential secondary mutations.

Immunohistochemical H&E staining in pieces of the original 134206B and 134206C tumours revealed that the 134206B section had no tumour (mostly fibrous tissue), while 134206C had only 10% tumour in the tissue section. These results highlight the issues that arise when not testing the same tumour piece in this type of analysis. Thus, *TP53* mutation sequencing should be carried out on the DNA samples originally tested for reversion mutations to more accurately estimate tumour purity of these DNA samples and interpret the reversion sequencing results.

Table 3.8. Reversion mutation screening results for patient and PDX 134206 tumours.

PDX	Sample	Primary mutation	Primary mutation frequency	Reversion mutation detected	Treatment
134206	7553	*BRCA1* :c.3817C>T	100%	N	Untreated
	7556		100%	N	Untreated
	7555		100%	N	Untreated
	206 Baseline		91%	NA	Post chemo
134206B	206B Baseline		88%	NA	Post chemo + PARPi
134206C	206C Baseline		57%	NA	Post chemo + PARPi

Only one of the three PDX 134141B samples tested was successfully sequenced, and there were not secondary mutations detected in this sample, confirming the findings from ARIEL2 (Kondrashova et al., 2017). Unfortunately, PDX 134141B was discontinued at T2 due to its extremely slow growth (with many transplants taking >6 months to reach measuring size).

3.4.3 BRCA1 methylation zygosity

The importance of *BRCA1* methylation (me*BRCA1*) zygosity in predicting PARPi response has been published by our group (Kondrashova et al., 2018). Using cell line models and PDX with either homozygous or heterozygous me*BRCA1*, we were able to show that all copies of *BRCA1* must be methylated for full gene silencing and PARPi response.

I performed the *BRCA1* qPCRs for this study, which demonstrated that *BRCA1* expression was present in models with one or more copies of unmethylated *BRCA1* (heterozygous me*BRCA1*), while models with all copies of *BRCA1* methylated (homozygous me*BRCA1*) did not have detectable *BRCA1* gene expression (**Figure 3.6**). The BROCA-WT PDX 134201 was used as a *BRCA1*-expressing positive control. The OVCAR8 cell line has been reported to have *BRCA1* methylation in the past, however our study demonstrated that this affects only two out of three copies of the gene. The one unmethylated copy was sufficient to restore gene expression (**Figure 3.6**).

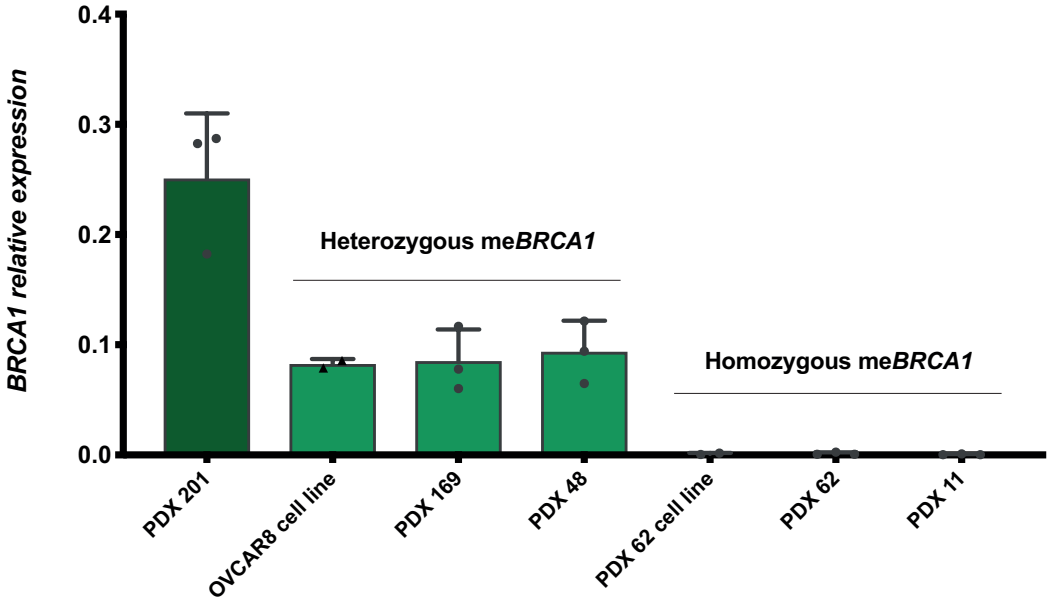


Figure 3.6. Relative BRCA1 expression in meBRCA1 homozygous and heterozygous models. *One copy of unmethylated BRAC1 is sufficient to restore expression of BRCA1 in PDX and cell line models (Kondrashova et al., 2018). Data shows mean +/- SD, where points represent individual PDX tumours or cell line passages.*

The two PDX models 134048 and 134169 were derived from previously platinum-treated patients, found to have 1 *BRCA1* copy methylated and 1 copy unmethylated. In these cases, again, one unmethylated copy of *BRCA1* was sufficient to restore gene expression. In contrast, samples from 100% me*BRCA1* (homozygous) models PDX 134062 and 134011, and the PDX 134062-derived cell line WEHI-CS62 had complete silencing of the *BRCA1* gene. This correlated with treatment responses for these PDX models, where heterozygous me*BRCA1* models 134048 and 134169 were more resistant to rucaparib *in vivo*, than PDX 134062 (**Table 3.1**; **Table 3.2**).

3.4.4 Constitutional BRCA1 methylation and BRCA1 methylation stability

In the me*BRCA1* study, it was also observed that some patients can lose methylation of one of their *BRCA1* alleles following chemotherapy, while others retain methylation following multiple treatment rounds (**Figure 3.7**). This suggests that there may be some underlying biological mechanism, perhaps epigenetic, that influences the stability *BRCA1* methylation under treatment pressure (Kondrashova et al., 2018).

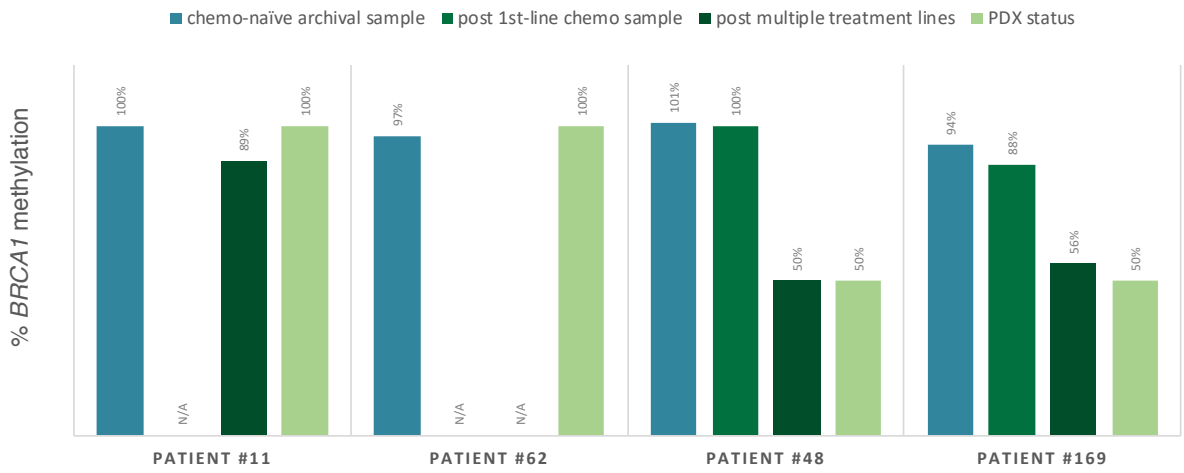


Figure 3.7. BRCA1 methylation can be lost following chemotherapy in patients.
Patient #169 and patient #48 developed heterozygous meBRCA1 after 2 and 3 lines of chemotherapy in the clinic, respectively. These post-treatment tumours were used to generate PDX #169 and PDX #48. Measurements displayed here are normalized to the tumour purity for each sample, which was estimated by targeted TP53 sequencing (Kondrashova et al., 2018).

I hypothesized that the presence of constitutional me*BRCA1* in patients may be associated with more stable me*BRCA1* in their tumours (**Figure 3.8**). Constitutional epimutations are aberrations in gene expression caused by altered epigenotypes that are widely distributed in normal tissues (though they are frequently mosaic). These can occur during development or can be inherited, and have been proposed as an alternative mechanism to genetic mutation for cancer predisposition (Dobrovic et al., 2009; Hitchins, 2015; Wong et al., 2011).

I tested me*BRCA1* in patient germline DNA from peripheral blood corresponding to our 4 me*BRCA1* PDX models, two with homozygous me*BRCA1* (134062 and 134011) and two with heterozygous me*BRCA1* (134048 and 134169) where methylation of one *BRCA1* allele was lost in patients following chemotherapy. Low level methylation was only detected in one patient blood sample, from which me*BRCA1* heterozygous PDX #48 was derived. Thus, though this test was done on a small sample size, the data does not support our hypothesis (**Table 3.9**).

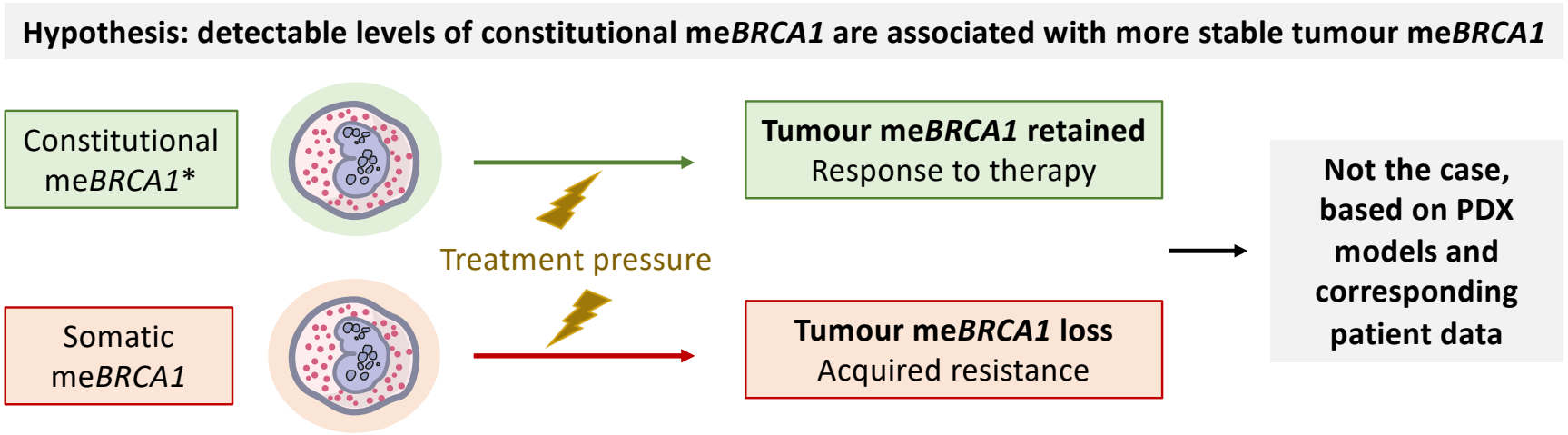


Figure 3.8. Hypothesis for constitutional methylation and stability of tumour methylation under treatment pressure.

*Constitutional BRCA1 methylation (meBRCA1), defined as *any methylation detected by BRCA1 MS-HRM in germline (blood) DNA sample of the patient, was hypothesized to lead to more stable tumour meBRCA1 under either PARPi or Platinum chemotherapy pressure.*

Table 3.9. Results of constitutional methylation analysis in patients with meBRCA1 HGSOC.

*Constitutional methylation, defined as *any methylation detected by BRCA1 MS-HRM in germline (blood) DNA sample of the patient, was only detected in patient #48 by meBRCA1 ddPCR, which does not support our hypothesis of an association between constitutional meBRCA1 and increased meBRCA1 stability under treatment pressure.*

PDX model	PDX derived from	PDX me*BRCA1* status	PDX PARPi (rucaparib) response	PDX cisplatin response	Constitutional me*BRCA1* in corresponding patient*
PDX #11	chemo-naïve tumour	Homozygous	responsive (patient data)	sensitive	Not detected
PDX #62	chemo-naïve tumour	Homozygous	some response (2/7 mice)	resistant	Not detected
PDX #48	post third-line platinum tumour	Heterozygous	refractory	refractory	Detected
PDX #169	post first-line carboplatin/paclitaxel tumour	Heterozygous	refractory	refractory	Not detected

As one of the requirements for an epimutation to be defined as constitutional is that it is present in all 3 germ layers (ectoderm, mesoderm and endoderm), other tissues (hair follicles and saliva or buccal mucosa) from this patient would need to be tested to confirm that the me*BRCA1* detected is due to true constitutional epimutation (Sloane et al., 2016). However, given that me*BRCA1* was not detected in other cases, true constitutional epimutations in these cases can probably be ruled out. It is, therefore, likely that other mechanisms are contributing to the relatively stable methylation in PDX 134062 and 134011. Perhaps there are tissue specific changes in methylation that may have influenced the development and stability of me*BRCA1* in these tumours, or perhaps stochastic events.

The WEHI-CS62 cell line derived from PDX 134062 retains its methylation in cell culture, providing another useful model for further study me*BRCA1* stability in HGSOC.

3.4.5 RAD51C methylation in PDX models

RAD51C methylation (me*RAD51C*) was also found in two PDX models from chemonaïve patients – one during our PDX cohort methylation screening (PDX 134183), and another as part of a collaboration with the Kaufmann group at the Mayo Clinic (a derivative of PDX model PH039; **Table 3.1**) (AlHilli et al., 2016). These models, their me*RAD51C* zygosity and responses to PARPi are investigated in more detail in chapters 5 and 6.

3.4.6 BRCA1 D11q isoform testing

As described in Chapter 1, mutations in the exon 11q region of *BRCA1*[1] are spliced out of certain, partially functional isoforms of *BRCA1*. One of these isoforms, *BRCA1* D11q, has been shown to contribute to cisplatin and PARPi resistance *in vitro* and i*n vivo* (cell line xenografts) (Wang et al., 2016) when overexpressed. The 11q region that is spliced out of canonical *BRCA1* (NM_007294.3) to make the D11q isoform (NM_007299.4) spans positions c.788 to 4096. Mutations within this region of *BRCA1* may, therefore, result in resistance via this splicing mechanism.

[1] Though *BRCA1* exon 11 is now called exon 10 in genome builds hg19 and hg38, to be consistent and avoid confusion with previously published work using exon 11 nomenclature, it will continue to be referred to as the "11q" region.

Within the HGSOC PDX cohort there are two models with deleterious mutations in this region of *BRCA1* exon 11: PDX 134056 and PDX 134206. Rucaparib-responsive PDX 134056 (stable disease) was derived from a chemonaïve patient, and 134206 (complete response) from a patient post-1st line of chemotherapy. I decided to investigate the presence of this alternative *BRCA1* isoform in these models, and how it impacted on PARPi responses *in vivo*.

3.4.6.1 Assay design

To examine D11q as a potential mechanism of PARPi resistance in these two models, I designed a qPCR-based assay for specific detection of the D11q isoform of *BRCA1*, as well as primers for only full exon 11-containing isoforms, and primers detecting all isoforms of *BRCA1*. As *BRCA1* exon 11 is now called exon 10 in genome builds hg19 and hg38, to avoid confusion I have chosen to remain consistent with previously published work referencing exon 11 and D11q instead of exon 10/10q. Thus, all exons described for the remainder of this section are shifted (+1) to be consistent with this older nomenclature.

To ensure that primers did not amplify genomic DNA, at least one primer of each primer pair was designed to cover an exon-exon boundary. As I was working with PDX samples, I also checked each primer set did not amplify any murine DNA/RNA sequences.

Primers to amplify only the *BRCA1* mRNA transcripts containing exon 11 were designed to target the exon 11q/11p boundary and a region within exon 11q (**Figure 3.9**). Thus, only *BRCA1* transcripts containing full exon 11 could be detected, as loss of either the exon 11q or 11p regions would prevent amplification. These were referred to as the "+exon 11" primers. To amplify the majority of common/functional full length transcripts of *BRCA1* (including D11q and canonical *BRCA1*), one primer was designed to cover the exon 13-14 boundary and the other within exon 14. These were referred to as the "*BRCA1* All" primers (**Figure 3.9**). The "D11q" primers were designed to only amplify transcripts with deleted 11q (i.e. D11q *BRCA1* isoforms). One primer was designed to target the exon 9-10 boundary and the other to target the exon 11p-12 boundary. This amplicon product would be too large to amplify in transcripts containing the 11q region, thus ensuring only D11q transcripts are detected (**Figure 3.9**).

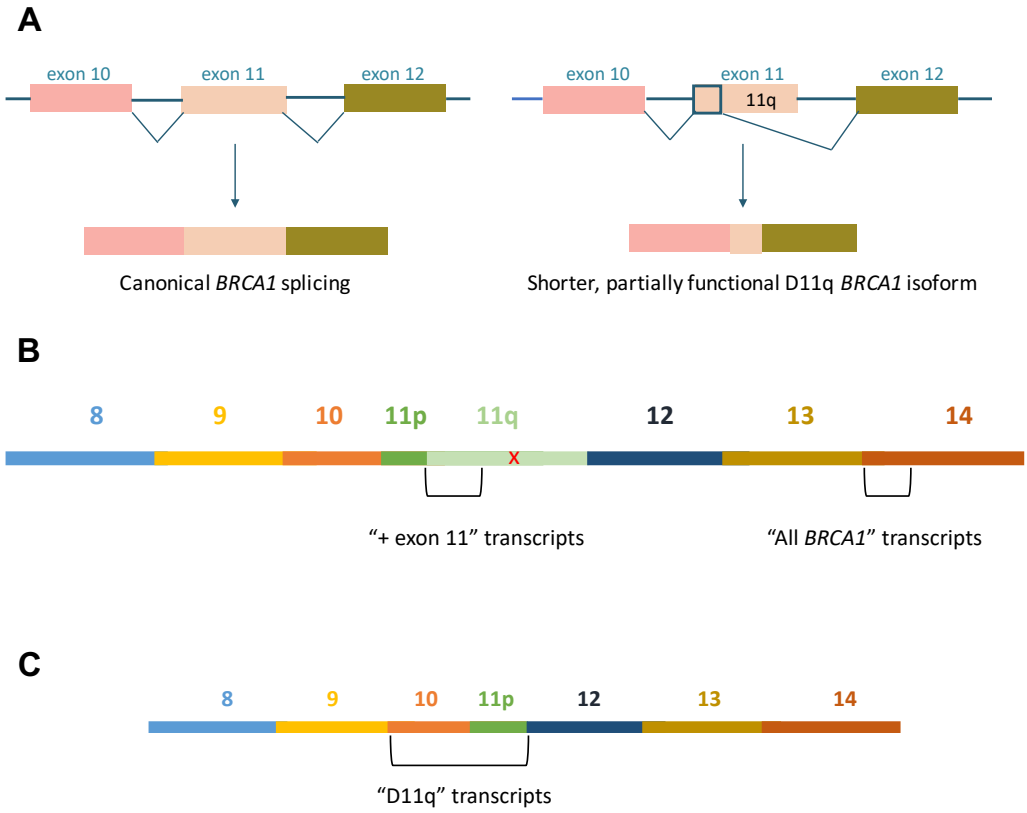


Figure 3.9. BRCA1 isoform qPCR primer design.

(A) *Canonical splicing of BRCA1 includes all of exon 11, while the D11q isoform has a large part of exon 11 (the 11q region) spliced out* ***(B)*** *Coloured and numbered blocks represent individual exons (8-14) of canonical BRCA1 transcript, and X marks the PDX 134056 primary mutation (not to scale). To amplify only exon 11 containing transcripts, one primer for "+ exon 11 transcripts", covers the exon 11q/11p boundary and the other sits within exon 11q. To amplify all BRCA1 transcripts (with or without D11q), one primer for "All BRCA1 transcripts", covers the exon 13-14 boundary and the other sits within exon 14.* ***(C)*** *Coloured and numbered blocks represent individual exons (8-14) of the D11q BRCA1 transcript (not to scale). To amplify only transcripts with deleted 11q, one primer for "D11q transcripts" covers the exon 9-10 boundary and the other sits across the exon 11p-12 boundary.*

Within-sample normalization was performed using average delta Ct values of four housekeeper genes (see methods section for details). As some tumours may have higher *BRCA1* expression than others, I did consider further normalizing the D11q expression values to the expression for "*BRCA1*-All" transcripts. However, I decided that this was not ideal as high total *BRCA1* expression is not reflective of functional *BRCA1*, and there may be other mechanisms governing the detection of these *BRCA1* transcripts by qPCR. Thus, the "D11q", "+ exon 11" and "*BRCA1* All" qPCR results for each tumour sample are shown individually.

During optimization of the primers, I found that our aliquots of the MDA-MB-231 breast cancer cell line (*BRCA*-WT) had relatively high transcript levels for all primer sets tested. Hence, I decided to use this cell line as a "D11q-high" technical control. I also uncovered a PDX 134091 (*BRCA*-WT) tumour sample with relatively low levels of D11q, and this was used as a "D11q-low" technical control.

Once the assay was established, I tested samples from both vehicle-treated and post-PARPi PDX tumours for several 134056-derived lineages (#56S, #56R and #56cis), and PDX 134206.

3.4.6.2 PDX 134056 results

Several lineages of PDX 134056 have been generated over time, some with varying degrees of PARPi sensitivity.

The original lineage of PDX 134056 (published as PDX #56) showed mixed responses to rucaparib (**Figure 3.10A**). From this original lineage, a cryopreserved T3 rucaparib 150mg/kg-treated tumour (#2272) was thawed and transplanted into mice to create a new rescue PDX lineage that was relatively sensitive to rucaparib (#56S; **Figure 3.10B-C**), except for one sub-lineage from mouse #6452 that appeared more rucaparib resistant (#56R; **Figure 3.10D**). The average rucaparib 300mg/kg treatment TTP for the #56S lineage was found to be >120 days, while the average TTP for the #56R lineage was found to be 46 days. The median TTH for #56S was also longer than that of #56R (141 and 81 respectively; **Table 3.10**).

Although the difference in rucaparib 300mg/kg treatment responses between these two lineages was not found to be statistically significant (*p*-value=0.187; **Figure 3.11**), I was still interested in whether the observed differences could be due to elevated *BRCA1* D11q expression in the #56R lineage.

No significant difference was observed in D11q expression between the #56S and #56R lineages when comparing standard 700mm^3 tumour volume harvest samples, termed here as long-term harvest (LTH) samples (**Figure 3.12**). There were also no significant differences in D11q expression of these lineages when compared to the *BRCA1*-mutant PDX control 134054 (**Figure 3.12**). Similar expression trends were observed for the "+ exon 11" and "*BRCA1* All" transcripts (**Figure 3.13**; **Figure 3.14**).

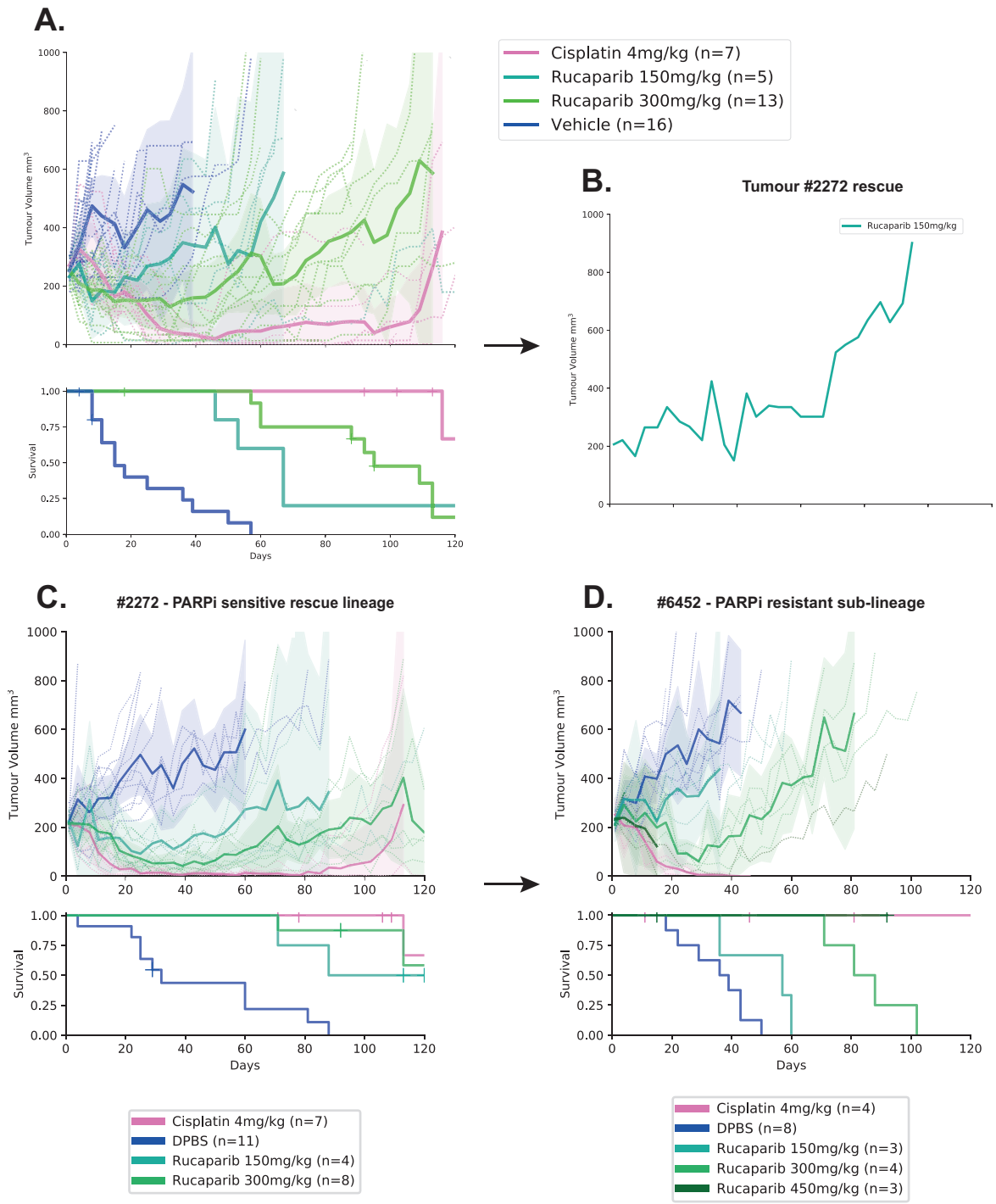


Figure 3.10. Two lineages with different PARPi sensitivity derived from PDX 134056.

*(**A**) The original in vivo data for PDX 134056 showed mixed responses to PARPi rucaparib. (**B**) from this original lineage, a post-rucaparib (150mg/kg) cryopreserved tumour was transplanted (rescued), and from this tumour two lineages emerged – (**C**) a PARPi sensitive lineage from the original rescued T3 tumour 2272 (#56S), and (**D**) a PARPi resistant lineage emerging from tumour 6452 (#56R). Tumour volume data presented is individual tumour measurements (dashed lines), with mean (bold line) +/- 95% CI (shaded area).*

Table 3.10. PDX 134056 lineage #56S and #56R rucaparib response p-values.

Table referencing data presented in figure 3.10. P-values calculated using Pairwise Log Rank Tests. Median TTH= median time (days) to harvest. NA – Not applicable as treatment not tested. NA – Not applicable as n<2 mice uncensored.*

	Treatment	#56S	#56R
p -value	Cisplatin	0.00	0.01
	Rucaparib 150mg/kg	0.02	0.07
	Rucaparib 300mg/kg	0.00	0.00
	Rucaparib 450mg/kg	NA	0.10
Median TTH	Vehicle (DPBS)	32	39
	Cisplatin	>120	>120
	Rucaparib 150mg/kg	88	57
	Rucaparib 300mg/kg	141	81
	Rucaparib 450mg/kg	NA	NA*

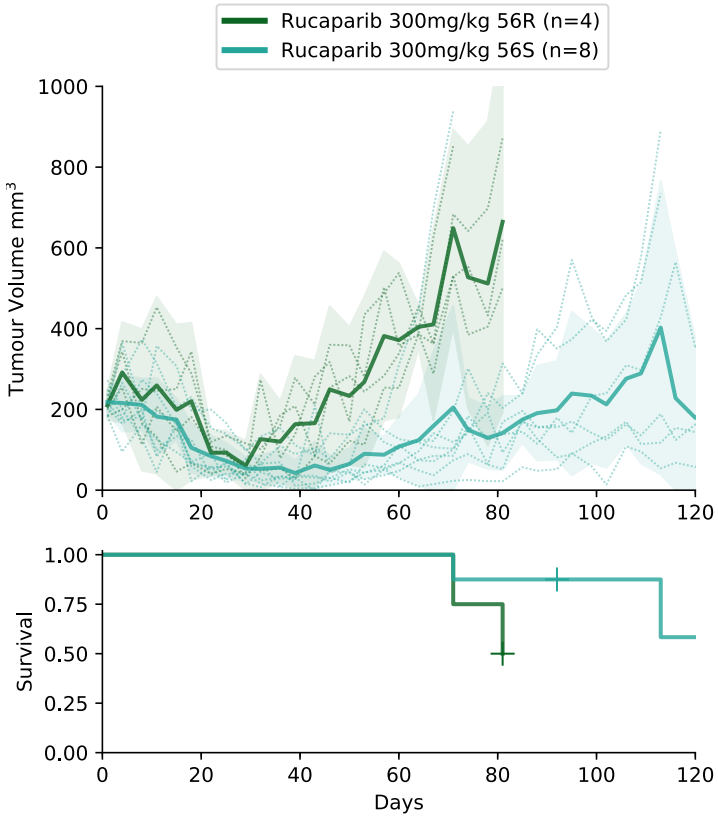


Figure 3.11. Direct comparison of PDX 134056 lineage #56S and #56R rucaparib 300mg/kg responses.

Although there is an observable difference between rucaparib responses in lineage #56S and #56R, this is not statistically significant (p-value=0.187). Tumour volume data presented is individual tumour measurements (dashed lines), with mean (bold line) +/- 95% CI (shaded area)

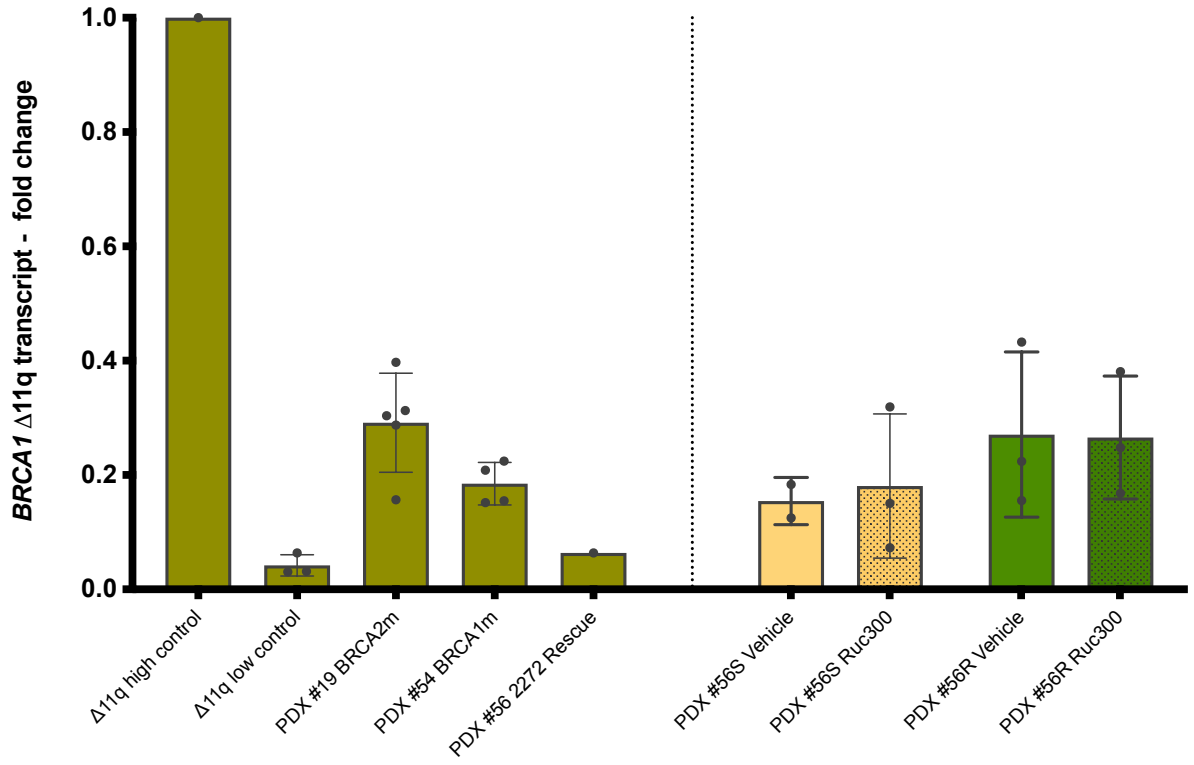


Figure 3.12. No elevated BRCA1 D11q expression in PDX 134056 LTH tumours.

BRCA1 D11q is not elevated in #56S or #56R relative to control PDX model 134054 (p-values 0.476 and 0.412, and average expression respectively). There is also no significant increase in #56S vs #56R vehicle samples (p= 0.30) or #56S vs #56R rucaparib 300mg/kg samples (p= 0.43). Fold-change expression from the D11q high control, the MDA-MB-231 cell line is presented. D11q low control is PDX 134091 sample. Data shows mean +/- SD, where points represent individual PDX tumours. Data normalized to D11q high control. Ruc300: rucaparib 300mg/kg treated; PDX #19 = 134019; PDX #54 = 134054; BRCA1m = BRCA1-mutant control; BRCA2m = BRCA2-mutant control; Δ11q = D11q; P-values calculated using an unpaired t-test with Welch's correction.

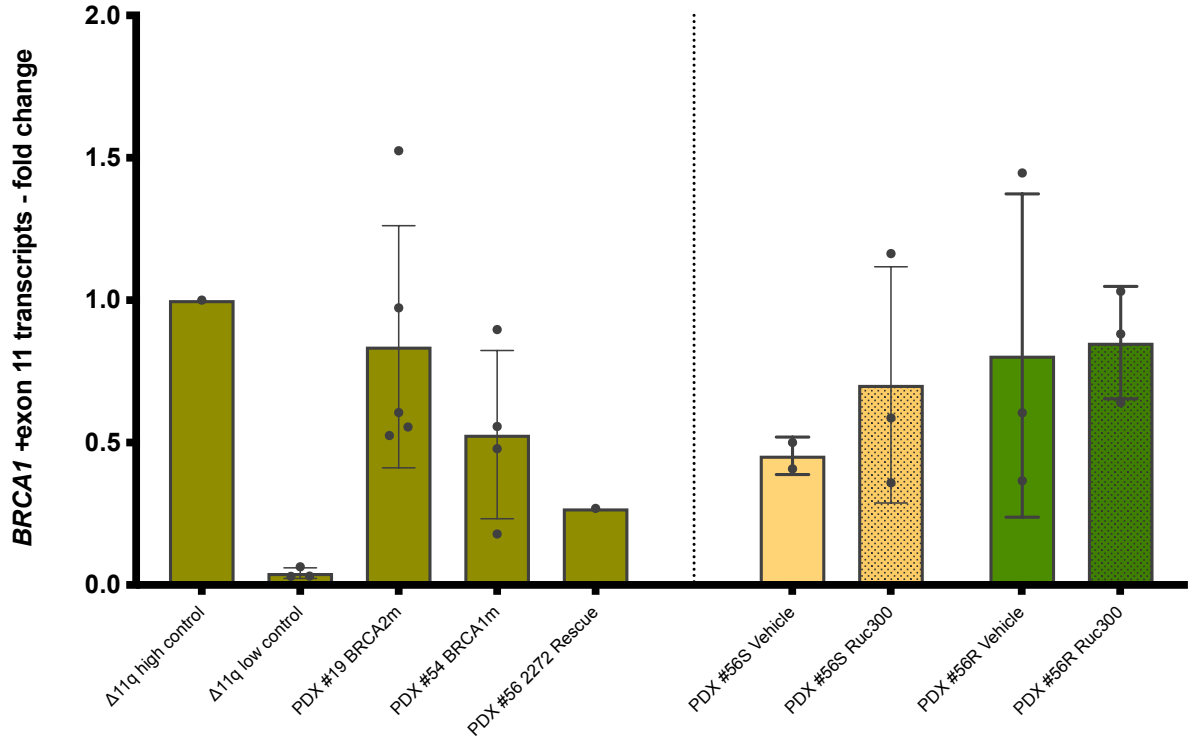


Figure 3.13. BRCA1 exon 11-containing transcript expression in LTH PDX 134056 lineage #56S and #56R tumours.

Fold-change expression from the D11q high control, the MDA-MB-231 cell line is presented. D11q low control is PDX 134091 sample. Data shows mean +/- SD, where points represent individual PDX tumours (except for D11q low control which are replicates from the same tumour). Data normalized to D11q high control. Ruc300: rucaparib 300mg/kg treated; Ruc450: rucaparib 450mg/kg treated; PDX #19 = 134019; PDX #54 = 134054; BRCA1m = BRCA1-mutant control; BRCA2m = BRCA2-mutant control; Δ11q = D11q; P-values calculated using an unpaired t-test with Welch's correction.

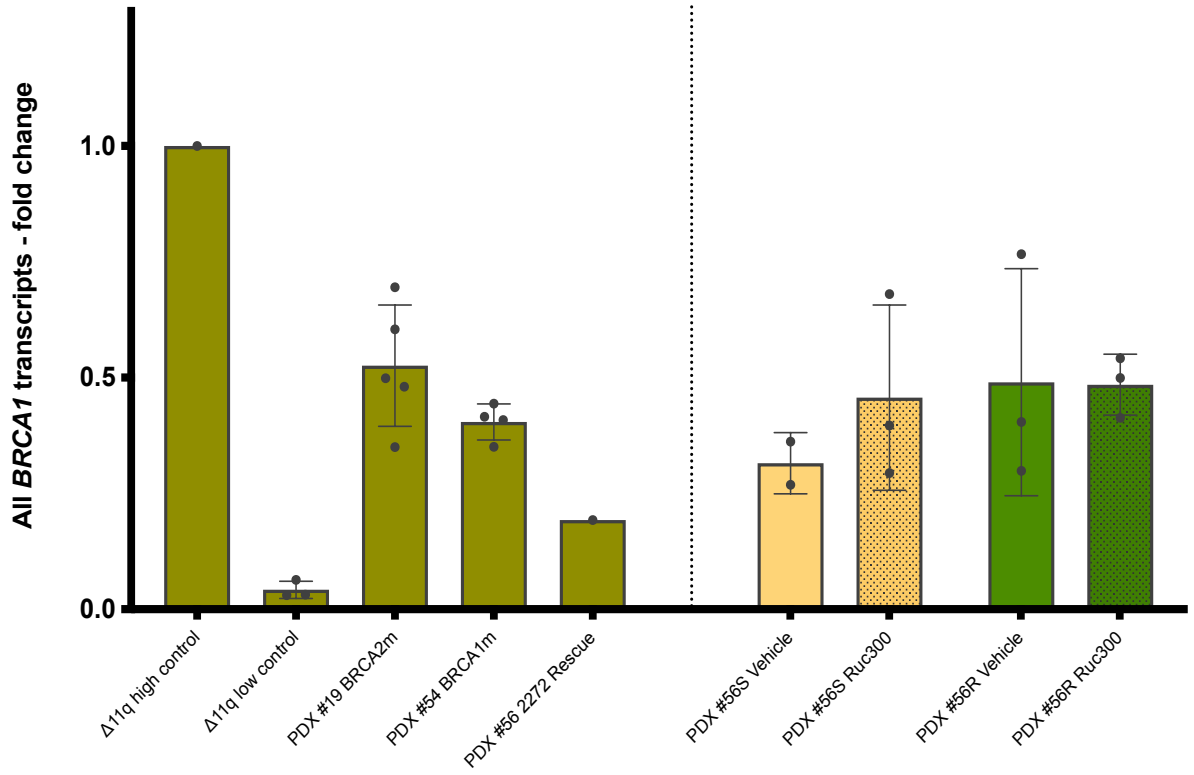


Figure 3.14. "BRCA1 All" expression in LTH PDX 134056 lineage #56S and #56R tumours.

Fold-change expression from the D11q high control, the MDA-MB-231 cell line is presented. D11q low control is PDX 134091 sample. Data shows mean +/- SD, where points represent individual PDX tumours (except for D11q low control which are replicates from the same tumour). Data normalized to D11q high control. Ruc300: rucaparib 300mg/kg treated; Ruc450: rucaparib 450mg/kg treated; PDX #19 = 134019; PDX #54 = 134054; BRCA1m = BRCA1-mutant control; BRCA2m = BRCA2-mutant control; Δ11q = D11q; P-values calculated using an unpaired t-test with Welch's correction.

However, since RNA expression can often be dynamic (Pisco et al., 2013), it was possible that the D11q expression may only initially spike during/just after treatment, and then stabilise or be selected against before harvest due to tumour volume. I therefore designed a "short-term harvest (STH)" experiment, where 14 PDX tumours (6 from #56R and 8 from #56S) were harvested 2-weeks post-treatment completion.

The STH experiment revealed a modest (0.1 mean fold-change difference), but statistically significant (p= 0.02), increase in D11q expression in the vehicle #56R lineage tumours relative to vehicle #56S (**Figure 3.15**). Though the same trend was visible for the rucaparib 300mg/kg-treated tumours, this difference was not statistically significant, possibly due to low sample number (n=2) in the rucaparib 300mg/kg-treated group (p= 0.13; **Figure 3.15**). *BRCA1* D11q was also found to be slightly elevated in vehicle #56R samples relative to control PDX model 134054 (p= 0.01), but not 134019 (p= 0.67; **Figure 3.15**).

Interestingly, expression "+ exon 11" transcripts also significantly increased in the #56R STH samples when comparing by treatment to the #56S STH samples (**Figure 3.16**), but this trend was not statistically significant when measuring the "*BRCA1* All" transcripts (**Figure 3.17**).

The reason canonical BRCA1 transcripts were still detected in all D11q-mutant PDX samples tested may be because the predicted nonsense-mediated decay of mRNA (based on the frameshift mutations in PDX 134056 and 134206) occurs at the ribosomes, when the mRNA is first translated, leaving some time for newly-transcribed mRNA molecules to be detected prior to degradation. Thus, the increase in mRNA expression of canonical BRCA1 would not be detected on a protein assay (western blot), but the increased D11q transcript expression would be detected. To confirm this, I selected a subset of PDX 134056 tumour samples western blotting with an established and validated assay run by our collaborators (Fox Chase Cancer Centre) due to the notorious difficulty of BRCA1 isoform western blotting. Indeed, only shorter D11q protein isoforms were detectable on this assay in these PDX 134056 samples (**Figure 3.18**).

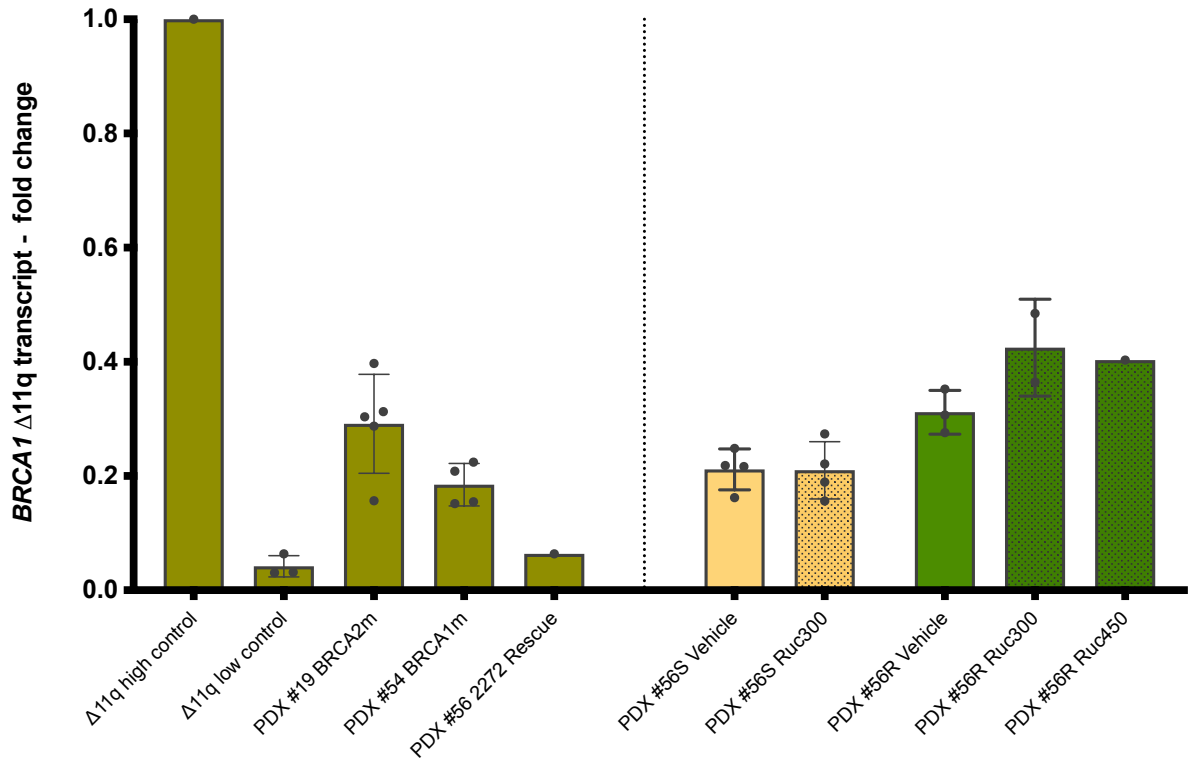


Figure 3.15. Slightly elevated BRCA1 D11q expression in PDX 134056 STH tumours.

BRCA1 D11q is slightly elevated in vehicle #56R samples relative to control PDX model 134054 (p= 0.01), but not 134019 (p= 0.67). There is a statistically significant increase in D11q expression in #56S vs #56R vehicle samples (p= 0.02) but not in #56S vs #56R rucaparib 300mg/kg samples (p= 0.13). Fold-change expression from the D11q high control, the MDA-MB-231 cell line is presented. D11q low control is PDX 134091 sample. Data shows mean +/- SD, where points represent individual PDX tumours (except for D11q low control which are replicates from the same tumour). Data normalized to D11q high control. Ruc300: rucaparib 300mg/kg treated; Ruc450: rucaparib 450mg/kg treated; PDX #19 = 134019; PDX #54 = 134054; BRCA1m = BRCA1-mutant control; BRCA2m = BRCA2-mutant control; Δ11q = D11q; P-values calculated using an unpaired t-test with Welch's correction.

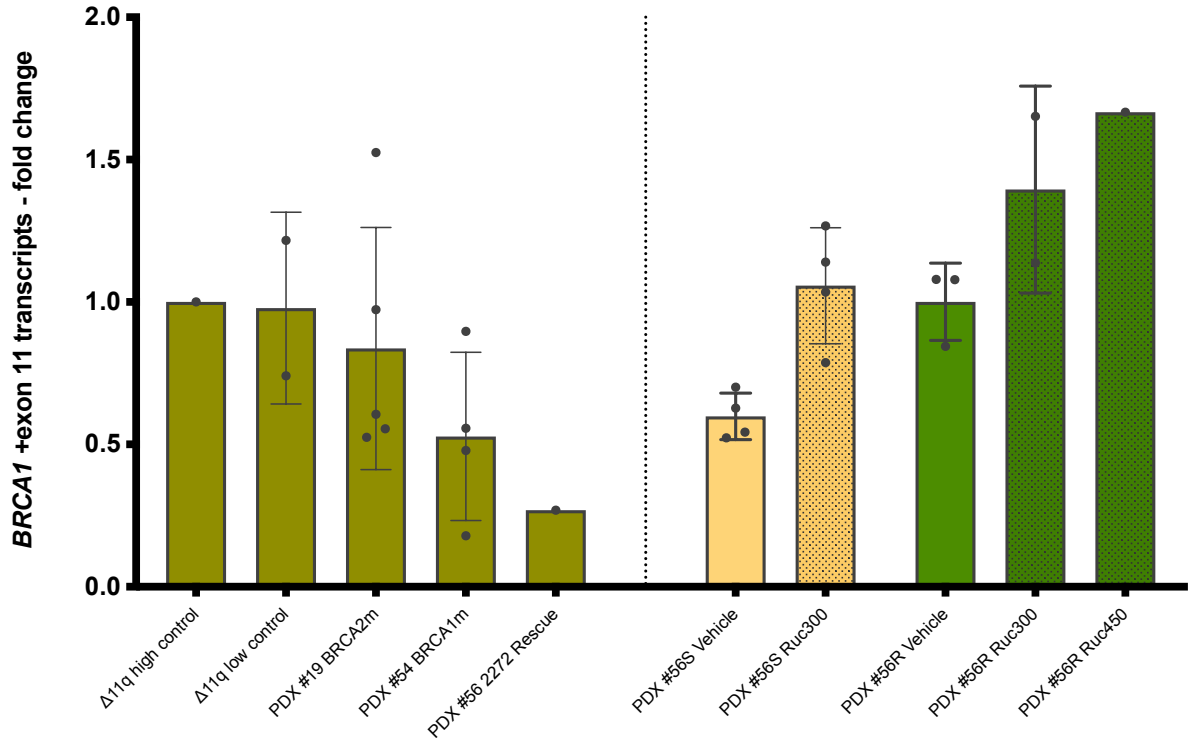


Figure 3.16. BRCA1 exon 11-containing transcript expression in STH PDX 134056 lineage #56S and #56R tumours.

BRCA1 "+ exon 11" transcript expression is higher in vehicle-treated 56R compared to 56S (p-value =0.019). BRCA1 "+ exon 11" transcript expression is not significantly higher in vehicle-treated 56R compared to 56S (p-value =0.396). There is an increase in "+ exon 11" transcript expression in rucaparib-treated #56S compared to vehicle #56S (p-value =0.014). Fold-change expression from the D11q high control, the MDA-MB-231 cell line is presented. D11q low control is PDX 134091 sample. Data shows mean +/- SD, where points represent individual PDX tumours (except for D11q low control which are replicates from the same tumour). Data normalized to D11q high control. Ruc300: rucaparib 300mg/kg treated; Ruc450: rucaparib 450mg/kg treated; PDX #19 = 134019; PDX #54 = 134054; BRCA1m = BRCA1-mutant control; BRCA2m = BRCA2-mutant control; Δ11q = D11q; P-values calculated using an unpaired t-test with Welch's correction.

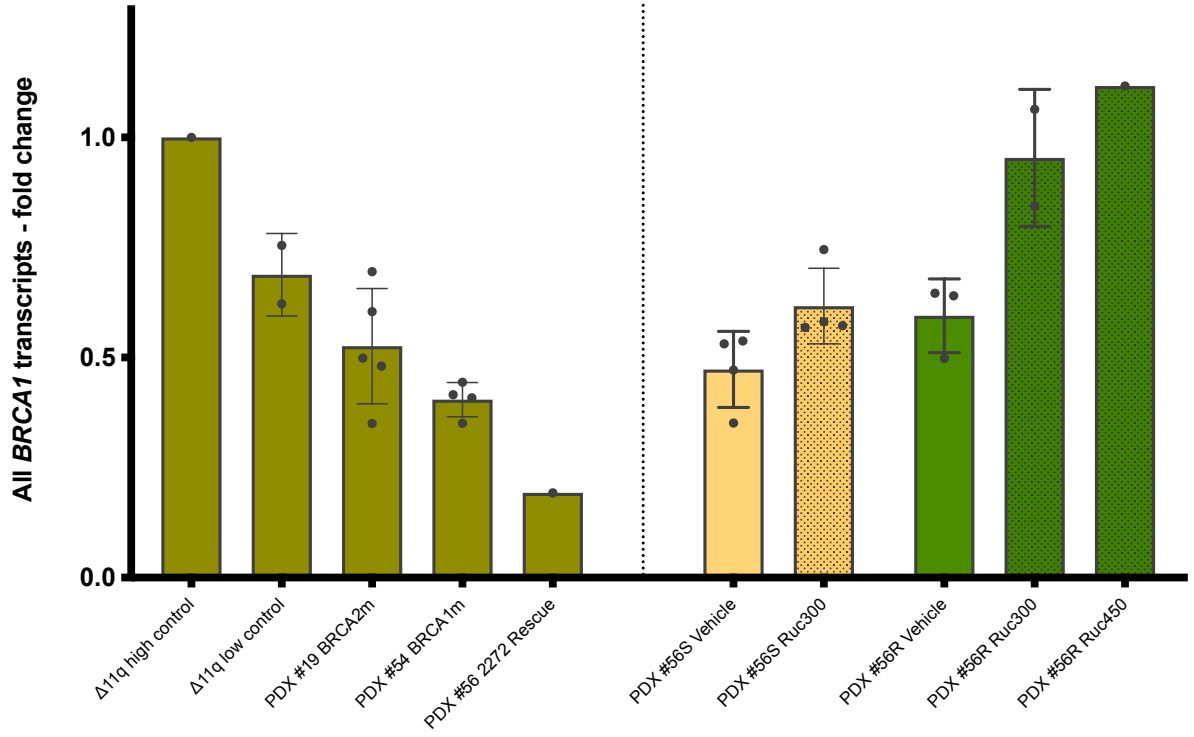


Figure 3.17. "BRCA1 All" expression in STH PDX 134056 lineage #56S and #56R tumours.
"BRCA1 All" transcript expression is not significantly higher in vehicle-treated 56R compared to 56S (p-value= 0.125), or in Ruc300-treated 56R compared to 56S (p-value =0.164). Though the mean expression is increased in Ruc300 #56R compared to vehicle #56R, this difference is not statistically significant (p-value= 0.145). Fold-change expression from the D11q high control, the MDA-MB-231 cell line is presented. D11q low control is PDX 134091 sample. Data shows mean +/- SD, where points represent individual PDX tumours (except for D11q low control which are replicates from the same tumour). Data normalized to D11q high control. Ruc300: rucaparib 300mg/kg treated; Ruc450: rucaparib 450mg/kg treated; PDX #19 = 134019; PDX #54 = 134054; BRCA1m = BRCA1-mutant control; BRCA2m = BRCA2-mutant control; Δ11q = D11q; P-values calculated using an unpaired t-test with Welch's correction.

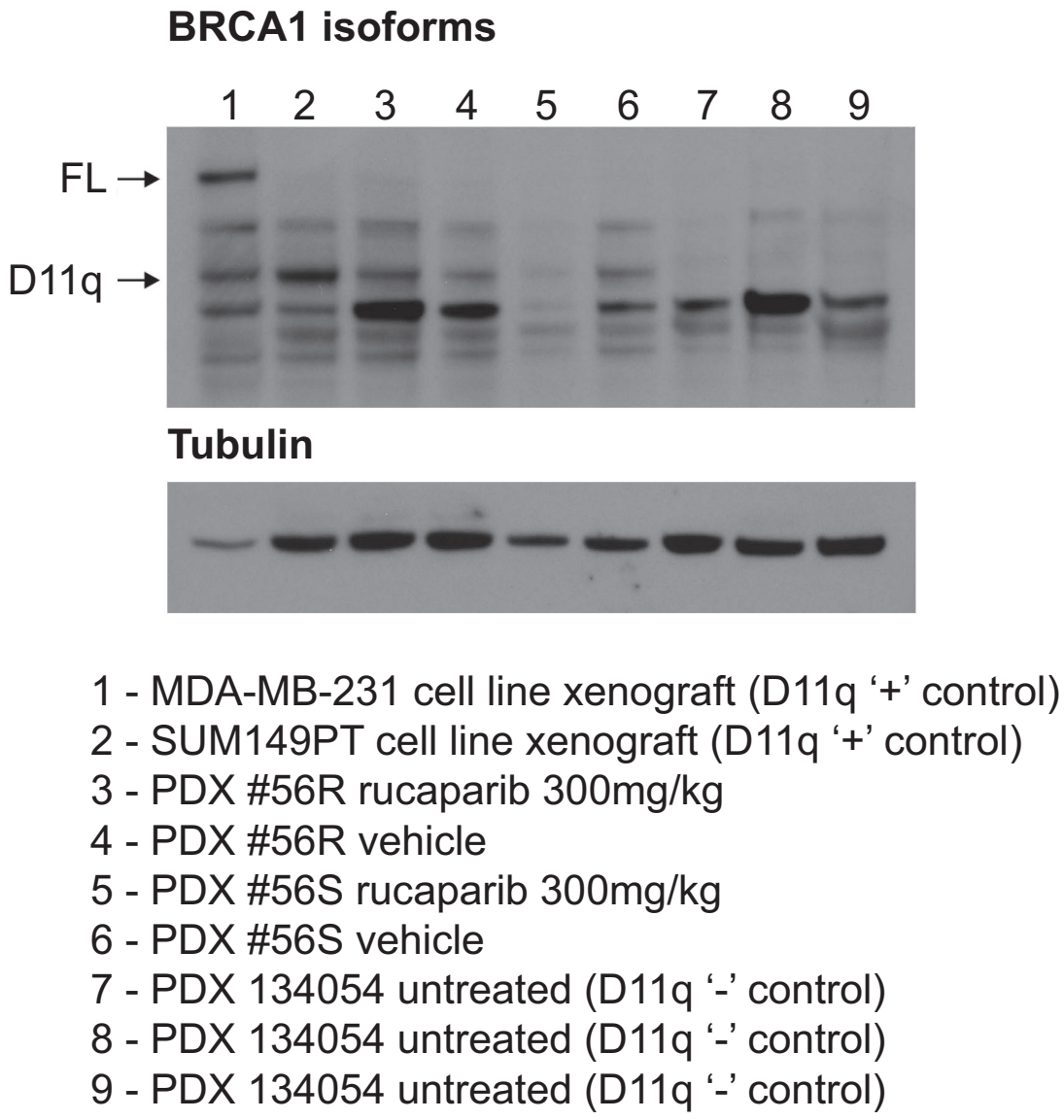


Figure 3.18. Western blot for BRCA1 isoforms in PDX 134056 lineage #56S and #56R tumours.

No full-length BRCA1 protein detected in any PDX 134056 lineage #56S and #56R samples (lanes 3-6), though the D11q isoform is detected. No full-length or D11q BRCA1 detected in PDX 134054 control (lanes 7-9). FL= full-length BRCA1 isoform.

This data suggested that the #56R lineage tumours produce more D11q compared to the #56S lineage, even when untreated. However, the difference in D11q expression could also be due to differences in PDX passage numbers, as most of the STH samples were of a later transplant, compared to the LTH samples. Thus, the relative *BRCA1* D11q transcript expression of each sample (marked by #56 lineage and transplant/passage number) was assessed (**Figure 3.19**).

Two late passage T8 samples, 8062 and 8063, that ended up being LTH in the 56R group ended up having relatively higher expression compared to the other two earlier passage LTH samples (T5-6). *BRCA1* D11q transcript expression was found to be higher in later passages of the #56R lineage compared earlier passages of #56R and also to all #56S tumours (early and late passages; **Figure 3.19**). This may be due to selection of more HR-competent clones with high D11q expression through PDX passaging, which happened to be more pronounced in #56R.

As mentioned earlier these *BRCA1* D11q expression changes are modest (<0.3 fold change expression difference in all D11q comparisons). Such subtle changes may not be biologically significant, thus more functional experiments are required to resolve this.

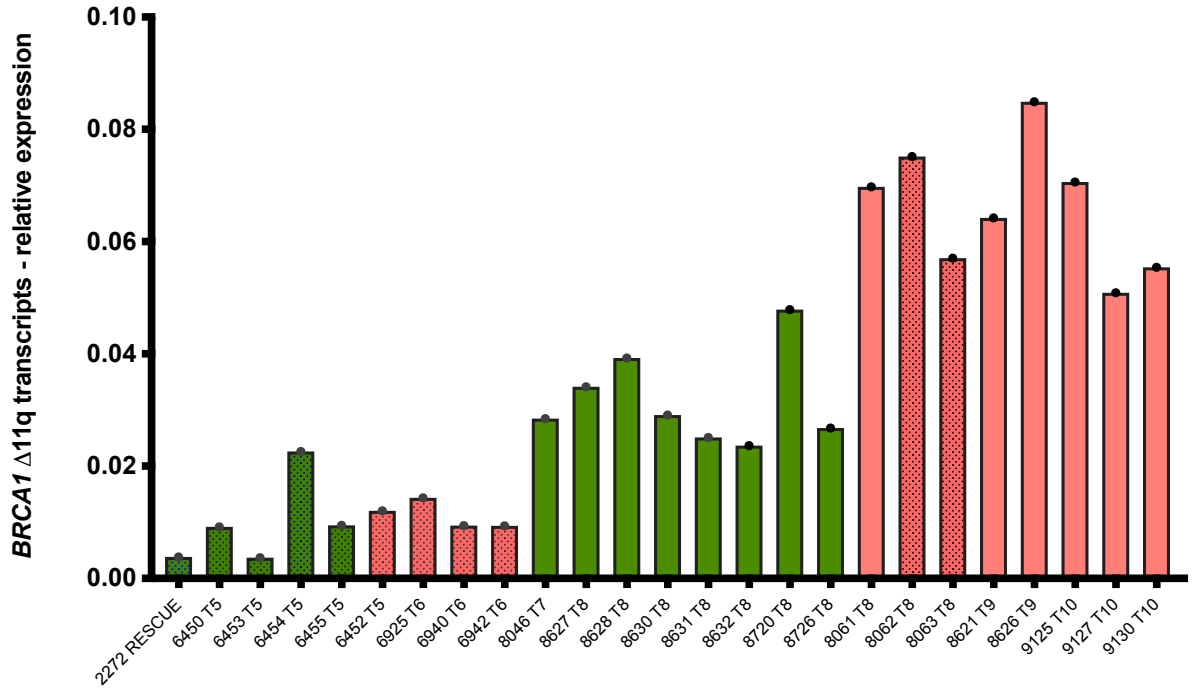


Figure 3.19. BRCA1 D11q expression in PDX 56 associated with higher passage number in the 56R.

Relative BRCA1 D11q transcript expression of both treated and untreated samples are presented here, named by tumour number and transplant number. Pink samples are #56R and green samples are #56S. Shaded samples were LTH, while unshaded samples were STH. Δ11q = D11q. Data shows mean +/- SD, where bars represent individual PDX tumours.

In addition to #56S and #56R lineages, another rescue lineage from a #56 cisplatin-treated mouse (#2105, T2 passage) was established - #56cis. This rescue lineage was shown to be refractory to rucaparib 300mg/kg, but sensitive to cisplatin (**Figure 3.20**; **Table 3.11**).

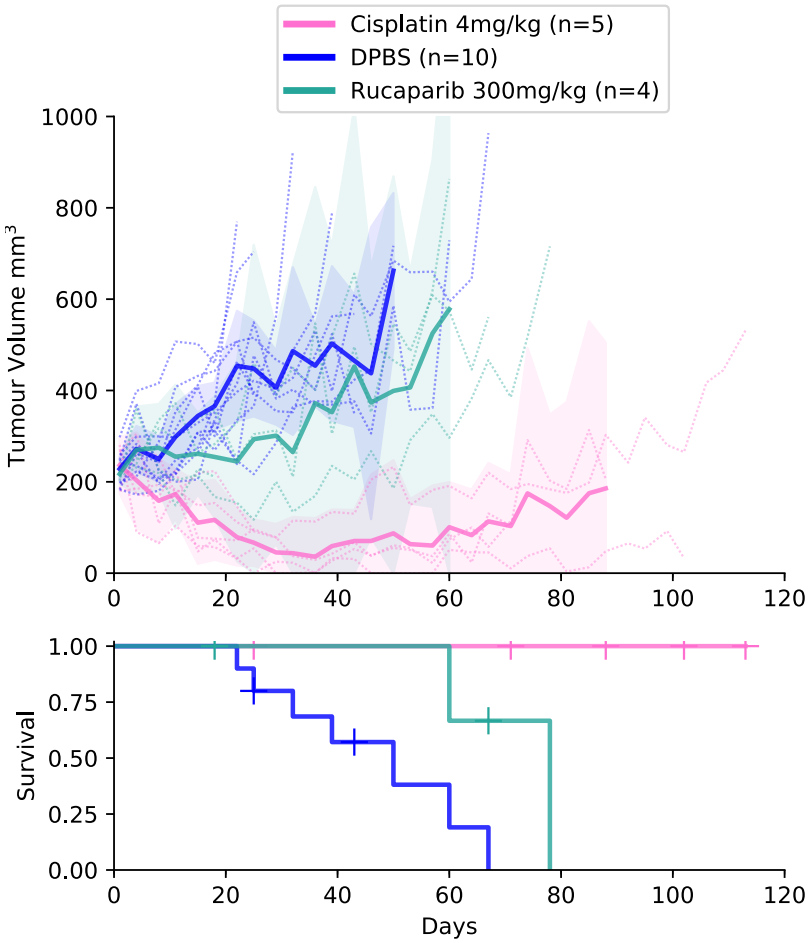


Figure 3.20. PDX 134056 rescue lineage #56cis is refractory to PARPi.

PDX 134056 lineage #56cis is rescued from a cisplatin-treated tumour from the original PDX 134056 PDX lineage and is unrelated to #56S and #56R lineages. This model is sensitive to cisplatin but refractory to rucaparib 300mg/kg. Tumour volume data presented is individual tumour measurements (dashed lines), with mean (bold line) +/- 95% CI (shaded area).

Table 3.11. P-values of PDX 134056 rescue lineage #56cis in vivo responses.

*Referencing data presented in Figure 3.20.*All treated mice censored early due to weight-loss or sickness, TTH measurements may not be reliable.*

Treatment	*p* -value	Median TTH
DPBS	NA	50
Cisplatin 4mg/kg	0.01	88*
Rucaparib 300mg/kg	0.05	78

BRCA1 D11q expression in vehicle-treated #56cis was not significant different to control 134054 (mean expression difference = 0.0232, *p*-value=0.303). Vehicle-treated LTH samples from the PDX #56cis lineage were found to have *BRCA1* D11q expression similar to LTH #56S and #56R samples (mean expression #56cis= 0.156, #56R= 0.154, #56S= 0.2708; **Figure 3.21**). No short-term harvest samples have yet been generated for this lineage, and therefore have not been tested.

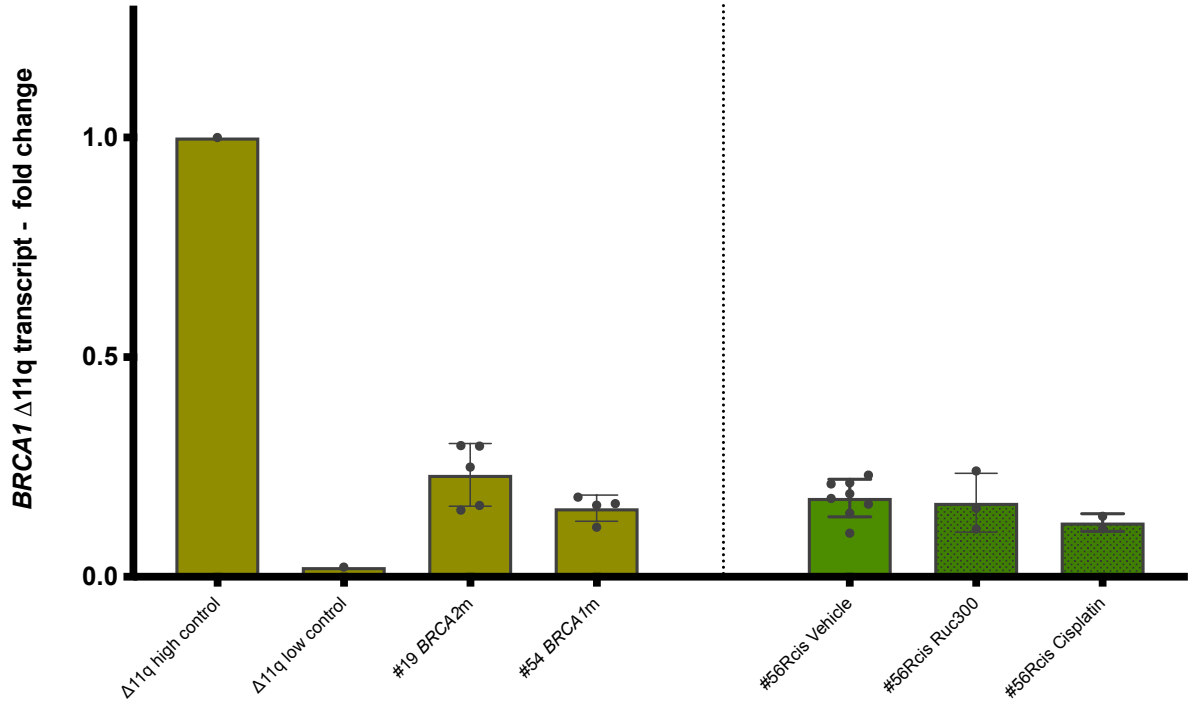


Figure 3.21. BRCA1 D11q isoform expression in LTH PDX 134056 lineage #56cis tumours. *Fold-change expression from the D11q high control, the MDA-MB-231 cell line is presented. D11q low control is PDX 134091 sample. Data shows mean +/- SD, where points represent individual PDX tumours (except for D11q low control which are replicates from the same tumour). Data normalized to D11q high control. Ruc300: rucaparib 300mg/kg treated; Ruc450: rucaparib 450mg/kg treated; PDX #19 = 134019; PDX #54 = 134054; BRCA1m = BRCA1-mutant control; BRCA2m = BRCA2-mutant control; Δ11q = D11q; P-values calculated using an unpaired t-test with Welch's correction.*

3.4.6.3 PDX 134206 results

PDX 134206 is sensitive to PARPi and cisplatin (**Figure 3.22**, **Table 3.12**), despite being derived from a pre-treated patient. LTH samples from the PDX model 134206 were also tested using this assay, and were found to have relatively low D11q expression, despite this model also having a mutation in the 11q region of *BRCA1* (**Figure 3.23**).

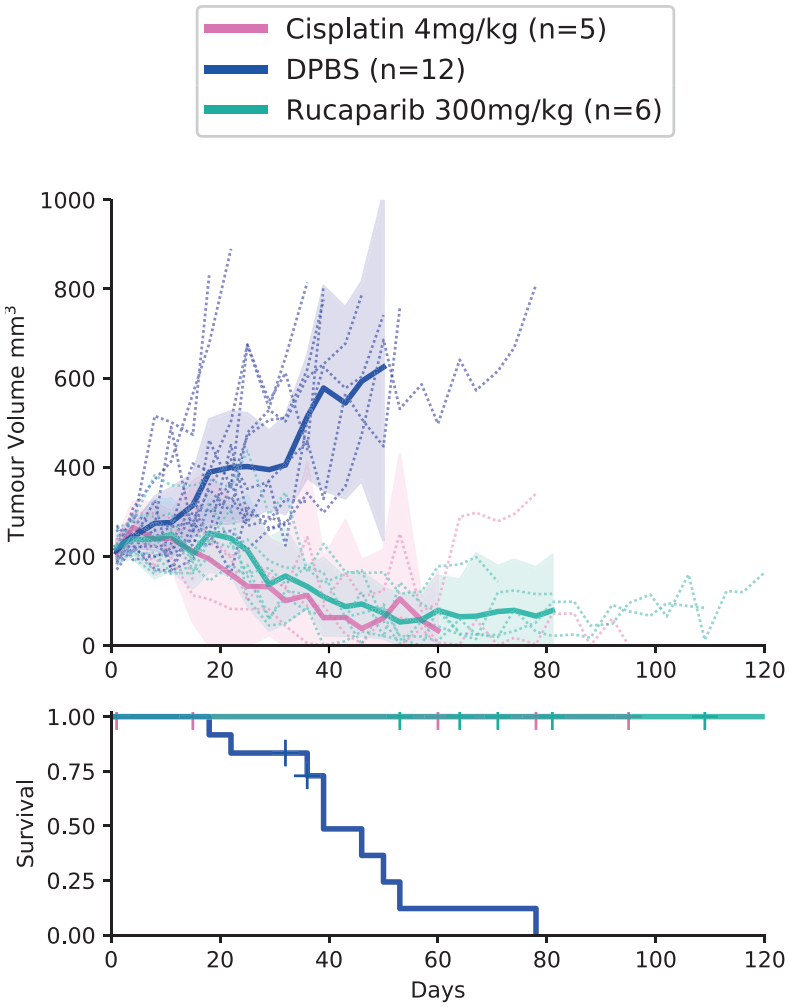


Figure 3.22. PDX 134206 is sensitive to cisplatin and rucaparib.

PDX is derived from a patient treated with 1st line chemotherapy in the clinic. Tumour volume data presented is individual tumour measurements (dashed lines), with mean (bold line) +/- 95% CI (shaded area).

Table 3.12. P-values of PDX 134206 in vivo responses.

*Referencing data presented in figure. *All treated mice censored early due to weight-loss or sickness, TTH measurements may not be reliable.*

Treatment	*p*-value	Median TTH
DPBS	NA	39
Cisplatin 4mg/kg	0.01	60*
Rucaparib 300mg/kg	0.00	76*

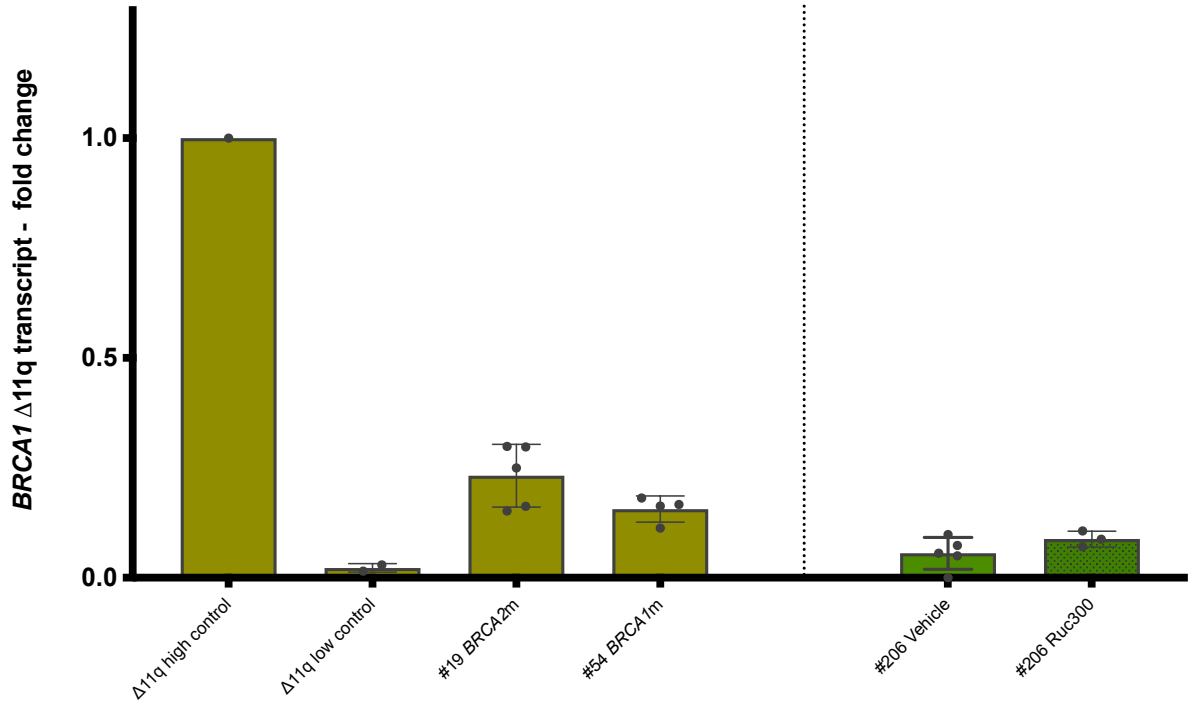


Figure 3.23. BRCA1 D11q isoform expression in LTH PDX 134206 tumours.
PDX 134206 vehicle has reduced D11q expression relative to control 134054 (mean expression values of 0.05547 and 0.1561 respectively, p-value = 0.003). Fold-change expression from the D11q high control, the MDA-MB-231 cell line is presented. D11q low control is PDX 134091 sample. Data shows mean +/- SD, where points represent individual PDX tumours (except for D11q low control which are replicates from the same tumour). Data normalized to D11q high control. Ruc300: rucaparib 300mg/kg treated; Ruc450: rucaparib 450mg/kg treated; PDX #19 = 134019; PDX #54 = 134054; PDX #206 = 134206; BRCA1m = BRCA1-mutant control; BRCA2m = BRCA2-mutant control; Δ11q = D11q; P-values calculated using an unpaired t-test with Welch's correction.

Interestingly, PDX 134206 had relatively high levels of *BRCA1* exon 11-containing transcripts compared to PDX controls (**Figure 3.24**), and this trend was not observed in the analysis of "All *BRCA1*" transcripts – perhaps due to the extremely low levels of D11q transcripts normalizing "All *BRCA1*" expression values. As these transcripts would not be expected to produce a protein due to the deleterious frameshift mutation in D11q, this PDX would still be considered HRD, and is, indeed, very sensitive to PARPi and cisplatin *in vivo* (**Figure 3.22**). However, it is still important to consider that these are LTH samples, and that STH samples may reveal different *BRCA1* expression profiles.

There were also more post-treatment samples (134206B and 134206C - post-second-line platinum and olaparib) subsequently acquired from the patient and transplanted into mice. However, no PDX models resulted from these transplants, and therefore there were no PDX samples to test.

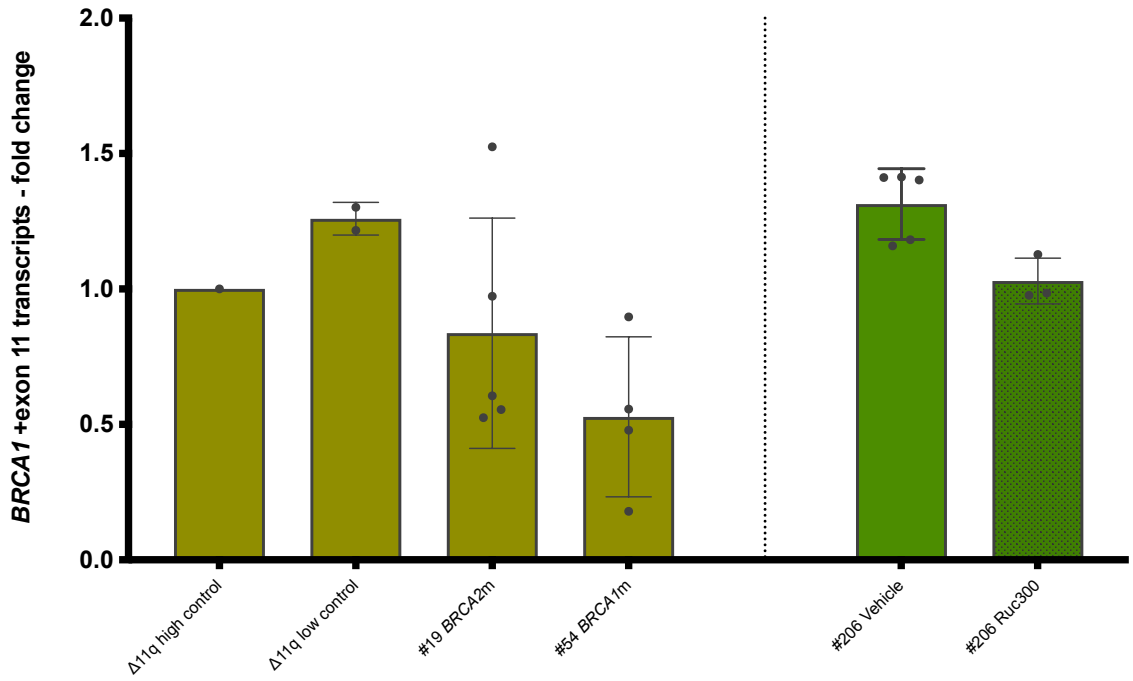


Figure 3.24. BRCA1 exon 11-containing transcript expression in LTH PDX 134206 tumours.

PDX 134206 vehicle has elevated "+exon 11" transcript expression relative to control 134054 (mean expression values of 1.314 and 0.5281 respectively, p-value = 0.008). Fold-change expression from the D11q high control, the MDA-MB-231 cell line is presented. D11q low control is PDX 134091 sample. Data shows mean +/- SD, where points represent individual PDX tumours (except for D11q low control which are replicates from the same tumour). Data normalized to D11q high control. Ruc300: rucaparib 300mg/kg treated; Ruc450: rucaparib 450mg/kg treated; PDX #19 = 134019; PDX #54 = 134054; PDX #206 = 134206; BRCA1m = BRCA1-mutant control; BRCA2m = BRCA2-mutant control; Δ11q = D11q.

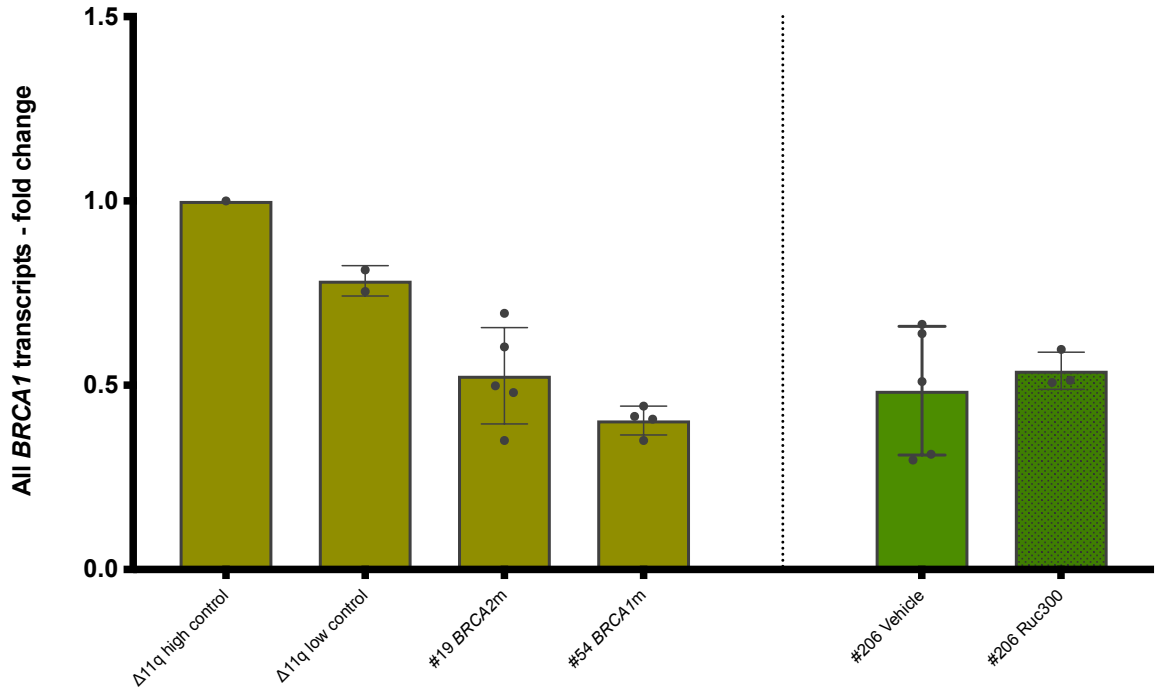


Figure 3.25. "BRCA1 All" expression in LTH PDX 134056 lineage #56cis tumours.
PDX 134206 vehicle has "BRCA1 All" transcript expression similar to that of control 134054 (mean expression values of 0.4852 and 0.4044 respectively, p-value = 0.37). Fold-change expression from the D11q high control, the MDA-MB-231 cell line is presented. D11q low control is PDX 134091 sample. Data shows mean +/- SD, where points represent individual PDX tumours (except for D11q low control which are replicates from the same tumour). Data normalized to D11q high control. Ruc300: rucaparib 300mg/kg treated; Ruc450: rucaparib 450mg/kg treated; PDX #19 = 134019; PDX #54 = 134054; PDX #206 = 134206; BRCA1m = BRCA1-mutant control; BRCA2m = BRCA2-mutant control; Δ11q = D11q.

3.4.7 Screening for C-NHEJ gene mutations

As described in Chapter 1, C-NHEJ DNA repair pathway genes have been shown to cause PARPi resistance in certain HRD contexts. Deleterious mutations in critical C-NHEJ genes *XRCC5*, *XRCC6*, *PRKDC*, *LIG4*, *XRCC4* and *DCLRE1C* were screened for using BROCA sequencing. No C-NHEJ gene mutations were detected in any of the PDX samples tested by BROCA (appendix A-C). As there are other mechanisms of protein inactivation beyond gene mutation, such as epigenetic silencing and targeted protein degradation, C-NHEJ protein screening was performed on our HGSOC PDX models and is covered in more detail in Chapter 4.

3.4.8 CHD4 mutation in PDX #134019

Loss of nucleosome remodelling factor CHD4 has been shown to cause resistance to DNA-damaging agents in *BRCA2*-mutant HGSOC cells *in vitro*, without restoration of HR DNA repair (Guillemette et al., 2015). This protein was identified in RNAi screening in *BRCA2*-mutant cancer cells, and further investigated using a panel of cell lines. Interestingly, clones of cell line PEO1 that were driven to cisplatin resistance were shown to still be HRD but had reduced *CHD4* expression. Authors demonstrated that this was due to RAD18-dependant trans-lesion synthesis bypass, leading to increased mutation frequency but reduced radial-chromosomes that would cause cell-cycle arrest. It was also found that low *CHD4* expression in the TCGA dataset correlated with poor survival in *BRCA2*-mutant cancers (Guillemette et al., 2015).

A *CHD4* mutation (NM_001273.5:c.4226_4236del; p.Asn1410Thrfs*4) was discovered at a variant allele frequency of 17.6% in a 100% purity in a vehicle-treated PDX 134019 tumour (mouse/tumour #2109) during BROCA screening. This mutation is located at the very end of exon 28, causing an out of frame deletion that creates a new, earlier donor splice site. This new donor splice site causes the frameshift to continue into the start of exon 29, which in turn leads to a premature stop codon after 4 bases (**Figure 3.26**). It is important to note, given the variant allele frequency of this *CHD4* mutation (17.6%), that this mutation was likely subclonal and may have been present in a heterozygous state, and thus only be leading to lower gene dosage in the cells with this mutation, instead of complete *CHD4* deficiency.

```
Wildtype: GGT.GGG.AAT.ATT.GAA^GTA.CTT.GGT.TTT.AAT = GGNIEVLGFN

Mutant:   GGT.G--------------^.GT.ACT.TGG.TTT.TAA = GGTWF*
```

Figure 3.26. Consequences of CHD4 mutation c.4226_4236del (p.Asn1410Thrfs*4).
Based on the human genome build hg38 sequence, codons for WT and mutant nucleotide sequences shown on left, and corresponding protein sequences on the right. ^exon 28 - exon 29 boundary. Highlighted in blue are the codons creating three new amino acids and a premature stop signal.

As there was no cryo-preserved material available for tumour #2109 for further transplantation (this tumour was harvested before reaching harvest tumour volume), I screened other tumours within this rucaparib and cisplatin sensitive PDX model (**Figure 3.27**) for *CHD4* variants. Tumours that were derived from the same source tumour as #2109 (tumour #645) along with a selection of treated and untreated tumours from other PDX 134019 lineages were tested on the BROCA panel (**Table 3.13**). Furthermore, treated and untreated tumours from a matched post-treatment PDX 134019B model were also screened. PDX 1340139B is a model derived from an AOCS patient 134019 tumour following 1st-line carboplatin/paclitaxel in the clinic, as opposed to PDX 134019 which was chemonaïve. Only one other tumour had a detected *CHD4* mutation, and it was different to the deletion detected in tumour #2109. PDX 134019 sample #3423 had a 16 base-pair frameshift insertion in exon 17 of *CHD4* (NM_001273.5:c.2425_2426ins16) detected in 4 reads, hence was likely a subclonal event. No deleterious *CHD4* mutations were detected in any other PDX 134019/134019B tumours screened by BROCA (**Table 3.13**).

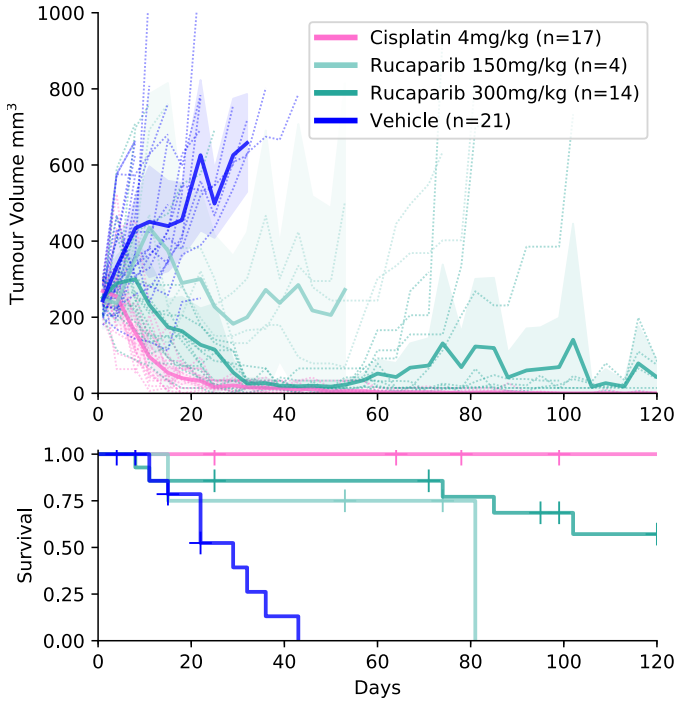


Figure 3.27. In vivo cisplatin and rucaparib responses of PDX 134019.
PDX 134019 is sensitive to both cisplatin (4mg/kg dose) and rucaparib (300mg/kg dose). Data published in (Kondrashova et al., 2018). Tumour volume data presented is individual tumour measurements (dashed lines), with mean (bold line) +/- 95% CI (shaded area).

Table 3.13. PDX 134019 and 134019B samples screened for CHD4 deletion.

*PDX 134019 samples 3423 and 2109 had detectable genomic defects in CHD4. *only deletion/insertion read number was provided in BROCA run MH80, without reference read #, thus deletion/insertion frequencies could not be calculated. The deletion/insertion sequences were also not provided.*

PDX	BROCA run (version)	Mouse/ tumour #	Treatment	Transplant number	Expected TP53 Mutation	TP53 Mutation Frequency	CHD4 defect (frequency/reads*)
134019	MH68 (v6)	2109	Vehicle	T3	c.463A>C p.T155P	1	c.4226_4236del (17.6%)
134019		2048	Untreated	T4		0.96	Undetected
134019	MH80 (v7)	2109	Vehicle	T3		1	c.4226_4236del (48 reads)
134019		2108	Untreated	T3		1	Undetected
134019		2110	Untreated	T3		1	Undetected
134019		2112	Untreated	T3		1	Undetected
134019		2113	Untreated	T3		1	Undetected
134019		3423	Rucaparib 300mg/kg	T4		0.97	c.2425_2426ins (4 reads)
134019		3042	Rucaparib 300mg/kg	T5		1	Undetected
134019		3046	Vehicle	T5		1	Undetected
134019		2342	Vehicle	T3		1	Undetected
134019		2280	Vehicle	T3		0.94	Undetected
134019B		4614	Rucaparib 300mg/kg	T3		0.97	Undetected
134019B		4694	Rucaparib 300mg/kg	T2		1	Undetected
134019B		3501	Cisplatin	T2		1	Undetected
134019B		3502	Cisplatin	T2		1	Undetected
134019B		3505	Cisplatin	T2		1	Undetected
134019B		3506	Cisplatin	T2		1	Undetected
134019B		3753	Vehicle	T2		1	Undetected
134019B		4698	Vehicle	T2		0.97	Undetected

3.5 Discussion

The characterisation work undertaken as part of my PhD has enabled us to explain PARPi treatment responses, and identify mechanisms of PARPi sensitivity and resistance within our HGSOC PDX cohort.

3.5.1 Reversion mutation screening is crucial for understanding platinum and PARPi responses in PDX

BRCA1 and *BRCA2* reversion mutations that restore functional HR DNA repair are the most commonly observed resistance mechanism in the clinic, but have mostly been reported post-platinum chemotherapy, with limited reports post-PARPi (Barber et al., 2013; Norquist et al., 2011). This was, therefore, an important mechanism of PARPi resistance to screen for within the HRD HGSOC PDX cohort. Two PDX models, 34931 and 134143B, were found to have such secondary HR gene mutations in *BRCA1* and *RAD51C* respectively. These are both from patients with recurrent tumours post-treatment.

Though this model was not screened by me, it is important to note that PDX 134143 had a *RAD51C* reversion mutation, originally detected in patient in the ARIEL2 clinical trial and characterized by our group (Kondrashova et al., 2017). This patient responded to 1st line platinum chemotherapy and was responding to PARPi until an enlarging groin lymph node was detected following 11 months of rucaparib treatment. This lymph node tumour sample contained four distinct secondary mutations that all restored the open reading frame of *RAD51C*, though only one of these was detected in the corresponding PDX (Kondrashova et al., 2017). In contrast, PDX 34931 was derived from a patient who had received 9 lines of chemotherapy and no PARPi. The secondary mutation in PDX 34931 explains why it is refractory to both PARPi and platinum *in vivo*.

Although PDX 134206 was post chemotherapy and did not have any detectable reversion mutations, it is possible that subsequent post-PARPi tumour samples 134206B and 134206C from the same patient may have reversion mutations in their *BRCA1* gene that revert sequence to WT, given their lower primary mutation frequencies (88% and 57% respectively). However, this is currently unclear due to human stroma contamination in these tumour samples. Unfortunately, H&E staining of a different piece of each tumour did not clarify these results,

with 134206B having no tumour in the section and 134206C having only 10% tumour. Thus, to enable interpretation of the WT sequencing reads in these samples, I will run *TP53* mutation sequencing to estimate the tumour purity in the same DNA samples.

These models not only allow us to characterize novel secondary mutations that have not been reported previously (e.g. in the *RAD51C* gene of PDX 134143B), but also now provide us with a platform to study novel therapeutic strategies for overcoming PARPi resistance these PDX. Several potential approaches for overcoming resistance caused by secondary mutations have been reported, though these are often based on pharmacological inactivation of HR using other drugs (Dhillon et al., 2011). Such combinations could be further trialled *in vivo* using our HGSOC PDX with restored HR DNA repair.

3.5.2 Tumour heterogeneity influences PARPi responses

The high degree of genomic instability in these tumours provides fertile ground for the development of new mutations and molecular defects that can, in turn, impact drug responses. Thus, re-testing the same models is critical for identifying mechanisms of resistance that may arise spontaneously or under treatment pressure, as we have examples of both in our HGSOC PDX cohort. However, this genomic instability also generates a large degree of molecular heterogeneity that must be considered when studying these models. For example, PDX 134056S and 134056R lineages were derived from the same rucaparib 150mg/kg- treated mouse, but ended up having strikingly different responses to rucaparib, despite the same degree of treatment pressure having been applied initially. The D11q isoform of *BRCA1* may be playing a role in this difference, or there may be additional contributing factors. Whatever the underlying mechanism, the divergence of treatment responses in these two lineages of PDX 134056 is likely to be driven by tumour heterogeneity.

In contrast, the *CHD4* mutation detected in a single untreated tumour of PDX 134019 appears to have arisen spontaneously. This mutation was only detected due to the comprehensive mutation screening strategy employed as part of my PhD, and underscores the impact that genomic instability-driven tumour heterogeneity can have on the evolution of drug resistance. It would be interesting to follow-up on the PDX 134019 *CHD4*-mutant tumour #3423, confirming whether this variant is real, perhaps using targeted sequencing approaches, and whether it can be detected in other parts of the tumour. If this variant is real and present at a

high enough frequency, the #3423 tumour material can be thawed and transplanted to establish a new lineage of PDX 134019 which harbours a *CHD4* defect. This would then provide us with an *in vivo* model to study the effects of *CHD4* deficiency on PARPi responses and replication fork stability. It would also be possible to induce these lesions in PDX 134019 directly using CRISPR gene editing, or in other models of *BRCA2*-mutant HGSOC. Genome-wide PARPi-resistance CRISPR screens have been performed on *BRCA2*-mutant cell line PEO1 as part of my PhD (results discussed in chapter 4), however *CHD4* loss was not found to be a resistance mechanism in these experiments.

3.5.3 The power of PDX models for the study of HR gene methylation

In contrast to the examples given above, some aspects of HGSOC PDX tumour biology have proven to be very homogeneous. This is most evident in our studies of HR gene methylation, where we have discovered that the zygosity *BRCA1* methylation predicts PARPi response in HGSOC (Kondrashova et al., 2018).

This discovery would not have been made without the PDX tumour samples from our cohort combined with human-specific methylation assays. This is due to the complexity of accurately measuring methylation of HR gene alleles when there is contaminating non-tumour tissue present in samples. PDX samples, in this sense, are clean as they are 100% human tumour, and enable very clear and consistent methylation and gene expression measurement. PDX models 134048 and 134169 with heterozygous gene methylation (one *BRCA1* allele methylated and one unmethylated) were consistently found to have 50% methylation on quantitative methylation assays, while homozygous me*BRCA1* PDX models 134062 and 134011 were found to consistently have 100% methylation (Kondrashova et al., 2018). This is reflected in the qPCR experiments presented in this chapter, where PDX 134048 and 134169 have *BRCA1* gene expression, while 134062 and 134011 do not. HR gene methylation zygosity is discussed in more detail in chapter 5, where I describe methylation of the *RAD51C* gene promoter in two unique HGSOC PDX models.

3.5.4 No PARP1 or C-NHEJ pathway mutations detected in PDX

Interestingly, no deleterious mutations in the *PARP1* gene were detected during BROCA screening of pre- and post- treatment PDX tumours. In one recent study, mutations affecting

DNA binding of *PARP1* were reported to cause PARPi resistance in *BRCA1* D11q-mutant pre-clinical models and in one *BRCA1/2* WT HGSOC patient via loss of PARP-trapping ability (Pettitt et al., 2016). The authors of this work proposed some residual HR activity is required for this resistance mechanism to develop, as it was not detected in HRD models, and inducing HRD by silencing *BRCA1/2* caused lethality in cell line models with *PARP1* mutations (Pettitt et al., 2016). Indeed, early studies of PARPi and HRD synthetic lethality showed that PARP1 silencing using siRNA was synthetic lethal with *BRCA1*/*2* loss, in both *TP53* proficient and deficient backgrounds (Bryant et al., 2005; Farmer et al., 2005). In contrast, other studies have shown that *PARP1* loss causes PARPi resistance in *BRCA1/2*-mutant cells via replication fork stabilization (Ding et al., 2016; Ray Chaudhuri et al., 2016). Though I have produced some *in vitro* evidence to suggest that PARP1 mutations can cause PARPi resistance in *BRCA2*-mutant cells (Chapter 4), this is yet to be confirmed/detected *in vivo* in our PDX models, or in patient samples we have screened.

There were also no C-NHEJ pathway gene mutations detected in any of the PDX samples screened by BROCA sequencing. As C-NHEJ loss has been described as a PARPi resistance mechanism, with more evidence available for early pathway proteins (e.g. *53BP1*) where their loss restores HR DNA repair in *BRCA1*-mutant cells (AlHilli et al., 2016; McCormick et al., 2017; Patel et al., 2011; Williamson et al., 2012), I interrogated the BROCA sequencing data for these hits. None of the PDX models screened during my PhD, and even before my PhD, were found to have any C-NHEJ gene defects. However, gene expression and protein defects can be missed when only considering gene mutations, therefore C-NHEJ protein losses were also screened for during my project, and these results are presented in more detail in Chapter 4.

3.5.5 Re-treatment studies to drive resistance

This study was potentially limited by the lack of PDX models where cyclical re-treatment with PARPi could be carried out. This would be an effective method for driving resistance in a given PDX model, and has been done for certain models within the cohort (*RAD51C* methylation project, presented in chapter 5). This was not carried out in many HRD models during my PhD due to limited space and resources for this type of *in vivo* study. In future, setting up more PARPi re-treatment experiments to drive resistance in different PDX models would be extremely informative. Some potentially interesting models to consider would be the

homozygous *BRCA1*-methylated models (in an effort to drive *BRCA1*methylation loss), and *BRCA1* D11q-mutant models PDX 134056 and 134206 (to drive increased *BRCA1* D11q expression). These re-treatment experiments should also be performed in PDX models with non-*BRCA1* defects, given that (excluding reversion mutations) resistance mechanisms in these models are less likely to involve restored HR DNA repair and are not as well-studied.

3.5.6 Measuring HR competence in PDX

Given the importance of HR DNA repair status in predicting responses to PARPi, a functional HR assay would be very informative in these studies. For example, the 134148 *BLM*-mutant PDX, would be extremely interesting to test for HR capacity given that *BLM* has not been established as a *bone fide* HR gene. Instead, it appears to play a more regulatory role in HR DNA repair, with its loss leading to increased sister-chromatid exchanges in cells – a marker of hyperactive HR DNA repair. Mutations in *BLM* are common in certain populations (e.g. Ashkenazi-Jewish) and are considered breast cancer pre-disposition genes. Given our PDX model of a *BLM*-mutant HGSOC did not respond to PARPi, it would be clinically important to understand its role in HR DNA repair and its potential for sensitizing tumour cells to PARPi.

RAD51 foci formation is considered the gold-standard marker for proficient HR DNA repair. This method can be performed on cell lines quite readily, but becomes more difficult when carried out on tissue samples. Through my PhD, I developed a novel, highly automated assay for the detection of foci, though this protocol has only been successfully applied to 3 PDX models (134183, PH039 and PH038 - results covered in Chapter 5), given the sensitivity of other PDX models to tumour digestion. Through further optimization, however, it is possible that this method could be used to measure DNA repair in remaining PDX models within our cohort in future.

3.5.7 Future studies of immune interactions in HGSOC PDX

A key limitation of the work presented in this chapter is that the PDX are engrafted into immune-compromised mice. The lack of a fully functioning immune system in these models is a limiting factor in studies of PARPi, given accumulating evidence that PARPi can be immunogenic, triggering the cGAS-STING response in tumours independently of *BRCA* gene

defects (Shen et al., 2019). Thus, humanized mice would be ideal for the study of PARPi and immune interactions, and are currently being investigated for other projects within our group.

3.5.8 Further characterisation of PDX models

Molecular and functional characterisation efforts will also continue for new HGSOC PDX models generated by our laboratory, thereby expanding on this already valuable resource for pre-clinical research. Most models have also been sequenced by WGS and RNA-seq, whereby their mutational and broader gene expression signatures can be interrogated. Full analysis of this data is currently underway and may reveal further biological mechanisms influencing platinum and PARPi responses in this HGSOC PDX cohort.

4 DNA repair pathways and PARPi sensitivity and resistance

4.1 Introduction

Since the discovery that PARPi exert a synthetic lethal effect in HRD cells, considerable effort has been invested in uncovering the underlying mechanism of this lethality and, consequently, potential mechanism of PARPi resistance. PARP1 has a well-known role in DNA repair and, given the sensitivity of HRD cells to PARPi, it was naturally believed that DNA repair balance was playing a primary role in PARPi toxicity in these cells. Multiple DNA repair pathways have been implicated in PARPi sensitivity and resistance contexts aside from HR, including BER, C-NHEJ and alt-EJ. It is possible that PARPi directly affect each of these pathways independently, or that there is some single overarching action of PARPi that in turn influences these pathways in HRD backgrounds. Unfortunately, due to their complexity, these interactions have not yet been fully explained. Thus, a better understanding of alternative DNA repair pathways taking over repair processes when PARP1 is inhibited in HRD cells is required in order to design more effective therapeutic approaches and overcome PARPi resistance in the clinic.

4.1.1 Role of C-NHEJ

Multiple theories have been proposed for PARPi-induced synthetic lethality (these are covered in detail in Chapter 1), however, none of these have been able to adequately explain the evidence of *in vitro* and *in vivo* resistance to PARPi that develops in HRD cells upon loss of C-NHEJ proteins Artemis, DNA-PKcs and Ku70/Ku80 (Patel et al., 2011; Jaspers et al., 2013; Somyajit et al., 2015; AlHilli et al., 2016). Upstream C-NHEJ factors 53BP1, REV7 and RIF1 have been demonstrated to cause resistance to PARPi in a *BRCA1* mutant setting, but this is via restored HR that is only possible in *BRCA1*-deficient cells due to the early pathway activity and competition of these proteins. Based on these studies, it appeared that functional C-NHEJ is a requirement for PARPi-induced cytotoxicity in HRD cells. Understanding the exact mechanism underlying C-NHEJ loss related resistance to PARPi could be crucial for improving PARPi responses in patients.

There is some evidence that PARPi-HRD synthetic lethality may depend on de-regulation of the C-NHEJ nuclease, Artemis. Artemis is a versatile exo- and endonuclease of the metallo-β-

lactamase protein family. It is involved in DNA DSB end-processing following endogenous or exogenous DNA damage, or during controlled V(D)J recombination in developing immune cells. All DNA breaks processed by Artemis are subsequently repaired by the C-NHEJ repair pathway. Artemis exerts 5' to 3' exonuclease activity upon phosphorylation by ATM, but its endonuclease activity is dependent on interaction with auto-phosphorylated DNA-PKcs (the catalytic subunit of DNA-PK) and the presence of Ku70/80 (Chang et al., 2015; Goodarzi et al., 2006; Lobrich et al., 2005; Ma et al., 2005; Riballo et al., 2004). Patients lacking Artemis suffer severe combined immunodeficiency (SCID) due to defects in antibody formation, and are extremely radiosensitive (Dvorak et al., 2010; Moshous et al., 2001). A study investigating the potential of Artemis gene-transfer for the treatment of SCID revealed that overexpression of Artemis induced DNA DSBs and apoptosis in mammalian cells as a result of excessive Artemis endonuclease activity (Multhaup et al., 2010). Later, Artemis overexpression was found to be responsible for the extreme radio-sensitivity and elevated apoptosis of human fibroblast cell lines 84BR and 175BR (Ulus-Senguloglu et al., 2012). Besides its role in the repair of DNA DSBs, Artemis has also been shown to contribute to break-down of high molecular weight DNA during early stages of apoptosis via its DNA-PK-dependent endonuclease activity (Abe et al., 2008; Britton et al., 2009). It is unclear whether this cleavage of high-molecular weight DNA is site-specific or random (Britton et al., 2009), and whether it occurs the same way in cells with deregulated Artemis endonuclease activity.

Thus, under certain conditions, Artemis transforms from a DNA DSB repair protein into a DNA DSB-generating nuclease. I hypothesized that in the context of HRD cells treated with PARPi, multiple negative regulators of C-NHEJ (HR pathway and PARP1 protein) are removed, disinhibiting DNA-PK and Artemis and resulting in C-NHEJ-driven degradation of the genome. I also hypothesized that other DNA repair inhibitors that further disinhibit C-NHEJ/Artemis may synergize with PARPi and present potential therapeutic options for PARPi-resistant patients.

4.1.2 Pre-clinical HGSOC models with C-NHEJ loss

To study C-NHEJ loss as a mechanism of PARPi resistance in *in vivo* setting, our group, in collaboration with the Kaufmann group at the Mayo Clinic, screened a selection of PDX models from our HGSOC PDX cohort (described in Chapter 3) for C-NHEJ protein loss by Western Blot (WB). Much of this work was carried out prior to my PhD.

Five HGSOC PDX models with a range of HR defects were sent for WB analysis of 7 C-NHEJ proteins: 53BP1, Ku70, Ku80, DNA-PKcs, XRCC4, Ligase 4 and Artemis. A total of 72 PDX samples were assessed by this WB multi-protein panel. A number of PDX models assessed showed loss of one or more C-NHEJ proteins (**Table 4.1**), suggesting that loss of C-NHEJ is a common event in HRD HGSOC.

Table 4.1. Summary of C-NHEJ western blot results for HRD PDX models.

PDX	PDX HR defect	PARPi response	Treatments tested	No Loss	Single Loss	Multi-Loss	If Single Loss
134019	***BRCA2* mutation**	Response, CR	Vehicle, rucaparib 150mg/kg, cisplatin	1	3	4	53BP1, Ligase 4 or Artemis
134056	***BRCA1* mutation**	Response, SD	Vehicle, rucaparib 150/300mg/kg, cisplatin	4	3	7	53BP1 or Ligase 4
134013	***BRCA2* mutation**	Response, SD	Vehicle, rucaparib 150/300mg/kg, cisplatin	8	9	7	Ku70, 53BP1, Ligase 4 or Artemis
134054	***BRCA1* mutation**	Refractory, PD	Vehicle, rucaparib 300mg/kg, cisplatin	2	2	4	53BP1
134062	***BRCA1* methylation**	Response, SD	Vehicle, rucaparib 150/300mg/kg, cisplatin	7	5	6	Ku70 or Artemis

Based on this data, our group established four lineages of *BRCA2*-deficient PDX 134013 from cryopreserved minced tumour material, where original tumours were found to have varying degrees of C-NHEJ loss by WB (lineages transplanted in 2015, **Table 4.2**). Lineage 1 (tumour 1373) was generated from a rucaparib 150mg/kg treated mouse where loss of Lig4 was detected. Lineage 2 (tumour 1440) was generated from a vehicle-treated tumour where C-NHEJ was intact. Lineage 3 (tumour 1734) was generated from a 2x cycle cisplatin-treated tumour where losses of Ku70 and Ku80 were detected. Lineage 4 (tumour 1616) was generated from a 3x cycle cisplatin-treated tumour where multiple C-NHEJ protein losses were detected (**Table 4.2**). We expected lineages 1,3 and 4 with C-NHEJ loss detected to be resistant to PARPi compared to Lineage 2 where C-NHEJ appeared to be intact. These four lineages of PDX134013, as well as initial WB results of the other PDX models, formed the foundation for the work presented in this chapter.

Table 4.2. Established PDX 134013 C-NHEJ loss lineages

PDX 134013 Lineage	Lineage 1	Lineage 2	Lineage 3	Lineage 4
Source tumour/ mouse	**1373**	**1440**	**1734**	**1616**
Passage	T4	T4	T4	T4
Line of treatment	Rucaparib 150mg/kg 1 cycle	Vehicle 1 cycle	Cisplatin 4mg/kg 2 cycles	Cisplatin 4mg/kg 3 cycles
Days to harvest	82	62	87	76
C-NHEJ losses	Lig4	None	Ku70, Ku80	"Multiple"

In this Chapter, I explored the regulation and interaction of DNA repair mechanisms in the context of HR deficiency and PARPi response. I did this by characterising *in vitro* and *in vivo* models with C-NHEJ protein loss, and by setting up genome-wide pooled CRISPR screens to identify genes that are potentially important for PARPi resistance and synergy. This CRISPR screen was designed to be completed in three PARPi-sensitive HGSOC cell lines, each with a different defect in its HR pathway: *BRCA1* mutation, *BRCA2* mutation and *BRCA1* methylation. In this Chapter, I present one completed CRISPR screen using *BRCA2* mutated cell line, with CRISPR screen conditions optimised for the other two cell lines, which are now ready for drug treatments.

4.2 Chapter 4 hypotheses

1. The C-NHEJ DNA repair pathway plays a critical role in PARPi toxicity in HRD cells.

2. Loss of both early and late C-NHEJ pathway proteins leads to PARPi resistance *in vitro* and *in vivo.*

4.3 Chapter 4 aims

1. Explore the role of C-NHEJ loss in PARP inhibitor resistance in *in vitro* and *in vivo* setting.

2. Uncover novel PARPi-resistance genes/pathways using *in vitro* genome-wide CRISPR screen in *BRCA2* mutated cell line.

3. Optimize CRISPR screen conditions for *BRCA*-mutated and *BRCA1* methylated cell lines to find which PARPi-resistance hits are specific to certain HRD contexts, and which are common across all contexts.

4.4 Results

4.4.1 C-NHEJ loss and PARPi resistance

To assess the role of C-NHEJ loss in PARPi resistance I utilised a selection of *in vitro* and *in vivo* models with reported C-NHEJ loss.

The *in vitro* model with C-NHEJ loss was a cell line generated by the Kaufmann/Haluska groups at the Mayo Clinic (AlHilli et al., 2016). They used CRISPR-Cas9 technology to knock out the Artemis gene (*DCLRE1C*) in the HGSOC cell line PEO1 with HRD (*BRCA2* mutation NM_000059.1:5193C>G, p.Tyr1655*). The Kaufmann group validated the Artemis knock-out by Sanger sequencing and WB (unpublished data). I aimed to characterise this model (referred to here as PEO1A2) in terms of drug response, and to confirm the knock-out of Artemis using NGS.

4.4.2 Characterisation of Artemis-deficient cell line

The *in vitro* drug responses of PEO1A2 to PARPi rucaparib and platinum-chemotherapy cisplatin were assessed using CTG Luminescent Cell Viability Assays (Promega), which use quantification of ATP as an indicator of metabolically active cells. A summary of all cell lines described in this chapter is presented in **Table 4.3**. This includes the control cell lines for this experiment, which were the parental *BRCA2*-mutant cell line PEO1, the *BRCA2*-revertant form of this cell line, PEO4, and a second HRD cell line control, PEO4 RAD51C KO, which is a PEO4 cell line where the *RAD51C* gene has been disrupted using targeted CRISPR (**Table 4.3**) (Kondrashova et al., 2017).

Based on the doubling time of our cell lines (**Table 4.3**), and the fact that PARPi-induced replication stress is exacerbated in rapidly dividing cells (Colicchia et al., 2017), a timepoint of seven days was chosen for all cell lines (except WEHI-CS62, which required a 14-day endpoint due to its slow growth). This ensured four-five cell divisions per seven-day CTG assay for PEO1 and PEO4, and their derivatives PEO1A2 and PEO4 RAD51C KO (which had the same cell culture passaging rates as their parental lines).

Table 4.3. Summary of all cell lines discussed in this chapter.

Cell doubling times calculated using IncuCyte platform. Rucaparib EC50 values calculated in PRISM (GraphPad) based on CTG experiments. NA – not applicable as cell line is sensitive to rucaparib.

Cell line	Primary HR defect	Cell doubling time (days)	Rucaparib EC50 (µM)	PARPi resistance mechanism
PEO1	*BRCA2* mutation	1.4	0.006	NA
PEO1A2	*BRCA2* mutation	See PEO1	0.479	Artemis (C-NHEJ) loss
PEO4	*BRCA2* mutation	1.8	1.444	*BRCA2* secondary mutation
PEO4 RAD51C KO	*RAD51C* mutation	See PEO4	0.007	NA
COV362	*BRCA1* mutations	2	6.248	Unclear
UWB1.289	*BRCA1* mutation	1.9	0.4072	NA
UWB1.289 +BRCA1	*BRCA1* mutation	1.4	6.869	Stable *BRCA1* expression vector
WEHI-CS62	*BRCA1* methylation	3.3	0.8439	NA
PEO1 Cas9	*BRCA2* mutation	1.2	See PEO1	NA
UWB1.289 Cas9	*BRCA1* mutation	1.7	See UWB1.289	NA
WEHI-CS62 Cas9	*BRCA1* methylation	3.1	See WEHI-CS62	NA

CTG cell viability assays demonstrated that PEO1A2 (EC50 = 0.479µM) was relatively rucaparib-resistant, compared to two HRD cell lines, PEO1 (EC50 = 0.006µM) and PEO4 RAD51C KO (EC50 = 0.007µM), though HR competent PEO4 was still the most rucaparib-resistant model (EC50 = 1.444µM; **Table 4.3**; **Figure 4.1**). Similar trends were observed for cisplatin, where PEO1A2 (EC50 = 0.496µM) was relatively cisplatin-resistant compared to PEO1 (EC50 = ~0.156µM) and PEO4 RAD51C KO (EC50 = 0.121µM), though HR competent PEO4 (EC50 = 1.25µM) was still the most cisplatin-resistant (**Figure 4.2**).

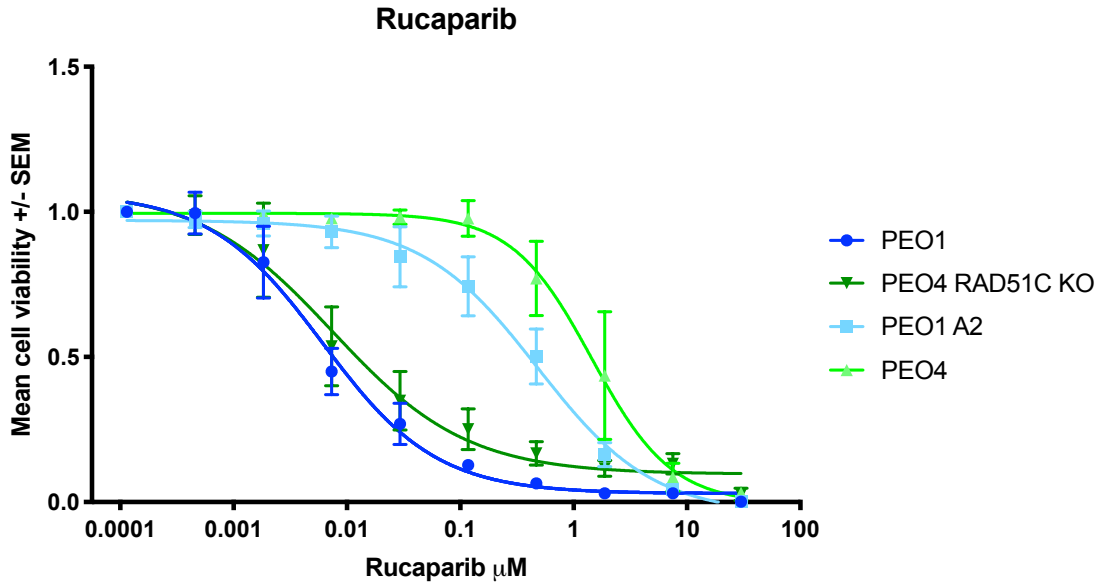


Figure 4.1. PEO1A2 is relatively rucaparib resistant.

CTG data presented is mean +/- SEM from n=3 independent experiments.

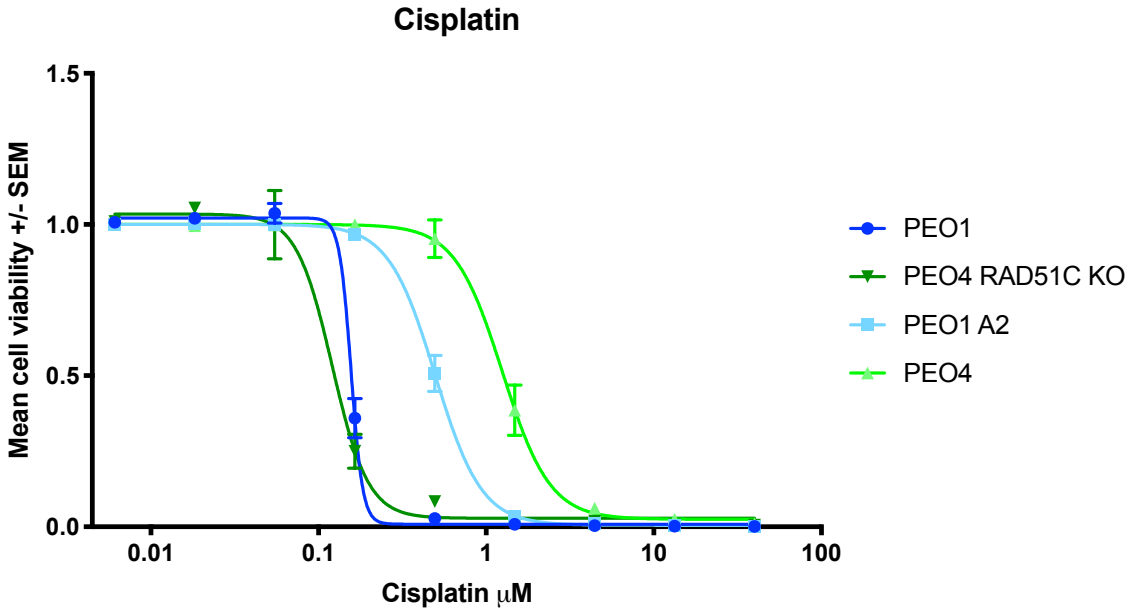


Figure 4.2. PEO1A2 is relatively cisplatin resistant.

CTG data presented is mean +/- SEM from n=3 independent experiments.

These results showed that PEO1A2 was relatively resistant to both rucaparib and cisplatin, compared to the two HRD cell lines without C-NHEJ loss. These findings were in line with previous findings by Patel et al (2011), where knockdown of C-NHEJ members resulted in resistance to PARPi veliparib, and AlHilli et al (2013), where the PEO1A2 cell line was first described and shown to be resistant to the PARPi niraparib.

Published data demonstrating HRD in PEO1 and HR competence in PEO4 was confirmed using the RAD51 foci assay, where PEO1 had impaired RAD51 foci formation following irradiation, while PEO4 was able to form RAD51 foci following DNA damage (**Figure 4.3**) (Patel et al., 2011; Sakai et al., 2009). PEO1A2 was also tested in this single experiment, and was found to also have impaired RAD51 foci formation, which aligns with published data for C-NHEJ deficient and *BRCA2*-mutant models (AlHilli et al., 2016; Patel et al., 2011).

Since the Kaufmann group previously validated the Artemis knock-out using Sanger sequencing (unpublished data), which is unable to discern multiple deletions in a single sample (as was the case for PEO1A2), I chose to confirm the knock-out status of Artemis by performing targeted NGS sequencing of *DCLRE1C* (Artemis) exon 1. Based on this NGS-based assay, I found that the PEO1A2 cell line contained one frameshift mutation and one in-frame deletion (loss of 21 nucleotides) in exon 1 (**Figure 4.4**).

Though one mutation is a frameshift, the other is an in-frame deletion of 21 nucleotides that is unlikely to cause nonsense-mediated decay of the resulting protein (**Figure 4.4**). Thus, despite the WB and drug response data from both laboratories suggesting PEO1A2 is Artemis deficient, it is possible that this cell line still has some Artemis nuclease activity, though it may be reduced or altered.

Due to this uncertainty, I did not to perform any additional follow-up functional studies of C-NHEJ pathway using this cell line and instead moved to validating the C-NHEJ protein status in our PDX models.

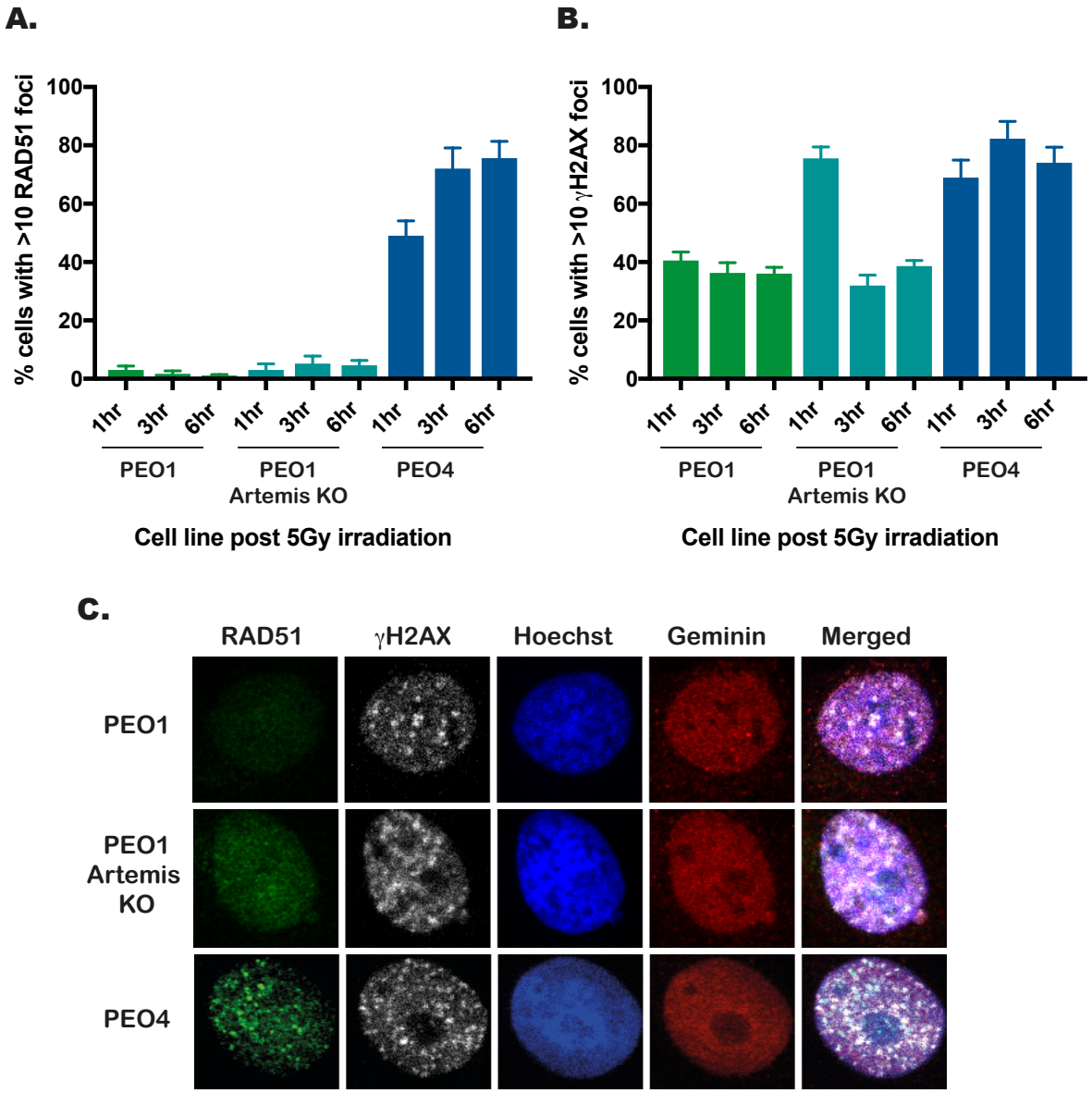


Figure 4.3. PEO1A2, like PEO1, has impaired RAD51 foci formation following DNA damage.

(A) Percentage of cells with >10 RAD51 foci counted per geminin positive cell. (B) Percentage of cells with >10 γH2AX foci counted per geminin positive cell. (C) Representative cell images at 3hrs post-irradiation. Based on n=1 experiment where an average of 140 cells were counted per experiment. Error bars are +/-SEM.

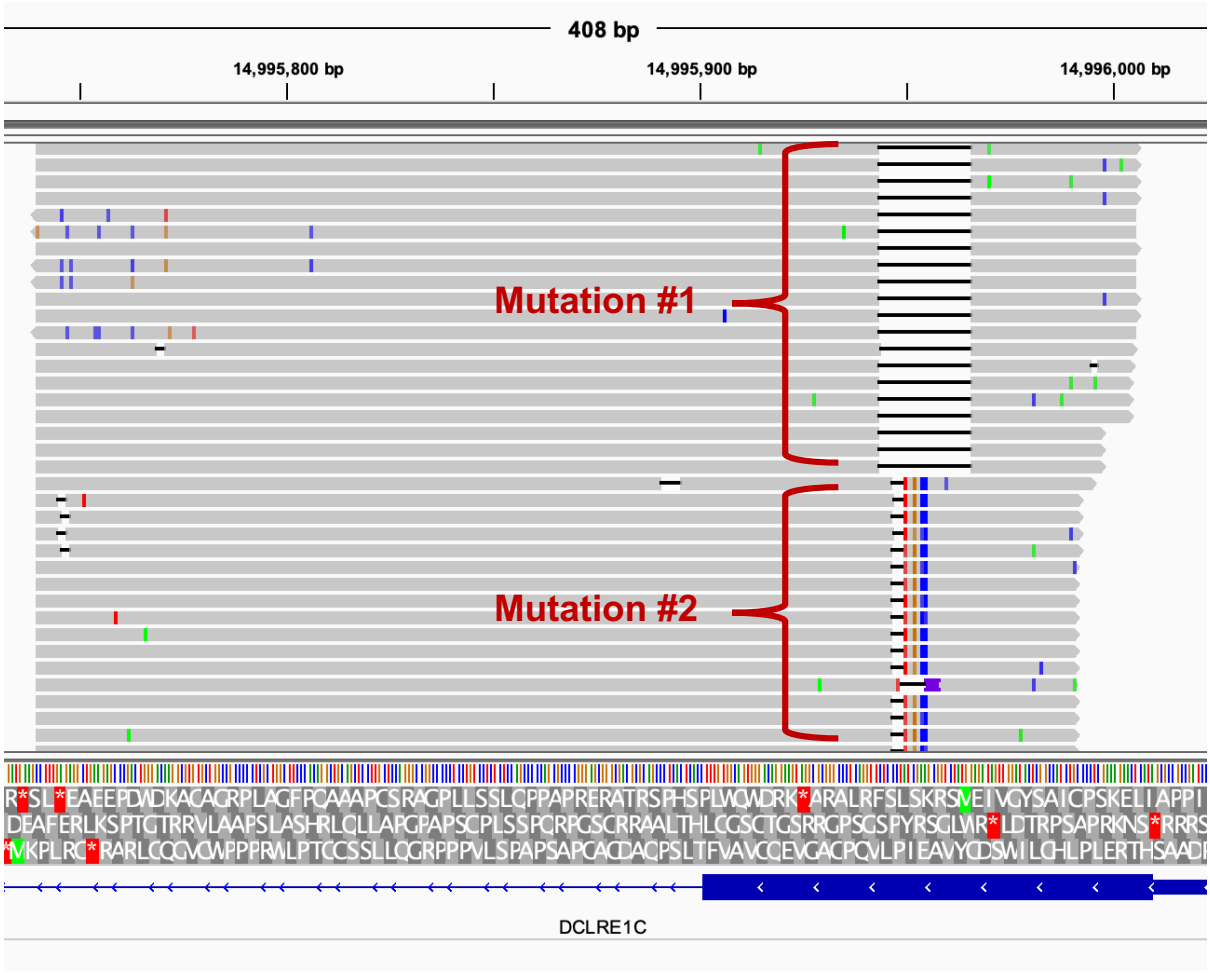


Figure 4.4. IGV visualisation of PEO1A2 CRISPR mutations in Artemis gene (DCLRE1C). *Mutation #1: In-frame deletion of [CTC CCT ATC GAA GCG GTC TAT G], insertion of [CGC CAT C]. Mutation #2: frame-shift deletion of [CTA TCG AA], insertion of [TTG GCC]. Though one mutation is a frameshift, the other is an in-frame deletion of 21 nucleotides that may not cause nonsense-mediated decay of the resulting protein.*

4.4.2.1 In vivo drug responses of PDX 134013 C-NHEJ lineages

As described in the introduction of this Chapter, 4 lineages of PDX 134013 were established, based on WB data for their source tumours, which suggested that each tumour had various degrees of C-NHEJ loss (**Table 4.2**). Based on our hypothesis of PARPi action, via Artemis and C-NHEJ, the "C-NHEJ-deficient" lineages 1,3 and 4 were expected to be PARPi resistant, while the "C-NHEJ intact" lineage 2 was expected to be PARPi sensitive.

Each of these new PDX lineages were expanded in mice and treated with standard regimens: cisplatin 4mg/kg or PARPi rucaparib 300mg/kg and 450mg/kg. All lineages were sensitive to

cisplatin (**Figure 4.5**; **Figure 4.6**; **Figure 4.7**; **Figure 4.8**) but had varying responses to rucaparib. Lineage 1 (predicted Ligase 4 loss) was refractory to rucaparib 450mg/kg with only a short delay in time to progression and harvest, and appeared to respond to 300mg/kg dose but these calculations were based on n=2 treated mice (**Figure 4.5**; **Table 4.4**). Lineage 2 (predicted intact C-NHEJ) was demonstrated a partial response to rucaparib doses 300mg/kg and 450mg/kg (**Figure 4.6**; **Table 4.4**). Lineage 3 (predicted Ku70 and Ku80 losses) was refractory to rucaparib 300mg/kg with a short delay in time to harvest (**Table 4.4**), and rucaparib 450mg/kg response could not be accurately estimated as only n=2 mice were treated (**Figure 4.7**; **Table 4.4**). Lineage 4 (predicted multiple C-NHEJ protein losses) was responsive to rucaparib 450mg/kg, with stable disease, while rucaparib 300mg/kg responses could not be accurately estimated as only n=2 tumours made it to harvest size (others censored; **Figure 4.8**; **Table 4.4**).

Some of these results were as expected based on the predicted C-NHEJ losses, with Lineage 2 (C-NHEJ intact) being the most responsive to rucaparib 450mg/kg treatment compared to other lineages (**Figure 4.6**; **Table 4.4**). Direct comparison of the rucaparib 450mg/kg treatments for each lineage shows that Lineage 2 and Lineage 1 are the only two that are significantly different statistically (p= 0.007; **Figure 4.9**; **Table 4.5**). These differences between Lineages were not observed when comparing rucaparib 300mg/kg responses both visibly (**Figure 4.10**) and statistically (all comparisons; $p > 0.1$).

It is important to note that responses to PARPi can be influenced by rates of cell division, with slower growing tumours appearing more resistant to treatment than fast growing tumours. Given that Lineage 2 and 3 had longer median days to harvest (both 57 days) compared to Lineage 1 and 4 (36 and 29 respectively) in the DPBS vehicle group, it was possible that slower tumour growth was making Lineages 2 and 3 appear more responsive to rucaparib 450mgkg (**Table 4.4**). To confirm that the differences in rucaparib responses were not due to differences in tumour growth rates between the lineages, control DPBS-treated tumour growth rates for each lineage were compared directly (**Figure 4.11**), and p-values determined for each comparison (**Table 4.6**). This comparison revealed some subtle differences in rates of tumour growth between lineages, with NHEJ 2 and 3 appearing to grow slightly slower than lineages 1 and 4 (**Figure 4.11**). However, these differences were very subtle, and none were statistically significant (**Table 4.6**). This could, therefore, be ruled out as a cause of the differential rucaparib responses between PDX 134013 C-NHEJ lineages.

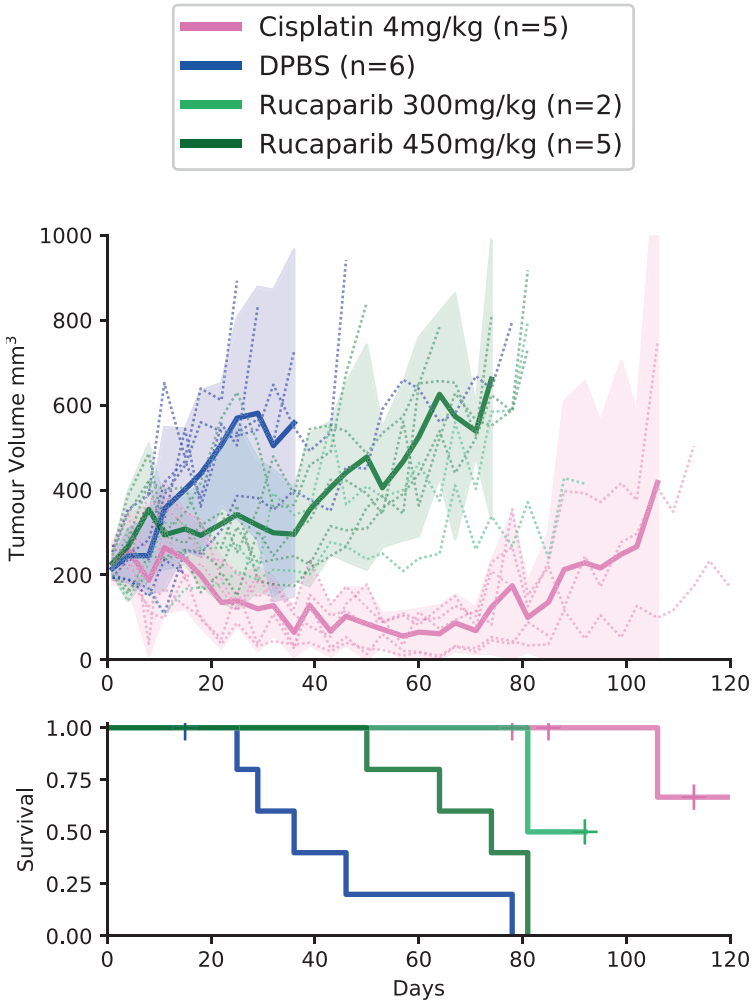


Figure 4.5. PDX 134013 C-NHEJ lineage 1 rucaparib and cisplatin responses.

Tumour volume data presented is individual tumour measurements (dashed lines), with mean (bold line) +/- 95% CI (shaded area).

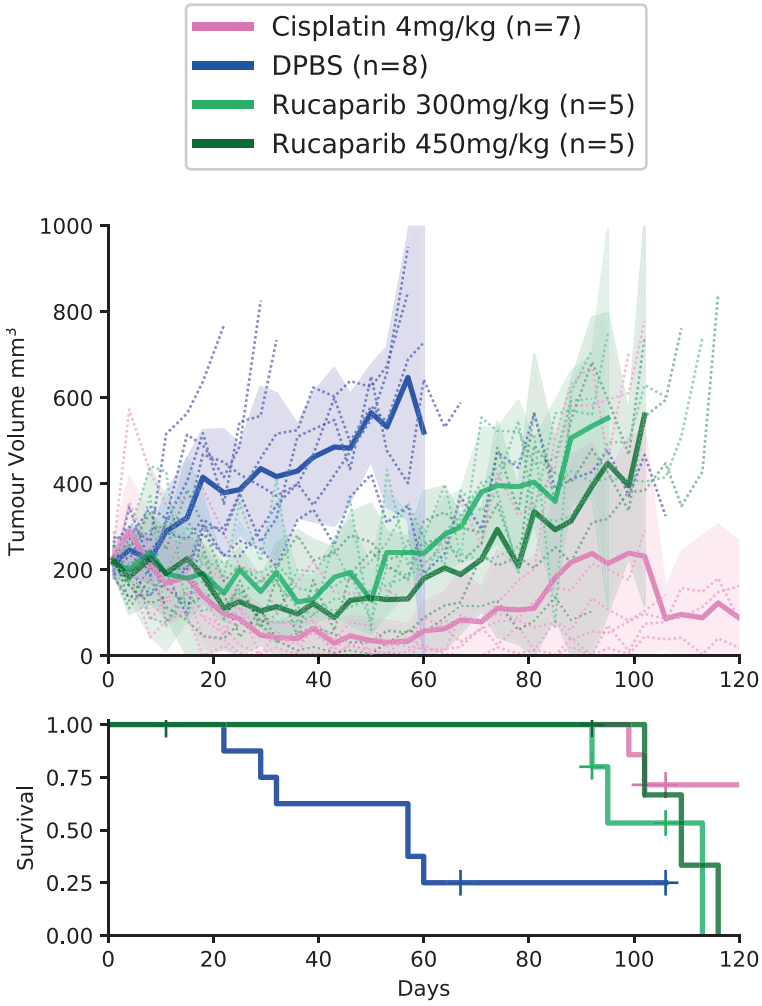


Figure 4.6. PDX 134013 C-NHEJ lineage 2 rucaparib and cisplatin responses.

Tumour volume data presented is individual tumour measurements (dashed lines), with mean (bold line) +/- 95% CI (shaded area).

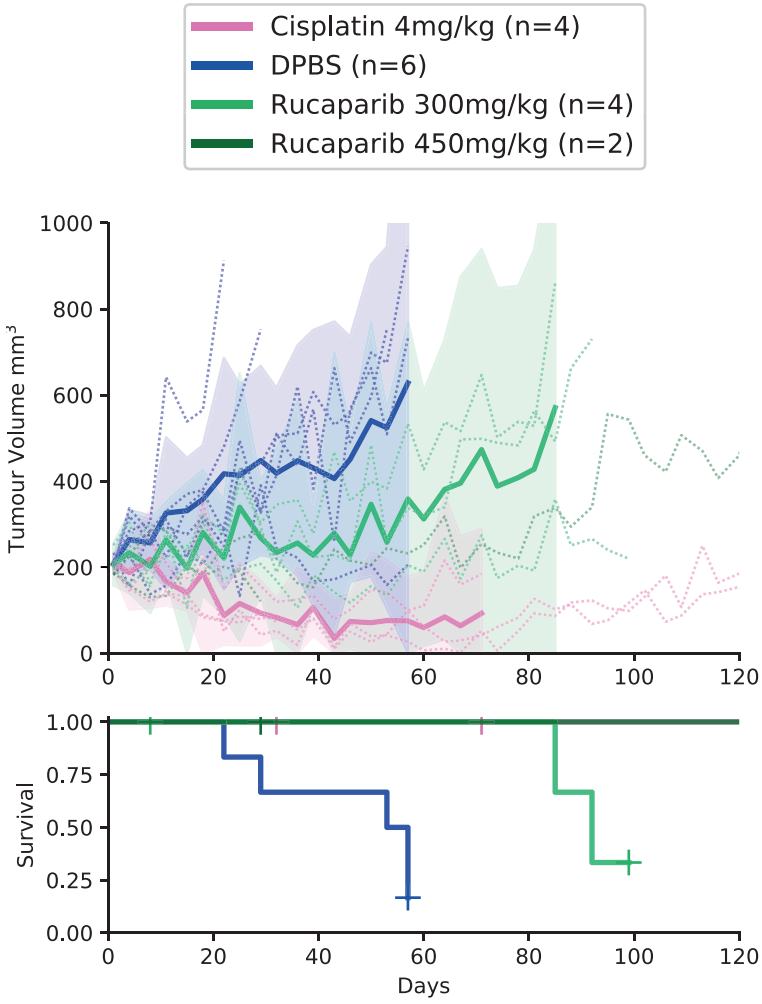


Figure 4.7. PDX 134013 C-NHEJ lineage 3 rucaparib and cisplatin responses.

Tumour volume data presented is individual tumour measurements (dashed lines), with mean (bold line) +/- 95% CI (shaded area).

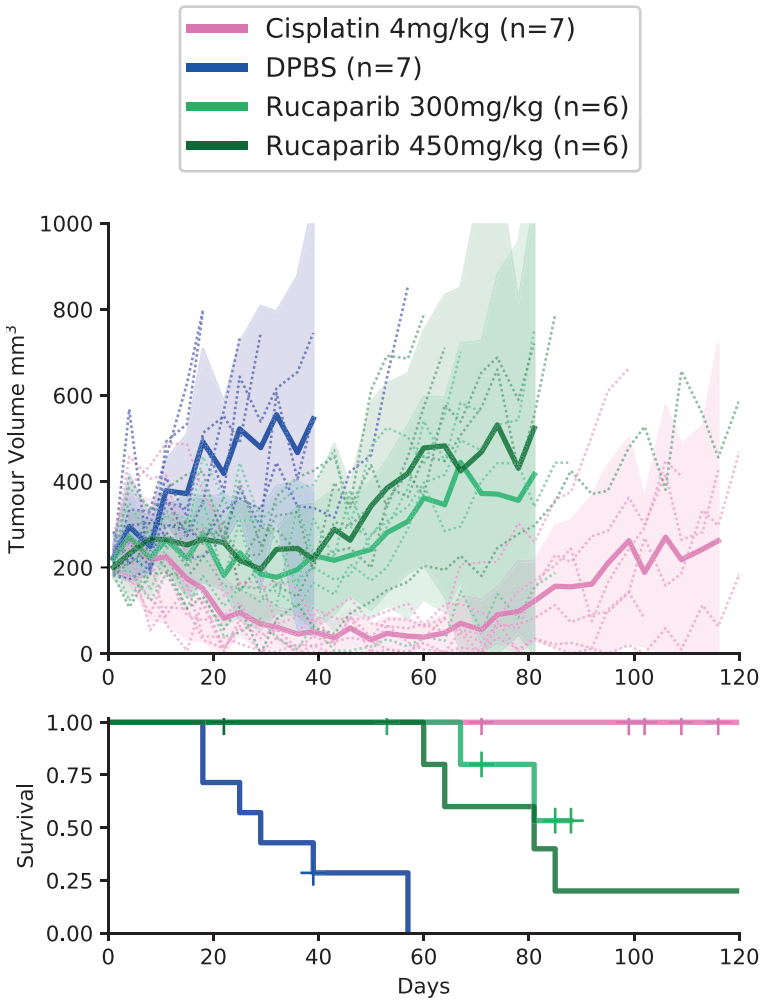


Figure 4.8. PDX 134013 C-NHEJ lineage 4 rucaparib and cisplatin responses.

Tumour volume data presented is individual tumour measurements (dashed lines), with mean (bold line) +/- 95% CI (shaded area).

Table 4.4. PDX 134013 C-NHEJ lineage treatment response summary.

All calculations based on n=3 unless specified: NA: n=2 mice treated/uncensored. TTH = time to harvest. TTP = time to progression. P-values for treatment group compared to DPBS vehicle control calculated using a Pairwise Log Rank Test.

PDX 134013 C-NHEJ lineage	Median TTH vehicle	PDX rucapraib 300mg/kg response				PDX rucapraib 450mg/kg response			
		Response	Median TTH (days)	Average TTP (days)	*p* -value	Response	Median TTH (days)	Average TTP (days)	*p* -value
1	36	NA	NA	NA	NA	Refractory, PD	74	8	0.057
2	57	Response, PR	113	54	0.061	Response, PR	109	82	0.065
3	57	Refractory, SD	92	19	0.042	NA	NA	NA	NA
4	29	NA	NA	NA	NA	Response, SD	81	44	0.003

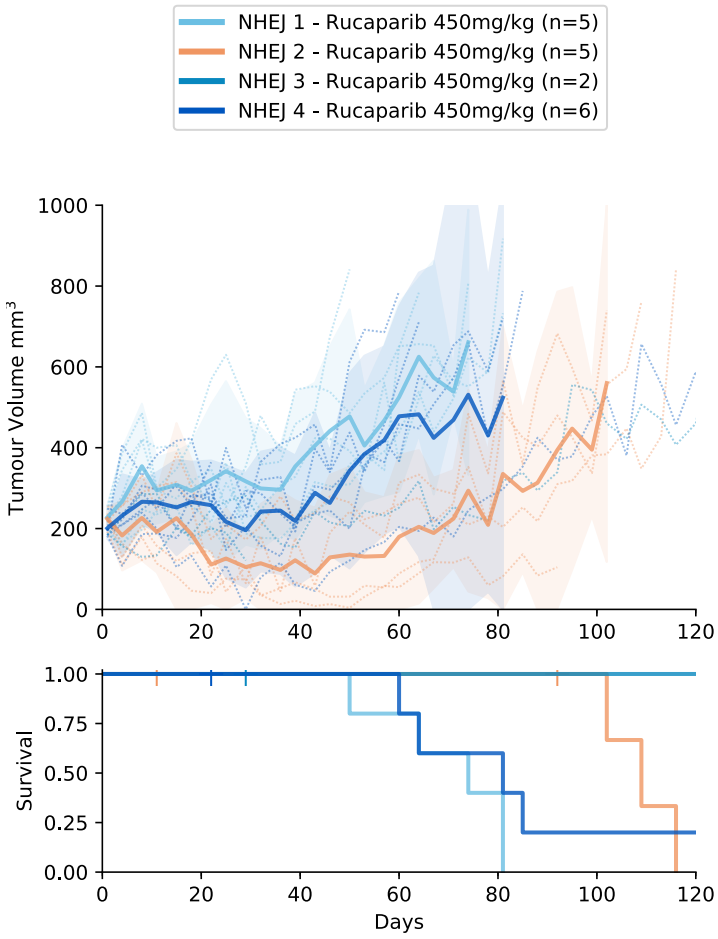


Figure 4.9. Comparison of PDX 134013 C-NHEJ lineage rucaparib 450mg/kg responses.

Tumour volume data presented is individual tumour measurements (dashed lines), with mean (bold line) +/- 95% CI (shaded area). Lineage 3 mean not visible as it is n=2.

Table 4.5. P-values of PDX 134013 C-NHEJ lineage rucaparib 450mg/kg response comparisons.

P-values calculated using Pairwise Log Rank Tests.

p- values	NHEJ 1	NHEJ 2	NHEJ 3	NHEJ 4
NHEJ 2	0.007			
NHEJ 3	0.127	0.182		
NHEJ 4	0.274	0.388	0.139	

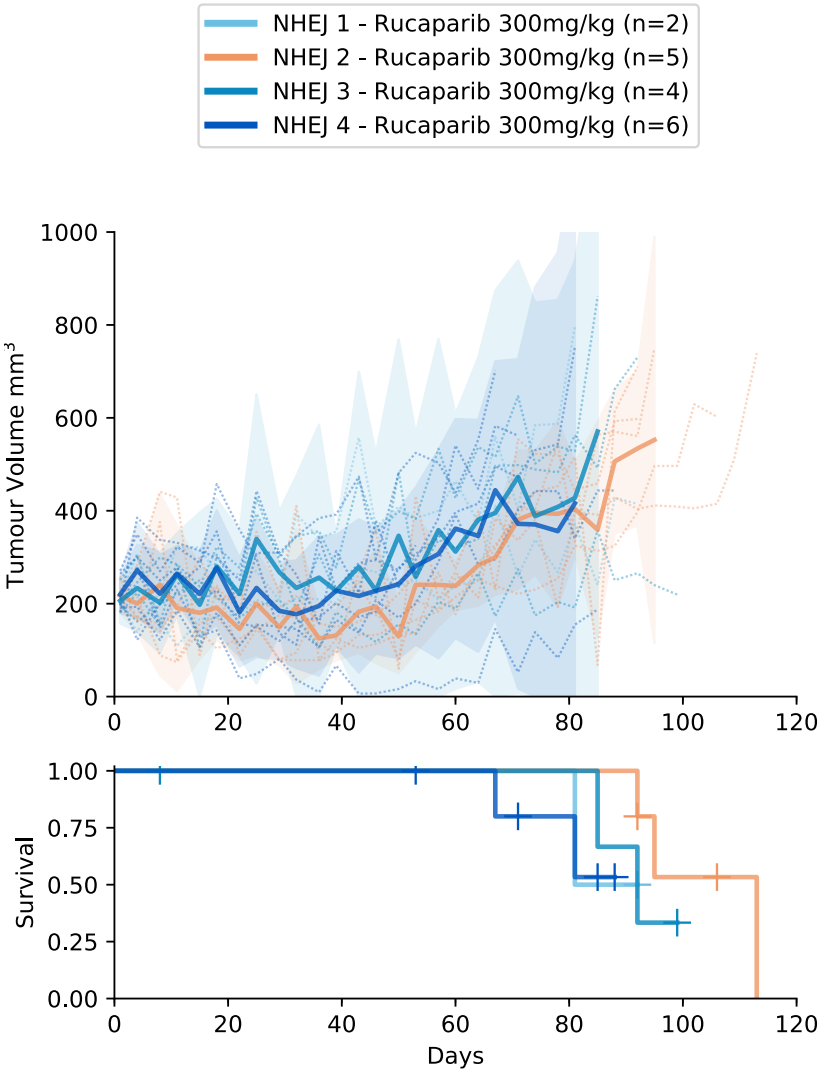


Figure 4.10. Comparison of PDX 134013 C-NHEJ lineage rucaparib 300mg/kg responses.

None of these differences were statistically significant (all comparisons were $p > 0.1$). Tumour volume data presented is individual tumour measurements (dashed lines), with mean (bold line) +/- 95% CI (shaded area). Lineage 1 mean not visible as it is n=2.

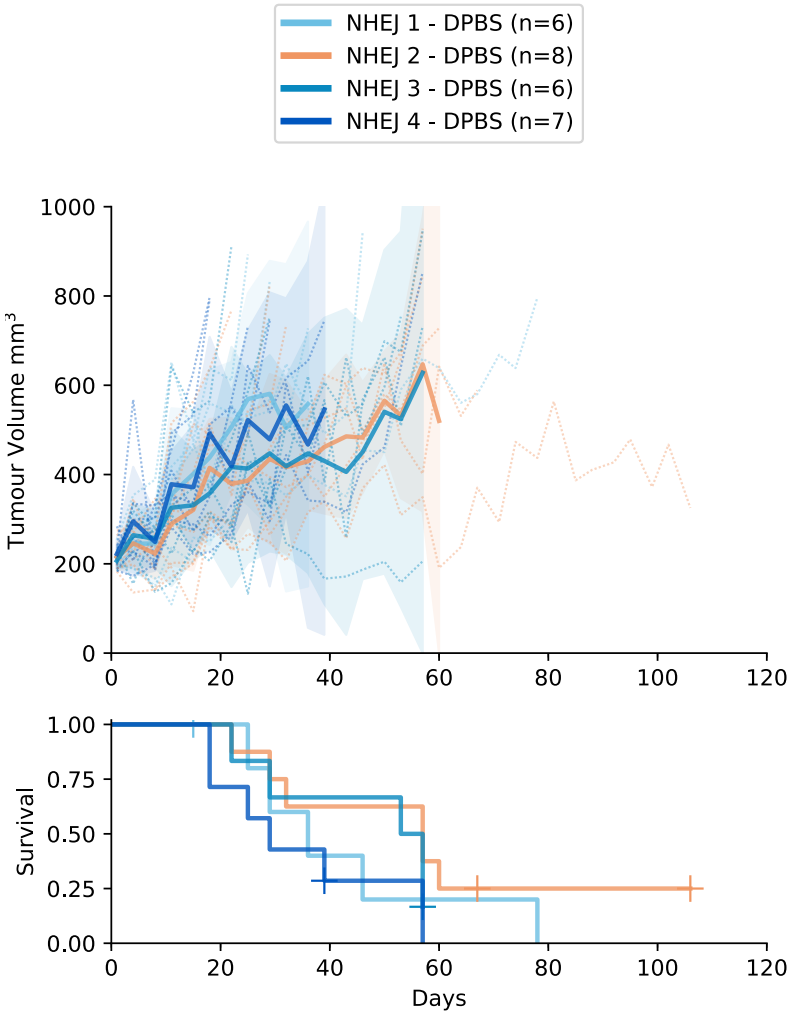


Figure 4.11. Comparison of PDX 134013 C-NHEJ lineage tumour growth rates.

Median time to harvest (TTH) is 57 days for Lineages 2 and 3, 36 days for Lineage 1 and 29 days for Lineage 4. Tumour volume data presented is individual tumour measurements (dashed lines), with mean (bold line) +/- 95% CI (shaded area).

Table 4.6. P-values of PDX 134013 C-NHEJ lineage growth rate comparison.

P-values calculated using Pairwise Log Rank Tests.

p- values	NHEJ 1	NHEJ 2	NHEJ 3	NHEJ 4
NHEJ 2	0.349			
NHEJ 3	0.605	0.486		
NHEJ 4	0.551	0.105	0.226	

Given that the rucaparib 450mg/kg results were suggesting that C-NHEJ loss may indeed be leading to PARPi resistance in these models, it was important to confirm that tumours within these lineages still represented the C-NHEJ profiles originally assigned to them. This was to be done using both a different method (IHC) and using the same method (WB) on different pieces of the original tumours. Results of this validation process are described in the following sections.

4.4.2.2 ***Immunohistochemistry scoring results***

To confirm the consistency of previously generated C-NHEJ WB results for PDX, and to assess the spatial heterogeneity of C-NHEJ staining, a selection of 33 of the samples was also stained by IHC staining for up to 8 proteins – the same proteins as WB, excluding Artemis, and with addition of RAD51 (HR pathway), PARP1 and Ki67 (proliferation marker). A total of 59 slides across 8 tumour samples were blindly scored by two people. This included 4 control PDX samples (2 tumours from PDX 134056 and 2 from PDX 134027) used as a training set, and the 4 original source samples for each PDX 134013 C-NHEJ lineage (tumours 1373, 1440, 1734 and 1616).

Digitised whole-slide images were analysed using the ImageScope software (Aperio, v12.3.2). Staining intensity (none, weak, moderate and strong) for XRCC4, Ku70, Ku80 and DNA-PKcs was determined using the IHC keys in **Figure 4.12**, **Figure 4.13**, **Figure 4.14** and **Figure 4.15**. Unfortunately, the Ligase 4 (Lig4) IHC stain was found to be consistently low across all samples and PDX models, thus it was deemed suboptimal and excluded from the rest of the analysis (total of 52 slides analysed excluding Ligase 4).

Given that staining was not always consistent throughout tissue sections likely due to intratumours heterogeneity, the percentage of staining intensity across the whole section was determined. This allowed H scores to be calculated for each slide: 3 x % of strongly stained nuclei + 2 x % of moderately stained nuclei + % of weakly stained nuclei, giving a range of 0 to 300 (Ishibashi et al., 2003; McCarty et al., 1985).

Each slide was scored in blinded fashion by me and another scorer. Discordance was reported when the difference in H score between the two scorers was ≥100. Slides where there was discordance between the two scorers were referred to a third scorer for clarification.

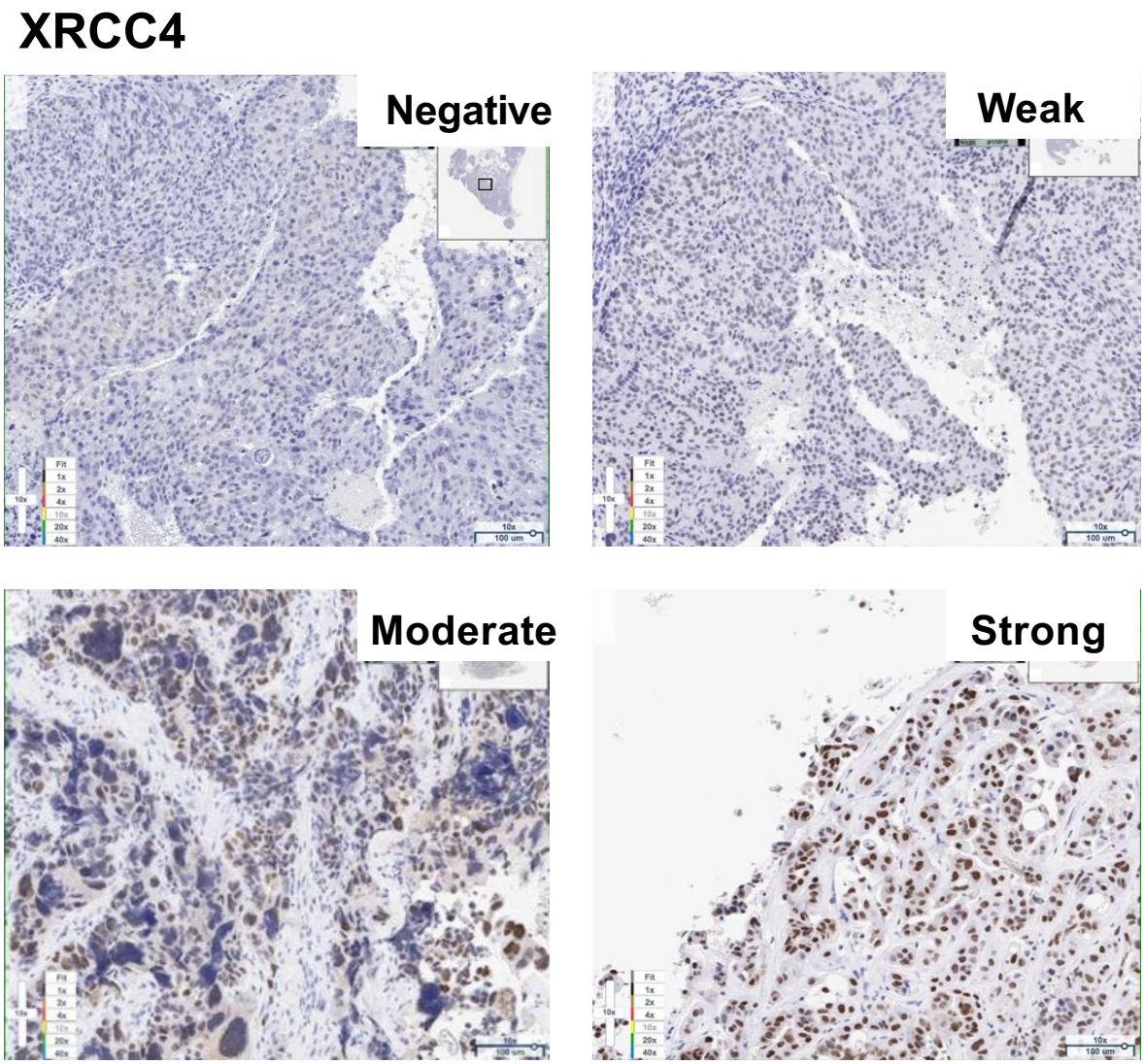


Figure 4.12. Key of XRCC4 staining intensity used to score PDX samples.

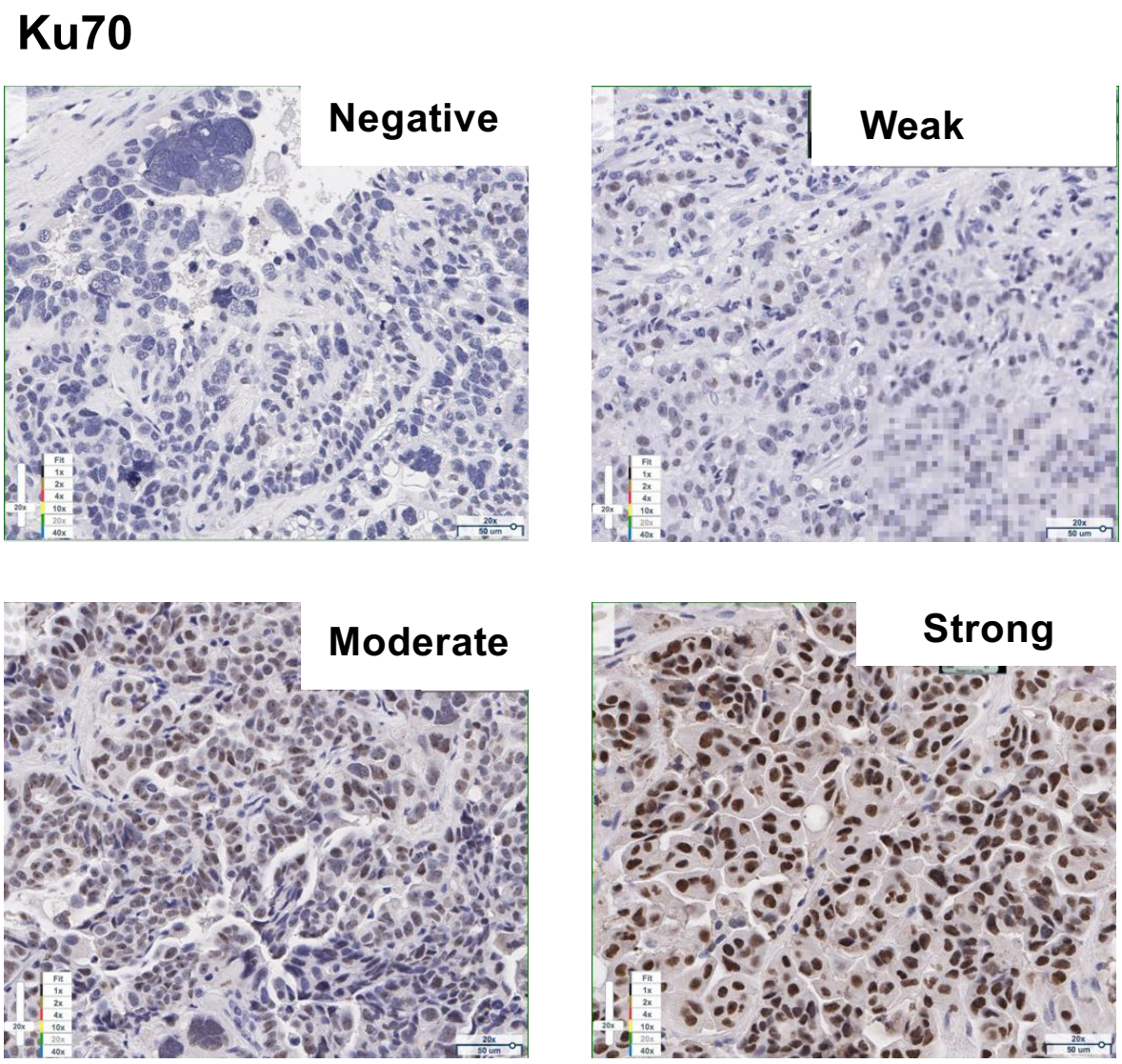


Figure 4.13. Key of Ku70 staining intensity used to score PDX samples.

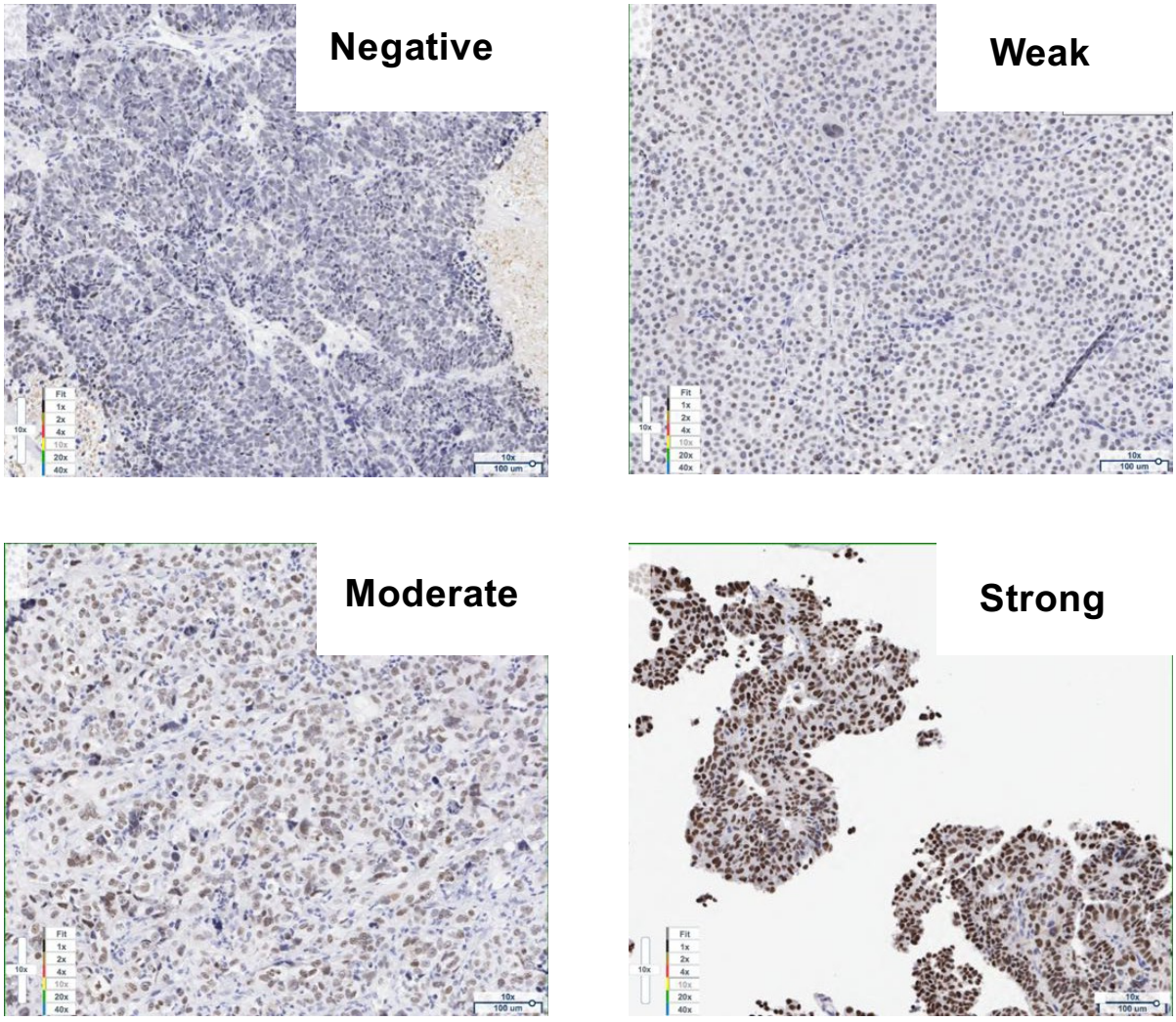


Figure 4.14. Key of Ku80 staining intensity used to score PDX samples.

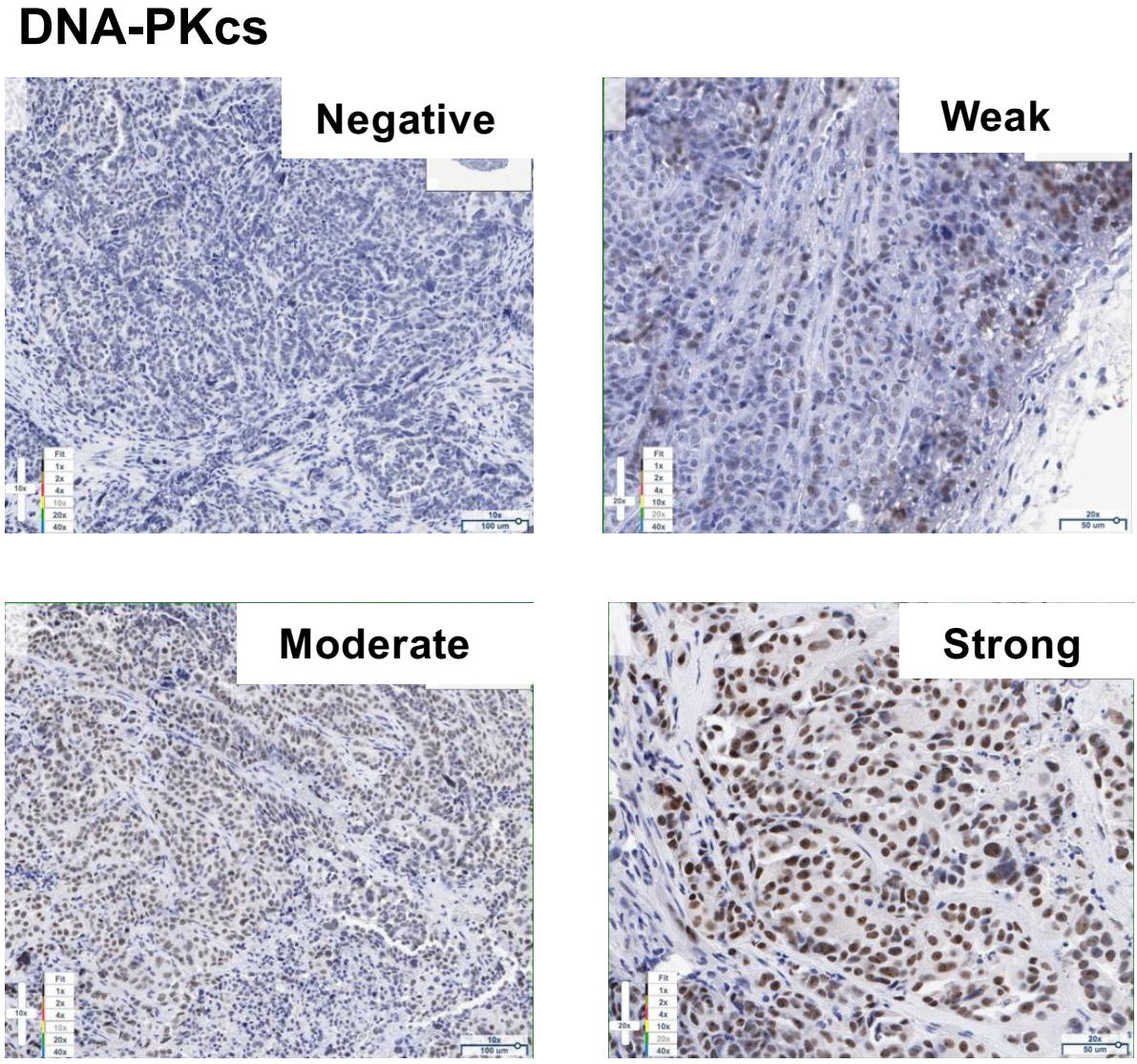


Figure 4.15. Key of DNA-PKcs staining intensity used to score PDX samples.

Though there was some discordance between primary scorers for certain slides in the PDX 134027 and 134056 training set samples, the majority of scores were found to be concordant (H score difference ≥100 in 5/32 slides scored; **Table 4.7**).

Table 4.7. IHC results of PDX 134027 and 134056 test samples.
H score 1= H score from scorer 1; H score 2= H score from scorer 2.

PDX	Tumour	Treatment	Days to harvest	Stain	H Score 1	H Score 2	Combined assessment	Difference in H scores	Average H score
134027	1566	1st line rucaparib 300mg/kg	29	53BP1	170	140	Weak-Moderate	30	155
				DNA-PKcs	40	80	No stain-weak	40	60
				Ki67	170	160	Patches Moderate-Strong	10	165
				Ku70	20	0	No stain-weak	20	10
				Ku80	150	60	Weak	90	105
				PARP	280	250	Moderate-Strong	30	265
				Rad51	10	10	Very Weak	0	10
				XRCC4	10	0	Very Weak	10	5
	3228	3rd line cisplatin 4mg/kg	131	53BP1	280	280	Moderate-Strong	0	280
				DNA-PKcs	290	260	Strong	30	275
				Ki67	200	280	Patches Strong	80	240
				Ku70	250	150	discordant	100	200
				Ku80	250	250	Moderate-Strong	0	250
				PARP	300	300	Strong	0	300
				Rad51	210	80	discordant	130	145
				XRCC4	280	200	Moderate-Strong	80	240
134056	2413	1st line vehicle	7	53BP1	280	220	Moderate-Strong	60	250
				DNA-PKcs	190	150	Weak-Moderate	40	170
				Ki67	170	150	Patches moderate-strong	20	160
				Ku70	200	130	Weak-Moderate	70	165
				Ku80	200	170	Large patches moderate-strong	30	185
				PARP	290	250	Moderate-Strong	40	270
				Rad51	140	150	Patches moderate-strong	10	145
				XRCC4	180	80	discordant	100	130
	2264	1st line cisplatin 4mg/kg	103	53BP1	250	180	Moderate-Strong	70	215
				DNA-PKcs	180	90	Weak-Moderate	90	135
				Ki67	170	130	Patches moderate-strong	40	150
				Ku70	250	120	discordant	130	185
				Ku80	250	250	Moderate-Strong	0	250
				PARP	280	300	Strong	20	290
				Rad51	80	90	Patches moderate-strong	10	85
				XRCC4	170	50	discordant	120	110

When comparing IHC results for stains within PDX models, it was observed that stains within HR competent model, PDX 134027, were greatly varied. For example DNA-PKcs having very weak signal in tumour #1566 but a strong signal in tumour #3228. Staining results for HRD model PDX 134056 were more consistent, however it is important to note that all of these tumours were exposed to different treatments, which means a direct comparison is not possible. Furthermore, we could not assess the consistency of these losses across tumour passages from these data, as these tumours were not derived from the same tumour transplants.

This set did, however, serve its purpose as a training set for validating our staining assessment protocol. Thus, we moved onto scoring the PDX 134013 C-NHEJ lineage tumours.

4.4.2.3 ***Validation of C-NHEJ lineages of PDX 134013***

Multiple new PDX tumour samples were sent for C-NHEJ protein analysis at the start of my PhD, including the first set of PDX 134013 C-NHEJ lineage (1-4) samples. I prepared protein lysates for 93 new tumour samples in total (with matched FFPE material sent for 60 samples). This included treated and untreated PDX 134013 C-NHEJ lineage 1-4 tumours, and tumours from PDX 134148, PDX 134056 lineage #56S and #56R, PDX 134019, PDX 134019B and control HRC PDX 134029 (full list of samples in appendix F).

Second lysates (*i.e*. same tumour, but a different piece used for new lysate) of the original PDX 134013 C-NHEJ lineage source tumours had been sent to the Kaufmann group before my PhD. These were intended to validate the initial WB results characterizing the C-NHEJ pathway of each lineage. We received WB results for these soon after I had sent the batches new tumour samples. Thus, before proceeding with WB of the new samples I had sent, I decided to prioritize validation of the original WB results for the PDX 134013 C-NHEJ lineage source tumour pieces.

The immunoblots of these PDX 134013 C-NHEJ lineage samples were not found to be concordant with assessments of the original tumours (**Table 4.8**). This was possibly due to tumour heterogeneity, or transient losses of expression of these proteins in the original samples. In an effort to gain some clarity, I then prioritized IHC analysis of these tumour samples.

Blind scoring of the IHC stains of the original PDX 134013 tumour samples (used to establish C-NHEJ lineages) and subsequent C-NHEJ lineages tumour samples was performed and a consensus score was determined, as described above. Scores for many of these slides were found to be discordant with the WB data, apart from lack of Ku70 staining in lineage 2 detected by IHC and by WB in the second tumour piece, but not in the first piece (**Table 4.8**).

Table 4.8. WB and IHC data discordant for PDX 134013 C-NHEJ lineage source tumours.

Summary table of results for 4 PDX tumours used to generate 4 different lineages of PDX 134013. The first set of WB results (tumour piece #1) were received and analysed before my PhD, while the second set of WB (tumour piece #2) were analysed at the start of my PhD, when discordance in stains between individual tumours was first observed. Discordance was seen again using a different method (IHC). TBC- Scoring to be completed.

PDX 134013 lineages				
Source tumour/ mouse	**1373**	**1440**	**1734**	**1616**
Passage	T4	T4	T4	T4
Line of treatment	Rucaparib 150mg/kg - 1 cycle	Vehicle - 1 cycle	Cisplatin 4mg/kg - 2 cycles	Cisplatin 4mg/kg - 3 cycles
Days to harvest	82	62	87	76
WB results - C-NHEJ losses				
Tumour piece #1	Lig4	None	Ku70, Ku80	"Multiple"
Tumour piece #2	None	Ku70	None	53BP1, Ku70, Ku80, Artemis, XRCC4, Lig4
IHC results - C-NHEJ losses				
53BP1	Weak-moderate (20-30%), strong (70-80%)	moderate-strong	TBC	Moderate (40-50%), Strong (50%)
Lig4	No stain 90%, weak-moderate 10%	No stain >90%, weak <10%	No stain >90%, weak <10%	TBC
DNA-PKcs	Weak-moderate	No stain 50%, weak 50%	discordant	discordant
Ku70	Weak (50%), Moderate (50%)	No stain 80-90%, weak 10-20%	No stain (40-50%), Weak-moderate (50-60%)	TBC
Ku80	Weak-moderate 70%, strong 30%	discordant	Weak-moderate (50-70%), strong (30-50%)	Weak-moderate (50-80%), strong (20-50%)
PARP	Moderate (10-20%), Strong (80-90%)	Weak-moderate	TBC	TBC
RAD51	mixed: no stain & moderate-strong	no stain-weak	TBC	TBC
XRCC4	Weak-moderate (20-50%), strong (50-80%)	discordant	TBC	Weak-moderate (20-40%), strong (60-80%)

It is likely that the observed variation was being caused by tumour heterogeneity or transient biological mechanisms, rather than stable and re-producible mechanisms that could be selected for under treatment pressure. Indeed, no PDX tumours screened on the BROCA sequencing panel were found to have deleterious mutations in any C-NHEJ pathway genes (described in section 3.4.7).

Unfortunately, given the inconsistencies observed between the screening methodologies, as well as no clear C-NHEJ protein loss observed by IHC in any PDX samples, I decided that it was not reasonable to continue with the characterisation and functional follow-up of the C-NHEJ "loss" PDX samples.

4.4.3 Identification of PARPi resistance through pooled CRISPR screen

To further elucidate the role of C-NHEJ in PARPi resistance and identify novel mechanisms of PARPi resistance, I prepared genome-wide pooled CRISPR screens with applied PARPi treatment on HR deficient HGSOC cell lines. For this screen, I chose three independent PARPi-sensitive HGSOC cell lines, each with a different defect in its HR pathway: *BRCA1* mutation, *BRCA2* mutation and *BRCA1* methylation. These cell lines represent the three most commonly detected HR defects in HGSOC, including both *BRCA1* and *BRCA2,* which have distinct biological roles. These two genes also have multiple previously reported PARPi resistance mechanisms that do not overlap, for example, *53BP1* and *REV7* losses cause resistance in *BRCA1* and not *BRCA2*-mutant cells (Bouwman et al., 2010; Jaspers et al., 2013), while *CHD4* cause resistance in *BRCA2*-mutant HGSOC, and not *BRCA1* (Guillemette et al., 2015).

The results of these screens would indicate which, if any, stable C-NHEJ protein losses are possible in each HRD context. We also aimed to investigate other identified hits, and determine whether these are unique to a particular HRD setting or detected in all cell lines (**Figure 4.16**).

Screening was completed for the *BRCA2*-mutant cell line (PEO1), while the *BRCA1*-mutant and methylated cell lines have been characterized, and parameters have been optimised for PARPi treatment and resistance screening in these lines.

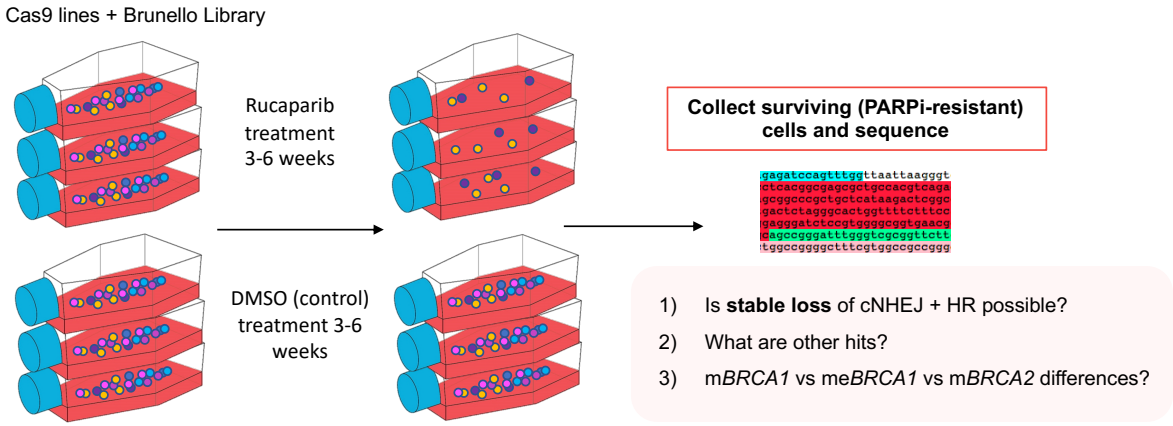


Figure 4.16. Outline of in vitro PARPi resistance CRISPR screen design.
PEO1, UWB1.289 and WEHI-CS62 Cas9-expressing cell lines infected with the Brunello library are cultured in the presence or absence of PARPi rucaparib for 3-6 weeks with escalating doses. Some cells are harvested each week at passaging so that multiple timepoint analyses can be performed. At the chosen timepoint, DNA is extracted from rucaparib- and control- treated cells, and libraries made for sequencing of the Brunello guides present within the cell population. This data is then analysed in silico to uncover the top enriched guides/genes in the treated samples, which represent genes or pathways that may cause PARPi resistance when lost.

4.4.3.1 Selection and characterisation of cell lines

The *BRCA2* mutant cell line selected for this experiment was the PEO1 line, with a frameshift *BRCA2* mutation NM_000059.1:5193C>G, p.Tyr1655*. PEO1 was prioritized as the *BRCA2*-mutant model for this study as it would allow us to validate whether complete Artemis CRISPR KO is possible, given the questions raised in the characterisation of the PEO1A2 cell line.

PEO1 is a platinum and PARPi-sensitive HRD cell line, making it ideal for PARPi resistance screening and possible future platinum resistance screening (**Table 4.3**; **Figure 4.17**; **Figure 4.18**). The platinum EC50 for this cell line was established to be ~0.156µM and the rucaparib EC50 was 0.006µM (**Table 4.3**). The choice of this cell line had the added advantage of the matched HR competent, PARPi resistant PEO4 cell line (with a *BRCA2* secondary mutation) from the same patient, that can be used as a control for any downstream CRISPR validation experiments. This cell line is PARPi and platinum resistant, with a cisplatin EC50 of 1.25µM and a rucaparib EC50 of 1.444µM (**Table 4.3**; **Figure 4.17**; **Figure 4.18**).

HGSOC cell lines lacking all *BRCA1* function are rare, and many instead carry mutations in the D11q region of *BRCA1*, resulting in partially functional splice variants (described in Chapter 3). Two HGSOC *BRCA1* mutant cell lines were considered for this experiment: UWB1.289 and COV362 cell lines, which are both *BRCA1* D11q mutants with possible residual *BRCA1* activity (**Table 4.3**) (Pettitt et al., 2016; Wang et al., 2016). UWB1.289 cell line has the *BRCA1* frameshift mutation NM_007294.1:c.2954delG, while COV362 cell line was reported to have two *BRCA1* mutations: NM_007294.1:c.2611fs and c.4095+1G>T (exon 11 splice donor). I also had acquired the UWB1.289+BRCA1 cell line, which is a version of UWB1.289 that contains a stably transfected pcDNA3 plasmid containing a *BRCA1* insert and may be useful for future validation experiments.

The COV362 and UWB1.289+BRCA1 cell lines were more resistant to rucaparib (EC50 = 6.248 and ~6.869μM respectively) compared to the HRC control cell line PEO4 (EC50 = 1.444μM), while UWB1.289 (EC50 = 0.407μM) was sensitive, though not as sensitive as PEO1 (EC50 = 0.006μM; **Table 4.3**; **Figure 4.17**). The COV362 cell line was also found to be more resistant to cisplatin treatment (EC50 = 0.598μM) compared to the PEO1 (EC50 = ~0.157μM), UWB1.289 (EC50 = 0.090μM) and UWB1.289+BRCA1 (EC50 = 0.174μM) cell lines, but not as resistant as HRC cell line PEO4 (EC50 = 1.250μM; **Table 4.3**; **Figure 4.18**).

Though the COV362 cell line was resistant to PARPi rucaparib, it still contained the *BRCA1* exon 11 splice donor mutation c.4095+1G>T at a 100% frequency (found via targeted amplicon sequencing – **Figure 4.19**). Presence of the exon 11 frameshift mutation in this line is yet to be confirmed, though it is possible that this mutation will also be present and resistance is due to other *BRCA1*-specific mechanisms (such as D11q expression or loss of C-NHEJ protein 53BP1).

Thus, I chose to proceed with the UWB1.289 cell line, as the cells were more responsive to PARPi than COV362, and also because I had acquired the isogenic UWB1.289+BRCA1 control cell line. This UWB1.289+BRCA1 cell line could be used as a HR competent control in subsequent validation experiments.

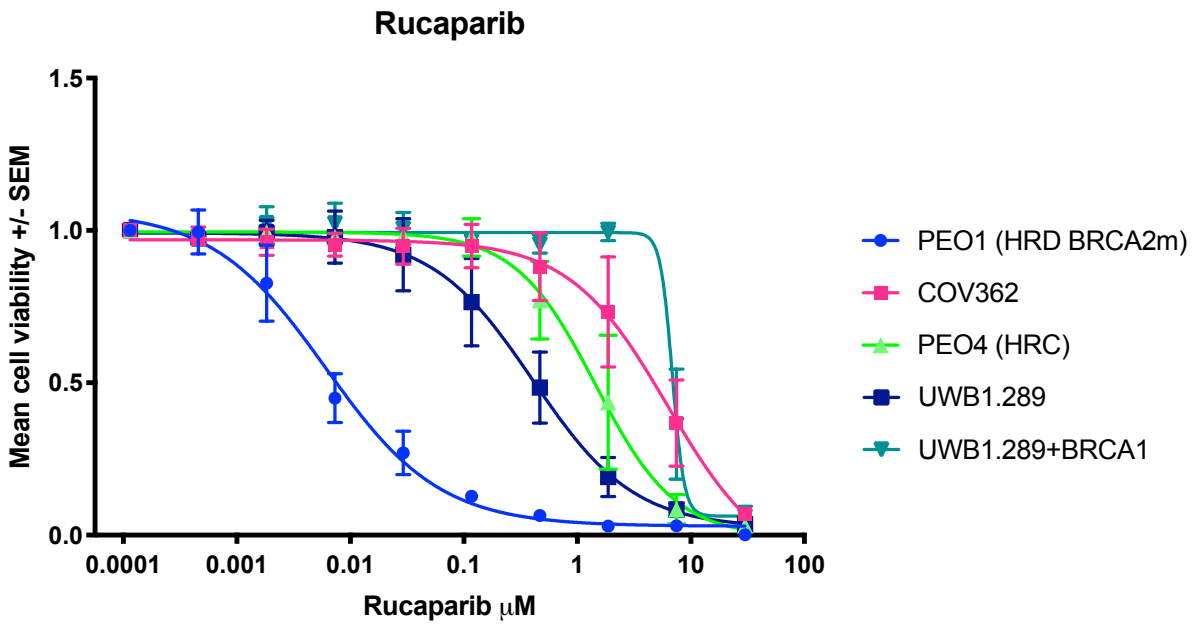


Figure 4.17. In vitro rucaparib responses in cell lines screened for CRISPR screen experiment.

CTG data presented is mean +/- SEM from n=3 independent experiments.

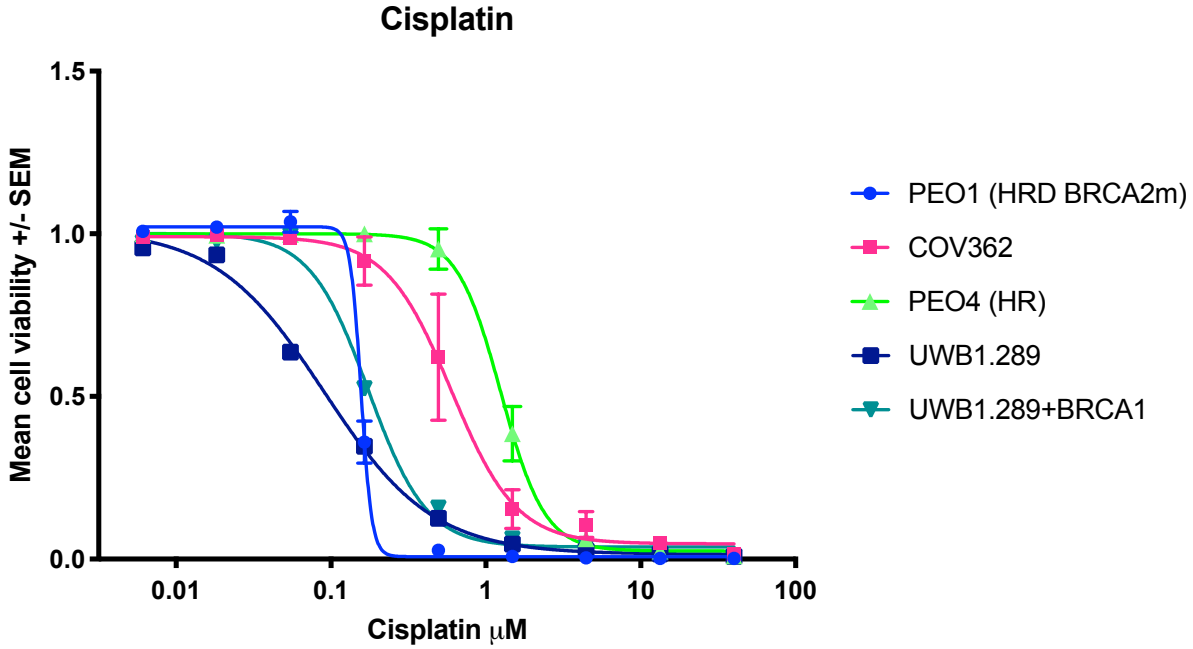


Figure 4.18. In vitro cisplatin responses in cell lines screened for CRISPR screen experiment.

CTG data presented is mean +/- SEM from n=3 independent experiments.

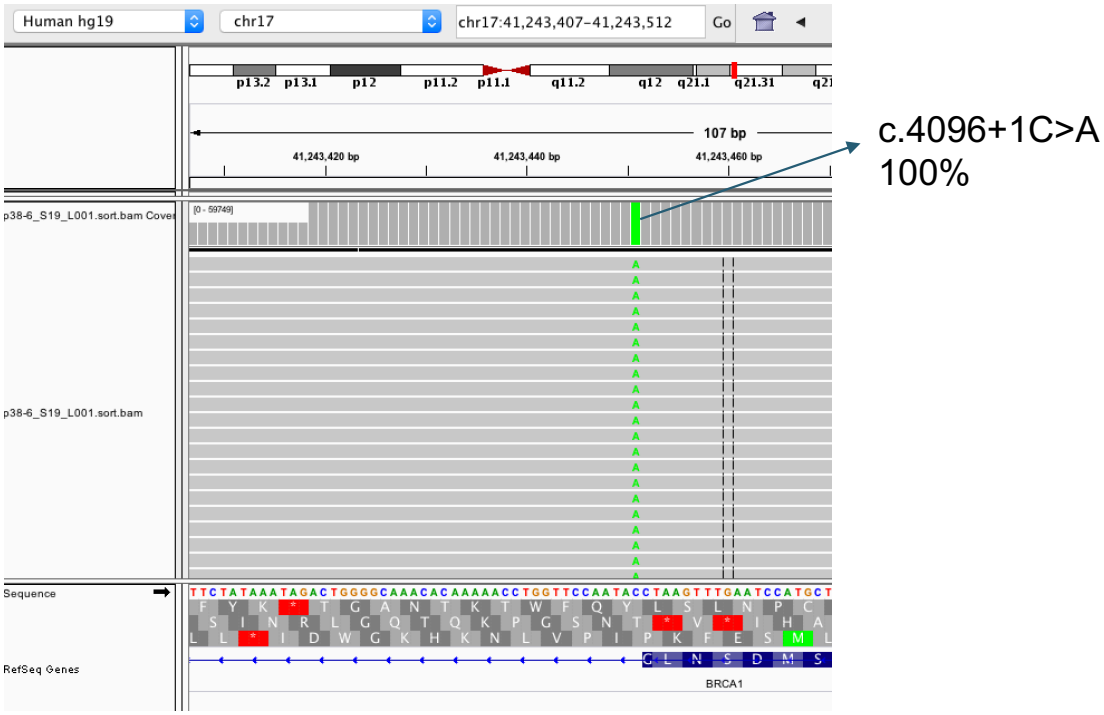


Figure 4.19. BRCA1 splice site mutation c.4096+1C>A detected at 100% frequency in COV362 cell line.

IGV screenshot of mutation BRCA1: c.4096+1C>A in COV362 cell line.

Selection of a homozygous *BRCA1* methylated cell line was straightforward, as our laboratory has the only HGSOC cell line (known to us) with this defect – WEHI-CS62 (Kondrashova et al., 2018). Although *BRCA1* methylation has been reported in the OVCAR8 cell line as well, this line has only heterozygous *BRCA1* methylation, and is therefore HR competent. In contrast, WEHI-CS62 has been shown to be HRD, maintaining its homozygous methylation in cell culture, and was rucaparib sensitive in two-week treatment experiments (Kondrashova et al., 2018).

I confirmed rucaparib response in WEHI-CS62 in independent experiments using CTG measured after two weeks of treatment. The longer rucaparib treatment was necessary due to the reduced doubling rate of the cell line (**Figure 4.20**). The cell line was found to be sensitive to rucaparib (EC50 = 0.844µM) and cisplatin (EC50 = 0. 0.168µM), and was thus prepared for CRISPR screening (**Table 4.3**).

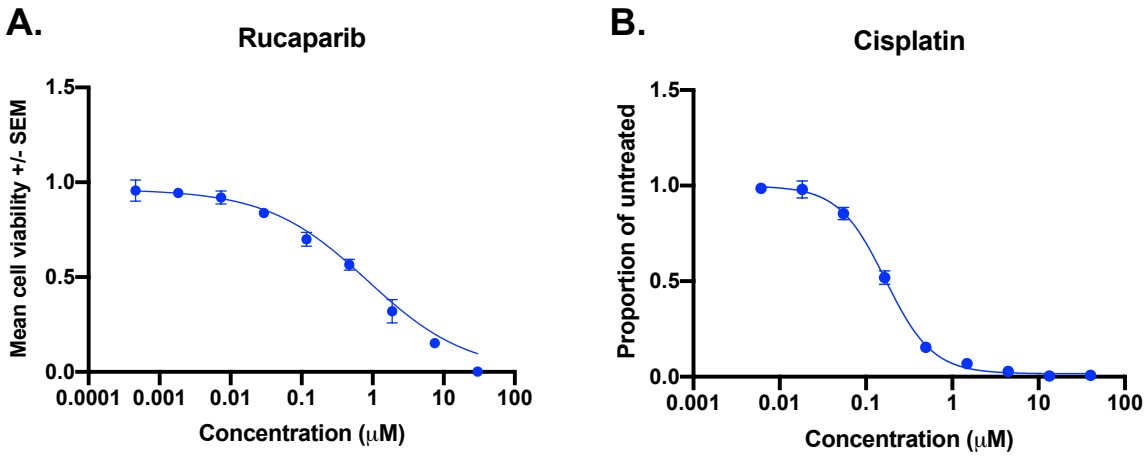


Figure 4.20. WEHI-CS62 rucaparib and cisplatin responses.
*CTG data presented is mean +/- SEM from n=2 independent experiments for **(A)** rucaparib response and **(B)** cisplatin response of WEHI-CS62 cell line. Assay run over 14 days (not seven days like other faster growing cell lines).*

4.4.3.2 Pooled PARPi-resistance CRISPR screen design and optimization

For the CRISPR screen, I chose to use the most recently validated genome-wide human CRISPR library from the BROAD institute, the Brunello library, targeting 19,114 genes using 76,441 single guide RNAs (average of 4 sgRNAs per gene) and containing 1000 non-coding control sgRNAs(Doench et al., 2016).

To generate versions of each cell line selected for CRISPR screening that stably express Cas9, I used transduction with the Cas9-mCherry lentiviral vector FUCas9Cherry. Resulting cells were FACS sorted for mCherry positivity twice to ensure purity of the lines (example FACS plot in **Figure 4.21**). I then visually determined the minimum concentration of puromycin required to kill cells of each line that are not infected with the Brunello CRISPR library (**Table 4.9**). To ensure that most cells only receive a single Brunello guide RNA during the infection, a 30-50% infection efficiency needed to be established for the screen (Doench et al., 2016). To do this, I set up lentiviral titrations of the Brunello virus and infected cells with viral titres of undiluted virus, to a 1:40 dilution of virus. Following infection, cells were incubated for 2 days, then re-plated at the same density onto 96-well plates, where each condition was treated with or without puromycin. After 3 days of incubation, cell viability was tested using the CTG cell viability assay.

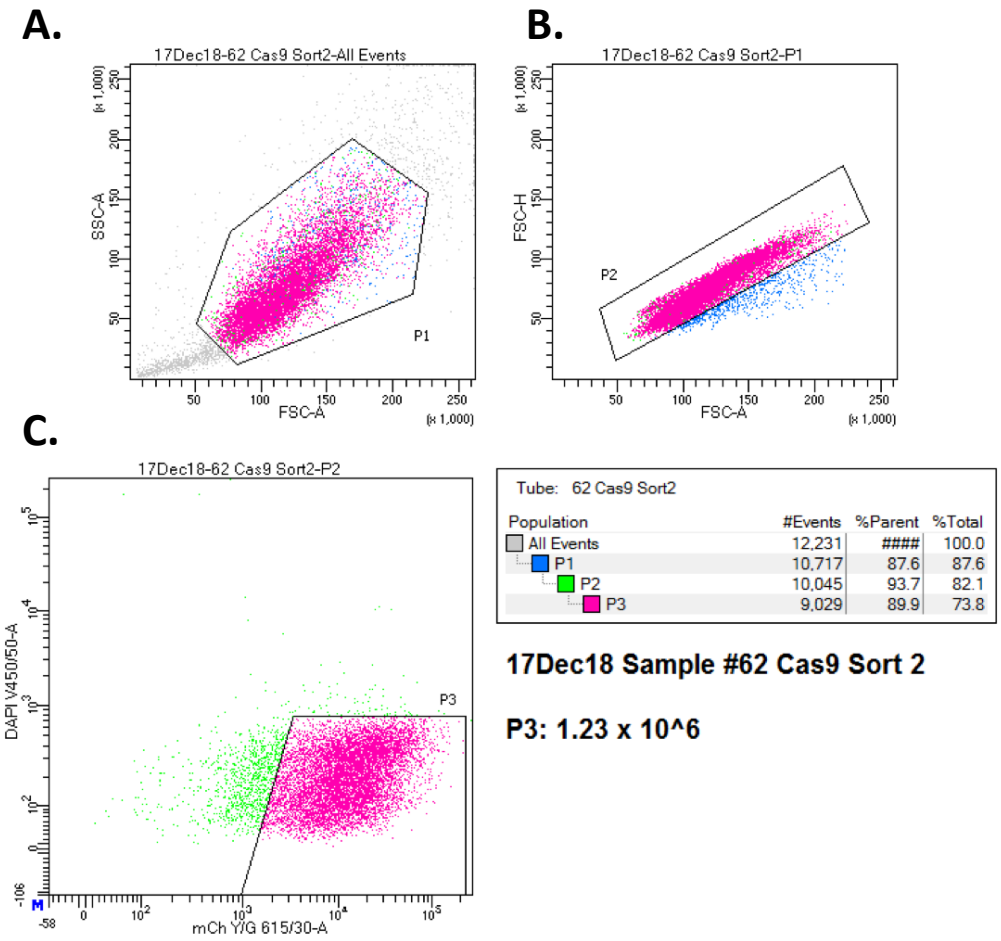


Figure 4.21. Example FACS plots of second mCherry sort for WEHI-CS62Cas9 cell line.
(A) *Scatter plot of SSC-A (side scatter area) vs. FSC-A (forward scatter area).* ***(B)*** *Scatter plot of FSC-H (forward scatter height) vs. FSC-A (forward scatter area).* ***(C)*** *Scatter plot of DAPI (4',6-diamidino-2-phenylindole) staining vs. mCh (mCherry) staining. A total of 1.23 million mCherry/Cas9 positive cells (population P3) were collected from this sort.*

Table 4.9. Minimum lethal dose of puromycin for each Cas9 cell line.
These concentrations of puromycin were used to select for cells containing integrated sgRNA's following Brunello CRISPR library infection.

Cell line	Minimum lethal puromycin concentration (µg/ml)
PEO1 cas9	0.8
UWB1.289 cas9	1.4
WEHI-CS62	1.4

CTG values obtained from these wells were then used to calculate the surviving fraction of cells under puromycin selection, where 30-50% survival would indicate a 30-50% infection efficiency. All three cell lines required a 1:40 dilution of lentivirus to fit within the appropriate infection efficiency range (**Table 4.10**).

Table 4.10. Infection efficiency calculations reveal 1:40 dilution of virus is optimal for all Cas9 cell lines.

All cell lines were found to require a Brunello virus dilution factor of 1:40 to fall within the desired infection efficiency range (30-50%) based on CTG assays.

Dilution factor	Cell line		
	PEO1	UWB1.289	WEHI-CS62
neat	93%	56%	94%
1 to 1	95%	74%	109%
1 to 2	67%	70%	107%
1 to 3	93%	63%	101%
1 to 4	83%	66%	102%
1 to 5	82%	59%	93%
1 to 10	73%	53%	87%
1 to 15	60%	50%	81%
1 to 20	58%	47%	69%
1 to 30	44%	36%	62%
1 to 40	34%	31%	49%
no virus	1%	6%	0%

These Cas9-expressing lines were then treated with rucaparib and cisplatin, along with their non-Cas9 counterparts, and run on the IncuCyte (Essen BioScience) live-cell analysis system for 7-14 days (14 days for WEHI-CS62) to confirm that the introduced Cas9 does not alter their responses to rucaparib, and that, therefore, the original EC50 and EC75 values for each line were not affected. The drug-response profiles of PEO1 and PEO1 Cas9 were not visibly different (**Figure 4.22**), nor were those for UWB1.289 and UWB1.289 Cas9 (**Figure 4.23**), or for WEHI-CS62 and WEHI-CS62 Cas9 (**Figure 4.24**).

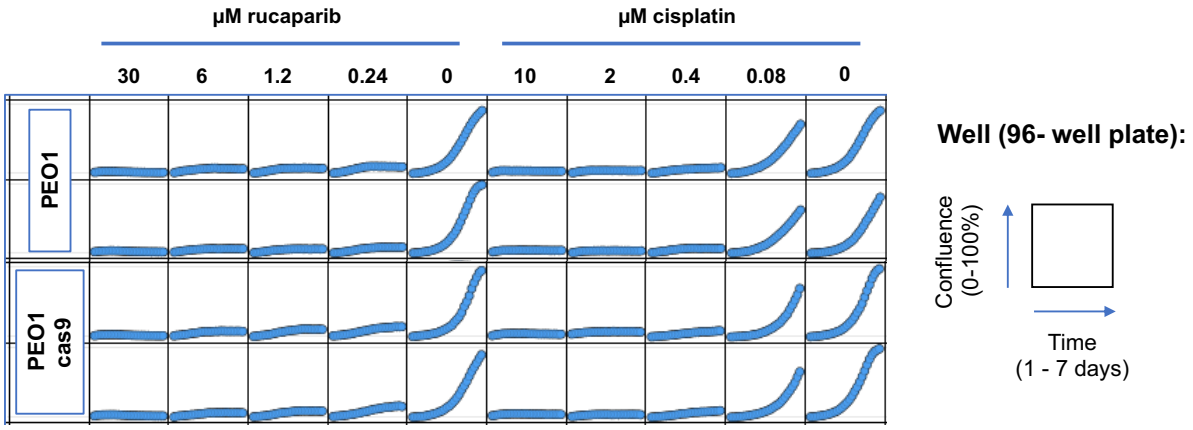


Figure 4.22. Cisplatin and rucaparib responses of PEO1 Cas9 unchanged compared to PEO1 cell line.

This figure shows confluence of cells over time in each well of plate in response to given concentrations of either rucaparib or cisplatin as measured on the IncuCyte S3 Live-Cell Analysis System (Sartorius). Each datapoint represents a well confluence measurement, where the assay was run for 7 days and n=2 wells per condition were imaged every 6 hours.

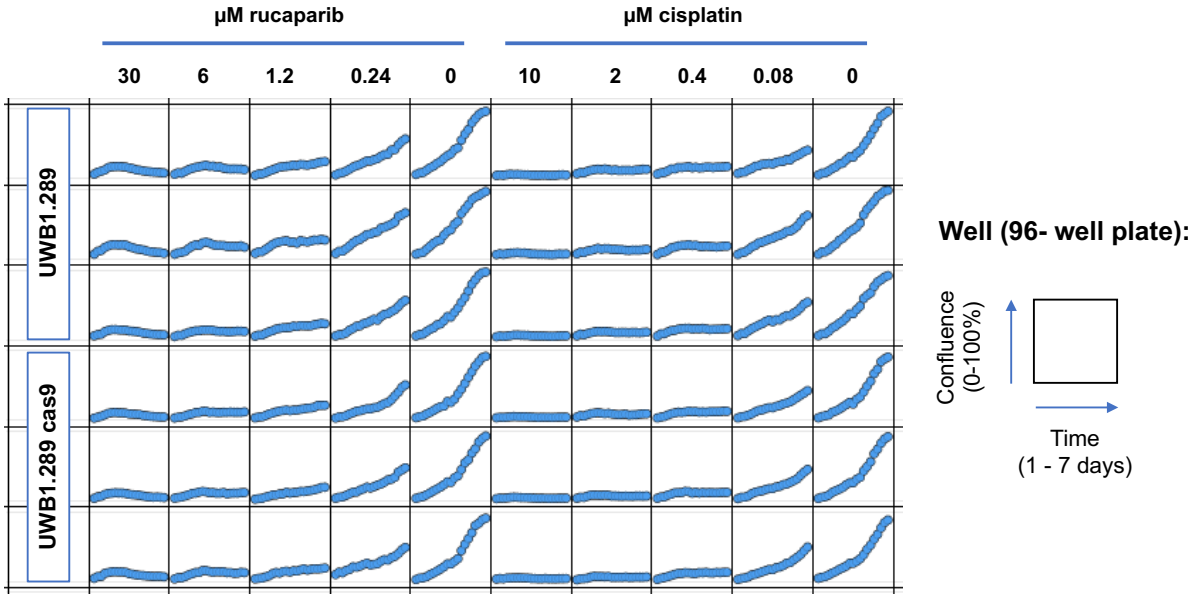


Figure 4.23. Cisplatin and rucaparib responses of UWB1.289 Cas9 unchanged compared to UWB1.289 cell line.

This figure shows confluence of cells over time in each well of plate in response to given concentrations of either rucaparib or cisplatin as measured on the IncuCyte S3 Live-Cell Analysis System (Sartorius). Each datapoint represents a well confluence measurement, where the assay was run for 7 days and n=3 wells per condition were imaged every 6 hours.

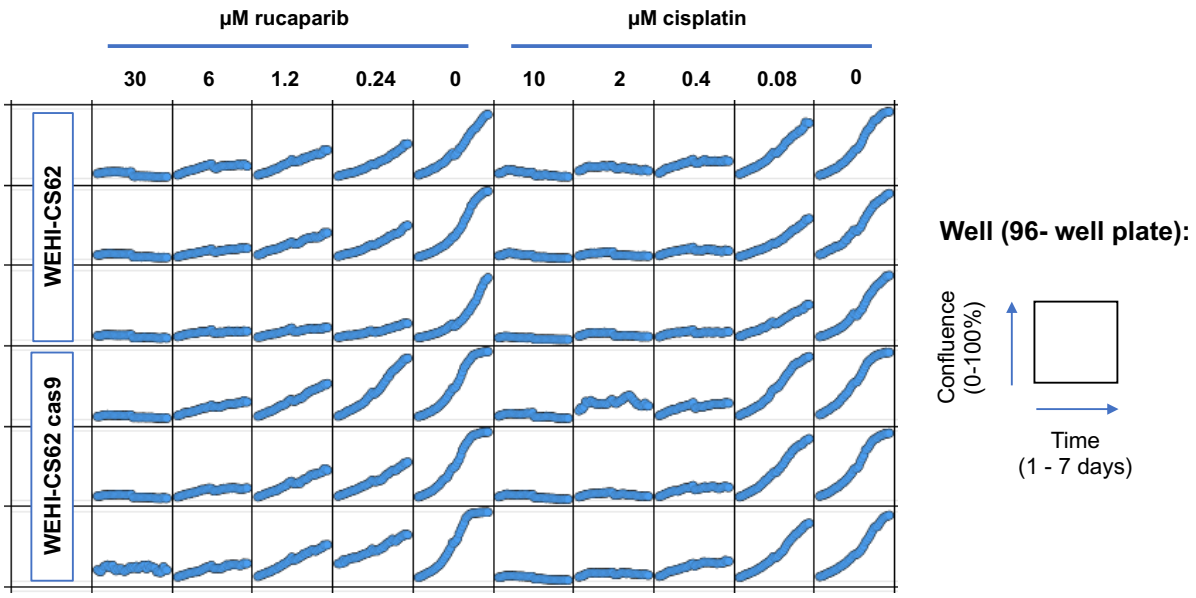


Figure 4.24. Cisplatin and rucaparib responses of WEHI-CS62 Cas9 unchanged compared to WEHI-CS62 cell line.

This figure shows confluence of cells over time in each well of plate in response to given concentrations of either rucaparib or cisplatin as measured on the IncuCyte S3 Live-Cell Analysis System (Sartorius). Each datapoint represents a well confluence measurement, where the assay was run for 7 days and and n=3 wells per condition were imaged every 6 hours.

Growth rates of these cell lines were also compared, and it was found that the Cas9 versions of each cell line were slightly faster (~0.2 days in all cases) than their non-Cas9 counterparts (**Figure 4.25**; **Table 4.11**). This was most likely due to the selection of sub-populations of cells following FACS sorting. As this difference was subtle and did not appear to significantly affect treatment responses, I was satisfied to proceed with the genome-wide CRISPR screens.

The next stage of the experiment was performing Brunello library infections of the Cas9-expressing cell lines. For the PEO1 Cas9 and UWB1.289 Cas9 cell lines, 100 million cells were infected using a 30% infection efficiency, as this would result in 30 million cells following puromycin selection which would provide sufficient diversity for this CRISPR library; 30 million cells would provide ~385x sequencing coverage per guide (Doench et al., 2016). Due to total number of cells harvested at 80-90% confluence for each cell line in culture, experiments needed to be performed in multiple multi-layer flasks to generate sufficient numbers for each infection, and infections required 2 separate spins, due to the number of culture plates required for these large cells.

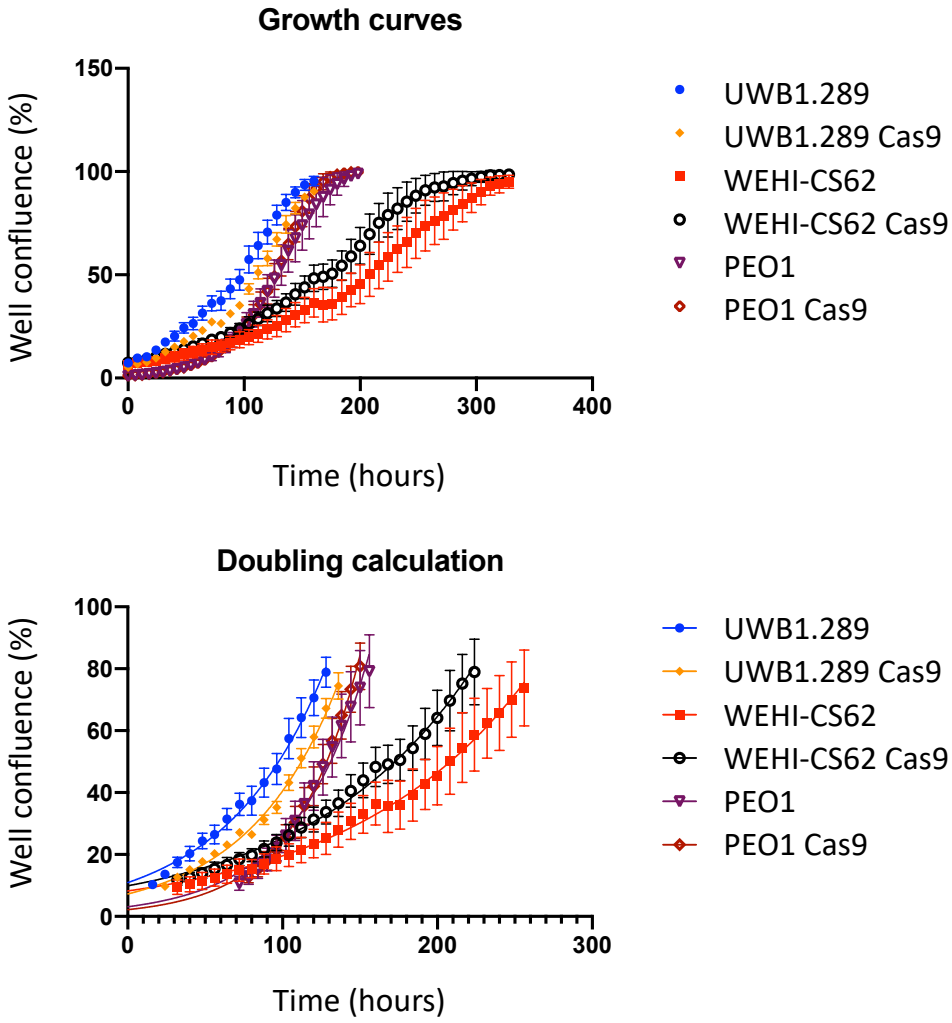


Figure 4.25. Growth and doubling rate curves of cell lines used for CRISPR screen.

(A) Growth curves and (B) exponential growth (doubling) calculation for cell lines are presented. Exponential growth calculation was performed using values between 10% and 80% confluence. Presented are mean +/-95% CI.

Table 4.11. Summary of doubling rates of cell lines used for CRISPR screen.

	PEO1	PEO1 Cas9	UWB1.289	UWB1.289 Cas9	WEHI-CS62	WEHI-CS62 Cas9
Cell doubling time (hours)	32.7	28.5	44.4	40.3	80.1	73.9
Cell doubling time (days)	1.4	1.2	1.9	1.7	3.3	3.1

For the WEHI-CS62 Cas9 cell line, 70 million cells were infected, as these cells could not yield the same numbers of cells as PEO1 Cas9 and UWB1.289 Cas9 lines from equivalent culture flasks, possibly due to increased contact-inhibition in cell culture compared to other lines (**Figure 4.26**). For WEHI-CS62 Cas9, 70 million cells infected with a 50% infection efficiency would result in >30 million cells following puromycin selection, thus equivalent to the other lines. The only consequence of a higher infection efficiency is an increased risk of cells carrying two guides, though an infection efficiency of 50% is still considered within an optimal infection efficiency (Doench et al., 2016). This also meant that only two spin infections would be required per experiment/infection replicate for all cell lines, including WEHI-CS62.

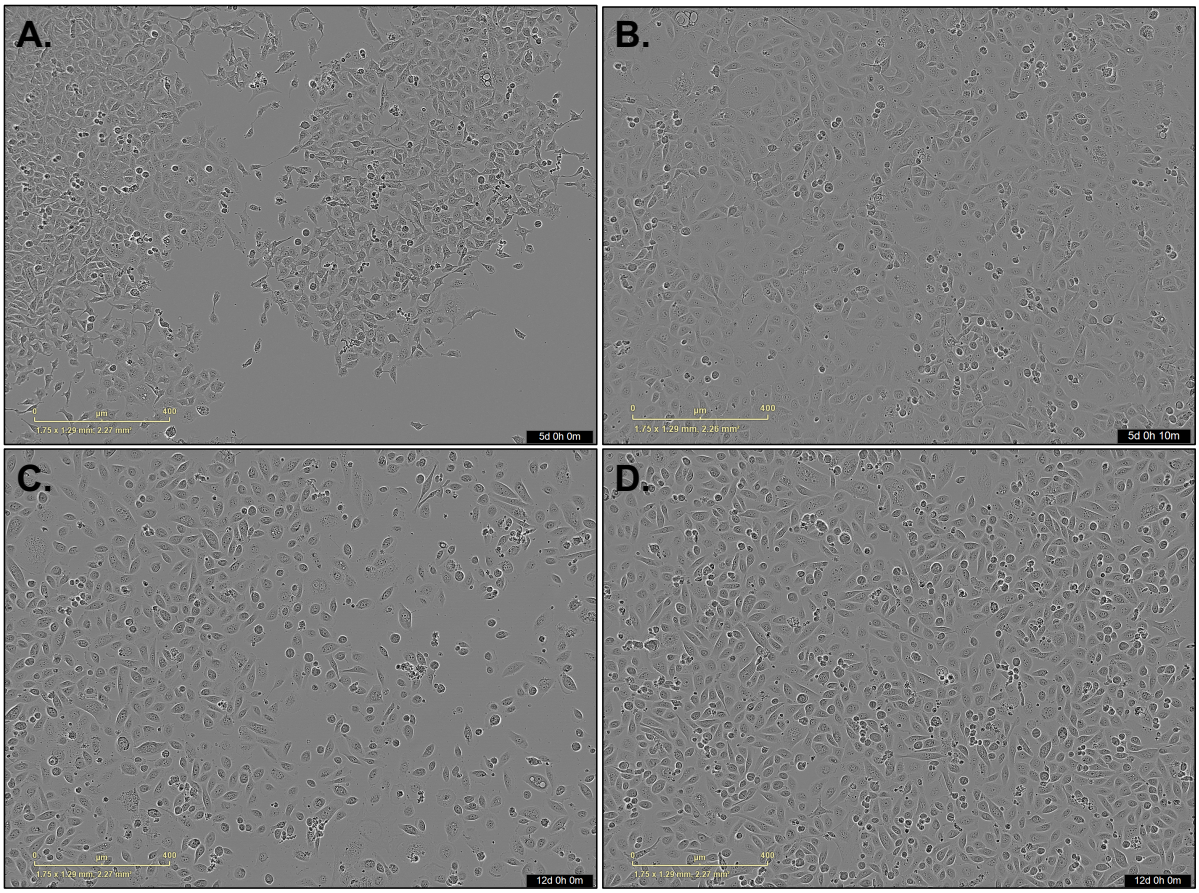


Figure 4.26. WEHI-CS62 Cas9 cells appear more dispersed in culture than the PEO1 Cas9 and UWB1.289 Cas9 cells .

*At 5 days of growth, when **(A)** PEO1 and **(B)** UWB1.289 cells are approaching well confluence, these cells appear to have less growth contact inhibition compared to **(C-D)** WEHI-CS62 cells approaching well confluence at 12 days of growth.*

PEO1 Cas9 Brunello cells were treated for 1 month with escalating doses of rucaparib (EC50 for 2 weeks and then EC75 for 2 weeks). The other screens have not been completed, but this is planned for the UWB1.289-Cas9 cells, while the WEHI-CS62-Cas9 Brunello cells will be treated for 2 months (1 month EC50 and 1 month EC75) due to their extremely slow doubling rate (3.1 days for WEHI-CS62 Cas9 vs 1.2 and 1.7 days for PEO1 Cas9 and UWB1.289 Cas9 respectively; **Table 4.11**). This way, the final results could be more comparable between these very different cell lines. DMSO control flasks were run in parallel, to be used in the final analysis (**Figure 4.16**).

The EC75 rucaparib concentrations used were considered sufficient to kill PARPi-sensitive cells, as these screens were performed as long-term culture experiments, while the CTG experiments used to calculate the EC values used were only run over 1-2 weeks (relatively short-term). Escalating doses were used to prevent massive die-off of cells, and loss of any more subtle resistance mechanisms that may develop over time.

4.4.3.3 Brunello CRISPR library diversity assessments

To establish library diversity and account for variation in infection efficiencies and resulting library representation, two independent replicate infections were created per cell line. From these two large Brunello infections, cells for treatment experiments were cryopreserved (25 million cells per vial) while 20 million infected puromycin-selected cells were harvested to check for library diversity.

Diversity-check libraries were prepared for sequencing on the Illumina NextSeq500 platform. The library diversity for each infection after >1 week of puromycin selection was calculated using a custom minimum read cut-off, which was adjusted based on the total sequencing reads. This was done to account for the inflated library diversity observed with increasing sequencing reads, most likely due to low-representation guides being missed at lower sequence coverage. Thus, the total number of unique guides was normalized by the total number of sequencing reads using a custom read cut-off of 5 reads per 10 million reads sequenced.

Sequencing of Brunello library guides in Cas9 cell lines post-infection reveals high degree of sgRNA diversity following puromycin selection, with the lowest adjusted guide count being 58,523 for PEO1 infection #2 (**Table 4.12**). The PEO1 infection #1 diversity (74,158 guides)

possibly looked better than infection #2 (58,523 guides) given it had a higher total number of reads in the sequencing (15,875,741 vs 6,961,426 respectively), meaning low-representation guides could be detected (**Table 4.12**). Slightly reduced diversity following the Brunello infection in all cell lines was expected (i.e. <76,441 – the total number of Brunello guides), as some genes that may be critical for cell survival would be lost through culture. The library diversity values for these infections were considered very high, thus I proceeded to the treatment experiments for the PEO1 Cas9 Brunello cells.

Table 4.12. All CRISPR Brunello infections demonstrate a high library diversity following puromycin selection.

Infection/Library	Total reads	Total # unique guides	Custom read cut-off (5 per 10 million)	Adjusted # unique guides	Mean coverage per guide	Median coverage per guide
PEO1 brunello #1	15,875,741	75,571	8	74,158	214.1	182
PEO1 brunello #2	6,961,426	63,926	3	58,523	118.9	96
WEHI-CS62 brunello #1	21,875,757	74,673	11	74,428	293.9	250
WEHI-CS62 brunello #2	27,666,592	76,008	14	75,848	364.7	310
UWB1.289 brunello #1	25,351,977	76,272	13	76,183	332.8	285
UWB1.289 brunello #2	36,265,832	76,381	18	76,315	475.2	393

4.4.3.4 WEHI-CS62 Cas9 did not lose BRCA1-methylation following Brunello infections

Another feature that I tested following Brunello library infections in the Cas9-expressing cell lines, was whether Brunello infections altered me*BRCA1* patterns in WEHI-CS62 Cas9. Brunello guides will still inactivate genes in Cas9-expressing cells before PARPi treatment, and cells with associated growth advantages can thus be enriched under puromycin selection. Given that there are likely to be multiple epigenetic mechanisms that can lead to loss of me*BRCA1* in these cells, it was possible that me*BRCA1* loss may be detectable even before PARPi treatment selection.

Thus, I tested me*BRCA1* status (using ddPCR) for the Brunello WEHI-CS62 Cas9 cells from each infection replicate (#1 and #2). Interestingly, Brunello infection #1 was found to be 99.9% *BRCA1* methylated, and infection #2 was found to be 99.7% *BRCA1* methylated. These values suggested that the majority of cells were still methylated at the *BRCA1* promoter.

As the two DNA samples used for testing were extracted from ~20 million cells each, I was able to estimate the number of cells within each sample that had unmethylated *BRCA1*: Infection #1 had approximately 20,000 cells with unmethylated *BRCA1* (out of ~2-million), while infection #2 had approximately 60,000 cells with unmethylated *BRCA1*.

This test will be repeated again on the Brunello WEHI-CS62 Cas9 cells following PARPi treatment, to see whether the proportion of unmethylated-*BRCA1* cells increases more significantly.

4.4.3.5 PEO1 Brunello CRISPR screen results

So far, drug treatments and screen analysis have only been completed for the PEO1 cell line, with other cell lines in progress. For each Brunello infection (#1 and #2), two treatment replicates were set-up (total of four screens). Infected cells for each replicate were treated with PARPi rucaparib EC50, or equivalent volume of DMSO for weeks #1-2, and then EC75 for weeks #3-4. To ensure some guide diversity during these experiments, a minimum 12.5 million cells maintained per passage for weeks 1-3.

Week #3 cells were selected for harvest and sequencing. Samples were sequenced on the Illumina NextSeq500 platform using the high-output kit, where the average number of reads was 32.7 million per sample, and an average of 557.9 reads per unique guide (across all samples). The data was analysed using the web-based software CRISPRAnalyzeR, which runs five analysis pipelines together (including EdgeR, DESeq2 and MAGeCK).

The analysis confirmed that there were more gene hits missing in the PARPi-treated samples than in the untreated (DMSO) controls, suggesting that many cells/guides were lost under PARPi pressure, and those left are truly PARPi-resistant (**Figure 4.27**). An average of 418 genes and 13,699 sgRNAs were missing in the untreated sample group compared to an average of 950 genes and 26,097 sgRNAs within the rucaparib-treated sample group (**Table 4.13**).



Figure 4.27. Gene count summary for PEO1 (BRCA2-mutant) CRISPR screen samples.
More target genes are missing in PARPi-treated samples compared to control (DMSO-treated) samples within each replicate run, indicating selection of only some guides in the treated samples. Suffix RUC indicates rucaparib-treated samples, while UT indicates control samples, and accompanying numbers 1-4 describe the replicate number for this cell line screen (i.e. screen replicates 1 to 4).

Table 4.13. Number of missing genes or sgRNAs for each PEO1 CRISPR screen sample.
RUC = rucaparib treated; UT = untreated (DMSO control); numerical suffix represents the experimental replicate.

PEO1 dataset	Genes missing	sgRNAs missing
Brunello_RUC_1	754	22951
Brunello_UT_1	325	10685
Brunello_RUC_2	893	25223
Brunello_UT_2	404	13204
Brunello_RUC_3	1008	27091
Brunello_UT_3	442	14659
Brunello_RUC_4	1144	29124
Brunello_UT_4	501	16249

4.4.3.6 CRISPRAnalyzeR enrichment analysis

The CRISPRAnalyzeR enrichment analysis showed genes that are likely to cause resistance when lost. Statistically significant hits detected in more than one pipeline were *PARP1* (MAGeCK and DESeq2 pipelines; **Figure 4.28**; **Table 4.14**), *KDM1A* (MAGeCK and EdgeR pipelines) and *BPTF* (DESeq2 and EdgeR pipelines; **Table 4.14**). Loss of *KDM1A* and *BPTF* has not been reported previously as a mechanism of PARPi resistance. Other hits only detected in one pipeline included *LAMTOR2*, *NDC1*, *COQ7*, *TUFM* and *RPS11*. None of these have been previously reported as PARPi-resistance genes. The only significant hit in the sgRSEA pipeline was a control guide, and was therefore not considered biologically relevant. No significant hits were observed in the Wilcox analysis. No C-NHEJ gene hits were observed as significant in any of the analyses.

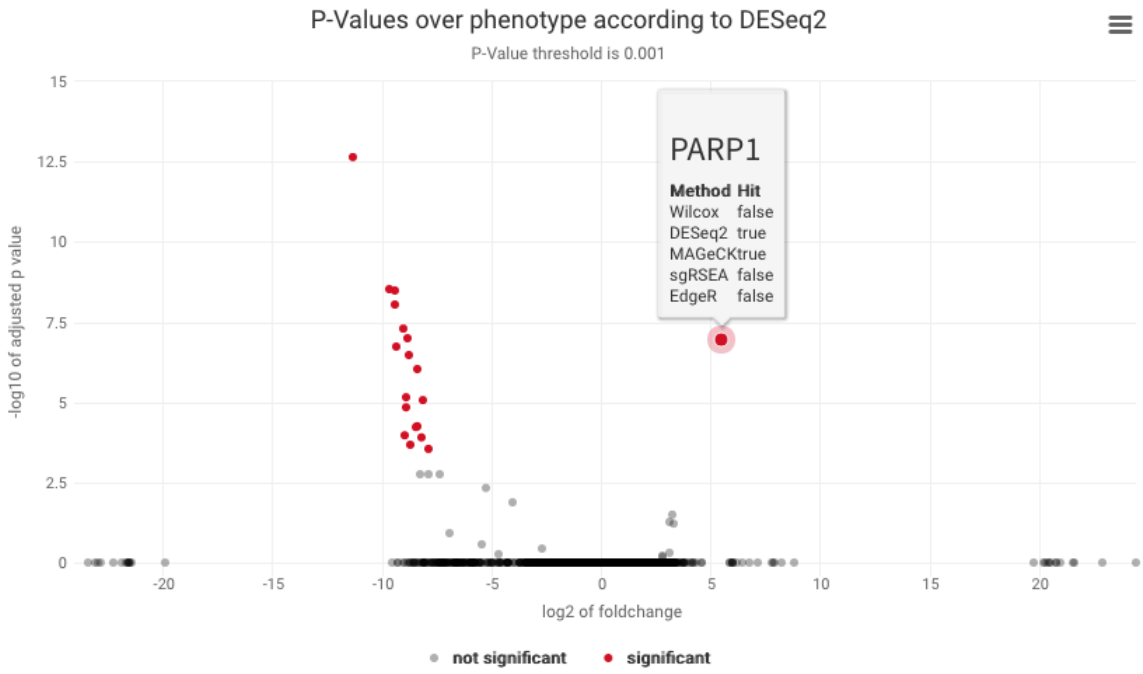


Figure 4.28. Example CRISPRAnalyzeR output for significantly enriched guides in PEO1 post-PARPi (DESeq2).

Red spots represent other statistically significant (p-value < 0.05) hits in the DESeq2 analysis pipeline, with PARP1 being one of the significant hits in this analysis and in the MAGeCK analysis.

Interestingly when the *BRCA1* and *BRCA2* genes were individually searched in the CRISPRAnalyzeR MAGeCK analysis, it was found that one of the two sgRNAs for *BRCA2* was enriched, while remaining sgRNAs for *BRCA1/2* were all depleted (**Figure 4.29**). It is possible that this enriched sgRNA was targeting a region proximal to the pathogenic *BRCA2* mutation in PEO1, resulting in a secondary or reversion mutation. However, CRISPRAnalyzeR software was not flexible enough to interrogate this hit further, therefore this hypothesis will need to be tested using alternative *in silico* methods.

Table 4.14. Significantly enriched gene hits and corresponding p-values across all analyses. *P-values <0.05 (significant) are highlighted in yellow. Only PARP1, BPTF and KDM1A are statistically significant hits in more than one analysis pipeline.*

Gene	Fold Change	P-values for each pipeline				
		Wilcox	DESeq2	MAGeCK	sgRSEA	EdgeR
PARP1	91.40	0.53	0.00	0.00	0.28	0.07
BPTF	14.72	0.53	0.00	0.81	0.41	0.04
KDM1A	5.88	0.53	0.93	0.02	0.77	0.04
TUFM	14325223.01	1.00	0.00	1.00	0.97	0.55
RPS11	4724300.46	1.00	0.00	1.00	0.97	0.62
NDC1	4.00	0.53	1.00	0.96	0.76	0.04
LAMTOR2	9.91	0.53	1.00	0.01	0.76	0.11
COQ7	5.79	0.53	1.00	0.02	0.81	0.11

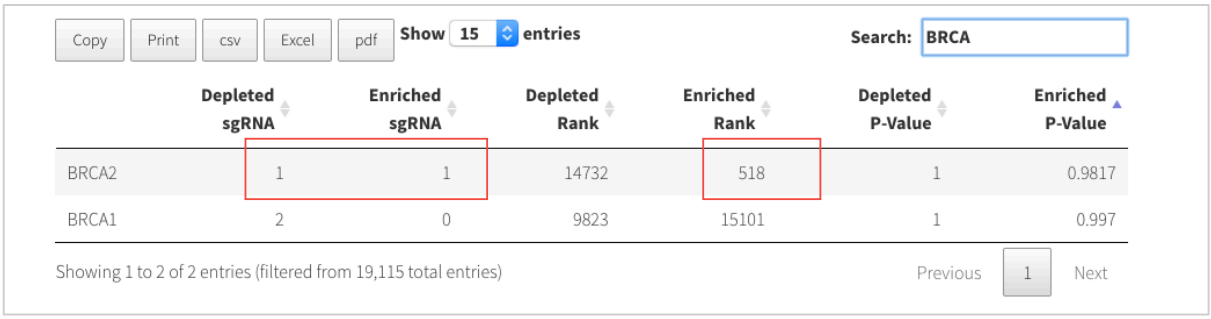


Figure 4.29. MAGeCK enriched guide results for BRCA1 and BRCA2 genes reveal one enriched single guide-RNA (sgRNA) detected in BRCA2.

4.4.3.7 CRISPRAnalyzeR depletion analysis

Another capability of the CRISPRAnalyzeR software is the ability to assess the most depleted guides/genes in the PARPi-treated samples relative to control-treated samples. These depleted hits represent genes where loss does not appear to be well tolerated in PARPi treated PEO1 cells, and thus it is possible that loss of these genes/protein would synergize with PARPi cytotoxicity in PEO1.

No significant hits were observed in the Wilcox pipeline. Given that EdgeR generated 224 statistically significant hits, and DESeq2 generated 20 statistically significant hits for the depletion analysis, only hits that were overlapping between these two pipelines are presented: C9orf27, TRAPPC5, UTP15, PSMB2, C1orf109 and DNPH1 (**Table 4.15**). The MAGeCK pipeline only produced one statistically significant gene hit – MAP4K4 (**Table 4.15**). This was also one of two significant hits in the sgRSEA analysis, where KEAP1 was also reported (**Table 4.15**). None of these genes have yet been directly reported as targets for enhancing PARPi response in the literature.

Table 4.15. Significantly depleted gene hits and corresponding p-values across all analyses. *Only mutual significant hits across EdgeR and DESeq2, DESeq2 and sgRSEA and one across MAGeCK and sgRSEA, are presented in this table as EdgeR generated 224 hits and DESeq2 generated 20 hits.*

Gene	Fold Change	Wilcox	DESeq2	MAGeCK	sgRSEA	EdgeR
C4orf27	0.07	0.53	0.00	0.24	0.07	0.04
TRAPPC5	0.00	0.53	0.00	1.00	0.99	0.04
UTP15	0.00	0.53	0.00	1.00	0.99	0.04
PSMB2	0.00	0.53	0.00	1.00	0.99	0.04
C1orf109	0.00	0.67	0.00	1.00	0.99	0.04
DNPH1	0.00	0.53	0.00	0.89	0.49	0.04
MAP4K4	0.28	0.53	1.00	0.04	0.02	0.07
KEAP1	0.07	0.75	0.01	0.69	0.05	0.07

4.5 Discussion

This project started with the observation that C-NHEJ may be playing a role in PARPi sensitivity and resistance in models of HRD HGSOC. However, attempts to validate stable/irreversible C-NHEJ loss as a *bone fide* mechanism of PARPi resistance in *BRCA2*-mutant PDX 134013 and cell line model PEO1A2 were not successful for various reasons.

4.5.1 PEO1A2 cell line characterisation raises questions

Though other groups have reported C-NHEJ loss as a PARPi resistance mechanism *in vitro*, this evidence was usually based on transient, and perhaps incompletely penetrant, silencing of core C-NHEJ proteins (McCormick et al., 2017; Patel et al., 2011). PEO1A2, where *DCLRE1C* (Artemis) was targeted using CRISPR, would have addressed this, but two main lines of evidence challenged its C-NHEJ null status. For one, PEO1A2,was found to contain a frameshift mutation in one *DCLRE1C* allele, but an in-frame 21-codon deletion in the other allele. Given that our collaborators could not detect the Artemis protein by WB in PEO1A2, I decided to check that the WB antibody does not target the same protein region targeted by CRISPR, as protein may be present but undetectable due to loss of binding epitope. I confirmed that the WB antibody does not target the same region as the sgRNA, as the Artemis rabbit polyclonal antibody (Orbigen – discontinued) targets amino acids 677-692 ([GESIAVKKRKCSLLDT], C-terminus of protein), while the CRISPR sgRNA targets nucleotides 134-146 (NM_001033855) in exon 1 (AlHilli et al., 2016). However, our collaborators later informed us that they had not been able to generate any other Artemis-deficient HRD clones, suggesting that perhaps some residual Artemis activity is indeed needed for HRD cell lines to survive, and that the protein was undetectable in PEO1A2 for other reasons.

4.5.2 Inconsistent C-NHEJ profiles of PDX 134013 tumours

Despite the initially promising *in vivo* results for the PDX 134013 C-NHEJ lineages, where lineages with C-NHEJ loss appeared more resistant to rucaparib than the one lineage with intact C-NHEJ, subsequent WB and IHC analysis that revealed discordance of C-NHEJ status in the source tumours cast doubt over these findings. However, though the source tumours appeared to have inconsistent C-NHEJ profiles spatially (as these were different tumour pieces

analysed), it is possible that the resulting PDX lineages did have some consistent C-NHEJ protein losses across passages. To address this I had prepared additional protein lysates and FFPE material of tumours from each of the C-NHEJ lineages, as well as control PDX models, and these were sent to the Kaufmann group (93 protein lysates and 60 FFPE samples in total). Unfortunately, processing and analysis of these was delayed due to limited funding and the conflicting *in vitro* and *in vivo* results both groups were observing for this project.

4.5.3 Rationale for genome-wide PARPi resistance CRISPR screens

Given that no other groups had yet reported a stable KO of any core C-NHEJ genes (i.e. excluding *53BP1* and *REV7*) in a HRD cell line, and we had not detected any C-NHEJ gene mutations in our HRD PDX during genomic screening (section 3.4.7, Chapter 3), we then started to question whether stable, long-term loss of C-NHEJ genes that do not restore HR DNA repair is possible in a HRD setting. Thus the following revised hypothesis was formed: Irreversible/stable C-NHEJ protein losses that do not restore HR are lethal to HRD HGSOC cells. The genome-wide PARPi resistance CRISPR screens were designed to address this hypothesis, but also provide additional data on other important PARPi resistance and sensitivity pathways. The cell line chosen for the first genome-wide CRISPR screen was the *BRCA2*-mutant PEO1 cell line, which was also used to create the PEO1A2 model.

4.5.4 C-NHEJ pathway hits absent in CRISPR screen

Most published studies implicating C-NHEJ loss in PARPi resistance were performed using gene knockdowns, which are transient and often incompletely penetrant gene silencing techniques. PEO1A2 was the first model reported to have KO of a core C-NHEJ gene (*DCLRE1C*) (AlHilli et al., 2016), but work from our collaboration with the Kaufmann group cast doubt over the validity of this KO. Thus, one of my primary questions in the PEO1 PARPi resistance CRISPR screen was whether any C-NHEJ gene hits were detected.

No core C-NHEJ pathway gene hits (*XRCC5*, *XRCC6*, *PRKDC*, *LIG4*, *XRCC4* and *DCLRE1C*) were observed as significant hits in this CRISPR screen enriched sgRNA analysis. This finding supports our modified hypothesis that stable/irreversible C-NHEJ pathway inactivation is not tolerated in HRD *BRCA2*-mutant cells. Whether loss of core C-NHEJ proteins (downstream of

53BP1 and REV7) can be tolerated in *BRCA1*-mutant and BRCA1-methylated HRD contexts remains to be confirmed in the UWB1.289 and WEHI-CS62 CRISPR screens, respectively.

4.5.5 Other hits absent in CRISPR screen

Interestingly, gene hits in *CHD4* or *PTIP* were also not observed as significant hits in this PEO1 CRISPR screen, although loss of these genes, like *PARP1*, has been described as a resistance mechanism in *BRCA2*-mutant ovarian cancer cells via replication fork stabilization (Guillemette et al., 2015; Ray Chaudhuri et al., 2016). In fact, *CHD4* depletion (via shRNA) was found to cause cisplatin and PARPi (olaparib) resistance in PEO1 by Guillemette et al., (2015). Given that this gene was not a hit in this CRISPR screen, it is possible that complete inactivation of this gene is not tolerated, while depletion may leave sufficient residual function for cell survival.

4.5.6 Interpretation of enriched gene hits

Here I discuss the biological relevance of the top eight statistically significant enriched gene hits across different analysis pipelines. Enriched gene hits may indicate genes that cause PARPi resistance in *BRCA2*-mutant cells when inactivated.

PARP1, *KDM1A* and *BPTF* were detected using at least two analysis methods, while *LAMTOR2*, *NDC1*, *COQ7*, *TUFM* and *RPS11* were detected in one pipeline each (**Table 4.14**). These genes are described in more detail in the following sections. Although PARP1 inactivation has been reported as a mechanism of PARPi resistance previously, each of these hits would still need to be validated using functional assays (such as targeted CRISPR, siRNA, cell viability and DNA repair assays) in PEO1 and other HRD cell lines. Matched HRC cell lines, in this case PEO4, could also be used as controls.

4.5.6.1 PARP1

One of the top gene hits observed in the enrichment analysis across the MAGeCK and DESeq2 analysis pipelines was *PARP1*. *PARP1* loss has been shown to cause PARPi resistance in *BRCA1/2*-mutant cells via replication fork stabilization (Ding et al., 2016; Ray Chaudhuri et al., 2016), though its knockdown using siRNA has been previously reported to be synthetic

lethal with *BRCA1*/*2* loss (Bryant et al., 2005; Farmer et al., 2005). Interestingly, Pettitt et al. (2018) showed that *PARP1* loss is a potent mechanism of PARPi resistance in *BRCA1* D11q mutants using genome-wide and targeted CRISPR screens. However, they did not see the same effects in non-D11q *BRCA1*-mutant cell lines. In fact, when they targeted *BRCA1* and *BRCA2* in the D11q cell lines with *PARP1* mutations, the cells were not viable. Therefore, they suggested that some residual function of *BRCA1*/*2* and HR DNA repair must be necessary for cells to survive *PARP1* loss. Our results and other published studies (Ding et al., 2016; Ray Chaudhuri et al., 2016) challenge this hypothesis. Our *BRCA2*-mutant PEO1 cells are very much deficient in HR DNA repair, based on published RAD51 foci data in PEO1 cells (Patel et al., 2011; Sakai et al., 2009), and confirmed by me in our version of this cell line. Furthermore, there is limited evidence of this resistance mechanism in patients, with only one reported case in a *BRCA1/2* WT ovarian cancer patient with acquired resistance to olaparib (Pettitt et al., 2016). Nonetheless, this gene hit will need to be validated in our PEO1 model.

4.5.6.2 KDM1A

KDM1A has not been previously reported in relation to PARPi resistance. *KDM1A* codes for lysine (K)-specific demethylase 1 (KDM1A/LSD1), which is an epigenetic transcriptional regulator. It targets gene promoters and enhancers primarily via demethylation of mono-methylated and di-methylated lysine 4 histone 3 (H3K4me1/me2), thereby remodelling the chromatin and promoting gene silencing or hormone receptor–mediated expression (Kozub et al., 2017). KDM1A was the first histone demethylase discovered and was found to play a central role in regulating pluripotency of embryonic stem cells and neurogenesis (Verigos et al., 2019). KDM1A expression has been found to be elevated in leukemias and multiple solid cancer types, including ovarian cancer, and is associated with poor prognosis (Chen et al., 2015; Konovalov et al., 2013; Verigos et al., 2019).

Apart from its role in gene regulation, KDM1A has been shown to be involved in the DNA damage response (Mosammaparast et al., 2013). This action of KDM1A is dependent on RNF168 (RING finger 168), an E3 ubiquitin-ligase that recruits DNA repair proteins to sites of damage (Bohgaki et al., 2013). Loss of KDM1A has been shown to cause hypersensitivity to γ-irradiation and increased HR DNA repair in HeLa cells, as well as impaired 53BP1 foci formation, suggesting a role for this protein in recruiting 53BP1 to sites of DNA damage (Mosammaparast et al., 2013). KDM1A overexpression has also been found to correlate with

down-regulation of *BRCA1* in triple negative breast cancer, which in turn sensitized cells to the PARPi olaparib (Nagasawa et al., 2015). Thus, loss of KDM1A would be expected to cause PARPi resistance in a *BRCA* wild-type context. However, this PARPi-resistance CRISPR screen was performed in a *BRCA2*-mutant context, and therefore this mechanism of resistance seems questionable. Furthermore, although 53BP1 loss has been shown to cause PARPi resistance in *BRCA1*-mutant cells, this finding has not been re-produced in *BRCA2*-mutant cells. How KDM1A loss would be causing resistance in *BRCA2*-mutant cells via these mechanism is unclear.

Interestingly, inhibition of KDM1A has been reported to inhibit proliferation and mediate platinum sensitivity in ovarian cancer cell line SKOV3 (Shao et al., 2018). This study suggests that KDM1A overexpression plays an unfavourable role in platinum-based chemotherapy. In contrast, based on the CRISPR screen results presented in this chapter, loss of KDM1A appears to be associated with PARPi resistance, and not sensitization. However, it is important to note that the SKOV3 cell line is considered a poor model of HGSOC based on its molecular profile (Domcke et al., 2013), and these published results may not be relevant to more accurate models of HGSOC (such as the PEO1 line used in this CRISPR screen).

KDM1A also mediates the de-methylation of multiple non-histone substrates, which include the tumour suppressor p53 – a key protein in HGSOC tumorigenesis, given its ubiquitous defects in this cancer type. KDM1A de-methylates di-methylated lysine 370 on p53, which disrupts its interaction with the C-NHEJ DNA repair protein 53BP1. 53BP1 and p53 cooperate to supress cancer (Morales et al., 2006). However, given that PEO1 cells carry a pathogenic loss of function missense mutation in *TP53* (NM_000546: c.731G>A), the effects of KDM1A loss on this pathway are ambiguous, and need to be validated.

4.5.6.3 BPTF

BPTF (Bromodomain PHD Finger Transcription Factor) is another novel PARPi resistance hit that was identified using the CRISPR screen. It is a core subunit of the NURF (nucleosome-remodelling factor) chromatin-remodelling complex. This protein recognizes H3K4me3 to facilitate transcription of chromatin and is critical for function of the transcription factor and oncogene c-MYC. *BPTF* expression correlates positively with activation of c-MYC gene signatures in human tumours, and is necessary for survival of c-MYC-overexpressing cells

(Richart et al., 2016). Although the effects of *BPTF* loss on PARPi sensitivity have not been described in the literature, studies have been published showing that MYC (c-MYC) blockade (using CDK12 inhibitor dinaciclib) is synthetic lethal with PARPi niraparib, independent of *BRCA* mutation status in triple-negative breast cancer (TNBC) (Carey et al., 2018). In this study, MYC was shown to directly regulate HR, and that MYC blockade was inducing a HR defect in TNBC cells. This contradicts our results, where *BPTF* loss (which may lead to reduced c-MYC levels/ HR) is instead causing resistance to PARPi.

Interestingly, PARP1 loss has been reported to cause both synthetic lethality with HRD and PARPi resistance in different studies/contexts. It is possible that both *KDM1A* and *BPTF* are, similarly, true biological hits, and can cause PARPi resistance. Indeed, it is interesting that both gene products play a role in chromatin remodelling via their interaction with H3K4, suggesting that perhaps, like PARP1, the PARPi resistance mechanism may be related to replication fork protection, which does not rely on restored HR function.

4.5.6.4 Other enriched gene hits

The following hits were only detected in one analysis pipeline, and thus require more thorough validation.

"Ragulator" complex protein LAMTOR2 was a significant hit (MAGeCK only) in the CRISPRAnalyzeR enrichment analysis, suggesting that loss of this protein (and impaired mTORC1 activation) leads to PARPi resistance in *BRCA2*-mutant HGSOC cells (Sancak et al., 2010). However, inhibition of mTOR has been shown to downregulate expression of DNA repair proteins and synergize with PARPi in models of *BRCA2*-mutated breast cancer (El Botty et al., 2018). Thus more work is required to resolve the relevance of this hit.

NDC1 codes for a critical component of the Nuclear Pore Complex (NPC). NPC export of certain proteins or drug targets has been described as a mechanism of resistance in cancer (Fabbro et al., 2003; Turner et al., 2012). It is, therefore, possible that this defect in the NPC may be affecting nuclear access of *PARP1*, or some other PARPi resistance protein, thereby leading to rucaparib resistance in this screen.

COQ7 (Coenzyme Q7, Hydroxylase) was another significant hit in the CRISPRAnalyzeR enrichment analysis (MAGeCK only). COQ7 is involved in biosynthesis of Coenzyme Q (CoQ), which is a critical component of the mitochondrial oxidative phosphorylation (OXPHOS) system (Lohman et al., 2014). There does not appear to be a clear link between PARPi resistance and COQ7 loss in the literature.

TUFM (Mitochondrial Tu translation elongation factor) is a nuclear-encoded factor involved in mitochondrial protein translation (Shi et al., 2012). There are no publications in the literature describing a direct link between TUFM and PARPi sensitivity and resistance. Therefore, this hit, along with COQ7, presents another defect in the OXPHOS pathway that has not been previously described as a mechanism of PARPi resistance. There are published links between PARP1 function and energy (ATP) depletion in cells, where overactivity of PARP1 leads to mitochondrial exhaustion and destabilization, which in turn leads to cell death (Morales et al., 2014). PARP inhibition has been shown to protect and stabilize the mitochondria, even in HRD contexts before cell death (Cseh et al., 2019; Hocsak et al., 2017). How OXPHOS or mitochondrial defects would promote PARPi resistance, however, is unclear.

RPS11 is a ribosomal protein gene of the smaller 40S ribosome subunit (Higa et al., 1999; Yong et al., 2015). Increased expression of RPS11 has been found to correlate with shorter patient survival in glioblastoma (Yong et al., 2015), with no other publications describing a role for this specific protein in the context of cancer. More broadly, targeting of ribosome biogenesis using the RNA polymerase I inhibitor CX-5461 has been shown to have some success in treatment of ovarian cancer in pre-clinical models, and is predicted to synergize with PARPi in the clinic (Higa et al., 1999; Sanij et al., 2020; Yong et al., 2015). Although there are multiple biological levels at which CX-5461 exerts its cytotoxic effects in HGSOC cells (Sanij et al., 2020), a defect in RPS11 perturbing ribosome function may mimic the effects of reduced ribosome biogenesis caused by CX-5461. However, this would be expected to enhance the effects of PARPi, rather than rescue the viability of HGSOC cells, which is what our PEO1 CRISPR screen indicates. Thus, more work is required to validate this gene hit and dissect the underlying biology.

4.5.7 Interpretation of depleted gene hits

Another valuable aspect of the CRISPR screen analysis is the ability to define guides/genes that are depleted instead of enriched in the PARPi-treated cell population. Depleted gene hits in the PEO1 CRISPR analysis may indicate gene losses that are not tolerated in *BRCA2* mutant cells treated with PARPi, and thus targets that, when inactivated, may synergize with PARPi. This could be validated using targeted CRISPR or siRNA knock-down, and even drug synergy analysis for targets where chemical inhibitors are available. Targets where inactivation synergizes with PARPi could then be investigated functionally to elucidate the underlying mechanisms of synergy (for example DNA repair changes). This is where HRC controls (like PEO4) become extremely useful, as they would reveal how specific/targeted the synergistic effects are to HRD cell lines and, consequently, to HRD HGSOC cancers.

Presented in the results section are the six statistically significant hits shared across the EdgeR and DESeq2 pipelines (as EdgeR analysis generated 224 hits and DESeq2 generated 20 hits), and the only significant hit from the MAGeCK analysis. In the following sections I will discuss the four top hits from EdgeR/DESeq2 (*C4orf27, DNPH1, C1orf109* and *UTP15*) and the one top hit from the MAGeCK analysis (*MAP4K4*) in more detail.

4.5.7.1 C4orf27 (HPF1)

C4orf27 codes for Histone PARylation Factor 1 (HPF1), a regulator of PARP1 required for histone serine ADP-ribosylation via PARP1 and PARP2 (Bonfiglio et al., 2017). HPF1 promotes histone serine ADP-ribosylation in response to DNA damage and limits DNA damage-induced hyper-automodification of PARP1, thereby ensuring genome stability (Bonfiglio et al., 2017; Gibbs-Seymour et al., 2016). Interestingly, HPF1 loss has been shown to cause PARPi-sensitivity in the past, with human cells lacking HPF1 displaying increased sensitivity to PARPi and other DNA damaging agents (Gibbs-Seymour et al., 2016). CRISPR knockout of *HPF1* sensitized U2-O-S (human bone osteosarcoma epithelial) cells to PARPi, but this phenotype was fully rescued with additional knockout of PARP-1. This suggests that the mechanism of sensitivity is dependent on the trapping of PARP1 by PARPi (Gibbs-Seymour et al., 2016). This makes *C4orf27* an exciting target to validate and will be prioritized.

4.5.7.2 DNPH1

DNPH1 (2'-Deoxynucleoside 5'-Phosphate N-Hydrolase 1; also known as Rcl) is an enzyme involved in nucleotide metabolism and has been described as a potential anti-cancer target given its role in cellular proliferation via c-Myc (Amiable et al., 2013; Lewis et al., 1997). No clear links between *DNPH1* loss and PARPi activity have yet been reported in the literature, thus this hit will require further validation.

4.5.7.3 C1orf109

There is currently limited information published on this gene, as the protein product of *C1orf109* was only characterized in 2012 (Liu et al., 2012). The C1ORF109 protein appears to be a target of the ubiquitous protein serine/threonine kinase CK2, which is essential for regulation of cell growth and proliferation. Exogenous expression of C1ORF109 *in vitro* leads to enhanced proliferation and colony forming capacity *in vitro* (Liu et al., 2012).

Furthermore, C1ORF109 was found to be overexpressed in multiple breast cancer cell lines and a melanoma cell line compared to non-cancer cell lines (Liu et al., 2012). Thus C1ORF109 may play a role in tumour cell proliferation. Based on the limited characterisation of this gene, however, it is unclear how loss of this gene would synergize with PARPi, especially as slower cell cycle progression tends to lead to PARPi resistance due to reduced replication stress, rather than PARPi synergy (Mateo et al., 2019).

4.5.7.4 UTP15

UTP15 codes for a small nucleolar RNA (snoRNA)-associated protein of the Small Subunit Processome (SSU) which is essential for 18S ribosomal RNA (rRNA) biogenesis. This ribosome biogenesis factor is involved in nucleolar processing of pre-18S rRNA and is required for optimal pre-rRNA transcription by RNA polymerase I (Prieto et al., 2007). No clear links have yet been made between this protein and PARPi action in the literature, thus this gene hit requires further validation.

4.5.7.5 MAP4K4

The MAP4K4 (Mitogen-Activated Protein 4 Kinase 4) protein is a member of the serine/threonine protein kinase family and has been found to be involved in a variety of cellular functions. Specifically in cancer cells, reduced MAP4K4 generally results in induction of apoptosis, cell cycle arrest, inhibition of cell growth and proliferation, and increased migration/invasion (Gao et al., 2016). However, knock-down of MAP4K4 in the ovarian carcinoma cell line SKOV3 resulted in reduced migration (Collins et al., 2006). It is not clear how loss of this gene would synergize with PARPi in PEO1 cells, and this hit therefore requires further validation.

4.5.7.6 KEAP1

The Keap1 protein regulates the activity of the Nrf2 transcription factor, which is involved in activation of cytoprotective gene expression programs in response to oxidative stress. Inactivation of KEAP1 or disruption of KEAP1-NRF2 interactions generally leads to drug resistance, increased cell proliferation and poor prognosis in the context of cancer (Kansanen et al., 2013). However, a recent study has demonstrated that mouse models of non-small cell lung cancer with knockout of KEAP1 have increased sensitivity to inhibitors targeting DNA damage response proteins ATR and ATM, and this is enhanced in combination with the PARPi olaparib (Galan-Cobo et al., 2019). As KEAP1 is a significant hit in the sgRSEA and DESeq2 depletion analyses, it is possible that defects in *BRCA2,* or indeed other HR defects, may allow KEAP1 loss to synergize with PARPi without the need for ATMi or ATRi. However, the effects of KEAP1 loss on PARPi response in HRD cells will need to be validated.

4.5.8 In silico validation of hits

One limitation of the current PEO1 CRISPR screen analysis is that it has only been performed by me using the web-based CRISPRAnalyzeR software. Although this software has proven extremely user-friendly and comprehensive (given the inclusion of multiple analysis pipelines), CRISPRAnalyzeR was not very flexible in terms of accounting for different experimental designs. For example, it was impossible to indicate that two treatment replicates for each of two infections were used in this screen, and instead they were listed as four replicates. The different analysis pipelines in CRISPRAnalyzeR also produced very different hits in both the

enrichment and depletion analyses, with only few overlapping genes between pipelines. Of note, the results presented here were using a cut-off of zero, because *PARP1*, the known resistance gene hit, was only observed with these parameters. However, different hits were observed when applying the recommended low-read cut-off, even the relatively low cut-off of 5-reads. It would, therefore, be critical to have this data re-analysed using a more complex, custom bioinformatics analysis pipeline that can take into account the experimental design of these CRISPR screens. Hits from the CRISPRAnalyzeR analysis could then be cross-validated *in silico* using this custom pipeline, before prioritizing hits for molecular and functional validation.

4.5.9 Future CRISPR screens

Given that the Brunello library diversity for the infections of the other two cell lines, *BRCA1*-mutant UWB1.289 and *BRCA1*-methylated WEHI-CS62, has been shown to be consistently high, it is now feasible to begin the drug treatment and control replicate experiments for these lines. Culture or these lines with and without treatment will last for one (UWB1.289) to two months (WEHI-CS62) per experimental replicate.

Expected hits for the CRISPR screen of *BRCA1*-mutant and *BRCA1*-methylated cell lines include the early C-NHEJ pathway genes *53B1*, *REV7* and *RIF1,* which are known PARPi resistance factors (Boersma et al., 2015; Bunting et al., 2010; Gupta et al., 2018; Lord et al., 2017; Xu et al., 2015). *DYNLL1* was uncovered and validated as a PARPi (olaparib)-resistance gene in the UWB1.289 cell line using a different CRISPR library (GeCKO library, BROAD institute) (He et al., 2018), and we would therefore expect to see it in the Brunello CRISPR screen of the same cell line, but with PARPi rucaparib. Some resistance genes detected in the Brunello CRISPR *BRCA2*-mutant screen and other studies, such as *PARP1*, may also be expected in the *BRCA1*-mutant and *BRCA1*-methylated screens, it will be interesting to see what gene hits are common across the three HRD backgrounds. However, the *BRCA1*-methylated cell line screen is expected to yield additional hits related to de-methylation of the *BRCA1* promoter. This may be in the form of DNA methyl-transferase defects, which would lead to *BRCA1* methylation loss, restored expression and PARPi resistance (Kondrashova et al., 2018).

CRISPR screening technology has proven powerful in the context of uncovering mechanisms of PARPi-resistance (He et al., 2018; Pettitt et al., 2016). However, no studies comparing hits across different HRD contexts have yet been published, nor have there been any screens carried out on a *BRCA1*-methylated model of HGSOC. The cell line panel selected in this project, including the WEHI-CS62 model with homozygous *BRCA1* methylation, provides a unique approach to genome-wide PARPi-resistance CRISPR screening in HGSOC, and is likely to uncover novel resistance genes/pathways, which may in turn reveal novel drug targets for combating PARPi-resistance.

5 *RAD51C* promoter methylation and PARPi response

5.1 Introduction

Although the impacts of deleterious HR gene mutations, e.g. in *BRCA1*, *BRCA2* and *RAD51C*, on platinum and PARPi responses are well recognised for HGSOC, the effects of HR gene promoter methylation in these contexts has remained more difficult to interpret (Bernards et al., 2018; Chiang et al., 2006; Cunningham et al., 2014; Ruscito et al., 2014; Stefansson et al., 2012). HR gene promoter methylation has only been shown to correlate with reduced gene expression for the *BRCA1* and *RAD51C* genes, with methylation of these genes often mutually exclusive of *BRCA1/2* mutation, excluding structural variants and aneuploidy (Bernards et al., 2018; Cancer Genome Atlas Research et al., 2013; Lheureux et al., 2017b; Ruscito et al., 2014; Swisher et al., 2009; Swisher et al., 2017).

Past pre-clinical studies have provided some evidence that silencing of these genes results in HRD (Drew et al., 2011; Min et al., 2013; Veeck et al., 2010). Genomic signatures related to *BRCA1/2* mutations have also been detected in some breast and ovarian cancer cases with *BRCA1* and *RAD51C* methylation, suggesting these events may indeed create HRD that could sensitise cells to platinum or PARPi treatment (George et al., 2013; Polak et al., 2017). However, based on mixed outcomes in several PARPi clinical studies that included screening for HR gene methylation, it was long unclear whether *BRCA1* and *RAD51C* methylation predicted PARPi response (Bernards et al., 2018; Lheureux et al., 2017b; Ruscito et al., 2014; Swisher et al., 2009; Swisher et al., 2017; TCGA, 2011).

Our group recently uncovered, using our cohort HGSOC PDX models, that the zygosity of methylation in the *BRCA1* promoter is a key factor for determining PARPi and platinum response in HGSOC (Kondrashova et al., 2018). This discovery was made possible by the fact that the only human cells propagated by PDX are tumour cells, and not stromal (non-tumour) human cells. Mouse stromal cells have been shown to replace human stromal cells as early as the second passage in NSG mouse PDX models (Maykel et al., 2014). One of the limitations of previous studies was the non-quantitative methods used, such as methylation-specific PCR (MS-PCR) (Bernards et al., 2018; Ruscito et al., 2014), as well as contaminating non-tumour tissue making it impossible to interpret the zygosity of HR gene methylation with human-specific assays (Cunningham et al., 2014). Our study demonstrated that all copies of *BRCA1*

must be methylated for PARPi response, that multiple methylated copies of *BRCA1* may be present, and that losing methylation of a single *BRCA1* copy was sufficient to restore HR DNA repair and cause PARPi resistance. This revealed an approach for predicting which patients with *BRCA1* methylation should respond to platinum or PARPi in the clinic, and this is now being investigated further in the EMBRACE study, a phase II clinical trial of olaparib in HRD metastatic breast and relapsed ovarian carcinomas lacking *BRCA1/2* mutations.

Though we are now beginning to better understand about *BRCA1* methylation stability under platinum or PARP inhibitor treatment pressure, very little is still known about *RAD51C* methylation (me*RAD51C*) in HGSOC. *RAD51C* is a *RAD51* paralog and is critical for HR DNA repair, playing a core role in resolution of DNA strand Holliday junctions during recombination (Liu et al., 2004). *RAD51C* is a known ovarian cancer susceptibility gene (Loveday et al., 2012; Meindl et al., 2010; Pelttari et al., 2011), and recently it was shown that deleterious mutations in this gene cause PARPi sensitivity, while secondary reversion mutations that restore function of at least a single *RAD51C* copy cause PARPi resistance (Kondrashova et al., 2017). This finding affirms *RAD51C* status as a *bone fide* PARPi-sensitising gene. The fact that the secondary mutations were observed on only one copy supports a model of genetic haplosufficiency for this gene.

RAD51C methylation is found in approximately 2% of HGSOC patients (Cunningham et al., 2014; TCGA, 2011), and its effects on PARPi response remain unclear (Bernards et al., 2018). This has likely been due to the same limitations as in clinical studies of *BRCA1* methylation – difficulty in assessing methylation zygosity in the presence of contaminating human stroma using human-specific assays and the ability of a single demethylated allele to cause therapy resistance (Kondrashova et al., 2018).

I hypothesised that the same mechanisms of zygosity influencing PARPi response in *BRCA1* methylated HGSOC tumours would predict PARPi response in me*RAD51C* tumours. I also hypothesised that homozygous me*RAD51C* can become heterozygous under PARPi or cisplatin treatment pressure, as was observed for *BRCA1* methylated patient samples in our previous work (Kondrashova et al., 2018). To address these questions, I studied two PDX models of me*RAD51C* (first described in Chapter 3) in great detail. I also analysed a large panel of patient samples collected by AOCS and University of Washington, where me*RAD51C* had

been previously detected, but not assessed for its zygosity (Bernards et al., 2018; Patch et al., 2015).

One of these HGSOC PDX models, 134183, was generated by our laboratory from a chemo-naive HGSOC patient (AOCS), while the other PDX, PH039, was sourced from collaborators at the Mayo Clinic (MN, USA), where its response to the PARPi niraparib has been described previously (AlHilli et al., 2016). PDX PH039 was derived from a chemonaïve stage III HGSOC that was found to be sensitive to platinum-based chemotherapy (Treatment Free Interval [TFI] = 11.7 months), but lacking any HR pathway mutations (AlHilli et al., 2016). The PDX was found to be sensitive to both carboplatin and the PARPi niraparib *in vivo*, with the carboplatin response reflecting the patient's sensitivity to platinum in the clinic (AlHilli et al., 2016).

Our collaborators at the Kaufmann group (Mayo Clinic) have subsequently driven resistance in a lineage of PDX PH039 they had generated in their laboratory (MAYO-PH039) using cyclical re-treatments with niraparib (**Figure 5.1**). They found that these tumours lost me*RAD51C* under niraparib treatment pressure, which correlated with restored expression of the *RAD51C* gene (**Figure 5.1**).

As we were studying zygosity of me*RAD51C* in 134183 PDX model, we decided to also test the resistance-driven MAYO-PH039 samples using Methylation-Specific High Resolution Melt (MS-HRM) and other quantitative assays. Moreover, through a past independent collaboration with the Haluska group (Mayo clinic), our laboratory had also established and characterised its own lineage of PDX PH039 in house (WEHI-PH039).

For this me*RAD51C* project, we also aimed to re-establish WEHI-PH039 (from cryopreserved material) and validate the niraparib re-treatment results of MAYO-PH039 in our WEHI-PH039 lineage using two PARPi – niraparib and rucaparib. We aimed to confirm that resistance was not unique to niraparib, the MAYO-PH039 lineage, or to the host PDX mouse strain, since MAYO-PH039 was grown in SCID Beige mice, while ours are in NOD/SCIDγ (NSG) mice.

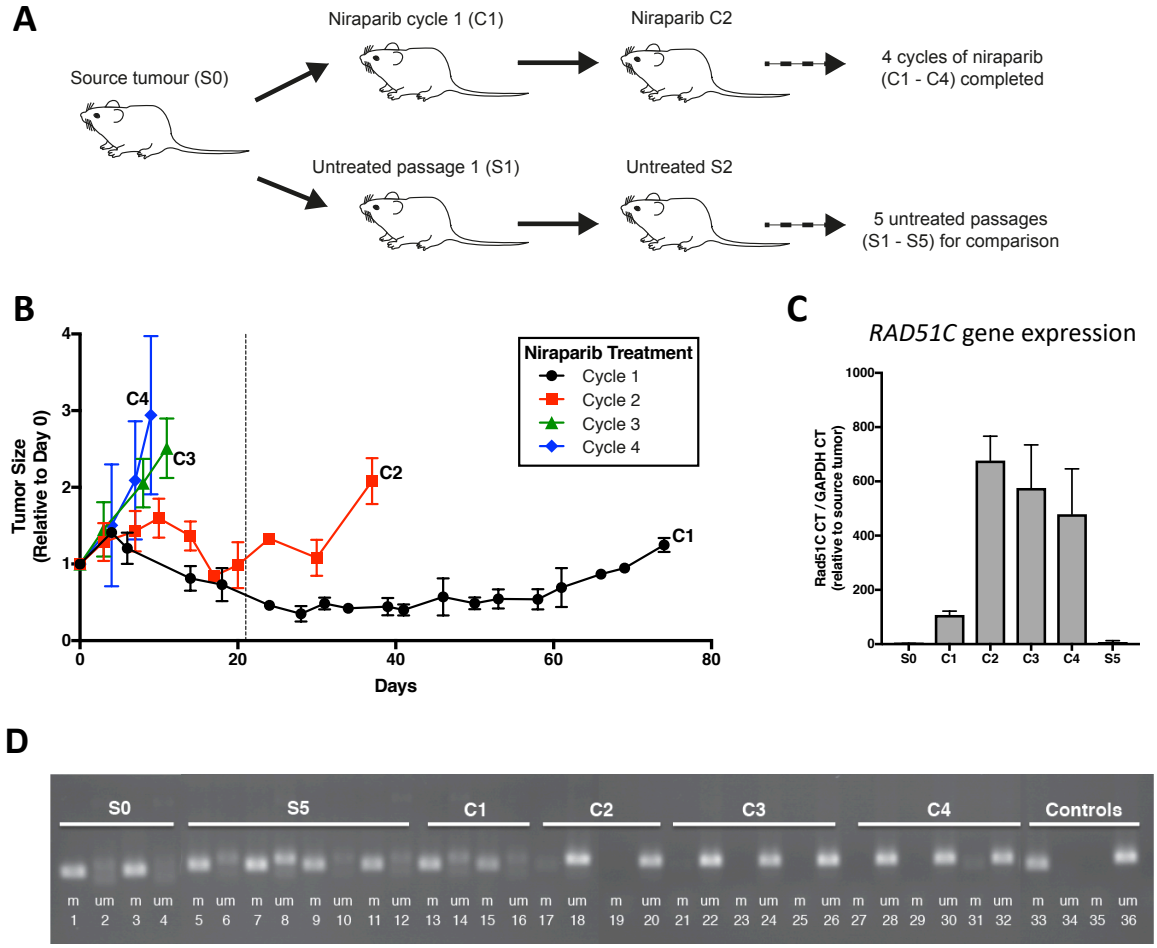


Figure 5.1. PDX MAYO-PH039 niraparib re-treatment experiments.

Unpublished data from the Kaufmann group (Mayo clinic). ***(A)*** *PDX were cyclically re-treated with 100mg/kg niraparib (cycles (C) 1-4) or passaged without treatment (Source (S) 1-5)* ***.(B)*** *PDX MAYO-PH039 became more resistant to PARPi niraparib with each treatment cycle, and this resistance correlated with* ***(C)*** *RAD51C gene expression and* ***(D)*** *meRAD51C loss by MS-PCR; m= methylated RAD51C, um= unmethylated.*

5.2 Chapter 5 hypotheses

1. Homozygous me*RAD51C* predicts platinum and PARPi responses in HGSOC.

2. Homozygous me*RAD51C* can become heterozygous or completely lost under platinum and PARPi pressure, leading to drug resistance.

5.3 Chapter 5 aims

1. To characterise novel HGSOC PDX models with *RAD51C* promoter methylation

2. To drive *RAD51C* promoter methylation loss in these models using PARPi or cisplatin and to screen for heterozygous methylation patterns

3. To screen for heterozygous *RAD51C* promoter methylation patterns in patient samples to determine whether this state is associated with platinum/PARPi resistance.

5.4 Results

5.4.1 PDX 134183 characterisation

PDX model 134183 was derived from a 65 year-old patient diagnosed with bulky stage III HGSOC diagnosed in 2015. This patient was treated with paclitaxel and carboplatin chemotherapy plus Avastin (bevacizumab) in the first-line. This patient responded to first-line treatment, with a TFI of 11 months. Second-line therapy of paclitaxel and carboplatin chemotherapy had a reduced TFI of 7 months. The TFI was shorter again for third-line therapy with carboplatin and gemcitabine, where it was 4 months. This patient eventually died from the disease, having never received PARPi.

The HGSOC PDX was derived prior to chemotherapy in this patient, and was found to be cisplatin sensitive ($p < 0.001$; **Table 5.1**; **Figure 5.2**), mirroring the initial response of the patient to platinum chemotherapy. This PDX also demonstrated some response to PARPi rucaparib (**Table 5.1**; **Figure 5.3**) and niraparib (**Table 5.1**;
Figure ***5.4***). However, only a nonsense *TP53* mutation NM_001126118:c.544G>T (p.E182X) was found by BROCA sequencing, with no other predicted pathogenic mutations detected. Given the moderate response of this PDX to PARPi *in vivo*, I tested this model for *BRCA1* and *RAD51C* promoter methylation.

Me*RAD51C* was detected by two independent methods, MS-PCR (collaborators at the University of Washington, USA) and MS-HRM (collaborators at the Oliva Newton John Cancer Centre, Australia). Interestingly MS-HRM analysis revealed homozygous me*RAD51C* status in both pre- and post-treatment samples (**Figure 5.5**). No *BRCA1* methylation was detected in this PDX.

PDX 134183 also demonstrated undetectable *RAD51C* gene expression in RNA sequencing compared to control PDX model 134013 (**Figure 5.6A**), and the absence of detectable protein expression by immunoblotting (**Figure 5.6B**), suggesting that the homozygous methylation of the *RAD51C* promoter was, indeed, causing gene silencing.

Table 5.1. Summary of PDX 134183 in vivo treatment responses compared to control.

The p-values for each treatment compared to DPBS-treated control tumours are presented. PDX 134183 is sensitive to cisplatin and shows some response to PARPi rucaparib and niraparib. TTH – Time to harvest, TTP – Time to progression.

PDX 134183	*p* - value	Median TTH (days)	Average TTP (days)
Cisplatin 4mg/kg	<0.001	183	145
Rucaparib 300mg/kg	0.067	71	43
Rucaparib 450mg/kg	0.043	74	47
Niraparib 100mg/kg	0.008	95	36

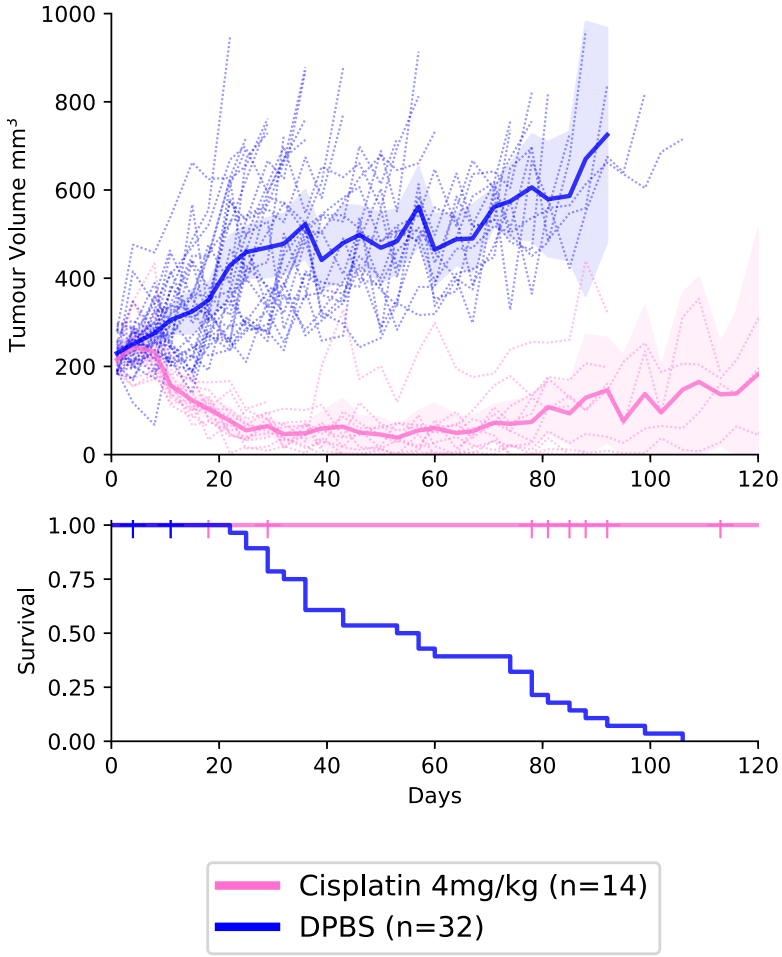


Figure 5.2. PDX 134183 is sensitive to cisplatin at a 4mg/kg dose.

Tumour volume data presented is individual tumours (dotted lines) and mean (thick line) +/- 95% CI (shaded area).

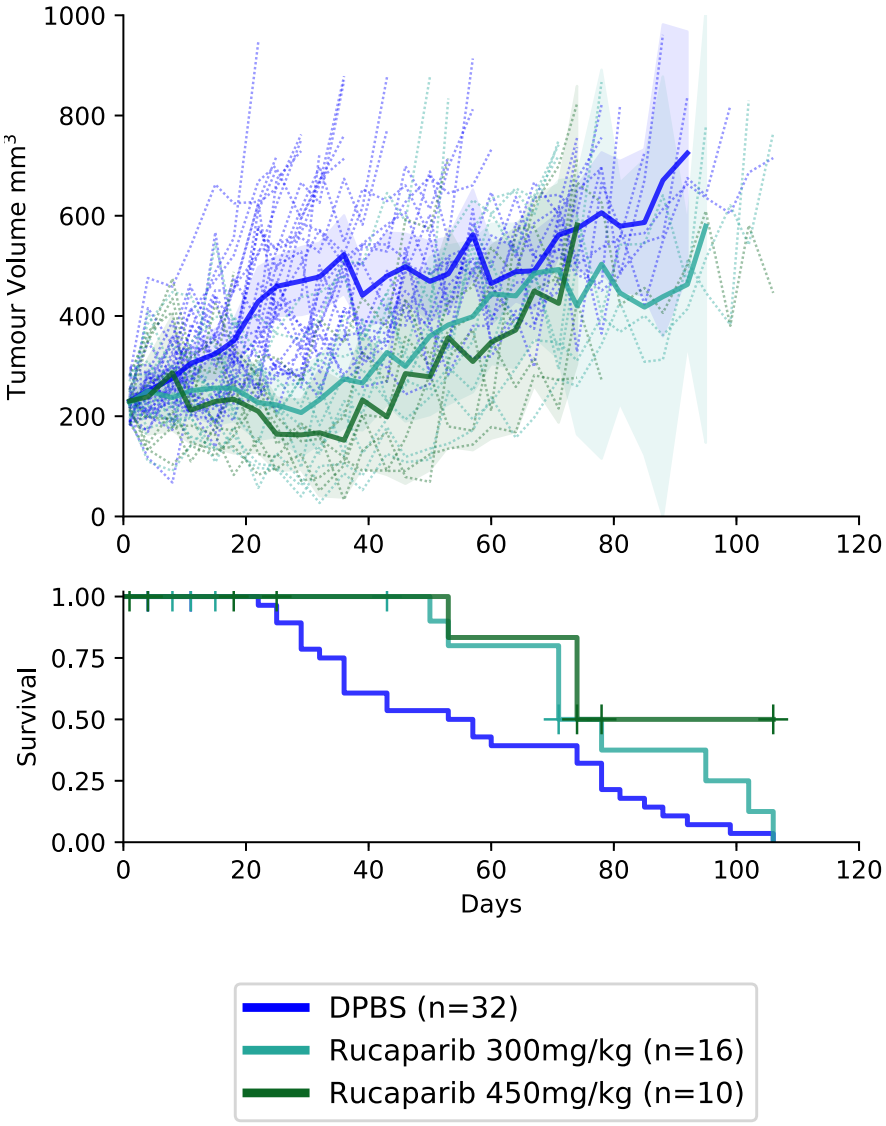


Figure 5.3. PDX 134183 shows some response to the PARPi rucaparib.

Tumour volume data presented is individual tumours (dotted lines) and mean (thick line) +/- 95% CI (shaded area).

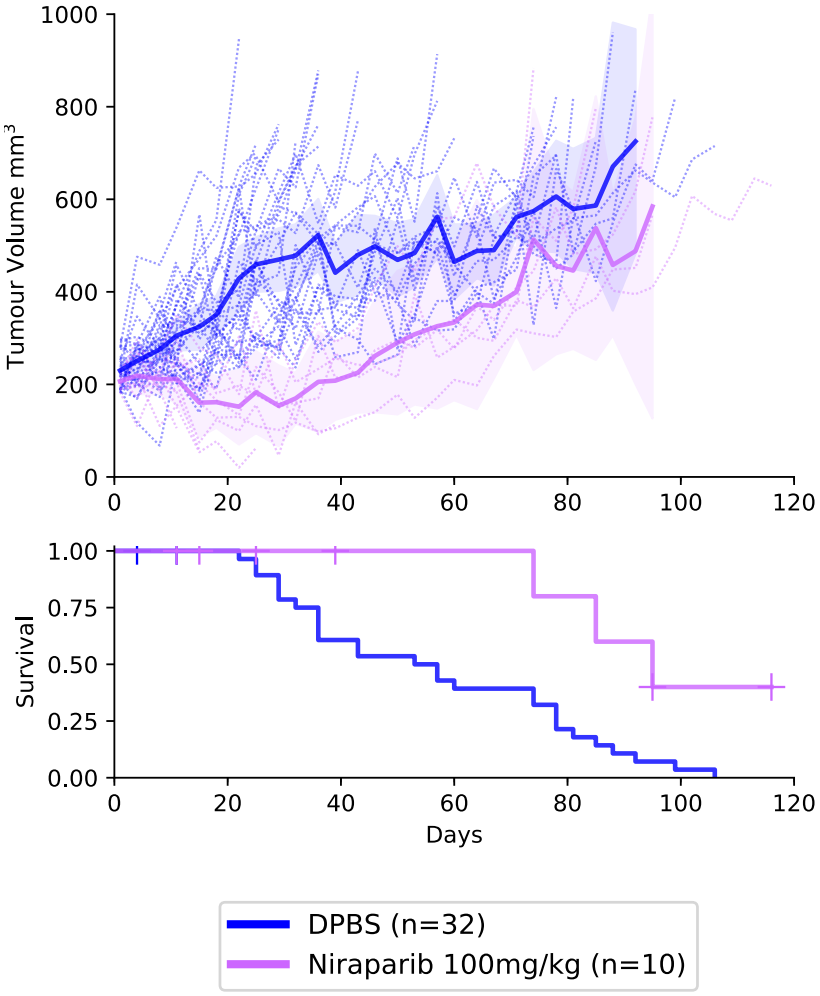


Figure 5.4. PDX 134183 shows some response to the PARPi niraparib.

Tumour volume data presented is individual tumours (dotted lines) and mean (thick line) +/- 95% CI (shaded area).

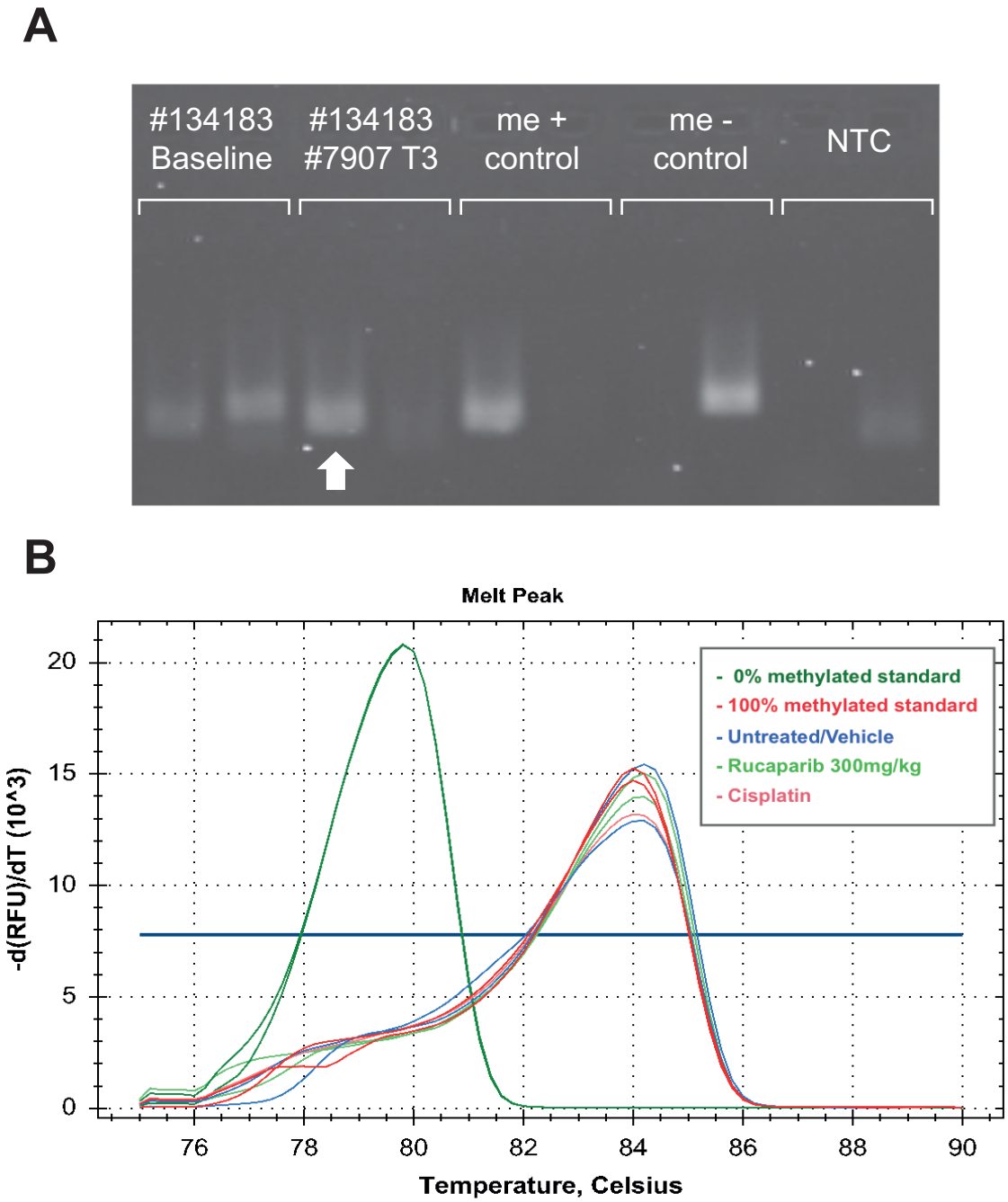


Figure 5.5. MS-PCR and MS-HRM show that PDX 134183 harbours RAD51C promoter methylation.

(A) *MS-PCR only shows the presence of methylation in PDX 134183 sample 7907 (arrow), but not the zygosity of this methylation.* ***(B)*** *MS-HRM shows one untreated sample, and two post-treatment PDX 134183 samples (rucaparib 300mg/kg and cisplatin 4mg/kg) are all 100% methylated, thus designated as homozygous for meRAD51C. Each line represents one of two measurements for a single tumour/sample. Positive meRAD51C control: "me +", negative meRAD51C control: "me –", NTC – Non-template control. RFU – Relative fluorescence units.*

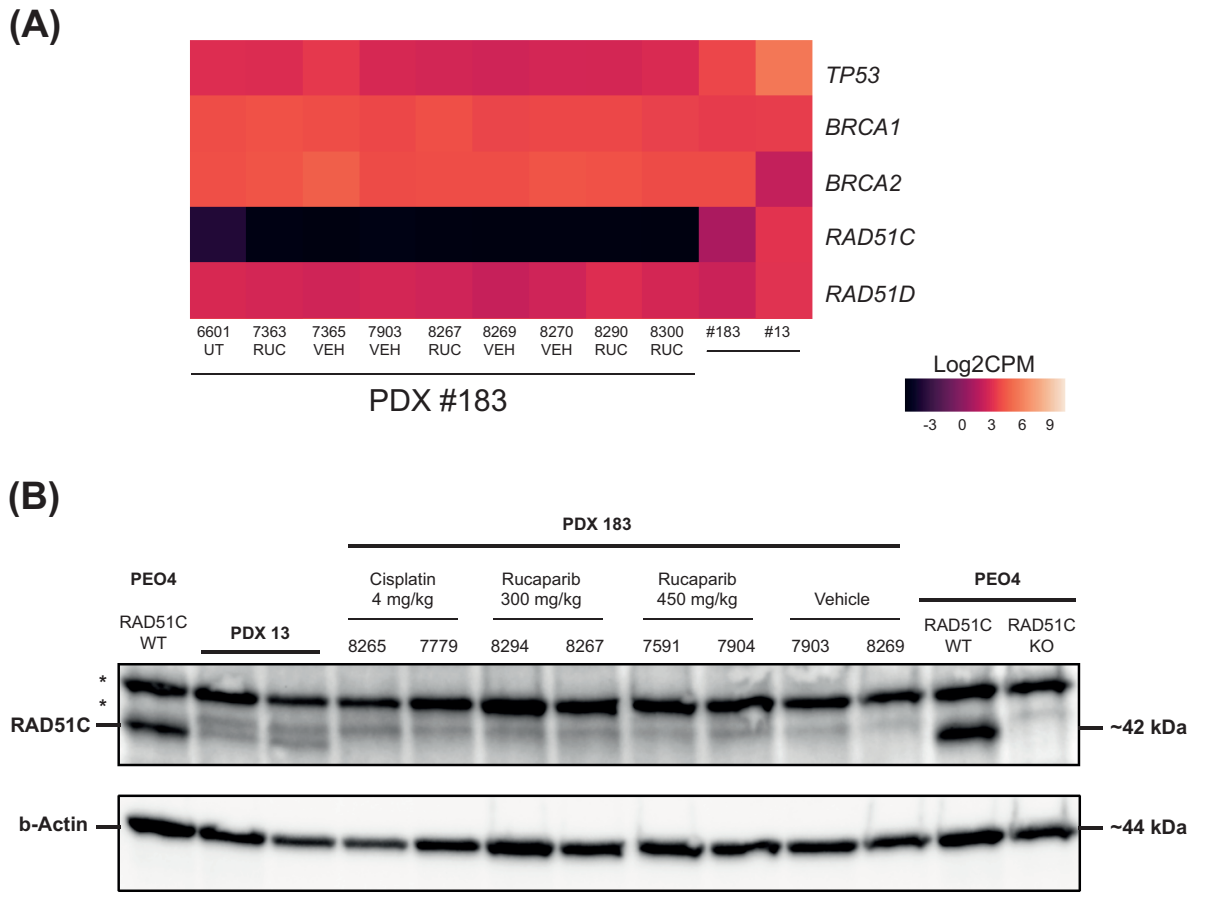


Figure 5.6. No RAD51C message or protein expression found in RNAseq and immunoblotting analysis of PDX 134183 treated and untreated samples.

(A) PDX 134183 (#183) samples show no expression of RAD51C message compared to control patient PDX 134013 (#13) sample. The patient #183 sample run (left of #13 control) appears to have some expression, but this is likely due to reduced tumour purity of the patient material ***(B)*** *PDX #183 has no detectable RAD51C protein by western blot. RAD51C protein is the lower band seen in PDX #13 positive control samples. Also included RAD51C positive (WT= "wild-type") PEO4 cell line controls, and a PEO4 RAD51C knock-out (KO) negative control.*

5.4.2 MAYO-PH039 characterisation

Although our collaborators had published the characterisation of this model, including detection of me*RAD51C* by MS-PCR and reduced gene expression (AlHilli et al., 2016), they did not have access to methylation assays that would allow assessment of me*RAD51C* zygosity, such as MS-HRM, or the expertise to analyse the resulting data. Given our recent work on *BRCA1* methylation zygosity and its impacts on PARPi responses, I coordinated equivalent testing on DNA from their model and analysed with our methods of me*RAD51C* zygosity assessment by Illumina EPIC methylation array (detailed results in Chapter 6) and *RAD51C* MS-HRM.

The MS-HRM results revealed an unexpected me*RAD51C* pattern in untreated PH039 samples. Rather than a homozygous pattern, like 134183, or a heterozygous pattern (two melt peaks – one methylated and one unmethylated), this model displayed a baseline heterogeneous pattern of me*RAD51C* (**Figure 5.7**).

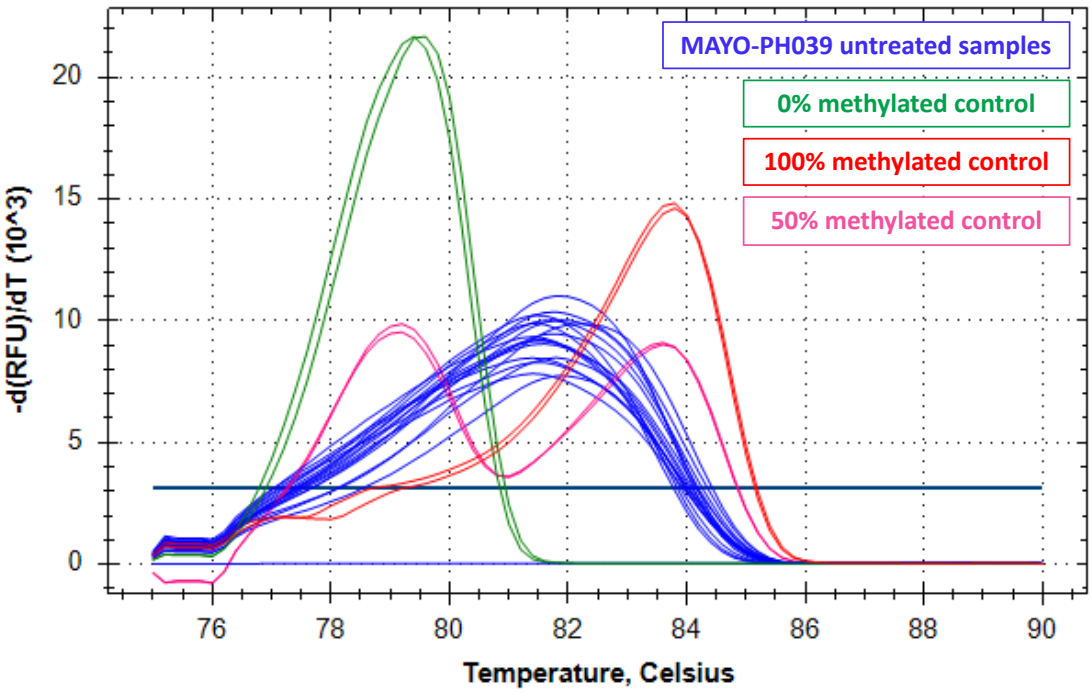


Figure 5.7. MS-HRM reveals heterogeneous meRAD51C of PDX MAYO-PH039.
PDX MAYO-PH039 untreated samples analysed by MS-HRM demonstrated a heterogeneous meRAD51C profile, rather a heterozygous profile (represented here by a 50% methylated control sample). Each line represents one of two measurements for a single tumour/sample. RFU – Relative fluorescence units.

The broadness of this MS-HRM peak suggested that, rather than the presence of a single partially methylated allele, there was a mix of many alleles with different methylation patterns. However, this could not be confirmed using MS-HRM, MS-PCR or even the EPIC methylation arrays (presented in Chapter 6). Elucidating the underlying me*RAD51C* pattern in this PDX instead required an assay that would enable interrogation of each CpG site within each individual epiallele. I therefore designed a targeted bisulfite amplicon sequencing assay to address this, and results of this analysis are described in detail in section 5.4.10 of this chapter.

5.4.3 WEHI-PH039 characterisation

Two lineages of WEHI-PH039 were re-established from two different T1 tumours of the original WEHI-PH039 – #1467 and #1471, which I defined as 'Lineage A' and 'Lineage B' respectively.

5.4.3.1 Two lineages of WEHI-PH039

As treatment PARPi data was generated, it became clear that the two lineages of WEHI-PH039, Lineage A and Lineage B, had different PARPi responses. Lineage A and Lineage B were both cisplatin sensitive, though Lineage A appeared to have slightly more durable response (**Figure 5.8**; **Table 5.2**). In contrast, Lineage A was found to be less responsive to PARPi rucaparib (**Figure 5.9**; **Table 5.3**; **Figure 5.10**; **Table 5.4**) and niraparib (**Figure 5.11**; **Table 5.5**) compared to Lineage B. The growth rates (measured by DPBS treated mice) of Lineages A and B were slightly different (TTH = 8 and 15 days, respectively; $p = 0.02$), but this difference was considered unlikely to have such a significant impact on PARPi responses.

It was possible that these differences in treatment responses were related to changes in me*RAD51C* status, so I assessed a number of untreated samples from each lineage by MS-HRM. The MS-HRM data revealed slightly different me*RAD51C* profiles of the two lineages for samples tested (**Figure 5.12**). These profiles were designated "LLS" (left-left-shift) for the less-methylated profile, and "LS" (left-shift) for the more-methylated profile. Vehicle-treated Lineage A samples appeared to have mostly "LLS" me*RAD51C* profiles, while vehicle-treated Lineage B samples were either "LS" or "LLS" (**Table 5.6**). The significance of these profiles is discussed further in subsequent sections of this chapter.

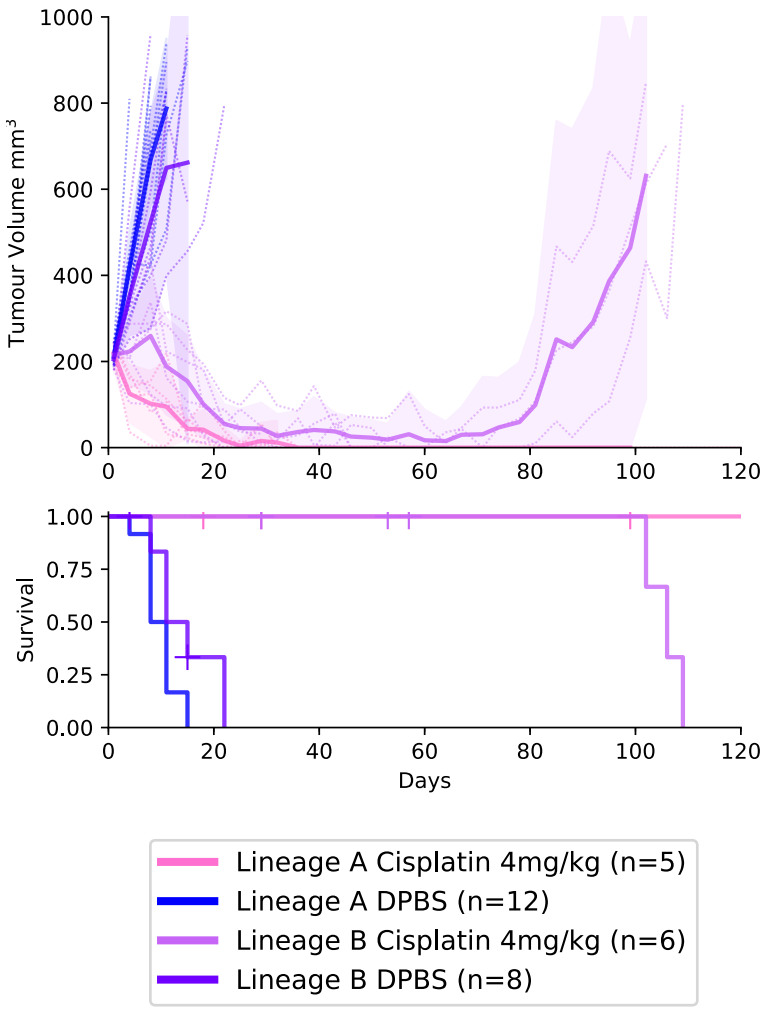


Figure 5.8. WEHI-PH039 Lineage A vs B in vivo cisplatin responses.

PDX WEHI-PH039 Lineages A and B are both sensitive to cisplatin, though Lineage B relapses sooner than Lineage A (TTP 95 vs >120 days respectively). Tumour volume data presented is mean +/- 95% CI.

Table 5.2. P-values of WEHI-PH039 Lineage A vs B in vivo cisplatin response differences.

Lineage A and B are both sensitive to cisplatin, and their cisplatin responses are not significantly different statistically (p= 0.063). TTH – Time to harvest, TTP – Time to progression.

WEHI-PH039	Cisplatin (*p* - value)	Median TTH (days)	Average TTP (days)	Lineage comparison (*p*- value)
Lineage A	<0.001	137	>120	0.063
Lineage B	0.002	109	85	

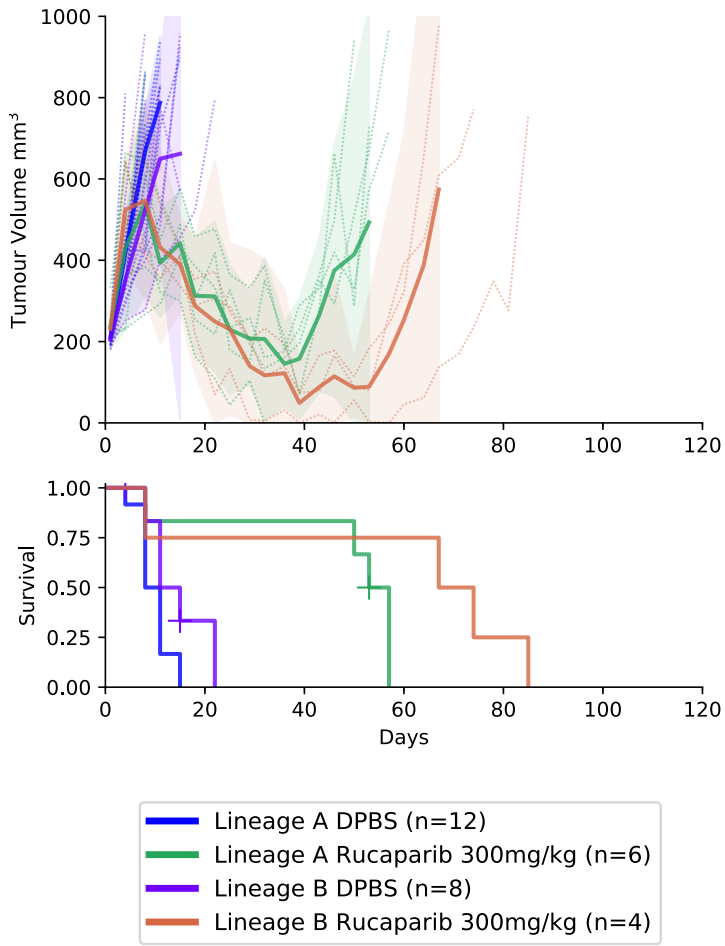


Figure 5.9. WEHI-PH039 Lineage A vs B in vivo rucaparib 300mg/kg responses.

PDX WEHI-PH039 Lineages A and B are both show some response to rucaparib (300mg/kg), though Lineage A relapses sooner than Lineage B (TTP 46 vs 64 days respectively). Tumour volume data presented is mean +/- 95% CI.

Table 5.3. P-values of WEHI-PH039 Lineage A vs B in vivo rucaparib 300mg/kg response differences.

Lineage A and B both have some response to rucaparib, and though their rucaparib 300mg/kg responses differ (Lineage A less responsive), this is not statistically significantly. TTH – Time to harvest, TTP – Time to progression.

WEHI-PH039	Rucaparib 300mg/kg (*p* - value)	Median TTH (days)	Average TTP (days)	Lineage comparison (*p*- value)
Lineage A	0.002	57	43	0.109
Lineage B	0.110	67	60	

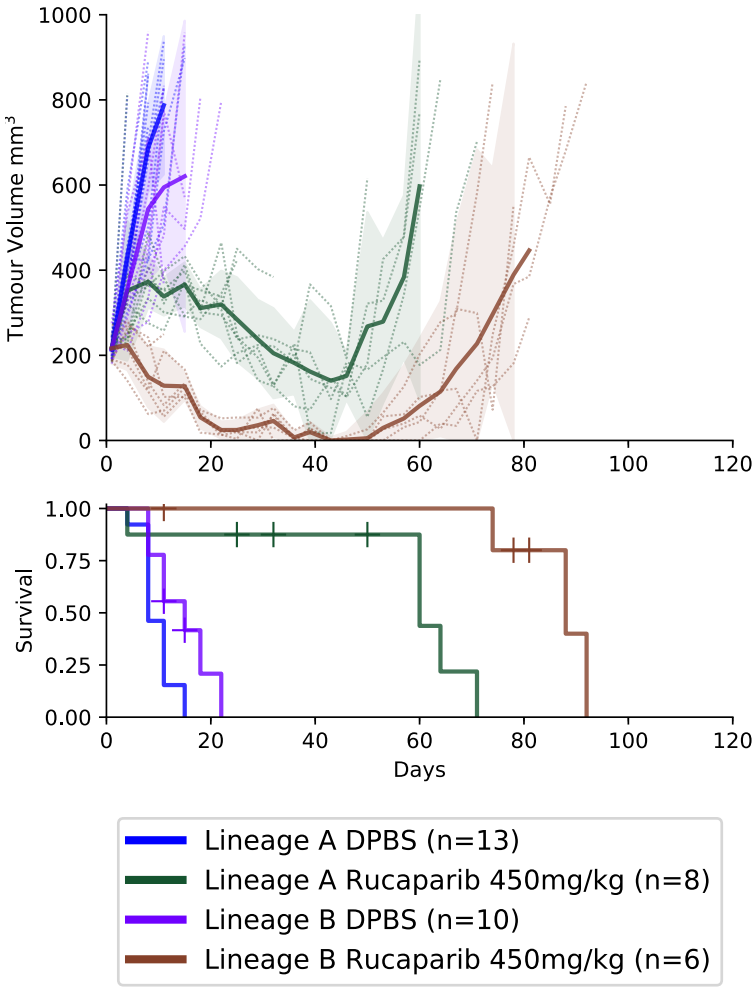


Figure 5.10. WEHI-PH039 Lineage A vs B in vivo rucaparib 450mg/kg responses.

PDX WEHI-PH039 Lineages A and B are both show some response to rucaparib (450mg/kg), though Lineage A relapses sooner than Lineage B (TTP 53 vs 71 days respectively). Tumour volume data presented is mean +/- 95% CI.

Table 5.4. P-values of WEHI-PH039 Lineage A vs B in vivo rucaparib 450mg/kg response differences.

Lineage A and B both have some response to rucaparib, though their rucaparib 450mg/kg responses differ (Lineage A less responsive), this is statistically significantly. TTH – Time to harvest, TTP – Time to progression.

WEHI-PH039	Rucaparib 450mg/kg (*p* - value)	Median TTH (days)	Average TTP (days)	Lineage comparison (*p*- value)
Lineage A	0.003	60	53	0.011
Lineage B	0.005	92	71	

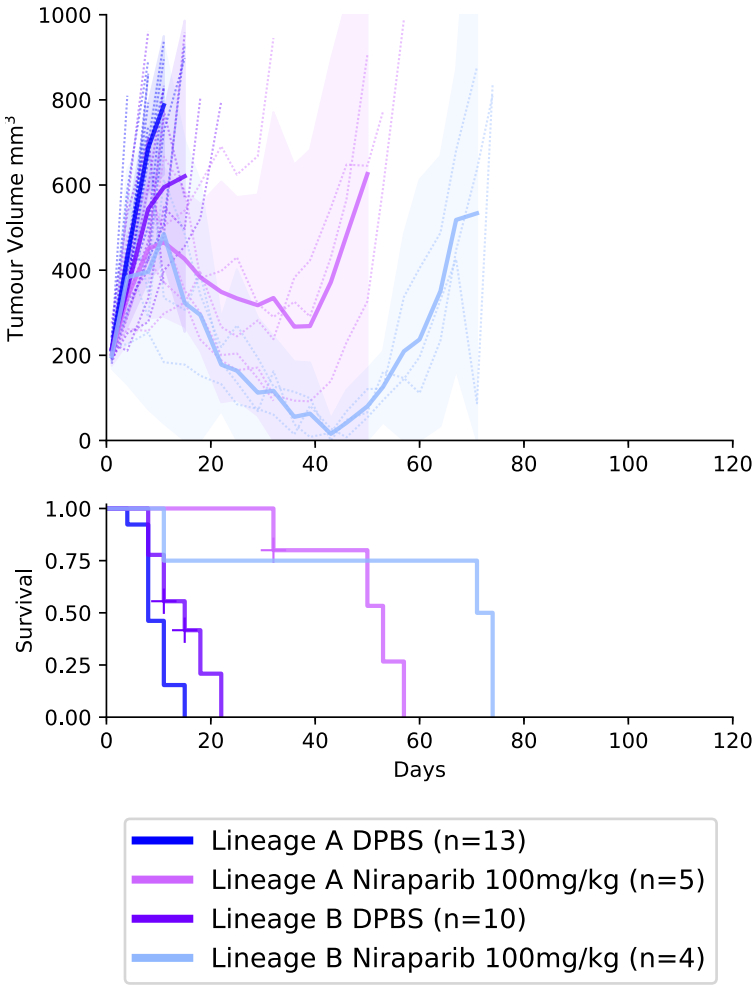


Figure 5.11. WEHI-PH039 Lineage A vs B in vivo niraparib responses.

PDX WEHI-PH039 Lineages A and B are both show some response to niraparib (100mg/kg), though Lineage A is less responsive than Lineage B (TTP 4 vs 57 days respectively). Tumour volume data presented is mean +/- 95% CI.

Table 5.5. P-values of WEHI-PH039 Lineage A vs B in vivo niraparib 100mg/kg response differences.

Lineage A and B both have some response to niraparib. Although Lineage A appears less responsive, this is not statistically significant. TTH – Time to harvest, TTP – Time to progression.

WEHI-PH039	Niraparib 100mg/kg (*p* - value)	Median TTH (days)	Average TTP (days)	Lineage comparison (*p*- value)
Lineage A	0.001	50	4	0.123
Lineage B	0.074	71	57	

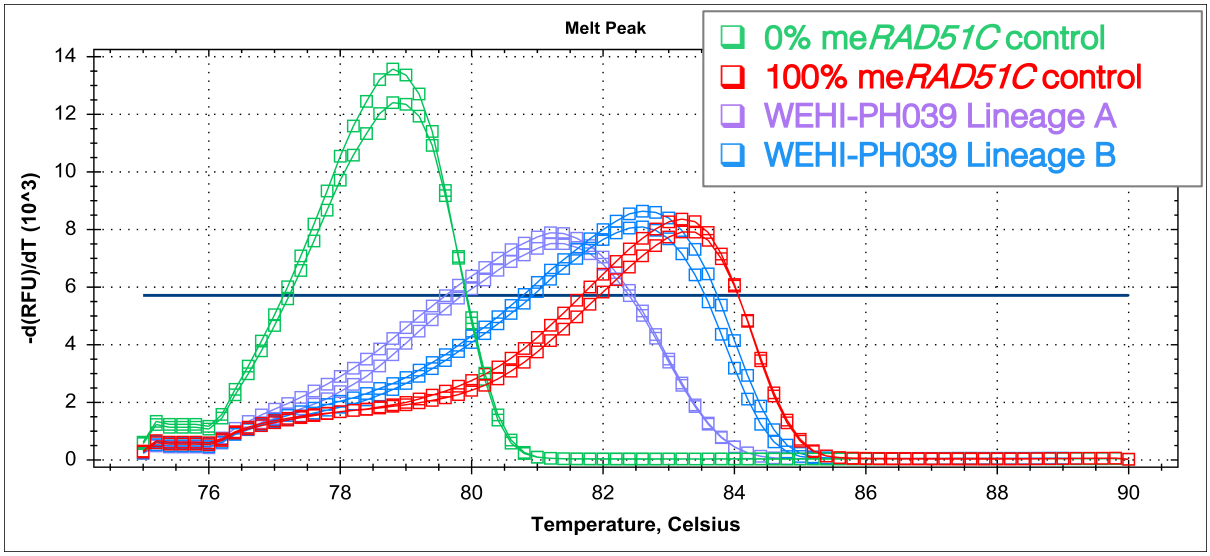


Figure 5.12. PH039 lineage A vs B RAD51C methylation patterns by MS-HRM.

Representative image of DPBS-treated PH039 lineage A and B methylation profiles as detected by RAD51C MS-HRM. Lineage A tumours tend to have a less methylated and more heterogeneous methylation profile compared to lineage B tumours, though there are some exceptions. Each line represents one of two measurements for a single tumour/sample. RFU – Relative fluorescence units.

Table 5.6. Vehicle-treated WEHI-PH039 Lineage B samples slightly more methylated at RAD51C promoter than Lineage A samples.

LLS: "left-left shift" profile indicates reduced methylation compared to LS: "left shift", which is closer to the 100% methylated control peak.

WEHI-PH039 Lineage	Tumour ID	Passage	Treatment	me*RAD51C* profile
A	12970	T4	DPBS	LLS
A	12971	T4	DPBS	LLS
A	13039	T4	DPBS	LLS
A	13288	T5	DPBS	LLS
A	14002	T7	DPBS	LLS
A	14179	T8	DPBS	LLS
B	13070	T4	DPBS	LLS
B	13071	T4	DPBS	LS
B	13368	T5	DPBS	LS
B	13381	T5	DPBS	LS
B	13939	T6	DPBS	LLS
B	14224	T7	DPBS	LLS

5.4.4 DNA repair capacity of RAD51C methylated PDX models

An interesting observation from published work on the me*RAD51C* PDX PH039 (AlHilli et al., 2016), was that authors reported this model formed RAD51 immunofluorescent foci, the gold-standard marker of functional HR DNA repair, following PARPi treatment *ex vivo*. This was an intriguing result, given that the absence of *RAD51C* RNA and protein was also reported in this model, yet work from our group on *RAD51C* primary and secondary gene mutations has shown that functional *RAD51C* is required for formation of RAD51 foci *in vitro*. I was, therefore, interested to assess the HR DNA repair capacity of our me*RAD51C* PDX 134183 using RAD51 foci staining.

Previously used protocol within our laboratory for measuring DNA repair foci in PDX tumours was found to be labour-intensive and difficult to image and interpret, compared to the cell line protocol. In previous studies from our group (Kondrashova et al., 2018) fragments of tumour were frozen in OCT blocks to preserve tissue and cell structure, then sectioned at 4µm thickness using a cryostat. These sections were then stained and imaged as previously described (Kondrashova et al., 2018), and analysed using a custom CellProfiler-based imaging analysis pipeline. However, these sections often contained overlapping cells and mouse stromal cells, making foci for some PDX difficult to measure. I wanted to explore whether using tumour digestions and FACS could clean-up the data by selecting only live human cells and then imaging these on a single plane, without overlapping cells.

I set up preliminary tests on irradiated tumours (to induce DNA damage) using our standard tumour digestion protocol, followed by FACS sorting of fixed cells stained with propidium iodide (PI) to sort for live cells and the epithelial marker EpCAM to select for human HGSOC tumour cells. The selected cells were attached to slides using cytospin and then stained using our standard immunofluorescent γH2AX foci staining protocol for cell lines. This initial experiment was successful, as I was able to detect γH2AX foci in both a PDX 134169 sample and a PDX PH039 sample on the confocal microscope (**Figure 5.13**). However, I found that the PI stain was not providing a clear enough separation for live and dead cells, likely because PI is not a suitable stain for cells undergoing fixation. I decided to test a fixable live/dead stain (LIVE/DEAD™ Fixable Aqua Dead Cell Stain Kit, Life Technologies), and found the sorting populations were more distinct (**Figure 5.14**).

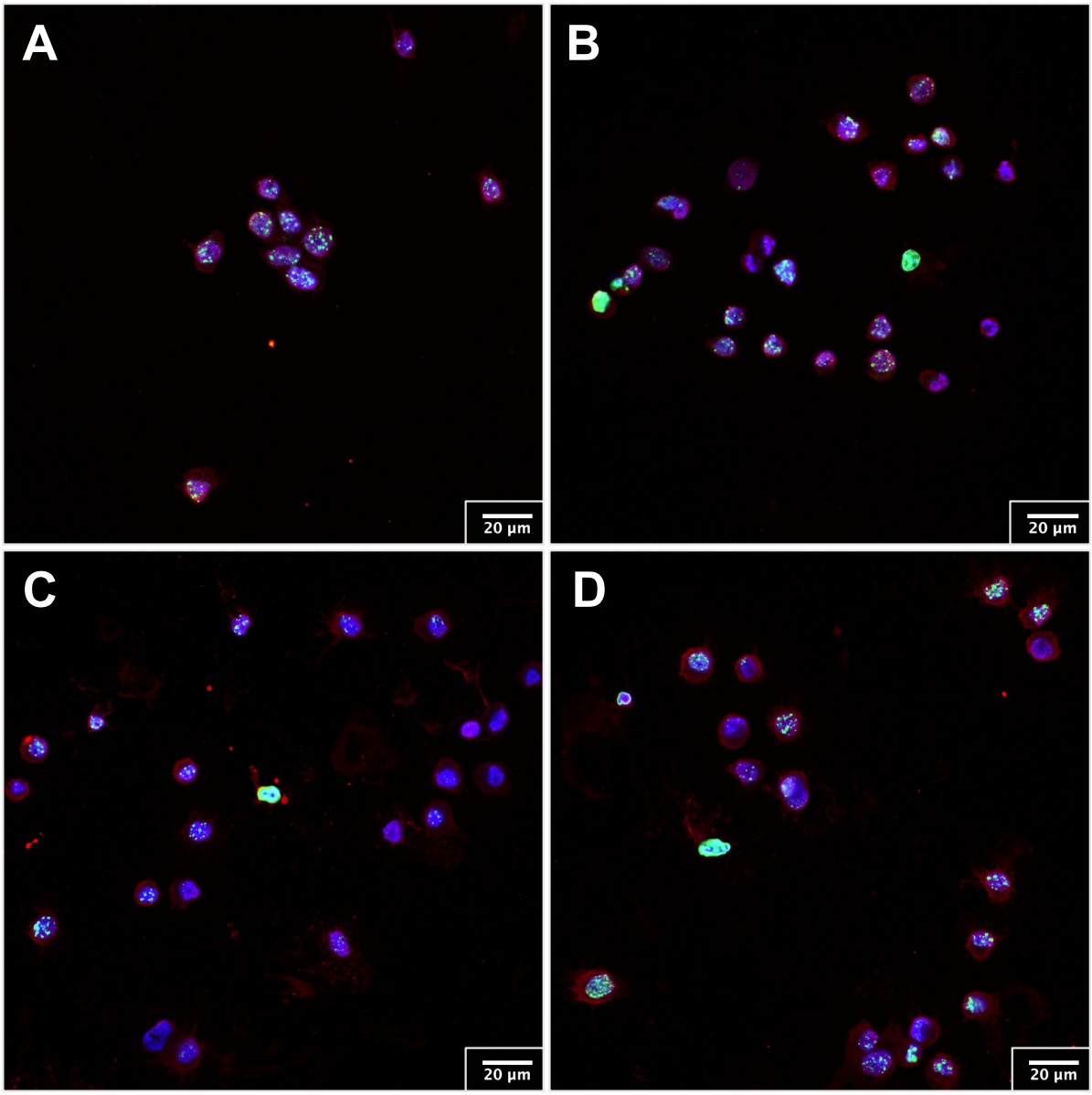


Figure 5.13. PDX tumour digested and FACS-sorted cells can be stained for DNA repair foci on cytospin slides and imaged on confocal microscope.

Proof of principal results showing that PDX tumours can be digested and FACS-sorted for live, human (EpCAM positive) cells and then attached to microscope slides via cytospin for subsequent immunofluorescent DNA repair foci staining and imaging protocols. ***(A)*** *and* ***(B)*** *show two different fields of view on a slide with 5Gy-irradiated post-sort PDX 134169 tumour cells stained for γH2AX foci (green spots), geminin (red) and Hoechst 33342 nuclear stain (blue).* ***(C)*** *and* ***(D)*** *show two different fields of view on a slide with 5Gy-irradiated post-sort PDX PH039 tumour cells stained for γH2AX foci (green spots), geminin (red) and Hoechst nuclear stain (blue).*

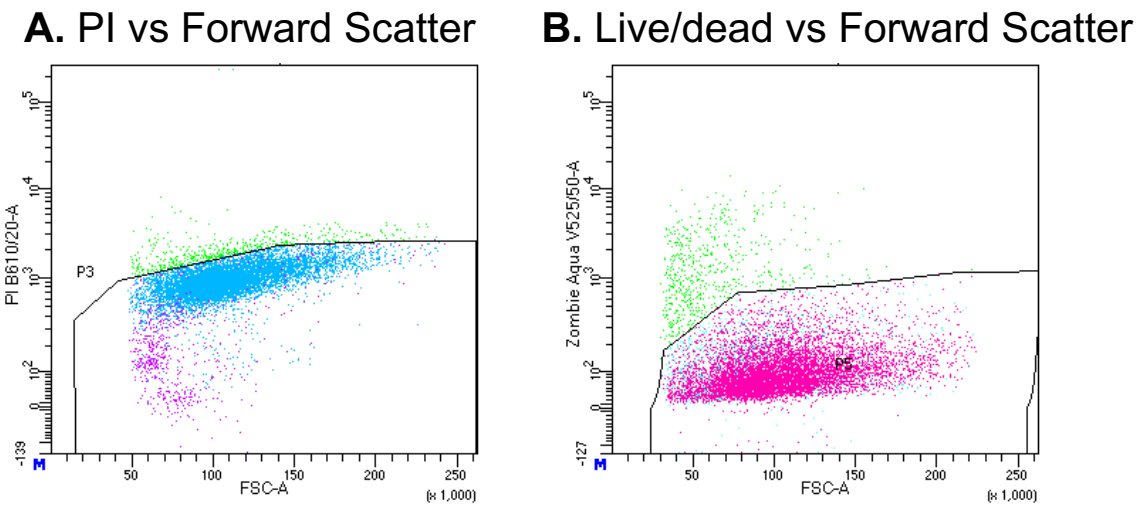


Figure 5.14. Improved separation of live and dead fixed cell populations using fixable stain. *(A) Non-fixable PI (dead cell) stain plotted against Forward scatter of cells does not allow for clear separation, unlike (B) the LIVE/DEAD Fixable Dead Cell Stain (Invitrogen), where two populations of cells (live and dead) were clearly separated.*

Another issue I had with the initial protocol was the time-consuming manual process of staining, then imaging individual slides for foci using confocal microscope (Zeiss LSM 780). Hence, I assessed whether it was possible to attach the fixed and sorted cells to wells of a 96-well plate for automated foci imaging on the Phenix OPERA platform, which had been successfully used by our group for cell line foci imaging. I tried a number of approaches for attaching the cells: high volumes of more diluted cells centrifuged briefly in liquid or left to settle at 4°C over time, lower volumes of less diluted cells centrifuged in liquid, and ultra-concentrated cells used to coat well, then centrifuged dry/no liquid (detailed in Chapter 3).

The most successful approach was found to be ultra-concentrated cells (collected cells resuspended in 10-15µl of DPBS) used to coat each well, and then centrifuged at 1800g for 10 minutes to dry. These cells were then stained for foci, and imaged on the OPERA instrument. This protocol was successful for both RAD51 and γH2AX foci staining in the HR competent, positive control PDX PH038 (**Figure 5.15A**), and could also be performed on PDX 134183 tumours successfully (**Figure 5.15B**). The established method also allowed for imaging and DNA repair foci detection in thousands of cells per tumour in an efficient way, with each assay assessing an average of 1000-3000 cells per well.

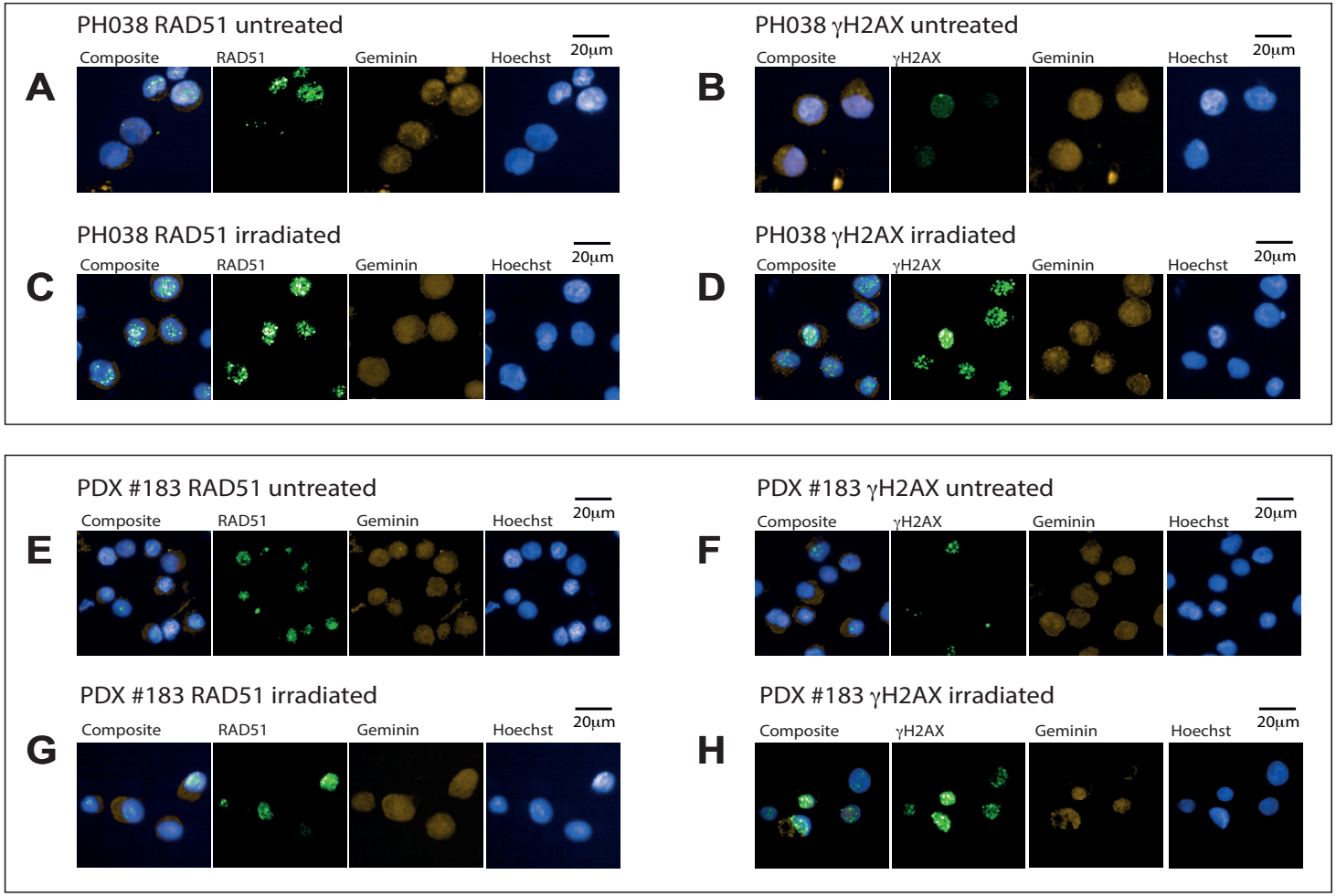


Figure 5.15. PDX tumour digested and FACS-sorted cells can be attached to 96-well plates for foci staining and imaging on OPERA platform. ***(A-D)*** *show example fields of view from 5Gy irradiated and untreated PDX PH038 (HR competent control) cells imaged on OPERA platform for RAD51 and γH2AX foci.* ***(E-H)*** *show example fields of view from 5Gy irradiated and untreated PDX 134183 (#183) cells imaged on OPERA platform for RAD51 and γH2AX foci.*

I then started processing treated (5Gy irradiated) and untreated tumours from the PDX PH038 control model and PDX 134183. The results indicated that PDX 134183 has impaired capacity for RAD51 foci formation following irradiation compared to the control model (**Figure 5.16**). In fact, PDX 134183 irradiated tumours generally had reduced RAD51 foci compared to the PDX 134183 untreated group (7.5% mean reduction; $p = 0.025$).

Using this assay I also found that RAD51 foci could form in some cells of WEHI-PH039 Lineages A and B. However, these did not increase in irradiated PH039 tumours like they did in the HR positive control PH038 tumours (**Figure 5.17**; **Table 5.7**). Interestingly, Lineage A (the more PARPi-resistant lineage) was found to have increased levels of RAD51 foci compared to Lineage B, both with and without irradiation (**Figure 5.17**; **Table 5.7**). These possibly represent spontaneously formed RAD51 foci, as they do not appear to be associated with a response to DNA damage.

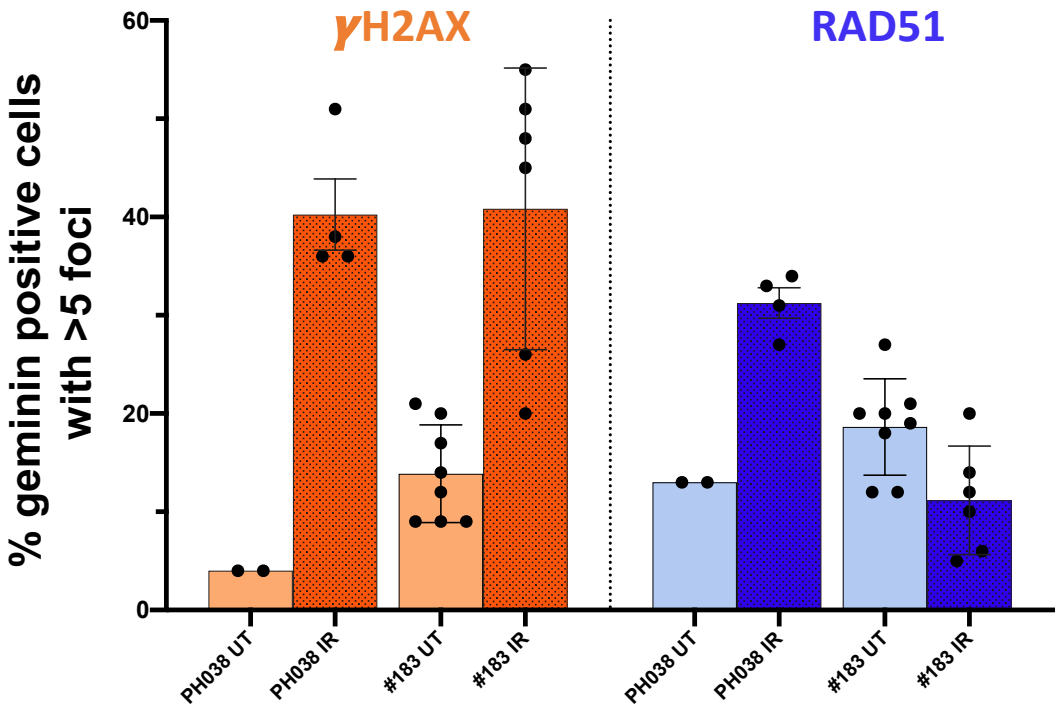


Figure 5.16. PDX 134183 does not form RAD51 DNA repair foci following DNA damage.
Presented is the percentage of geminin positive cells analysed with >5 γH2AX or RAD51 foci counted in their nucleus. "PH038" is the HR competent control and "#183" is PDX 134183. IR = Irradiated, UT = untreated. PDX 134183 untreated vs irradiated RAD51 foci = -7.5% mean difference (p = 0.025), PH038 untreated vs irradiated RAD51 foci = +18.25% mean difference (p = 0.001). P-values calculated using Welch's two-tailed t test in PRISM.

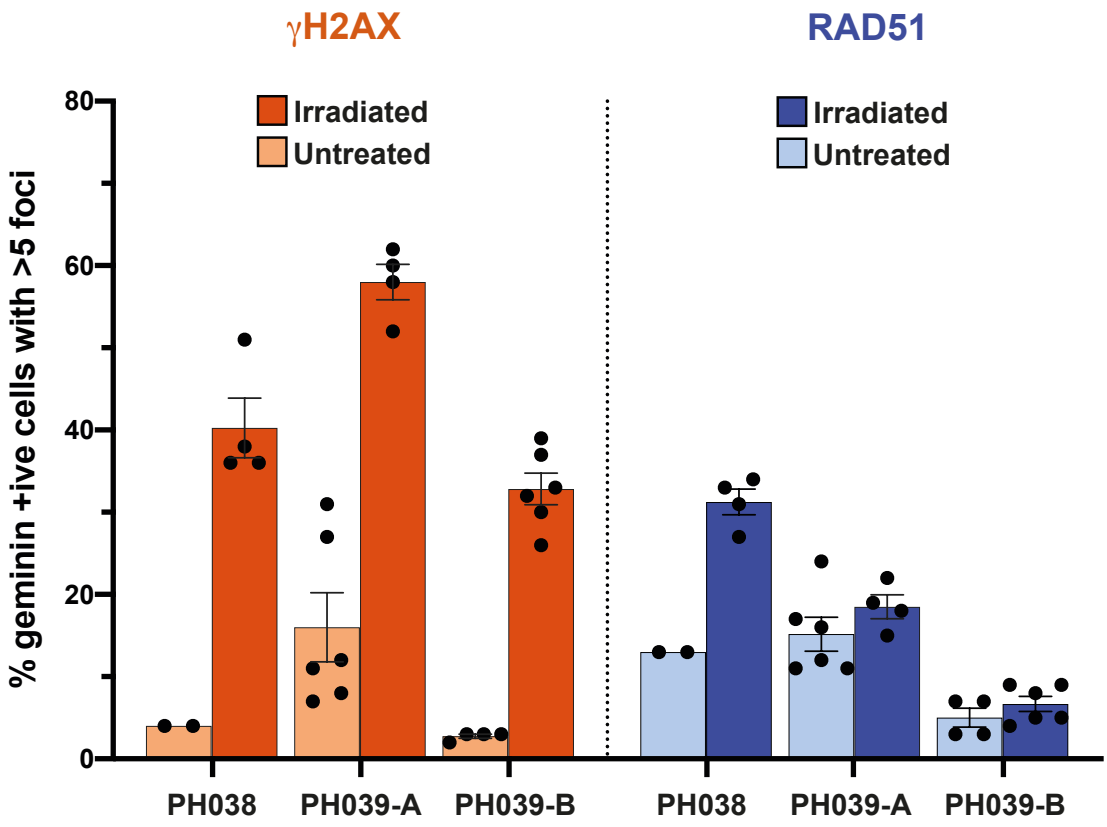


Figure 5.17. PH039 Lineage A and B have impaired RAD51 DNA repair foci forming capacity following DNA damage.

Presented is the percentage of geminin positive cells analysed with >5 γH2AX or RAD51 foci counted in their nucleus. "PH038" is the HR competent control, "PH039-A" is WEHI-PH039 Lineage A and "PH039-B" is WEHI-PH039 Lineage B. Same positive control is used in Figure 5.16. PH039-A untreated vs irradiated RAD51 foci = +3.33% mean difference (p = 0.222); PH039-B untreated vs irradiated RAD51 foci = +1.67% mean difference (p = 0.299). P-values calculated using Welch's two-tailed t test in PRISM.

Table 5.7. Mean RAD51 foci value comparison between irradiated PDX groups.

"PH038" is the HR competent control, "PH039-A" is WEHI-PH039 Lineage A and "PH039-B" is WEHI-PH039 Lineage B. P-values calculated using Welch's two-tailed t test in PRISM.

Irradiated treatment group comparison		Mean difference (%)	*p* -value
PH038	134183	20.08 ± 2.74	<0.001
PH038	PH039-A	12.75 ± 2.12	0.001
PH038	PH039-B	24.58 ± 1.80	<0.001
PH039-A	PH039-B	11.83 ± 1.711	<0.001

5.4.5 Bisulfite capture sequencing using methyl-BROCA

During this project, our collaborators at the University of Washington (Swisher group) optimised a BROCA-style capture-based sequencing panel for measuring methylation in bisulfite-converted DNA samples. Unlike MS-HRM and MS-PCR, this test allowed us to look at average methylation values for each individual CpG site within the captured regions – similar to a chip-based methylation array (e.g. EPIC array data in Chapter 6), but covering all CpG sites across our regions of interest.

This panel covered HR genes, including *BRCA1* and *RAD51C.* Despite the absence of *RAD51C* expression in untreated PH039 tumours, we were still interested in what the heterogeneous *RAD51C* methylation patterns detected in MS-HRM actually represented at a molecular level, so I coordinated the methyl-BROCA analysis of MAYO-PH039 tumours and PDX 134183, for comparison. In total, 12 samples from PDX 134183 and 12 samples from MAYO-PH039 were tested using the novel assay (**Table 5.8**).

So far, six PDX 134183 samples have been run on this assay (**Table 5.8**; note that #7363 failed sequencing). Methyl-BROCA analysis confirmed the homozygous methylation pattern of most PDX 134183 samples (examples presented in **Figure 5.18**). Sample #8294 was consistently highly methylated across all CpG sites, while sample #7904 had slightly reduced methylation at site 56769937 (**Figure 5.18**), though this was not detectable as a shift in MS-HRM curve for this sample.

Interestingly, one sample, #7907, appeared to be heterozygous for me*RAD51C* (**Figure 5.18**). This finding was validated in this same DNA sample by MS-HRM, however a second DNA extraction from another tumour piece of #7907 sample revealed that the me*RAD51C* loss was in fact homozygous (**Figure 5.19**). This result suggested that the initial "heterozygous" measurement was an effect of tumour purity (i.e. the initial piece tested had 50% of cells with complete me*RAD51C* loss). To confirm that these measurements were not due to contamination of another PDX, *TP53* amplicon sequencing was performed on DNA from the first piece of tumour. The identity of this tumour piece was confirmed to be 100% PDX 134183 (**Figure 5.20**).

Table 5.8. Samples selected for methyl-BROCA analysis.

Samples highlighted green are those that have been tested so far.

PDX	PDX tumour sample	Treatment
MAYO-PH039	C1.1	Niraparib Cycle 1
	C1.2	Niraparib Cycle 1
	C2.1	Niraparib Cycle 2
	C2.2	Niraparib Cycle 2
	C3.1	Niraparib Cycle 3
	C3.3	Niraparib Cycle 3
	S0.1	Source tumour
	S0.2	Source tumour
	S1.3	Untreated passage 1
	S1.4	Untreated passage 1
	S6.1	Untreated passage 6
	S6.4	Untreated passage 6
134183	8265	Cisplatin
	7779	Cisplatin
	7907	Cisplatin
	7363	Rucaparib 300mg/kg
	8294	Rucaparib 300mg/kg
	8267	Rucaparib 300mg/kg
	7591	Rucaparib 450mg/kg
	7904	Rucaparib 450mg/kg
	8266	Rucaparib 450mg/kg
	7903	DPBS
	8270	DPBS
	8269	DPBS

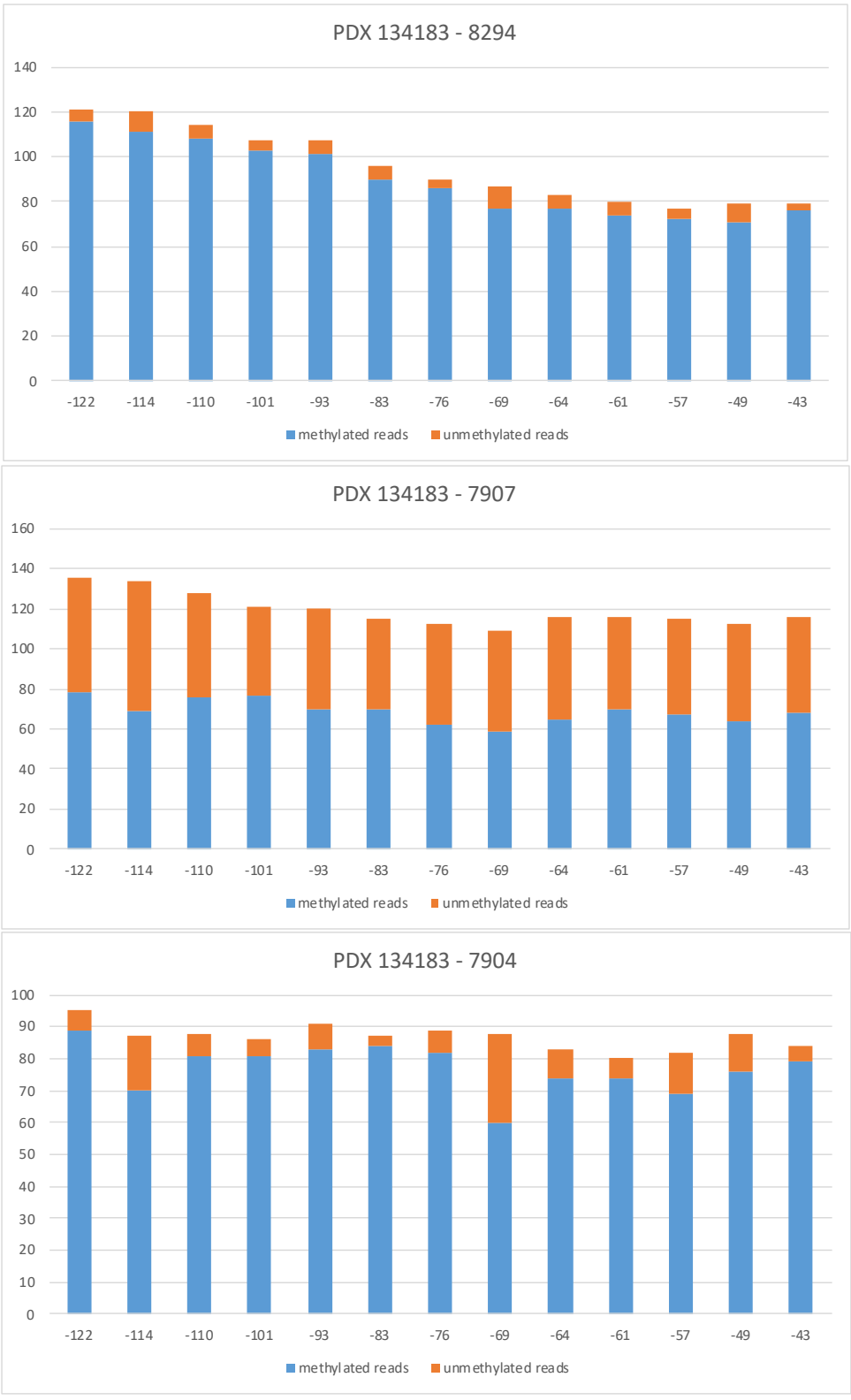


Figure 5.18. Example PDX 134183 meRAD51C profiles by methyl-BROCA.

Figure shows the total methylated and unmethylated reads (y-axis) for each CpG position (x-axis- labelled by nucleotide distance from promoter) along the RAD51C gene promoter region covered by RAD51C MS-HRM. Sample 8294 is rucaparib 300mg/kg-treated, sample 7907 is cisplatin-treated and sample 7904 is rucaparib 450mg/kg-treated.

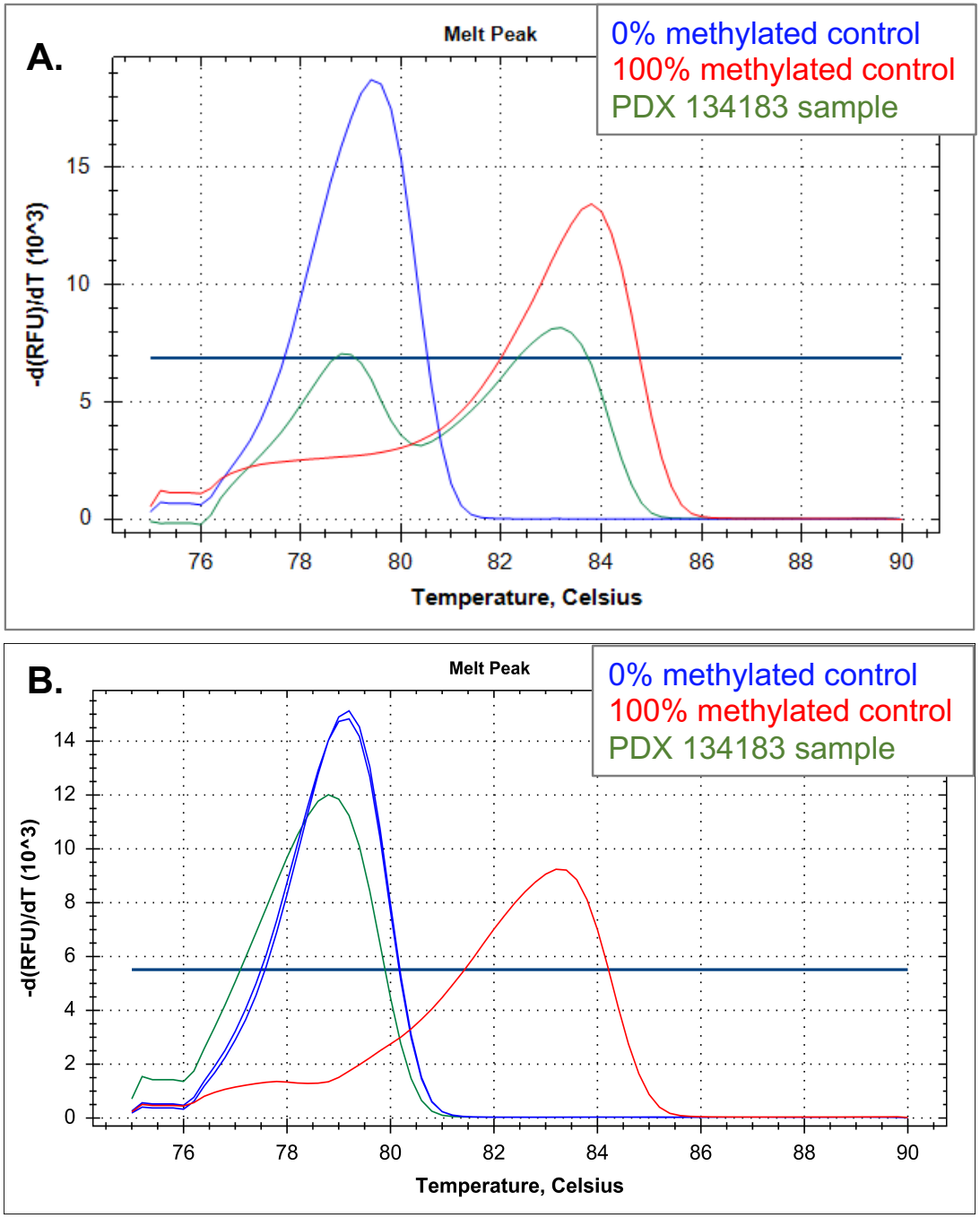


Figure 5.19. Tumour heterogeneity influences meRAD51C measurements.

MS-HRM profiles of cisplatin-treated PDX 134183 #7907 tumour reveal 50% meRAD51C loss in one piece of tumour and (B) 100% meRAD51C loss in a different piece of the same tumour. Each line represents measurements per tumour/sample. RFU – Relative fluorescence units.

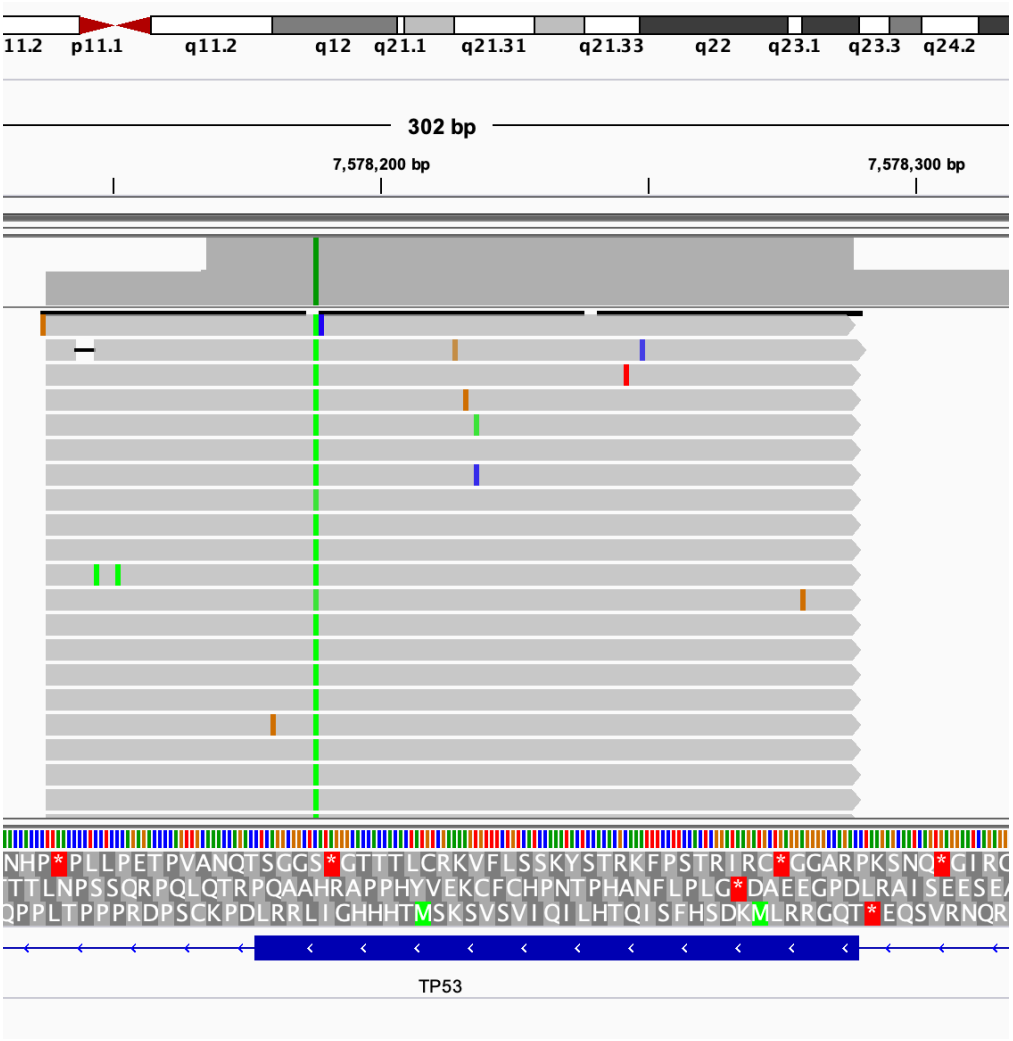


Figure 5.20. Tumour with 50% meRAD51C loss is 100% PDX 134183 based on TP53 mutation.

IGV screenshot of TP53 mutation (NM_000546:c.661G>T) found in amplicon sequencing reveals that the first piece of tumour sample #7907 with 50% meRAD51C loss is 100% PDX 134183 identity. Green column indicates c.661G>T mutation, detected at a 99% frequency.

As observed in the MS-HRM assay, MAYO-PH039 samples presented with increasing methylation loss with each subsequent cycle of niraparib treatment – with the entire region losing methylation at the third treatment cycle (**Figure 5.21**). In the untreated MAYO-PH039 samples, however, we could now observe that certain CpG sites were consistently less methylated (**Figure 5.21**), thereby in part explaining the heterogenous profile observed in MS-HRM for these samples (**Figure 5.7**).



Figure 5.21. Methyl-BROCA profile reveals some RAD51C CpG sites less methylated than others in untreated MAYO-PH039.

Figure shows the total methylated and unmethylated reads (y-axis) for each CpG position (x-axis- labelled by nucleotide distance from promoter) along the RAD51C gene promoter region covered by RAD51C MS-HRM. S0.1: untreated (source) MAYO-PH039, C1.2: post-one cycle of niraparib, C2.2: post-two cycles of niraparib.

Given that untreated MAYO-PH039 tumours still have *RAD51C* gene silencing with these heterogeneous me*RAD51C* profiles, it is possible that these particular CpG sites are less critical for *RAD51C* gene silencing. Interestingly, one vehicle-treated PDX 134183 sample known to have gene silencing (#8269, **Figure 5.6**) was also found to have a heterogeneous me*RAD51C* profile by MS-HRM (**Figure 5.22**). When comparing the methyl-BROCA me*RAD51C* profile of this PDX 134183 sample with that of untreated MAYO-PH039 source tumour, the same CpG sites appear to have reduced methylation in these samples (**Figure 5.23**). This suggested that these two CpG sites may be less important for *RAD51C* gene silencing.

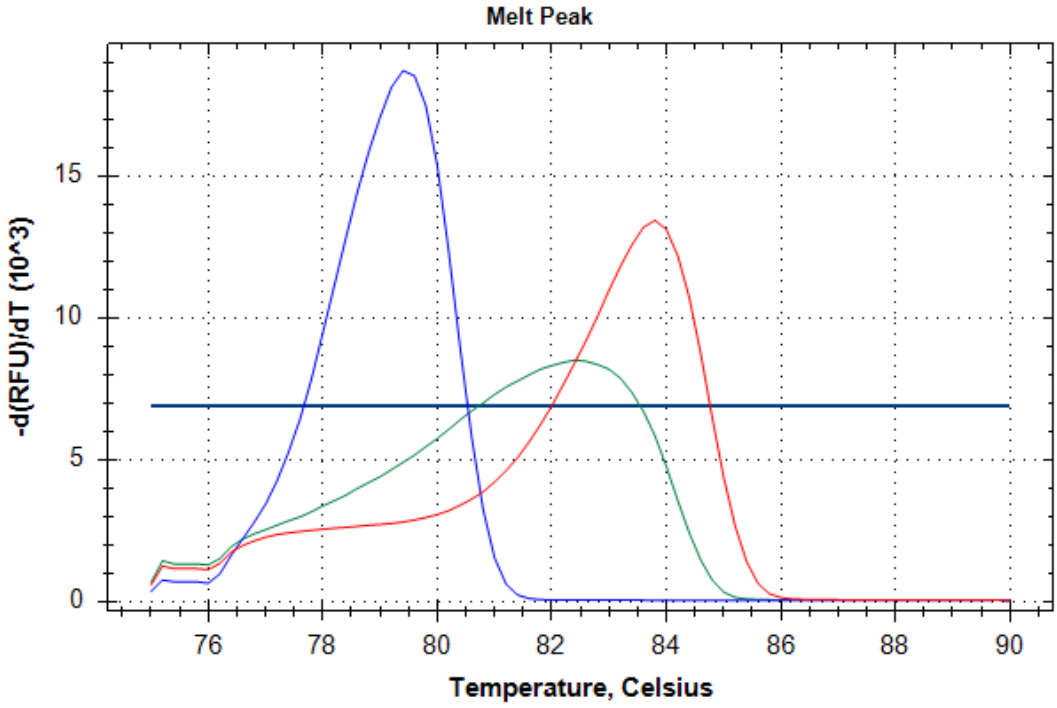


Figure 5.22. Vehicle-treated PDX 134183 sample #8269 has heterogeneous meRAD51C profile.

Sample found in MS-HRM testing. Each line represents a measurements per tumour/sample. RFU – Relative fluorescence units.

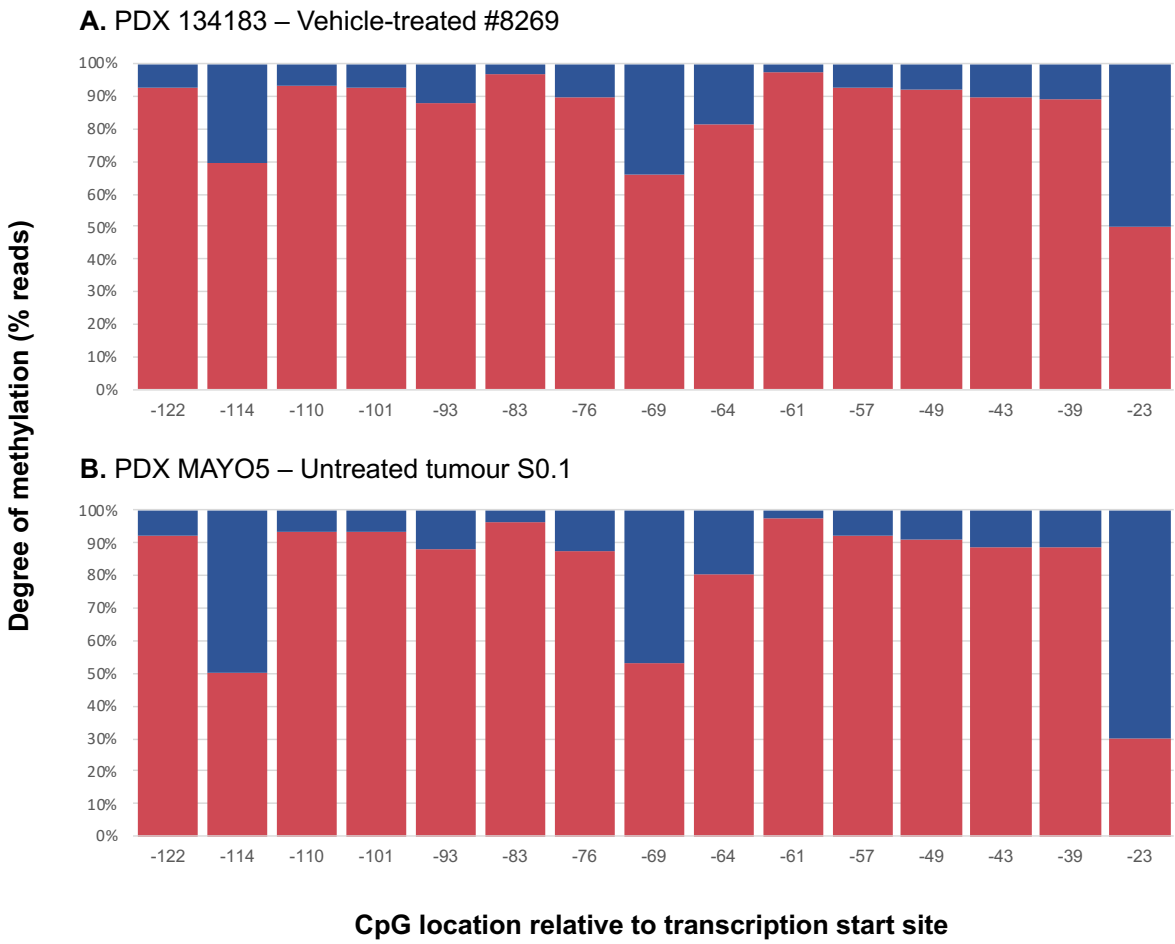


Figure 5.23. PDX 134183 sample meRAD51C profile that matches that of MAYO-PH039.
Methyl-BROCA results for (A) Vehicle-treated PDX 134183 sample #8269 and (B) MAYO-PH039 source tumour sample. CpG -114 and -69 from transcription start site have reduced methylation compared to other sites within these samples. Figure shows the % of methylated and unmethylated reads (y-axis) for each CpG position (x-axis- labelled by nucleotide distance from promoter) along the RAD51C gene promoter region covered by RAD51C MS-HRM.

5.4.6 Driving RAD51C methylation loss in PDX 134183

Given that most standard PARPi/cisplatin treatment tumours initially tested for me*RAD51C* in PDX 134183 were all still fully methylated, we were interested in whether we could drive loss more consistently in these tumours using cyclical re-treatments with cisplatin or PARPi, similar to MAYO-PH039 model. To do this, PDX 134183 mice were treated with rucaparib at a dose of 300mg/kg for a total of 3 weeks for cycle one (5/7 days per week) and again for 2 weeks for cycle 2 (5/7 days per week) when tumours reached 500mm^3. Tumours were then transplanted into new mice where treatments were repeated (cycles 3 and 4), to give a total of 4 cycles of rucaparib at the end-point (**Figure 5.24A**). Tumour fragments were snap frozen at transplant (2 cycles) and at final harvest (4 cycles).

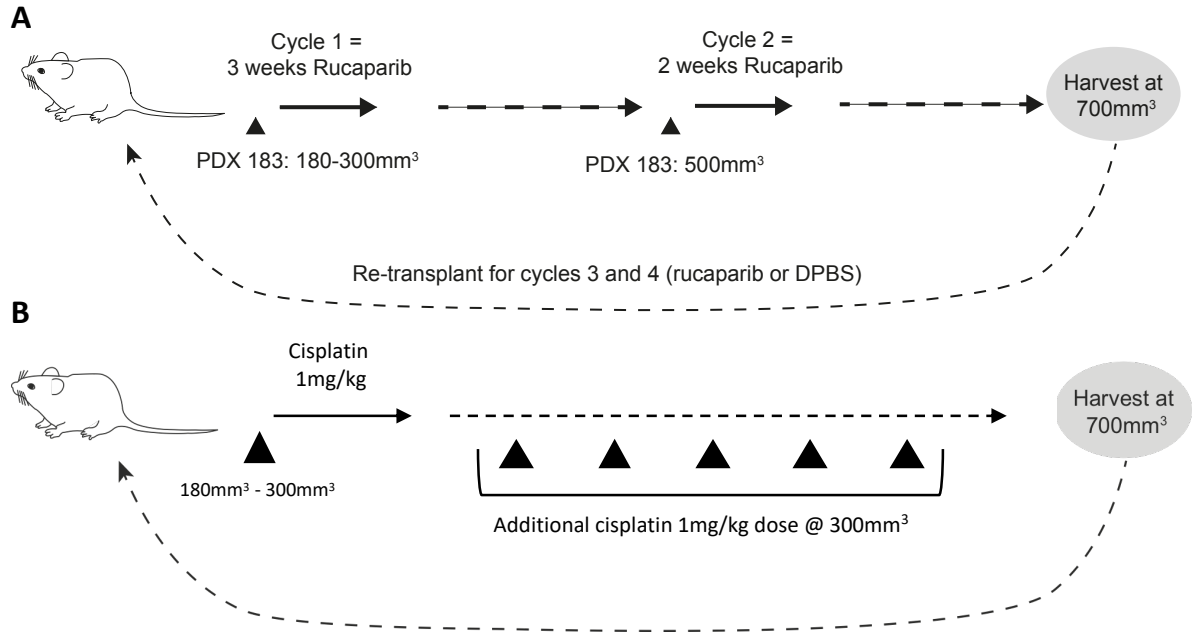


Figure 5.24. Rucaparib and cisplatin retreatments of PDX 134183.

(A) Rucaparib re-treatment strategy for PDX 134183 (#183), where tumours were treated with 2 cycles of rucaparib (300mg/kg) in first mouse/passage, and two more in second passage for a maximum of 4 cycles per tumour. (B) Cisplatin re-treatment strategy for PDX #183, where mice were re-treated with a lower dose if cisplatin (1mg/kg) each time tumour volume reached 300mm^3 for up to 6 doses per mouse, across two passages.

Cisplatin re-treatments were also designed (**Figure 5.24B**), as we were aware from our studies on *BRCA1* methylation that platinum therapy in patients could lead to loss of *BRCA1* methylation in one allele, causing restored HR DNA repair and PARPi resistance. The cisplatin re-treatment strategy for PDX 134183 involved re-treating PDX with a lower dose of cisplatin (1mg/kg) each time tumour volume reached 300mm^3 (given the high sensitivity of this model to standard cisplatin dosing) for up to 6 doses per mouse, and this was across two passages, with tumours harvested at transplant and final harvest.

DNA was extracted from these tumours, along with previously untested standard treatment cisplatin and PARPi tumours, and me*RAD51C* loss was then screened for using MS-HRM assay. "Me*RAD51C* loss" was defined as any shift in the HRM curve away from the 100% methylated control/vehicle-treated controls, towards the unmethylated control peak. There was no minimum methylation loss cut-off introduced, given that other pieces of the same tumour may have different *meRAD51C* profiles due to tumour heterogeneity (as was observed for tumour #7907, **Figure 5.19**).

A total of 102 tumours from PDX 134183 were screened for methylation loss, and the results are presented in **Table 5.9**.

Table 5.9. Results of meRAD51C loss MS-HRM screening in PDX 134183 tumours by treatment.

Loss of methylation was defined as any shift in the MS-HRM curve towards the unmethylated standard (MS-HRM example curve in Figure 5.25).

	PDX #183 tumours with me*RAD51C* loss	
Vehicle	1/21	4.8%
Niraparib 100mg/kg	2/7	28.6%
Rucaparib 300mg/kg	1/12	8.3%
Rucaparib 450mg/kg	0/8	0.0%
Cisplatin 4mg/kg	2/9	22.2%
Rucaparib re-treatments	3/23	13.0%
Cisplatin re-treatments	1/22	4.5%

Some tumour samples were found to range in their degree of me*RAD51C* loss, for example, tumour #7907 had complete me*RAD51C* loss in one of the tumour pieces (**Figure 5.19**) ,while tumour #13290 had around 50% me*RAD51C* loss (**Figure 5.25**). Interestingly, the PARPi and cisplatin re-treatment strategy did not enrich for me*RAD51C* loss compared to standard treatments, with PARPi niraparib-treated tumours resulting in the largest proportion of cases with some degree of methylation loss, followed by cisplatin (**Table 5.9**).

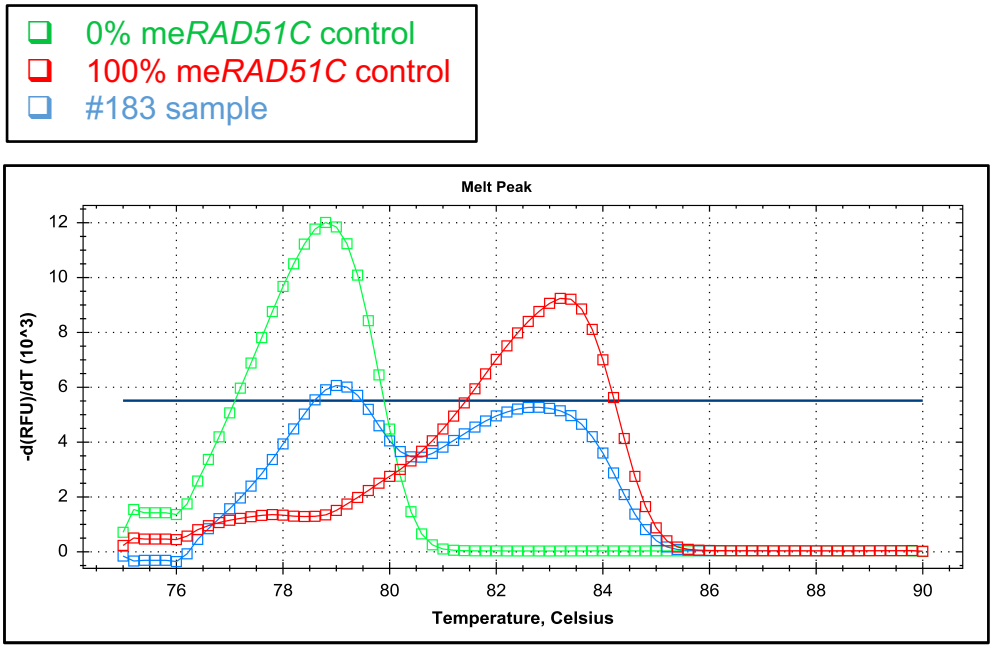


Figure 5.25. Example MS-HRM curve of rucaparib-treated 134183 sample with ~50% meRAD51C loss.

Piece of PDX 134183 tumour #13290 was found to have ~50% meRAD51C loss by MS-HRM following standard treatment with rucaparib (300mg/kg dose). Each line represents a measurements per tumour/sample. RFU – Relative fluorescence units.

5.4.7 Driving RAD51C methylation loss in PDX WEHI-PH039

We then attempted the same rucaparib treatment regimen for both lineages of PDX WEHI-PH039, but due to fast tumour growth, we were unable to complete cycle 1/standard PARPi treatment (**Table 5.10**). Our collaborators did not report the same problem for MAYO-PH039 treated with niraparib at a 100mg/kg dose (**Figure 5.1**). This is possibly due to the different mouse strains used for treatment, or, more likely, selection of a more resistant tumour following rescue of our lineages from cryo-preserved minced tumours.

Table 5.10. WEHI-PH039 samples grow too fast for standard treatments.

Half of the WEHI-PH039 samples that started treatment when over 250mm^3 in volume were harvested before 15 days. Cisplatin treatments end at 18 days, but PARPi treatments end at 21 days.

PDX	Treatment group	Tmour ID and transplant	Days from treatment start				
			1	4	8	11	15
WEHI-PH039 Lineage A	Cisplatin 1mg/kg (Retreat)	13043 T4	292.42	411.63	599.25	618.69	350.85
	Cisplatin 4mg/kg	13376 T5	252.05	313.46	313.37	172.84	132.69
	Cisplatin 4mg/kg	13378 T5	297.74	179.90	175.75	49.15	0.00
	Vehicle (DPBS)	12970 T4	282.27	484.22	973.72		
	Vehicle (DPBS)	12971 T4	261.43	372.24	937.09		
	Vehicle (DPBS)	13538 T6	278.23	453.27	341.15	483.77	860.79
	Vehicle (DPBS)	13574 T6	292.55	587.63	860.85		
	Rucaparib 300mg/kg	13293 T5	254.89	353.67	555.16	511.94	551.52
	Rucaparib 300mg/kg	13537 T6	298.52	324.49	494.36	432.02	316.23
	Rucaparib 300mg/kg	13577 T6	277.07	427.27	427.64	477.10	609.27
WEHI-PH039 Lineage B	Cisplatin 1mg/kg (Retreat)	13366 T5	284.99	447.78	418.80	535.13	513.93
	Vehicle (DPBS)	13070 T4	283.16	442.34	688.08	714.73	
	Vehicle (DPBS)	13071 T4	290.95	387.74	550.81	843.09	
	Niraparib 100mg/kg	13072 T4	271.79	551.82	488.15	738.30	
	Niraparib 100mg/kg	13369 T5	270.68	415.12	836.20		
	Rucaparib 300mg/kg	13364 T5	263.75	376.72	632.09	785.41	

To address this, I modified the treatment regimen used for the WEHI-PH039 mice. These mice were started on treatments at a smaller tumour size (180-250mm^3 instead of standard 180-300mm^3), received a higher dose of rucaparib (450mg/kg), and were re-treated in cycle 2 at a smaller tumour size of 300mm^3 (**Figure 5.26A**). I also designed cisplatin re-treatments for WEHI-PH039 (**Figure 5.26B**). As WEHI-PH039 tumours responded better to cisplatin than PARPi (**Figure 5.8**; **Figure 5.10**), the re-treatment regimen was started on tumours with the standard tumour volume of 180-300mm^3, like PDX 134183.

WEHI-PH039 tumours from the standard treatment and re-treatment studies were then screened for me*RAD51C* loss using MS-HRM analysis. A total of 24 and 29 samples were tested from Lineage A and B, respectively, and results are presented in **Table 5.11**. Example MS-HRM curves of samples with me*RAD51C* losses ranging from 50-100% are shown in **Figure 5.27**, **Figure 5.28** and **Figure 5.29**. Interestingly, it appears that Lineage A of WEHI-PH039 was more susceptible to loss of me*RAD51C* compared to Lineage B, with me*RAD51C* loss (defined as any shift in the HRM curve towards the unmethylated state) observed in more post-treatment Lineage A samples compared to Lineage B (**Table 5.11**).

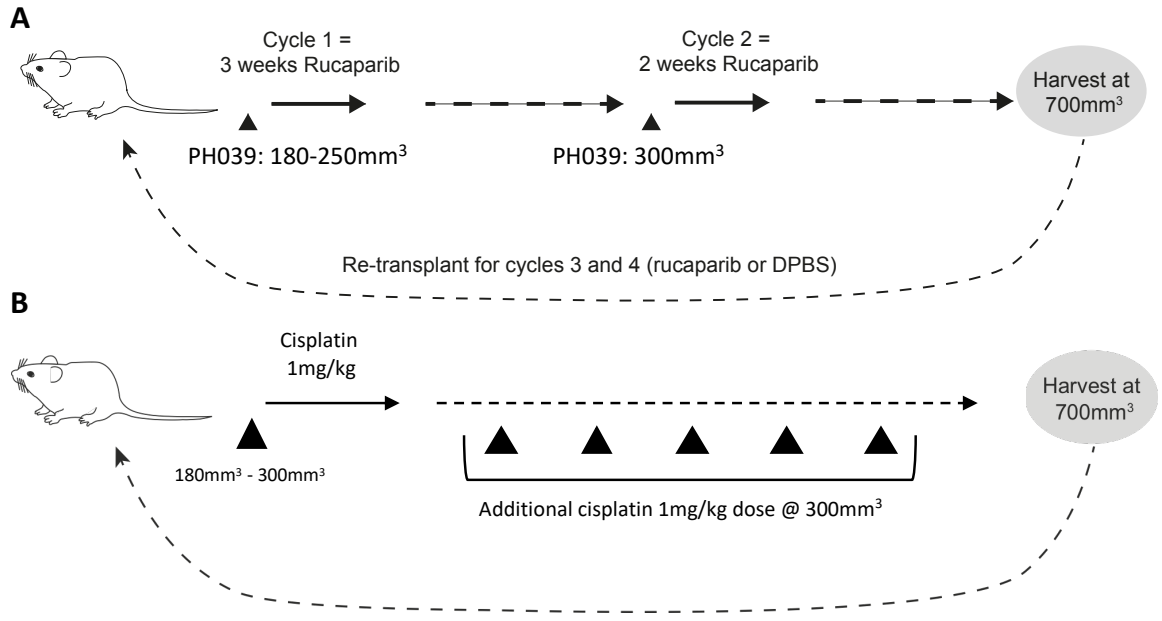


Figure 5.26. Rucaparib and cisplatin retreatments of PDX WEHI-PH039.

(A) *Rucaparib re-treatment strategy for PDX WEHI-PH039, where tumours were treated with 2 cycles of rucaparib (450mg/kg) in first mouse/passage, and two more in second passage for a maximum of 4 cycles per tumour.* ***(B)*** *Cisplatin re-treatment strategy for PDX WEHI-PH039, where mice were treated with a lower, single dose of cisplatin (1mg/kg) and re-treated with this dose each time tumour volume reached 300mm^3 for up to 6 doses per mouse, across two passages.*

Table 5.11. WEHI-PH039 Lineage A loses meRAD51C more readily than Linage B.

*Results of meRAD51C loss MS-HRM screening in WEHI-PH039 Lineage A and B tumours by treatment. *Lineage A samples were found to be too sensitive to cisplatin, and there was no material to harvest at ethical harvest endpoint. Loss of methylation was defined as any shift in the MS-HRM curve towards the unmethylated standard (MS-HRM example curves shown in Figure 5.27, Figure 5.28 and Figure 5.29).*

	Tumours with me*RAD51C* loss:			
	WEHI-PH039 Lineage A		**WEHI-PH039 Lineage B**	
Vehicle	0/6	0.0%	0/6	0.0%
Niraparib 100mg/kg	1/4	25.0%	0/4	0.0%
Rucaparib 300mg/kg	3/5	60.0%	0/4	0.0%
Rucaparib 450mg/kg	3/5	60.0%	1/3	33.3%
Cisplatin 4mg/kg	NA*	NA*	1/3	33.3%
Rucaparib re-treatments	1/3	33.3%	2/9	22.2%
Cisplatin re-treatments	1/1	100.0%	NA	NA

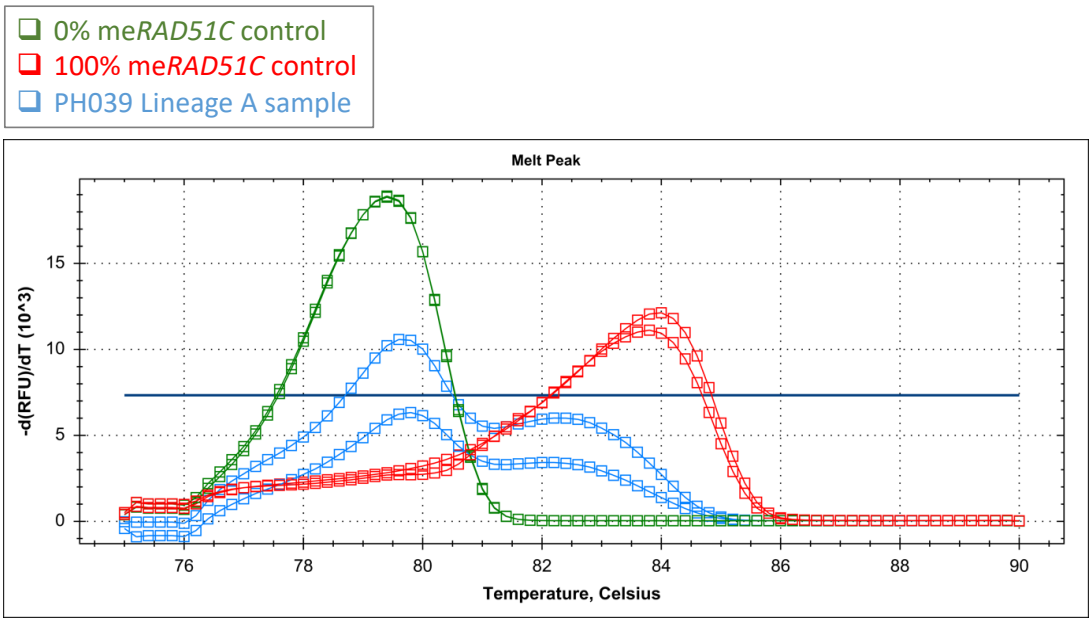


Figure 5.27. Example MS-HRM curve of rucaparib-treated WEHI-PH039 Lineage A sample with >50% meRAD51C loss.

Piece of PDX WEHI-PH039 Lineage A tumour 14419 found to have >50% meRAD51C loss by MS-HRM following standard treatment with rucaparib (450mg/kg dose). Each line represents a measurements per tumour/sample. RFU – Relative fluorescence units.

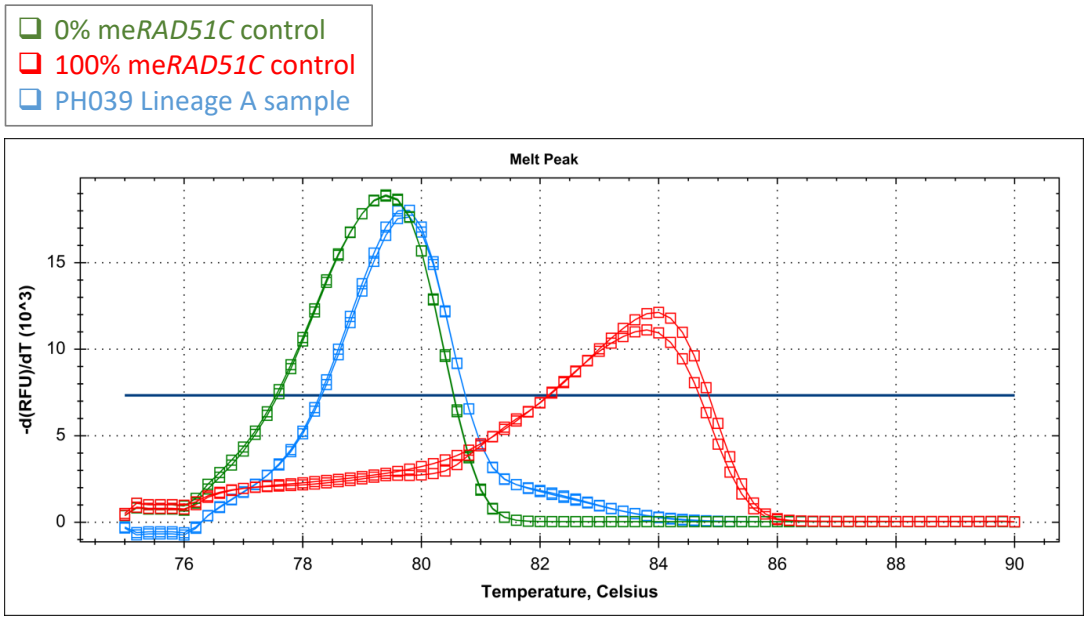


Figure 5.28. Example MS-HRM curve of rucaparib-treated WEHI-PH039 Lineage A sample with 100% meRAD51C loss.

Piece of PDX WEHI-PH039 Lineage A tumour 14186 found to have 100% meRAD51C loss by MS-HRM following re-treatment with rucaparib (450mg/kg dose, 2 cycles). Each line represents a measurements per tumour/sample. RFU – Relative fluorescence units.

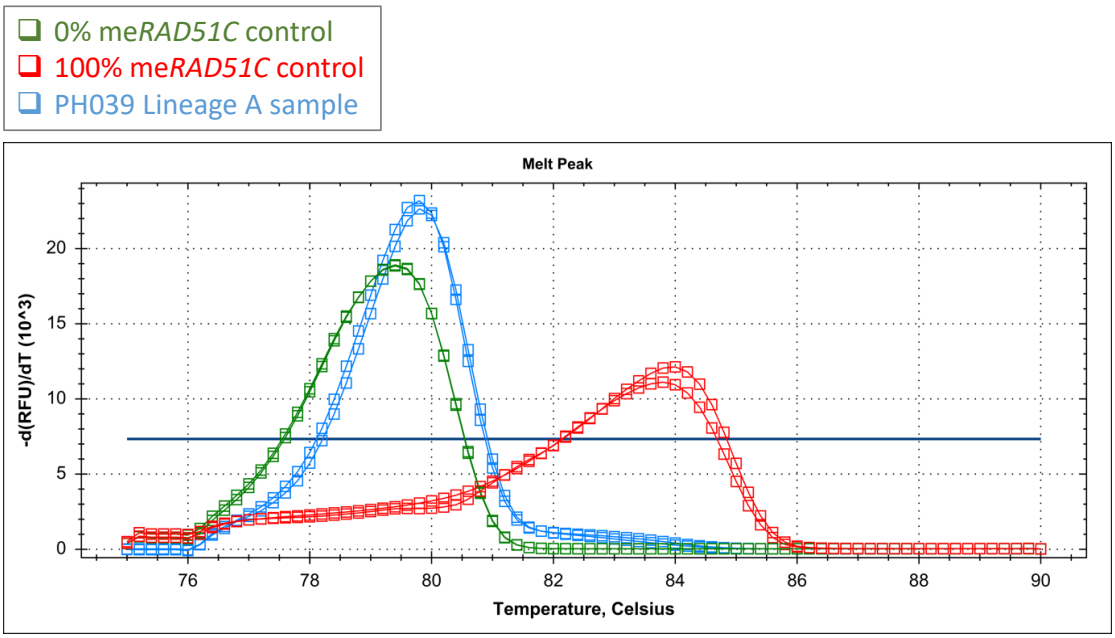


Figure 5.29. Example MS-HRM curve of rucaparib-treated WEHI-PH039 Lineage B sample with 100% meRAD51C loss.

Piece of PDX WEHI-PH039 Lineage A tumour 14225 found to have 100% meRAD51C loss by MS-HRM following re-treatment with rucaparib (450mg/kg dose, 2 cycles). Each line represents a measurements per tumour/sample. RFU – Relative fluorescence units.

5.4.8 RAD51C promoter methylation and gene expression in PDX

Given that I established a substantial collection of tumours with me*RAD51C* loss in both PDX 134183 and WEHI-PH039, I was also interested in whether these losses correlated with restored *RAD51C* gene expression as they did for PDX MAYO-PH039 (**Figure 5.1**). To address this, I tested *RAD51C* expression in RNA extracted from PDX tumours using qRT-PCR.

All untreated PDX 134183 samples had undetectable *RAD51C* expression by qRT-PCR (**Figure 5.30**), including the heterogeneous me*RAD51C* sample #8269 (described in **Figure 5.23**). Some post-PARPi and post-cisplatin PDX 134183 samples were found to have a low level of *RAD51C* gene expression (**Figure 5.30**), and this was found to correlate strongly ($p < 0.001$) with loss of me*RAD51C* (**Figure 5.31**).

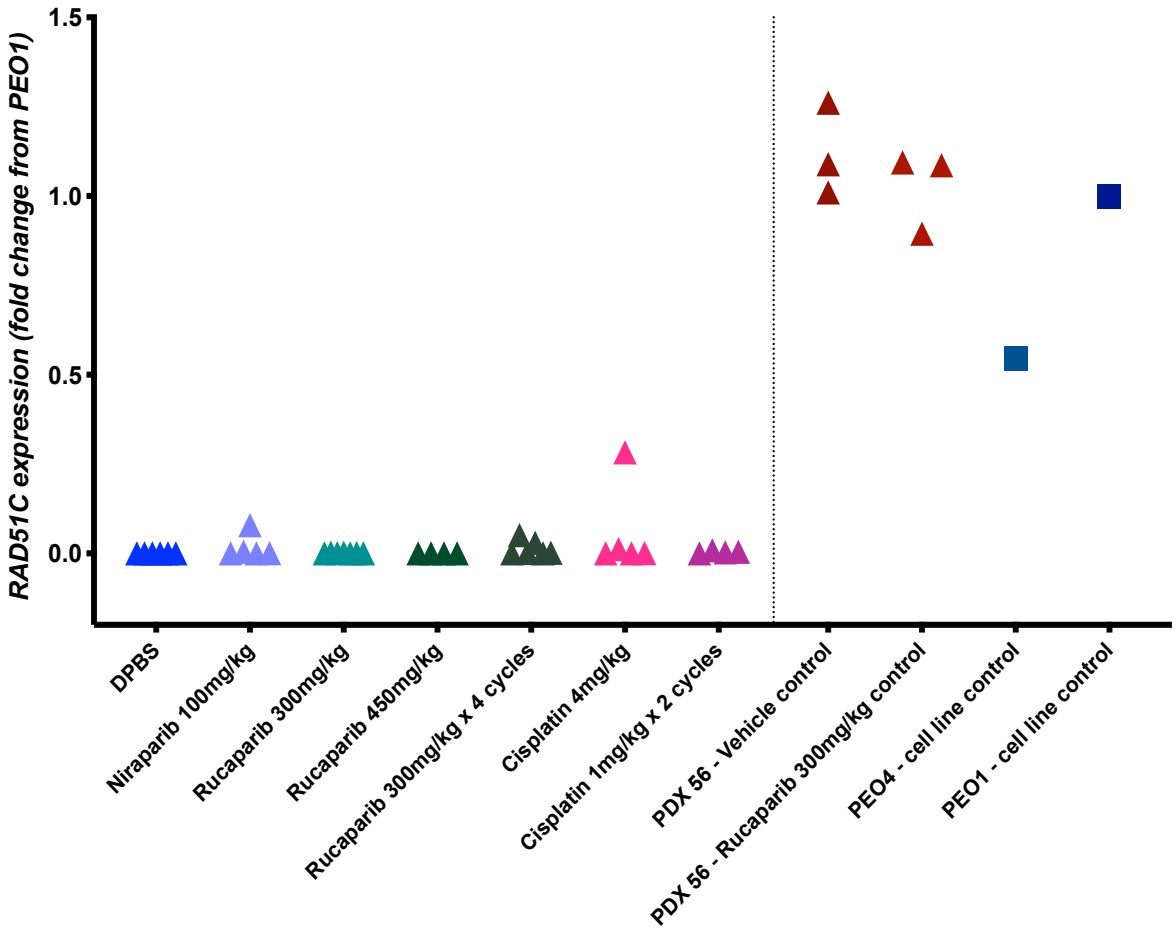


Figure 5.30. Untreated PDX 134183 samples lack detectable RAD51C gene expression while some post-treatment samples demonstrate elevated RAD51C gene expression.

Each point represents an individual tumour measurement. RAD51C expression values were normalised to GAPDH values for each sample. Fold change from control cell line PEO1 sample is presented.

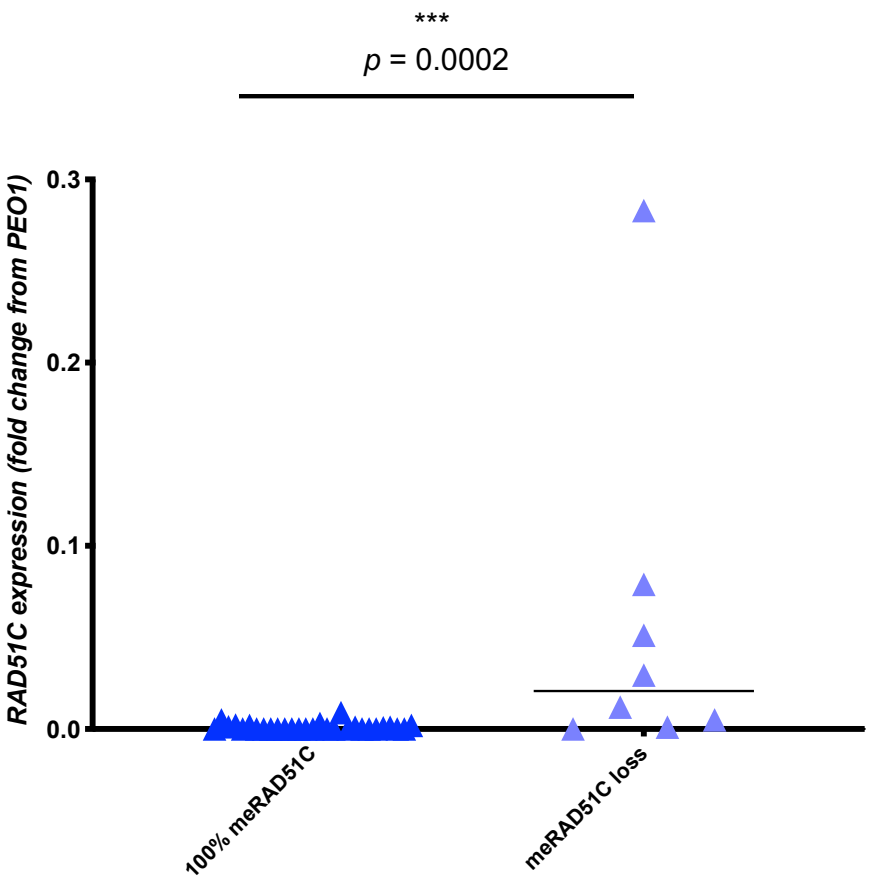


Figure 5.31. PDX 134183 tumours with meRAD51C loss have increased RAD51C expression compared to tumours without meRAD51C loss.

All PDX 134183 samples without any detectable meRAD51C loss (MS-HRM) across all treatments were grouped, and compared to all the grouped samples with detectable loss. Each point represents individual PDX tumour sample. Data normalised to housekeeper gene GAPDH, and fold change from RAD51C-expressing control PEO1 is presented. P-value calculated using the Mann–Whitney U nonparametric test.

Untreated WEHI-PH039 Lineage A tumours also demonstrated undetectable *RAD51C* expression on this assay (**Figure 5.32**), while the post-treatment samples with elevated expression were from tumours with me*RAD51C* loss (**Table 5.12**). This correlation between *RAD51C* expression and me*RAD51C* loss was found to be statistically significant (p-value = 0.011; **Table 5.12**), despite the small number of samples with me*RAD51C* loss tested by qPCR. This corroborated the findings for niraparib-treated PDX MAYO-PH039 samples with me*RAD51C* loss (**Figure 5.1**).

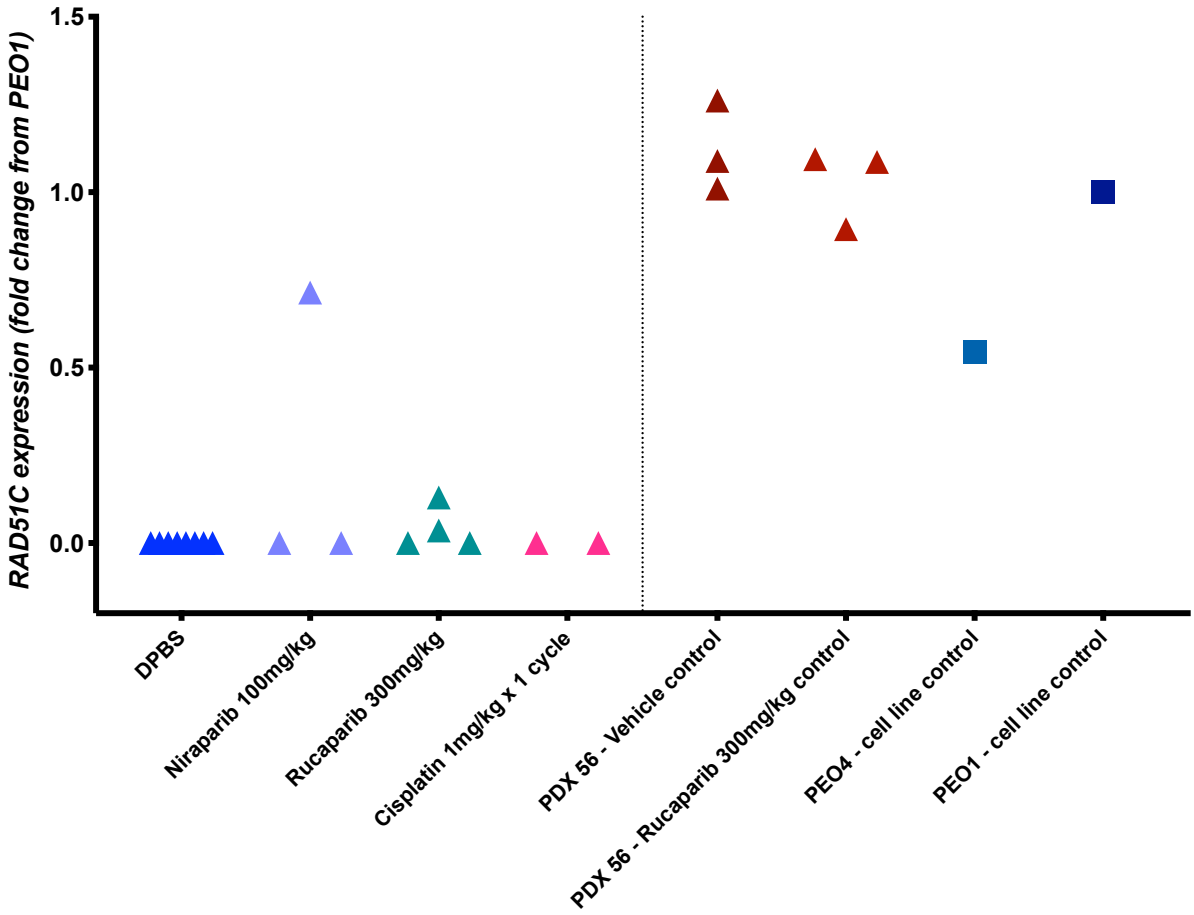


Figure 5.32. PARPi-treated PH039 Lineage A tumours regain RAD51C gene expression.
Each point represents individual PDX tumour sample/cell line passage. Data normalised to house keeper gene GAPDH, and fold-change from RAD51C-expressing control PEO1 is presented.

Table 5.12. RAD51C gene expression observed in PH039 Lineage A tumours with meRAD51C loss.

Tumour sample #	Treatment	me*RAD51C* loss (MS-HRM)	*RAD51C* expression (fold-change)
13375	Niraparib 100mg/kg	Yes	0.714
13874	Niraparib 100mg/kg	No	0.000
13877	Niraparib 100mg/kg	No	0.000
13290	Rucaparib 300mg/kg	Yes	0.130
13575	Rucaparib 300mg/kg	Yes	0.036
13876	Rucaparib 300mg/kg	Yes	0.000
14421	Rucaparib 300mg/kg	No	0.000
13041	Cisplatin-retreat cycle 1	No	0.000
13294	Cisplatin-retreat cycle 1	No	0.000

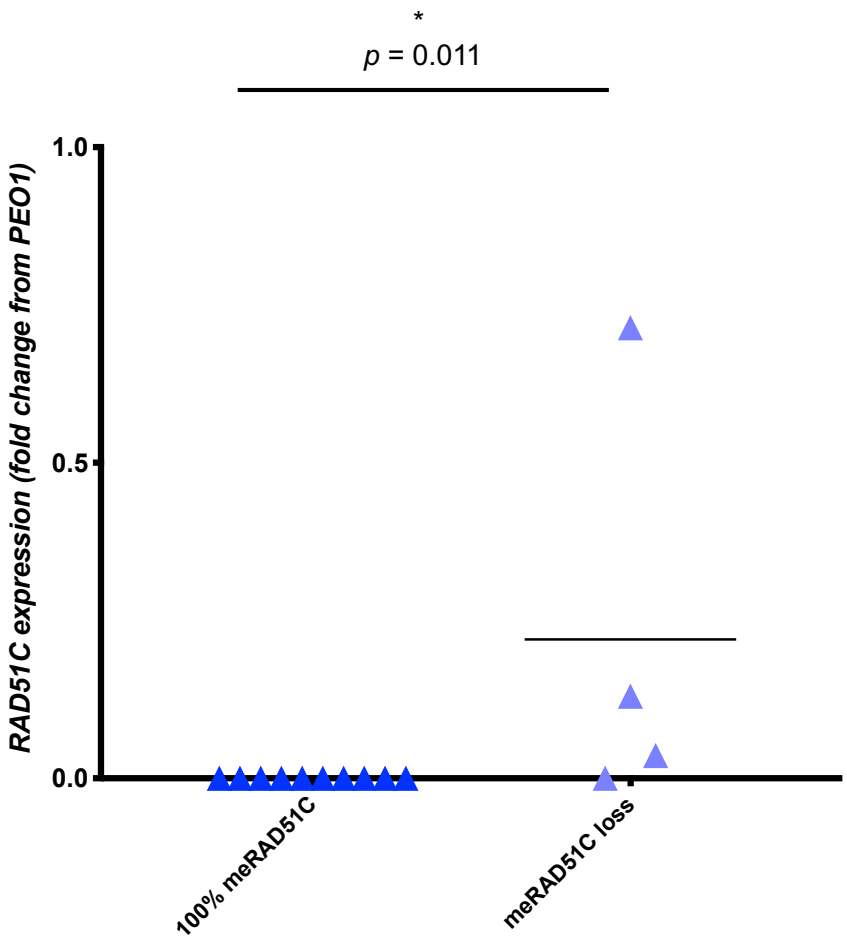


Figure 5.33. WEHI-PH039 Lineage A tumours with meRAD51C loss have increased RAD51C expression compared to tumours without meRAD51C loss.

All WEHI-PH039 Lineage A samples without any detectable meRAD51C loss (MS-HRM) across all treatments were grouped, and compared to all the grouped samples with detectable loss. Each point represents individual PDX tumour sample. Data normalised to housekeeper gene GAPDH, and fold change from RAD51C-expressing control PEO1 is presented. P-value calculated using the Mann–Whitney U nonparametric test.

All WEHI-PH039 Lineage B samples tested on qRT-PCR were from samples that had no evidence of me*RAD51C* loss, and this was evident in the lack of *RAD51C* gene expression in the qPCR results (**Figure 5.34**). Interestingly, this data also allowed us to establish that the DPBS-treated (vehicle) samples with different me*RAD51C* profiles on MS-HRM (less-methylated "LLS" and more-methylated "LS" curves) all appeared to have *RAD51C* gene silencing (**Table 5.13**).

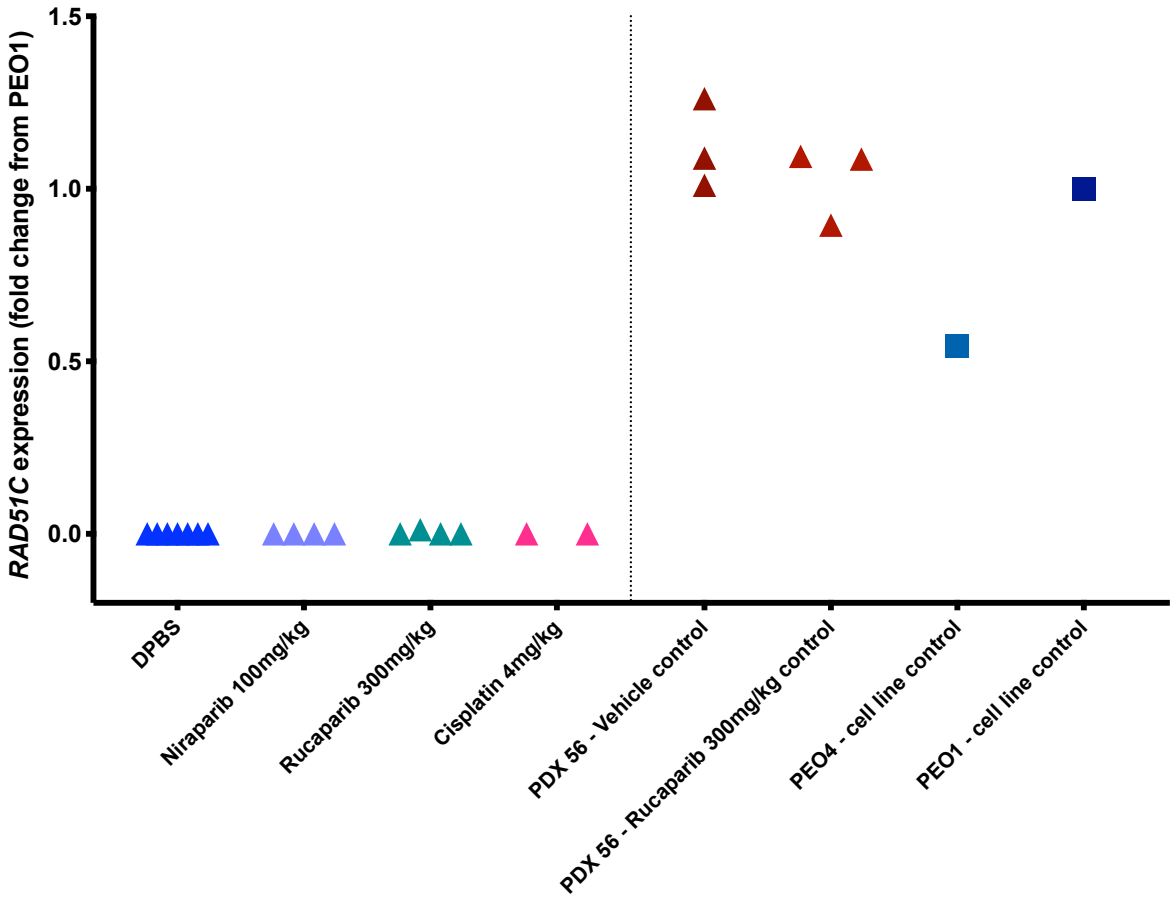


Figure 5.34. No RAD51C gene expression detected in highly methylated PH039 Lineage B samples.

Each point represents individual PDX tumour sample/cell line passage. Data normalised to housekeeper gene GAPDH, and fold change from RAD51C-expressing control PEO1 is presented.

Table 5.13. WEHI-PH039 Lineage B meRAD51C LS and LLS profiles result in RAD51C gene silencing.

No RAD51C gene expression detected in the following DPBS-treated samples with "LS" and "LLS" meRAD51C profiles. NA: sample not tested by MS-HRM.

Tumour sample #	me*RAD51C* profile (MS-HRM)
13071	LS
13368	LS
13381	LS
13365	NA
13939	LLS
13070	LLS
14224	LLS

5.4.9 RAD51C copy-number analysis in PDX 134183 and WEHI-PH039

To determine if the observed loss of methylation in PDX was due to change in zygosity (homozygous to heterozygous) or tumour heterogeneity, I needed to determine the *RAD51C* copy number status of the two PDX models. MLPA (Multiplex ligation-dependent probe amplification) is a common approach for testing gene copy number in cells. This approach was recently developed into a simplified NGS amplicon-based assay, "MLPA-seq", which can incorporate multiple probes for a single gene to interrogate gene copy number in a relatively straightforward way (Kondrashova et al., 2015a). Three probes for *RAD51C* were selected and used for MLPA-seq testing. Unfortunately, the test results were inconclusive, with both models appearing to have 1.4-1.6 copies of *RAD51C* (**Table 5.14**).

Table 5.14. MLPA-seq results for RAD51C copy number are inconclusive.
Average copy number estimate for control probes calculated using the average values of all 8 control probes across different genes, while copy number estimate for RAD51C calculated using the average values of 3 RAD51C probes (in exons 2, 6 and 9).

PDX	Sample	Average of control probes	Average of *RAD51C* probes	*RAD51C* copy number estimate
-	Control 1	0.99	1.03	2.1
-	Control 2	1.01	1.00	2.0
-	Control 3	1.00	0.98	2.0
134183	8290	1.04	0.69	1.4
134183	8292	1.06	0.78	1.6
MAYO-PH039	C3	0.97	0.67	1.3
MAYO-PH039	S2	0.98	0.70	1.4

Thus, I turned to whole genome sequencing (WGS) data generated for both models, where results suggested one copy of *RAD51C* per cell in both PDX models (**Table 5.15**). These results were later confirmed using SNP arrays (**Table 5.16**).

Although I had observed some samples that appeared heterozygous in MS-HRM (~50% methylation; **Figure 5.25**), given the *RAD51C* copy number estimates, this was more likely to be due to tumour heterogeneity rather than changes in me*RAD51C* zygosity. Indeed, PDX 134183 sample #7907 appeared to have heterozygous me*RAD51C* initially, but was later found to have complete loss of me*RAD51C* in a different tumour piece (**Figure 5.19**).

Table 5.15. Both PDX models have one copy of RAD51C per cell in WGS analysis.

The copy number estimation of two in PH039 patient tumour could be inaccurate due to lower tumour purity compared with PDX samples, given that WEHI-PH039 PDX samples consistently had a copy number of one. PDX tumour samples have passage number in brackets. ASCAT = Allele-Specific Copy number Analysis of Tumours; cnLOH = copy number-neutral loss of heterozygosity; Del = deletion.

Model	Sample	Copy number	ASCAT call
PH039	Patient tumour	2	cnLOH
PH039	13288 (T5)	1	Del
PH039	13368 (T5)	1	Del
134183	7903 (T3)	1	Del
134183	Patient tumour	1	Del

Table 5.16. Both PDX models have one copy of RAD51C per cell in SNP array analysis.

PDX 134183 sample #7365 is a T2 passage, while WEHI-PH039 Lineage A samples 13288 is a T5 passage.

PDX	Sample	*RAD51C* copy number
134183	7365	1
WEHI-PH039-A	13288	1

5.4.10 Targeted bisulfite meRAD51C sequencing

Unfortunately, MS-HRM and methyl-BROCA assays only provide information on the average methylation of all the bisulfite-converted *RAD51C* promoter amplicons or CpG sites, respectively, and not on how this methylation is distributed per amplicon/allele or what types of alleles exist in this mixture. Understanding the methylation state of each individual epiallele would allow to uncover if there are any pre-existing unmethylated alleles within the untreated PH039 tumours, elucidating the mechanism of resistance – pre-existing or acquired.

To address the need for an epiallele-specific assay, I set up a targeted next generation sequencing assay for me*RAD51C* amplicons within our samples. I based primer design on the

MS-HRM *RAD51C* assay and Illumina Nextera adapters, and then optimised sequencing of these bisulphite converted amplicons on the Illumina MiSeq platform. This straightforward assay can generate a large amount of information per sample, and allowed us to uncover the underlying me*RAD51C* epialleles present in our two models.

To ensure the developed assay is accurate and quantitative, I used PDX 134183 DNA (homozygous me*RAD51C*), and WEHI-CS62 cell line DNA (unmethylated *RAD51C*) and a 50:50 mix of the two. I wanted to make sure there would be no amplification bias introduced with the addition of the Illumina sequencing adapters. The results of this test were very encouraging, with little-to-no bias observed in these controls (**Figure 5.35**).

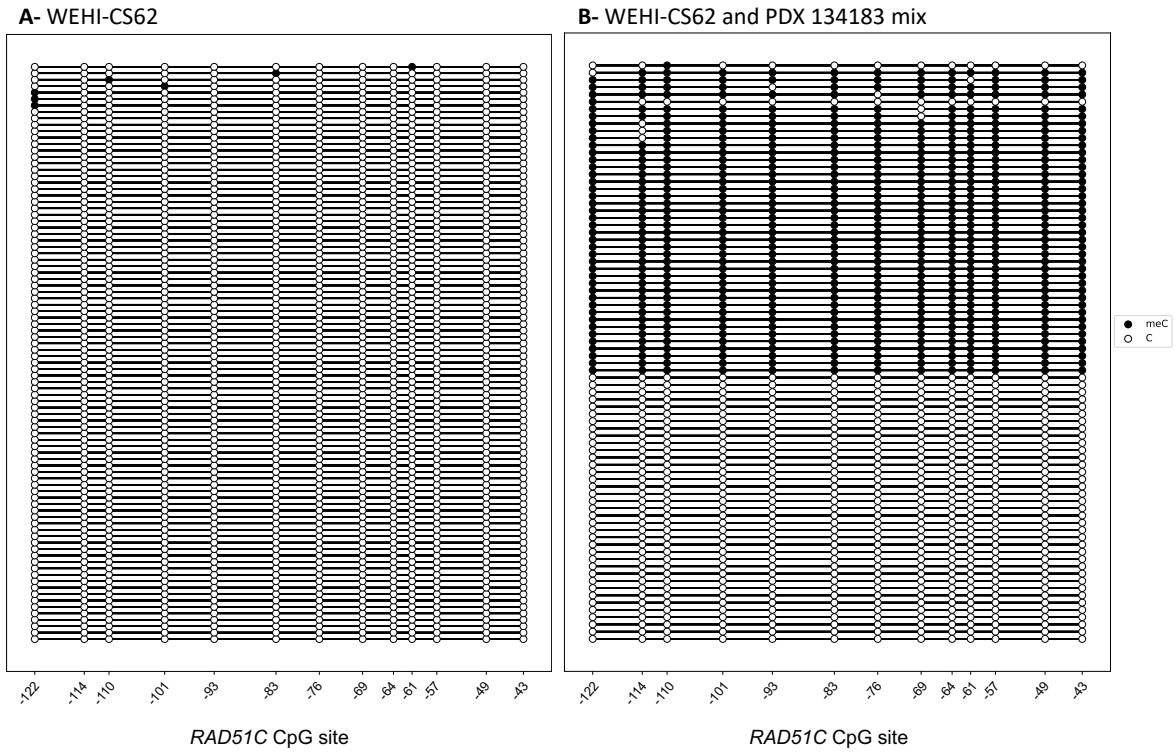


Figure 5.35. No apparent bias in targeted meRAD51C sequencing

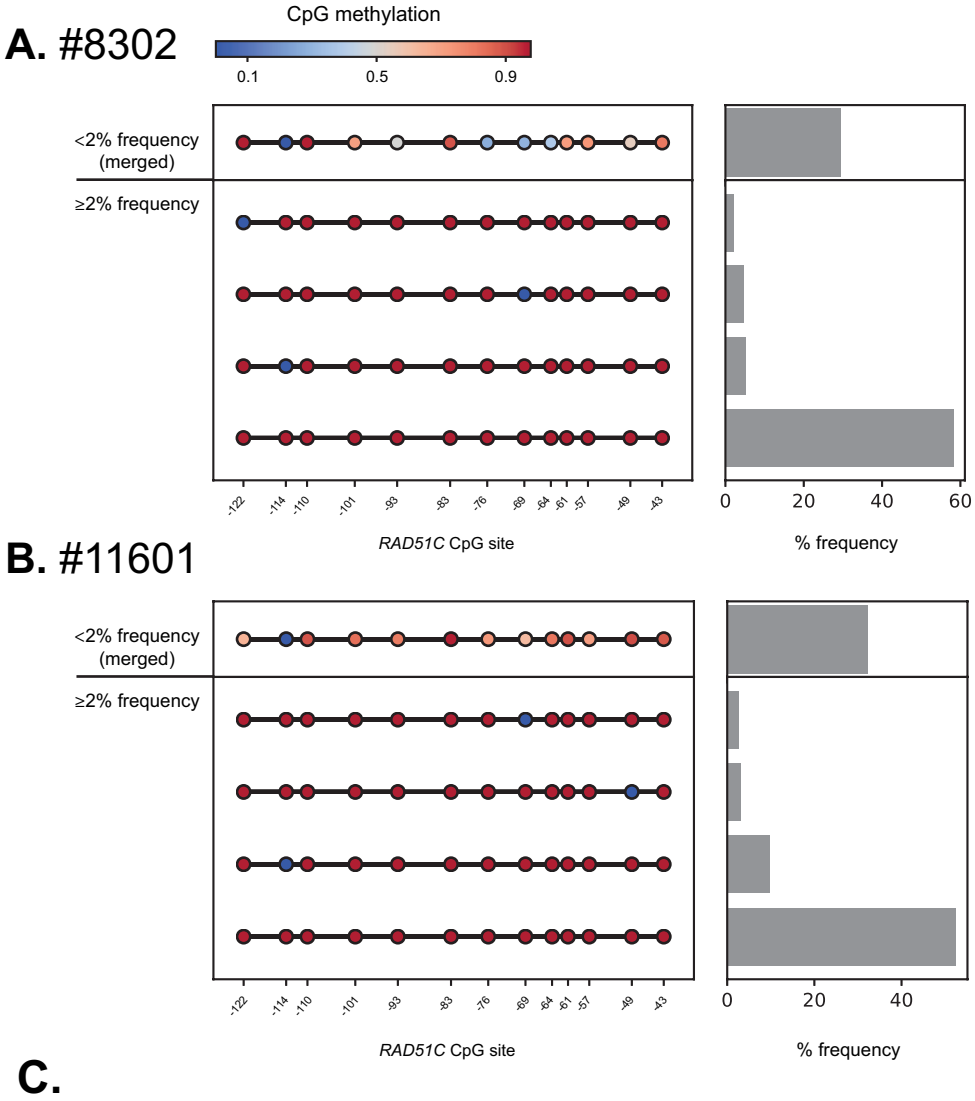
(A) *WEHI-CS62 sample is fully unmethylated, while* ***(B)*** *a 50:50 mix of WEHI-CS62 and PDX 134183 shows approximately 50:50 methylated alleles by sequencing. Using a >1% amplicon frequency threshold, all detected amplicons are presented. meC= methylated CpG, C= unmethylated CpG.*

An amplicon frequency threshold of 1% was used in this initial test to exclude any sequence errors introduced during bisulfite conversion or PCR amplification, and to limit the number of analysed amplicons. For subsequent analyses this was changed so that all amplicons were included, but those at a frequency of <2% were merged as a summary amplicon. This was done because such sequence errors would likely only affect a single CpG site along the amplicon, with the remaining CpG sites being an accurate representation of the original amplicon. Merging low frequency amplicons thus gives a representative view of these alleles, without losing any information.

An example of this type of representation is presented for two PDX 134183 tumours (#8302 and #11601), which were found to be 100% methylated by RAD51C MS-HRM assay (**Figure *5.36***). These two samples also demonstrated that long-term storage of samples at -30°C does not significantly affect results of this assay. Vehicle-treated tumour #8302 (sequenced 18 months post-bisulfite conversion) and rucaparib 300mg/kg-treated tumour #11601 (sequenced only 2 months post-bisulfite conversion) having only marginal (≤0.02%) differences in amplicon/epiallele representation when considering proportions of ≥40%, <40% and 0% methylated epialleles in each sample (**Figure *5.36*C**). This is reassuring, given published reports that bisulfite-converted DNA is less stable than unconverted DNA (Li et al., 2011).

Using this assay, I also assessed the me*RAD51C* differences between WEHI-PH039 Lineages A and B in more detail. MS-HRM assay previously uncovered that vehicle-treated Lineage A tumours tended to have a less methylated "LLS" profile compared to Lineage B tumours, which were a mix of "LLS" and more methylated "LS" profiles (**Figure 5.12**; **Table 5.6**). Lineage A was also more resistant to PARPi than Lineage B (**Figure 5.9**; **Figure 5.10**) and tended to lose me*RAD51C* (**Table 5.11**), thereby re-gaining *RAD51C* expression (**Figure 5.32**), compared to Lineage B (**Figure 5.34**).

Targeted me*RAD51C* sequencing of a Lineage A "LLS" tumour sample, and a Lineage B "LS" tumour sample revealed that the difference in melt curves was due to methylation of one CpG site at position -69. Tumours with "LLS" me*RAD51C* had reduced methylation of CpG sites -114 and -69, while "LS" tumours had reduced methylation of only site -114 (**Figure 5.37**).



C.

Sample	>=40% meCpG	<40% meCpG	0% meCpG
8302	99.78%	0.17%	0.05%
11601	99.80%	0.16%	0.05%

Figure 5.36. Long-term storage of bisulfite-converted DNA samples does not affect results of meRAD51C sequencing.

Targeted meRAD51C sequencing of PDX 134183 samples reveals ***(A)*** *vehicle-treated tumour #8302, run 18 months post-bisulfite conversion and* ***(B)*** *rucaparib 300mg/kg-treated tumour #11601, run 2 months post-bisulfite conversion have comparable methylation profiles, summarized in table* ***(C)*** *showing % of alleles with ≥ 40% CpG sites methylated, showing % of alleles with <40% CpG sites methylated and fully unmethylated alleles. Lollipop diagrams display merged amplicon summaries for amplicons present at <2% frequency, and individual amplicon profiles for those present at >2%, with degree of CpG methylation calculated using β-values.*

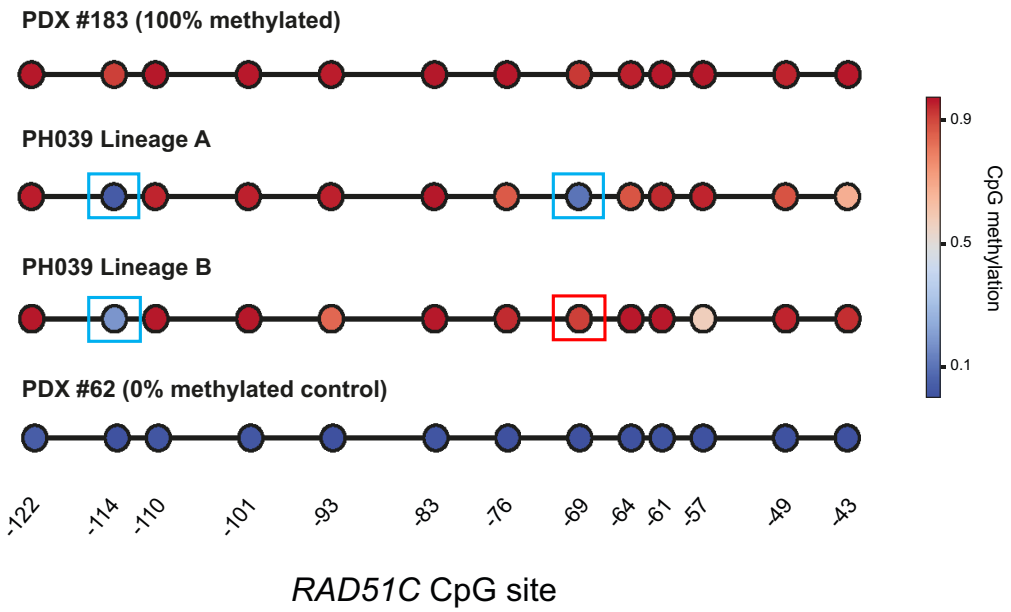


Figure 5.37. WEHI-PH039 Lineage A and B have slightly different methylation profiles due to differential methylation of single CpG site.

Targeted amplicon sequencing reveals that WEHI-PH039 Lineage B is frequently methylated at CpG -69, while Lineage A is not. Boxes indicate CpG sites that are consistently and inconsistently unmethylated (-114 and -69 respectively) between the lineages. Lollipop diagrams display merged total amplicon summaries for each PDX model, with degree of CpG methylation based on β-values.

I then prepared samples from MAYO-PH039 at different cycles of niraparib treatment, with different degrees of methylation loss, as I was interested in whether we could detect any fully unmethylated epialleles in the untreated PH039 samples. Detection of such epialleles would point to clonal selection as the main mechanism of me*RAD51C* loss and PARPi resistance in this model. No fully unmethylated epialleles were detected at ≥2% frequency using the detailed amplicon/lollipop plot style (**Figure 5.38**), though these plot did highlight the high degree of molecular me*RAD51C* heterogeneity in untreated MAYO-PH039 PDX. To see if there were any fully unmethylated me*RAD51C* molecules present in these samples at <2%, I interrogated the % of fully unmethylated epialleles per sample, along with epialleles with <40% methylation and epialleles with ≥40% methylation. The ≥40% methylation value was chosen to represent highly methylated alleles based on previous studies examining heterogeneous promoter methylation patterns and gene silencing of other genes (Cameron et al., 1999). No fully unmethylated epialleles were reported in the untreated MAYO-PH039 samples analysed (**Figure 5.39**). Fully unmethylated epialleles of *RAD51C* could be detected at a low proportion after one cycle of niraparib and at a high proportion after two cycles (**Figure 5.39**), suggesting this was an acquired mechanism of PARPi resistance.

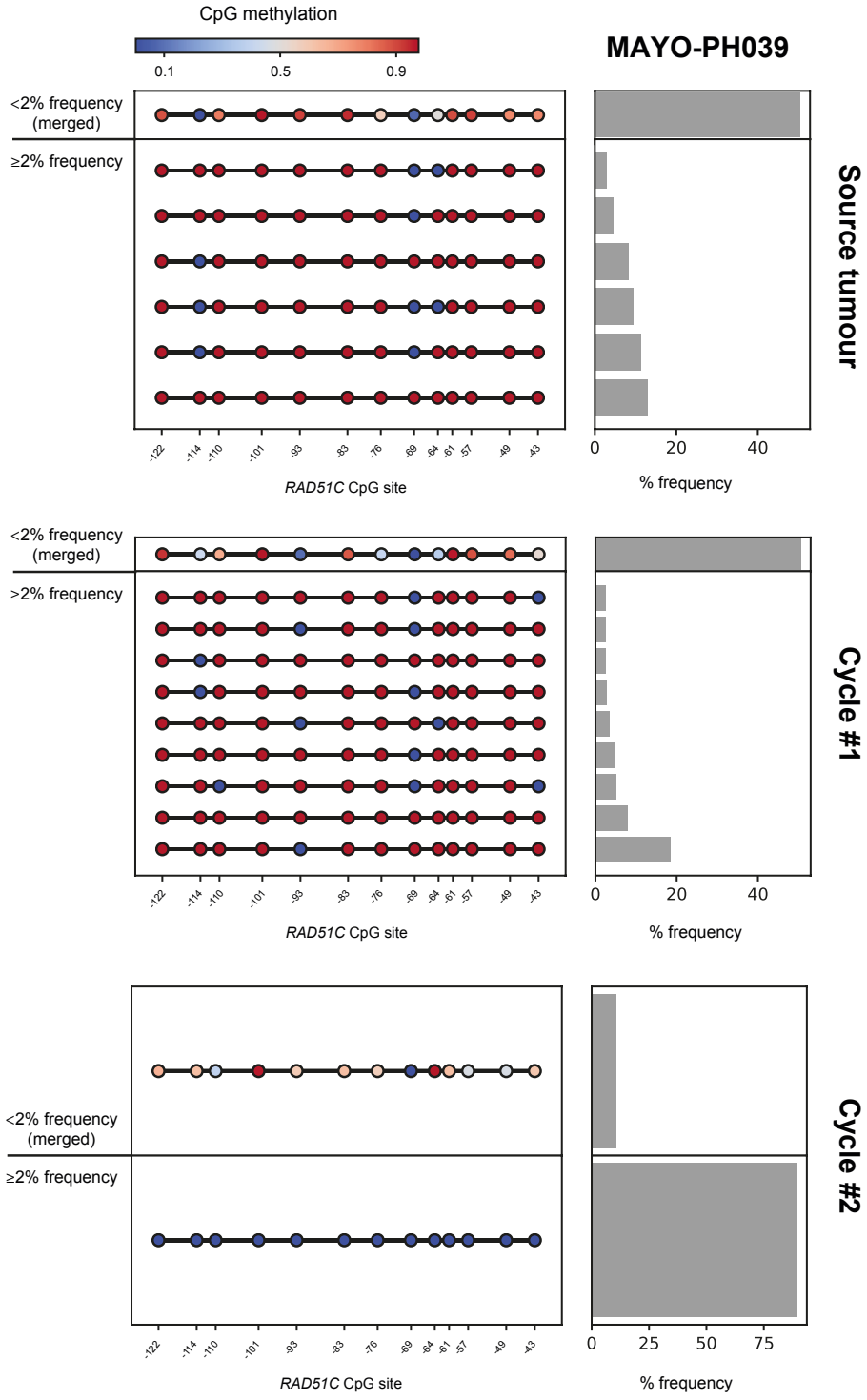


Figure 5.38. High degree of RAD51C epiallele heterogeneity in source PDX MAYO-PH039.

Targeted bisulfite sequencing of untreated (source), cycle #1 niraparib-treated and cycle #2 niraparib-treated MAYO-PH039 samples. Lollipop diagrams display merged amplicon summaries for amplicons present at <2% frequency, and individual amplicon profiles for those present at >2%, with degree of CpG methylation based on β-values.

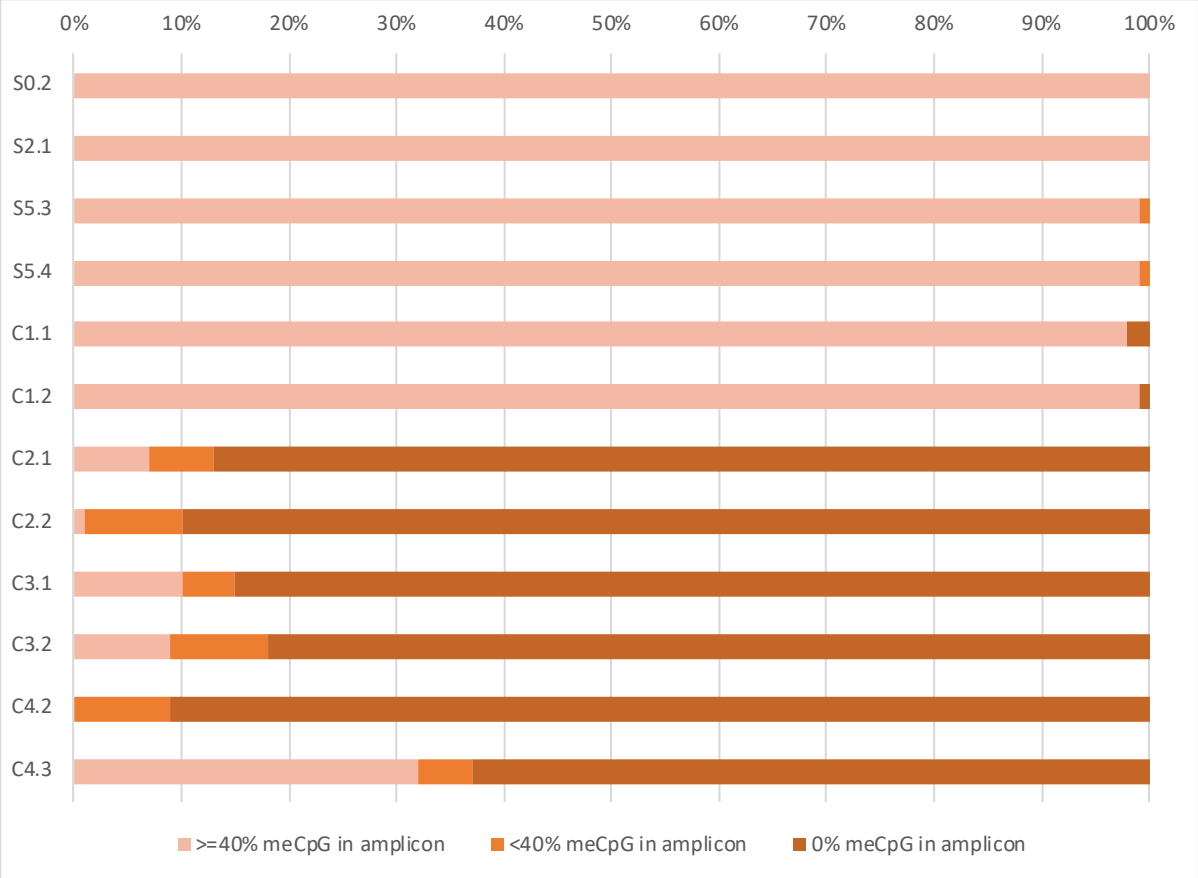


Figure 5.39. Unmethylated RAD51C promoter epialleles first detected after cycle 1 of niraparib in MAYO-PH039.

Bar chart shows the % of fully unmethylated (0% meCpG) epialleles, epialleles with <40% methylation (<40% meCpG) and epialleles with ≥40% methylation (≥40% meCpG) per sample. There were <2% fully unmethylated meRAD51C alleles detected in niraparib cycle one (C1.1 and C1.2) samples, and this jumps to ~88-90% fully unmethylated meRAD51C alleles at cycle two of niraparib (C2.1 and C2.2). S prefix = untreated samples, C prefix = treated samples.

5.4.11 Patterns of RAD51C methylation in clinical samples

Given I had characterised two PDX models with different patterns of me*RAD51C*, I wanted to investigate what the most common patterns of me*RAD51C* observed in the clinic are. Perhaps the heterogenous me*RAD51C* pattern detected in PDX PH039 is very common, or perhaps it is a rare or unique case. Furthermore, if found in patients, I wanted to assess whether this heterogenous pattern is associated with any particular pathological features or clinical outcomes. I also wanted to determine if any *meRAD51C* loss (from homozygous to

heterozygous or to complete loss) could be detected in clinical samples. To address these questions, I sourced DNA samples from known me*RAD51C* patient samples for detailed methylation assessment on my targeted sequencing platform. Nine me*RAD51C* samples were acquired from the Swisher Group at the University of Washington (WA, USA) (Bernards et al., 2018), and an additional three me*RAD51C* samples, identified in publicly available ICGC data (discussed in chapter 6) (Patch et al., 2015), were sourced via AOCS. Of all these tumour samples, only four were post-platinum chemotherapy, three of these being post neoadjuvant chemotherapy (**Table 5.17**).

These samples were tested by both MS-HRM and targeted me*RAD51C* sequencing to assess me*RAD51C* in both a qualitative and quantitative manner. Both heterogeneous and homogeneous me*RAD51C* profiles were detected across all samples (**Table 5.17**; **Figure 5.40**), and this did not correlate with personal/family history, stage, histology, platinum response or previous chemotherapy (**Table 5.17**).

Interestingly, it was not always the same CpG sites that had reduced methylation in these samples. Many samples displayed reduced methylation at either one or both of the CpG sites, that were also previously observed in PDX MAYO-PH039 and WEHI-PH039 Lineage A (position -114 and -69; **Figure 5.41**). However, some other samples with heterogeneous me*RAD51C* had reduced methylation at other CpG positions within the promoter, such as AOCS-41170 (sites -93 and -49) and LS472 (site -43; **Figure 5.41**). Thus, heterogeneity of me*RAD51C* was not linked to any particular sites across the promoter region, though it remains to be confirmed whether these other heterogeneous profiles still lead to gene silencing, as they did in PDX PH039. Although *RAD51C* gene expression had been previously reported for AOCS samples, the inverse correlation of DNA methylation and gene expression was associated with the CpG probe cg04582861, located within the *BRCA1* gene and not *RAD51C* (Patch et al., 2015). This is possibly due to a typographical error in the publication, but it means that this association should be confirmed independently.

Targeted me*RAD51C* sequencing data was also used to determine methylation zygosity. The percentage of fully unmethylated epialleles, epialleles with <40% methylation (low methylation) and epialleles with ≥40% methylation (highly methylated) was calculated per sample (**Figure 5.42**). It was found that each sample contained only 1-4% (mean of 2%) epialleles with low methylation, with remaining alleles being either highly methylated (≥40%

meCpG) or fully unmethylated. Thus the "% methylated alleles" used to calculate zygosity in **Table 5.17** refers to all methylated alleles, which had either homogeneous or heterogeneous profiles on NGS and MS-HRM (**Figure 5.40**).

Tumour purity was then assessed for all samples using our standard in-house *TP53* mutation sequencing assay, as well as SNP arrays for the LS samples. AOCS samples had published qpure tumour purity estimates available, so these were not re-run on SNP arrays (Patch et al., 2015; Song et al., 2012). *TP53* mutation sequencing tumour purity did not always align with the SNP array-based tumour purity. SNP array tumour purity estimates were, ultimately, considered more accurate measures given that they do not rely on a single gene/mutation. It is possible that PCR amplification bias during NGS library preparations or *TP53* gene copy-number changes may have affected the cellularity estimates from the *TP53* sequencing. Thus, SNP array estimates were used for calculating the adjusted percentage of me*RAD51C* within tumours, using the formula: % methylated alleles/ tumour purity.

Once methylation percentage was adjusted, all samples but one were found to be ~100% methylated at the *RAD51C* promoter (**Table 5.17**). This one tumour sample AOCS-34059, a primary platinum-resistant tumour, was estimated to have ~60% me*RAD51C* based on qpure tumour purity and targeted me*RAD51C* sequencing, hence was classified as heterozygous. This patient had received neo-adjuvant platinum chemotherapy, and tumour sample was acquired during interval de-bulking surgery. This patient progressed rapidly after primary treatment (PFS of 1.6 months) and eventually died from disease progression (OS of 12.3 months). Unfortunately, no pre-treatment samples exist for this patient. Thus, it is not clear whether it was the neo-adjuvant chemotherapy that caused this heterozygous me*RAD51C* state to develop, or whether this was the primary state of the chemonaïve tumour.

Interestingly, tumour AOCS-34059 was described as *RAD51C* methylated in the (Patch et al., 2015) paper, while the me*RAD51C* case AOCS-34932 (100% methylation by assessment in this project) was not reported as methylated in that study. Case AOCS-34059 was identified by my independent analysis of the published 450K methylation array data (presented in chapter 6). This may be because in the initial study, only one *RAD51C* CpG site was considered for methylation assessment (Patch et al., 2015).

Table 5.17. Summary of clinical information and meRAD51C profiles of PDX and patient samples.

Clinical and pathological characteristics, including Family Hx (family history), Personal Hx Breast Cancer (personal history of breast cancer), stage, histology and platinum sensitivity are as reported by Patch et al., 2015 for AOCS samples, and Bernards et al., 2018/personal communication with Swisher group for LS samples. NA = data not yet available.*

Sample	Family Hx*	Personal Hx Breast Cancer	Chemotherapy before sample taken	Stage	Histology	Platinum Sensitivity	me*RAD51C* profile	TP53 NGS - Tumour Purity %	SNP array/qpure - Tumour Purity %	*RAD51C* copy number	Unmethylated alleles %	Methylated alleles %	Adjusted me*RAD51C*
LS-467	None	No	No	2b	Serous & Clear Cell	Unknown	Heterogeneous	59	75.91	3	12	88	100%
LS-158	NA	No	No	3c	Serous Carcinoma	Sensitive	Homogeneous	88	90.26	2	7	93	100%
LS-215	Weak	No	No	4	Poorly Differentiated	Sensitive	Homogeneous	50	56.43	2	28	72	100%
AOCS-41170	Yes	No	No	NA	Serous Carcinoma	Sensitive	Heterogeneous	39	78.30	NA	19	81	100%
PDX 183	None	No	No	3	Serous Carcinoma	Sensitive	Homogeneous	100	100.00	1	0	100	100%
PDX PH039	NA	NA	No	3c	Serous Carcinoma	Sensitive	Heterogeneous	100	100.00	1	0	100	100%
LS-376	Strong	No	No	3c	Serous Carcinoma	Resistant	Homogeneous	67	95.56	3	11	89	93%
LS-473	Strong	No	Neo-adjuvant	3c	Serous Carcinoma	Resistant	Homogeneous	40	79.43	4	14	86	100%
AOCS-34059	NA	NA	Neo-adjuvant	NA	Serous Carcinoma	Resistant	Homogeneous	26	92.14	NA	45	55	60%
AOCS-34932	NA	NA	Yes (relapse sample)	NA	Serous Carcinoma	Resistant	Heterogeneous	83	92.87	NA	4	96	100%
LS-28	Strong	No	No	3c	Serous Carcinoma	Refractory	Homogeneous	37	NA	NA	28	72	NA
LS-267	Weak	Yes	No	3c	Serous Carcinoma	Refractory	Homogeneous	37	58.93	2	25	75	100%
LS-472	None	No	No	3c	Serous Carcinoma	Refractory	Heterogeneous	97	97.36	1	6	94	97%
LS-475	None	No	Neo-adjuvant	3c	Serous Carcinoma	Refractory	Homogeneous	27	89.08	4	20	80	90%

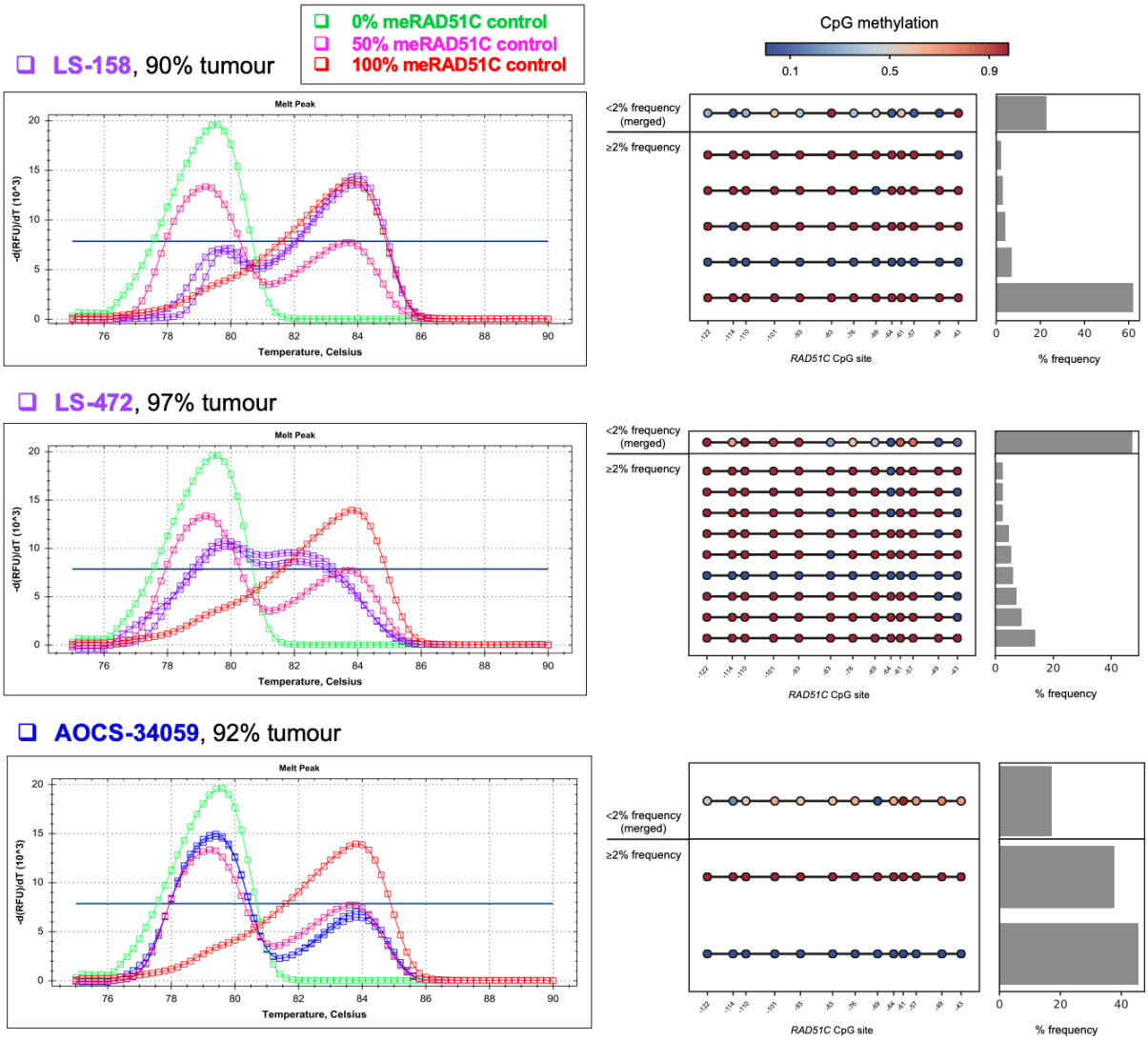


Figure 5.40. Example MS-HRM curves and corresponding meRAD51C amplicon plots of clinical samples.

LS-158 has a homogeneous methylation pattern and is predicted to be homozygous based on tumour purity (90%), while LS-472 has a heterogeneous methylation profile, but is still predicted to be highly methylated for meRAD51C (predicted tumour purity of 97%). In contrast, AOCS-34059 is predicted to have heterozygous meRAD51C based on tumour purity estimates (92%) and meRAD51C sequencing.

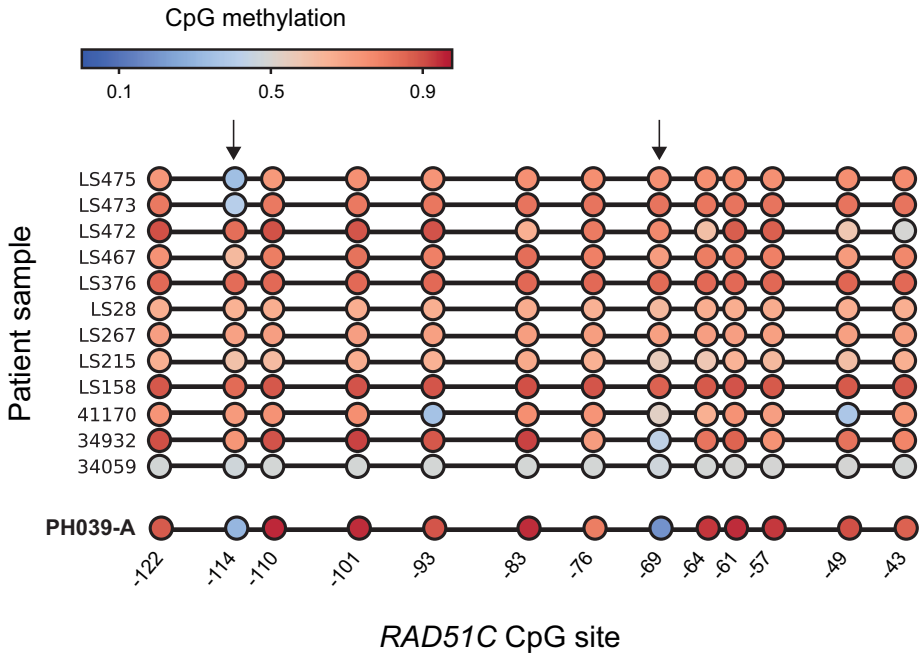


Figure 5.41. Not all patient samples with heterogeneous meRAD51C have the same unmethylated CpG sites as PDX PH039.

Lollipop diagrams display merged total amplicon summaries for each clinical sample and PDX PH039 Linage A. Degree of CpG methylation based on β-values. Arrows indicate CpG sites 114 and -69, which are consistently unmethylated in untreated PH039 Linage A.

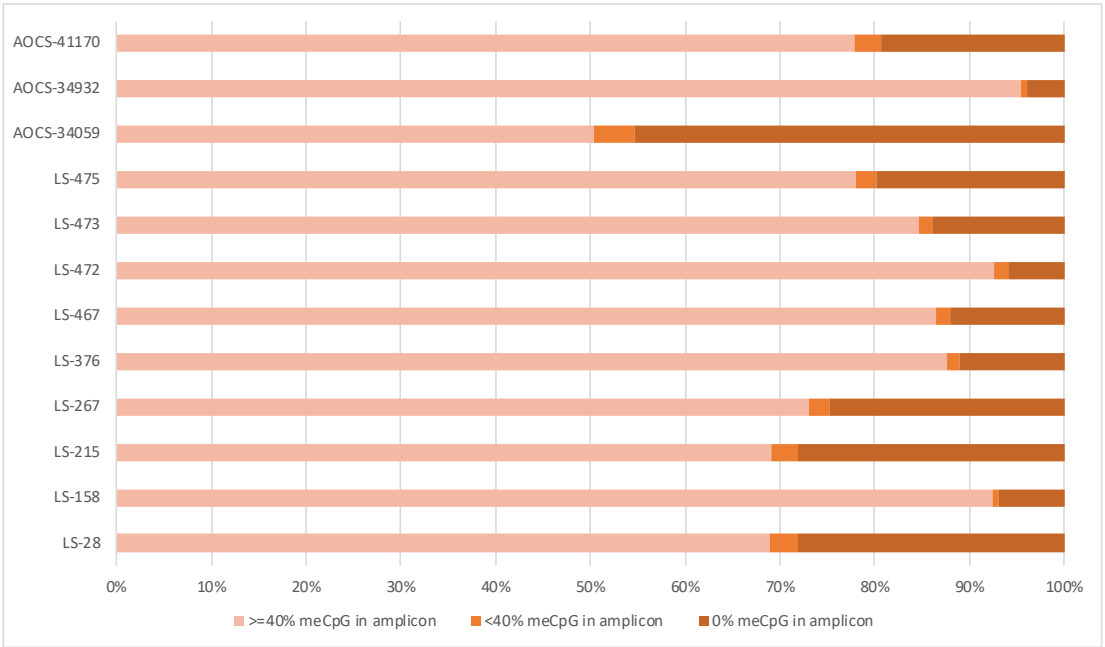


Figure 5.42. Majority of meRAD51C epialleles detected in clinical samples are highly methylated, containing ≥40% methylated CpG sites.

Bar chart shows the % of fully unmethylated (0% meCpG) epialleles, epialleles with <40% methylation (<40% meCpG) and epialleles with ≥40% methylation (≥40% meCpG) per sample.

5.5 Discussion

This study demonstrates that complete, or homozygous, me*RAD51C* can predict PARPi response in HGSOC, but that me*RAD51C* can be lost under PARPi or cisplatin treatment pressure. This work also demonstrates haplosufficiency of single *RAD51C* allele in PDX models, as *RAD51C* qPCR and PARPi resistance data illustrates that one copy of unmethylated *RAD51C* is sufficient to cause restored gene expression (WEHI-PH039 and 134183) and drive PARPi resistance (MAYO-PH039). This aligns with what has been observed for correcting *RAD51C* secondary mutations and PARPi resistance (Kondrashova et al., 2017), and suggests that classical heterozygous methylation patterns (presence of both methylated and unmethylated alleles) would also lead to PARPi resistance. Unfortunately the latter could not be definitively validated in the PDX models as they both carried a single copy of *RAD51C* per cell. Although a heterozygous methylation pattern was uncovered in one patient sample (post-chemotherapy), it has not yet been confirmed that this sample was originally homozygous, or that this me*RAD51C* pattern resulted in restored expression. Gene expression for this sample should be checked in future, however contaminating normal tissue may affect these measurements.

This work also revealed unique patterns of methylation at the *RAD51C* promoter – homogeneous or heterogeneous. Although the heterogeneous and homogeneous methylation patterns both still led to gene silencing in our models, knowledge of these patterns will be extremely important for other groups assessing me*RAD51C*. For example, the me*RAD51C* AOCS samples presented in this chapter were chosen by me based on methylation array data for three CpG sites at the *RAD51C* promoter (described in chapter 6). I found four samples in total, and I was able to source three of these. In contrast, Patch et al. (2015) only reported three of these four me*RAD51C* samples, as case AOCS-34932 was not described as methylated in their study. Patch et al. were only considering a single CpG site in their assessment of me*RAD51C* (though it is not clear which one). It is possible that this site was CpG -69, which is highly unmethylated in case AOCS-34932, though the rest of the promoter region is highly methylated. Thus, my works illustrates the importance of covering the entire *RAD51C* promoter region when assessing me*RAD51C* in tumour samples, as heterogeneous methylation patterns can lead to cases being missed when too few CpG sites are considered.

Ultimately, the findings from this study support the relevance of me*RAD51C* status for platinum and PARPi responses, though there is still much work to do in understanding the mechanisms governing me*RAD51C* stability under treatment pressure.

5.5.1 Analysis of new PDX lineages

Cryopreserved material from PDX tumours with 100% me*RAD51C* loss has now been transplanted into mice in an attempt to create new lineages of PDX 134183 and WEHI-PH039 (Lineages A and B) that lack me*RAD51C* and, should be, resistant to platinum and PARPi.

Given the moderate responses of PDX 134183 to PARPi, it will be important to confirm that me*RAD51C* leads to PARPi response in this PDX and loss leads to resistance, as it has been observed in the MAYO-PH039 PDX. Given that tumour #7907 was observed to have the most striking losses in me*RAD51C*, this cryopreserved tumour was selected for future follow-up experiments, and now has been re-tested for *meRAD51C* loss, thawed and transplanted into mice for expansion.

It will also be important to validate the PARPi resistance findings from MAYO-PH039 in our WEHI-PH039 models. As with the PDX 134183 experimental plans, tumours found to have full me*RAD51C* loss in WEHI-PH039 Lineages A and B have recently been re-transplanted from cryopreserved material for follow-up treatment experiments. The transplanted material will also have to be tested for me*RAD51C* loss, as tumour heterogeneity may mean that this material is not lacking me*RAD51C* to the same degree as the tumour pieces originally tested.

Once these new unmethylated lineages are established, our group would then have a valuable renewable resource for further study of PARPi and platinum resistance in PDX with me*RAD51C* loss.

5.5.2 Further optimization of the DNA repair foci assay

In this chapter, I describe a novel, highly automated protocol for the detection of DNA repair foci in PDX models, relying on digestion of tumours, FACS sorting for tumour epithelial cells and subsequent plating and RAD51 foci analysis (Detailed method described in Chapter 2). The PDX models tested in this project (134183, PH039 and PH038) worked well using this

method, as there were many live-fixed cells collected during FACS. However, while testing this protocol on other models (results not presented here), it was found that many other PDX tumours experience significant cell death during digestion, thus too few cells are collected following FACS. Future testing of more gentle digestion methods is therefore warranted, if this assay is to be used for other PDX models. Potentially useful alternatives include more gentle, cold-digestion protocols, used for single-cell RNA-seq protocols in order to minimise conserved collagenase-associated stress responses (O'Flanagan et al., 2019).

5.5.3 Interpretation of DNA repair foci results

Published data characterising the MAYO-PH039 model (AlHilli et al., 2016) demonstrated that the model presented with high RAD51 foci (marker of active HR repair pathway) relative to controls. PDX tumours in this study were digested and cultured briefly *in vitro* before irradiation and foci staining. The explanation provided by the authors for the foci detection was that RAD51C participates in the HR pathway after RAD51, thus allowing formation of RAD51 foci in the absence of RAD51C. However, our group's work on *RAD51C* gene primary and secondary mutations demonstrated that loss of *RAD51C* by mutation correlates with reduced/absent RAD51 foci, while correcting secondary *RAD51C* mutations result in restored RAD51 foci (Kondrashova et al., 2017).

My assessment of WEHI-PH039 Lineages A and B showed that me*RAD51C*-based gene silencing did lead to an impaired ability to form RAD51 foci following DNA damage, in line with our previous work on *RAD51C* mutations. Furthermore, our collaborators from the Kaufman group recently reported (via internal communication) that they were unable to reproduce the findings published by (AlHilli et al., 2016). However, to confirm that me*RAD51C* is the true cause of deficient HR in our PDX models, it would be extremely valuable to run these DNA repair foci experiments in any new unmethylated-*RAD51C* PDX 134183 and WEHI-PH039 lineages that arise, as these would be the best controls for this set of experiments.

Another interesting observation in these experiments was that WEHI-PH039 Lineage A (the more PARPi-resistant lineage) was found to have generally increased levels of RAD51 foci compared to Lineage B, in cells both, with and without irradiation.

Given that Lineage A tends to lose methylation more readily than Lineage B, it is possible that this spontaneous formation of RAD51 foci could be marker of less stable me*RAD51C*. This will be an interesting follow-up experiment.

5.5.4 Potential of targeted meRAD51C sequencing assay

The targeted me*RAD51C* sequencing assay that was developed as part of this project is a powerful technique that enables interrogation of methylation at individual CpG sites on individual alleles/DNA molecules in a given sample.

Initially, the baseline me*RAD51C* profiles of the PDX PH039 samples seemed suggestive of only certain CpG sites being important for gene silencing, given that two sites -114 and -69, were largely unmethylated in MAYO-PH039 and WEHI-PH039 Lineage A. However, analysis of clinical samples shown that other sites can also be less methylated possibly without an impact on *RAD51C* re-expression. Case AOCS-41170 having reduced methylation of sites -93 and -49, and (Patch et al., 2015) reported reduced *RAD51C* expression in this sample, with an inverse correlation of gene expression and methylation of one *RAD51C* CpG site. Although, since it was unclear which CpG site was used for this analysis, this result needs to be confirmed.

It is possible that instead of methylation of specific CpG sites in this region determining gene silencing, it is instead the density of methylation across the CpG island that dictates gene expression. Indeed, this has been observed in other gene promoters exhibiting heterogeneous methylation patterns. Previous work examining heterogeneous methylation patterns at the $p15^{INK4B}$ gene promoter in leukemias has demonstrated that ~40% of promoter CpG sites on each allele must be methylated for complete gene silencing. Any methylation density less than this led to reduced but variable expression of the gene (Cameron et al., 1999).

In our PDX samples, however, complete regional loss of methylation appeared to be selected for under treatment pressure, with fully unmethylated alleles present in all samples with restored *RAD51C* expression. This was especially obvious in MAYO-PH039 samples re-treated with niraparib, where cyclical re-treatment led to the gradual selection of fully unmethylated alleles. Thus, it is likely that such fully unmethylated *RAD51C* alleles are required for restored gene expression and HR DNA repair. Fortunately, the established sequencing assay allowed us to measure both fully unmethylated alleles and alleles with <40%

methylation. So far, all samples with <40% me*RAD51C* alleles detected also had fully unmethylated alleles present. This simplified analysis approach can continue to be applied to future samples tested, as they may yield different results.

5.5.5 Patterns of meRAD51C in clinical samples

All but one patient sample had a high degree of me*RAD51C.* Homozygous me*RAD51C* was predominantly observed in patient samples, with heterogeneous patterns observed in four of the 12 cases. The only case with predicted heterozygous me*RAD51C* was pre-treated with platinum chemotherapy. This was an encouraging result, given that most of these samples were chemonaïve, suggesting that most me*RAD51C* tumours begin with homozygous methylation, and, thus, have potential to respond to PARPi. Furthermore, knowing that homozygous me*RAD51C* is the typical zygosity state at diagnosis means that, in future, novel therapies may be developed to stabilize me*RAD51C* to prevent it being lost under treatment pressure.

One major limitation of the clinical sample analysis was that all cases only had one tumour sample available, and many of these were chemonaïve samples. This is most likely why most samples were found to have homozygous and homogeneous *RAD51C* methylation, with only one post-neoadjuvant chemotherapy tumour found to have a heterozygous methylation profile. Unfortunately, due to a lack of archival material, collected at diagnosis, for this patient, we could not confirm that the tumour was originally homozygous and that chemotherapy is what caused the heterozygosity, as was observed in our heterozygous me*BRCA1* cases (Kondrashova et al., 2018).

Access to serially sampled patient tumour material would be extremely valuable for this study, as it may allow us to prove this principle of zygosity and gene silencing for the *RAD51C* gene. In addition to me*RAD51C* zygosity and *RAD51C* gene expression measurements, functional assays for HR DNA repair could also be investigated to infer or validate gene silencing. Future PARPi clinical trials may enable this, through collection of archival, pre-screen and post-progression biopsies. One particular phase II trial of the PARPi olaparib in HRD metastatic breast and relapsed ovarian cancer lacking *BRCA*-mutations (EMBRACE) is including me*RAD51C* screening, and may be a potential source of such samples.

5.5.6 Mechanisms influencing DNA methylation states at RAD51C promoter

It would be interesting in future to investigate any mechanisms that may be influencing me*RAD51C* pattern and stability in our PDX models, such as defects in the DNA methylation machinery or underlying chromatin modifications at the *RAD51C* promoter.

Both PDX 134183 and WEHI-PH039 Lineages A and B, and their corresponding germline DNA samples, have recently been run on WGS. This data has been analysed for *RAD51C* copy number, but other analyses have not yet been completed. WGS data will allow us to look at genomic scarring/signatures in these models, and also identify mutations and genome rearrangements (not identified in BROCA sequencing) that may affect the epigenetic machinery. For example, defects in epigenetic regulators such as *EZH2* may be detected. The EZH2 methyltransferase catalyses the formation of a di- or trimethyl mark on lysine 27 of Histone H3 (H3K27me3), and has been shown to cause silencing of RAD51 family members, including *RAD51C*, when upregulated (Zeidler et al., 2005). This protein has also been reported to directly control DNA methylation of its target gene promoters via the DNA methyltransferases DNMT1, DNMT3A and DNMT3B (Viré et al., 2006). *EZH2* overexpression is a common feature of EOC, and is associated with increased levels of H3K27me3 in EOC cell lines (Li et al., 2010) and can lead to PARPi sensitivity *in vitro*(Min et al., 2013). Gain of function mutations in EZH2 have been detected in blood cancers (Majer et al., 2012; Ryan et al., 2011), and may be contributing to gene silencing in our models.

Another way of detecting or validating such events would be to look more locally at histone methylation patterns of the *RAD51C* promoter. Histone modifications, including H3K27me3, can influence DNA methylation patterns (Cedar et al., 2009). The future directions of this project are to test several histone marks known to be associated with DNA methylation and/or gene silencing in the me*RAD51C* PDX models, including H3K27me3, H3K4me1 and H3K9me3 (Cedar et al., 2009; Du et al., 2015; Pisanic et al., 2017; Skvortsova et al., 2019).

Ultimately, understanding the mechanisms governing me*RAD51C* stability may pave the way for development of therapeutic strategies to prevent loss of me*RAD51C* under treatment pressure, thereby preventing or overcoming PARPi resistance in patients with these defects.

6 Genome-wide DNA methylation profiling of HGSOC PDX models

6.1 Introduction

DNA methylation via the addition of a methyl group at the 5th position of a cytosine nucleotide at CpG sites is one of the best studied mechanisms of epigenetic control in mammals. This methylation contributes to the epigenetic control of chromatin in cell differentiation and is essential for normal development (Moore et al., 2013). Methylation has roles in many different contexts of cell development and maintenance, including silencing of genes or repetitive DNA elements, maintaining genomic stability during mitosis, alternative gene splicing, genomic imprinting and stem cell differentiation (Jones, 2012). Methylation of DNA can also be reflective of other chromatin processes that are not as well understood, such as methylation in the body of actively transcribed genes, which correlates positively with gene expression (Yang et al., 2014). During normal development, three highly conserved enzymes are primarily responsible for the placement and maintenance of methyl groups to CpG site: DNMT1, DNMT3A and DNMT3B (Bestor, 2000). The DNMT1 enzyme recognizes hemi-methylated DNA (one strand methylated) following replication, and coordinates methylation of the new DNA strand via methyltransferases. DNMT1 loss, thus, results in global hypomethylation. DNMT3A and DNMT3B are, in contrast, believed to be involved in *de novo* DNA methylation, rather than maintenance (Moore et al., 2013).

CpG islands are regions dense with CG nucleotides, and are generally associated with the transcriptional promoters of developmental and housekeeping genes (Bird et al., 1985; Gardiner-Garden et al., 1987). Under normal circumstances, these tend to be protected from DNA methylation-based gene silencing by a variety of mechanisms (Brandeis et al., 1994; Gebhard et al., 2010; Moore et al., 2013). In the context of cancer, however, this is not the case. Global methylation, or "methylome", profiling of cancers has demonstrated significant changes in this epigenetic mark compared to normal tissues. Cancers generally present with global hypomethylation of their genomes, with the exception of gene promoters, which tend to gain methylation and result in gene silencing (Esteller, 2008), though the patterns of hyper- and hypo-methylation do not appear to be linked in this context (Ehrlich, 2002). A significant proportion of these gene promoters are believed to be key developmental genes (Keita et al., 2013). Promoter methylation of tumour suppressors has been studied in great detail over many

cancer types, including HGSOC, where the breast/ovarian cancer predisposition genes *BRCA1* and *RAD51C* are susceptible to promoter methylation and gene silencing (Esteller, 2008; Prieske et al., 2017; Vos et al., 2018). However, the impacts of global hypomethylation on tumour development, progression and therapy are not as well understood (Ehrlich, 2002; Ehrlich, 2009).

Global hypomethylation in cancer is generally associated with reduced genomic stability, and tends to occur at moderately-highly repetitive DNA sequences within the genome (Ehrlich, 2002). De-methylation of these normally repressed heterochromatic regions of DNA can wreak havoc on the genome, via erroneous mitotic recombination or direct mutagenesis caused by transposable elements (Ehrlich, 2002). Hypomethylation can also influence the expression of oncogenes, for example by occurring at transcriptional promoters (Kanwal et al., 2016; Tao et al., 2000) or by causing loss of parental imprinting (Jelinic et al., 2007).

It is therefore unsurprising that global hypomethylation has been demonstrated to be a common feature of advanced-stage ovarian cancers, correlating with more advanced and more aggressive disease (Keita et al., 2013; Watts et al., 2008; Wei et al., 2002; Widschwendter et al., 2004). It is possible that this feature is directly selected for during tumour evolution or under treatment pressure, given its potential to generate increased genetic diversity via genomic instability.

Both hypermethylation and hypomethylation of certain genomic regions have been associated with OC resistance to standard platinum-based therapies (Chang et al., 2010; Koukoura et al., 2014). For example, DNA hypermethylation-based silencing of Wnt antagonist *SFRP5* (Su et al., 2010), DNA repair gene *MLH1* (Strathdee et al., 1999) or the argininosuccinate synthetase gene *ASS1* (Nicholson et al., 2009) have been associated with platinum-resistance in OC cells, while hypomethylation-induced gene expression of myelin and lymphocyte *MAL* gene (Lee et al., 2010) or multidrug transporter gene *ABCG2* (Bram et al., 2009; Yan et al., 2016) have also been linked to platinum resistance in OC. Additionally, as described in detail in Chapter 1, loss of promoter methylation in HR DNA repair gene *BRCA1* has also been shown to cause resistance to both platinum and PARPi (Kondrashova et al., 2018).

Given the clear role of global methylation patterns in promoting cancer growth and drug resistance, we were interested in characterizing this within our HGSOC PDX cohort. In

addition to their accurate molecular representation of corresponding patient tumours, HGSOC PDX have been shown to be epigenomically stable over passaging and when compared to the original patient sample (Tomar et al., 2016). Furthermore, like single gene promoter methylation patterns, global methylation signals can be affected by contaminating normal tissue in patient tumour samples (e.g. patient stroma). These non-cancer human cells do not grow with the HGSOC PDX. Thus, HGSOC PDX present a useful model system for the study of the ovarian carcinoma methylome and its relationship to treatment responses.

As our laboratory developed a highly characterised cohort of *BRCA1* and *RAD51C* methylated PDX, including treated and untreated samples, we decided to set up an exploratory study to look at the methylation landscape of these HGSOC PDX models with HR gene methylation, and compare the samples with and without methylation loss of their HR gene promoter. To do this, we ran a panel of our PDX samples on Illumina's Infinium MethylationEPIC BeadChip microarrays (referred to as EPIC methylation arrays in this chapter). These arrays measure the degree of methylation at over 850,000 CpG sites across the genome, making them less comprehensive but more cost-effective than bisulphite whole genome sequencing.

We hypothesised that it may be possible to detect differences in the global methylomes of tumours/PDX that readily lost methylation of their HR gene, compared to the more "stable" models that retained HR gene methylation under treatment pressure. For example, there may be possible global methylation differences between the me*BRCA1* tumours that lose methylation of one or more alleles more readily under treatment pressure in the PDX or patient (PDX 134169 and 134048) and those that appear to have more stable homozygous *BRCA1*/*RAD51C* methylation (PDX 134011 and 134062). We then wanted to investigate whether any differences found in methylome profiles between different tumours could provide evidence of some common underlying mechanisms that may be influencing the stability of HR gene promoter methylation.

We were also interested in methylome changes within models that lost HR gene methylation following treatment, such as MAYO-PH039, as these may also provide evidence of mechanisms influencing methylation stability, or to the types of cell populations that may be selected for under PARPi pressure.

6.1.1 PDX samples selected for EPIC array

A total of 32 samples with *BRCA1* or *RAD51C* methylation were run across two Infinium MethylationEPIC BeadChip Kits, as each kit runs 16 samples (**Table 6.1**), and I performed the bioinformatic analysis of resulting data in R.

Table 6.1. Samples analysed using EPIC array.
PH039 samples listed here were generated at the Mayo Clinic (PDX MAYO-PH039). Hom = homozygous; het = heterozygous.

PDX	Sample #	Treatment	Model of
PH039	S0.1	Untreated	me*RAD51C*
PH039	S0.2	Untreated	me*RAD51C*
PH039	S2.1	Untreated	me*RAD51C*
PH039	S2.3	Untreated	me*RAD51C*
PH039	C1.2	Niraparib 100mg/kg round 1	me*RAD51C* loss
PH039	C2.1	Niraparib 100mg/kg round 2	me*RAD51C* loss
PH039	C2.2	Niraparib 100mg/kg round 2	me*RAD51C* loss
PH039	C3.1	Niraparib 100mg/kg round 3	me*RAD51C* loss
134183	8269	Vehicle	me*RAD51C*
134183	8270	Vehicle	me*RAD51C*
134183	7365	Vehicle	me*RAD51C*
134183	7903	Vehicle	me*RAD51C*
134183	7363	Rucaparib 300mg/kg	me*RAD51C*
134183	8267	Rucaparib 300mg/kg	me*RAD51C*
134183	8300	Rucaparib 300mg/kg	me*RAD51C*
134183	8290	Rucaparib 300mg/kg	me*RAD51C*
134011	1550	Vehicle	hom me*BRCA1*
134011	1450	Vehicle	hom me*BRCA1*
134011	1459	Vehicle	hom me*BRCA1*
134062	2238	Vehicle	hom me*BRCA1*
134062	1930	Vehicle	hom me*BRCA1*
134062	9172	Vehicle	hom me*BRCA1*
134048	7795	Vehicle	het me*BRCA1*
134048	7388	Vehicle	het me*BRCA1*
134048	6517	Vehicle	het me*BRCA1*
134169	7202	Vehicle	het me*BRCA1*
134169	7347	Vehicle	het me*BRCA1*
134169	7182	Vehicle	het me*BRCA1*
WEHICS62 cell line	p8.5.4	Untreated	100% human control
Murine sample	148B-7136	Untreated	100% murine control
50:50 mix	50:50 mix	Untreated	Human:murine mix control

The sample list included MAYO-PH039 samples, where cyclical re-treatment using the PARPi niraparib was used to generate PARPi resistant clones with me*RAD51C* loss and restored *RAD51C* expression. PDX 134183 samples were also screened – either untreated, or following standard treatments with 300mg/kg of PARPi rucaparib, where no loss of *RAD51C* methylation/restored gene expression had been detected by other assays (PDX 134183 samples with loss of RAD51C methylation had not been detected at this time, more detail provided in Chapter 5). All samples from me*BRCA1* PDX were vehicle-treated, as the PDX were derived from either chemonaïve or pre-treated patients (me*BRCA1* homozygous and me*BRCA1* heterozygous models, respectively; **Table 6.1**).

I also included PDX-derived me*BRCA1* cell line WEHI-CS62 (Kondrashova et al., 2018), a murine control sample, and a 50:50 mix of the two, to determine the effects of murine DNA contamination on this assay (**Table 6.1**).

6.2 Chapter 6 hypotheses:

1. HGSOC PDX models with homozygous vs heterozygous me*BRCA1* will have different global methylation profiles

2. Global methylomes of HGSOC PDX change under PARPi pressure

6.3 Chapter 6 aims:

1. Characterize global methylation profiles of HGSOC PDX models with *RAD51C* or *BRCA1* promoter methylation

2. Search for changes in global methylation profiles of PDX tumours following PARPi-treatment

3. Search for global methylation signatures that may be associated with *RAD51C* or *BRCA1* promoter methylation profiles

6.4 Results

6.4.1 Validation of EPIC array for PDX samples

Given that previously published work has suggested that human EPIC methylation arrays can be successfully used to assess methylation in mouse tissues (Needhamsen et al., 2017), there was a concern that the contaminating mouse stroma in the harvested PDX tumours may interfere significantly with the results for the human tumour component. To address this, I analysed data for control samples of 100% murine DNA (from a PDX that we discovered to be 100% murine cells), 100% human DNA (from WEHI-CS62 cell line) and a 50:50 mix of the two DNA samples (**Table 6.1**). The global β value (methylation) distributions for these samples were compared using quantile-quantile plots in R, and it was confirmed that the 100% murine sample distribution was highly dissimilar to the 100% human and 50:50 mix samples, while the 100% human and mixed sample were extremely similar (**Figure 6.1**).

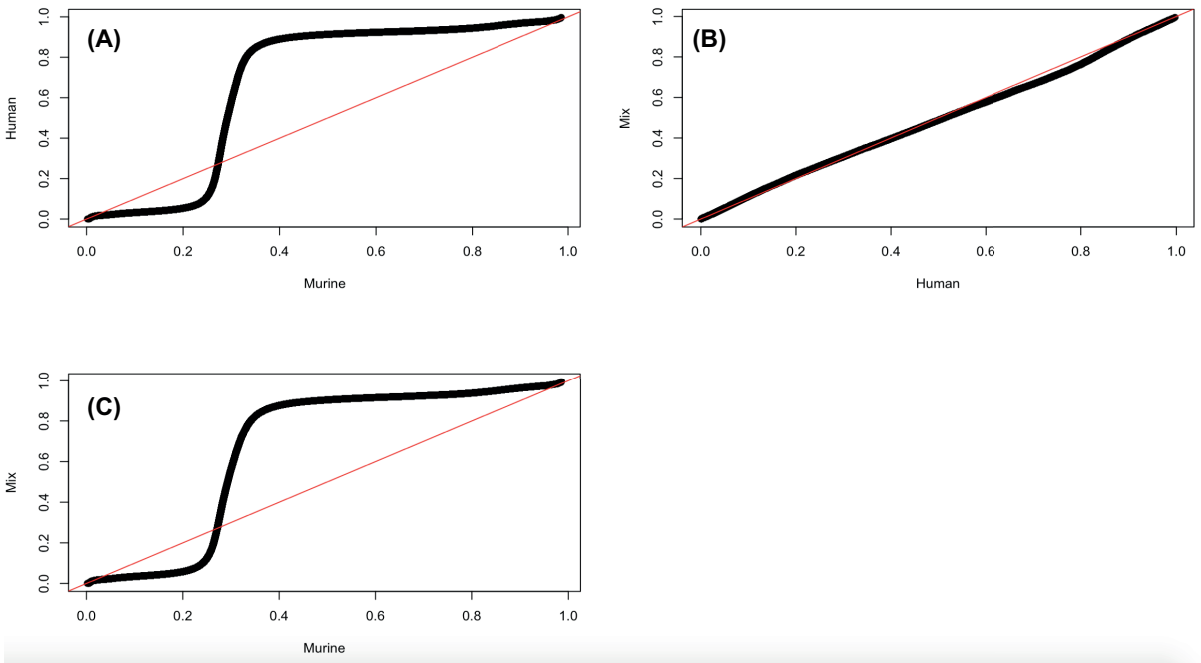


Figure 6.1. Contaminating murine DNA in PDX DNA samples does not significantly affect methylation measurements.
*Quantile-quantile plots comparing the β values for **(A)** human vs murine controls, **(B)** human vs 50:50 mix controls and the **(C)** murine vs 50:50 mix controls demonstrated that the human only and mixed samples largely correlated, while the murine only vs human only or mixed samples were extremely different.*

This suggests that the murine component in the 50:50 mix does not significantly affect the β value distribution, and is unlikely to significantly affect the methylation measurements in our PDX samples. This result is consistent with the β value distribution of murine DNA being non-bimodal, and not contributing to detection in mixed samples (**Figure 6.2**). I thus proceeded with analysis of other samples.

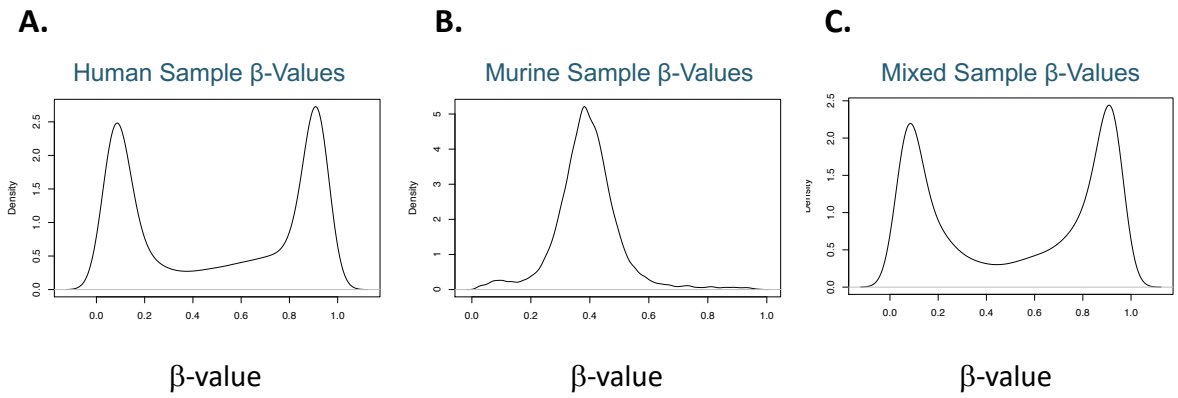


Figure 6.2. Global methylation value distributions of control samples.
Distributions of all CpG probes in ***(A)*** *human* ***(B)*** *murine and* ***(C)*** *50:50 mix controls reveal that the murine DNA sample lacks the expected bimodal β value distribution observed in the human sample, and that the mixed sample is largely unaffected by murine contamination.*

6.4.2 Clustering of PDX samples run on EPIC array

The next item queried in this dataset was how the individual samples clustered using Multidimensional Scaling (MDS) plots. Samples from the same PDX model are expected to be very similar in their global methylation profiles, and should thus cluster together on the plots, even across multiple dimensions. This was confirmed, with PDX samples clustering together across multiple dimensions by models (Dimension 1 vs 2 shown in **Figure 6.3**). Interestingly, the WEHI-CS62 cell line clustered closely with 134062 PDX samples until comparing dimensions 5 and 6, suggesting that the cell line of this model has undergone changes in its global methylation pattern during its adaptation to 2D *in vitro* culture conditions, or a reduction in cell type diversity (**Figure 6.4**).

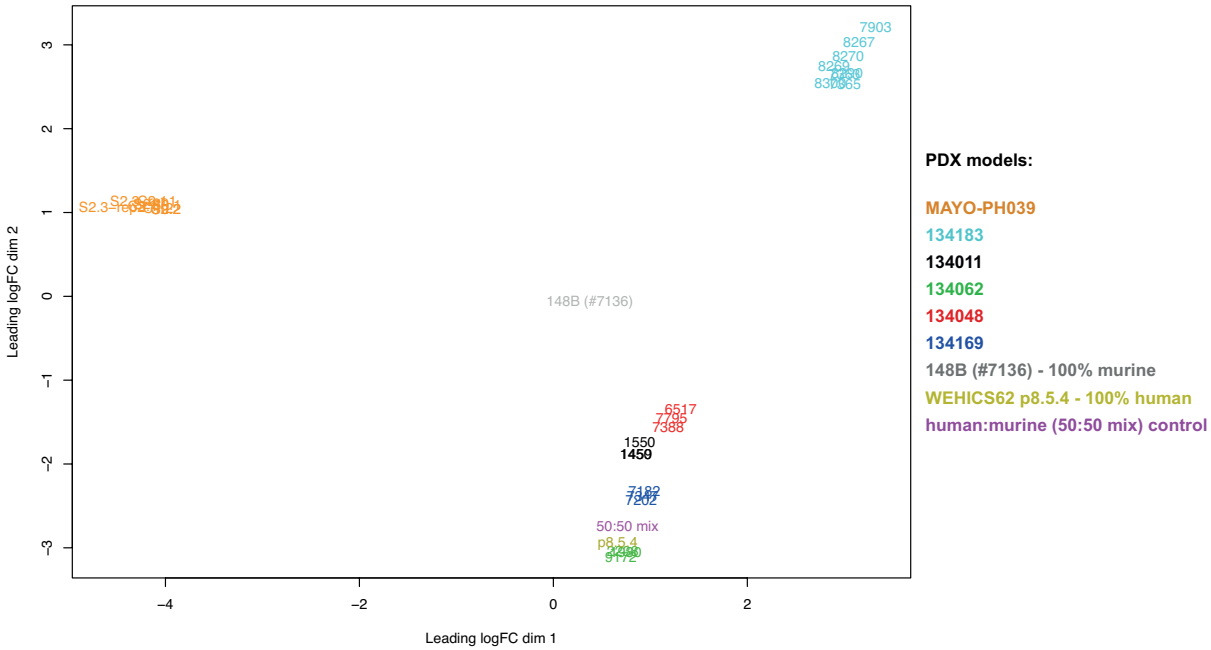


Figure 6.3. PDX samples cluster together on MDS plot of dimensions 1 vs 2.
The same clusters appear in all dimensions up to dimension 5 vs 6, where WEHICS62 no longer groups with PDX #134062 samples (shown in Figure 3).

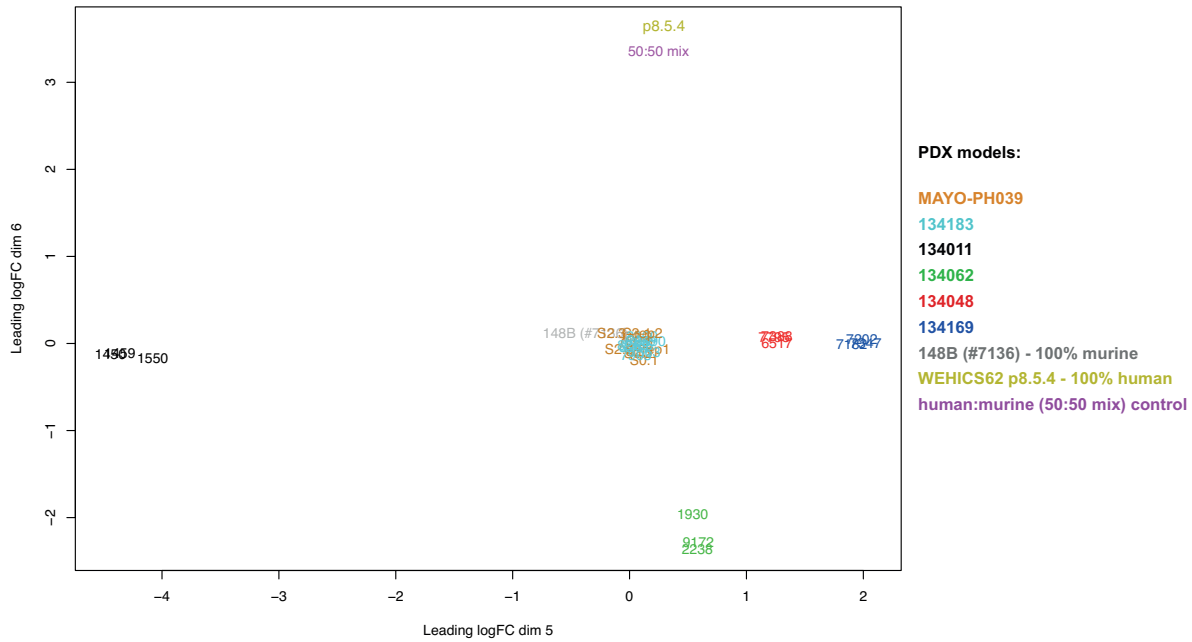


Figure 6.4. MDS clustering reveals WEHI-CS62 cell line has different methylation profile to PDX #134062.
Methylation profile PDX #134062-derived cell line WEHI-CS62 is significantly different to its corresponding PDX in dimension 5 vs 6 of MDS plot. The 50:50 mix sample was generated by mixing WEHI-CS62 cell line DNA with murine DNA.

This was confirmed when creating scatter plots for correlation of each CpG site between PDX 134062 samples and the PDX and cell line samples (**Figure 6.5**). Both the comparison of WEHI-CS62 cell line vs 50:50 mix control sample (**Figure 6.5A**), and the comparison of two untreated PDX 134062 samples (**Figure 6.5B**) yielded a cleaner correlation of CpG global methylation values than the comparison of PDX 134062 to the WEHI-CS62 cell line (**Figure 6.5C**).

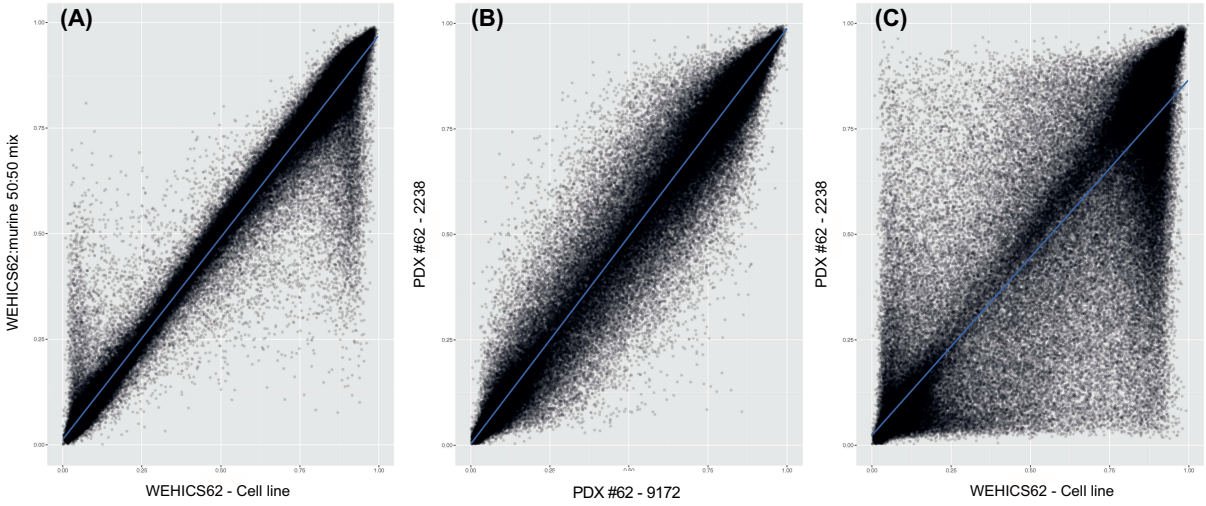


Figure 6.5. WEHICS62 cell line has substantially different methylome to PDX #134062 tumours.
Scatter plots of CpG site β values were created to measure the correlation of EPIC array probe β values for (A) the WEHICS62 cell line sample and the 50:50 mix of the cell line with murine DNA sample, (B) two vehicle-treated PDX #62 tumours (mouse # 9172 and 2238) and (C) a PDX #62 tumour 2238 compared to the cell line, where fewer points were found to correlate.

6.4.3 RAD51C and BRCA1 gene promoter methylation patterns

I then wanted to confirm that the local patterns of *RAD51C* and *BRCA1* promoter methylation in each of the samples correlated with results from other assays such as *RAD51C* MS-HRM and *BRCA1* ddPCR. Heatmaps were initially created for all CpG-sites/probes related to the *RAD51C* and *BRCA1* genes for a broader view of methylation patterns across these loci (**Figure 6.6** and **Figure 6.7**).

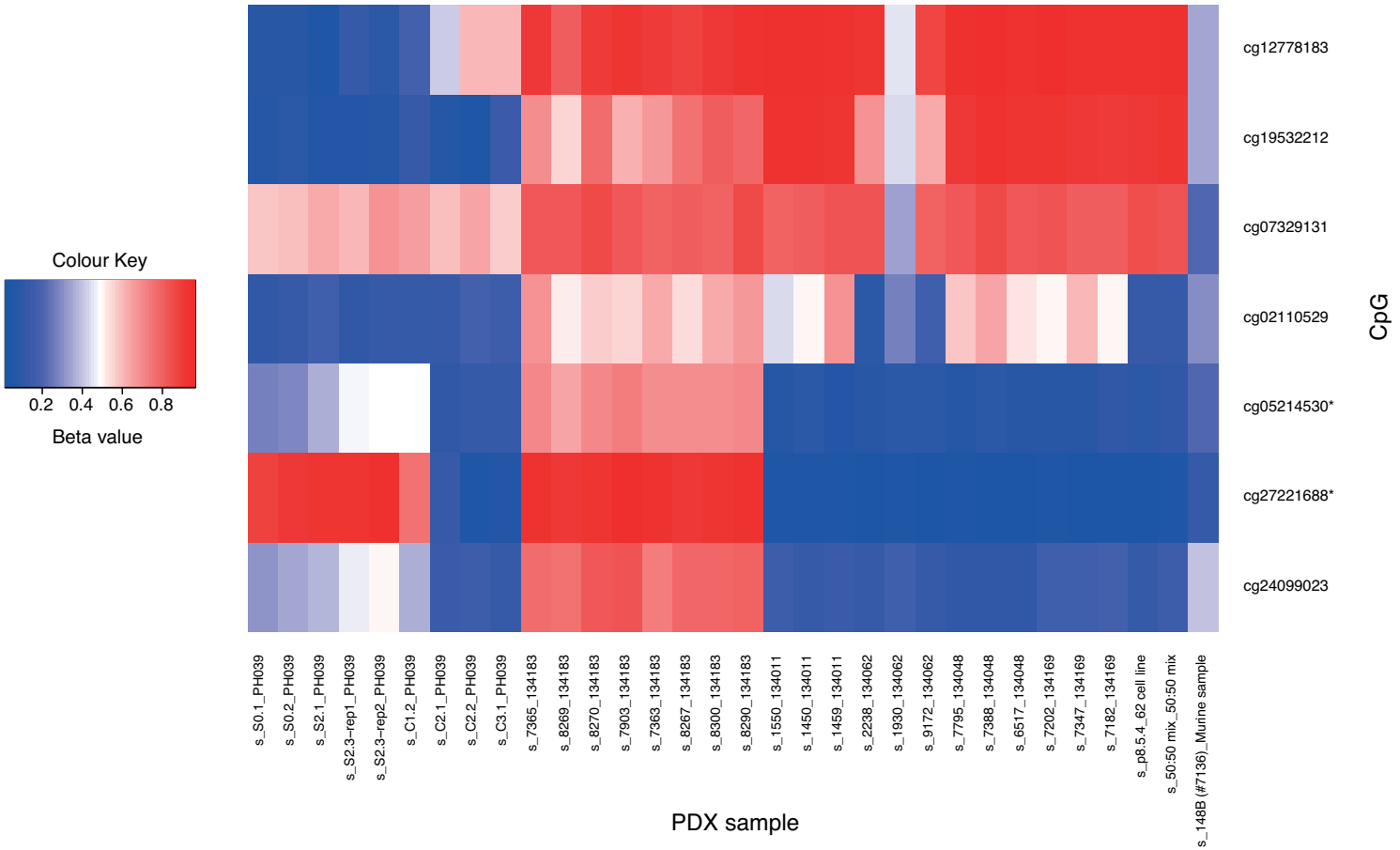


Figure 6.6. Methylation heatmap of all RAD51C CpG probes in EPIC array.

Heatmap shows β values of all CpG probes associated with the RAD51C gene in the EPIC array. CpG's marked with "" indicate the two probes covered by both the RAD51C MS-HRM assay and EPIC array. Probes cg05214530, cg27221688 and cg24099023 are the only ones that appear to correlate with RAD51C gene expression and MS-HRM assays across all samples.*

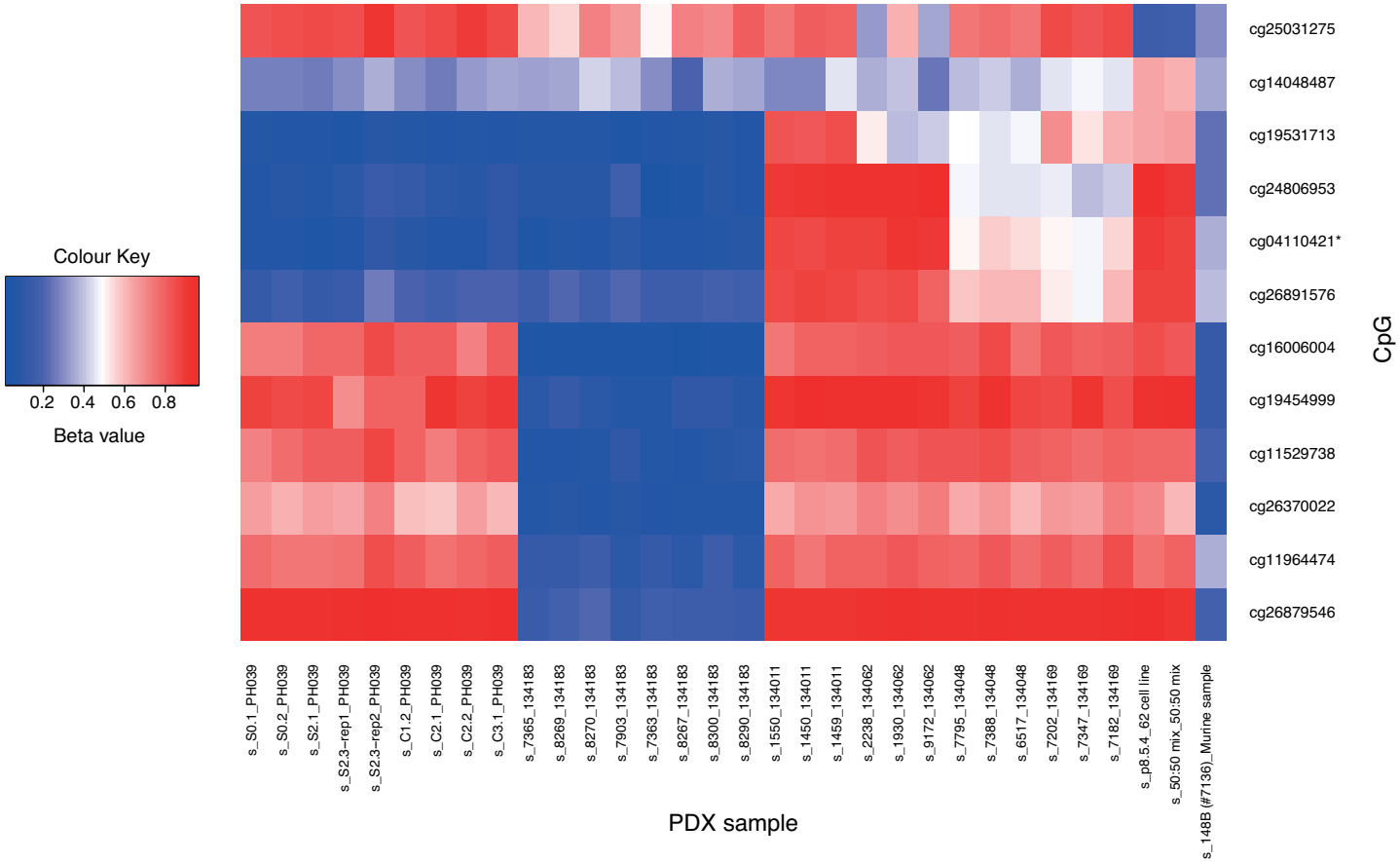


Figure 6.7. Methylation heatmap of all BRCA1 CpG probes in EPIC array.

Heatmap shows β values of CpG probes associated with the BRCA1 gene in the EPIC array. CpG marked with "" indicates the probe covered by both the BRCA1 MS-HRM assay and EPIC array. Probes cg24806953, cg04110421 and cg26891576 are the only ones that appear to correlate with BRCA1 gene expression and MS-HRM and ddPCR assays across all samples, including clear separation of the homozygous and heterozygous BRCA1 methylated models (Kondrashova et al., 2018).*

PDX 134183 appeared to have larger regions of DNA either fully methylated (at the *RAD51C* locus), or fully unmethylated (at the *BRCA1* locus) compared to other models. I then created subsets of these based on CpG probes covered in the other assays and others that appear to correlate with the results for other probes for *RAD51C* (**Figure 6.8**) and *BRCA1* (**Figure 6.9**). Heterozygous me*BRCA1* PDX models had moderate methylation of relevant CpG probes (cg24806953, cg04110421 and cg26891576) in the *BRCA1* promoter, while homozygous me*BRCA1* PDX models were highly methylated at these 3 CpG probes, and me*RAD51C* PDX models were fully unmethylated at these probes (**Figure 6.9**)(Kondrashova et al., 2018).

The three CpG probes that correlated with *RAD51C* gene silencing (cg05214530, cg27221688 and cg24099023) were found to be highly methylated in all PDX 134183 samples, but not in the MAYO-PH039 samples (**Figure 6.8**). Instead, MAYO-PH039 had two CpG probes (cg05214530 and cg24099023) that were moderately methylated in untreated samples, while cg27221688 was fully methylated. However, all 3 of these *RAD51C* CpG probes lost methylation under PARPi treatment pressure (**Figure 6.8**; see Chapter 5 for more detail).

Thus, it was clear that the methylation patterns detected by MS-HRM, ddPCR and targeted bisulfite sequencing were the same as observed for selected CpG probes in the EPIC array (me*RAD51C* results in Chapter 5, me*BRCA1* results in (Kondrashova et al., 2018)).

6.4.4 Methylation patterns of other genes

I also created heatmaps for other genes that are known to frequently present with promoter methylation in HGSOC. These included *MLH1, CDH13, CDKN2A, CDKN2B, ESR1, RASSF1, TIMP3, ATM* and *APC* (Ozdemir et al., 2012), with example heatmaps of *MLH1* and *CDH13* presented in **Figure 6.10** and **Figure 6.11**, respectively. Although interpretation was clear for some PDX models, such as all PDX 134183 samples being completely unmethylated across all CpG probes related to *CDH13*, other PDX samples tended to have some methylated and some unmethylated CpG probes. Unfortunately, information regarding which CpG probes are actually relevant for gene silencing is not readily available for these genes and may include cell type specific effects, making conclusions about the significance of these results beyond the scope of this study.

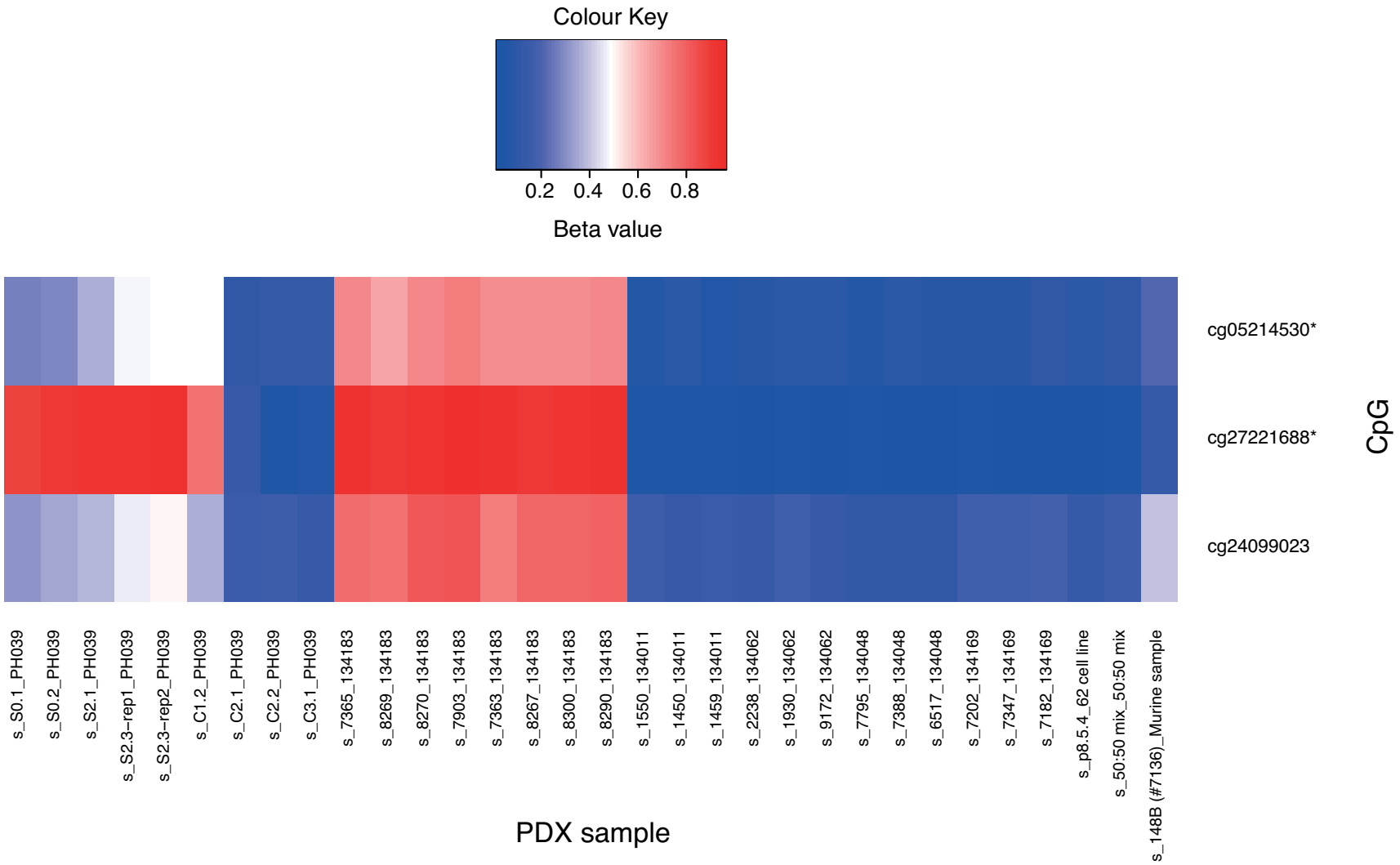


Figure 6.8. EPIC array RAD51C CpG probes associated with gene silencing.

Summary β value heatmap of RAD51C CpG probes associated with RAD51C gene expression in PDX models. CpG's marked with "" indicate the two probes covered by both the RAD51C MS-HRM assay and EPIC array.*

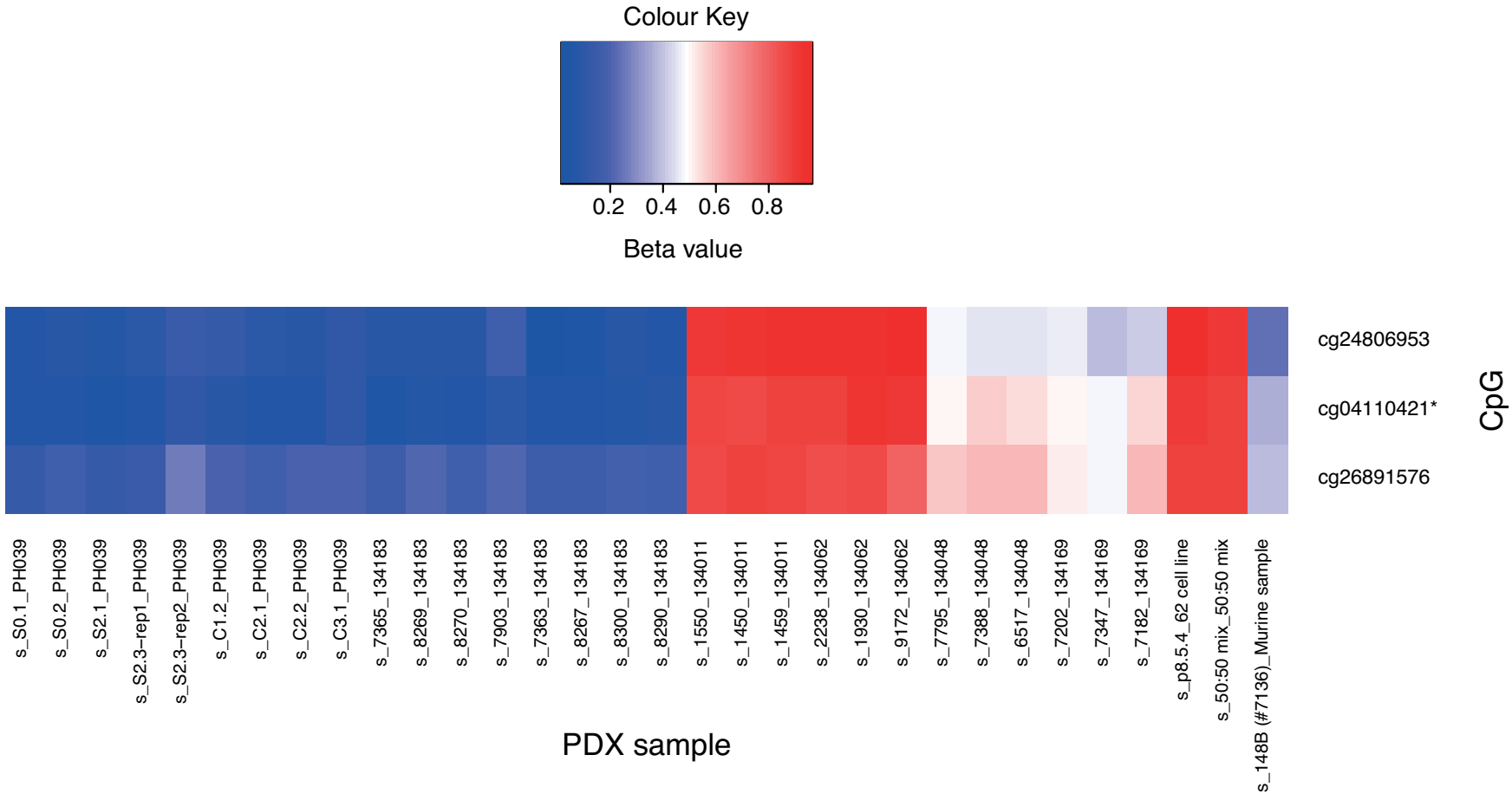


Figure 6.9. EPIC array BRCA1 CpG probes associated with gene silencing.

Summary β value heatmap of BRCA1 CpG probes (cg24806953, cg04110421 and cg26891576) associated with BRCA1 gene expression in PDX models. Heterozygous BRCA1 methylated models 134048 and 134169 have β values closer to 0.5, while homozygous models 134011 and 134062 have β values closer to 1 for these CpG probes. CpG marked with "" indicates the probe covered by both the BRCA1 MS-HRM assay and EPIC array.*

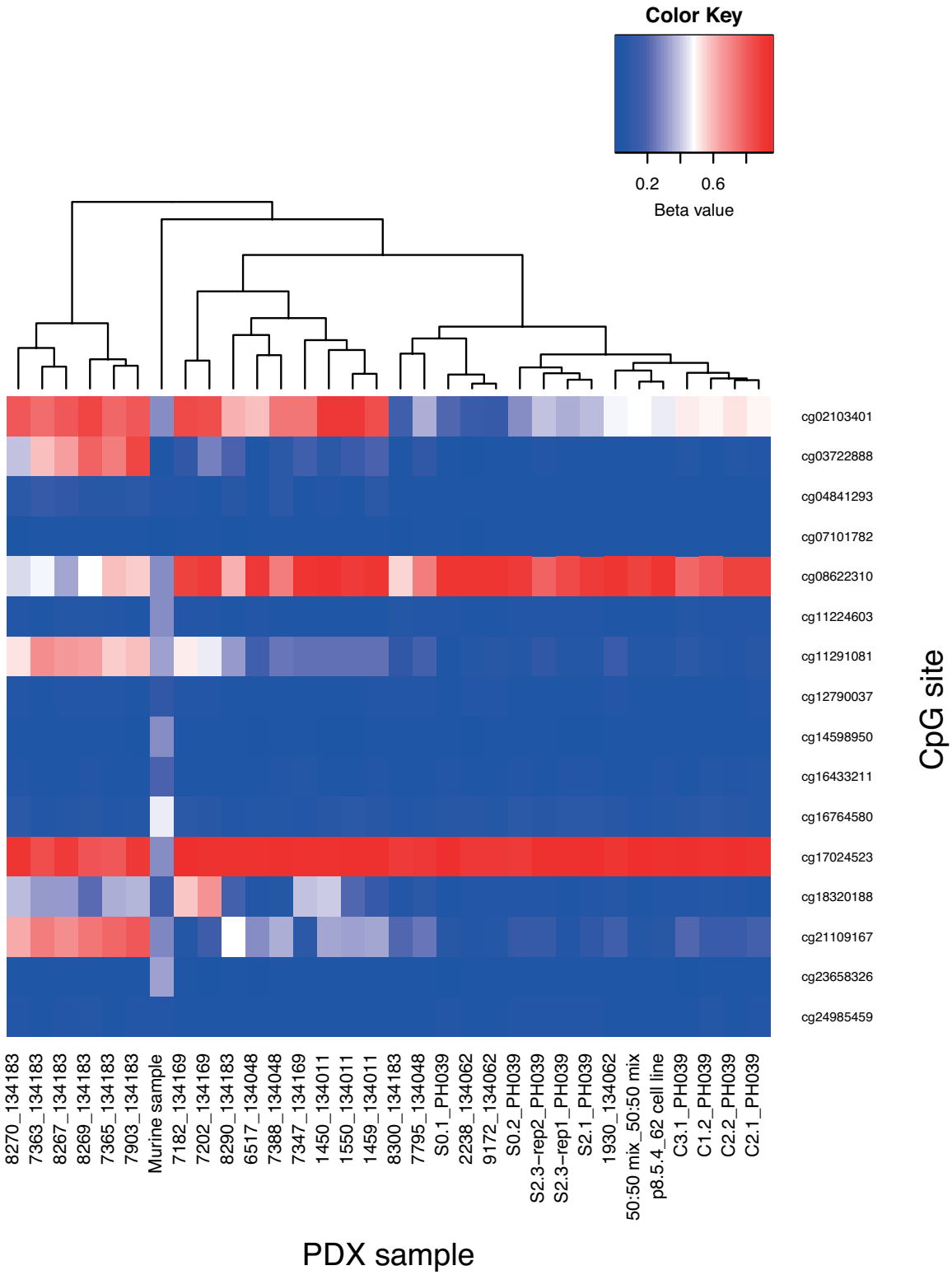


Figure 6.10. Methylation heatmap of all MLH1 CpG probes in EPIC array.
Heatmap shows β values of CpG probes associated with the MLH1 gene in the EPIC array, with samples ordered by MLH1 methylation similarity using dendrogram.

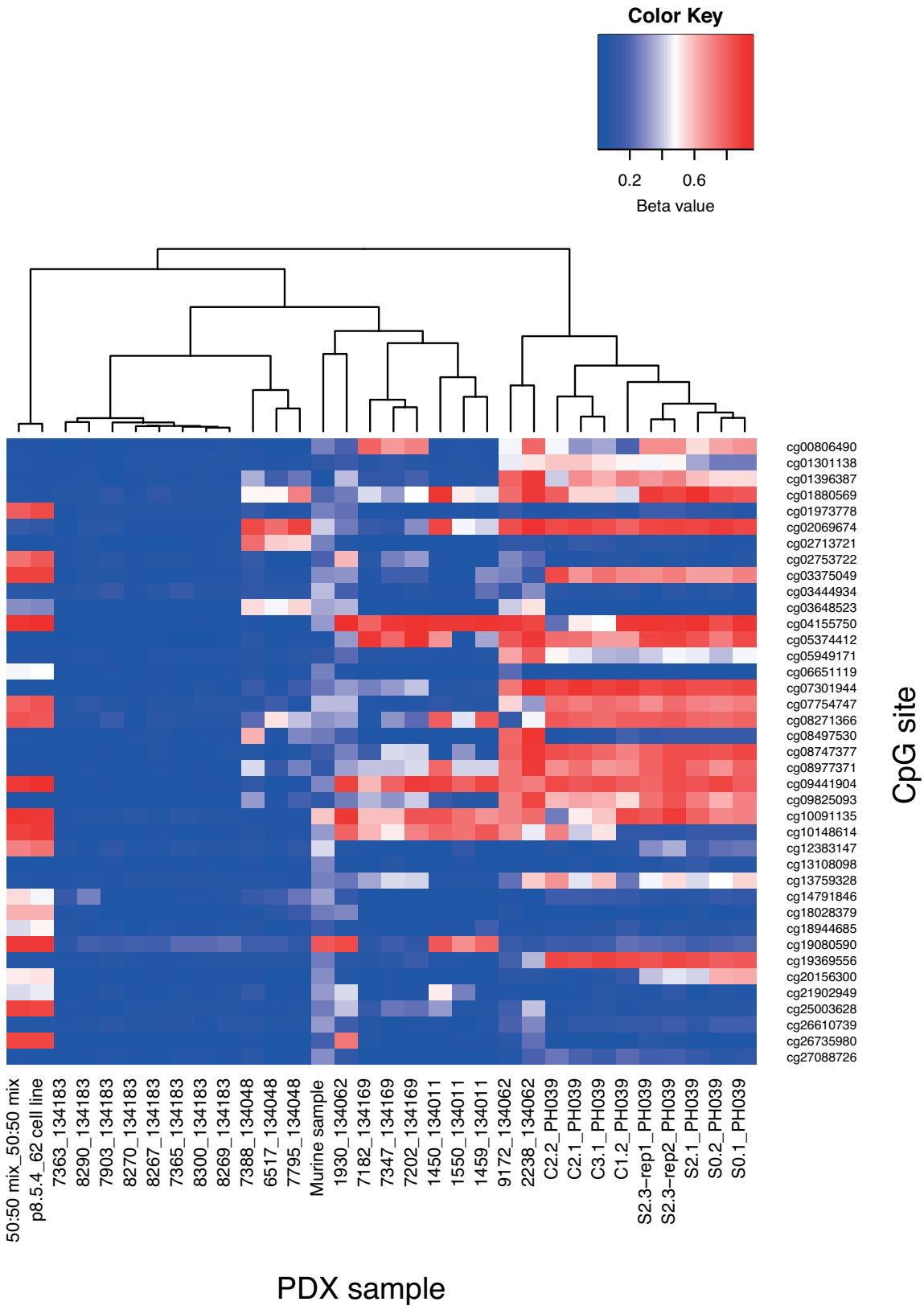


Figure 6.11. Methylation heatmap of all CDH13 CpG probes in EPIC array.
Heatmap shows β values of CpG probes associated with the CDH13 gene in the EPIC array, with samples ordered by CDH13 methylation similarity using dendrogram.

6.4.5 Global methylation profiles of PDX

I was then interested in looking at global patterns of methylation in each of the models and comparing them to each other. **Figure 6.12** shows boxplots of global β values for each sample (all CpG probes), coloured by PDX model. Models PDX 134011 and PDX 134169 were found to have much higher levels of methylation globally compared to other models (median β value ~0.5-0.6), while global methylation means were slightly lower for PDX models MAYO-PH039, 134062 and 134048 (mean β value ~0.3-0.5), and PDX 134183 tumours had the lowest relative median global methylation values (mean β value ~0.25-0.30). However, when restricting the global β methylation analysis to CpG island regions within the genome, a different pattern emerges. MAYO-PH039 PDX samples had a wider range of β values CpG island methylation compared to other samples, although the median β values for all samples appeared to align (**Figure 6.13**).

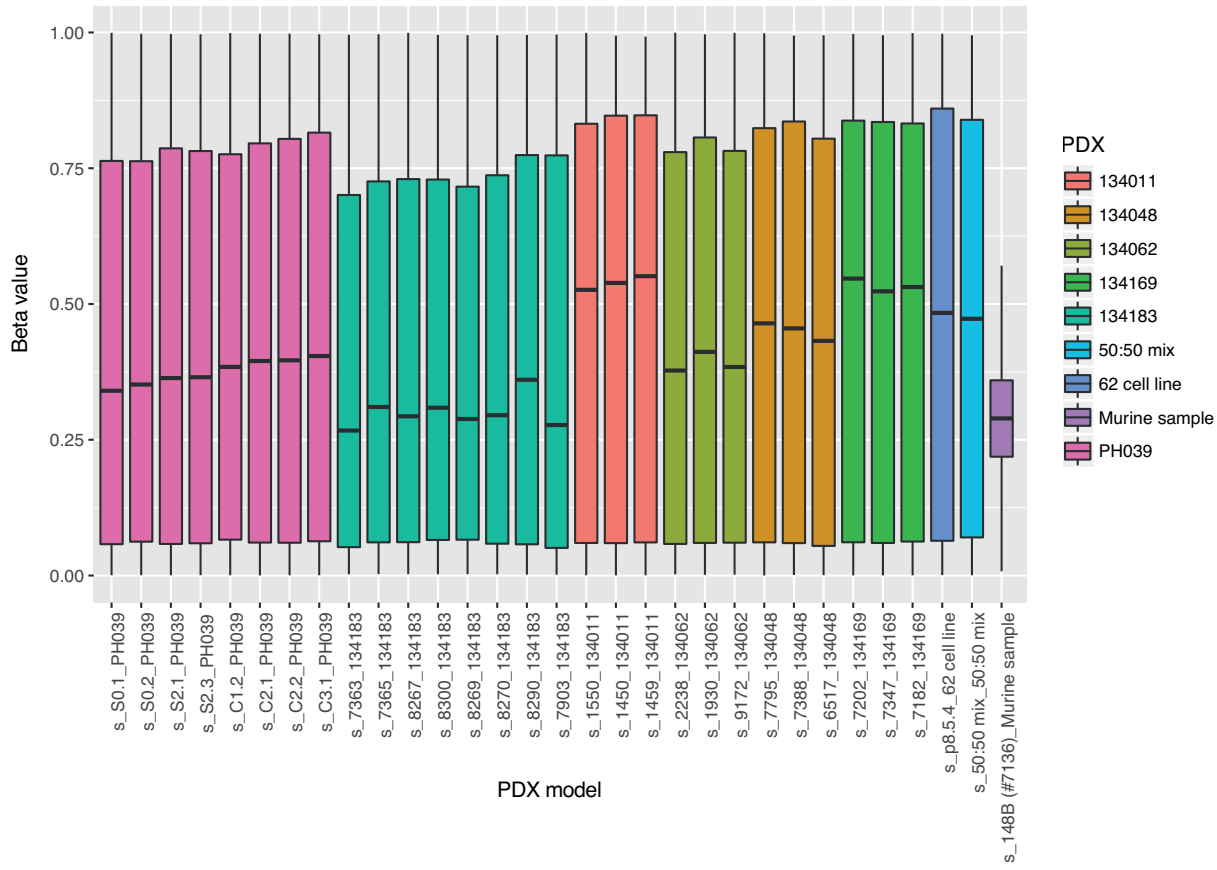


Figure 6.12. Methylome profiling of HGSOC PDX models by all CpG regions.
Boxplots of all β values for each PDX sample tested on EPIC array, coloured by PDX .

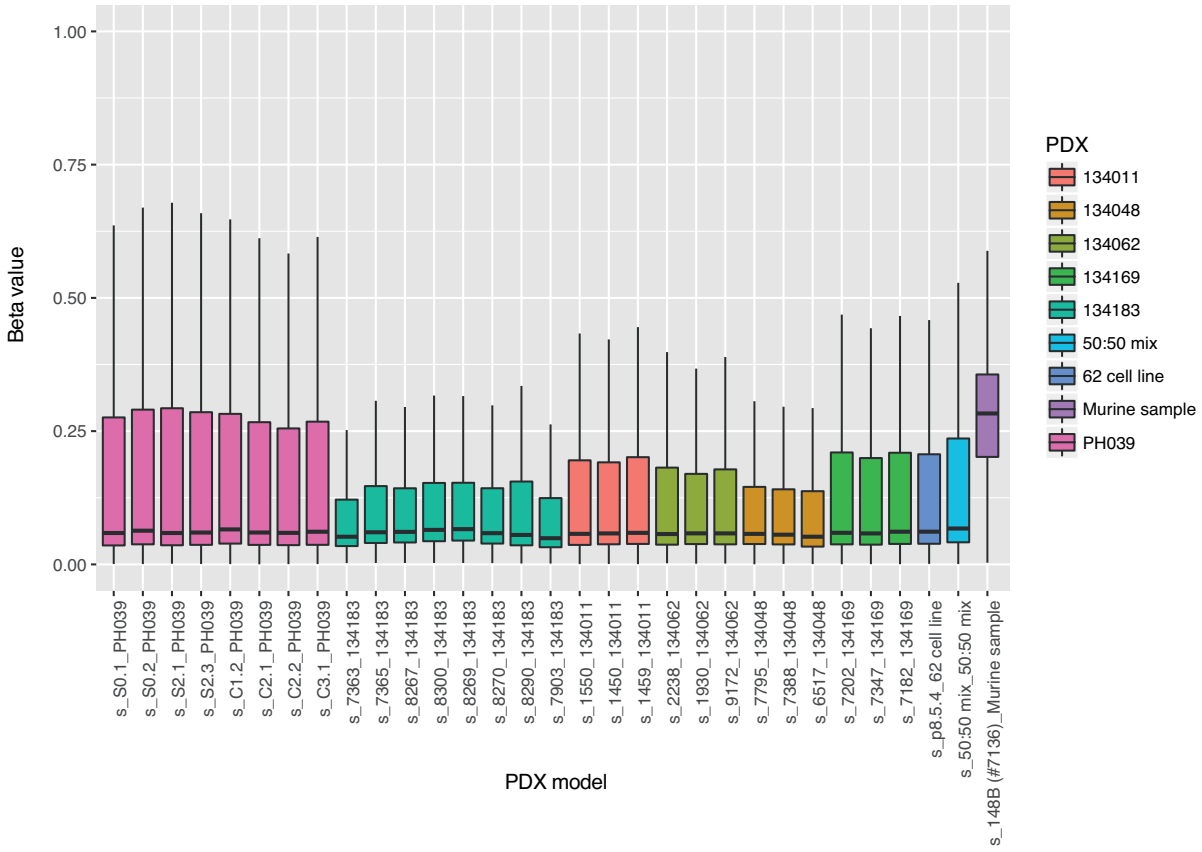


Figure 6.13. Methylome profiling of HGSOC PDX models by CpG islands.
Boxplots of β values related to CpG islands reveal that PDX MAYO-PH039 has higher global CpG island methylation relative to other PDX models.

When considering changes in median β values within models, it was observed that PDX MAYO-PH039 global methylation levels appear to increase with transplantation and with treatment when comparing untreated source tumours (S0.1 and S0.2) to second transplant untreated tumours (S2.1 and S2.3), and comparing treated transplant/cycle 1 (C1.2), cycle 2 (C2.1 and C2.2) and cycle 3 (C3.1) tumours (**Figure 6.12**). However, this trend was subtle, and was not observed when only considering methylation within CpG islands of MAYO-PH039 tumours (**Figure 6.13**).

6.4.6 Differential methylation analysis in RAD51C-methylated PDX models

I compared methylation profiles for treated and untreated samples that were run for the *RAD51C* methylated models, MAYO-PH039 and PDX 134183. The MAYO-PH039 samples were particularly interesting, as these were samples where PARPi resistance and *RAD51C* methylation loss had been driven by cyclical *in vivo* PARPi re-treatments. I started by grouping the treated (1-4 cycles of niraparib) samples and untreated samples (from transplants 1-2) and

then running a differential methylation analysis comparing these two groups. This analysis reported 256 top differentially-methylated probes with an adjusted *p*-value < 0.05, including several *RAD51C* gene probes. When plotting these across the genome for treated vs untreated, there appeared to be a trend towards methylation loss in the treated MAYO-PH039 samples both around the *RAD51C* locus on chromosome 17 (**Figure 6.14**) and globally (across all chromosomes; **Figure 6.15**) . This was demonstrated more clearly by presenting the boxplots of β values of these differentially methylated probes for each sample (**Figure 6.16**), where increasing losses of methylation with each cycle of PARPi niraparib were observed.

When separating the CpG hits by the epigenomic regions, the same patterns emerges, indicating that loss of methylation was not restricted to one type of epigenomic region (**Figure 6.17**). This included CpG islands, CpG shores (~2Kb from islands), CpG shelves (~4Kb from islands) and open sea (>4Kb from islands). Interestingly, despite the overall trend, some differentially methylated probes/CpG probes gained methylation following PARPi treatment/re-treatment (**Figure 6.18**).

In contrast, differential methylation analysis (using the same parameters) on the PDX 134183 treated vs untreated samples yielded only 34 differentially methylated CpG probes. Given that 20 of these probes gained methylation and 14 lost methylation, there appeared to be a trend towards gain of methylation across the genome (**Figure 6.19**), when looking at individual samples (**Figure 6.20**) or individual CpG probes (**Figure 6.21**).

However, given the small number of CpG observations for this analysis, any trends observed are low confidence. This low number of hits is possibly due to the fact that the PDX 134183 treated samples were only exposed to a single treatment of rucaparib 300mg/kg (as the re-treatment studies outlined in Chapter 5 had not yet been completed for this model), which may not be sufficient to drive global methylation changes in this model. Indeed, there were no me*RAD51C* losses in these samples.

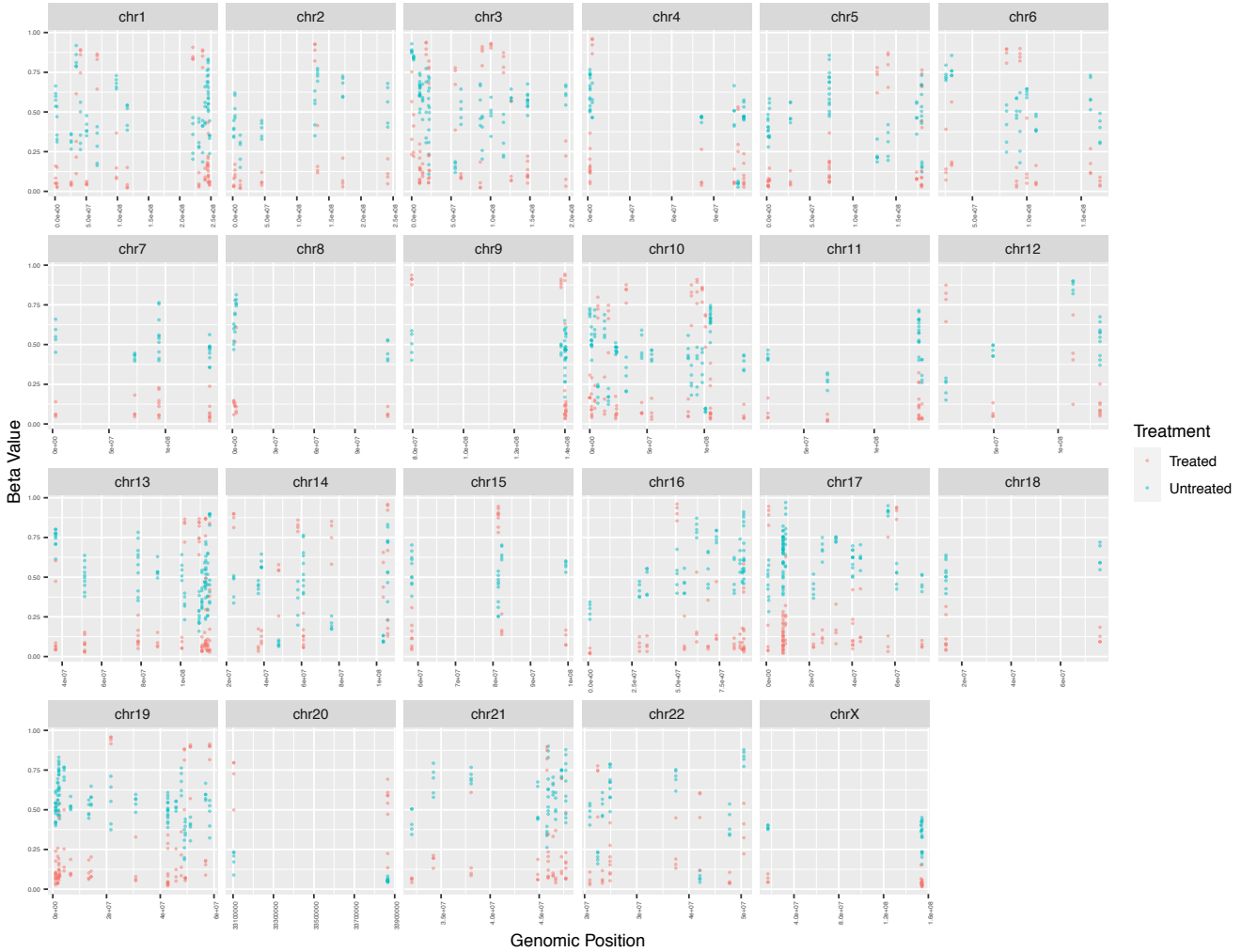


Figure 6.14. Treated PDX MAYO-PH039 samples appear to lose methylation at differentially methylated CpG probes globally.
Presented are β values for differentially methylated CpG probes reported in the PDX MAYO-PH039 treated vs untreated differential methylation analysis (256 hits), plotted across the genome. "Chr" =chromosome.

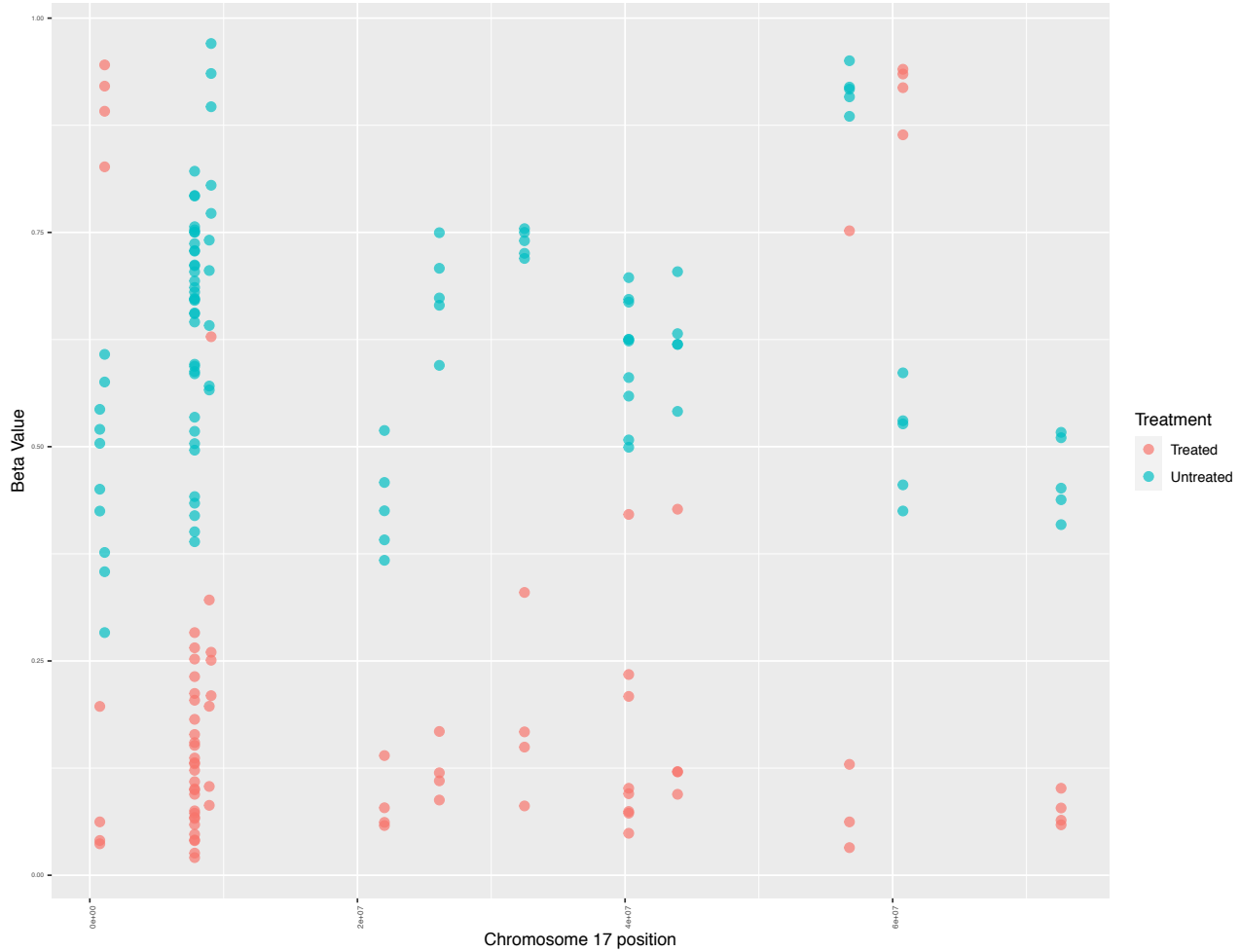


Figure 6.15. Treated PDX MAYO-PH039 samples appear to lose methylation at differentially methylated CpG probes, including chromosome 17.

Presented are the β values for the top differentially methylated CpG probes reported in the MAYO-PH039 treated vs untreated differential methylation analysis, plotted across chromosome 17 (which includes the RAD51C locus).

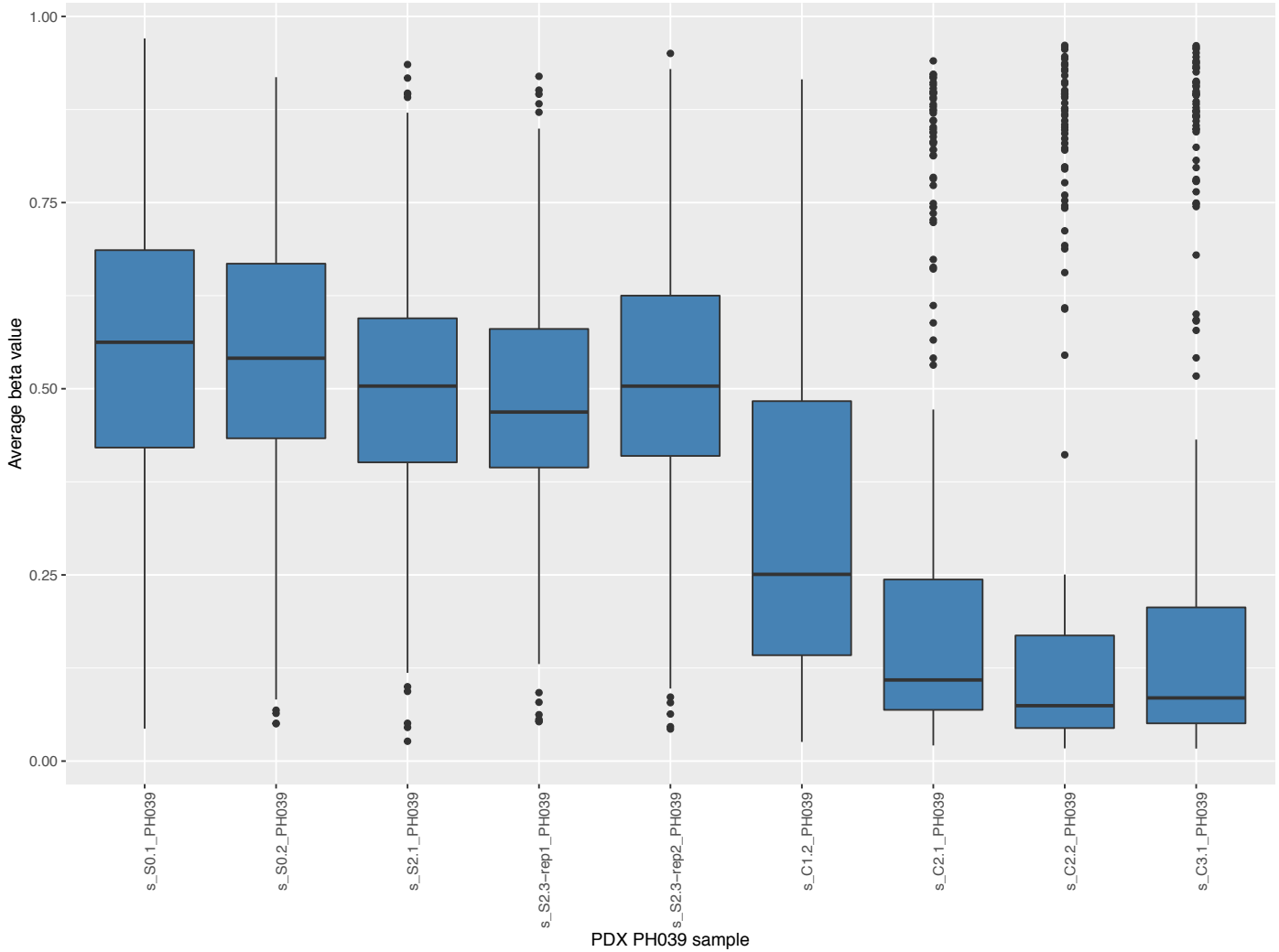


Figure 6.16. Increasing global methylation loss with each subsequent round of niraparib treatment in PDX MAYO-PH039.
Average β value of all differentially methylated CpG probes (256) within each MAYO-PH039 sample.

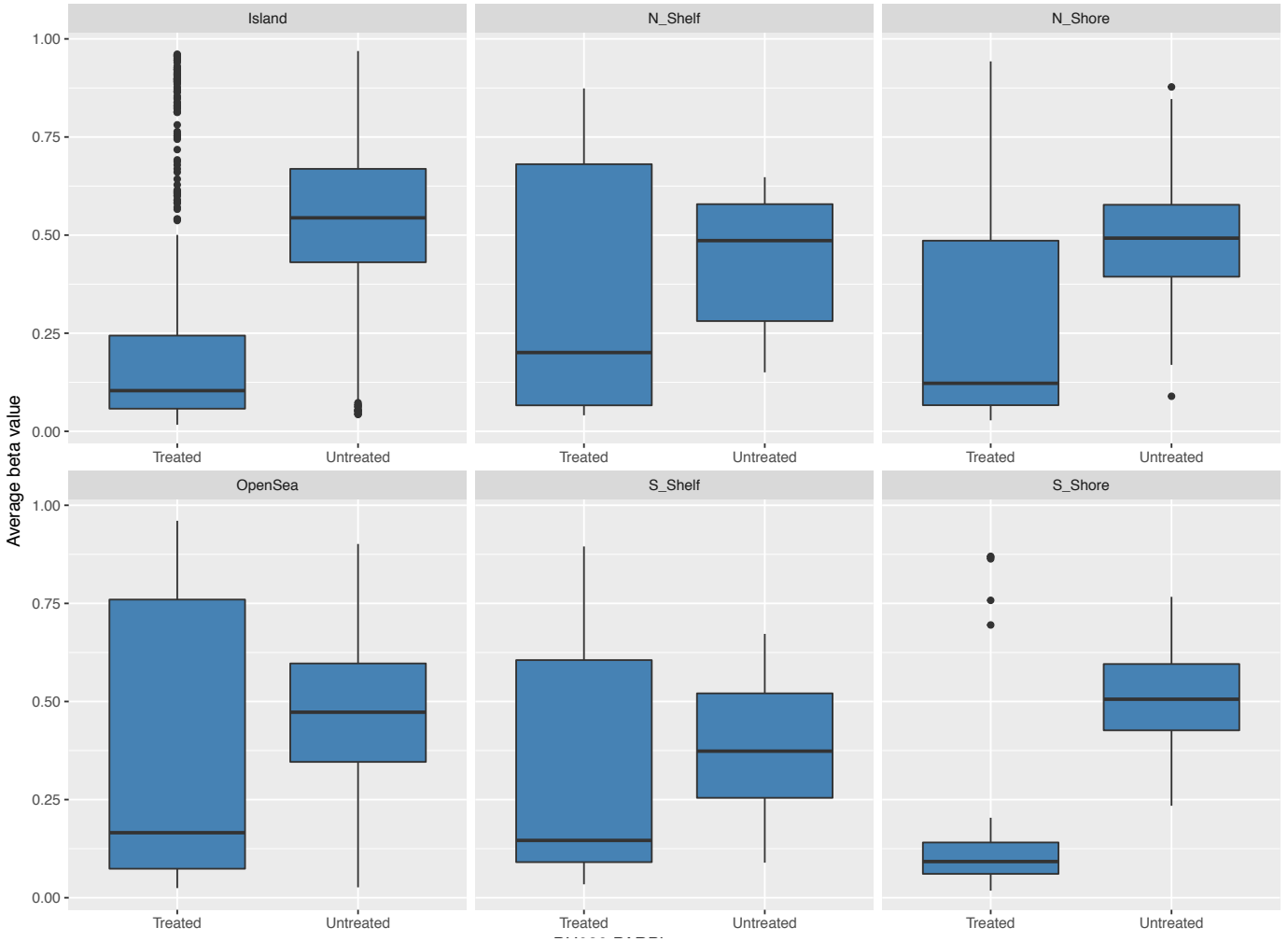


Figure 6.17. Increasing global methylation losses associated with increasing rounds of niraparib treatment in PDX MAYO-PH039 are not specific to a single epigenomic region.

Methylation losses in top differentially methylated probes are observed across all epigenomic regions: CpG islands, Northern (N)-shelves, Northern (N)-shores. Open Seas, Southern (S)-shelves and Southern (S)-shores.



Figure 6.18. Some differentially methylated CpG probes in MAYO-PH039 gain methylation.
Comparing the average β value for each differential methylation analysis CpG site within the treated vs untreated groups shows that most CpG probes in this list lose methylation following niraparib treatment (n=200), but some also gain methylation (n=56).

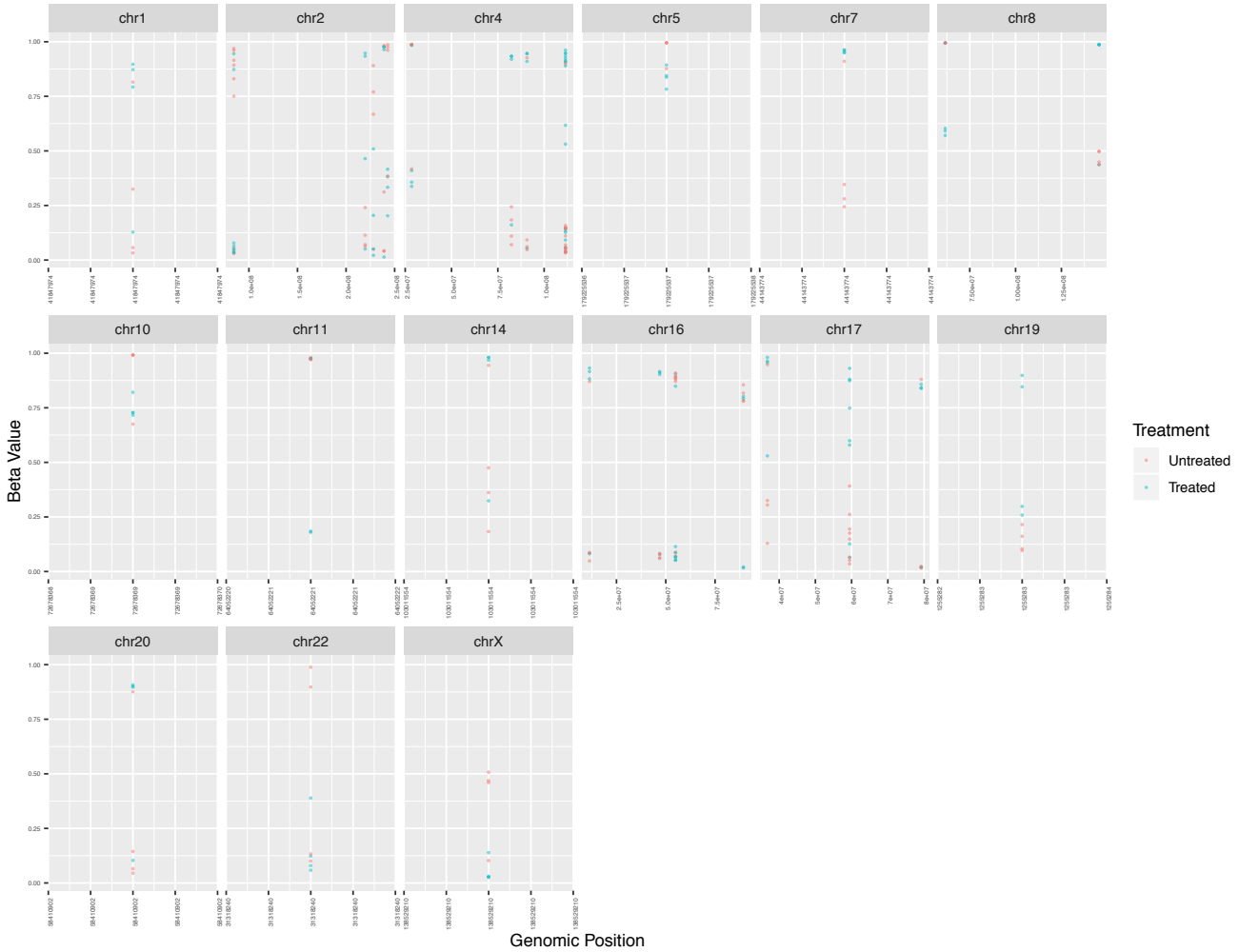


Figure 6.19. Global distribution of differentially methylated CpG probes for PDX 134183 treated vs untreated samples.
Presented are β values for the top differentially methylated CpG probes (34 hits) reported in the PDX 134183 treated vs untreated differential methylation analysis, plotted across the genome. "Chr" =chromosome.

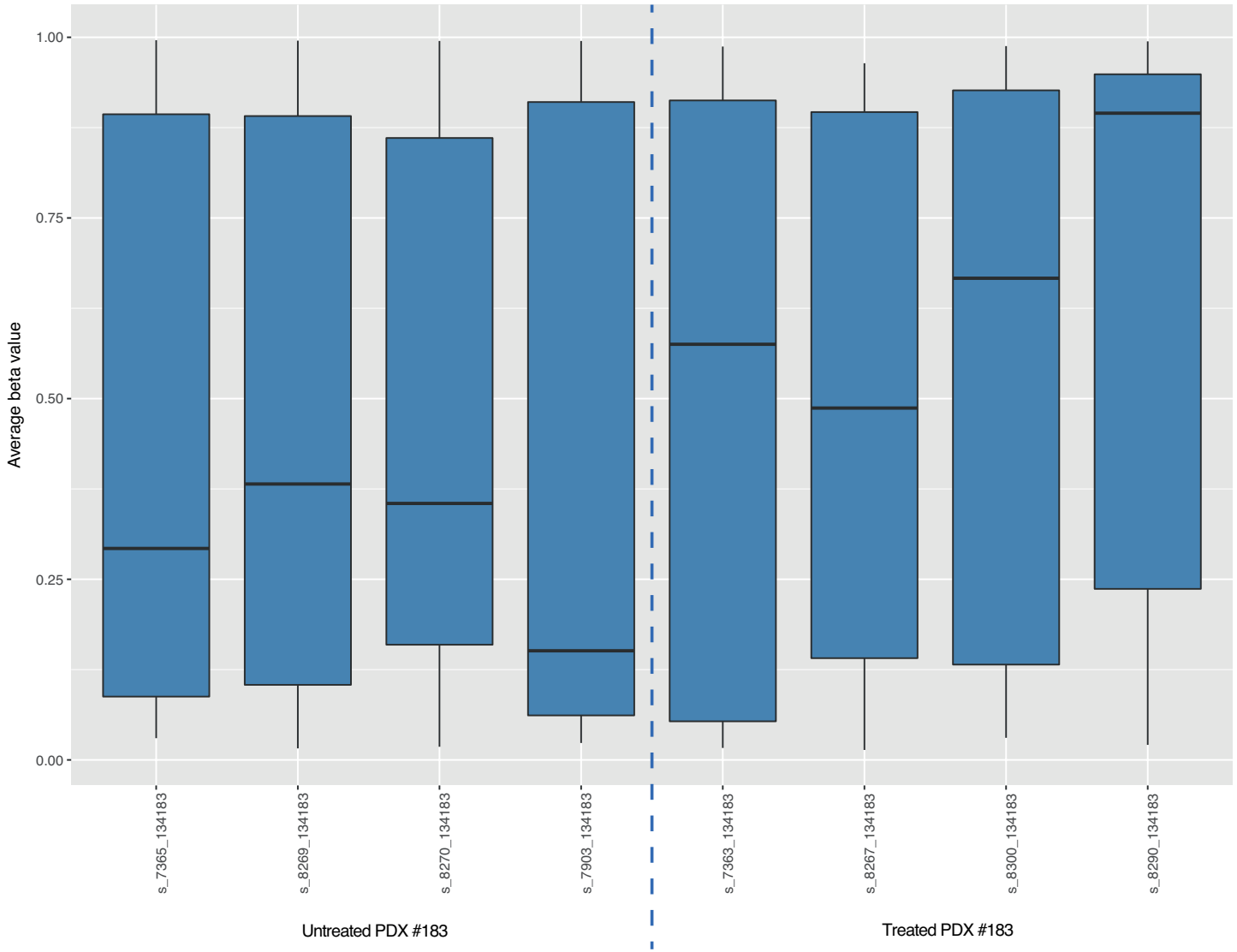


Figure 6.20. Trend towards gain of methylation in differentially methylated CpG probes for PDX 134183 treated samples compared to untreated samples.

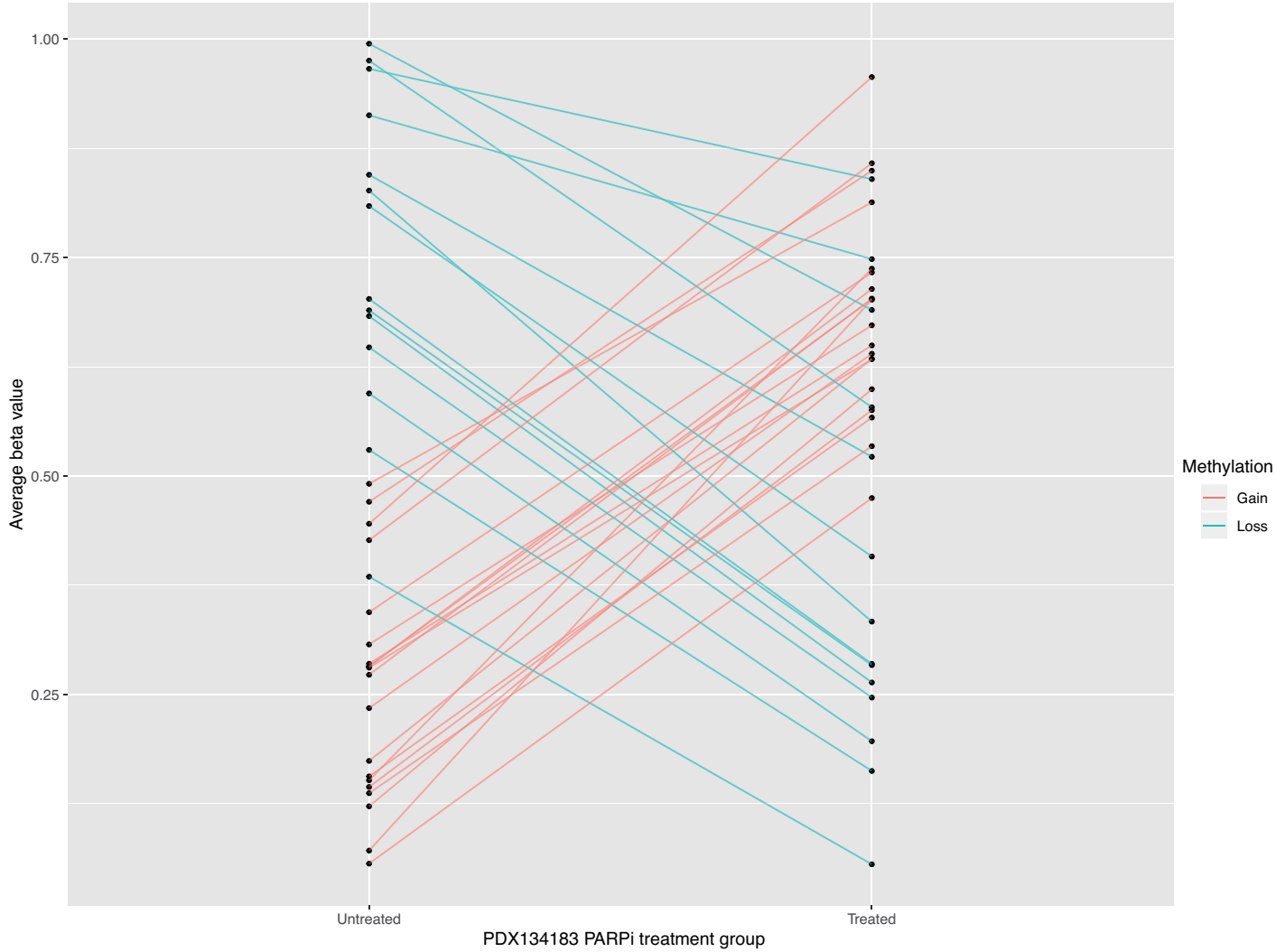


Figure 6.21. Subtle gains of methylation in differentially methylated CpG probes in PDX 134183 treated samples.
Average β value shown for n = 34 differentially methylated CpG probes.

6.4.7 Gene ontology terms for MAYO-PH039 differential methylation analysis

Given that there were CpG probes in the MAYO-PH039 differential methylation analysis that gained methylation post-PARPi or lost methylation post-PARPi, I was interested in whether these methylation changes were linked to any particular pathways or biological processes within the tumour cells. I therefore performed a Gene Ontology (GO) analysis on the CpG probes in the "gained" methylation group and in the "lost" methylation group.

When the GO terms for the CpG hits that gained methylation post-PARPi were interrogated, there was a clear enrichment of terms related to cell-cell interactions and plasma membrane features (**Table 6.2**).

Table 6.2. Enrichment of cell-cell interaction GO terms in CpG probes that gain methylation under niraparib pressure in MAYO-PH039.
Presented are terms with p-values less than 0.002. N = number of genes, DE = number of genes in differential methylation analysis. P.DE = p-value for in differential methylation analysis, FDR = False discovery rate, Ont = Ontology group, where "BP" = biological process, "CC" = cellular component, "MF" = molecular function.

GO term ID	GO Term	Ont	N	DE	P.DE	FDR
GO:0098609	cell-cell adhesion	BP	773	20	0.000	0.00
GO:0098742	cell-cell adhesion via plasma-membrane adhesion molecules	BP	242	19	0.000	0.00
GO:0007156	homophilic cell adhesion via plasma membrane adhesion molecules	BP	158	19	0.000	0.00
GO:0005887	integral component of plasma membrane	CC	1657	22	0.000	0.00
GO:0031226	intrinsic component of plasma membrane	CC	1720	22	0.000	0.00
GO:0005509	calcium ion binding	MF	694	21	0.000	0.00
GO:0007155	cell adhesion	BP	1340	21	0.000	0.00
GO:0022610	biological adhesion	BP	1348	21	0.000	0.00
GO:0007267	cell-cell signaling	BP	1652	20	0.000	0.00
GO:0044459	plasma membrane part	CC	2761	23	0.000	0.00
GO:0007399	nervous system development	BP	2287	22	0.000	0.00
GO:0046872	metal ion binding	MF	4077	26	0.000	0.00
GO:0043169	cation binding	MF	4170	26	0.000	0.01
GO:0031224	intrinsic component of membrane	CC	5340	26	0.000	0.02
GO:0043167	ion binding	MF	6086	31	0.000	0.02
GO:0016021	integral component of membrane	CC	5204	25	0.000	0.03
GO:0071944	cell periphery	CC	5316	28	0.000	0.04
GO:0048731	system development	BP	4734	27	0.000	0.06
GO:0005886	plasma membrane	CC	5206	27	0.000	0.07
GO:0032501	multicellular organismal process	BP	7382	32	0.000	0.09
GO:0032502	developmental process	BP	6219	30	0.000	0.14
GO:0007275	multicellular organism development	BP	5322	27	0.000	0.29
GO:0048856	anatomical structure development	BP	5803	28	0.000	0.40
GO:0044425	membrane part	CC	6569	27	0.000	0.46
GO:0031449	regulation of slow-twitch skeletal muscle fiber contraction	BP	1	1	0.002	1.00

The top 5 most significant GO terms for this group were “cell-cell adhesion, cell-cell adhesion via plasma-membrane adhesion molecules”, “homophilic cell adhesion via plasma membrane adhesion molecules”, “integral component of plasma membrane” and “intrinsic component of plasma membrane”. Methylation gains may be associated with gene silencing in these pathways or cellular processes. In contrast, gene ontology terms enriched for the CpG hits that lost methylation post-PARPi were mostly related to neuronal function and development (**Table 6.3**). The top 5 most significant GO terms for this group were “chemical synaptic transmission”, “anterograde trans-synaptic signalling”, “trans-synaptic signalling”, “synaptic signalling” and “forebrain development”. Methylation losses may be associated with gained gene expression in these pathways or cellular processes.

Table 6.3. Enrichment of neuronal pathway GO terms in CpG probes that lose methylation under niraparib pressure in MAYO-PH039.

Presented are terms with p-values less than 0.002. N = number of genes, DE = number of genes in differential methylation analysis. P.DE = p-value for in differential methylation analysis, FDR = False discovery rate, Ont = Ontology group, where "BP" = biological process, "CC" = cellular component, "MF" = molecular function.

GO term ID	GO Term	Ont	N	DE	P.DE	FDR
GO:0007268	chemical synaptic transmission	BP	664	15	0.00017569	1
GO:0098916	anterograde trans-synaptic signaling	BP	664	15	0.00017569	1
GO:0099537	trans-synaptic signaling	BP	667	15	0.00019131	1
GO:0099536	synaptic signaling	BP	668	15	0.00019333	1
GO:0030900	forebrain development	BP	366	11	0.00027643	1
GO:0043457	regulation of cellular respiration	BP	23	3	0.00055501	1
GO:0007420	brain development	BP	695	15	0.0005676	1
GO:0043005	neuron projection	CC	1216	21	0.00075808	1
GO:0007097	nuclear migration	BP	19	3	0.00080877	1
GO:0060322	head development	BP	735	15	0.00096087	1
GO:0030902	hindbrain development	BP	143	6	0.00104156	1
GO:0097458	neuron part	CC	1524	24	0.00109032	1
GO:0009064	glutamine family amino acid metabolic process	BP	73	4	0.00121439	1
GO:0051963	regulation of synapse assembly	BP	88	5	0.00125521	1
GO:0051647	nucleus localization	BP	23	3	0.00142639	1
GO:0090101	negative regulation of transmembrane receptor protein serine/threonine kinase signaling pathway	BP	117	5	0.0014988	1
GO:0009719	response to endogenous stimulus	BP	1600	22	0.00155737	1
GO:0007610	behavior	BP	582	12	0.00165067	1
GO:0098797	plasma membrane protein complex	CC	568	12	0.00193516	1

6.4.8 Differential methylation analysis in BRCA1-methylated PDX models

I then looked for differences between heterozygous and homozygous *BRCA1* methylated PDX models, to see if I could identify any methylome features distinguishing the two groups. I decided to perform a differential methylation analysis comparing the homozygous and heterozygous PDX models, to see if any pattern emerged (like that observed in the MAYO-PH039 treated vs untreated differential methylation analysis). I grouped the homozygous models (PDX 134011 and 134062) and the heterozygous models (PDX 134048 and 134169) using a contrast matrix (specifying individual PDX samples) and then performed a differential methylation analysis on these groups. Using the same parameters as used for the *RAD51C* analysis (+/- log-fold change (LFC) of >3), there were 14396 differentially methylated probes identified, which included only one of the three *BRCA1* CpG probes associated with gene silencing in PDX: cg24806953 (detected with a *p*-value of 0.09, adjusted p-value of 0.97 and LFC of 3.7). The two probes cg04110421 and cg26891576 were most likely excluded from this list because the change of methylation from homozygous to heterozygous state is not as pronounced as a homozygous methylation to unmethylated state, and their methylation changes were more subtle than cg24806953 (**Figure 6.9**). This was confirmed by changing the LFC parameter to +/- LFC >2, where cg04110421 was then detected with a LFC of 2.7, *p*-value = 0.21 and adjusted *p*-value of 1 (total of 28144 observations), though cg26891576 was still undetectable.

I assessed β value distribution across the genome for CpG probes reported for the initial differential methylation analysis (+/- LFC of >3) to see if there were any patterns. However, 14396 observations was too many points to visualise clearly, so I subset the data based on a *p*-value threshold of <0.01, which resulted in 620 observations. These differentially methylated CpG probes were then plotted across the genome (**Figure 6.22**) and chromosome 17/*BRCA1* locus (**Figure 6.23**) for each sample in "homozygous" and "heterozygous" groups. There were no obvious patterns visible based on chromosomal position. I also assessed the overall β value distribution of all differentially methylated CpG for each sample. Grouping by samples revealed that the differentially methylated CpG probes had much lower methylation in PDX 134062 relative to other models (**Figure 6.24**). This trend was also reflected in the global methylation profiles of all CpG probes per sample and PDX model in **Figure 6.12**.

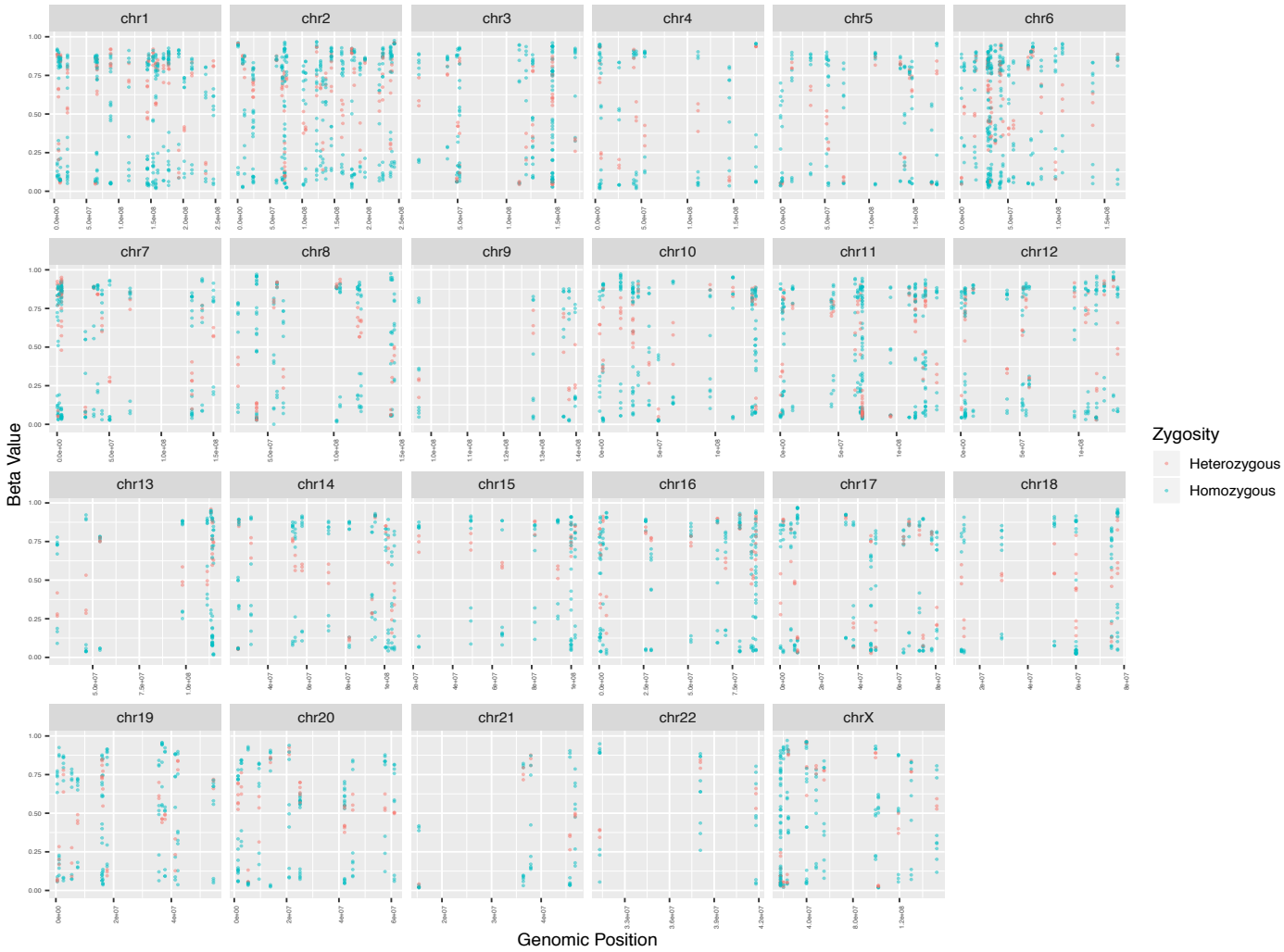


Figure 6.22. No global trends observed comparing differentially methylated CpG probes in homozygous and heterozygous PDX.

Presented are β values for the top differentially methylated CpG probes (n =256) reported in the BRCA1 homozygous vs heterozygous differential methylation analysis, plotted across the genome. "Chr" =chromosome.

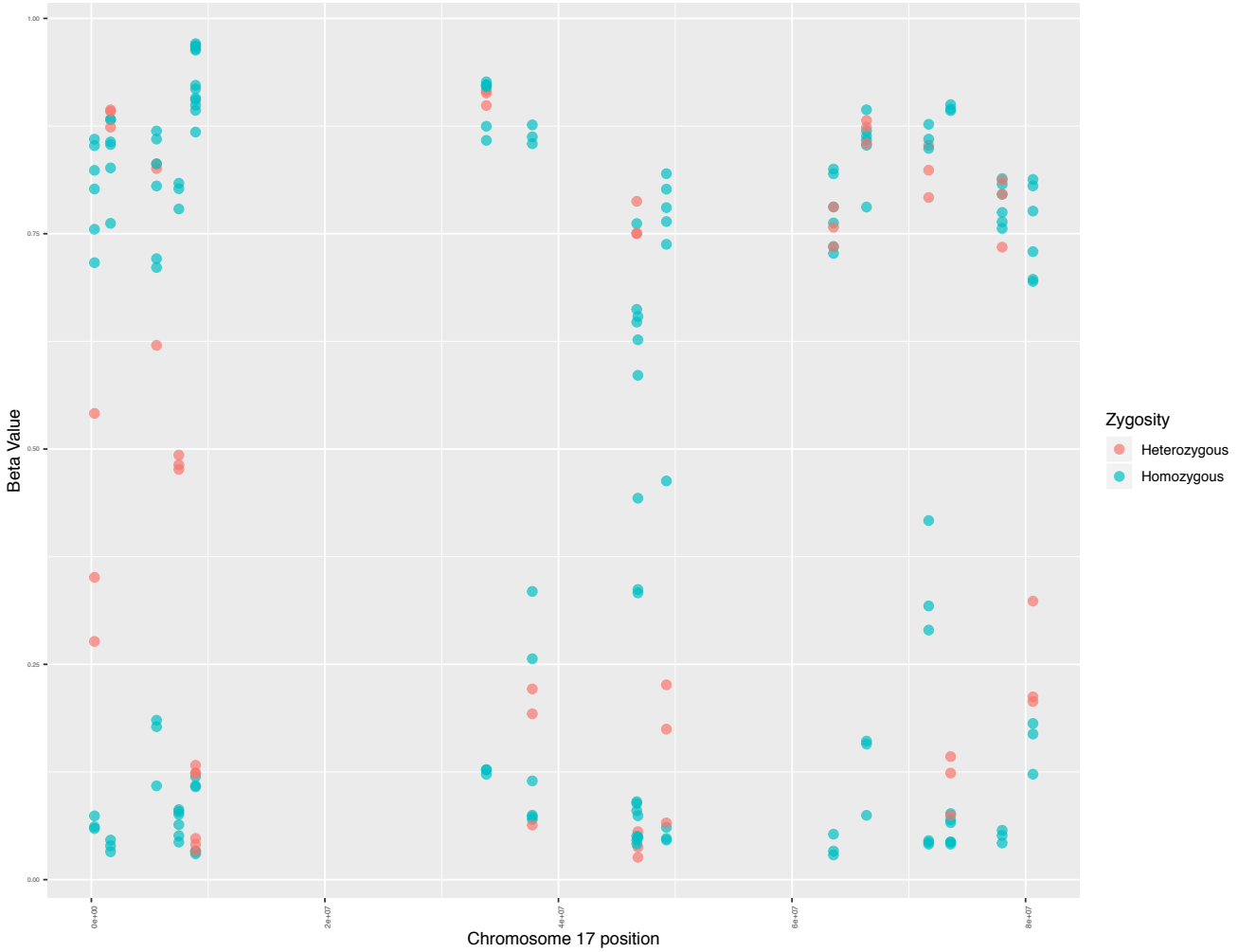


Figure 6.23. No trends observed comparing differentially methylated CpG probes in homozygous and heterozygous PDX across chromosome 17.

Presented are the β values for the top differentially methylated CpG probes reported in the BRCA1 homozygous vs heterozygous differential methylation analysis, plotted across chromosome 17 (which includes the BRCA1 locus).

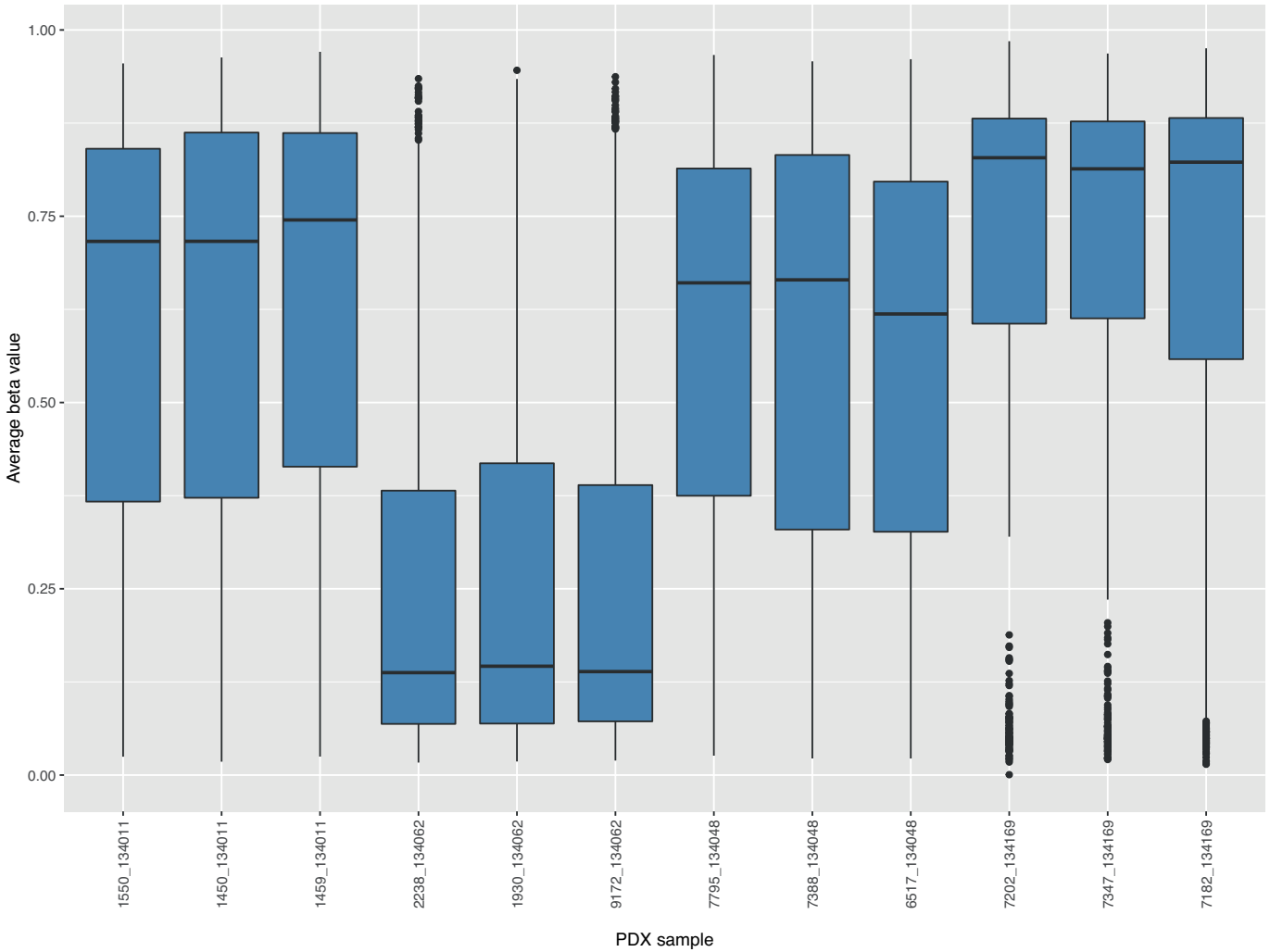


Figure 6.24. PDX 134062 has reduced methylation of CpG probes from BRCA1 homozygous vs heterozygous differentially methylation analysis

These results were, however, difficult to interpret as not all CpG probes of the internal positive control (me*BRCA1*) were picked up by this analysis. Furthermore, there was added biological variance when comparing these samples given that different PDX models are being compared, unlike the me*RAD51C* analysis of MAYO-PH039 where matched samples were used (treated vs untreated). Hence, I decided to explore publicly available methylation array data, as I postulated a larger cohort of samples may help to overcome these issues.

6.4.9 Searching for signatures: ICGC differential methylation analysis

To further explore whether there were any gene promoters or regions commonly co-methylated/unmethylated with *RAD51C* or *BRCA1* in HGSOC, a dataset larger than the PDX cohort was needed, so I accessed publicly available methylation array data for 122 HGSOC samples, published by Patch et al. (2015) as part of the International Cancer Genome Consortium (ICGC). These samples, however, were run on the discontinued Illumina Infinium Human Methylation 450 Bead array (the '450K' array), which only quantifies DNA methylation at ~450,000 loci across the human genome.

The purpose of this analysis was to use the larger ICGC dataset to identify genes that may be frequently co-methylated or co-unmethylated with *RAD51C* or *BRCA1* in HGSOC tumours, and then checking this list of genes within the PDX EPIC array dataset. I hypothesized that methylation patterns found to be associated with *BRCA1* and *RAD51C* promoter methylation could provide evidence of common mechanisms for initiation and maintenance of HR gene methylation in HGSOC.

No obvious batch effects were observed from MDS plots in dimensions 1 and 2 for arrays (**Figure 6.25**) or for slides (**Figure 6.26**) within this ICGC dataset, thus I proceeded with the analysis.

The degree of methylation at CpG probes known to be associated with *BRCA1* and *RAD51C* silencing in each ICGC 450K array sample was assessed using β value heatmaps. The CpG probes interrogated were as described above (i.e. those associated with MS-HRM results and gene silencing for PDX cohort) – cg24806953, cg04110421 and cg26891576 for *BRCA1,* and cg05214530, cg27221688 and cg24099023 for *RAD51C*.

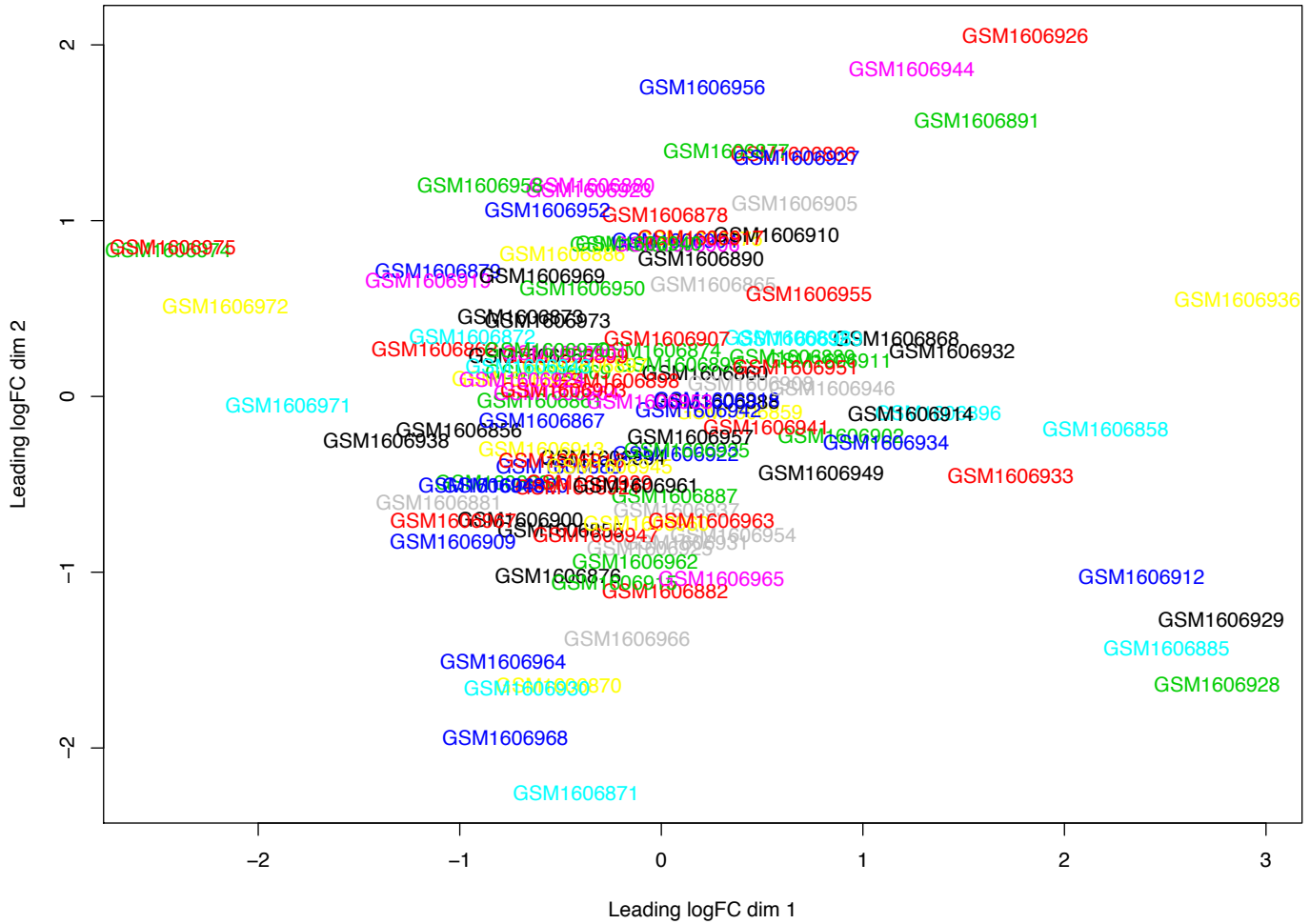


Figure 6.25. No batch effects produced by array for ICGC samples.
MDS plot where samples are coloured by their array run.

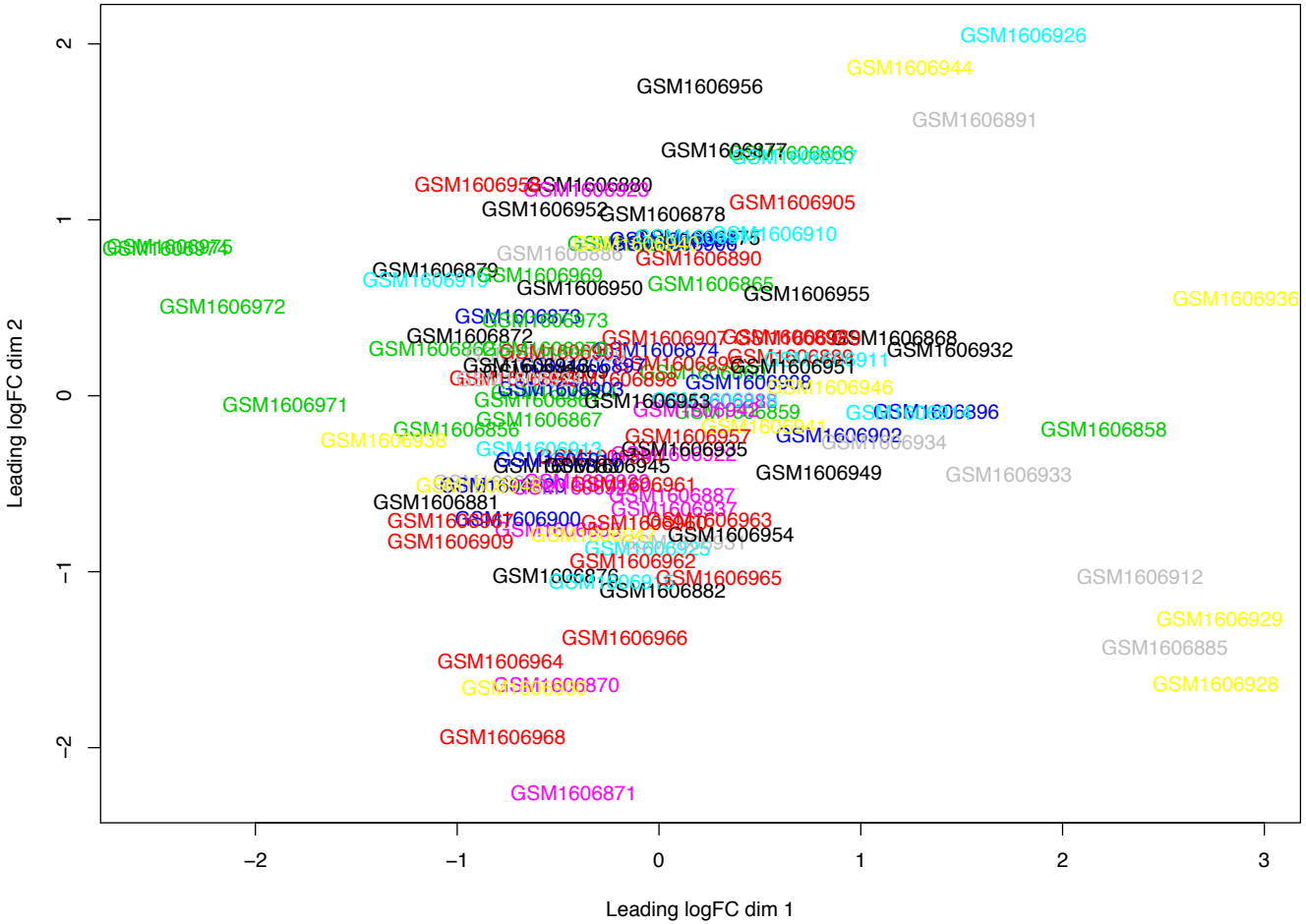


Figure 6.26. No batch effects produced by slide for ICGC samples.

MDS plot where samples are coloured by their slide run.

In this dataset this approach was used to identify samples that may have epigenetic silencing of these HR genes. Samples that were defined as "methylated" and selected for further analysis had at least one of these CpG probes with a β value of >0.4. This generous cut-off value was selected to ensure that true methylated samples with heterozygous/heterogeneous methylation profiles or lower tumour purity were not missed. This resulted in 16 samples defined as "*BRCA1*-methylated" (including the 12 reported in Patch et al., 2015; **Figure 6.27**), and 4 samples defined as "*RAD51C*-methylated" (including the 3 reported in Patch et al., 2015; **Figure 6.28**).

These samples were then used to create 2 subsets of the ICGC 450K array data: a *BRCA1* methylated subset containing all un-methylated samples and *BRCA1*-methylated samples (excluding *RAD51C*-methylated samples), and a *RAD51C* methylated subset containing all un-methylated samples and *RAD51C*-methylated samples (excluding *BRCA1*-methylated samples). This was done to create the cleanest dataset possible for the identification of *BRCA1/RAD51C*-associated methylation signatures.

These sample subsets were then re-processed and re-normalized before testing for differential methylation using the MissMethyl package. The cut-offs of LFC >2 and *p*-value <0.05 were used for sub-setting the differentially methylated CpG probes found in the *BRCA1* methylated vs unmethylated sample comparison, and the *RAD51C* methylated vs unmethylated sample comparison.

Nineteen CpG probes were detected in the *RAD51C* differential methylation analysis: nine unmethylated and ten methylated CpG probes (seven related to *RAD51C*) that are associated with *RAD51C* methylation (**Table 6.4**). Only five of these were found to overlap with CpG probes covered by the EPIC array, and three of these were related to the *RAD51C* promoter. The two CpG probes that are not within the *RAD51C* locus and are covered by the EPIC array were thus expected to be methylated in me*RAD51C* PDX samples within our EPIC array cohort if a true association existed between them. This was not the case as the two CpG probes were not methylated in any of the EPIC array samples (**Figure 6.29**), thus this particular analysis was concluded at this point.

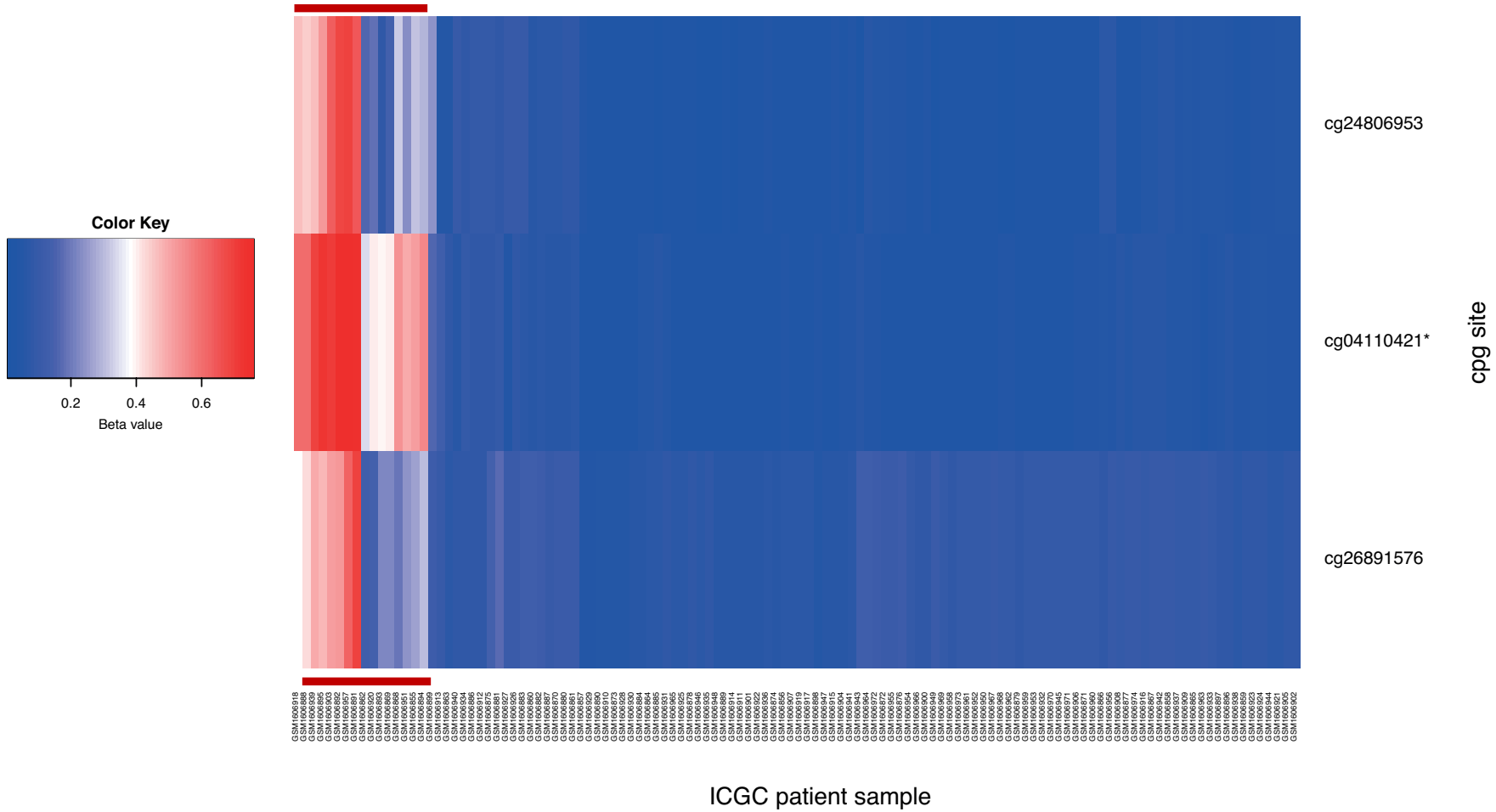


Figure 6.27. BRCA1 methylation heatmap of ICGC samples indicates 16 samples with possible homozygous or heterozygous BRCA1 promoter methylation.

Summary β value heatmap of BRCA1 CpG probes (cg24806953, cg04110421 and cg26891576) in ICGC samples associated with BRCA1 gene expression in PDX models. Red bar indicates 16 samples with BRCA1 methylation. CpG marked with "" indicates the probe covered by both the BRCA1 MS-HRM assay and EPIC array.*

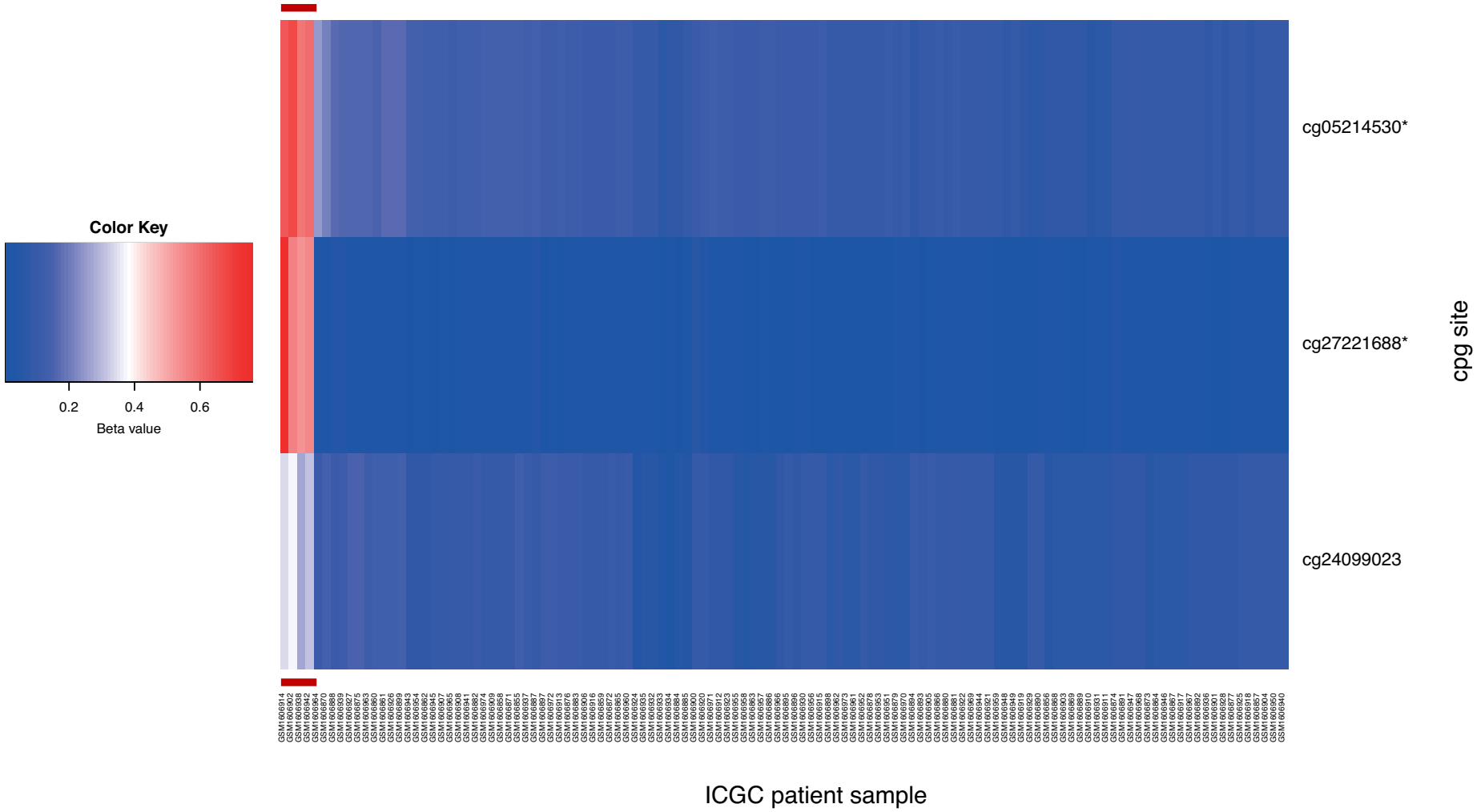


Figure 6.28. RAD51C methylation heatmap of ICGC samples indicates four samples with RAD51C promoter methylation.

Summary β value heatmap of ICGC patient samples run on the Illumina 405K array. Presented are the three RAD51C CpG probes associated with RAD51C gene expression and MS-HRM results in PDX models (cg05214530, cg27221688 and cg24099023). Red bar indicates 4 samples with RAD51C methylation. CpG's marked with "" indicate the two probes covered by both the RAD51C MS-HRM assay and EPIC array,*

Table 6.4. CpG probes outside RAD51C promoter that are possibly associated with RAD51C methylation.

List of CpG probes from differential methylation analysis comparing meRAD51C ICGC samples to RAD51C-unmethylated samples using LFC (log fold change) >2 and a p-value <0.05 cut-off. Highlighted in blue are CpG probes where unmethylated state may be associated with meRAD51C, though none of these are covered by the EPIC array (for validation). Highlighted in pink are CpG probes where methylated state may be associated with meRAD51C, where two probes unrelated to RAD51C are covered by the EPIC array and can thus be validated in the meRAD51C PDX samples: cg21046967 (NEUROD2 gene) and cg16306190 (LRRC34 gene).

CpG probe	Associated gene	LFC	Chromosome	Chromosomal position	CpG covered by EPIC array?
cg09667067		-3.79847156	chr10	2453191	No
cg03531388		-3.253760811	chr13	27077539	No
cg26576978		-2.885638216	chr6	138718522	No
cg11699126	TCF3;TCF3	-2.872775508	chr19	1646212	No
cg09192412	CASP6;CASP6	-2.745682511	chr4	110621006	No
cg23291158	KCNMA1;KCNMA1;KCNMA1;KCNMA1	-2.448378288	chr10	79006384	No
cg21114725		-2.163648955	chr3	132115350	No
cg17165444		-2.116877267	chr15	101405961	No
cg05660197	BTNL3	-2.063424445	chr5	180433174	No
cg09672890		2.053787317	chr17	70536484	No
cg21046967	NEUROD2	2.082739644	chr17	37762455	Yes
cg16306190	LRRC34	2.184219809	chr3	169530268	Yes
cg24099023	TEX14;RAD51C;TEX14;RAD51C	2.202726093	chr17	56770189	Yes
cg23436779	TEX14;RAD51C;TEX14;RAD51C	3.12703567	chr17	56769830	No
cg10487724	TEX14;RAD51C;TEX14;RAD51C	3.522912031	chr17	56770010	No
cg05214530	TEX14;RAD51C;TEX14;RAD51C	3.569103274	chr17	56769891	Yes
cg14066645	TEX14;RAD51C;TEX14;RAD51C	4.156048836	chr17	56770424	No
cg02118635	RAD51C;TEX14;RAD51C;TEX14;RAD51C;RAD51C	4.732402142	chr17	56770003	No
cg27221688	TEX14;RAD51C;TEX14;RAD51C	5.699308654	chr17	56769904	Yes

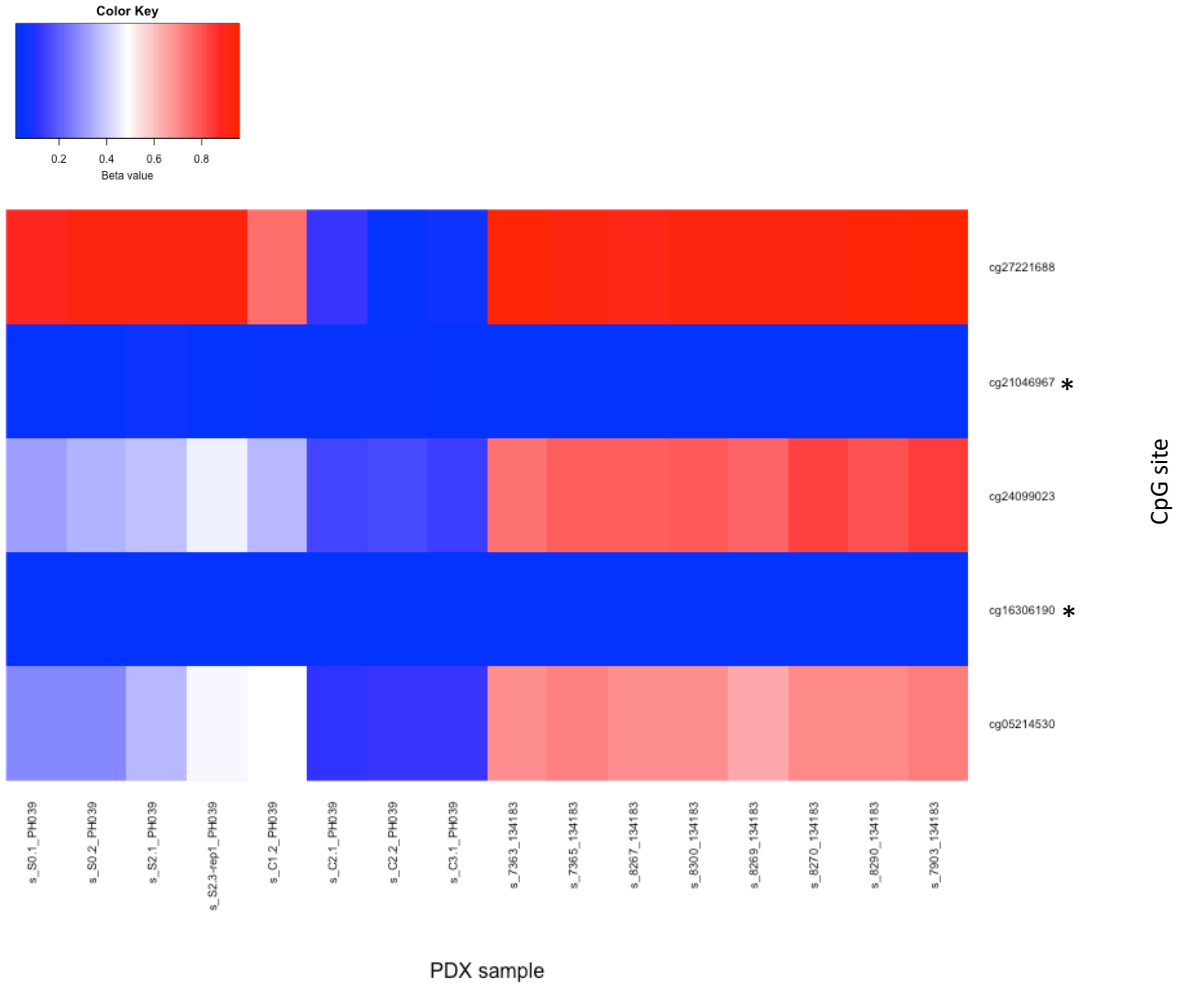


Figure 6.29. CpG probes associated with RAD51C promoter methylation in 450K differential methylation analysis are not methylated in EPIC array PDX samples.
*CpG probes marked with * indicate the two probes where methylation is associated with meRAD51C in the ICGC data: cg21046967 (NEUROD2 gene) and cg16306190 (LRRC34 gene). Remaining CpG probes presented are the three RAD51C CpG probes associated with RAD51C gene expression and MS-HRM results in PDX models (cg05214530, cg27221688 and cg24099023). The two query probes (*) are fully unmethylated across all PDX samples, suggesting no association between these and meRAD51C in the meRAD51C PDX models.*

Only two non-*BRCA1* CpG hits appeared in the me*BRCA1* differential methylation analysis (cg17574785 and cg16463564), one of which is proximal to the *BRCA1* promoter, and the other was not associated with any genes. As the primary objective of these analyses was to find broader patterns of methylation that are consistently associated with *BRCA1* promoter methylation in the majority of samples and could indicate underlying mechanisms of HR gene methylation initiation and maintenance, this analysis was also concluded at this point.

6.4.10 Searching for signatures: ICGC manual methylation analysis

Since the differential methylation analysis grouping samples by HR methylation state was unsuccessful, I attempted manual sub-setting of 450K array me*BRCA1* data that may detect more subtle gene signatures associated HR gene methylation. To do this, I manually defined all CpG probes that were differentially methylated between the two groups using the mean β-value for each CpG within the me*BRCA1* vs non-me*BRCA1* cancer samples. I extracted the CpG probes with a mean β-value difference over 0.15 between the two groups. I then used these CpG probes to perform a clustering analysis (heatmap.2 dendrogram using gplots in R), where 4 main clusters were identified (**Figure 6.30**). When highlighting the *BRCA1* samples within this clustering analysis, 10 samples fell in cluster 2, while 5 samples were in cluster 3 and 1 in cluster 4 (**Table 6.5**). By assessing the *BRCA1* methylation status of these samples in more detail, I found that cluster 2 samples generally appeared to be more methylated at the *BRCA1* locus than those in clusters 3 and 4 (**Figure 6.31**), and this was also observed at the 3 CpG probes associated with *BRCA1* gene silencing in the PDX data (cg24806953, cg04110421, cg26891576; **Figure 6.32**). It appeared that a signature associated with homozygous vs heterozygous *BRCA1* methylation had been identified. However, when I interrogated the reported tumour purity measurements for these same samples published in Patch et al., 2015, carefully ensuring that the same DNA sample had been used in both assays, I found that cluster 2 samples tended to have higher tumour purity that cluster 3 samples, while the cluster 4 sample had no tumour purity measurement available (**Table 6.5**).

This suggested that the clustering of the *BRCA1* methylated tumours was instead based mostly on their tumour purity, and not on a novel signature of *BRCA1* methylation zygosity. This tumour purity information was, however, useful in identifying patient tumour samples that may have heterozygous *BRCA1* methylation for further study and validation of the *BRCA1* methylation zygosity hypothesis (Kondrashova et al., 2018). The 450K array β values for the *BRCA1* CpG probes cg24806953, cg04110421, cg26891576 were retrieved and then divided by the tumour purity proportion to generate a β values normalized by tumour purity (**Table 6.6**).

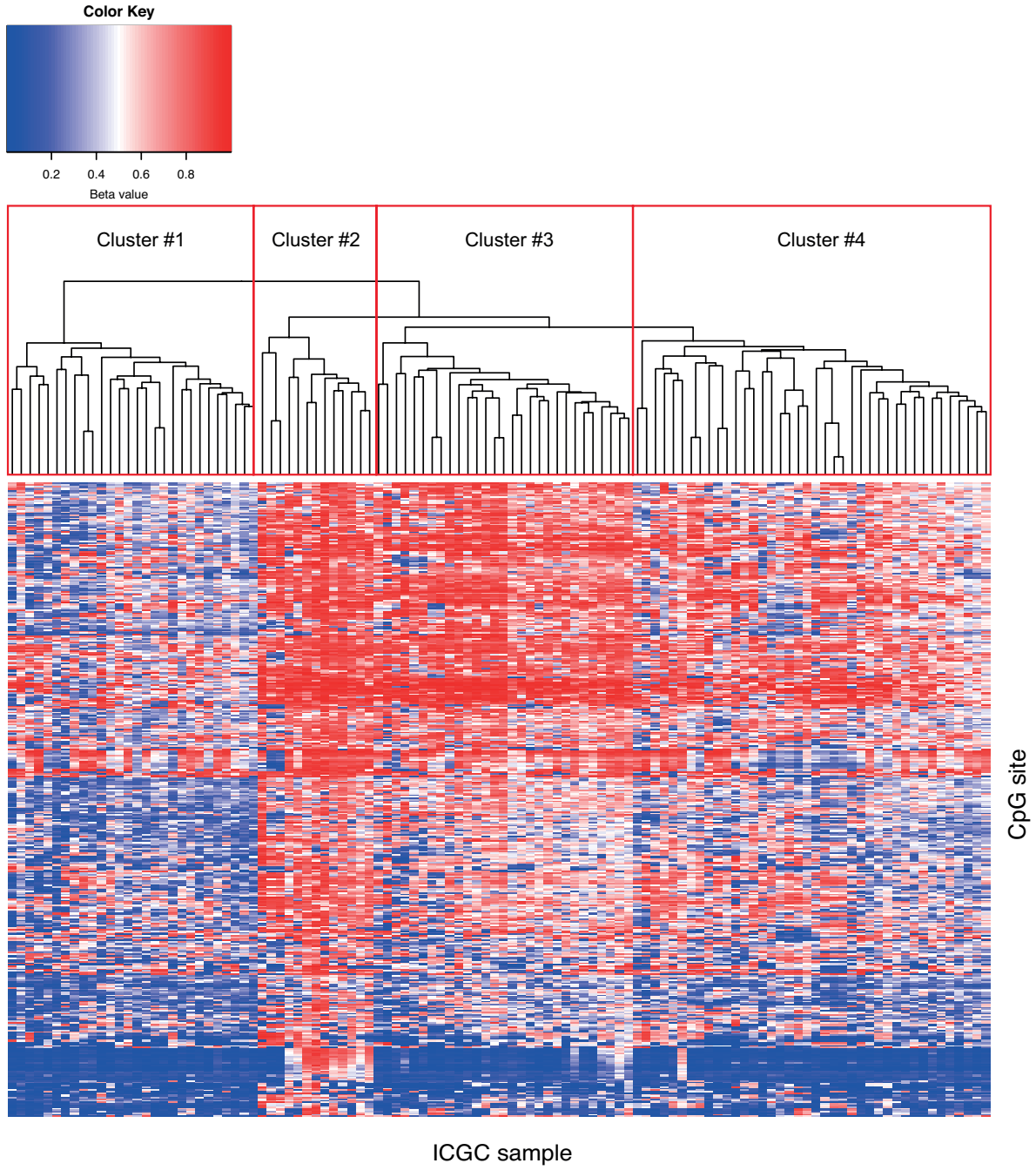


Figure 6.30. Four sample clusters identified in manual BRCA1 clustering analysis of ICGC samples.

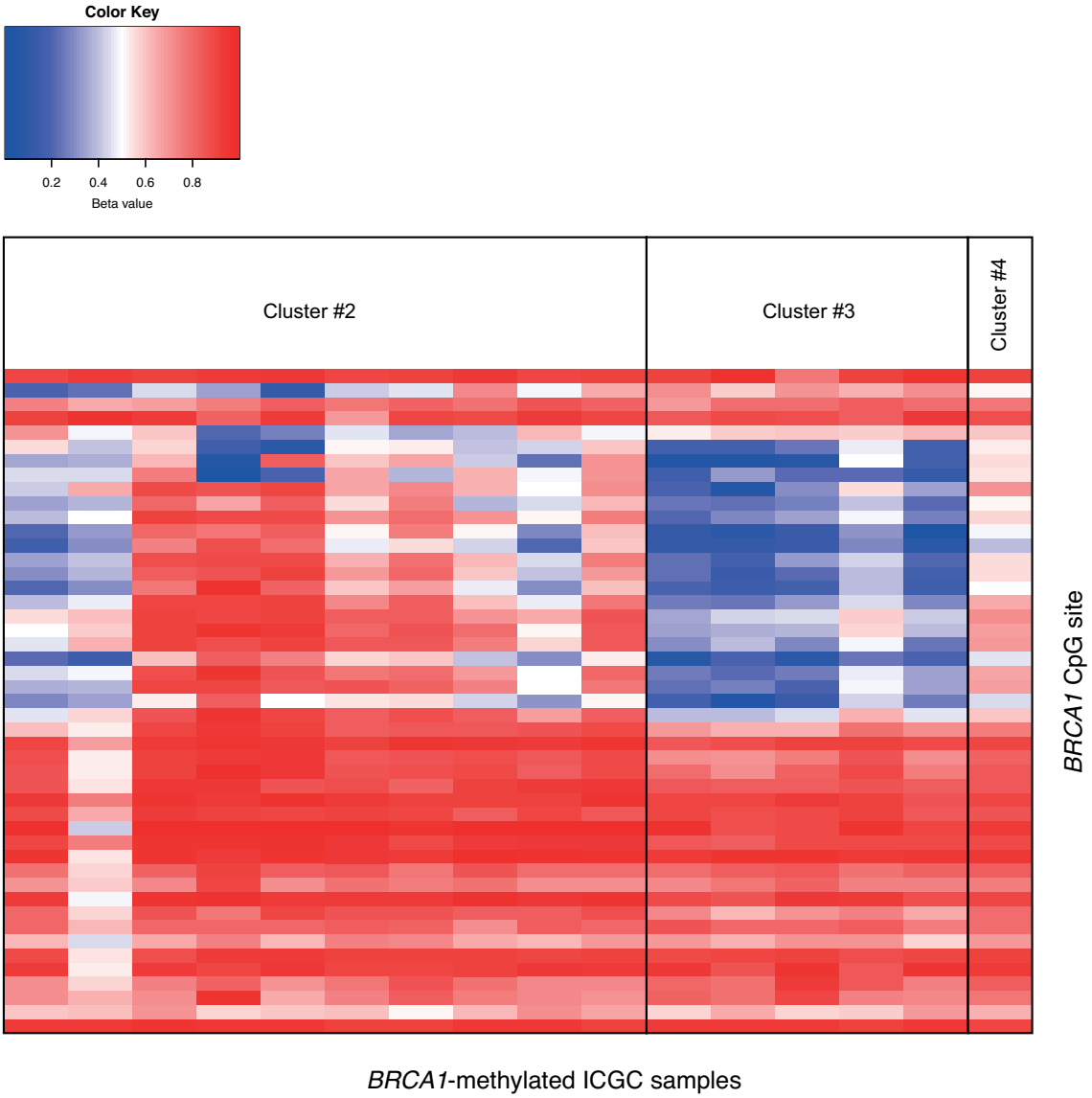


Figure 6.31. Apparent association between identified clusters and broad BRCA1 methylation patterns.

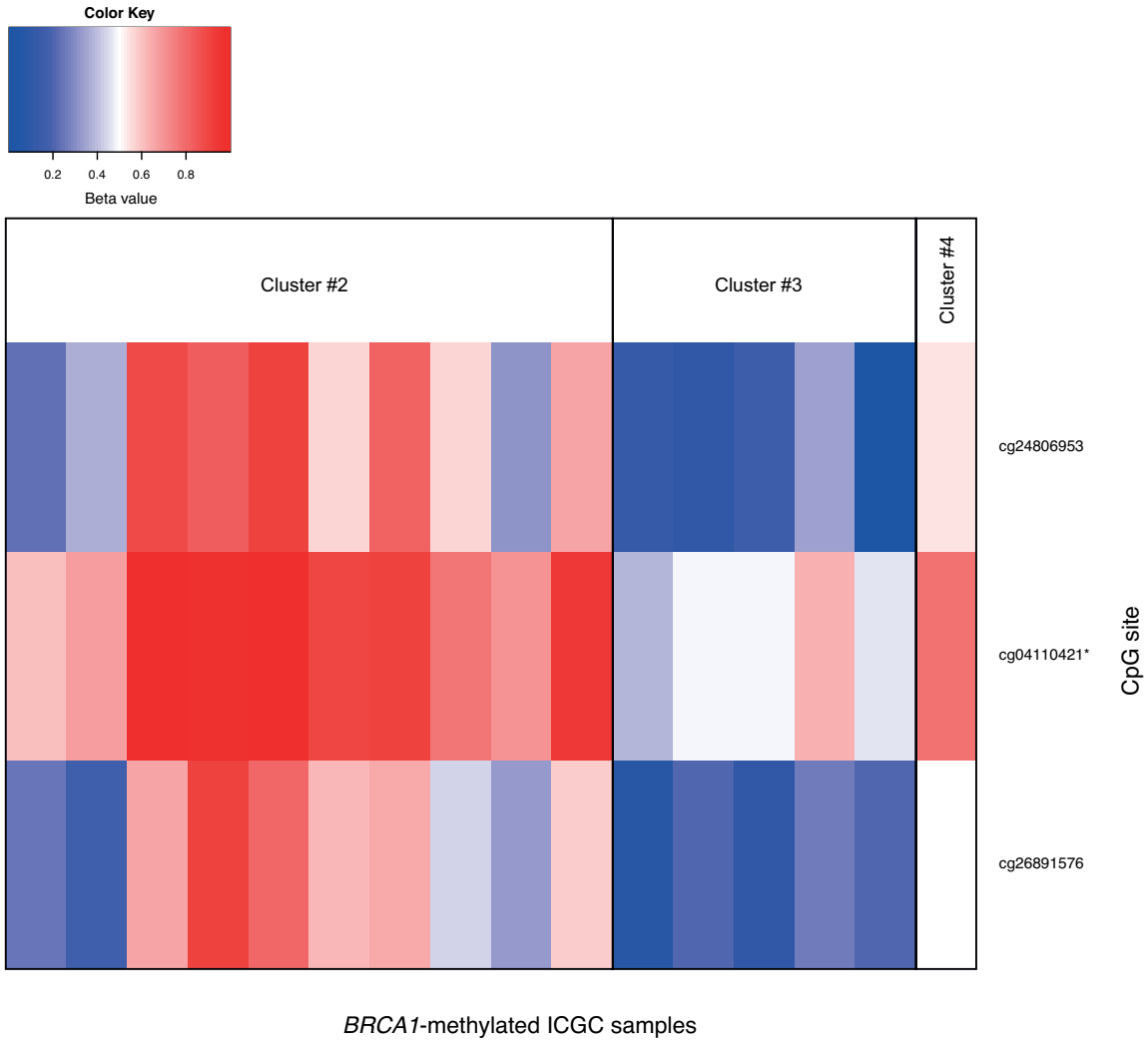


Figure 6.32. Apparent association between identified clusters and methylation of BRCA1 CpG probes relevant to gene silencing.

Table 6.5. BRCA1 clusters are associated with sample tumour purity rather than unique BRCA1-associated methylation signatures.

Cluster	Array_ID	AOCS_ID	Tumour type	Cisplatin response	Tumour source	Tumor Purity (%)
#2	GSM1606951_9445229094_R01C02	AOCS_158	primary	refractory	Primary Tumour	94.4
	GSM1606868_9298768174_R01C01	AOCS_064	relapse	resistant	Ascites	91
	GSM1606892_9298768178_R03C01	AOCS_093	relapse	resistant	Ascites	NA
	GSM1606891_9445229078_R06C01	AOCS_093	Primary	sensitive	Ascites	61
	GSM1606957_9445229158_R01C01	AOCS_164	primary	resistant	Primary Tumour	94.9
	GSM1606939_9341679080_R05C02	AOCS_144	primary	sensitive	Primary Tumour	84.1
	GSM1606903_9341679070_R01C02	AOCS_107	primary	resistant	Primary Tumour	92.7
	GSM1606918_9341679075_R02C02	AOCS_125	primary	sensitive	Primary Tumour	89.4
	GSM1606894_9298768178_R05C01	AOCS_094	relapse	resistant	Tumour Local Recurrence	87.7
	GSM1606895_9298768178_R06C01	AOCS_094	primary	sensitive	Primary Tumour	NA
#3	GSM1606862_9305216078_R01C02	AOCS_057	primary	resistant	Primary Tumour	68.5
	GSM1606869_9298768174_R02C01	AOCS_064	primary	sensitive	Primary Tumour	NA
	GSM1606920_9341679070_R06C02	AOCS_128	primary	resistant	Primary Tumour	49.7
	GSM1606855_9341679080_R01C01	AOCS_001	primary	refractory	Primary Tumour	63.5
	GSM1606893_9298768178_R04C01	AOCS_093	primary	sensitive	Primary Tumour	NA
#4	GSM1606888_9341679080_R05C01	AOCS_091	primary	sensitive	Primary Tumour	NA

Table 6.6. Potential BRCA1 methylation zygosity of AOCS patient samples based on 450K array results and tumour purity estimates.

*Sample information from Patch et al., 2015, while β values are from my MissMethyl analysis. Adjusted tumour purity: CpG b value divided by the tumour purity proportion.*Zygosity calculated assuming two copies BRCA1 in tumour, and based only on the adjusted CpG cg04110421 (^) value given this site is the only one covered by MS-HRM, where homozygous is adjusted b value >0.75, heterozygous is adjusted b value ≤0.75. 'Low confidence' describes samples where tumour purity is <70%.*

Array_ID	AOCS_ID	Tumour type	Cisplatin response	Tumour source	Beta value:			Tumor Purity (%)	Beta value adjusted for tumor purity:			Possible me*BRCA1* Zygosity*
					cg24806953	cg04110421	cg26891576		cg24806953	cg04110421^	cg26891576	
GSM1606951_9445229094_R01C02	AOCS_158	primary	refractory	Primary Tumour	0.28	0.58	0.29	94.4	0.30	0.62	0.31	Heterozygous
GSM1606868_9298768174_R01C01	AOCS_064	relapse	resistant	Ascites	0.39	0.63	0.23	91	0.43	0.69	0.25	Heterozygous
GSM1606891_9445229078_R06C01	AOCS_093	Primary	sensitive	Ascites	0.77	0.89	0.83	61	1.27	1.46	1.37	Homozygous
GSM1606957_9445229158_R01C01	AOCS_164	primary	resistant	Primary Tumour	0.83	0.90	0.75	94.9	0.88	0.95	0.79	Homozygous
GSM1606939_9341679080_R05C02	AOCS_144	primary	sensitive	Primary Tumour	0.55	0.83	0.59	84.1	0.66	0.98	0.71	Homozygous
GSM1606903_9341679070_R01C02	AOCS_107	primary	resistant	Primary Tumour	0.76	0.83	0.62	92.7	0.82	0.90	0.67	Homozygous
GSM1606918_9341679075_R02C02	AOCS_125	primary	sensitive	Primary Tumour	0.55	0.71	0.45	89.4	0.62	0.80	0.50	Homozygous
GSM1606894_9298768178_R05C01	AOCS_094	relapse	resistant	Tumour Local Recurrence	0.35	0.66	0.36	87.7	0.40	0.75	0.41	Heterozygous
GSM1606862_9305216078_R01C02	AOCS_057	primary	resistant	Primary Tumour	0.20	0.41	0.16	68.5	0.29	0.59	0.23	Low Confidence Heterozygous
GSM1606920_9341679070_R06C02	AOCS_128	primary	resistant	Primary Tumour	0.22	0.49	0.17	49.7	0.45	0.98	0.35	Low confidence Homozygous
GSM1606855_9341679080_R01C01	AOCS_001	primary	refractory	Primary Tumour	0.37	0.61	0.31	63.5	0.58	0.97	0.49	Low confidence Homozygous
GSM1606892_9298768178_R03C01	AOCS_093	relapse	resistant	Ascites	0.81	0.90	0.63	NA				
GSM1606895_9298768178_R06C01	AOCS_094	primary	sensitive	Primary Tumour	0.63	0.86	0.56	NA				
GSM1606869_9298768174_R02C01	AOCS_064	primary	sensitive	Primary Tumour	0.17	0.48	0.27	NA				
GSM1606893_9298768178_R04C01	AOCS_093	primary	sensitive	Primary Tumour	0.10	0.47	0.26	NA				
GSM1606888_9341679080_R05C01	AOCS_091	primary	sensitive	Primary Tumour	0.53	0.72	0.50	NA				

The predicted zygosity of these samples was based only on the adjusted β value for CpG cg04110421, given this site is the only one covered by MS-HRM, and the other two CpG probes had lower β values inconsistent with cg04110421. Samples with adjusted cg04110421 β values >0.7 were considered likely homozygous, with the assumption that *BRCA1* copy number was 2, while samples with adjusted cg04110421 β values <0.7 were considered likely heterozygous.

Samples with tumour purity estimates below 70% and lower β values were considered "low confidence" calls. Of the three high confidence heterozygous calls, two were from relapsed cisplatin-resistant tumours, and one was from a primary cisplatin-refractory tumour. Though not all predicted-homozygous tumours were cisplatin-sensitive, the only three cisplatin-sensitive tumours where zygosity could be calculated were predicted to be homozygous, which aligns with the findings of our *BRCA1* methylation project (Kondrashova et al., 2018). The three low confidence samples were from primary cisplatin-resistant/refractory tumours, with one predicted heterozygous (primary resistant) and the other two predicted to be homozygous. Sample AOCS_093 was reported as having a tumour purity of 61%, while the un-adjusted CpG β values were reported 0.77, 0.89 and 0.83, making the sample appear more-than homozygous. It is possible that the assumed tumour *BRCA1* gene copy number of 2 may be causing an overestimated methylation prediction.

6.5 Discussion

Genomic hypomethylation and hypermethylation are both features of HGSOC known to be associated with disease pathology and drug responses. We were interested in studying these features in our HGSOC PDX models, specifically focussing on the changes in global methylation that occur under treatment pressure (MAYO-PH039 and 134183), or differences between models that lost HR gene methylation readily (heterozygous me*BRCA1* PDX) compared to those that did not (homozygous me*BRCA1* PDX).

6.5.1 RAD51C and BRCA1 methylation profiles of PDX

The EPIC array data for *BRCA1* and *RAD51C* in these PDX models confirms what was observed in these models using other methylation assays (bisulfite sequencing, MS-HRM and ddPCR – Chapter 5 and (Kondrashova et al., 2018)), but also allows us to look more broadly as it includes other local CpG probes related to *BRCA1* and *RAD51C*. Interestingly, PDX 134183 has a broader region of DNA around the *RAD51C* promoter that is fully methylated compared to PDX MAYO-PH039, which has more heterogeneity. Given that DNA methylation can be associated with histone modifications, these differences in methylation patterns may suggest different underlying epigenetic mechanisms establishing or maintaining *RAD51C* promoter methylation in these models. The presence of various histone marks at the *RAD51C* promoter is discussed in more detail in Chapter 5 - Discussion, and will be investigated in these models in future.

6.5.2 Methylation profiles of other genes

Though I have produced methylation heatmaps for other genes that are known to be silenced by promoter methylation in ovarian cancer, it is not yet clear which CpG probes included by the EPIC array analysis are actually relevant for gene silencing. Clarification would require either literature searches to identify the most relevant CpG probes, or analysis of gene expression data for these models. RNAseq data is available for some models (PDX 134183, MAYO-PH039 and 134062) and could be analysed in future.

6.5.3 Characterisation of PDX by global methylation profiles

Through the assessment of global methylation profiles of each sample, it was found that some PDX models are more methylated than others. For example, MAYO-PH039 samples have higher global methylation when compared to PDX 134183 tumours. This may be associated with how differentiated/un-differentiated the tumours are, with less differentiated/more stem-like tumours presenting with a more "cancer-like" profile of global hypomethylation, while tumours with relatively hypermethylated profiles may be more differentiated and less stem-like (Ehrlich, 2009). Unfortunately we did not have access to the most appropriate normal tissue control, which would be PAX8 positive secretory cells from human fallopian tubes, currently considered the most-likely cell of origin for HGSOC (Perets et al., 2013). Fallopian tube controls would represent the global methylation profile of fully differentiated cells, and would be a good reference point in an analysis looking at how relatively undifferentiated the tumours are based on their methylomes. Another way to confirm the significance of these global methylation profiles would be to compare the RNAseq gene expression profiles of these PDX to assess the relative "stemness" of these models. This is something that would require additional RNA sequencing of several *BRCA1* methylated PDX models (PDX 134011, 134048 and 134169), and should be considered for future work on these mechanisms.

6.5.4 Global methylation losses in MAYO-PH039 with niraparib re-treatment

Differential methylation analysis of MAYO-PH039 untreated vs niraparib-treated samples revealed 256 top differentially-methylated CpG probes, and although most of these probes lost methylation following PARPi treatment, there were still some that gained methylation. This potentially implied that, instead of a change in underlying mechanisms of methylation maintenance for all cells within the tumour under PARPi pressure, there has been selection of one population of cells with its own global methylation profile, that is already lacking me*RAD51C*. This begged the question: is PARPi treatment causing these changes in methylation, or is it simply selecting for a pre-existing PARPi-resistant clone within the tumour?

PARPi have been shown to cause both global hypomethylation via reduced *DNMT* activity in some contexts (Cramer et al., 2019), but also global hypermethylation (possibly via increase *DNMT* expression) in other contexts (Zardo et al., 2002). It appears that both global

methylation losses and gains are observed in MAYO-PH039 post-PARPi, depending on the way the data is analysed. Though PDX MAYO-PH039 tumours presented subtle gains in methylation following PARPi treatment, methylation losses were predominantly detected in the most significantly differentially methylated CpG probes, which may be more biologically relevant given the greater shifts in β values at individual probes. It is, therefore, possible that PARPi activity was leading to direct changes in methylation in MAYO-PH039 tumours but, given that both gains and losses of methylation were observed in the differentially methylated CpG probes, some clonal selection for a rare subset of cells where this change has taken place could also occur. In parallel to this work, I investigated whether fully unmethylated *RAD51C* alleles were present at low frequency prior to PARPi treatment (presented in detail in Chapter 5). Using deep targeted bisulfite sequencing of the *RAD51C* promoter I searched for any fully unmethylated *RAD51C* alleles in untreated MAYO-PH039 tumours, as these would be the alleles selected for under PARPi pressure. I found no fully unmethylated alleles in the pre-treated tumour samples, suggesting that this was an acquired feature of the PARPi resistant MAYO-PH039 tumours. It is likely that these resistant cells were then selected for with each subsequent treatment.

6.5.5 Gene ontology analysis of MAYO-PH039 treated samples

The GO-term analysis of the 256 top differentially-methylated CpG probes revealed an enrichment of neuronal pathway genes related to CpG probes that lose methylation under niraparib pressure in MAYO-PH039, suggesting a possible activation of these pathways. Abnormal expression of specific neuronal pathway genes due to methylation changes has previously been reported as a feature of ovarian oncogenesis (Bruening et al., 2000; Czekierdowski et al., 2006; Gupta et al., 2003). Global hypomethylation of neuronal-system genes has also been reported as a feature of breast cancers in younger women, where it was postulated that they may play a role in modulating the tumour microenvironment(Oltra et al., 2019; Venkatesh et al., 2017). However, this study in breast cancer also reported hypomethylation of genes related to matrix organisation and cell communication(Oltra et al., 2019), while our GO term analysis instead revealed hypermethylation, and possible silencing, of genes within these pathways. Silencing of cell adhesion molecules, such as tumour suppressor E-cadherin, is a critical feature of epithelial-mesenchymal transition (EMT) (Larue et al., 2005), and suggests that the population of MAYO-PH039 cells selected for under PARPi pressure may have been less differentiated than those present in the untreated tumours. The

best way to confirm this would be to interrogate the RNAseq data of these MAYO-PH039 samples, to confirm silencing or activation of genes with differential methylation, or by searching for a mesenchymal signature in the post-PARPi tumours. This is something that could be done in collaboration with the Kaufmann group (Mayo clinic) in future.

Another question that arises from these experiments is whether the MAYO-PH039 cell population selected for under PARPi pressure is pre-existing, or whether PARPi induce these changes in cells. This could be investigated by repeating the EPIC array experiment on a new set of PH039 samples where me*RAD51C* has been lost following PARPi. If the observed global methylation patterns are reproduced exactly in this second set of samples, this would suggest selection of a very rare clone that is undetectable by sequencing (see section 5.4.10 of chapter 5). On the other hand, if the methylation changes are similar but not exactly the same, this would indicate changes in biologically relevant pathways that occur either following PARPi or with loss of me*RAD51C* (restored HR DNA repair). If the methylation changes are completely different, this may suggest that the observed changes were random effects of PARPi/me*RAD51C* loss on the epigenome.

6.5.6 Differential methylation analysis of homozygous vs heterozygous BRCA1 methylated PDX

No trends in global methylation related to *BRCA1* methylation zygosity could be discerned, possibly because there were not enough models used for comparison, with only 2 models per group. There was a much greater background signal in this analysis compared to the MAYO-PH039 analysis, where treated and untreated MAYO-PH039 samples were compared within the one PDX model. Comparing the me*BRCA1* heterozygous vs homozygous PDX models led to a much larger set of differentially methylated CpG hits identified (14,396 observations), compared to the same analysis performed in MAYO-PH039 (256 observations). This makes sense, given that each model has a unique methylome profile. Thus, to uncover any biologically relevant methylation patterns consistently associated with me*BRCA1* homozygous or heterozygous samples, this analysis should be performed in a much larger set of high tumour purity samples, where me*BRCA1* zygosity has been confidently assigned, or in models with matched samples with and without treatment (like MAYO-PH039). Unfortunately, we are unaware of such sample set existing at this point.

It should also be noted that another limitation of this type of differential methylation analysis is that homozygous to heterozygous methylation shifts may be missed, depending on LFC threshold values. Higher LFC thresholds, or lower LFC thresholds with added adjusted *p*-value thresholds, might exclude these transitions, though we know that heterozygous methylation can allow gene expression and is, therefore, biologically relevant. Low LFC thresholds on their own can result in too many observations, many of which may not be biologically significant. Thus the balance between false positives and false negatives will be an important consideration for future analyses, along with the use of larger sample sets which may remove a lot of background effects.

6.5.7 ICGC sample methylation analysis

Though in this instance both the MissMethyl and manual differential methylation analyses for *RAD51C* and *BRCA1* were not useful in identifying broader methylation signatures related to methylation of these HR genes, through this process I was able to uncover me*BRCA1* samples with possible heterozygous methylation using tumour purity measurements. The zygosity of these ICGC samples should, however, be validated using other methods that cover other critical *BRCA1* (and *RAD51C*) promoter probes, like MS-HRM or ddPCR, and gene expression analysis (using RNAseq data or qPCR). This has been done for 3 of the 4 me*RAD51C* ICGC samples presented in this Chapter (described Chapter 5), where MS-HRM and targeted bisulfite sequencing of the *RAD51C* promoter have revealed unique methylation patterns. Based on the targeted me*RAD51C* sequencing and corresponding tumour purity estimates, two samples were found to be homozygous for me*RAD51C,* while one was found to have heterozygous me*RAD51C* (see section 5.4.11 of Chapter 5). The me*BRCA1* samples described in this Chapter, however, will need to be sourced and analysed using these alternative methods in future.

It may also be interesting to return to the exploratory cluster analysis, given that cluster 1 contained high tumour purity samples, but none with me*BRCA1*, while cluster 2 contained high tumour purity samples including those with me*BRCA1*. This difference in clustering may be related to the methylation surrounding the *BRCA1* promoter region, but this would need to be confirmed in future, perhaps using a differential methylation analysis comparing the two cluster groups. Gene expression analysis (e.g. RNAseq) could also be used to assess gene expression changes in these clusters.

Another analysis that should be done on these datasets in future would be a reverse-search; checking the status of the differentially methylated CpG probes from the PH039/ 134183 differential methylation analyses in the four ICGC me*RAD51C* samples.

7 Discussion and Conclusions

7.1 Introduction

Prognosis for most women with OC remains poor, with dismal improvements in survival compared to other cancer types over the last few decades (Siegel et al., 2014). This can largely be attributed to several key factors related to this disease: late stage diagnosis, limited therapeutic options and a history of poor quality pre-clinical models being available for research.

Given limited improvements in early diagnosis and screening, much effort has been invested in validating new approaches for the treatment and management of late-stage metastatic OC. This includes work to find better surgical approaches, more effective first-line therapies, novel targeted therapeutics or drug combinations for relapsed disease. Since the 1970's, platinum-based chemotherapy was the only option available for all women diagnosed with OC, regardless of histological or molecular subtype. PARPi have shown great promise in the treatment of EOC, in particular in HRD and/or platinum-sensitive contexts. For example, the phase 3 SOLO1 trial (evaluating olaparib maintenance therapy in patients with newly diagnosed advanced ovarian cancers with germline or somatic mutation *BRCA*-mutations who had a complete or partial clinical response to platinum-based chemotherapy) demonstrated a median time to first subsequent therapy or death was 51.8 months in the olaparib group compared to 15.1 months in the placebo group (Friedlander et al., 2018). Such responses to targeted therapies in EOC are unprecedented. Although the cure-rates of PARPi cannot yet be determined as data is not yet available, results such as these are extremely encouraging.

Unfortunately, despite an understanding that PARPi illicit their effects via a mechanism of synthetic lethality, where loss of HR DNA repair and inhibition of PARP1 alone can be tolerated but are cytotoxic in combination, it is still impossible to predict whether a patient will respond to PARPi and how durable their response will be. Many patients treated with PARPi either do not respond at all, or do respond but eventually develop drug resistance. Thus, more work is required to understand the forces influencing PARPi response and how to improve the response durability in patients (Oza et al., 2015b; Tewari et al., 2019). Understanding the underlying mechanism of this synthetic lethality has been difficult to elucidate, with multiple different theories being put forward over the years (De Lorenzo et al., 2013; Scott et al., 2015).

These include increased DNA DSB's that overwhelm the cell, PARP1 trapping on DNA by PARPi leading to replication fork collapse, or increased dependence on genotoxic forms of DNA repair. It is possible that some or all of these mechanisms contribute to PARPi toxicity, but to improve PARPi responses and combat resistance, we need to know which mechanisms are most relevant and in what contexts.

Progress in uncovering these underlying mechanisms has been slow due to years of suboptimal or inaccurate pre-clinical models of disease, which persisted largely due to a generally limited understanding of ovarian cancer biology. For a long time, invasive EOC was widely considered a single disease, and was therefore treated as such in the laboratory and in the clinic, with little effort invested in histological or molecular stratification of subtypes. For example, a 2013 study revealed that several of the most published cell line models of HGSOC were actually more likely to be other EOC subtypes (endometrioid or clear cell) based on molecular profiling.

Ultimately, it was two crucial discoveries that led to a shift in the way this set of diseases was studied and treated in the clinic. The first was the finding that the ovarian surface epithelium, long considered to be the origin of all EOC, was in fact not likely to be the primary site of carcinogenesis. The second was uncovering the molecular heterogeneity that existed within EOC using novel massively parallel sequencing approaches and, recognising that these data could be used to define several distinct disease subtypes. We now understand that these subtypes of EOC all have unique molecular drivers, clinical outcomes and therapeutic vulnerabilities, thus these findings were critical for the advancement of EOC research and clinical management.

7.2 Outcomes of PhD project

HGSOC, the most common EOC subtype, is characterized by ubiquitous mutations in the *TP53* tumour suppressor gene and frequent defects in the HR DNA repair pathway. These features both contribute to a high degree of disease-promoting genomic instability in these cells, but they also act as an Achilles heel. HRD HGSOC is highly sensitive to treatment with DNA-damaging platinum chemotherapy, and has recently also been found to be vulnerable to treatment with PARPi. Though PARPi present as an ideal targeted therapy for HRD HGSOC, not all patients expected to respond do respond, and of those patients that do respond, most eventually develop resistance to therapy and relapse.

My PhD has focussed on both what makes a HGSOC tumour sensitive to PARPi, but also what makes it resistant. Due to the broad nature of these questions, my work has utilized *in vivo* and *in vitro* techniques for the detailed study of both genomic and epigenomic regulation of DNA repair in HGSOC.

7.2.1 PDX are a valuable resource for the study of PARPi sensitivity and resistance HGSOC

Given our appreciation of past errors in models used for pre-clinical studies of OC, HGSOC PDX and cell line models within our cohort have been comprehensively (and regularly) characterized molecularly, histologically, functionally and therapeutically. These have also been tracked using molecular identity checking protocols. This meticulous approach to managing the pre-clinical models enabled me to track samples and uncover novel lineages of our PDX that have developed either sporadically or following treatment pressure.

Working with a large cohort of HGSOC PDX models was important for ensuring recapitulation of the heterogeneity observed between tumours in the clinic. This heterogeneity was reflected in the platinum and PARPi responses of each model, tumour growth characteristics and molecular features. However, some PDX models within this cohort also enabled the study of intra-tumoural heterogeneity, where different tumour lineages within PDX were found to have different molecular features and treatment responses. Our PDX cohort, thus, provides a robust, highly characterized, clinically relevant and renewable resource for the study of HGSOC, and has been used to elucidate multiple aspects of PARPi sensitivity and resistance (Kondrashova et al., 2017; Kondrashova et al., 2018; Topp et al., 2014).

Work carried out in my PhD has underscored the molecular complexity of HGSOC tumours, but also shed some light on some of the pathways and mechanisms that influence responses to PARPi. The HGSOC PDX cohort included a variety of HRD backgrounds with which to study effects of PARPi therapy *in vivo*, but also multiple putative mechanisms of PARPi resistance.

Through this work, secondary mutations in two post-chemotherapy PDX models were uncovered; 34931 (*BRCA2*-reversion) and 134143B (*RAD51C* reversions). Unfortunately, 134143B could not be expanded beyond T3 due to extremely slow tumour growth and could

not be followed up more extensively *in vivo*. PDX 34931, however, was expanded and has been shown to be refractory to both platinum and PARPi treatment *in vivo*. To our knowledge, these are the only existing characterized PDX models derived directly from patients with confirmed HR gene secondary mutations, making PDX 34931 a unique and powerful model to study therapeutics of potential utility in the "post-PARPi" space.

This model could be used to study novel therapies, either alone or in combination with PARPi. Indeed, some studies have reported that it is possible to re-sensitize HGSOC cell lines with HR reversions to PARPi using agents that target DNMT1 by inducing an HR defect via increased PARP1 trapping capacity, and accumulation of reactive oxygen species (ROS) and modulation of the ROS-cAMP/PKA metabolic signalling axis (Pulliam et al., 2018). Other studies have demonstrated that both HR competent and PARPi-resistant HRD tumour models can be sensitized to PARPi using Cyclin-Dependent Kinase (CDK) inhibitors by induction of a "BRCA-ness" phenotype (Johnson et al., 2011; Johnson et al., 2016). PDX 34931 would enable such combinations to be trialled *in vivo,* in a highly characterised model of PARPi resistance caused by reversion mutation.

Newly characterized PARPi resistant models could also be investigated further within our existing collaborations; for example, our work with the Pearson laboratory (Peter MacCallum Cancer Centre, VIC, AUS) testing compound CX-5461 in our PDX cohort. CX-5461 is an inhibitor of RNA polymerase I transcription of ribosomal RNA genes, which causes competition for proteins essential in replication stress response, leading to DNA damage involving replication fork collapse and degradation by MRE11. This drug is currently being tested in phase I clinical trials in haematological malignancies and solid tumours (Khot et al., 2019; Xu et al., 2017). CX-5461 has been shown to synergize with PARPi in our HRD HGSOC PDX model 134019, and exhibits single agent activity in our PARPi-resistant HRD PDX model 134062 (Sanij et al., 2020). However, as this compound has shown efficacy in both HRD and HR competent cell lines when combined with PARPi, it would be important to also test this combination in our HR-reverted PDX models such as 134011/134048 (heterozygous me*BRCA1*) and 34931 (*BRCA2* secondary mutation). Determining whether this combination can overcome HR reversion and PARPi resistance *in vivo* would be of high clinical relevance.

Our laboratory has also been investigating the CHK1 inhibitor SRA737 (Sierra Oncology) in our HR competent HGSOC PDX models, in collaboration with the Simpkins laboratory (University of Pennsylvania, PA, US). This drug has been shown to induce replication stress and synergize with PARPi to kill HGSOC cell line models with acquired PARPi resistance (Xu et al., 2018). Thus, our work focusses on overcoming PARPi-resistance in PDX models by testing either single-agent SRA737 or SRA737 in combination with PARPi. So far, single agent SRA737 has demonstrated impressive activity in several PDX models, while the PARPi combination work is ongoing.

The PARPi sensitive HGSOC PDX models within our cohort also have the potential to be driven to PARPi resistance *in vivo*. This approach has already been utilized in studies of *RAD51C* promoter methylation, but has potential in other PDX models with HR gene mutations. This includes the PDX expressing alternative isoforms of *BRCA1* that lack a portion of exon 11. *BRCA1* D11q mutant tumours have been shown to exhibit resistance to PARPi *in vitro* and *in vivo* (though this was using cell line xenografts) (Wang et al., 2016). Our two *BRCA1* D11q PDX models, 134056 and 134206, represent a more clinically relevant model of resistance than previously published models, given these PDX were engrafted without any prior *in vitro* manipulation.

The original lineage of PDX 134056 had mixed responses to PARPi. A PARPi-treated tumour from this lineage was transplanted to created two new lineages with different responses to PARPi – one sensitive (#56S) and one resistant (#56R). Interestingly, both lineages appeared to have increasing D11q expression with successive tumour passaging, though this was more pronounced in the PARPi resistant lineage. However, these differences in D11q levels were subtle, and may not be biologically significant at these levels. PDX 134206 was very cisplatin and PARPi sensitive and was found to have relatively low D11 expression. Though there are human tumour samples available for this patient following additional treatments (including PARPi), D11q transcript measurements in these would be complicated by contaminating normal tissue in the sample. One potential way to overcome this would be to perform a co-extraction of DNA and RNA from the same tumour piece, so that tumour purity and gene expression can be assessed on the same tissue sample, and this will be explored in future.

In addition, using rucaparib re-treatment to drive PARPi resistance in both PDX models will also be examined, as having *in vivo* models with high D11q expression would facilitate testing

of novel compounds with the potential to overcome this resistance mechanism (e.g. splicing inhibitors) (Wang et al., 2016). Other models that could be driven to PARPi resistance using *in vivo* re-treatments would be the two homozygous me*BRCA1* models, 134011 and 134062, which may lose me*BRCA1* and re-gain *BRCA1* expression if kept under PARPi treatment pressure for an extended number of cycles. The PARPi-sensitive *BRCA2*-mutant model 134019 would also be an interesting model for such re-treatment studies, as we may uncover some PARPi resistance mechanisms that are unique to *BRCA2*-mutant HGSOC, such as *CHD4* defects that enable replication fork stabilization under PARPi treatment.

An added advantage of driving PARPi resistance in these models is that we can then create a renewable resource for studying various resistance mechanisms by cryopreserving material from the resulting PARPi resistant tumours. This material can then be used to establish new PDX lineages, where specific features can be selected for (such as a particular mutation or drug response). This then expands the cohort of models available for study and enables new studies to be conducted.

7.2.2 Types of PARPi resistance mechanisms observed in PDX models

Interestingly, the only PARPi resistance mechanisms we have confirmed in our PDX cohort thus far have involved restoration of HR DNA repair. These include the PDX 34931 and 134143B secondary HR gene mutations, and heterozygous me*BRCA1* observed in PDX 134048 and 134169 in which loss of methylation had occurred, resulting in resistance to PARPi. Other potential PARPi resistance mechanisms that do not restore HR were detected, such as the low frequency *CHD4* mutations in two PDX 134019 tumours. However, these *CHD4* mutations were unique and isolated cases, and their impacts on PARPi responses could not be confirmed. The fact that one of these mutations occurred in a vehicle-treated sample suggests that this may have even been a passenger mutation. The zygosity of these defects also could not be determined, thus it is possible that these were heterozygous mutations that did not inactivate all copies of the *CHD4* gene.

The contribution of the *BRCA1* D11q isoform in causing PARPi resistance in PDX 134056 lineages and PDX 134206 also remains to be established. Though there were some subtle differences in D11q expression between the resistant #56R and sensitive #56S lineages of

134056, these were so minimal that they were unlikely to be restoring HR repair and enabling PARPi resistance.

Although of potential functional interest, there were no core C-NHEJ pathway mutations detected in any of the PDX samples screened. There appeared to be C-NHEJ protein losses observed in some tumours based on WB and IHC, however these measurements were found to be inconsistent within PDX and even within tumour samples. Given that no C-NHEJ mutations were detected in PDX screening, or in the PARPi-resistance CRISPR screen of PEO1, it is likely that these changes were due to heterogeneous spatial/temporal expression of these proteins within tumour samples rather than sustained/permanent defects or losses of these proteins. Indeed, *in vitro* work using the PEO1A2 cell line suggested that haploinsufficiency of the C-NHEJ protein Artemis contributed to rucaparib resistance, but complete knockout of Artemis was not possible. Such reversible mechanisms of PARPi resistance may be more difficult to track and directly link to PARPi resistance, though they may still be relevant.

Thus, from these PDX cohort studies, it appears that HR-restoring mechanisms may be the more common form of platinum and PARPi resistance mechanism in the clinic. Development of a simple and robust test for measure of HR capacity of patient tumour cells would, therefore, be extremely valuable for predicting PARPi responses and monitoring patients for development of PARPi resistance mechanisms. Given that genomic scarring and mutational signatures give a historical measure of DNA repair defects in tumours, these are not ideal for measuring the present state of active HR DNA repair in tumour cells. RAD51 foci are also difficult to measure in patient tumour samples that have been fixed or frozen (the most common methods of preserving patient tissue samples). For such cases, co-staining with gH2AX would be critical to assess the presence of DNA damage in cases where RAD51 repair foci are absent. In cases with no gH2AX foci and no RAD51 foci, HR capacity could not be properly determined. Even for cases where fresh samples are available, irradiation (to induce DNA damage) and processing of tissues before fixation and immunofluorescent staining of each sample would be time-intensive and not very scalable. Consequently, new biomarkers of active HR DNA repair need to be investigated.

Furthermore, it is clear from my work in these PDX models that approvals of PARPi in later treatment lines are, theoretically, less likely to be successful than using them in the first-line maintenance setting. The majority of PARPi-refractory HRD PDX were derived from patients

who had undergone multiple lines of platinum chemotherapy (134048, 134169, 23133, 34931). PARPi were more effective in tumours that had not been exposed to multiple lines of platinum chemotherapy, where HR-restoring resistance mechanisms were acquired and selected for. This is supported by clinical trials of PARPi in the first-line, where exciting data shows unprecedented prolongation of PFS and TFST (Coleman et al., 2019; González-Martín et al., 2019; Moore et al., 2018; Ray-Coquard et al., 2019).

7.2.3 Genome-wide PARPi resistance CRISPR screens may uncover novel biological aspects of PARPi action

The PARP1-resistance CRISPR screen performed on the PEO1 (*BRCA2*-mutant) cell line in this project has already provided some valuable information regarding mechanisms of PARPi action, as described below. Furthermore, the two additional cell line screens (*BRCA1* mutation/methylation) that have been optimized, but not yet completed, will provide novel data but also add valuable insight into the results of the initial screen. We have chosen to study these three cell lines as we expect them to complement one another by allowing us to look for hits specific to each cell line/HRD context and some which will be common across all three cell lines/HR defects.

PARP1 was one of the most significant hits in the PEO1 CRISPR screen and has been reported as a PARPi resistance mechanisms in the past. Interestingly, *PARP1* mutations have not been observed in any HGSOC PDX models screened thus far. Thus, it is important to remember that, although these may be true resistance mechanisms, their frequency in the clinic is the ultimate indicator of how relevant these are for patients with PARPi resistance. Nonetheless, such hits are extremely useful for our understanding of biological mechanisms of PARPi action. The fact that *PARP1* was a top hit in this screen strongly supports the PARP1-trapping and replication-fork stabilization model of PARPi action, where the PARP1 protein is required for PARPi toxicity. Other significant hits, such as *KDM1A* and *BPTF,* have not been reported in the context of PARPi resistance previously, and may provide exciting novel insights into PARPi action during their functional validation.

These screens may also allow us to uncover novel targets which, when inactivated, synergize with PARPi in a *BRCA2*-mutant background. For example, the depleted gene hit, Histone PARylation Factor 1 (*HPF1*), where its loss appears to not be tolerated in PEO1 cells treated

with PARPi. Indeed, *HPF1* is an especially exciting hit, as its loss has been shown to sensitize cells to PARPi in other studies (Gibbs-Seymour et al., 2016). Unfortunately, there are currently no chemical inhibitors available for *HPF1*, although further validation of this target for PARPi synergy may justify the development of such compounds in future. Knock-down of *HPF1* will be an important first experimental step to determine whether this could represent a potential combination therapeutic for the clinic.

Another aspect to validation of these hits involves looking at whether they occur in other HRD contexts or whether they are unique to *BRCA2*-mutant HGSOC. This will be investigated through the additional CRISPR screens in *BRCA1*-mutated/methylated models (UWB1.289 and WEHI-CS62 respectively) but can also be tested directly in the other HGSOC cell lines within our cohort (including the PEO4 *RAD51C* and *RAD51D*-KO cell lines).

These two future CRISPR screens may also reveal novel hits that were not detected in the PEO1 screen. This is especially true for the unique *BRCA1*-methylated WEHI-CS62 cell line, where we would expect to observe hits that cause loss of *BRCA1* methylation, such as defects in DNA methyltransferases. Such hits may provide clues as to how to stabilize methylation in this model. These could then be tested directly in both the me*BRCA1* and me*RAD51C* models to see if these are broad mechanisms that apply to methylation of other HR genes.

7.2.4 RAD51C promoter methylation influences PARPi responses

The work done during this project on HGSOC PDX models with me*RAD51C* has enabled extensive characterisation of methylation patterns at the *RAD51C* promoter, and clarification as to what these patterns mean for PARPi responses *in vivo*. It is now clear that both heterogenous and homogeneous patterns of me*RAD51C* cause HRD and vulnerability to PARPi-treatment. However, these me*RAD51C* patterns can be lost under PARPi or cisplatin pressure. This was shown to cause resistance in the MAYO-PH039 PDX and will soon be shown for PDX 134183 and WEHI-PH039 lineages, where unmethylated tumours have been transplanted for expansion in mice.

For this project, I have also developed a targeted assay for highly sensitive and comprehensive analysis of me*RAD51C*, which has been applied to both PDX samples and patient samples. This assay has the power to distinguish individual molecules at the *RAD51C* promoter and their

methylation patterns. The potential of this assay has been demonstrated in PDX samples, where me*RAD51C* loss in MAYO-PH039 samples was tracked and correlated with PARPi resistance. I also studied this in a series of patient samples and found an example of a heterozygous case of me*RAD51C* (AOCS #34059), proving that this can occur.

As the me*RAD51C* PDX models in our study only had a single copy of *RAD51C*, we could propose haplosufficiency of a single *RAD51C* copy given the PARPi resistance observed in MAYO-PH039 samples where methylation was lost. Thus, it is likely that this heterozygous methylation pattern in patient tumour #34059 would result in a single copy of unmethylated *RAD51C* that is sufficient to restore HR DNA repair and cause PARPi/platinum resistance. However, although this patient sample received neoadjuvant chemotherapy prior to the surgery and sample collection, it cannot be proven that this tumour had homozygous me*RAD51C* prior to treatment as there are no other tumour samples available. We were fortunate in our studies of me*BRCA1* zygosity to have archival, pre-screening and post-treatment samples available for most cases. Unfortunately, me*RAD51C* is a much rarer defect, and these samples are currently lacking for this study.

There is, however, potential to acquire such samples in future through clinical trials or additional collaborations. Our group is currently involved in the design of the EMBRACE clinical trial – a phase II trial of the PARPi olaparib in HRD metastatic breast and relapsed ovarian cancer without *BRCA*-mutations. This trial is currently recruiting patients, and our feedback has ensured testing of me*RAD51C* is included in the patient screening process. This will, hopefully, result in new me*RAD51C* cases where multiple tumour samples are collected both before and over the course of treatment. These samples will then be analysed using methods described in chapter 5 to identify tumours that have lost me*RAD51C* under treatment pressure, and potentially fresh material may be sourced and used to generate new PDX models for further pre-clinical studies.

7.2.5 Relationship between DNA methylation stability and underlying histone marks

Another important follow-up question regarding me*RAD51C* loss in our PDX samples is what underlying mechanisms are governing the stability or instability of this DNA methylation. Histone marks and DNA methylation are known to influence one another, with DNA methylation often being a mark of underlying repressive chromatin marks (Cedar et al., 2009).

A better understanding of the fundamental mechanisms governing *RAD51C* silencing in the me*RAD51C* PDX models may facilitate discovery of novel methods to enhance the stability of gene silencing, thereby leading to more durable PARPi responses (for example, inhibition of histone methyl-transferases or acetyl-transferases).

This could be investigated by testing whether there are differences in histone modifications in *RAD51C* promoter regions in PDX 134183 and WEHI-PH039 lineages, before and after methylation loss. I have already identified several histone marks that may of interest for such an experiment. For example, the EZH2 methyltransferase, which catalyses the formation of a di- or trimethyl mark on lysine 27 of Histone H3 (H3K27me3), has been shown to cause silencing of RAD51 family members, including *RAD51C*, when upregulated (Min et al., 2013; Zeidler et al., 2005). Other histone marks that have been reported to be associated with DNA methylation in some contexts include H3K4me1 and H3K9me3, and these could also be investigated if H3K27me is not detected (Du et al., 2015; Pisanic et al., 2017) as discussed in chapter 5, section 5.5.6.

7.3 Closing remarks

My PhD has focussed on elucidating mechanisms of PARPi sensitivity and resistance in HGSOC, which would in turn enable development of novel therapeutic strategies to enhance the durability of PARPi responses in the clinic and improve patient outcomes. As early diagnosis methods for ovarian cancer remain unreliable, management of advanced disease is crucial. PARPi are an exciting targeted therapy for HGSOC with HRD, given their high efficacy and limited side-effects. The unprecedented efficacy observed for PARPi in the first-line maintenance setting demonstrates that the majority of women should receive PARPi in that setting. However, although some patients will derive long-term benefits from such first-line maintenance PARPi therapy, many patients are likely to eventually develop PARPi resistance unless they receive appropriate combination first-line maintenance therapy, tailored to their HGSOC. Much work remains to be done to determine which combinations are appropriate to avert resistance to PARPi, for which HGSOC. Many women today have not received the advantage of first-line maintenance PARPi therapy and hence need other salvage therapies.

To study underlying PARPi-response biology, I have characterised and employed a range of highly clinically relevant models of disease, including both PDX and cell lines. From this work, the importance of HR-restoring mechanisms of resistance has been clearly demonstrated *in vivo*. This includes detection of HR secondary mutations, and the detailed study of HR gene methylation zygosity and its impacts on PARPi responses. My work has therefore shown that maintenance therapy is more likely to be successful in first remission rather than in subsequent remissions, when the chance of emergence of resistance mechanisms would be higher (such as reversion/secondary mutations or loss of methylation, for example). Furthermore, characterisation of existing models and creation of HR competent versions of these models creates a platform for further studies of these resistance mechanism and potential PARPi combination therapies to prevent development of resistance or to overcome resistance once it has developed. Other mechanisms of resistance observed *in vitro* using genome-wide PARPi-resistance CRISPR screens, remain to be detected or validated in our PDX cohort, but nonetheless provide important information on underlying mechanisms of PARPi action within HRD cells. These have also uncovered novel molecular targets that may potentially synergize with PARPi when inhibited in HRD cancer cells.

In future, the hope is that molecular characterisation of HGSOC will allow for selection of the most appropriate and effective targeted single-agent or combination therapies for each individual ovarian cancer patient, leading to reduced side-effects, better quality of life and improved overall survival. This will only be possible with continued high quality pre-clinical and clinical research into understanding and enhancing the effects of monotherapies and combination therapies for various ovarian cancer subtypes and molecular contexts. In this way, we may finally move closer to curing more individual women with advanced ovarian cancer, or managing ovarian cancer as a chronic disease rather than a terminal illness.

8 References

Aghajanian, C., Goff, B., Nycum, L. R., Wang, Y. V., Husain, A., & Blank, S. V. (2015). Final overall survival and safety analysis of OCEANS, a phase 3 trial of chemotherapy with or without bevacizumab in patients with platinum-sensitive recurrent ovarian cancer. *Gynecol Oncol, 139*(1), 10-16. doi:10.1016/j.ygyno.2015.08.004

Aguilar-Quesada, R., Munoz-Gamez, J. A., Martin-Oliva, D., Peralta, A., Valenzuela, M. T., Matinez-Romero, R.*, et al.* (2007). Interaction between ATM and PARP-1 in response to DNA damage and sensitization of ATM deficient cells through PARP inhibition. *BMC Mol Biol, 8*, 29. doi:10.1186/1471-2199-8-29

Ahmed, A. A., Etemadmoghadam, D., Temple, J., Lynch, A. G., Riad, M., Sharma, R.*, et al.* (2010). Driver mutations in TP53 are ubiquitous in high grade serous carcinoma of the ovary. *J Pathol, 221*(1), 49-56. doi:10.1002/path.2696

Alexandrov, L., Kim, J., Haradhvala, N. J., Huang, M. N., Ng, A. W., Boot, A.*, et al.* (2018). The repertoire of mutational signatures in human cancer. *bioRxiv*, 322859.

Alexandrov, L. B., Nik-Zainal, S., Wedge, D. C., Aparicio, S. A., Behjati, S., Biankin, A. V.*, et al.* (2013). Signatures of mutational processes in human cancer. *Nature, 500*(7463), 415-421. doi:10.1038/nature12477

AlHilli, M. M., Becker, M. A., Weroha, S. J., Flatten, K. S., Hurley, R. M., Harrell, M. I.*, et al.* (2016). In vivo anti-tumor activity of the PARP inhibitor niraparib in homologous recombination deficient and proficient ovarian carcinoma. *Gynecol Oncol, 143*(2), 379-388. doi:10.1016/j.ygyno.2016.08.328

Ali, R., Alabdullah, M., Alblihy, A., Miligy, I., Mesquita, K. A., Chan, S. Y.*, et al.* (2020). PARP1 blockade is synthetically lethal in XRCC1 deficient sporadic epithelial ovarian cancers. *Cancer letters, 469*, 124-133.

Alsop, K., Fereday, S., Meldrum, C., deFazio, A., Emmanuel, C., George, J.*, et al.* (2012). BRCA mutation frequency and patterns of treatment response in BRCA mutation-positive women with ovarian cancer: a report from the Australian Ovarian Cancer Study Group. *J Clin Oncol, 30*(21), 2654-2663. doi:10.1200/JCO.2011.39.8545

Amiable, C., Pochet, S., Padilla, A., Labesse, G., & Kaminski, P. A. (2013). N6-Substituted AMPs Inhibit Mammalian Deoxynucleotide N-Hydrolase DNPH1. *PloS one, 8*(11), e80755. doi:10.1371/journal.pone.0080755

Aryee, M. J., Jaffe, A. E., Corrada-Bravo, H., Ladd-Acosta, C., Feinberg, A. P., Hansen, K. D.*, et al.* (2014). Minfi: a flexible and comprehensive Bioconductor package for the analysis of Infinium DNA methylation microarrays. *Bioinformatics, 30*(10), 1363-1369.

Ashworth, A. (2008). A synthetic lethal therapeutic approach: poly(ADP) ribose polymerase inhibitors for the treatment of cancers deficient in DNA double-strand break repair. *J Clin Oncol, 26*(22), 3785-3790. doi:10.1200/JCO.2008.16.0812

Athuluri-Divakar, S. K., Vasquez-Del Carpio, R., Dutta, K., Baker, S. J., Cosenza, S. C., Basu, I.*, et al.* (2016). A Small Molecule RAS-Mimetic Disrupts RAS Association with Effector Proteins to Block Signaling. *Cell, 165*(3), 643-655. doi:10.1016/j.cell.2016.03.045

Au-Yeung, G., Lang, F., Azar, W. J., Mitchell, C., Jarman, K. E., Lackovic, K.*, et al.* (2017). Selective Targeting of Cyclin E1-Amplified High-Grade Serous Ovarian Cancer by Cyclin-Dependent Kinase 2 and AKT Inhibition. *Clin Cancer Res, 23*(7), 1862-1874. doi:10.1158/1078-0432.CCR-16-0620

Audeh, M. W., Carmichael, J., Penson, R. T., Friedlander, M., Powell, B., Bell-McGuinn, K. M.*, et al.* (2010). Oral poly(ADP-ribose) polymerase inhibitor olaparib in patients with

BRCA1 or BRCA2 mutations and recurrent ovarian cancer: a proof-of-concept trial. *Lancet, 376*(9737), 245-251. doi:10.1016/S0140-6736(10)60893-8

Bajrami, I., Frankum, J. R., Konde, A., Miller, R. E., Rehman, F. L., Brough, R.*, et al.* (2014). Genome-wide profiling of genetic synthetic lethality identifies CDK12 as a novel determinant of PARP1/2 inhibitor sensitivity. *Cancer Res, 74*(1), 287-297. doi:10.1158/0008-5472.CAN-13-2541

Baker, N. M., & Der, C. J. (2013). Cancer: Drug for an 'undruggable' protein. *Nature, 497*(7451), 577-578. doi:10.1038/nature12248

Balmana, J., Tung, N. M., Isakoff, S. J., Grana, B., Ryan, P. D., Saura, C.*, et al.* (2014). Phase I trial of olaparib in combination with cisplatin for the treatment of patients with advanced breast, ovarian and other solid tumors. *Ann Oncol, 25*(8), 1656-1663. doi:10.1093/annonc/mdu187

Banerjee, S., & Kaye, S. (2011). The role of targeted therapy in ovarian cancer. *Eur J Cancer, 47 Suppl 3*, S116-130. doi:10.1016/S0959-8049(11)70155-1

Bankert, R. B., Balu-Iyer, S. V., Odunsi, K., Shultz, L. D., Kelleher Jr, R. J., Barnas, J. L.*, et al.* (2011). Humanized mouse model of ovarian cancer recapitulates patient solid tumor progression, ascites formation, and metastasis. *PloS one, 6*(9), e24420.

Barber, L. J., Sandhu, S., Chen, L., Campbell, J., Kozarewa, I., Fenwick, K.*, et al.* (2013). Secondary mutations in BRCA2 associated with clinical resistance to a PARP inhibitor. *J Pathol, 229*(3), 422-429. doi:10.1002/path.4140

Beaufort, C. M., Helmijr, J. C., Piskorz, A. M., Hoogstraat, M., Ruigrok-Ritstier, K., Besselink, N.*, et al.* (2014). Ovarian cancer cell line panel (OCCP): clinical importance of in vitro morphological subtypes. *PloS one, 9*(9), e103988.

Bernards, S. S., Pennington, K. P., Harrell, M. I., Agnew, K. J., Garcia, R. L., Norquist, B. M.*, et al.* (2018). Clinical characteristics and outcomes of patients with BRCA1 or RAD51C methylated versus mutated ovarian carcinoma. *Gynecologic oncology, 148*(2), 281-285. doi:doi.org/10.1016/j.ygyno.2017.12.004

Berndt, N., Hamilton, A. D., & Sebti, S. M. (2011). Targeting protein prenylation for cancer therapy. *Nat Rev Cancer, 11*(11), 775-791. doi:10.1038/nrc3151

Berti, M., Ray Chaudhuri, A., Thangavel, S., Gomathinayagam, S., Kenig, S., Vujanovic, M.*, et al.* (2013). Human RECQ1 promotes restart of replication forks reversed by DNA topoisomerase I inhibition. *Nat Struct Mol Biol, 20*(3), 347-354. doi:10.1038/nsmb.2501

Bestor, T. H. (2000). The DNA methyltransferases of mammals. *Human Molecular Genetics, 9*(16), 2395-2402.

Betermier, M., Bertrand, P., & Lopez, B. S. (2014). Is non-homologous end-joining really an inherently error-prone process? *PLoS Genet, 10*(1), e1004086. doi:10.1371/journal.pgen.1004086

Bindra, R. S., Gibson, S. L., Meng, A., Westermark, U., Jasin, M., Pierce, A. J.*, et al.* (2005). Hypoxia-induced down-regulation of BRCA1 expression by E2Fs. *Cancer Research, 65*(24), 11597-11604.

Bindra, R. S., Schaffer, P. J., Meng, A., Woo, J., Måseide, K., Roth, M. E.*, et al.* (2004). Down-regulation of Rad51 and decreased homologous recombination in hypoxic cancer cells. *Molecular and cellular biology, 24*(19), 8504-8518.

Binkhathlan, Z., & Lavasanifar, A. (2013). P-glycoprotein inhibition as a therapeutic approach for overcoming multidrug resistance in cancer: current status and future perspectives. *Curr Cancer Drug Targets, 13*(3), 326-346. doi:10.2174/15680096113139990076

Bird, A., Taggart, M., Frommer, M., Miller, O. J., & Macleod, D. (1985). A fraction of the mouse genome that is derived from islands of nonmethylated, CpG-rich DNA. *Cell, 40*(1), 91-99.

Boboila, C., Oksenych, V., Gostissa, M., Wang, J. H., Zha, S., Zhang, Y., *et al.* (2012). Robust chromosomal DNA repair via alternative end-joining in the absence of X-ray repair cross-complementing protein 1 (XRCC1). *Proc Natl Acad Sci U S A, 109*(7), 2473-2478. doi:10.1073/pnas.1121470109

Boersma, V., Moatti, N., Segura-Bayona, S., Peuscher, M. H., van der Torre, J., Wevers, B. A., *et al.* (2015). MAD2L2 controls DNA repair at telomeres and DNA breaks by inhibiting 5' end resection. *Nature, 521*(7553), 537-540. doi:10.1038/nature14216

Bohgaki, M., Bohgaki, T., El Ghamrasni, S., Srikumar, T., Maire, G., Panier, S., *et al.* (2013). RNF168 ubiquitylates 53BP1 and controls its response to DNA double-strand breaks. *Proceedings of the National Academy of Sciences, 110*(52), 20982-20987. doi:10.1073/pnas.1320302111

Bollag, G., & McCormick, F. (1992). Ras regulation. NF is enough of GAP. *Nature, 356*(6371), 663-664. doi:10.1038/356663a0

Bonfiglio, J. J., Fontana, P., Zhang, Q., Colby, T., Gibbs-Seymour, I., Atanassov, I., *et al.* (2017). Serine ADP-Ribosylation Depends on HPF1. *Mol Cell, 65*(5), 932-940.e936. doi:10.1016/j.molcel.2017.01.003

Bookman, M. A. (2010). The addition of new drugs to standard therapy in the first-line treatment of ovarian cancer. *Ann Oncol, 21 Suppl 7*, vii211-217. doi:10.1093/annonc/mdq368

Bouchard, V. J., Rouleau, M., & Poirier, G. G. (2003). PARP-1, a determinant of cell survival in response to DNA damage. *Exp Hematol, 31*(6), 446-454. doi:10.1016/s0301-472x(03)00083-3

Bouwman, P., Aly, A., Escandell, J. M., Pieterse, M., Bartkova, J., van der Gulden, H., *et al.* (2010). 53BP1 loss rescues BRCA1 deficiency and is associated with triple-negative and BRCA-mutated breast cancers. *Nat Struct Mol Biol, 17*(6), 688-695. doi:10.1038/nsmb.1831

Bowtell, D. D., Bohm, S., Ahmed, A. A., Aspuria, P. J., Bast, R. C., Jr., Beral, V., *et al.* (2015). Rethinking ovarian cancer II: reducing mortality from high-grade serous ovarian cancer. *Nat Rev Cancer, 15*(11), 668-679. doi:10.1038/nrc4019

Bowtell, D. D. L. (2010). The genesis and evolution of high-grade serous ovarian cancer. *Nature Reviews Cancer, 10*(11), 803-808. doi:10.1038/nrc2946

Bram, E. E., Stark, M., Raz, S., & Assaraf, Y. G. (2009). Chemotherapeutic drug-induced ABCG2 promoter demethylation as a novel mechanism of acquired multidrug resistance. *Neoplasia (New York, N.Y.), 11*(12), 1359-1370. doi:10.1593/neo.91314

Brandeis, M., Frank, D., Keshet, I., Siegfried, Z., Mendelsohn, M., Temper, V., *et al.* (1994). Spl elements protect a CpG island from de novo methylation. *Nature, 371*(6496), 435-438.

Brandsma, I., & Gent, D. C. (2012). Pathway choice in DNA double strand break repair: observations of a balancing act. *Genome Integr, 3*(1), 9. doi:10.1186/2041-9414-3-9

Brosh, R., & Rotter, V. (2009). When mutants gain new powers: news from the mutant p53 field. *Nat Rev Cancer, 9*(10), 701-713. doi:10.1038/nrc2693

Brosh, R. M., Jr. (2013). DNA helicases involved in DNA repair and their roles in cancer. *Nat Rev Cancer, 13*(8), 542-558. doi:10.1038/nrc3560

Bruening, W., Giasson, B. I., Klein-Szanto, A. J., Lee, V. M. Y., Trojanowski, J. Q., & Godwin, A. K. (2000). Synucleins are expressed in the majority of breast and ovarian carcinomas and in preneoplastic lesions of the ovary. *Cancer: Interdisciplinary International Journal of the American Cancer Society, 88*(9), 2154-2163.

Bryant, H. E., Schultz, N., Thomas, H. D., Parker, K. M., Flower, D., Lopez, E., *et al.* (2005). Specific killing of BRCA2-deficient tumours with inhibitors of poly(ADP-ribose) polymerase. *Nature, 434*(7035), 913-917. doi:10.1038/nature03443

Buisson, R., Dion-Cote, A. M., Coulombe, Y., Launay, H., Cai, H., Stasiak, A. Z., *et al.* (2010). Cooperation of breast cancer proteins PALB2 and piccolo BRCA2 in stimulating homologous recombination. *Nat Struct Mol Biol, 17*(10), 1247-1254. doi:10.1038/nsmb.1915

Bunting, S. F., Callen, E., Wong, N., Chen, H. T., Polato, F., Gunn, A., *et al.* (2010). 53BP1 inhibits homologous recombination in Brca1-deficient cells by blocking resection of DNA breaks. *Cell, 141*(2), 243-254. doi:10.1016/j.cell.2010.03.012

Burma, S., Chen, B. P., & Chen, D. J. (2006). Role of non-homologous end joining (NHEJ) in maintaining genomic integrity. *DNA Repair (Amst), 5*(9-10), 1042-1048. doi:10.1016/j.dnarep.2006.05.026

Cameron, E. E., Baylin, S. B., & Herman, J. G. (1999). p15(INK4B) CpG island methylation in primary acute leukemia is heterogeneous and suggests density as a critical factor for transcriptional silencing. *Blood, 94*(7), 2445-2451.

Cancer Genome Atlas Research, N., Kandoth, C., Schultz, N., Cherniack, A. D., Akbani, R., Liu, Y., *et al.* (2013). Integrated genomic characterization of endometrial carcinoma. *Nature, 497*(7447), 67-73. doi:10.1038/nature12113

Candido-dos-Reis, F. J., Song, H., Goode, E. L., Cunningham, J. M., Fridley, B. L., Larson, M. C., *et al.* (2015). Germline mutation in BRCA1 or BRCA2 and ten-year survival for women diagnosed with epithelial ovarian cancer. *Clin Cancer Res, 21*(3), 652-657. doi:10.1158/1078-0432.CCR-14-2497

Carey, J. P., Karakas, C., Bui, T., Chen, X., Vijayaraghavan, S., Zhao, Y., *et al.* (2018). Synthetic lethality of PARP inhibitors in combination with MYC blockade is independent of BRCA status in triple-negative breast cancer. *Cancer Research, 78*(3), 742-757.

Carrano, A. C., Eytan, E., Hershko, A., & Pagano, M. (1999). SKP2 is required for ubiquitin-mediated degradation of the CDK inhibitor p27. *Nat Cell Biol, 1*(4), 193-199. doi:10.1038/12013

Catteau, A., Harris, W. H., Xu, C. F., & Solomon, E. (1999). Methylation of the BRCA1 promoter region in sporadic breast and ovarian cancer: correlation with disease characteristics. *Oncogene, 18*(11), 1957-1965. doi:10.1038/sj.onc.1202509

Ceccaldi, R., Liu, J. C., Amunugama, R., Hajdu, I., Primack, B., Petalcorin, M. I., *et al.* (2015). Homologous-recombination-deficient tumours are dependent on Poltheta-mediated repair. *Nature, 518*(7538), 258-262. doi:10.1038/nature14184

Ceccaldi, R., Rondinelli, B., & D'Andrea, A. D. (2016). Repair Pathway Choices and Consequences at the Double-Strand Break. *Trends Cell Biol, 26*(1), 52-64. doi:10.1016/j.tcb.2015.07.009

Cedar, H., & Bergman, Y. (2009). Linking DNA methylation and histone modification: patterns and paradigms. *Nature Reviews Genetics, 10*(5), 295-304.

Chan, N., & Bristow, R. G. (2010). "Contextual" synthetic lethality and/or loss of heterozygosity: tumor hypoxia and modification of DNA repair. *Clinical Cancer Research, 16*(18), 4553-4560.

Chang, H. H., Watanabe, G., & Lieber, M. R. (2015). Unifying the DNA end-processing roles of the artemis nuclease: Ku-dependent artemis resection at blunt DNA ends. *J Biol Chem, 290*(40), 24036-24050. doi:10.1074/jbc.M115.680900

Chang, X., Monitto, C. L., Demokan, S., Kim, M. S., Chang, S. S., Zhong, X., *et al.* (2010). Identification of hypermethylated genes associated with cisplatin resistance in human cancers. *Cancer Research, 70*(7), 2870-2879.

Chen, C., Ge, J., Lu, Q., Ping, G., Yang, C., & Fang, X. (2015). Expression of Lysine-specific demethylase 1 in human epithelial ovarian cancer. *J Ovarian Res, 8*, 28. doi:10.1186/s13048-015-0155-1

Chen, L., Nievera, C. J., Lee, A. Y., & Wu, X. (2008). Cell cycle-dependent complex formation of BRCA1.CtIP.MRN is important for DNA double-strand break repair. *J Biol Chem, 283*(12), 7713-7720. doi:10.1074/jbc.M710245200

Cheon, J. Y., Mozersky, J., & Cook-Deegan, R. (2014). Variants of uncertain significance in BRCA: a harbinger of ethical and policy issues to come? *Genome Med, 6*(12), 121. doi:10.1186/s13073-014-0121-3

Chiang, J. W., Karlan, B. Y., & Baldwin, R. L. (2006). BRCA1 promoter methylation predicts adverse ovarian cancer prognosis. *Gynecologic oncology, 101*(3), 403-410.

Clements, K. E., Thakar, T., Nicolae, C. M., Liang, X., Wang, H. G., & Moldovan, G. L. (2018). Loss of E2F7 confers resistance to poly-ADP-ribose polymerase (PARP) inhibitors in BRCA2-deficient cells. *Nucleic Acids Res, 46*(17), 8898-8907. doi:10.1093/nar/gky657

Cohen, J. D., Li, L., Wang, Y., Thoburn, C., Afsari, B., Danilova, L.*, et al.* (2018). Detection and localization of surgically resectable cancers with a multi-analyte blood test. *Science, 359*(6378), 926-930. doi:10.1126/science.aar3247

Coleman, R. L., Fleming, G. F., Brady, M. F., Swisher, E. M., Steffensen, K. D., Friedlander, M.*, et al.* (2019). Veliparib with First-Line Chemotherapy and as Maintenance Therapy in Ovarian Cancer. *New England Journal of Medicine, 381*(25), 2403-2415. doi:10.1056/NEJMoa1909707

Coleman, R. L., Oza, A. M., Lorusso, D., Aghajanian, C., Oaknin, A., Dean, A.*, et al.* (2017). Rucaparib maintenance treatment for recurrent ovarian carcinoma after response to platinum therapy (ARIEL3): a randomised, double-blind, placebo-controlled, phase 3 trial. *Lancet, 390*(10106), 1949-1961. doi:10.1016/S0140-6736(17)32440-6

Colicchia, V., Petroni, M., Guarguaglini, G., Sardina, F., Sahún-Roncero, M., Carbonari, M.*, et al.* (2017). PARP inhibitors enhance replication stress and cause mitotic catastrophe in MYCN-dependent neuroblastoma. *Oncogene, 36*(33), 4682-4691. doi:10.1038/onc.2017.40

Collins, C. S., Hong, J., Sapinoso, L., Zhou, Y., Liu, Z., Micklash, K.*, et al.* (2006). A small interfering RNA screen for modulators of tumor cell motility identifies MAP4K4 as a promigratory kinase. *Proceedings of the National Academy of Sciences of the United States of America, 103*(10), 3775-3780. doi:10.1073/pnas.0600040103

Collins, N., Wooster, R., & Stratton, M. R. (1997). Absence of methylation of CpG dinucleotides within the promoter of the breast cancer susceptibility gene BRCA2 in normal tissues and in breast and ovarian cancers. *Br J Cancer, 76*(9), 1150-1156. doi:10.1038/bjc.1997.526

Cramer, T., Rosenberg, T., Kisliouk, T., & Meiri, N. (2019). PARP Inhibitor Affects Long-term Heat-stress Response via Changes in DNA Methylation. *Neuroscience, 399*, 65-76. doi:doi.org/10.1016/j.neuroscience.2018.12.018

Cruz, C., Bustos, L., Gris, A., Palafox, M., Castroviejo, M., Llop, A.*, et al.* (2016). Abstract P4-07-05: PARP inhibition in breast and ovarian patient-derived tumor xenografts (PDX) harboring germline BRCA1/2 mutations unveils mechanisms of primary and acquired resistance that restore homologous recombination (HR). *Cancer Research, 76*(4 Supplement), P4-07-05-P04-07-05. doi:10.1158/1538-7445.Sabcs15-p4-07-05

Cseh, A. M., Fabian, Z., Quintana-Cabrera, R., Szabo, A., Eros, K., Soriano, M. E.*, et al.* (2019). PARP Inhibitor PJ34 Protects Mitochondria and Induces DNA-Damage Mediated Apoptosis in Combination With Cisplatin or Temozolomide in B16F10 Melanoma Cells. *Frontiers in Physiology, 10*(538). doi:10.3389/fphys.2019.00538

Cunningham, J. M., Cicek, M., Larson, N., Davila, J., Wang, C., Larson, M.*, et al.* (2014). Clinical characteristics of ovarian cancer classified by BRCA1, BRCA2, and RAD51C status. *Scientific Reports, 4*, 4026.

Czekierdowski, A., Czekierdowska, S., Wielgos, M., Smolen, A., Kaminski, P., & Kotarski, J. (2006). The role of CpG islands hypomethylation and abnormal expression of neuronal protein synuclein-γ (SNCG) in ovarian cancer. *Neuroendocrinology Letters, 27*(3), 381-386.

Dai, C. H., Chen, P., Li, J., Lan, T., Chen, Y. C., Qian, H.*, et al.* (2016). Co-inhibition of pol theta and HR genes efficiently synergize with cisplatin to suppress cisplatin-resistant lung cancer cells survival. *Oncotarget, 7*(40), 65157-65170. doi:10.18632/oncotarget.11214

Dantzer, F., Schreiber, V., Niedergang, C., Trucco, C., Flatter, E., De La Rubia, G.*, et al.* (1999). Involvement of poly(ADP-ribose) polymerase in base excision repair. *Biochimie, 81*(1-2), 69-75. doi:10.1016/s0300-9084(99)80040-6

Davies, H., Glodzik, D., Morganella, S., Yates, L. R., Staaf, J., Zou, X.*, et al.* (2017). HRDetect is a predictor of BRCA1 and BRCA2 deficiency based on mutational signatures. *Nat Med, 23*(4), 517-525. doi:10.1038/nm.4292

Davis, A. J., & Chen, D. J. (2013). DNA double strand break repair via non-homologous end-joining. *Transl Cancer Res, 2*(3), 130-143. doi:10.3978/j.issn.2218-676X.2013.04.02

De Lorenzo, S. B., Patel, A. G., Hurley, R. M., & Kaufmann, S. H. (2013). The Elephant and the Blind Men: Making Sense of PARP Inhibitors in Homologous Recombination Deficient Tumor Cells. *Front Oncol, 3*, 228. doi:10.3389/fonc.2013.00228

De Vos, M., Schreiber, V., & Dantzer, F. (2012). The diverse roles and clinical relevance of PARPs in DNA damage repair: current state of the art. *Biochem Pharmacol, 84*(2), 137-146. doi:10.1016/j.bcp.2012.03.018

de Vries, A., Flores, E. R., Miranda, B., Hsieh, H. M., van Oostrom, C. T., Sage, J.*, et al.* (2002). Targeted point mutations of p53 lead to dominant-negative inhibition of wild-type p53 function. *Proc Natl Acad Sci U S A, 99*(5), 2948-2953. doi:10.1073/pnas.052713099

Dent, R. A., Lindeman, G. J., Clemons, M., Wildiers, H., Chan, A., McCarthy, N. J.*, et al.* (2013). Phase I trial of the oral PARP inhibitor olaparib in combination with paclitaxel for first- or second-line treatment of patients with metastatic triple-negative breast cancer. *Breast Cancer Res, 15*(5), R88. doi:10.1186/bcr3484

Dhillon, K. K., Swisher, E. M., & Taniguchi, T. (2011). Secondary mutations of BRCA1/2 and drug resistance. *Cancer Science, 102*(4), 663-669. doi:10.1111/j.1349-7006.2010.01840.x

Ding, L., Kim, H.-J., Wang, Q., Kearns, M., Jiang, T., Ohlson, C. E.*, et al.* (2018). PARP Inhibition Elicits STING-Dependent Antitumor Immunity in Brca1-Deficient Ovarian Cancer. *Cell Reports, 25*(11), 2972-2980.e2975. doi:10.1016/j.celrep.2018.11.054

Ding, X., Chaudhuri, A. R., Callen, E., Pang, Y., Biswas, K., Klarmann, K. D.*, et al.* (2016). Synthetic viability by BRCA2 and PARP1/ARTD1 deficiencies. *Nature Communications, 7*(1), 12425. doi:10.1038/ncomms12425

Dittami, G. M., Sethi, M., Rabbitt, R. D., & Ayliffe, H. E. (2012). Determination of mammalian cell counts, cell size and cell health using the Moxi Z mini automated cell counter. *Journal of visualized experiments : JoVE*(64), 3842. doi:10.3791/3842

Dittmer, D., Pati, S., Zambetti, G., Chu, S., Teresky, A. K., Moore, M.*, et al.* (1993). Gain of function mutations in p53. *Nat Genet, 4*(1), 42-46. doi:10.1038/ng0593-42

Dobrovic, A., & Kristensen, L. S. (2009). DNA methylation, epimutations and cancer predisposition. *Int J Biochem Cell Biol, 41*(1), 34-39. doi:10.1016/j.biocel.2008.09.006

Dobzhansky, T. (1946). Genetics of natural populations; recombination and variability in populations of Drosophila pseudoobscura. *Genetics, 31*, 269-290.

Doench, J. G., Fusi, N., Sullender, M., Hegde, M., Vaimberg, E. W., Donovan, K. F., *et al.* (2016). Optimized sgRNA design to maximize activity and minimize off-target effects of CRISPR-Cas9. *Nature Biotechnology, 34*(2), 184-191. doi:10.1038/nbt.3437

Domchek, S. M., Friebel, T. M., Singer, C. F., Evans, D. G., Lynch, H. T., Isaacs, C., *et al.* (2010). Association of risk-reducing surgery in BRCA1 or BRCA2 mutation carriers with cancer risk and mortality. *JAMA, 304*(9), 967-975. doi:10.1001/jama.2010.1237

Domcke, S., Sinha, R., Levine, D. A., Sander, C., & Schultz, N. (2013). Evaluating cell lines as tumour models by comparison of genomic profiles. *Nat Commun, 4*, 2126. doi:10.1038/ncomms3126

Drew, Y., Mulligan, E. A., Vong, W. T., Thomas, H. D., Kahn, S., Kyle, S., *et al.* (2011). Therapeutic potential of poly(ADP-ribose) polymerase inhibitor AG014699 in human cancers with mutated or methylated BRCA1 or BRCA2. *J Natl Cancer Inst, 103*(4), 334-346. doi:10.1093/jnci/djq509

du Bois, A., Lück, H.-J., Meier, W., Adams, H.-P., Möbus, V., Costa, S., *et al.* (2003). A Randomized Clinical Trial of Cisplatin/Paclitaxel Versus Carboplatin/Paclitaxel as First-Line Treatment of Ovarian Cancer. *JNCI: Journal of the National Cancer Institute, 95*(17), 1320-1329. doi:10.1093/jnci/djg036

Du, J., Johnson, L. M., Jacobsen, S. E., & Patel, D. J. (2015). DNA methylation pathways and their crosstalk with histone methylation. *Nature reviews. Molecular cell biology, 16*(9), 519-532. doi:10.1038/nrm4043

Dungrawala, H., Bhat, K. P., Le Meur, R., Chazin, W. J., Ding, X., Sharan, S. K., *et al.* (2017). RADX Promotes Genome Stability and Modulates Chemosensitivity by Regulating RAD51 at Replication Forks. *Mol Cell, 67*(3), 374-386.e375. doi:10.1016/j.molcel.2017.06.023

Durmus, S., Sparidans, R. W., van Esch, A., Wagenaar, E., Beijnen, J. H., & Schinkel, A. H. (2015). Breast cancer resistance protein (BCRP/ABCG2) and P-glycoprotein (P-GP/ABCB1) restrict oral availability and brain accumulation of the PARP inhibitor rucaparib (AG-014699). *Pharm Res, 32*(1), 37-46. doi:10.1007/s11095-014-1442-z

Dvorak, C. C., & Cowan, M. J. (2010). Radiosensitive severe combined immunodeficiency disease. *Immunology and allergy clinics of North America, 30*(1), 125-142. doi:10.1016/j.iac.2009.10.004

Edwards, S. L., Brough, R., Lord, C. J., Natrajan, R., Vatcheva, R., Levine, D. A., *et al.* (2008). Resistance to therapy caused by intragenic deletion in BRCA2. *Nature, 451*(7182), 1111-1115. doi:10.1038/nature06548

Ehrlich, M. (2002). DNA methylation in cancer: too much, but also too little. *Oncogene, 21*(35), 5400-5413. doi:10.1038/sj.onc.1205651

Ehrlich, M. (2009). DNA hypomethylation in cancer cells. *Epigenomics, 1*(2), 239-259. doi:10.2217/epi.09.33

El Botty, R., Coussy, F., Hatem, R., Assayag, F., Chateau-Joubert, S., Servely, J. L., *et al.* (2018). Inhibition of mTOR downregulates expression of DNA repair proteins and is highly efficient against BRCA2-mutated breast cancer in combination to PARP inhibition. *Oncotarget, 9*(51), 29587-29600. doi:10.18632/oncotarget.25640

Elias, K. M., Fendler, W., Stawiski, K., Fiascone, S. J., Vitonis, A. F., Berkowitz, R. S., *et al.* (2017). Diagnostic potential for a serum miRNA neural network for detection of ovarian cancer. *eLife, 6*, e28932. doi:10.7554/eLife.28932

Elkas, J. C., Baldwin, R. L., Pegram, M., Tseng, Y., Slamon, D., & Karlan, B. Y. (2002). A human ovarian carcinoma murine xenograft model useful for preclinical trials. *Gynecologic oncology, 87*(2), 200-206.

Erickson, B. K., Conner, M. G., & Landen, C. N., Jr. (2013). The role of the fallopian tube in the origin of ovarian cancer. *Am J Obstet Gynecol, 209*(5), 409-414. doi:10.1016/j.ajog.2013.04.019

Esteller, M. (2008). Epigenetics in Cancer. *New England Journal of Medicine, 358*(11), 1148-1159. doi:10.1056/NEJMra072067

Esteller, M., Silva, J. M., Dominguez, G., Bonilla, F., Matias-Guiu, X., Lerma, E.*, et al.* (2000). Promoter hypermethylation and BRCA1 inactivation in sporadic breast and ovarian tumors. *J Natl Cancer Inst, 92*(7), 564-569. doi:10.1093/jnci/92.7.564

Etemadmoghadam, D., Au-Yeung, G., Wall, M., Mitchell, C., Kansara, M., Loehrer, E.*, et al.* (2013a). Resistance to CDK2 inhibitors is associated with selection of polyploid cells in CCNE1-amplified ovarian cancer. *Clin Cancer Res, 19*(21), 5960-5971. doi:10.1158/1078-0432.CCR-13-1337

Etemadmoghadam, D., deFazio, A., Beroukhim, R., Mermel, C., George, J., Getz, G.*, et al.* (2009). Integrated Genome-Wide DNA Copy Number and Expression Analysis Identifies Distinct Mechanisms of Primary Chemoresistance in Ovarian Carcinomas. *Clinical Cancer Research, 15*(4), 1417-1427. doi:10.1158/1078-0432.Ccr-08-1564

Etemadmoghadam, D., Weir, B. A., Au-Yeung, G., Alsop, K., Mitchell, G., George, J.*, et al.* (2013b). Synthetic lethality between CCNE1 amplification and loss of BRCA1. *Proc Natl Acad Sci U S A, 110*(48), 19489-19494. doi:10.1073/pnas.1314302110

Fabbro, M., & Henderson, B. R. (2003). Regulation of tumor suppressors by nuclear-cytoplasmic shuttling. *Exp Cell Res, 282*(2), 59-69. doi:10.1016/s0014-4827(02)00019-8

Falconer, H., Yin, L., Gronberg, H., & Altman, D. (2015). Ovarian cancer risk after salpingectomy: a nationwide population-based study. *J Natl Cancer Inst, 107*(2). doi:10.1093/jnci/dju410

Farmer, H., McCabe, N., Lord, C. J., Tutt, A. N., Johnson, D. A., Richardson, T. B.*, et al.* (2005). Targeting the DNA repair defect in BRCA mutant cells as a therapeutic strategy. *Nature, 434*(7035), 917-921. doi:10.1038/nature03445

Feng, Z., Scott, S. P., Bussen, W., Sharma, G. G., Guo, G., Pandita, T. K.*, et al.* (2011). Rad52 inactivation is synthetically lethal with BRCA2 deficiency. *Proc Natl Acad Sci U S A, 108*(2), 686-691. doi:10.1073/pnas.1010959107

Findlay, G. M., Daza, R. M., Martin, B., Zhang, M. D., Leith, A. P., Gasperini, M.*, et al.* (2018). Accurate classification of BRCA1 variants with saturation genome editing. *Nature, 562*(7726), 217-222. doi:10.1038/s41586-018-0461-z

Fraser, M., Zhao, H., Luoto, K. R., Lundin, C., Coackley, C., Chan, N.*, et al.* (2012). PTEN deletion in prostate cancer cells does not associate with loss of RAD51 function: implications for radiotherapy and chemotherapy. *Clin Cancer Res, 18*(4), 1015-1027. doi:10.1158/1078-0432.CCR-11-2189

Friedlander, M., Moore, K., Colombo, N., Scambia, G., Kim, B. G., Oaknin, A.*, et al.* (2018). LBA3Maintenance olaparib following platinum-based chemotherapy in newly diagnosed patients (pts) with advanced ovarian cancer (OC) and a BRCA1/2 mutation (BRCAm): Phase III SOLO1 trial. *Annals of Oncology, 29*(suppl_9). doi:10.1093/annonc/mdy483.002

Friend, S. H., Bernards, R., Rogelj, S., Weinberg, R. A., Rapaport, J. M., Albert, D. M.*, et al.* (1986). A human DNA segment with properties of the gene that predisposes to retinoblastoma and osteosarcoma. *Nature, 323*(6089), 643-646. doi:10.1038/323643a0

Gagne, J. P., Hendzel, M. J., Droit, A., & Poirier, G. G. (2006). The expanding role of poly(ADP-ribose) metabolism: current challenges and new perspectives. *Curr Opin Cell Biol, 18*(2), 145-151. doi:10.1016/j.ceb.2006.02.013

Galan-Cobo, A., Pottetee, A., & Heymach, J. V. (2019). Abstract 3507: LKB1 deficiency and KEAP1/NRF2 pathway alterations as biomarkers of response for ATR and ATM inhibitors and other inhibitors of DNA damage response (DDR) in NSCLC. *Cancer Research, 79*(13 Supplement), 3507-3507. doi:10.1158/1538-7445.Am2019-3507

Gao, X., Gao, C., Liu, G., & Hu, J. (2016). MAP4K4: an emerging therapeutic target in cancer. *Cell & Bioscience, 6*(1), 56. doi:10.1186/s13578-016-0121-7

Gardiner-Garden, M., & Frommer, M. (1987). CpG islands in vertebrate genomes. *Journal of molecular biology, 196*(2), 261-282.

Garsed, D. W., Alsop, K., Fereday, S., Emmanuel, C., Kennedy, C. J., Etemadmoghadam, D.*, et al.* (2018). Homologous recombination DNA repair pathway disruption and retinoblastoma protein loss are associated with exceptional survival in high-grade serous ovarian cancer. *Clinical Cancer Research, 24*(3), 569-580.

Gaymes, T. J., Mohamedali, A. M., Patterson, M., Matto, N., Smith, A., Kulasekararaj, A.*, et al.* (2013). Microsatellite instability induced mutations in DNA repair genes CtIP and MRE11 confer hypersensitivity to poly (ADP-ribose) polymerase inhibitors in myeloid malignancies. *Haematologica, 98*(9), 1397-1406. doi:10.3324/haematol.2012.079251

Gebhard, C., Benner, C., Ehrich, M., Schwarzfischer, L., Schilling, E., Klug, M.*, et al.* (2010). General transcription factor binding at CpG islands in normal cells correlates with resistance to de novo DNA methylation in cancer cells. *Cancer Research, 70*(4), 1398-1407.

Gelmon, K. A., Hirte, H. W., Robidoux, A., Tonkin, K. S., Tischkowitz, M., Swenerton, K.*, et al.* (2010). Can we define tumors that will respond to PARP inhibitors? A phase II correlative study of olaparib in advanced serous ovarian cancer and triple-negative breast cancer. *Journal of Clinical Oncology, 28*(15_suppl), 3002-3002. doi:10.1200/jco.2010.28.15_suppl.3002

Gelmon, K. A., Tischkowitz, M., Mackay, H., Swenerton, K., Robidoux, A., Tonkin, K.*, et al.* (2011). Olaparib in patients with recurrent high-grade serous or poorly differentiated ovarian carcinoma or triple-negative breast cancer: a phase 2, multicentre, open-label, non-randomised study. *Lancet Oncol, 12*(9), 852-861. doi:10.1016/S1470-2045(11)70214-5

George, J., Alsop, K., Etemadmoghadam, D., Hondow, H., Mikeska, T., Dobrovic, A.*, et al.* (2013). Nonequivalent gene expression and copy number alterations in high-grade serous ovarian cancers with BRCA1 and BRCA2 mutations. *Clinical Cancer Research, 19*(13), 3474-3484.

Gibbs-Seymour, I., Fontana, P., Rack, J. G. M., & Ahel, I. (2016). HPF1/C4orf27 Is a PARP-1-Interacting Protein that Regulates PARP-1 ADP-Ribosylation Activity. *Mol Cell, 62*(3), 432-442. doi:10.1016/j.molcel.2016.03.008

Gilks, C. B. (2010). Molecular abnormalities in ovarian cancer subtypes other than high-grade serous carcinoma. *J Oncol, 2010*, 740968. doi:10.1155/2010/740968

Goff, B. A., Mandel, L. S., Drescher, C. W., Urban, N., Gough, S., Schurman, K. M.*, et al.* (2007). Development of an ovarian cancer symptom index. *Cancer, 109*(2), 221-227. doi:10.1002/cncr.22371

Gogola, E., Duarte, A. A., de Ruiter, J. R., Wiegant, W. W., Schmid, J. A., de Bruijn, R.*, et al.* (2018). Selective Loss of PARG Restores PARylation and Counteracts PARP Inhibitor-Mediated Synthetic Lethality. *Cancer Cell, 33*(6), 1078-1093 e1012. doi:10.1016/j.ccell.2018.05.008

González-Martín, A., Pothuri, B., Vergote, I., DePont Christensen, R., Graybill, W., Mirza, M. R.*, et al.* (2019). Niraparib in Patients with Newly Diagnosed Advanced Ovarian Cancer. *New England Journal of Medicine, 381*(25), 2391-2402. doi:10.1056/NEJMoa1910962

Goodarzi, A. A., Yu, Y., Riballo, E., Douglas, P., Walker, S. A., Ye, R., *et al.* (2006). DNA-PK autophosphorylation facilitates Artemis endonuclease activity. *EMBO J, 25*(16), 3880-3889. doi:10.1038/sj.emboj.7601255

Goodrich, D. W., Wang, N. P., Qian, Y. W., Lee, E. Y., & Lee, W. H. (1991). The retinoblastoma gene product regulates progression through the G1 phase of the cell cycle. *Cell, 67*(2), 293-302. doi:10.1016/0092-8674(91)90181-w

Gottipati, P., Vischioni, B., Schultz, N., Solomons, J., Bryant, H. E., Djureinovic, T., *et al.* (2010). Poly(ADP-ribose) polymerase is hyperactivated in homologous recombination-defective cells. *Cancer Res, 70*(13), 5389-5398. doi:10.1158/0008-5472.CAN-09-4716

Guillemette, S., Serra, R. W., Peng, M., Hayes, J. A., Konstantinopoulos, P. A., Green, M. R., *et al.* (2015). Resistance to therapy in BRCA2 mutant cells due to loss of the nucleosome remodeling factor CHD4. *Genes Dev, 29*(5), 489-494. doi:10.1101/gad.256214.114

Gupta, A., Godwin, A. K., Vanderveer, L., Lu, A., & Liu, J. (2003). Hypomethylation of the Synuclein γ Gene CpG Island Promotes Its Aberrant Expression in Breast Carcinoma and Ovarian Carcinoma. *Cancer Research, 63*(3), 664-673.

Gupta, R., Somyajit, K., Narita, T., Maskey, E., Stanlie, A., Kremer, M., *et al.* (2018). DNA Repair Network Analysis Reveals Shieldin as a Key Regulator of NHEJ and PARP Inhibitor Sensitivity. *Cell, 173*(4), 972-988.e923. doi:10.1016/j.cell.2018.03.050

He, Y. J., Meghani, K., Caron, M.-C., Yang, C., Ronato, D. A., Bian, J., *et al.* (2018). DYNLL1 binds to MRE11 to limit DNA end resection in BRCA1-deficient cells. *Nature, 563*(7732), 522-526. doi:10.1038/s41586-018-0670-5

Hegan, D. C., Lu, Y., Stachelek, G. C., Crosby, M. E., Bindra, R. S., & Glazer, P. M. (2010). Inhibition of poly (ADP-ribose) polymerase down-regulates BRCA1 and RAD51 in a pathway mediated by E2F4 and p130. *Proceedings of the National Academy of Sciences, 107*(5), 2201-2206.

Henneman, L., van Miltenburg, M. H., Michalak, E. M., Braumuller, T. M., Jaspers, J. E., Drenth, A. P., *et al.* (2015). Selective resistance to the PARP inhibitor olaparib in a mouse model for BRCA1-deficient metaplastic breast cancer. *Proc Natl Acad Sci U S A, 112*(27), 8409-8414. doi:10.1073/pnas.1500223112

Herrera, R. E., Makela, T. P., & Weinberg, R. A. (1996). TGF beta-induced growth inhibition in primary fibroblasts requires the retinoblastoma protein. *Mol Biol Cell, 7*(9), 1335-1342. doi:10.1091/mbc.7.9.1335

Higa, S., Yoshihama, M., Tanaka, T., & Kenmochi, N. (1999). Gene organization and sequence of the region containing the ribosomal protein genes RPL13A and RPS11 in the human genome and conserved features in the mouse genome. *Gene, 240*(2), 371-377.

Hitchins, M. P. (2015). Constitutional epimutation as a mechanism for cancer causality and heritability? *Nat Rev Cancer, 15*(10), 625-634. doi:10.1038/nrc4001

Hocsak, E., Szabo, V., Kalman, N., Antus, C., Cseh, A., Sumegi, K., *et al.* (2017). PARP inhibition protects mitochondria and reduces ROS production via PARP-1-ATF4-MKP-1-MAPK retrograde pathway. *Free Radical Biology and Medicine, 108*, 770-784. doi:doi.org/10.1016/j.freeradbiomed.2017.04.018

Holloman, W. K. (2011). Unraveling the mechanism of BRCA2 in homologous recombination. *Nat Struct Mol Biol, 18*(7), 748-754. doi:10.1038/nsmb.2096

Hopkins, T. A., Ainsworth, W. B., Ellis, P. A., Donawho, C. K., DiGiammarino, E. L., Panchal, S. C., *et al.* (2019). PARP1 Trapping by PARP Inhibitors Drives Cytotoxicity in Both Cancer Cells and Healthy Bone Marrow. *Mol Cancer Res, 17*(2), 409-419. doi:10.1158/1541-7786.MCR-18-0138

Howlader, N., Noone, A. M., Krapcho, M., Miller, D., Brest, A., Yu, M., *et al.* (2019). SEER Cancer Statistics Review, 1975-2016, National Cancer Institute. Bethesda, MD, https://seer.cancer.gov/csr/1975_2016/, based on November 2018 SEER data submission, posted to the SEER web site, April 2019.

Hsu, A. L., Kondrashova, O., Lunke, S., Love, C. J., Meldrum, C., Marquis-Nicholson, R., *et al.* (2015). AmpliVar: mutation detection in high-throughput sequence from amplicon-based libraries. *Hum Mutat, 36*(4), 411-418. doi:10.1002/humu.22763

Huang, H. J., Yee, J. K., Shew, J. Y., Chen, P. L., Bookstein, R., Friedmann, T., *et al.* (1988). Suppression of the neoplastic phenotype by replacement of the RB gene in human cancer cells. *Science, 242*(4885), 1563-1566. doi:10.1126/science.3201247

Huertas, P. (2010). DNA resection in eukaryotes: deciding how to fix the break. *Nat Struct Mol Biol, 17*(1), 11-16. doi:10.1038/nsmb.1710

Hunn, J., & Rodriguez, G. C. (2012). Ovarian cancer: etiology, risk factors, and epidemiology. *Clin Obstet Gynecol, 55*(1), 3-23. doi:10.1097/GRF.0b013e31824b4611

Iba, T., Kigawa, J., Kanamori, Y., Itamochi, H., Oishi, T., Simada, M., *et al.* (2004). Expression of the c-myc gene as a predictor of chemotherapy response and a prognostic factor in patients with ovarian cancer. *Cancer Science, 95*(5), 418-423.

Iglehart, J. D., & Silver, D. P. (2009). Synthetic lethality--a new direction in cancer-drug development. *N Engl J Med, 361*(2), 189-191. doi:10.1056/NEJMe0903044

Indraccolo, S., Tisato, V., Agata, S., Moserle, L., Ferrari, S., Callegaro, M., *et al.* (2006). Establishment and characterization of xenografts and cancer cell cultures derived from BRCA1−/− epithelial ovarian cancers. *European Journal of Cancer, 42*(10), 1475-1483.

Ishibashi, H., Suzuki, T., Suzuki, S., Moriya, T., Kaneko, C., Takizawa, T., *et al.* (2003). Sex steroid hormone receptors in human thymoma. *The Journal of Clinical Endocrinology & Metabolism, 88*(5), 2309-2317.

Jaspers, J. E., Kersbergen, A., Boon, U., Sol, W., van Deemter, L., Zander, S. A., *et al.* (2013). Loss of 53BP1 causes PARP inhibitor resistance in Brca1-mutated mouse mammary tumors. *Cancer Discov, 3*(1), 68-81. doi:10.1158/2159-8290.CD-12-0049

Jelinic, P., & Shaw, P. (2007). Loss of imprinting and cancer. *J Pathol, 211*(3), 261-268. doi:10.1002/path.2116

Jiang, X., Li, W., Li, X., Bai, H., & Zhang, Z. (2019). Current status and future prospects of PARP inhibitor clinical trials in ovarian cancer. *Cancer management and research, 11*, 4371-4390. doi:10.2147/CMAR.S200524

Jiao, S., Xia, W., Yamaguchi, H., Wei, Y., Chen, M.-K., Hsu, J.-M., *et al.* (2017). PARP Inhibitor Upregulates PD-L1 Expression and Enhances Cancer-Associated Immunosuppression. *Clinical Cancer Research, 23*(14), 3711-3720. doi:10.1158/1078-0432.Ccr-16-3215

Johnson, N., Johnson, S. F., Yao, W., Li, Y. C., Choi, Y. E., Bernhardy, A. J., *et al.* (2013). Stabilization of mutant BRCA1 protein confers PARP inhibitor and platinum resistance. *Proc Natl Acad Sci U S A, 110*(42), 17041-17046. doi:10.1073/pnas.1305170110

Johnson, N., Li, Y.-C., Walton, Z. E., Cheng, K. A., Li, D., Rodig, S. J., *et al.* (2011). Compromised CDK1 activity sensitizes BRCA-proficient cancers to PARP inhibition. *Nature medicine, 17*(7), 875-882. doi:10.1038/nm.2377

Johnson, S. F., Cruz, C., Greifenberg, A. K., Dust, S., Stover, D. G., Chi, D., *et al.* (2016). CDK12 Inhibition Reverses De Novo and Acquired PARP Inhibitor Resistance in BRCA Wild-Type and Mutated Models of Triple-Negative Breast Cancer. *Cell Reports, 17*(9), 2367-2381. doi:doi.org/10.1016/j.celrep.2016.10.077

Jokinen, E., & Koivunen, J. P. (2015). MEK and PI3K inhibition in solid tumors: rationale and evidence to date. *Ther Adv Med Oncol, 7*(3), 170-180. doi:10.1177/1758834015571111

Jones, P. A. (2012). Functions of DNA methylation: islands, start sites, gene bodies and beyond. *Nature Reviews Genetics, 13*(7), 484-492. doi:10.1038/nrg3230

Joshi, P. M., Sutor, S. L., Huntoon, C. J., & Karnitz, L. M. (2014). Ovarian cancer-associated mutations disable catalytic activity of CDK12, a kinase that promotes homologous recombination repair and resistance to cisplatin and poly(ADP-ribose) polymerase inhibitors. *J Biol Chem, 289*(13), 9247-9253. doi:10.1074/jbc.M114.551143

Kano, Y., Cook, J. D., Lee, J. E., & Ohh, M. (2016). New structural and functional insight into the regulation of Ras. *Semin Cell Dev Biol, 58*, 70-78. doi:10.1016/j.semcdb.2016.06.006

Kansanen, E., Kuosmanen, S. M., Leinonen, H., & Levonen, A.-L. (2013). The Keap1-Nrf2 pathway: Mechanisms of activation and dysregulation in cancer. *Redox Biology, 1*(1), 45-49. doi:doi.org/10.1016/j.redox.2012.10.001

Kanwal, A., Kaur, M., Singh, A., Gupta, S., & Sachan, M. (2016). Hypo/unmethylated promoter status of Cdk2 gene correlates with its over-expression in ovarian cancer in north Indian population. *Cell Mol Biol (Noisy-le-grand), 62*(1), 67-72.

Kaplan, A. R., Gueble, S. E., Liu, Y., Oeck, S., Kim, H., Yun, Z.*, et al.* (2019). Cediranib suppresses homology-directed DNA repair through down-regulation of BRCA1/2 and RAD51. *Science Translational Medicine, 11*(492), eaav4508. doi:10.1126/scitranslmed.aav4508

Kaufman, B., Shapira-Frommer, R., Schmutzler, R. K., Audeh, M. W., Friedlander, M., Balmana, J.*, et al.* (2015). Olaparib monotherapy in patients with advanced cancer and a germline BRCA1/2 mutation. *J Clin Oncol, 33*(3), 244-250. doi:10.1200/JCO.2014.56.2728

Keita, M., Wang, Z.-Q., Pelletier, J.-F., Bachvarova, M., Plante, M., Gregoire, J.*, et al.* (2013). Global methylation profiling in serous ovarian cancer is indicative for distinct aberrant DNA methylation signatures associated with tumor aggressiveness and disease progression. *Gynecologic oncology, 128*(2), 356-363.

Khot, A., Brajanovski, N., Cameron, D. P., Hein, N., Maclachlan, K. H., Sanij, E.*, et al.* (2019). First-in-Human RNA Polymerase I Transcription Inhibitor CX-5461 in Patients with Advanced Hematologic Cancers: Results of a Phase I Dose-Escalation Study. *Cancer Discovery, 9*(8), 1036-1049. doi:10.1158/2159-8290.Cd-18-1455

Kim, G., Ison, G., McKee, A. E., Zhang, H., Tang, S., Gwise, T.*, et al.* (2015). FDA Approval Summary: Olaparib Monotherapy in Patients with Deleterious Germline BRCA-Mutated Advanced Ovarian Cancer Treated with Three or More Lines of Chemotherapy. *Clin Cancer Res, 21*(19), 4257-4261. doi:10.1158/1078-0432.Ccr-15-0887

Kim, H., George, E., Ragland, R., Rafail, S., Zhang, R., Krepler, C.*, et al.* (2017). Targeting the ATR/CHK1 Axis with PARP Inhibition Results in Tumor Regression in BRCA-Mutant Ovarian Cancer Models. *Clin Cancer Res, 23*(12), 3097-3108. doi:10.1158/1078-0432.Ccr-16-2273

Kim, M. Y., Zhang, T., & Kraus, W. L. (2005). Poly(ADP-ribosyl)ation by PARP-1: 'PAR-laying' NAD+ into a nuclear signal. *Genes Dev, 19*(17), 1951-1967. doi:10.1101/gad.1331805

Kindelberger, D. W., Lee, Y., Miron, A., Hirsch, M. S., Feltmate, C., Medeiros, F.*, et al.* (2007). Intraepithelial carcinoma of the fimbria and pelvic serous carcinoma: Evidence for a causal relationship. *Am J Surg Pathol, 31*(2), 161-169. doi:10.1097/01.pas.0000213335.40358.47

Kolasa, I. K., Rembiszewska, A., Felisiak, A., Ziolkowska-Seta, I., Murawska, M., Moes, J., *et al.* (2009). PIK3CA amplification associates with resistance to chemotherapy in ovarian cancer patients. *Cancer Biol Ther, 8*(1), 21-26. doi:10.4161/cbt.8.1.7209

Kolfschoten, G. M., Pinedo, H. M., Scheffer, P. G., Schlüper, H. M., Erkelens, C. A., & Boven, E. (2000). Development of a panel of 15 human ovarian cancer xenografts for drug screening and determination of the role of the glutathione detoxification system. *Gynecologic oncology, 76*(3), 362-368.

Kondrashova, O., Love, C. J., Lunke, S., Hsu, A. L., Australian Ovarian Cancer Study, G., Waring, P. M., *et al.* (2015a). High-Throughput Amplicon-Based Copy Number Detection of 11 Genes in Formalin-Fixed Paraffin-Embedded Ovarian Tumour Samples by MLPA-Seq. *PloS one, 10*(11), e0143006. doi:10.1371/journal.pone.0143006

Kondrashova, O., Love, C. J., Lunke, S., Hsu, A. L., Waring, P. M., & Taylor, G. R. (2015b). High-Throughput Amplicon-Based Copy Number Detection of 11 Genes in Formalin-Fixed Paraffin-Embedded Ovarian Tumour Samples by MLPA-Seq. *PloS one, 10*(11), e0143006. doi:10.1371/journal.pone.0143006

Kondrashova, O., Nguyen, M., Shield-Artin, K., Tinker, A. V., Teng, N. N. H., Harrell, M. I., *et al.* (2017). Secondary Somatic Mutations Restoring RAD51C and RAD51D Associated with Acquired Resistance to the PARP Inhibitor Rucaparib in High-Grade Ovarian Carcinoma. *Cancer Discov, 7*(9), 984-998. doi:10.1158/2159-8290.CD-17-0419

Kondrashova, O., & Scott, C. L. (2019). Clarifying the role of EMSY in DNA repair in ovarian cancer. *Cancer, 125*(16), 2720-2724. doi:10.1002/cncr.32135

Kondrashova, O., Topp, M., Nesic, K., Lieschke, E., Ho, G. Y., Harrell, M. I., *et al.* (2018). Methylation of all BRCA1 copies predicts response to the PARP inhibitor rucaparib in ovarian carcinoma. *Nat Commun, 9*(1), 3970. doi:10.1038/s41467-018-05564-z

Konovalov, S., & Garcia-Bassets, I. (2013). Analysis of the levels of lysine-specific demethylase 1 (LSD1) mRNA in human ovarian tumors and the effects of chemical LSD1 inhibitors in ovarian cancer cell lines. *J Ovarian Res, 6*(1), 75. doi:10.1186/1757-2215-6-75

Konstantinopoulos, P. A., Spentzos, D., Karlan, B. Y., Taniguchi, T., Fountzilas, E., Francoeur, N., *et al.* (2010). Gene expression profile of BRCAness that correlates with responsiveness to chemotherapy and with outcome in patients with epithelial ovarian cancer. *J Clin Oncol, 28*(22), 3555-3561. doi:10.1200/JCO.2009.27.5719

Konstantinopoulos, P. A., Waggoner, S. E., Vidal, G. A., Mita, M. M., Fleming, G. F., Holloway, R. W., *et al.* (2018). TOPACIO/Keynote-162 (NCT02657889): a phase 1/2 study of niraparib+ pembrolizumab in patients (pts) with advanced triple-negative breast cancer or recurrent ovarian cancer (ROC)—results from ROC cohort. In: American Society of Clinical Oncology.

Koukoura, O., Spandidos, D. A., Daponte, A., & Sifakis, S. (2014). DNA methylation profiles in ovarian cancer: implication in diagnosis and therapy (Review). *Molecular medicine reports, 10*(1), 3-9. doi:10.3892/mmr.2014.2221

Kozub, M. M., Carr, R. M., Lomberk, G. L., & Fernandez-Zapico, M. E. (2017). LSD1, a double-edged sword, confers dynamic chromatin regulation but commonly promotes aberrant cell growth. *F1000Research, 6*, 2016-2016. doi:10.12688/f1000research.12169.1

Krishnakumar, R., & Kraus, W. L. (2010). The PARP side of the nucleus: molecular actions, physiological outcomes, and clinical targets. *Mol Cell, 39*(1), 8-24. doi:10.1016/j.molcel.2010.06.017

Kuhn, E., Kurman, R. J., Vang, R., Sehdev, A. S., Han, G., Soslow, R.*, et al.* (2012). TP53 mutations in serous tubal intraepithelial carcinoma and concurrent pelvic high-grade serous carcinoma--evidence supporting the clonal relationship of the two lesions. *J Pathol, 226*(3), 421-426. doi:10.1002/path.3023

LaFargue, C. J., Dal Molin, G. Z., Sood, A. K., & Coleman, R. L. (2019). Exploring and comparing adverse events between PARP inhibitors. *The Lancet Oncology, 20*(1), e15-e28. doi:doi.org/10.1016/S1470-2045(18)30786-1

Laird, C. D., Pleasant, N. D., Clark, A. D., Sneeden, J. L., Hassan, K. M. A., Manley, N. C.*, et al.* (2004). Hairpin-bisulfite PCR: Assessing epigenetic methylation patterns on complementary strands of individual DNA molecules. *Proceedings of the National Academy of Sciences, 101*(1), 204-209. doi:10.1073/pnas.2536758100

Lampert, E. J., Hays, J. L., Kohn, E. C., Annunziata, C. M., Minasian, L., Yu, M.*, et al.* (2019). Phase I/Ib study of olaparib and carboplatin in heavily pretreated recurrent high-grade serous ovarian cancer at low genetic risk. *Oncotarget, 10*(30), 2855-2868. doi:10.18632/oncotarget.26869

Landen, C. N., Jr., Birrer, M. J., & Sood, A. K. (2008). Early events in the pathogenesis of epithelial ovarian cancer. *J Clin Oncol, 26*(6), 995-1005. doi:10.1200/JCO.2006.07.9970

Landrum, M. J., Lee, J. M., Benson, M., Brown, G., Chao, C., Chitipiralla, S.*, et al.* (2015). ClinVar: public archive of interpretations of clinically relevant variants. *Nucleic Acids Research, 44*(D1), D862-D868. doi:10.1093/nar/gkv1222

Larue, L., & Bellacosa, A. (2005). Epithelial–mesenchymal transition in development and cancer: role of phosphatidylinositol 3′ kinase/AKT pathways. *Oncogene, 24*(50), 7443-7454. doi:10.1038/sj.onc.1209091

Lavin, M. F. (2008). Ataxia-telangiectasia: from a rare disorder to a paradigm for cell signalling and cancer. *Nat Rev Mol Cell Biol, 9*(10), 759-769. doi:10.1038/nrm2514

Ledermann, J., Harter, P., Gourley, C., Friedlander, M., Vergote, I., Rustin, G.*, et al.* (2012). Olaparib maintenance therapy in platinum-sensitive relapsed ovarian cancer. *N Engl J Med, 366*(15), 1382-1392. doi:10.1056/NEJMoa1105535

Ledermann, J., Harter, P., Gourley, C., Friedlander, M., Vergote, I., Rustin, G.*, et al.* (2014). Olaparib maintenance therapy in patients with platinum-sensitive relapsed serous ovarian cancer: a preplanned retrospective analysis of outcomes by BRCA status in a randomised phase 2 trial. *Lancet Oncol, 15*(8), 852-861. doi:10.1016/S1470-2045(14)70228-1

Ledermann, J. A., Raja, F. A., Fotopoulou, C., Gonzalez-Martin, A., Colombo, N., & Sessa, C. (2013). Newly diagnosed and relapsed epithelial ovarian carcinoma: ESMO Clinical Practice Guidelines for diagnosis, treatment and follow-up. *Ann Oncol, 24 Suppl 6*, vi24-32. doi:10.1093/annonc/mdt333

Lee, P. S., Teaberry, V. S., Bland, A. E., Huang, Z., Whitaker, R. S., Baba, T.*, et al.* (2010). Elevated MAL expression is accompanied by promoter hypomethylation and platinum resistance in epithelial ovarian cancer. *Int J Cancer, 126*(6), 1378-1389. doi:10.1002/ijc.24797

Lee, Y., Miron, A., Drapkin, R., Nucci, M., Medeiros, F., Saleemuddin, A.*, et al.* (2007). A candidate precursor to serous carcinoma that originates in the distal fallopian tube. *The Journal of Pathology: A Journal of the Pathological Society of Great Britain and Ireland, 211*(1), 26-35.

Lengyel, E. (2010). Ovarian cancer development and metastasis. *Am J Pathol, 177*(3), 1053-1064. doi:10.2353/ajpath.2010.100105

Leo, E., Johannes, J., Illuzzi, G., Zhang, A., Hemsley, P., Bista, M. J.*, et al.* (2018). Abstract LB-273: A head-to-head comparison of the properties of five clinical PARP inhibitors

identifies new insights that can explain both the observed clinical efficacy and safety profiles. *Cancer Research, 78*(13 Supplement), LB-273-LB-273. doi:10.1158/1538-7445.Am2018-lb-273

Leslie, A., Carey, F. A., Pratt, N. R., & Steele, R. J. (2002). The colorectal adenoma-carcinoma sequence. *Br J Surg, 89*(7), 845-860. doi:10.1046/j.1365-2168.2002.02120.x

Lewis, B. C., Shim, H., Li, Q., Wu, C. S., Lee, L. A., Maity, A.*, et al.* (1997). Identification of putative c-Myc-responsive genes: characterization of rcl, a novel growth-related gene. *Mol Cell Biol, 17*(9), 4967-4978. doi:10.1128/mcb.17.9.4967

Lheureux, S., Bruce, J. P., Burnier, J. V., Karakasis, K., Shaw, P. A., Clarke, B. A.*, et al.* (2017a). Somatic BRCA1/2 Recovery as a Resistance Mechanism After Exceptional Response to Poly (ADP-ribose) Polymerase Inhibition. *Journal of Clinical Oncology, 35*(11), 1240-1249. doi:10.1200/JCO.2016.71.3677

Lheureux, S., Lai, Z., Dougherty, B. A., Runswick, S., Hodgson, D. R., Timms, K. M.*, et al.* (2017b). Long-Term Responders on Olaparib Maintenance in High-Grade Serous Ovarian Cancer: Clinical and Molecular Characterization. *Clin Cancer Res, 23*(15), 4086-4094. doi:10.1158/1078-0432.Ccr-16-2615

Lhomme, C., Joly, F., Walker, J. L., Lissoni, A. A., Nicoletto, M. O., Manikhas, G. M.*, et al.* (2008). Phase III study of valspodar (PSC 833) combined with paclitaxel and carboplatin compared with paclitaxel and carboplatin alone in patients with stage IV or suboptimally debulked stage III epithelial ovarian cancer or primary peritoneal cancer. *J Clin Oncol, 26*(16), 2674-2682. doi:10.1200/jco.2007.14.9807

Li, H., Cai, Q., Godwin, A. K., & Zhang, R. (2010). Enhancer of zeste homolog 2 promotes the proliferation and invasion of epithelial ovarian cancer cells. *Mol Cancer Res, 8*(12), 1610-1618. doi:10.1158/1541-7786.Mcr-10-0398

Li, N. F., Broad, S., Lu, Y. J., Yang, J. S., Watson, R., Hagemann, T.*, et al.* (2007). Human ovarian surface epithelial cells immortalized with hTERT maintain functional pRb and p53 expression. *Cell Prolif, 40*(5), 780-794. doi:10.1111/j.1365-2184.2007.00462.x

Li, X., & Heyer, W.-D. (2008). Homologous recombination in DNA repair and DNA damage tolerance. *Cell research, 18*(1), 99-113. doi:10.1038/cr.2008.1

Li, Y., & Tollefsbol, T. O. (2011). DNA methylation detection: bisulfite genomic sequencing analysis. In *Epigenetics Protocols* (pp. 11-21): Springer.

Li, Z., Owonikoko, T. K., Sun, S.-Y., Ramalingam, S. S., Doetsch, P. W., Xiao, Z.-Q.*, et al.* (2012). c-Myc suppression of DNA double-strand break repair. *Neoplasia (New York, N.Y.), 14*(12), 1190-1202. doi:10.1593/neo.121258

Lieber, M. R. (2010). The mechanism of double-strand DNA break repair by the nonhomologous DNA end-joining pathway. *Annu Rev Biochem, 79*, 181-211. doi:10.1146/annurev.biochem.052308.093131

Lieber, M. R., Ma, Y., Pannicke, U., & Schwarz, K. (2004). The mechanism of vertebrate nonhomologous DNA end joining and its role in V(D)J recombination. *DNA Repair (Amst), 3*(8-9), 817-826. doi:10.1016/j.dnarep.2004.03.015

Lieschke, E., Wang, Z., Kelly, G. L., & Strasser, A. (2019). Discussion of some 'knowns' and some 'unknowns' about the tumour suppressor p53. *J Mol Cell Biol, 11*(3), 212-223. doi:10.1093/jmcb/mjy077

Litton, J. K., Scoggins, M. E., Hess, K. R., Adrada, B. E., Murthy, R. K., Damodaran, S.*, et al.* (2019). Neoadjuvant Talazoparib for Patients With Operable Breast Cancer With a Germline BRCA Pathogenic Variant. *Journal of Clinical Oncology*, JCO.19.01304. doi:10.1200/JCO.19.01304

Liu, J., Barry, W. T., Birrer, M. J., Lee, J.-m., Buckanovich, R. J., Fleming, G. F.*, et al.* (2014). A randomized phase 2 trial comparing efficacy of the combination of the PARP inhibitor olaparib and the antiangiogenic cediranib against olaparib alone in recurrent

platinum-sensitive ovarian cancer. *Journal of Clinical Oncology, 32*(18_suppl), LBA5500-LBA5500. doi:10.1200/jco.2014.32.18_suppl.lba5500

Liu, J. F., Tolaney, S. M., Birrer, M., Fleming, G. F., Buss, M. K., Dahlberg, S. E.*, et al.* (2013). A Phase 1 trial of the poly(ADP-ribose) polymerase inhibitor olaparib (AZD2281) in combination with the anti-angiogenic cediranib (AZD2171) in recurrent epithelial ovarian or triple-negative breast cancer. *European Journal of Cancer, 49*(14), 2972-2978. doi:doi.org/10.1016/j.ejca.2013.05.020

Liu, S. S., Zheng, H. X., Jiang, H. D., He, J., Yu, Y., Qu, Y. P.*, et al.* (2012). Identification and characterization of a novel gene, c1orf109, encoding a CK2 substrate that is involved in cancer cell proliferation. *J Biomed Sci, 19*, 49. doi:10.1186/1423-0127-19-49

Liu, Y., Masson, J.-Y., Shah, R., O'Regan, P., & West, S. C. (2004). RAD51C is required for Holliday junction processing in mammalian cells. *Science, 303*(5655), 243-246.

Lobrich, M., & Jeggo, P. A. (2005). Harmonising the response to DSBs: a new string in the ATM bow. *DNA Repair (Amst), 4*(7), 749-759. doi:10.1016/j.dnarep.2004.12.008

Lohman, D. C., Forouhar, F., Beebe, E. T., Stefely, M. S., Minogue, C. E., Ulbrich, A.*, et al.* (2014). Mitochondrial COQ9 is a lipid-binding protein that associates with COQ7 to enable coenzyme Q biosynthesis. *Proceedings of the National Academy of Sciences, 111*(44), E4697-E4705. doi:10.1073/pnas.1413128111

Lok, B. H., Carley, A. C., Tchang, B., & Powell, S. N. (2013). RAD52 inactivation is synthetically lethal with deficiencies in BRCA1 and PALB2 in addition to BRCA2 through RAD51-mediated homologous recombination. *Oncogene, 32*(30), 3552-3558. doi:10.1038/onc.2012.391

Long, H. J. (1994). Paclitaxel (Taxol): A Novel Anticancer Chemotherapeutic Drug. *Mayo Clinic Proceedings, 69*(4), 341-345. doi:doi.org/10.1016/S0025-6196(12)62219-8

Lord, C. J., & Ashworth, A. (2017). PARP inhibitors: Synthetic lethality in the clinic. *Science, 355*(6330), 1152-1158. doi:10.1126/science.aam7344

Lord, C. J., McDonald, S., Swift, S., Turner, N. C., & Ashworth, A. (2008). A high-throughput RNA interference screen for DNA repair determinants of PARP inhibitor sensitivity. *DNA Repair (Amst), 7*(12), 2010-2019. doi:10.1016/j.dnarep.2008.08.014

Loveday, C., Turnbull, C., Ramsay, E., Hughes, D., Ruark, E., Frankum, J. R.*, et al.* (2011). Germline mutations in RAD51D confer susceptibility to ovarian cancer. *Nat Genet, 43*(9), 879-882. doi:10.1038/ng.893

Loveday, C., Turnbull, C., Ruark, E., Xicola, R. M., Ramsay, E., Hughes, D.*, et al.* (2012). Germline RAD51C mutations confer susceptibility to ovarian cancer. *Nat Genet, 44*(5), 475-476; author reply 476. doi:10.1038/ng.2224

Ma, Y., Schwarz, K., & Lieber, M. R. (2005). The Artemis:DNA-PKcs endonuclease cleaves DNA loops, flaps, and gaps. *DNA Repair (Amst), 4*(7), 845-851. doi:10.1016/j.dnarep.2005.04.013

Magnusson, J., & Ramel, C. (1990). Inhibitor of poly(ADP-ribose)transferase potentiates the recombinogenic but not the mutagenic action of alkylating agents in somatic cells in vivo in Drosophila melanogaster. *Mutagenesis, 5*(5), 511-514. doi:10.1093/mutage/5.5.511

Majer, C. R., Jin, L., Scott, M. P., Knutson, S. K., Kuntz, K. W., Keilhack, H.*, et al.* (2012). A687V EZH2 is a gain-of-function mutation found in lymphoma patients. *FEBS Lett, 586*(19), 3448-3451. doi:10.1016/j.febslet.2012.07.066

Malu, S., Malshetty, V., Francis, D., & Cortes, P. (2012). Role of non-homologous end joining in V(D)J recombination. *Immunol Res, 54*(1-3), 233-246. doi:10.1007/s12026-012-8329-z

Marchetti, C., Muzii, L., Romito, A., & Benedetti Panici, P. (2019). First-line treatment of women with advanced ovarian cancer: focus on bevacizumab. *OncoTargets and therapy, 12*, 1095-1103. doi:10.2147/OTT.S155425

Mari, R., Mamessier, E., Lambaudie, E., Provansal, M., Birnbaum, D., Bertucci, F.*, et al.* (2019). Liquid Biopsies for Ovarian Carcinoma: How Blood Tests May Improve the Clinical Management of a Deadly Disease. *Cancers, 11*(6), 774. doi:10.3390/cancers11060774

Marquard, A. M., Eklund, A. C., Joshi, T., Krzystanek, M., Favero, F., Wang, Z. C.*, et al.* (2015). Pan-cancer analysis of genomic scar signatures associated with homologous recombination deficiency suggests novel indications for existing cancer drugs. *Biomark Res, 3*, 9. doi:10.1186/s40364-015-0033-4

Marth, C., Reimer, D., & Zeimet, A. G. (2017). Front-line therapy of advanced epithelial ovarian cancer: standard treatment. *Annals of Oncology, 28*(suppl_8), viii36-viii39. doi:10.1093/annonc/mdx450

Mateo, J., Carreira, S., Sandhu, S., Miranda, S., Mossop, H., Perez-Lopez, R.*, et al.* (2015). DNA-Repair Defects and Olaparib in Metastatic Prostate Cancer. *N Engl J Med, 373*(18), 1697-1708. doi:10.1056/NEJMoa1506859

Mateo, J., Lord, C. J., Serra, V., Tutt, A., Balmaña, J., Castroviejo-Bermejo, M.*, et al.* (2019). A decade of clinical development of PARP inhibitors in perspective. *Annals of Oncology, 30*(9), 1437-1447. doi:10.1093/annonc/mdz192

Mateos-Gomez, P. A., Gong, F., Nair, N., Miller, K. M., Lazzerini-Denchi, E., & Sfeir, A. (2015). Mammalian polymerase theta promotes alternative NHEJ and suppresses recombination. *Nature, 518*(7538), 254-257. doi:10.1038/nature14157

Mathieu, K. B., Bedi, D. G., Thrower, S. L., Qayyum, A., & Bast, R. C., Jr. (2018). Screening for ovarian cancer: imaging challenges and opportunities for improvement. *Ultrasound Obstet Gynecol, 51*(3), 293-303. doi:10.1002/uog.17557

Maykel, J., Liu, J. H., Li, H., Shultz, L. D., Greiner, D. L., & Houghton, J. (2014). NOD-scidIl2rgtm1Wjland NOD-Rag1nullIl2rgtm1Wjl: A Model for Stromal Cell–Tumor Cell Interaction for Human Colon Cancer. *Digestive Diseases and Sciences, 59*(6), 1169-1179. doi:10.1007/s10620-014-3168-5

McCabe, N., Turner, N. C., Lord, C. J., Kluzek, K., Bialkowska, A., Swift, S.*, et al.* (2006). Deficiency in the repair of DNA damage by homologous recombination and sensitivity to poly(ADP-ribose) polymerase inhibition. *Cancer Res, 66*(16), 8109-8115. doi:10.1158/0008-5472.CAN-06-0140

McCarty, J. K., Miller, L., Cox, E., Konrath, J., & McCarty, S. K. (1985). Estrogen receptor analyses. Correlation of biochemical and immunohistochemical methods using monoclonal antireceptor antibodies. *Archives of pathology & laboratory medicine, 109*(8), 716-721.

McCluggage, W. G. (2011). Morphological subtypes of ovarian carcinoma: a review with emphasis on new developments and pathogenesis. *Pathology, 43*(5), 420-432. doi:10.1097/PAT.0b013e328348a6e7

McCormick, A., Donoghue, P., Dixon, M., O'Sullivan, R., O'Donnell, R. L., Murray, J.*, et al.* (2017). Ovarian Cancers Harbor Defects in Nonhomologous End Joining Resulting in Resistance to Rucaparib. *Clin Cancer Res, 23*(8), 2050-2060. doi:10.1158/1078-0432.CCR-16-0564

McGuire, W. P., Hoskins, W. J., Brady, M. F., Kucera, P. R., Partridge, E. E., Look, K. Y.*, et al.* (1996). Cyclophosphamide and Cisplatin Compared with Paclitaxel and Cisplatin in Patients with Stage III and Stage IV Ovarian Cancer. *New England Journal of Medicine, 334*(1), 1-6. doi:10.1056/nejm199601043340101

Meindl, A., Hellebrand, H., Wiek, C., Erven, V., Wappenschmidt, B., Niederacher, D., *et al.* (2010). Germline mutations in breast and ovarian cancer pedigrees establish RAD51C as a human cancer susceptibility gene. *Nat Genet, 42*(5), 410-414. doi:10.1038/ng.569

Mendes-Pereira, A. M., Martin, S. A., Brough, R., McCarthy, A., Taylor, J. R., Kim, J. S., *et al.* (2009). Synthetic lethal targeting of PTEN mutant cells with PARP inhibitors. *EMBO Mol Med, 1*(6-7), 315-322. doi:10.1002/emmm.200900041

Menisser-de Murcia, J., Mark, M., Wendling, O., Wynshaw-Boris, A., & de Murcia, G. (2001). Early embryonic lethality in PARP-1 Atm double-mutant mice suggests a functional synergy in cell proliferation during development. *Mol Cell Biol, 21*(5), 1828-1832. doi:10.1128/MCB.21.5.1828-1832.2001

Mesquita, K. A., Alabdullah, M., Griffin, M., Toss, M. S., Fatah, T. M. A., Alblihy, A., *et al.* (2019). ERCC1-XPF deficiency is a predictor of olaparib induced synthetic lethality and platinum sensitivity in epithelial ovarian cancers. *Gynecologic oncology, 153*(2), 416-424.

Mignogna, C., Staropoli, N., Botta, C., De Marco, C., Rizzuto, A., Morelli, M., *et al.* (2016). Aurora Kinase A expression predicts platinum-resistance and adverse outcome in high-grade serous ovarian carcinoma patients. *J Ovarian Res, 9*(1), 31. doi:10.1186/s13048-016-0238-7

Miki, Y., Swensen, J., Shattuck-Eidens, D., Futreal, P. A., Harshman, K., Tavtigian, S., *et al.* (1994). A strong candidate for the breast and ovarian cancer susceptibility gene BRCA1. *Science, 266*(5182), 66-71. doi:10.1126/science.7545954

Milea, A., George, S. H., Matevski, D., Jiang, H., Madunic, M., Berman, H. K., *et al.* (2014). Retinoblastoma pathway deregulatory mechanisms determine clinical outcome in high-grade serous ovarian carcinoma. *Mod Pathol, 27*(7), 991-1001. doi:10.1038/modpathol.2013.218

Millot, G. A., Carvalho, M. A., Caputo, S. M., Vreeswijk, M. P., Brown, M. A., Webb, M., *et al.* (2012). A guide for functional analysis of BRCA1 variants of uncertain significance. *Hum Mutat, 33*(11), 1526-1537. doi:10.1002/humu.22150

Mimitou, E. P., & Symington, L. S. (2011). DNA end resection--unraveling the tail. *DNA Repair (Amst), 10*(3), 344-348. doi:10.1016/j.dnarep.2010.12.004

Min, A., Im, S.-A., Yoon, Y.-K., Song, S.-H., Nam, H.-J., Hur, H.-S., *et al.* (2013). RAD51C-deficient cancer cells are highly sensitive to the PARP inhibitor olaparib. *Molecular cancer therapeutics, 12*(6), 865-877.

Min, W., & Wang, Z. Q. (2009). Poly (ADP-ribose) glycohydrolase (PARG) and its therapeutic potential. *Front Biosci (Landmark Ed), 14*, 1619-1626. doi:10.2741/3329

Mirza, M. R., Avall-Lundqvist, E., Birrer, M. J., Christensen, R. d., Nyvang, G.-B., Malander, S., *et al.* (2019). Combination of niraparib and bevacizumab versus niraparib alone as treatment of recurrent platinum-sensitive ovarian cancer: A randomized controlled chemotherapy-free study—NSGO-AVANOVA2/ENGOT-OV24. *Journal of Clinical Oncology, 37*(15_suppl), 5505-5505. doi:10.1200/JCO.2019.37.15_suppl.5505

Mirza, M. R., Monk, B. J., Herrstedt, J., Oza, A. M., Mahner, S., Redondo, A., *et al.* (2016). Niraparib Maintenance Therapy in Platinum-Sensitive, Recurrent Ovarian Cancer. *375*(22), 2154-2164.

Montoni, A., Robu, M., Pouliot, E., & Shah, G. M. (2013). Resistance to PARP-Inhibitors in Cancer Therapy. *Front Pharmacol, 4*, 18. doi:10.3389/fphar.2013.00018

Moore, K., Colombo, N., Scambia, G., Kim, B. G., Oaknin, A., Friedlander, M., *et al.* (2018). Maintenance Olaparib in Patients with Newly Diagnosed Advanced Ovarian Cancer. *N Engl J Med, 379*(26), 2495-2505. doi:10.1056/NEJMoa1810858

Moore, L. D., Le, T., & Fan, G. (2013). DNA methylation and its basic function. *Neuropsychopharmacology : official publication of the American College of Neuropsychopharmacology, 38*(1), 23-38. doi:10.1038/npp.2012.112

Morales, J., Li, L., Fattah, F. J., Dong, Y., Bey, E. A., Patel, M.*, et al.* (2014). Review of poly (ADP-ribose) polymerase (PARP) mechanisms of action and rationale for targeting in cancer and other diseases. *Critical reviews in eukaryotic gene expression, 24*(1), 15-28. doi:10.1615/critreveukaryotgeneexpr.2013006875

Morales, J. C., Franco, S., Murphy, M. M., Bassing, C. H., Mills, K. D., Adams, M. M.*, et al.* (2006). 53BP1 and p53 synergize to suppress genomic instability and lymphomagenesis. *Proc Natl Acad Sci U S A, 103*(9), 3310-3315. doi:10.1073/pnas.0511259103

Mosammaparast, N., Kim, H., Laurent, B., Zhao, Y., Lim, H. J., Majid, M. C.*, et al.* (2013). The histone demethylase LSD1/KDM1A promotes the DNA damage response. *J Cell Biol, 203*(3), 457-470. doi:10.1083/jcb.201302092

Moshous, D., Callebaut, I., de Chasseval, R., Corneo, B., Cavazzana-Calvo, M., Le Deist, F.*, et al.* (2001). Artemis, a novel DNA double-strand break repair/V(D)J recombination protein, is mutated in human severe combined immune deficiency. *Cell, 105*(2), 177-186. doi:10.1016/s0092-8674(01)00309-9

Moynahan, M. E., Chiu, J. W., Koller, B. H., & Jasin, M. (1999). Brca1 controls homology-directed DNA repair. *Mol Cell, 4*(4), 511-518. doi:10.1016/s1097-2765(00)80202-6

Moynahan, M. E., & Jasin, M. (2010). Mitotic homologous recombination maintains genomic stability and suppresses tumorigenesis. *Nat Rev Mol Cell Biol, 11*(3), 196-207. doi:10.1038/nrm2851

Mukhopadhyay, A., Elattar, A., Cerbinskaite, A., Wilkinson, S. J., Drew, Y., Kyle, S.*, et al.* (2010). Development of a functional assay for homologous recombination status in primary cultures of epithelial ovarian tumor and correlation with sensitivity to poly(ADP-ribose) polymerase inhibitors. *Clin Cancer Res, 16*(8), 2344-2351. doi:10.1158/1078-0432.CCR-09-2758

Multhaup, M., Karlen, A. D., Swanson, D. L., Wilber, A., Somia, N. V., Cowan, M. J.*, et al.* (2010). Cytotoxicity associated with artemis overexpression after lentiviral vector-mediated gene transfer. *Hum Gene Ther, 21*(7), 865-875. doi:10.1089/hum.2009.162

Murai, J., Huang, S. Y., Das, B. B., Renaud, A., Zhang, Y., Doroshow, J. H.*, et al.* (2012). Trapping of PARP1 and PARP2 by Clinical PARP Inhibitors. *Cancer Res, 72*(21), 5588-5599. doi:10.1158/0008-5472.CAN-12-2753

Murai, J., Huang, S. Y., Renaud, A., Zhang, Y., Ji, J., Takeda, S.*, et al.* (2014). Stereospecific PARP trapping by BMN 673 and comparison with olaparib and rucaparib. *Mol Cancer Ther, 13*(2), 433-443. doi:10.1158/1535-7163.MCT-13-0803

Nagasawa, S., Sedukhina, A. S., Nakagawa, Y., Maeda, I., Kubota, M., Ohnuma, S.*, et al.* (2015). LSD1 overexpression is associated with poor prognosis in basal-like breast cancer, and sensitivity to PARP inhibition. *PloS one, 10*(2), e0118002.

Nakayama, K., Kanzaki, A., Terada, K., Mutoh, M., Ogawa, K., Sugiyama, T.*, et al.* (2004). Prognostic value of the Cu-transporting ATPase in ovarian carcinoma patients receiving cisplatin-based chemotherapy. *Clin Cancer Res, 10*(8), 2804-2811. doi:10.1158/1078-0432.ccr-03-0454

Nakayama, N., Nakayama, K., Shamima, Y., Ishikawa, M., Katagiri, A., Iida, K.*, et al.* (2010). Gene amplification CCNE1 is related to poor survival and potential therapeutic target in ovarian cancer. *Cancer: Interdisciplinary International Journal of the American Cancer Society, 116*(11), 2621-2634.

Nanjundan, M., Nakayama, Y., Cheng, K. W., Lahad, J., Liu, J., Lu, K.*, et al.* (2007). Amplification of MDS1/EVI1 and EVI1, located in the 3q26. 2 amplicon, is associated

with favorable patient prognosis in ovarian cancer. *Cancer Research, 67*(7), 3074-3084.
Needhamsen, M., Ewing, E., Lund, H., Gomez-Cabrero, D., Harris, R. A., Kular, L.*, et al.* (2017). Usability of human Infinium MethylationEPIC BeadChip for mouse DNA methylation studies. *BMC bioinformatics, 18*(1), 486.
Neelsen, K. J., & Lopes, M. (2015). Replication fork reversal in eukaryotes: from dead end to dynamic response. *Nat Rev Mol Cell Biol, 16*(4), 207-220. doi:10.1038/nrm3935
Nesic, K., Wakefield, M., Kondrashova, O., Scott, C. L., & McNeish, I. A. (2018). Targeting DNA repair: the genome as a potential biomarker. *J Pathol, 244*(5), 586-597. doi:10.1002/path.5025
Nicholson, L. J., Smith, P. R., Hiller, L., Szlosarek, P. W., Kimberley, C., Sehouli, J.*, et al.* (2009). Epigenetic silencing of argininosuccinate synthetase confers resistance to platinum-induced cell death but collateral sensitivity to arginine auxotrophy in ovarian cancer. *Int J Cancer, 125*(6), 1454-1463. doi:10.1002/ijc.24546
Nickoloff, J. A., Jones, D., Lee, S. H., Williamson, E. A., & Hromas, R. (2017). Drugging the Cancers Addicted to DNA Repair. *J Natl Cancer Inst, 109*(11). doi:10.1093/jnci/djx059
Nik-Zainal, S., Davies, H., Staaf, J., Ramakrishna, M., Glodzik, D., Zou, X.*, et al.* (2016). Landscape of somatic mutations in 560 breast cancer whole-genome sequences. *Nature, 534*(7605), 47-54. doi:10.1038/nature17676
Norquist, B., Wurz, K. A., Pennil, C. C., Garcia, R., Gross, J., Sakai, W.*, et al.* (2011). Secondary somatic mutations restoring BRCA1/2 predict chemotherapy resistance in hereditary ovarian carcinomas. *J Clin Oncol, 29*(22), 3008-3015. doi:10.1200/JCO.2010.34.2980
O'Bryan, J. P. (2019). Pharmacological targeting of RAS: Recent success with direct inhibitors. *Pharmacological research, 139*, 503-511. doi:10.1016/j.phrs.2018.10.021
O'Flanagan, C. H., Campbell, K. R., Zhang, A. W., Kabeer, F., Lim, J. L., Biele, J.*, et al.* (2019). Dissociation of solid tumour tissues with cold active protease for single-cell RNA-seq minimizes conserved collagenase associated stress responses. *bioRxiv*, 683227.
Oltra, S. S., Peña-Chilet, M., Flower, K., Martinez, M. T., Alonso, E., Burgues, O.*, et al.* (2019). Acceleration in the DNA methylation age in breast cancer tumours from very young women. *Scientific Reports, 9*(1), 14991. doi:10.1038/s41598-019-51457-6
Orelli, B. J., & Bishop, D. K. (2001). BRCA2 and homologous recombination. *Breast Cancer Res, 3*(5), 294-298. doi:10.1186/bcr310
Oza, A. M., Cibula, D., Benzaquen, A. O., Poole, C., Mathijssen, R. H., Sonke, G. S.*, et al.* (2015a). Olaparib combined with chemotherapy for recurrent platinum-sensitive ovarian cancer: a randomised phase 2 trial. *Lancet Oncol, 16*(1), 87-97. doi:10.1016/s1470-2045(14)71135-0
Oza, A. M., Cook, A. D., Pfisterer, J., Embleton, A., Ledermann, J. A., Pujade-Lauraine, E.*, et al.* (2015b). Standard chemotherapy with or without bevacizumab for women with newly diagnosed ovarian cancer (ICON7): overall survival results of a phase 3 randomised trial. *The Lancet Oncology, 16*(8), 928-936. doi:10.1016/S1470-2045(15)00086-8
Ozdemir, F., Altinisik, J., Karateke, A., Coksuer, H., & Buyru, N. (2012). Methylation of tumor suppressor genes in ovarian cancer. *Experimental and therapeutic medicine, 4*(6), 1092-1096. doi:10.3892/etm.2012.715
Ozols, R. F., Bundy, B. N., Greer, B. E., Fowler, J. M., Clarke-Pearson, D., Burger, R. A.*, et al.* (2003). Phase III trial of carboplatin and paclitaxel compared with cisplatin and paclitaxel in patients with optimally resected stage III ovarian cancer: a Gynecologic Oncology Group study. *Journal of Clinical Oncology, 21*(17), 3194-3200.

Parmar, K., Kochupurakkal, B. S., Lazaro, J. B., Wang, Z. C., Palakurthi, S., Kirschmeier, P. T., *et al.* (2019). The CHK1 Inhibitor Prexasertib Exhibits Monotherapy Activity in High-Grade Serous Ovarian Cancer Models and Sensitizes to PARP Inhibition. *Clin Cancer Res, 25*(20), 6127-6140. doi:10.1158/1078-0432.Ccr-19-0448

Parrales, A., & Iwakuma, T. (2015). Targeting Oncogenic Mutant p53 for Cancer Therapy. *Front Oncol, 5*, 288. doi:10.3389/fonc.2015.00288

Patch, A. M., Christie, E. L., Etemadmoghadam, D., Garsed, D. W., George, J., Fereday, S., *et al.* (2015). Whole-genome characterization of chemoresistant ovarian cancer. *Nature, 521*(7553), 489-494. doi:10.1038/nature14410

Patel, A. G., Sarkaria, J. N., & Kaufmann, S. H. (2011). Nonhomologous end joining drives poly(ADP-ribose) polymerase (PARP) inhibitor lethality in homologous recombination-deficient cells. *Proc Natl Acad Sci U S A, 108*(8), 3406-3411. doi:10.1073/pnas.1013715108

Patel, D. S., Misenko, S. M., Her, J., & Bunting, S. F. (2017). BLM helicase regulates DNA repair by counteracting RAD51 loading at DNA double-strand break sites. *The Journal of Cell Biology, 216*(11), 3521-3534. doi:10.1083/jcb.201703144

Paull, T. T. (2010). Making the best of the loose ends: Mre11/Rad50 complexes and Sae2 promote DNA double-strand break resection. *DNA Repair (Amst), 9*(12), 1283-1291. doi:10.1016/j.dnarep.2010.09.015

Pelttari, L. M., Heikkinen, T., Thompson, D., Kallioniemi, A., Schleutker, J., Holli, K., *et al.* (2011). RAD51C is a susceptibility gene for ovarian cancer. *Human Molecular Genetics, 20*(16), 3278-3288. doi:10.1093/hmg/ddr229

Pennington, K. P., Walsh, T., Harrell, M. I., Lee, M. K., Pennil, C. C., Rendi, M. H., *et al.* (2014). Germline and somatic mutations in homologous recombination genes predict platinum response and survival in ovarian, fallopian tube, and peritoneal carcinomas. *Clin Cancer Res, 20*(3), 764-775. doi:10.1158/1078-0432.CCR-13-2287

Perets, R., Wyant, G. A., Muto, K. W., Bijron, J. G., Poole, B. B., Chin, K. T., *et al.* (2013). Transformation of the fallopian tube secretory epithelium leads to high-grade serous ovarian cancer in Brca;Tp53;Pten models. *Cancer Cell, 24*(6), 751-765. doi:10.1016/j.ccr.2013.10.013

Perren, T. J., Swart, A. M., Pfisterer, J., Ledermann, J. A., Pujade-Lauraine, E., Kristensen, G., *et al.* (2011). A phase 3 trial of bevacizumab in ovarian cancer. *N Engl J Med, 365*(26), 2484-2496. doi:10.1056/NEJMoa1103799

Petitjean, A., Mathe, E., Kato, S., Ishioka, C., Tavtigian, S. V., Hainaut, P., *et al.* (2007). Impact of mutant p53 functional properties on TP53 mutation patterns and tumor phenotype: lessons from recent developments in the IARC TP53 database. *Hum Mutat, 28*(6), 622-629. doi:10.1002/humu.20495

Pettitt, S., Krastev, D. B., Song, F., Ashworth, A., & Lord, C. J. (2016). Abstract 2743: Finding determinants of PARP inhibitor sensitivity using genome-wide and focused CRISPR screens. *Cancer Research, 76*(14 Supplement), 2743-2743. doi:10.1158/1538-7445.Am2016-2743

Phipson, B., Maksimovic, J., & Oshlack, A. (2016). missMethyl: an R package for analyzing data from Illumina's HumanMethylation450 platform. *Bioinformatics, 32*(2), 286-288.

Piccart, M. J., Bertelsen, K., James, K., Cassidy, J., Mangioni, C., Simonsen, E., *et al.* (2000). Randomized Intergroup Trial of Cisplatin–Paclitaxel Versus Cisplatin–Cyclophosphamide in Women With Advanced Epithelial Ovarian Cancer: Three-Year Results. *JNCI: Journal of the National Cancer Institute, 92*(9), 699-708. doi:10.1093/jnci/92.9.699

Piek, J. M., van Diest, P. J., Zweemer, R. P., Jansen, J. W., Poort-Keesom, R. J., Menko, F. H., *et al.* (2001a). Dysplastic changes in prophylactically removed Fallopian tubes of

women predisposed to developing ovarian cancer. *J Pathol, 195*(4), 451-456. doi:10.1002/path.1000

Piek, J. M., Van Diest, P. J., Zweemer, R. P., Jansen, J. W., Poort-Keesom, R. J., Menko, F. H.*, et al.* (2001b). Dysplastic changes in prophylactically removed Fallopian tubes of women predisposed to developing ovarian cancer. *The Journal of Pathology: A Journal of the Pathological Society of Great Britain and Ireland, 195*(4), 451-456.

Pilié, P. G., Gay, C. M., Byers, L. A., O'Connor, M. J., & Yap, T. A. (2019). PARP Inhibitors: Extending Benefit Beyond BRCA-Mutant Cancers. *Clinical Cancer Research, 25*(13), 3759-3771. doi:10.1158/1078-0432.Ccr-18-0968

Pisanic, T. R., 2nd, Athamanolap, P., & Wang, T.-H. (2017). Defining, distinguishing and detecting the contribution of heterogeneous methylation to cancer heterogeneity. *Seminars in cell & developmental biology, 64*, 5-17. doi:10.1016/j.semcdb.2016.08.030

Pisco, A. O., Brock, A., Zhou, J., Moor, A., Mojtahedi, M., Jackson, D.*, et al.* (2013). Non-Darwinian dynamics in therapy-induced cancer drug resistance. *Nature Communications, 4*, 2467-2467. doi:10.1038/ncomms3467

Polak, P., Kim, J., Braunstein, L. Z., Karlic, R., Haradhavala, N. J., Tiao, G.*, et al.* (2017). A mutational signature reveals alterations underlying deficient homologous recombination repair in breast cancer. *Nat Genet, 49*(10), 1476-1486. doi:10.1038/ng.3934

Polo, S. E., & Jackson, S. P. (2011). Dynamics of DNA damage response proteins at DNA breaks: a focus on protein modifications. *Genes Dev, 25*(5), 409-433. doi:10.1101/gad.2021311

Polterauer, S., Vergote, I., Concin, N., Braicu, I., Chekerov, R., Mahner, S.*, et al.* (2012). Prognostic value of residual tumor size in patients with epithelial ovarian cancer FIGO stages IIA-IV: analysis of the OVCAD data. *Int J Gynecol Cancer, 22*(3), 380-385. doi:10.1097/IGC.0b013e31823de6ae

Pommier, Y., O'Connor, M. J., & de Bono, J. (2016). Laying a trap to kill cancer cells: PARP inhibitors and their mechanisms of action. *Science Translational Medicine, 8*(362), 362ps317-362ps317. doi:10.1126/scitranslmed.aaf9246

Prat, J. (2012a). New insights into ovarian cancer pathology. *Ann Oncol, 23 Suppl 10*, x111-117. doi:10.1093/annonc/mds300

Prat, J. (2012b). Ovarian carcinomas: five distinct diseases with different origins, genetic alterations, and clinicopathological features. *Virchows Arch, 460*(3), 237-249. doi:10.1007/s00428-012-1203-5

Prieske, K., Prieske, S., Joosse, S. A., Trillsch, F., Grimm, D., Burandt, E.*, et al.* (2017). Loss of BRCA1 promotor hypermethylation in recurrent high-grade ovarian cancer. *Oncotarget, 8*(47), 83063.

Prieto, J. L., & McStay, B. (2007). Recruitment of factors linking transcription and processing of pre-rRNA to NOR chromatin is UBF-dependent and occurs independent of transcription in human cells. *Genes Dev, 21*(16), 2041-2054. doi:10.1101/gad.436707

Printz, C. (2015). NCI launches exceptional responders initiative: researchers will attempt to identify why some patients respond to treatment so much better than others. *Cancer, 121*(6), 803-804.

Pujade-Lauraine, E., Ledermann, J. A., Selle, F., Gebski, V., Penson, R. T., Oza, A. M.*, et al.* (2017). Olaparib tablets as maintenance therapy in patients with platinum-sensitive, relapsed ovarian cancer and a BRCA1/2 mutation (SOLO2/ENGOT-Ov21): a double-blind, randomised, placebo-controlled, phase 3 trial. *Lancet Oncol, 18*(9), 1274-1284. doi:10.1016/s1470-2045(17)30469-2

Pulliam, N., Fang, F., Ozes, A. R., Tang, J., Adewuyi, A., Keer, H.*, et al.* (2018). An Effective Epigenetic-PARP Inhibitor Combination Therapy for Breast and Ovarian Cancers

Independent of BRCA Mutations. *Clinical Cancer Research, 24*(13), 3163-3175. doi:10.1158/1078-0432.Ccr-18-0204

Qiao, G., Jia, X., Zhang, Y., & Chen, B. (2019). Neurofibromin 1 expression is negatively correlated with malignancy and prognosis of epithelial ovarian cancer. *International journal of clinical and experimental pathology, 12*(5), 1702-1712.

Radziszewska, A. U., Karczmarek-Borowska, B., Wójcik, S., & Kluz, T. (2018). Survival rates among women with ovarian cancers diagnosed in the area of Podkarpacie province in the years 1990-2015. *Contemporary oncology (Poznan, Poland), 22*(3), 151-157. doi:10.5114/wo.2018.78935

Rafnar, T., Gudbjartsson, D. F., Sulem, P., Jonasdottir, A., Sigurdsson, A., Jonasdottir, A.*, et al.* (2011). Mutations in BRIP1 confer high risk of ovarian cancer. *Nat Genet, 43*(11), 1104-1107. doi:10.1038/ng.955

Raja, F. A., Chopra, N., & Ledermann, J. A. (2012). Optimal first-line treatment in ovarian cancer. *Annals of Oncology, 23*(suppl_10), x118-x127. doi:10.1093/annonc/mds315

Ray Chaudhuri, A., Callen, E., Ding, X., Gogola, E., Duarte, A. A., Lee, J.-E.*, et al.* (2016). Replication fork stability confers chemoresistance in BRCA-deficient cells. *Nature, 535*(7612), 382-387. doi:10.1038/nature18325

Ray Chaudhuri, A., Hashimoto, Y., Herrador, R., Neelsen, K. J., Fachinetti, D., Bermejo, R.*, et al.* (2012). Topoisomerase I poisoning results in PARP-mediated replication fork reversal. *Nat Struct Mol Biol, 19*(4), 417-423. doi:10.1038/nsmb.2258

Ray-Coquard, I., Pautier, P., Pignata, S., Pérol, D., González-Martín, A., Berger, R.*, et al.* (2019). Olaparib plus Bevacizumab as First-Line Maintenance in Ovarian Cancer. *New England Journal of Medicine, 381*(25), 2416-2428.

Rebbeck, T. R., Kauff, N. D., & Domchek, S. M. (2009). Meta-analysis of risk reduction estimates associated with risk-reducing salpingo-oophorectomy in BRCA1 or BRCA2 mutation carriers. *J Natl Cancer Inst, 101*(2), 80-87. doi:10.1093/jnci/djn442

Rhyasen, G. W., Yao, Y., Zhang, J., Dulak, A., Castriotta, L., Jacques, K.*, et al.* (2018). BRD4 amplification facilitates an oncogenic gene expression program in high-grade serous ovarian cancer and confers sensitivity to BET inhibitors. *PloS one, 13*(7), e0200826. doi:10.1371/journal.pone.0200826

Riballo, E., Kuhne, M., Rief, N., Doherty, A., Smith, G. C., Recio, M. J.*, et al.* (2004). A pathway of double-strand break rejoining dependent upon ATM, Artemis, and proteins locating to gamma-H2AX foci. *Mol Cell, 16*(5), 715-724. doi:10.1016/j.molcel.2004.10.029

Richards, S., Aziz, N., Bale, S., Bick, D., Das, S., Gastier-Foster, J.*, et al.* (2015). Standards and guidelines for the interpretation of sequence variants: a joint consensus recommendation of the American College of Medical Genetics and Genomics and the Association for Molecular Pathology. *Genet Med, 17*(5), 405-424. doi:10.1038/gim.2015.30

Richart, L., Carrillo-de Santa Pau, E., Río-Machín, A., de Andrés, M. P., Cigudosa, J. C., Lobo, V. J. S.-A.*, et al.* (2016). BPTF is required for c-MYC transcriptional activity and in vivo tumorigenesis. *Nature Communications, 7*(1), 10153. doi:10.1038/ncomms10153

Riley, R. S., June, C. H., Langer, R., & Mitchell, M. J. (2019). Delivery technologies for cancer immunotherapy. *Nature reviews. Drug discovery, 18*(3), 175-196. doi:10.1038/s41573-018-0006-z

Ronaghi, M., Uhlén, M., & Nyrén, P. (1998). A sequencing method based on real-time pyrophosphate. *Science, 281*(5375), 363-365.

Rondinelli, B., Gogola, E., Yucel, H., Duarte, A. A., van de Ven, M., van der Sluijs, R.*, et al.* (2017). EZH2 promotes degradation of stalled replication forks by recruiting MUS81

through histone H3 trimethylation. *Nat Cell Biol, 19*(11), 1371-1378. doi:10.1038/ncb3626

Roy, R., Chun, J., & Powell, S. N. (2012). BRCA1 and BRCA2: different roles in a common pathway of genome protection. *Nature Reviews Cancer, 12*(1), 68-78.

Rubin, G., Vedsted, P., & Emery, J. (2011). Improving cancer outcomes: better access to diagnostics in primary care could be critical. *British Journal of General Practice, 61*(586), 317-318. doi:10.3399/bjgp11X572283

Ruscito, I., Dimitrova, D., Vasconcelos, I., Gellhaus, K., Schwachula, T., Bellati, F.*, et al.* (2014). BRCA1 gene promoter methylation status in high-grade serous ovarian cancer patients–a study of the tumour Bank ovarian cancer (TOC) and ovarian cancer diagnosis consortium (OVCAD). *European Journal of Cancer, 50*(12), 2090-2098.

Ryan, R. J., Nitta, M., Borger, D., Zukerberg, L. R., Ferry, J. A., Harris, N. L.*, et al.* (2011). EZH2 codon 641 mutations are common in BCL2-rearranged germinal center B cell lymphomas. *PloS one, 6*(12), e28585. doi:10.1371/journal.pone.0028585

Sage, J. (2012). The retinoblastoma tumor suppressor and stem cell biology. *Genes Dev, 26*(13), 1409-1420. doi:10.1101/gad.193730.112

Sakai, W., Swisher, E. M., Jacquemont, C., Chandramohan, K. V., Couch, F. J., Langdon, S. P.*, et al.* (2009). Functional restoration of BRCA2 protein by secondary BRCA2 mutations in BRCA2-mutated ovarian carcinoma. *Cancer Res, 69*(16), 6381-6386. doi:10.1158/0008-5472.CAN-09-1178

Sakai, W., Swisher, E. M., Karlan, B. Y., Agarwal, M. K., Higgins, J., Friedman, C.*, et al.* (2008). Secondary mutations as a mechanism of cisplatin resistance in BRCA2-mutated cancers. *Nature, 451*(7182), 1116-1120. doi:10.1038/nature06633

Saleh-Gohari, N., Bryant, H. E., Schultz, N., Parker, K. M., Cassel, T. N., & Helleday, T. (2005). Spontaneous homologous recombination is induced by collapsed replication forks that are caused by endogenous DNA single-strand breaks. *Mol Cell Biol, 25*(16), 7158-7169. doi:10.1128/MCB.25.16.7158-7169.2005

Salhab, M., Bismohun, S., & Mokbel, K. (2010). Risk-reducing strategies for women carrying BRCA1/2 mutations with a focus on prophylactic surgery. *BMC Womens Health, 10*, 28. doi:10.1186/1472-6874-10-28

Samimi, G., Safaei, R., Katano, K., Holzer, A. K., Rochdi, M., Tomioka, M.*, et al.* (2004). Increased expression of the copper efflux transporter ATP7A mediates resistance to cisplatin, carboplatin, and oxaliplatin in ovarian cancer cells. *Clin Cancer Res, 10*(14), 4661-4669. doi:10.1158/1078-0432.CCR-04-0137

Samstein, R. M., Lee, C.-H., Shoushtari, A. N., Hellmann, M. D., Shen, R., Janjigian, Y. Y.*, et al.* (2019). Tumor mutational load predicts survival after immunotherapy across multiple cancer types. *Nature Genetics, 51*(2), 202-206. doi:10.1038/s41588-018-0312-8

Sancak, Y., Bar-Peled, L., Zoncu, R., Markhard, A. L., Nada, S., & Sabatini, D. M. (2010). Ragulator-Rag complex targets mTORC1 to the lysosomal surface and is necessary for its activation by amino acids. *Cell, 141*(2), 290-303. doi:10.1016/j.cell.2010.02.024

Saner, F. A. M., Herschtal, A., Nelson, B. H., deFazio, A., Goode, E. L., Ramus, S. J.*, et al.* (2019). Going to extremes: determinants of extraordinary response and survival in patients with cancer. *Nat Rev Cancer, 19*(6), 339-348. doi:10.1038/s41568-019-0145-5

Sanij, E., Hannan, K. M., Xuan, J., Yan, S., Ahern, J. E., Trigos, A. S.*, et al.* (2020). CX-5461 activates the DNA damage response and demonstrates therapeutic efficacy in high-grade serous ovarian cancer. *Nat Commun, 11*(1), 2641. doi:10.1038/s41467-020-16393-4

Sankaranarayanan, R., & Ferlay, J. (2006). Worldwide burden of gynaecological cancer: the size of the problem. *Best practice & research Clinical obstetrics & gynaecology, 20*(2), 207-225.

Sartori, A. A., Lukas, C., Coates, J., Mistrik, M., Fu, S., Bartek, J.*, et al.* (2007). Human CtIP promotes DNA end resection. *Nature, 450*(7169), 509-514. doi:10.1038/nature06337

Satoh, M. S., & Lindahl, T. (1992). Role of poly(ADP-ribose) formation in DNA repair. *Nature, 356*(6367), 356-358. doi:10.1038/356356a0

Scarabelli, C., Gallo, A., Franceschi, S., Campagnutta, E., De Piero, G., Giorda, G.*, et al.* (2000). Primary cytoreductive surgery with rectosigmoid colon resection for patients with advanced epithelial ovarian carcinoma. *Cancer, 88*(2), 389-397. doi:10.1002/(SICI)1097-0142(20000115)88:2<389::AID-CNCR21>3.0.CO;2-W

Schlacher, K., Wu, H., & Jasin, M. (2012). A distinct replication fork protection pathway connects Fanconi anemia tumor suppressors to RAD51-BRCA1/2. *Cancer Cell, 22*(1), 106-116. doi:10.1016/j.ccr.2012.05.015

Schreiber, V., Hunting, D., Trucco, C., Gowans, B., Grunwald, D., De Murcia, G.*, et al.* (1995). A dominant-negative mutant of human poly(ADP-ribose) polymerase affects cell recovery, apoptosis, and sister chromatid exchange following DNA damage. *Proc Natl Acad Sci U S A, 92*(11), 4753-4757. doi:10.1073/pnas.92.11.4753

Schultz, N., Lopez, E., Saleh-Gohari, N., & Helleday, T. (2003). Poly(ADP-ribose) polymerase (PARP-1) has a controlling role in homologous recombination. *Nucleic Acids Res, 31*(17), 4959-4964. doi:10.1093/nar/gkg703

Schwarz, J. M., Cooper, D. N., Schuelke, M., & Seelow, D. (2014). MutationTaster2: mutation prediction for the deep-sequencing age. *Nature Methods, 11*(4), 361-362. doi:10.1038/nmeth.2890

Scott, C., Becker, M. A., Haluska, P., & Samimi, G. (2013). Patient-derived xenograft models to improve targeted therapy in epithelial ovarian cancer treatment. *Frontiers in oncology, 3*, 295.

Scott, C. L., Swisher, E. M., & Kaufmann, S. H. (2015). Poly (ADP-ribose) polymerase inhibitors: recent advances and future development. *J Clin Oncol, 33*(12), 1397-1406. doi:10.1200/JCO.2014.58.8848

Semionov, A., Cournoyer, D., & Chow, T. Y. (1999). Inhibition of poly(ADP-ribose)polymerase stimulates extrachromosomal homologous recombination in mouse Ltk-fibroblasts. *Nucleic Acids Res, 27*(22), 4526-4531. doi:10.1093/nar/27.22.4526

Shao, G., Wan, X., Lai, W., Wu, C., Jin, J., Liu, X.*, et al.* (2018). Inhibition of lysine-specific demethylase 1 prevents proliferation and mediates cisplatin sensitivity in ovarian cancer cells. *Oncol Lett, 15*(6), 9025-9032. doi:10.3892/ol.2018.8511

Shen, J., Zhao, W., Ju, Z., Wang, L., Peng, Y., Labrie, M.*, et al.* (2019). PARPi triggers the STING-dependent immune response and enhances the therapeutic efficacy of immune checkpoint blockade independent of BRCAness. *Cancer Research, 79*(2), 311-319.

Shewell, L. K., Wang, J. J., Paton, J. C., Paton, A. W., Day, C. J., & Jennings, M. P. (2018). Detection of N-glycolylneuraminic acid biomarkers in sera from patients with ovarian cancer using an engineered N-glycolylneuraminic acid-specific lectin SubB2M. *Biochem Biophys Res Commun, 507*(1-4), 173-177. doi:10.1016/j.bbrc.2018.11.001

Shi, H., Hayes, M., Kirana, C., Miller, R., Keating, J., Macartney-Coxson, D.*, et al.* (2012). TUFM is a potential new prognostic indicator for colorectal carcinoma. *Pathology, 44*(6), 506-512. doi:10.1097/PAT.0b013e3283559cbe

Shima, N., Munroe, R. J., & Schimenti, J. C. (2004). The mouse genomic instability mutation chaos1 is an allele of Polq that exhibits genetic interaction with Atm. *Mol Cell Biol, 24*(23), 10381-10389. doi:10.1128/MCB.24.23.10381-10389.2004

Siegel, R., Ma, J., Zou, Z., & Jemal, A. (2014). Cancer statistics, 2014. *CA: A Cancer Journal for Clinicians, 64*(1), 9-29. doi:10.3322/caac.21208

Simsek, D., Brunet, E., Wong, S. Y., Katyal, S., Gao, Y., McKinnon, P. J.*, et al.* (2011). DNA ligase III promotes alternative nonhomologous end-joining during chromosomal translocation formation. *PLoS Genet, 7*(6), e1002080. doi:10.1371/journal.pgen.1002080

Singer, G., Kurman, R. J., Chang, H. W., Cho, S. K., & Shih Ie, M. (2002). Diverse tumorigenic pathways in ovarian serous carcinoma. *Am J Pathol, 160*(4), 1223-1228. doi:10.1016/s0002-9440(10)62549-7

Skvortsova, K., Masle-Farquhar, E., Luu, P.-L., Song, J. Z., Qu, W., Zotenko, E.*, et al.* (2019). DNA Hypermethylation Encroachment at CpG Island Borders in Cancer Is Predisposed by H3K4 Monomethylation Patterns. *Cancer Cell, 35*(2), 297-314.e298. doi:doi.org/10.1016/j.ccell.2019.01.004

Sloane, M. A., Ward, R. L., & Hesson, L. B. (2016). Defining the criteria for identifying constitutional epimutations. *Clinical epigenetics, 8*, 39-39. doi:10.1186/s13148-016-0207-4

Smith, M. A., Hampton, O. A., Reynolds, C. P., Kang, M. H., Maris, J. M., Gorlick, R.*, et al.* (2015). Initial testing (stage 1) of the PARP inhibitor BMN 673 by the pediatric preclinical testing program: PALB2 mutation predicts exceptional in vivo response to BMN 673. *Pediatr Blood Cancer, 62*(1), 91-98. doi:10.1002/pbc.25201

Snell, C., Krypuy, M., Wong, E. M., kConFab, i., Loughrey, M. B., & Dobrovic, A. (2008). BRCA1 promoter methylation in peripheral blood DNA of mutation negative familial breast cancer patients with a BRCA1 tumour phenotype. *Breast cancer research : BCR, 10*(1), R12-R12. doi:10.1186/bcr1858

Song, S., Nones, K., Miller, D., Harliwong, I., Kassahn, K. S., Pinese, M.*, et al.* (2012). qpure: A Tool to Estimate Tumor Cellularity from Genome-Wide Single-Nucleotide Polymorphism Profiles. *PloS one, 7*(9), e45835. doi:10.1371/journal.pone.0045835

Sousa, F. G., Matuo, R., Soares, D. G., Escargueil, A. E., Henriques, J. A., Larsen, A. K.*, et al.* (2012). PARPs and the DNA damage response. *Carcinogenesis, 33*(8), 1433-1440. doi:10.1093/carcin/bgs132

Stefansson, O. A., Villanueva, A., Vidal, A., Martí, L., & Esteller, M. (2012). BRCA1 epigenetic inactivation predicts sensitivity to platinum-based chemotherapy in breast and ovarian cancer. *Epigenetics, 7*(11), 1225-1229.

Stewart, J. M., Shaw, P. A., Gedye, C., Bernardini, M. Q., Neel, B. G., & Ailles, L. E. (2011). Phenotypic heterogeneity and instability of human ovarian tumor-initiating cells. *Proceedings of the National Academy of Sciences, 108*(16), 6468-6473.

Stracker, T. H., & Petrini, J. H. (2011). The MRE11 complex: starting from the ends. *Nat Rev Mol Cell Biol, 12*(2), 90-103. doi:10.1038/nrm3047

Strathdee, G., MacKean, M. J., Illand, M., & Brown, R. (1999). A role for methylation of the hMLH1 promoter in loss of hMLH1 expression and drug resistance in ovarian cancer. *Oncogene, 18*(14), 2335-2341. doi:10.1038/sj.onc.1202540

Strickland, K. C., Howitt, B. E., Shukla, S. A., Rodig, S., Ritterhouse, L. L., Liu, J. F.*, et al.* (2016). Association and prognostic significance of BRCA1/2-mutation status with neoantigen load, number of tumor-infiltrating lymphocytes and expression of PD-1/PD-L1 in high grade serous ovarian cancer. *Oncotarget, 7*(12), 13587.

Strom, C. E., Johansson, F., Uhlen, M., Szigyarto, C. A., Erixon, K., & Helleday, T. (2011). Poly (ADP-ribose) polymerase (PARP) is not involved in base excision repair but PARP inhibition traps a single-strand intermediate. *Nucleic Acids Res, 39*(8), 3166-3175. doi:10.1093/nar/gkq1241

Su, H. Y., Lai, H. C., Lin, Y. W., Liu, C. Y., Chen, C. K., Chou, Y. C., *et al.* (2010). Epigenetic silencing of SFRP5 is related to malignant phenotype and chemoresistance of ovarian cancer through Wnt signaling pathway. *Int J Cancer, 127*(3), 555-567. doi:10.1002/ijc.25083

Sugimura, K., Takebayashi, S., Taguchi, H., Takeda, S., & Okumura, K. (2008). PARP-1 ensures regulation of replication fork progression by homologous recombination on damaged DNA. *J Cell Biol, 183*(7), 1203-1212. doi:10.1083/jcb.200806068

Sullivan-Reed, K., Bolton-Gillespie, E., Dasgupta, Y., Langer, S., Siciliano, M., Nieborowska-Skorska, M., *et al.* (2018). Simultaneous Targeting of PARP1 and RAD52 Triggers Dual Synthetic Lethality in BRCA-Deficient Tumor Cells. *Cell Rep, 23*(11), 3127-3136. doi:10.1016/j.celrep.2018.05.034

Sun, C., Fang, Y., Yin, J., Chen, J., Ju, Z., Zhang, D., *et al.* (2017). Rational combination therapy with PARP and MEK inhibitors capitalizes on therapeutic liabilities in RAS mutant cancers. *Sci Transl Med, 9*(392). doi:10.1126/scitranslmed.aal5148

Swisher, E. M., Gonzalez, R. M., Taniguchi, T., Garcia, R. L., Walsh, T., Goff, B. A., *et al.* (2009). Methylation and protein expression of DNA repair genes: association with chemotherapy exposure and survival in sporadic ovarian and peritoneal carcinomas. *Mol Cancer, 8*, 48. doi:10.1186/1476-4598-8-48

Swisher, E. M., Lin, K. K., Oza, A. M., Scott, C. L., Giordano, H., Sun, J., *et al.* (2017). Rucaparib in relapsed, platinum-sensitive high-grade ovarian carcinoma (ARIEL2 Part 1): an international, multicentre, open-label, phase 2 trial. *Lancet Oncol, 18*(1), 75-87. doi:10.1016/S1470-2045(16)30559-9

Taglialatela, A., Alvarez, S., Leuzzi, G., Sannino, V., Ranjha, L., Huang, J. W., *et al.* (2017). Restoration of Replication Fork Stability in BRCA1- and BRCA2-Deficient Cells by Inactivation of SNF2-Family Fork Remodelers. *Mol Cell, 68*(2), 414-430.e418. doi:10.1016/j.molcel.2017.09.036

Tan, T. Z., Miow, Q. H., Huang, R. Y., Wong, M. K., Ye, J., Lau, J. A., *et al.* (2013). Functional genomics identifies five distinct molecular subtypes with clinical relevance and pathways for growth control in epithelial ovarian cancer. *EMBO Mol Med, 5*(7), 1051-1066. doi:10.1002/emmm.201201823

Tang, Z., Yuan, X., Du, R., Cheung, S. H., Zhang, G., Wei, J., *et al.* (2015). BGB-283, a Novel RAF Kinase and EGFR Inhibitor, Displays Potent Antitumor Activity in BRAF-Mutated Colorectal Cancers. *Mol Cancer Ther, 14*(10), 2187-2197. doi:10.1158/1535-7163.MCT-15-0262

Tao, L., Yang, S., Xie, M., Kramer, P. M., & Pereira, M. A. (2000). Hypomethylation and overexpression of c-jun and c-myc protooncogenes and increased DNA methyltransferase activity in dichloroacetic and trichloroacetic acid-promoted mouse liver tumors. *Cancer Lett, 158*(2), 185-193. doi:10.1016/s0304-3835(00)00518-8

TCGA, C. G. A. R. N. (2011). Integrated genomic analyses of ovarian carcinoma. *Nature, 474*(7353), 609.

Tentler, J. J., Tan, A. C., Weekes, C. D., Jimeno, A., Leong, S., Pitts, T. M., *et al.* (2012). Patient-derived tumour xenografts as models for oncology drug development. *Nature reviews Clinical oncology, 9*(6), 338.

Tentori, L., Lacal, P. M., Muzi, A., Dorio, A. S., Leonetti, C., Scarsella, M., *et al.* (2007). Poly (ADP-ribose) polymerase (PARP) inhibition or PARP-1 gene deletion reduces angiogenesis. *European Journal of Cancer, 43*(14), 2124-2133.

Tewari, K. S., Burger, R. A., Enserro, D., Norquist, B. M., Swisher, E. M., Brady, M. F., *et al.* (2019). Final Overall Survival of a Randomized Trial of Bevacizumab for Primary Treatment of Ovarian Cancer. *J Clin Oncol, 37*(26), 2317-2328. doi:10.1200/jco.19.01009

To, C., Kim, E.-H., Royce, D. B., Williams, C. R., Collins, R. M., Risingsong, R.*, et al.* (2014). The PARP inhibitors, veliparib and olaparib, are effective chemopreventive agents for delaying mammary tumor development in BRCA1-deficient mice. *Cancer prevention research (Philadelphia, Pa.), 7*(7), 698-707. doi:10.1158/1940-6207.CAPR-14-0047

Tomar, T., de Jong, S., Alkema, N. G., Hoekman, R. L., Meersma, G. J., Klip, H. G.*, et al.* (2016). Genome-wide methylation profiling of ovarian cancer patient-derived xenografts treated with the demethylating agent decitabine identifies novel epigenetically regulated genes and pathways. *Genome medicine, 8*(1), 107.

Topp, M. D., Hartley, L., Cook, M., Heong, V., Boehm, E., McShane, L.*, et al.* (2014). Molecular correlates of platinum response in human high-grade serous ovarian cancer patient-derived xenografts. *Mol Oncol, 8*(3), 656-668. doi:10.1016/j.molonc.2014.01.008

Torre, L. A., Trabert, B., DeSantis, C. E., Miller, K. D., Samimi, G., Runowicz, C. D.*, et al.* (2018). Ovarian cancer statistics, 2018. *CA Cancer J Clin, 68*(4), 284-296. doi:10.3322/caac.21456

Tothill, R. W., Tinker, A. V., George, J., Brown, R., Fox, S. B., Lade, S.*, et al.* (2008). Novel molecular subtypes of serous and endometrioid ovarian cancer linked to clinical outcome. *Clin Cancer Res, 14*(16), 5198-5208. doi:10.1158/1078-0432.CCR-08-0196

Trucco, C., Oliver, F. J., de Murcia, G., & Menissier-de Murcia, J. (1998). DNA repair defect in poly(ADP-ribose) polymerase-deficient cell lines. *Nucleic Acids Res, 26*(11), 2644-2649. doi:10.1093/nar/26.11.2644

Turner, J. G., Dawson, J., & Sullivan, D. M. (2012). Nuclear export of proteins and drug resistance in cancer. *Biochemical pharmacology, 83*(8), 1021-1032. doi:10.1016/j.bcp.2011.12.016

Turner, N., Tutt, A., & Ashworth, A. (2004). Hallmarks of 'BRCAness' in sporadic cancers. *Nat Rev Cancer, 4*(10), 814-819. doi:10.1038/nrc1457

Tutt, A., Bertwistle, D., Valentine, J., Gabriel, A., Swift, S., Ross, G.*, et al.* (2001). Mutation in Brca2 stimulates error-prone homology-directed repair of DNA double-strand breaks occurring between repeated sequences. *EMBO J, 20*(17), 4704-4716. doi:10.1093/emboj/20.17.4704

Tutt, A., Robson, M., Garber, J. E., Domchek, S. M., Audeh, M. W., Weitzel, J. N.*, et al.* (2010). Oral poly(ADP-ribose) polymerase inhibitor olaparib in patients with BRCA1 or BRCA2 mutations and advanced breast cancer: a proof-of-concept trial. *Lancet, 376*(9737), 235-244. doi:10.1016/S0140-6736(10)60892-6

Ulus-Senguloglu, G., Arlett, C. F., Plowman, P. N., Parnell, J., Patel, N., Bourton, E. C.*, et al.* (2012). Elevated expression of artemis in human fibroblast cells is associated with cellular radiosensitivity and increased apoptosis. *British journal of cancer, 107*(9), 1506-1513. doi:10.1038/bjc.2012.443

van de Ven, M., van der Burg, E., van der Gulden, H., Klarenbeek, S., Bouwman, P., & Jonkers, J. (2017a). Prophylactic window therapy with the clinical poly(ADP-ribose) polymerase inhibitor olaparib delays BRCA1-deficient mammary tumour formation in mice. *The Journal of Pathology, 241*(4), 511-521. doi:10.1002/path.4857

van de Ven, M., van der Burg, E., van der Gulden, H., Klarenbeek, S., Bouwman, P., & Jonkers, J. (2017b). Prophylactic window therapy with the clinical poly(ADP-ribose) polymerase inhibitor olaparib delays BRCA1-deficient mammary tumour formation in mice. *J Pathol, 241*(4), 511-521. doi:10.1002/path.4857

van Gent, D. C., Hoeijmakers, J. H., & Kanaar, R. (2001). Chromosomal stability and the DNA double-stranded break connection. *Nat Rev Genet, 2*(3), 196-206. doi:10.1038/35056049

Vasey, P. A., Jayson, G. C., Gordon, A., Gabra, H., Coleman, R., Atkinson, R.*, et al.* (2004). Phase III Randomized Trial of Docetaxel–Carboplatin Versus Paclitaxel–Carboplatin as First-line Chemotherapy for Ovarian Carcinoma. *JNCI: Journal of the National Cancer Institute, 96*(22), 1682-1691. doi:10.1093/jnci/djh323

Vaughan, S., Coward, J. I., Bast, R. C., Jr., Berchuck, A., Berek, J. S., Brenton, J. D.*, et al.* (2011). Rethinking ovarian cancer: recommendations for improving outcomes. *Nat Rev Cancer, 11*(10), 719-725. doi:10.1038/nrc3144

Veeck, J., Ropero, S., Setien, F., Gonzalez-Suarez, E., Osorio, A., Benitez, J.*, et al.* (2010). BRCA1 CpG island hypermethylation predicts sensitivity to poly(adenosine diphosphate)-ribose polymerase inhibitors. *J Clin Oncol, 28*(29), e563-564; author reply e565-566. doi:10.1200/JCO.2010.30.1010

Venkatesh, H., & Monje, M. (2017). Neuronal Activity in Ontogeny and Oncology. *Trends in Cancer, 3*(2), 89-112. doi:10.1016/j.trecan.2016.12.008

Verigos, J., Karakaidos, P., Kordias, D., Papoudou-Bai, A., Evangelou, Z., Harissis, H. V.*, et al.* (2019). The Histone Demethylase LSD1/KappaDM1A Mediates Chemoresistance in Breast Cancer via Regulation of a Stem Cell Program. *Cancers (Basel), 11*(10). doi:10.3390/cancers11101585

Villarroel, M. C., Rajeshkumar, N. V., Garrido-Laguna, I., De Jesus-Acosta, A., Jones, S., Maitra, A.*, et al.* (2011). Personalizing cancer treatment in the age of global genomic analyses: PALB2 gene mutations and the response to DNA damaging agents in pancreatic cancer. *Mol Cancer Ther, 10*(1), 3-8. doi:10.1158/1535-7163.MCT-10-0893

Viré, E., Brenner, C., Deplus, R., Blanchon, L., Fraga, M., Didelot, C.*, et al.* (2006). The Polycomb group protein EZH2 directly controls DNA methylation. *Nature, 439*(7078), 871-874. doi:10.1038/nature04431

Vogelstein, B., Lane, D., & Levine, A. J. (2000). Surfing the p53 network. *Nature, 408*(6810), 307-310. doi:10.1038/35042675

Vos, S., van Diest, P. J., & Moelans, C. B. (2018). A systematic review on the frequency of BRCA promoter methylation in breast and ovarian carcinomas of BRCA germline mutation carriers: Mutually exclusive, or not? *Critical reviews in oncology/hematology, 127*, 29-41.

Wakefield, M. J. (2016). SurvivalVolume: interactive volume threshold survival graphs. *J. Open Source Software, 1*(8), 111.

Waldman, A. S., & Waldman, B. C. (1991). Stimulation of intrachromosomal homologous recombination in mammalian cells by an inhibitor of poly(ADP-ribosylation). *Nucleic Acids Res, 19*(21), 5943-5947. doi:10.1093/nar/19.21.5943

Walsh, T., Casadei, S., Lee, M. K., Pennil, C. C., Nord, A. S., Thornton, A. M.*, et al.* (2011). Mutations in 12 genes for inherited ovarian, fallopian tube, and peritoneal carcinoma identified by massively parallel sequencing. *Proc Natl Acad Sci U S A, 108*(44), 18032-18037. doi:10.1073/pnas.1115052108

Wang, H., Bauzon, F., Ji, P., Xu, X., Sun, D., Locker, J.*, et al.* (2010). Skp2 is required for survival of aberrantly proliferating Rb1-deficient cells and for tumorigenesis in Rb1+/- mice. *Nat Genet, 42*(1), 83-88. doi:10.1038/ng.498

Wang, H., Zeng, Z.-C., Perrault, A. R., Cheng, X., Qin, W., & Iliakis, G. (2001). Genetic evidence for the involvement of DNA ligase IV in the DNA-PK-dependent pathway of non-homologous end joining in mammalian cells. *Nucleic Acids Research, 29*(8), 1653-1660. doi:10.1093/nar/29.8.1653

Wang, M., Wu, W., Wu, W., Rosidi, B., Zhang, L., Wang, H.*, et al.* (2006). PARP-1 and Ku compete for repair of DNA double strand breaks by distinct NHEJ pathways. *Nucleic Acids Res, 34*(21), 6170-6182. doi:10.1093/nar/gkl840

Wang, Y., Bernhardy, A. J., Cruz, C., Krais, J. J., Nacson, J., Nicolas, E., *et al.* (2016). The BRCA1-Delta11q Alternative Splice Isoform Bypasses Germline Mutations and Promotes Therapeutic Resistance to PARP Inhibition and Cisplatin. *Cancer Res, 76*(9), 2778-2790. doi:10.1158/0008-5472.CAN-16-0186

Watts, G. S., Futscher, B. W., Holtan, N., Degeest, K., Domann, F. E., & Rose, S. L. (2008). DNA methylation changes in ovarian cancer are cumulative with disease progression and identify tumor stage. *BMC Med Genomics, 1*, 47. doi:10.1186/1755-8794-1-47

Wei, S. H., Chen, C.-M., Strathdee, G., Harnsomburana, J., Shyu, C.-R., Rahmatpanah, F., *et al.* (2002). Methylation microarray analysis of late-stage ovarian carcinomas distinguishes progression-free survival in patients and identifies candidate epigenetic markers. *Clinical Cancer Research, 8*(7), 2246-2252.

Widschwendter, A., Müller, H. M., Fiegl, H., Ivarsson, L., Wiedemair, A., Müller-Holzner, E., *et al.* (2004). DNA methylation in serum and tumors of cervical cancer patients. *Clinical Cancer Research, 10*(2), 565-571.

Wilkerson, P. M., Dedes, K. J., Wetterskog, D., Mackay, A., Lambros, M. B., Mansour, M., *et al.* (2011). Functional characterization of EMSY gene amplification in human cancers. *J Pathol, 225*(1), 29-42. doi:10.1002/path.2944

Williamson, C. T., Kubota, E., Hamill, J. D., Klimowicz, A., Ye, R., Muzik, H., *et al.* (2012). Enhanced cytotoxicity of PARP inhibition in mantle cell lymphoma harbouring mutations in both ATM and p53. *EMBO Mol Med, 4*(6), 515-527. doi:10.1002/emmm.201200229

Winter, J., Schwering, M., Pelz, O., Rauscher, B., Zhan, T., Heigwer, F., *et al.* (2017). CRISPRAnalyzeR: Interactive analysis, annotation and documentation of pooled CRISPR screens. *bioRxiv*, 109967. doi:10.1101/109967

Wong, E. M., Southey, M. C., Fox, S. B., Brown, M. A., Dowty, J. G., Jenkins, M. A., *et al.* (2011). Constitutional methylation of the BRCA1 promoter is specifically associated with BRCA1 mutation-associated pathology in early-onset breast cancer. *Cancer Prev Res (Phila), 4*(1), 23-33. doi:10.1158/1940-6207.CAPR-10-0212

Wooster, R., Bignell, G., Lancaster, J., Swift, S., Seal, S., Mangion, J., *et al.* (1995). Identification of the breast cancer susceptibility gene BRCA2. *Nature, 378*(6559), 789-792. doi:10.1038/378789a0

Wooster, R., Neuhausen, S. L., Mangion, J., Quirk, Y., Ford, D., Collins, N., *et al.* (1994). Localization of a breast cancer susceptibility gene, BRCA2, to chromosome 13q12-13. *Science, 265*(5181), 2088-2090. doi:10.1126/science.8091231

Wyman, C., Ristic, D., & Kanaar, R. (2004). Homologous recombination-mediated double-strand break repair. *DNA Repair (Amst), 3*(8-9), 827-833. doi:10.1016/j.dnarep.2004.03.037

Xian, W., Miron, A., Roh, M., Semmel, D. R., Yassin, Y., Garber, J., *et al.* (2010). The Li–Fraumeni syndrome (LFS): a model for the initiation of p53 signatures in the distal fallopian tube. *The Journal of Pathology: A Journal of the Pathological Society of Great Britain and Ireland, 220*(1), 17-23.

Xu, G., Chapman, J. R., Brandsma, I., Yuan, J., Mistrik, M., Bouwman, P., *et al.* (2015). REV7 counteracts DNA double-strand break resection and affects PARP inhibition. *Nature, 521*(7553), 541-544. doi:10.1038/nature14328

Xu, H., Di Antonio, M., McKinney, S., Mathew, V., Ho, B., O'Neil, N. J., *et al.* (2017). CX-5461 is a DNA G-quadruplex stabilizer with selective lethality in BRCA1/2 deficient tumours. *Nat Commun, 8*, 14432. doi:10.1038/ncomms14432

Xu, H., Medvedev, S., Pandya, A., Kim, H., Kinose, Y., Brown, E., *et al.* (2018). Abstract LB-265: The novel oral Chk1 inhibitor, SRA737, is active in both PARP inhibitor resistant and CCNE1 amplified high grade serous ovarian cancers. *Cancer*

Research, 78(13 Supplement), LB-265-LB-265. doi:10.1158/1538-7445.Am2018-lb-265

Yan, B., Yin, F., Wang, Q. I., Zhang, W., & Li, L. I. (2016). Integration and bioinformatics analysis of DNA-methylated genes associated with drug resistance in ovarian cancer. *Oncology letters, 12*(1), 157-166. doi:10.3892/ol.2016.4608

Yang, X., Han, H., De Carvalho, D. D., Lay, F. D., Jones, P. A., & Liang, G. (2014). Gene body methylation can alter gene expression and is a therapeutic target in cancer. *Cancer Cell, 26*(4), 577-590. doi:10.1016/j.ccr.2014.07.028

Yap, T. A., Sandhu, S. K., Carden, C. P., & de Bono, J. S. (2011). Poly(ADP-ribose) polymerase (PARP) inhibitors: Exploiting a synthetic lethal strategy in the clinic. *CA Cancer J Clin, 61*(1), 31-49. doi:10.3322/caac.20095

Yong, W. H., Shabihkhani, M., Telesca, D., Yang, S., Tso, J. L., Menjivar, J. C.*, et al.* (2015). Ribosomal proteins RPS11 and RPS20, two stress-response markers of glioblastoma stem cells, are novel predictors of poor prognosis in glioblastoma patients. *PloS one, 10*(10).

Youn, C. K., Kim, M. H., Cho, H. J., Kim, H. B., Chang, I. Y., Chung, M. H.*, et al.* (2004). Oncogenic H-Ras up-regulates expression of ERCC1 to protect cells from platinum-based anticancer agents. *Cancer Res, 64*(14), 4849-4857. doi:10.1158/0008-5472.CAN-04-0348

Zardo, G., Reale, A., Passananti, C., Pradhan, S., Buontempo, S., De Matteis, G.*, et al.* (2002). Inhibition of poly(ADP-ribosyl)ation induces DNA hypermethylation: a possible molecular mechanism. *Faseb j, 16*(10), 1319-1321. doi:10.1096/fj.01-0827fje

Zeidler, M., Varambally, S., Cao, Q., Chinnaiyan, A. M., Ferguson, D. O., Merajver, S. D.*, et al.* (2005). The Polycomb group protein EZH2 impairs DNA repair in breast epithelial cells. *Neoplasia, 7*(11), 1011-1019. doi:10.1593/neo.05472

Zellweger, R., Dalcher, D., Mutreja, K., Berti, M., Schmid, J. A., Herrador, R.*, et al.* (2015). Rad51-mediated replication fork reversal is a global response to genotoxic treatments in human cells. *J Cell Biol, 208*(5), 563-579. doi:10.1083/jcb.201406099

Zisowsky, J., Koegel, S., Leyers, S., Devarakonda, K., Kassack, M. U., Osmak, M.*, et al.* (2007). Relevance of drug uptake and efflux for cisplatin sensitivity of tumor cells. *Biochem Pharmacol, 73*(2), 298-307. doi:10.1016/j.bcp.2006.10.003

Zou, Y., Liu, Y., Wu, X., & Shell, S. M. (2006). Functions of human replication protein A (RPA): from DNA replication to DNA damage and stress responses. *J Cell Physiol, 208*(2), 267-273. doi:10.1002/jcp.20622

9 Appendices

List of appendices:

Appendix A:

Batch 1 of PDX tumour samples run on BROCA (version 6) sequencing during my PhD.

Appendix B:

Batch 2 of PDX tumour samples run on BROCA (version 6) sequencing during my PhD.

Appendix C:

Batch 3 of PDX tumour samples run on BROCA (version 7) sequencing during my PhD.

Appendix D:

Genes covered by BROCA versions 6 and 7.

Appendix E:

Samples tested for secondary mutations using my targeted sequencing assays.

Appendix F:

Tumour samples where protein lysates and FFPE material were sent to the Mayo clinic for C-NHEJ protein analysis.

Appendix A

Batch 1 of PDX tumour samples run on BROCA (version 6) sequencing during my PhD.

Cyclo25 = cyclophosphamide (25mg/kg) treatment; NA = not applicable.

PDX	Tumour	Transplant	Treatment
134019	2109	T3	Vehicle
134019	2048	T4	None
134054	2931	T3	Rucaparib 300mg/kg
23133	6456	T2	Vehicle
23133	6464	T2	Cisplatin 4mg/kg
23133	6459	T2	Cisplatin 4mg/kg
23133	6465	T2	Cisplatin 4mg/kg
23133	6463	T2	Cisplatin 4mg/kg
23133	6462	T2	Vehicle
23133	6458	T2	Vehicle
23133	6466	T2	Vehicle
23133	6461	T2	Vehicle
23133	6457	T2	Vehicle
23133	6460	T2	Rucaparib 450mg/kg
134169	7202	T3	Rucaparib 450mg/kg
134048	7388	T2	Vehicle
134143B	6394	T1	None
134011	1450	T4	Vehicle
134062	1844	T2	None
134062	2509	T3	Cisplatin 4mg/kg
134062	1927	T2	None
134062	2598	T3	Cyclo25
134062	3190	T3	Rucaparib 300mg/kg
134062	3878	T4	Rucaparib 300mg/kg
134140	Baseline	NA	NA

Appendix B

Batch 2 of PDX tumour samples run on BROCA (version 6) sequencing during my PhD.

NA = not applicable.

PDX	Tumour	Transplant	Treatment
134018	Baseline primary frozen	NA	NA
134056	6583	T5	Cisplatin 4mg/kg
134056	6539	T6	Cisplatin 4mg/kg
134056	6544	T6	Cisplatin 4mg/kg
134056	6577	T6	Cisplatin 4mg/kg
134056	6450	T5	Vehicle
134056	6537	T6	Vehicle
134056	6540	T6	Vehicle
134056	2625	T4	Rucaparib 150mg/kg
134056	6128	T5	Rucaparib 150mg/kg
134056	6129	T5	Rucaparib 150mg/kg
134056	6454	T5	Rucaparib 300mg/kg
134056	6453	T5	Rucaparib 300mg/kg
134056	6535	T6	Rucaparib 300mg/kg
134056	6541	T6	Rucaparib 300mg/kg
134056	6542	T6	Rucaparib 300mg/kg
134056	6580	T6	Rucaparib 300mg/kg
134056	6582	T6	Rucaparib 300mg/kg
134056	6585	T6	Rucaparib 300mg/kg
134056	6850	T7	Rucaparib 450mg/kg
134056	6797	T7	Rucaparib 450mg/kg
134056	6543	T6	Vehicle
134056	6545	T6	Vehicle
134056	6578	T6	Vehicle
134056	6579	T6	Vehicle
134107	Baseline ascites frozen	NA	NA
134199	Baseline tumour	NA	NA
134201	Baseline tumour	NA	NA
134206	Baseline tumour	NA	NA
134205C	Baseline tumour	NA	NA
SFRC01021	Baseline FFPE	NA	NA
SFRC01023	Baseline FFPE	NA	NA
SFRC01027B	Baseline FFPE	NA	NA
SFRC01032	Baseline FFPE	NA	NA

Appendix C

Batch 3 of PDX tumour samples run on BROCA (version 7) sequencing during my PhD.

NA = not applicable.

PDX	Tumour	PDX Transplant	PDX Treatment
34931	Baseline	NA	NA
34931	7132	T2	None
34939	Baseline	NA	NA
34939	8518	T3	Vehicle
134019	2109	T3	Vehicle
134019	2280	T3	Vehicle
134019	2342	T3	Vehicle
134019	2108	T3	None
134019	2110	T3	None
134019	2112	T3	None
134019	3423	T4	Rucaparib 300mg/kg
134019	3042	T5	Rucaparib 300mg/kg
134019	3046	T5	Vehicle
134019	2113	T3	None
134183	Baseline	NA	NA
134183	7903	T3	Vehicle
134220	Baseline	NA	NA
134220	7341	T1	None
134019B	3501	T2	Cisplatin 4mg/kg
134019B	3502	T2	Cisplatin 4mg/kg
134019B	3505	T2	Cisplatin 4mg/kg
134019B	3506	T2	Vehicle
134019B	4698	T2	Vehicle
134019B	4614	T3	Rucaparib 300mg/kg
134019B	3753	T2	Cisplatin 4mg/kg
134019B	4694	T3	Rucaparib 300mg/kg
34939B	Baseline	NA	NA
34939B	7900	T2	None

Appendix D

Genes covered by BROCA versions 6 and 7.

HRv6 = BROCA version 6; HRv7 = BROCA version 7; 1 = gene covered; 0 = gene not covered.

Gene	HRv6	HRv7	Gene	HRv6	HRv7	Gene	HRv6	HRv7
ATM	1	1	**FANCB**	1	1	**POLQ**	1	1
ATR	1	1	**FANCC**	1	1	**PPM1D**	1	1
BABAM1	1	1	**FANCD2**	1	0	**PRKDC**	1	0
BAP1	1	1	**FANCE**	1	1	**PTEN**	1	1
BARD1	1	1	**FANCF**	1	1	**RAD50**	1	1
BLM	1	1	**FANCG**	1	1	**RAD51**	1	1
BRCA1	1	1	**FANCI**	1	1	**RAD51B**	1	1
BRCA2	1	1	**FANCL**	1	1	**RAD51C**	1	1
BRCC3	1	1	**FANCM**	1	1	**RAD51D**	1	1
BRE	1	1	**GEN1**	1	1	**RBBP8**	1	1
BRIP1	1	1	**HELQ**	1	1	**RECQL**	1	1
C11ORF30	1	0	**ID4**	1	1	**RIF1**	1	1
CDH4	1	1	**KMT2C**	1	0	**RINT1**	1	1
CDK12	1	1	**KMT2D**	1	0	**SLX4**	1	1
CHD4	1	1	**LIG4**	1	1	**SMARCA4**	1	1
CHEK1	1	1	**MAD2L2**	0	1	**TOPBP1**	1	1
CHEK2	1	1	**MLH1**	1	1	**TP53**	1	1
DCLRE1C	1	1	**MRE11**	1	1	**TP53BP1**	1	1
DDB1	1	1	**MSH2**	1	1	**UBE2T**	0	1
ERCC1	1	1	**MSH6**	1	1	**UIMC1**	1	1
ERCC2	1	1	**NBN**	1	1	**USP28**	1	1
ERCC3	1	1	**NEIL1**	1	1	**WRN**	1	1
ERCC4	1	1	**PALB2**	1	1	**XPA**	1	1
ERCC5	1	1	**PARP1**	1	1	**XPC**	1	1
ERCC6	1	1	**PAXIP1**	1	1	**XRCC2**	1	1
EZH2	0	1	**PIK3CA**	1	1	**XRCC3**	1	1
FAM175A	1	1	**PMS2**	1	1	**XRCC4**	1	1
FANCA	1	1	**POLD1**	1	1	**XRCC5**	1	1
			POLE	1	1	**XRCC6**	1	1

Appendix E

Samples tested for secondary mutations using my targeted sequencing assays.

NA = not available (could not be determined for baseline samples)

PDX	Sample	Primary mutation	Primary mutation frequency	Reversion mutation detected	Treatment
134019	3423	*BRCA2* :c.2323delT	100%	N	Rucaparib 300mg/kg
	3042		100%	N	Rucaparib 300mg/kg
	3202		100%	N	Rucaparib 300mg/kg
	3046		100%	N	Vehicle
	2342		100%	N	Vehicle
	2280		100%	N	Vehicle
	19 Baseline		60%	NA	Chemo-naïve
134019B	3501	*BRCA2:* c.2323delT	100%	N	Cisplatin
	3502		100%	N	Cisplatin
	3505		100%	N	Cisplatin
	3753		100%	N	Cisplatin
	4614		100%	N	Rucaparib 300mg/kg
	4694		100%	N	Rucaparib 300mg/kg
	4617		Failed	N	Rucaparib 300mg/kg
	4615		100%	N	Vehicle
	3503		100%	N	Vehicle
	3506		100%	N	Vehicle
	4698		100%	N	Vehicle
	19B Baseline		29%	NA	Post chemo
134148	6066	*BLM* :c.2207_2212delinsTAGATTC	100%	N	Rucaparib 300mg/kg
	6265		100%	N	Rucaparib 450mg/kg
	6408		100%	N	Rucaparib 450mg/kg
	6065		100%	N	Vehicle
	6085		100%	N	Vehicle
	148 Baseline		78%	NA	None
23133	6459	*BRCA1* :c.181T>G	100%	N	Cisplatin
	6463		100%	N	Cisplatin
	6464		100%	N	Cisplatin
	6465		100%	N	Cisplatin
	6457		100%	N	Vehicle
	6458		100%	N	Vehicle
	6461		100%	N	Vehicle
	6462		100%	N	Vehicle
	6460		100%	N	Rucaparib 450mg/kg
	23133 Baseline		88%	NA	Post chemo + PARPi
134141B	7978	*BRCA1* :c.5346G>A	93%	N	Untreated
	9088		Failed	NA	Untreated
	10054		Failed	NA	Untreated
	141B BL		54%	NA	Post chemo + PARPi
34931	7132	*BRCA2* :c.1313dupA	49%	Y	Untreated
	7133		48%	Y	Untreated
	7948		48%	Y	Untreated
	7865		49%	Y	Untreated
	34931 Baseline		24%	Y	Untreated
134206	7553	*BRCA1* :c.3817C>T	100%	N	Untreated
	7556		100%	N	Untreated
	7555		100%	N	Untreated
	206 Baseline		91%	NA	Post chemo
134206B	206B Baseline		88%	NA	Post chemo + PARPi
134206C	206C Baseline		57%	NA	Post chemo + PARPi

Appendix F

Tumour samples where protein lysates and FFPE material were sent to the Mayo clinic for C-NHEJ protein analysis.

Samples highlighted yellow did not have matched FFPE material sent. 134013 NHEJ1- 134013 NHEJ4 represent PDX 134013 C-NHEJ lineages 1-4.

PDX model	Tumour #	Transplant	Treatment	PDX model	Tumour #	Transplant	Treatment
134148	6070	T3	Cisplatin	134019	3423	T4	Ruc300
134148	6084	T4	Cisplatin	134019	7968	T5	Ruc300
134148	6433	T4	Cisplatin	134056 #56R	8621	T9	Ruc300 STH
134148	6436	T4	Cisplatin	134056 #56R	8626	T9	Ruc300 STH
134148	6086	T4	Cisplatin	134056 #56R	9125	T10	Ruc450 STH
134148	6087	T4	Vehicle	134056 #56R	8061	T8	Vehicle STH
134148	6088	T3	Vehicle	134056 #56R	9127	T10	Vehicle STH
134148	6414	T4	Vehicle	134056 #56R	9130	T10	Vehicle STH
134148	6432	T4	Vehicle	134056 #56R	8063	T8	Ruc300 STH
134148	6435	T4	Vehicle	134056 #56R	8062	T6	Vehicle STH
134148	6793	T5	Vehicle	134056 #56S	8046	T7	Ruc300 STH
134148	6065	T3	Vehicle	134056 #56S	8627	T8	Ruc300 STH
134148	6085	T3	Vehicle	134056 #56S	8628	T8	Ruc300 STH
134148	6413	T4	Cyclo25	134056 #56S	8720	T8	Ruc300 STH
134148	6794	T5	Cyclo25	134056 #56S	8630	T8	Vehicle STH
134148	6803	T5	Cyclo25	134056 #56S	8631	T8	Vehicle STH
134148	6792	T5	Cyclo25+Ruc300	134056 #56S	8632	T8	Vehicle STH
134148	6795	T5	Cyclo25+Ruc300	134056 #56S	8726	T8	Vehicle STH
134148	6824	T5	Cyclo25+Ruc300	134029	1817	T3	Ruc300
134148	6066	T3	Ruc300	134029	2554	T3	Ruc300
134148	6067	T3	Ruc300	134029	3175	T4	Ruc300
134148	6264	T4	Ruc300	134029	1610	T3	Cisplatin
134148	6412	T4	Ruc300	134029	1514	T4	Cisplatin
134148	6416	T4	Ruc300	134029	1434	T3	Cisplatin
134148	6437	T4	Ruc300	134029	1766	T3	Vehicle
134148	6265	T4	Ruc450	134029	1749	T3	Vehicle
134148	6408	T4	Ruc450	134029	1751	T3	Vehicle
134148	6411	T4	Ruc450	134013 NHEJ4	1616 (#1)	T4	3rd line cisplatin
134148	6417	T4	Ruc450	134013 NHEJ4	1616 (#2)	T4	3rd line cisplatin
134148	6418	T4	Ruc450	134013 NHEJ1	7160	T5	NA
134148	6419	T4	Ruc450	134013 NHEJ1	7825	T6	NA
134148	6790	T5	Ruc150+Zalc	134013 NHEJ1	7829	T6	Vehicle
134148	6804	T5	Ruc450+Zalc	134013 NHEJ2	7161	T5	NA
134148	7277	T3	Ruc450+Zalc	134013 NHEJ2	7162	T5	NA
134019B	3913	T2	Cisplatin	134013 NHEJ2	7163	T5	NA
134019B	3501	T2	Cisplatin	134013 NHEJ2	7526	T6	Ruc300
134019B	3502	T2	Cisplatin	134013 NHEJ2	7523	T6	Cisplatin
134019B	4694	T2	Ruc300	134013 NHEJ2	7535	T6	Ruc450
134019B	4617	T3	Ruc300	134013 NHEJ2	7539	T6	Cisplatin
134019B	4614	T3	Ruc300	134013 NHEJ3	7821	T6	Vehicle
134019B	4615	T3	Vehicle	134013 NHEJ3	7819	T6	NA
134019B	5058	T4	Vehicle	134013 NHEJ3	7154	T5	NA
134019B	4698	T2	Vehicle	134013 NHEJ4	8085	T6	Vehicle
134019	3547	T4	Vehicle	134013 NHEJ4	8086	T6	NA
134019	2144	T3	Vehicle	134013 NHEJ4	7155	T5	NA
134019	2962	T3	Ruc150	134013 NHEJ4	8073	T6	Ruc450
134019	2276	T3	Ruc150	***93 samples prepared and shipped in total***			